SURSAT ICE EXPERIMENT REPORT

Surveillance Satellite Project Workshop

on

Active and Passive Microwave Measurements

of

Sea Ice and Icebergs

Atmospheric Environment Service

Toronto, June 23-27, 1980

Summary Report

Edited by: René O.Ramseier

David J. Lapp

Rec'd: Jan 26/82
Order No.: WF
Price:
Acc. No.: Atmospheric
Env. Service

BOREAL INSTITUTE
LIBRARY
45613

TABLE OF CONTENTS

1. Summary of Workshop Panel Discussions

2. O.A.O. Workshop Summary

3. Acknowledgements

4. Editorial Note

5. Papers Presented at Workshop

    5.1 Single and Multiple Parameter Microwave Signatures of Sea Ice, Hawkins, R.K., C.E. Livingstone, A.L. Gray, K. Okamoto, L. Drapier Arsenault, D. Pearson and T.L. Wilkinson

    5.2 Eastern Arctic SURSAT SAR Ice Experiment, Radar Signatures of Sea Ice Features, Ketchum Jr., R.D. and L.D. Farmer

    5.3 Intermediate Results of the Radar Backscatter Study of Sea Ice in the Beaufort Sea, Delker, C.V., R.G. Onstott and R.K. Moore

    5.4 Microwave Signatures of Sea Ice in the Marginal Ice Zone, Skou, N.

    5.5 Classification of Beaufort Sea Ice Using Active and Passive Microwave Sensors, Livingstone, C.E., R.K. Hawkins, A.L. Gray, K. Okamoto, T.L. Wilkinson, S. Young, L. Drapier Arsenault, D. Pearson

    5.6 West Greenland Sea Ice Experiment, SURSAT Report No. 1, Gray, L., P. Gudmansen, S. Overgaard, N. Skou, F. Sondergaard Pederson

    5.7 Depression Angle Study, SURSAT Report No. 2, Gray, L.

    5.8 Qualitative Comparison of SLAR and SAR Data Sets, Hengeveld, H.G.

    5.9 X-Band SAR Image Response From First-Year Ice Off Newfoundland, Wedler, E. and J.R. Rossiter

    5.10 The Implications of Meltponds to the Remote Sensing of Sea Ice, Kirby, M.E., R.O. Ramseier, D.E. Pearson and R.G Dixon

    5.11 Ridge Height Measurement With SAR, Inkster, D.R. and R.T. Lowry

5.12 Radar Detection of Sea Ice Ridges and Icebergs in Frozen Oceans at Incidence Angles from 0° to 90°, Pearson, D., C.E. Livingstone, R.K. Hawkins, A.L. Gray, L. Drapier Arsenault, T.L. Wilkinson, K. Okamoto

5.13 Iceberg Detectability Problems Using SAR and SLAR Systems, Kirby, M.E. and R.T. Lowry

5.14 Digital Image Analysis of SAR Imagery for the Detection of Icebergs, Kirby, M.E.

5.15 Quantitative Analysis of Ice Radar Images Using Digital Image Processing Techniques, Tang, G.Y.

5.16 Sea Ice Detectability as a Function of Resolution and Mixed Integration, Luther, C.A. and R. Schuchmann

5.17 Optimizing Imaging Radar Parameters for Ice Reconnaissance, Lowry, R.T. and H.G. Hengeveld

5.18 Experimental Use of Real-Time SAR Imagery in Support of Oil Exploration in the Beaufort Sea, Mercer, J.B., R.T. Lowry, and S.K. Leung

5.19 Airborne Impulse Radar Soundings of Sea Ice - Rossiter, J.R., K.A. Butt, J.B. Gamberg and T.F. Ridings

5.20 Impulse Radar Profile Over T-3, Rossiter, J.R., K.A. Butt and J.B. Mercer

5.21 Labrador Ice Dynamics Experiment (LIDEX), Denner, W.W. and T.E. Keliher

5.22 The Special Sensor Microwave Imager (SSM/I) for the Defense Meteorological Satellite Program (DMSP), Burke, H.K., K.R. Hardy and J.C. Barnes

5.23 List of Participants

6. SURSAT Ice Experiment Report

6.1 Introduction

6.2 Experimental Procedures

6.3 Discussion of Final SURSAT Meeting Contributions

6.4 Marine (Ice) Environmental Information Program

6.5 General Conclusions

6.6 Acknowledgements

6.7 References

Appendix 6.1 Interdepartmental Task Force on Surveillance Satellite Census of Surveillance Requirements

Appendix 6.2 Remote Estimation of the Properties of Sea Ice Publication List - March 1980

7. RADAR Satellite Program

Appendix 7.1 Bilateral SAR Satellite Mission Requirement Study Program Implementation Plan Appropval

Appendix 7.2 Joint NASA/DEM&R SAR Satellite Mission Requirement Study Program Implementation Plan Scope/Content

1. SUMMARY OF WORKSHOP PANEL DISCUSSIONS

On the last day of the workshop, June 26, 1980, panel discussions were held to outline analysis and experimental priorities as well as programs presently ongoing and planned for the future. The workshop broke into four panels:

1. *Experiments - Active and Passive (L. Jones, C. Swift, Co-Chair.)*
2. *Microwave Theory and Ice Modelling (J. Rossiter, R. Moore, Co-Chair.)*
3. *Industrial Requirements (B. Mercer, Chair.)*
4. *Present and Future Programs (F. Carsey, H. Hengeveld, Co-Chair.)*

The results of each panel discussion are summarized mostly in point form in the following sections:

PANEL 1 - EXPERIMENTS - ACTIVE AND PASSIVE

1.1 Problem Areas Requiring Research

a. *The effect of snow on the backscatter coefficient*
b. *Wet ice and snow*
c. *Dielectric properties*
d. T_b *for thin ice*
e. *Emissivity/temperature dependence*
f. *Ice type identification and frequency dependence*
g. *Meltponds*

1.2 Research Priorities and Policy

a. *Continue development of combined active/passive remote sensing ice algorithms.*

b. *Explore the middle microwave band (3-8.6 Hz) and develop 5-6 GHz scatterometer.*

c. *Develop remote sensing packages for on-site field experiments and aircraft experiments with:*

- *near real-time capability - requires minicomputer*
- *participation by hardware sponsors and manufacturers*
- *availability of technical staff and expertise to repair and modify system*
- *supporting services on-site*

This could be addressed in the form of a remote sensing facility with available sensors that can be utilized in the field or on aircraft.

d. *Processing of SEASAT ice data including*

- *SASS*
- *SMMR (at least to* T_b *level)*
- *Altimeter*

Orbits for future processing and analysis still have to be prioritized.

e. Utilize the NASA C-130, 990, AES Electra, CCRS Convair 580 and other aircraft of opportunity for future programs and experiments.

f. Require aircraft and field experiments as well as lab experiments.

g. Data sets should be available within a national archive.

1.3 5-10 Year Plan

a. Aircraft Field Experiments

- *Locations - Beaufort Sea, Bering Sea, East Greenland, Labrador Sea, Lancaster Sound*

- *Timing - Canadian yearly*
  - *Joint US/Canadian cooperation in even years beginning in 1982.*

b. Surface Based Field Experiments

- *Locations - Beaufort Sea, Bering Sea, Barents Sea, East Greenland, Pond Inlet and Greenland ice sheet*

- *Timing - yearly.*

PANEL 2 - MICROWAVE THEORY AND ICE MODELLING

Although it is clear that radar imaging can give much information about sea ice, many unresolved questions remain. Most of the existing data are either in the form of image interpretations or empirical curves of variation of scattering coefficient with different parameters. With regard to the latter, even though many empirical curves exist for scattering coefficient versus angle frequency, polarization and ice type, serious gaps exist in the information because of a lack of observation during the fall and summer seasons and apparent differences that have not been reconciled between the observations made in the Beaufort Sea and those made off Labrador.

Carefully controlled experiments both in the laboratory and in the field need to be continued for some time if we are to resolve the as yet unanswered questions. Particular emphasis needs to be placed on determining whether the properties of radar return from sea ice depend strongly on differences in the ice characteristics in different parts of the Arctic and certainly emphasis needs to be placed on summer and fall measurements, which are indeed rare.

2.1 Overview

a. EM properties of ice and snow cover

b. Evaluate dielectric constant for varying frequency, salinity, temperature, structure and free water content.

c. Spacial distribution of dielectric constant

   - fine scale differences
   - horizontal and vertical variations particularly near the surface
   - varying ice types and structures including multi-year, first-year, ridges, and new ice forms

d. Measurement technique evaluation and development required.

e. Measurement frequencies - 0.1 - 16 GHz as well as 37 GHz.

f. Standardized reporting scheme for the above results applied to theory for scatter and emission.

2.2 Suggested Lab Environment Experiments

a. Grow sea ice under multiple conditions and examine:

   - dielectric profiles
   - backscatter vs frequency, incidence angle, polarization
   - brightness temperature vs. frequency, incidence angle, polarization
   - measure radar profiles
   - examine all feasible environmental conditions

b. Frequency range (1-2), 2-16, 35 GHz

c. Incidence angle - 0^{o} to the limit possible

d. Horizontal, vertical and cross polarization

2.3 Suggested Field Experiments

a. Measurements of dielectric constant, radar profiles as for lab experiments

b. Measurements of backscatter and brightness temperature versus frequency, incidence angle and polarization as for lab experiments

c. These measurements require surface truth

   - surface roughness of snow and ice
   - snow - depth, density, temperature, free water content and grain structure
   - ice - thickness,salinity, temperature, grain structure, density and history

d. Varying measurement conditions

   - temperal,- melt, freeze, mid-winter
   - locations - Beaufort Sea, multi-ice zones, perennial pack

e. *Varying types of ice*

- *types of pack exceeding ½ m thickness*
- *thin ice where signatures are ambiguous*
- *first-year and multi-year ridges especially their azimuthal response*
- *blocks and rubble*
- *icebergs*

f. *Cell size should be small (in order of meters) but large enough to see features.*

g. *Resolution studied should be guided by forecasting and pattern recognition (Moore's tradeoff paper)*

h. *Analyse multi-sensor data for total needs*

2.4 *Pattern Recognition and Processing Considerations*

a. *How can we enhance results to pull out parameters of interest*

b. *Multi-sensor requirement*

c. *Display requirements*

PANEL 3 - INDUSTRY REQUIREMENTS

3.1 *Policy*

a. *Industrial requirements should serve as guidelines for research and development effort. This happens reasonably successfully in Canada, less so in the United States.*

b. *Industry must make a more determined effort to exactly define its requirements.*

c. *The time scale of R&D efforts should be linked to the time scale of industrial requirements. An example of this is the 1985 Arctic LNG tanker route startup.*

d. *For tactical support, all-weather capability is an operational necessity.*

3.2 *Research Priorities*

a. *Development of ship-borne remote sensing systems for hazard detection is an industry priority and should be within the mandate for R&D activities of the remote sensing community if not SURSAT itself.*

b. *Iceberg detection by SAR/SLAR and/or passive microwave images should be a priority R&D activity.*

c. *Seastate, currents and other similar environmental data on the East Coast are an industry priority.*

3.3 Conclusions

a. *In certain areas such as the Beaufort Sea, we have sufficient understanding to commence operational use of airborne SAR/SLAR systems now. This does not appear to apply to East Coast regions.*

PANEL 4 - PRESENT AND FUTURE PROGRAMS

4.1 Program Issues

a. *Timetable considerations required for each program*

- *remote sensor development*
- *ship/aircraft availability*
- *measurement and analysis techniques required*
- *principal investigators*
- *need*
- *physical and financial resources*

b. *Interagency/industry collaboration*

- *more communication needed*

c. *Priorities*

d. *Research issues relating to programs*

e. *Present and future programs (Table 4.1)*

4.2 Other Required Studies

a. *Summer transition ice experiment*

- *microwave properties of summer melt ice*
- *pilot study under way in Beaufort Sea by CCRS, also AES meltpond study*

b. *Lake/river ice*

- *more research on freshwater ice*

c. *SEASAT data*

- *continue ongoing analysis and processing of SEASAT data bank*

d. *Coastal zone ice*

- *cross-correlation between existing sensors and microwave required*

e. *Historical data*

- *Survey various ice people to see what data exists, where it is and its availability.*

TABLE 4.1: PRESENT AND FUTURE PROGRAMS

PROGRAM/PARAMETER IDENTIFICATION	PLANNED TIME OF PROGRAM	GEOGRAPHICAL LOCATION	PRINCIPAL DRIVER	ADDITIONAL COMMENTS
Climate				Analysis of historical data banks
Southern Oceans	1980 (October)	Fringe areas of Antarctic	CRREL	Near ice zone studies
	1981	"	US/USSR	"
	1982	"	US/GDR	"
Fram III	March-May 1981-1989		US Military	
YMER 80	1980		Sweden	X-band scatterometer study
Baltic Sea	Ongoing	Baltic Sea	Scandinavia, GDR	Expt. phase Ericsson SLAR + observers mapping ice
Swiss Expedition	March - April 1982	North Pole	Switzerland	Willing to collect surface data
North Water	Ongoing	Smith Sound	Polar Continental Shelf Project (PCSP)	
Marine Radar	1980	Lancaster Sound	Petrocan/AES	Detection of ice hazards
Thickness Radar	Ongoing		C-CORE, MPB Technologies NRC	Synthetic Pulse/Impulse radar Test flown Spring 1979-1980
MIZEX (Marginal Ice Zone Expt.)	Spring 1982	Barrants Sea	US Navy	Similar to NORSEX

TABLE 4.1: PRESENT AND FUTURE PROGRAMS

PROGRAM/PARAMETER IDENTIFICATION	PLANNED TIME OF PROGRAM	GEOGRAPHICAL LOCATION	PRINCIPAL DRIVER	ADDITIONAL COMMENTS
LIDEX (Labrador Ice Dynamics Expt.)	March 1982 - Pilot Study	Labrador Coast	C-CORE Memorial University	Drifting buoys for ice movement
WIEBS (Winter Ice Experiment in Beaufort Sea)	Winter 1981, 1982	Beaufort Sea	AES/Intera	Ice modelling effort
Bering Strait	1981-initial work 1982 - experiment	Bering Strait	Univ. of Washington	Bottom buoys
Pond Inlet	Spring 1981 - start	Pond Inlet, N.W.T.	AES/NASA Langley	- radiometer attached to tower - long term project for complete ice cycle
Fixed Based Radar	1980	Lancaster Sound - Bylot Basin	AES/Petrocanada	Ship + land radar discrimination of sea ice at high incidence angles
Radar Parameters SAR mission C-band High angle scatterometer High frequency systems	1981-1983	Various areas	CCRS Convair 580 pgm	- weather effects of higher frequency systems - partly in support of RADARSAT pgm.
Icebergs	Presently ongoing	Atlantic Ocean	US Coast Guard	Work on microwave signatures required
Canadian Ice Reconnaissance	Ongoing	Canadian Arctic/Gulf of St. Lawrence	AES Ice Branch	Operational pgm. using SLAR

TABLE 4.1: PRESENT AND FUTURE PROGRAMS

PROGRAM/PARAMETER IDENTIFICATION	PLANNED TIME OF PROGRAM	GEOGRAPHICAL LOCATION	PRINCIPAL DRIVER	ADDITIONAL COMMENTS
W. Weeks Experiment	1981-82	CRREL laboratory	CRREL	
Over the Horizon Radar	1980-81	Labrador Sea, Grand Banks	C-CORE, CRC (DFO)	HF skyborne and ground-borne radar to estimate ocean parameters and to detect ice and icebergs
RADARSAT	1980-1990	Arctic Regions	AES/EMR and NASA	Operational satellite with C-Band SAR Launch in 1988

FINAL DISCUSSIONS

After panel deliberations and their reports to the participants, the floor was opened for general discussion.

V. Nerella stated that, in order to communicate with the remote sensing community interested in ice research, an informative newsletter with planned programs, schedules of experiments, highlights of results of analyses, data set availability, etc., would be extremely useful.

W. Denner suggested exploring the possibility of communicating with other researchers in the remote sensing of ice, through the C-CORE Bulletin.

B. Mercer suggested pursuing this idea through CCRS Newsletter.

R. Ramseier stated that he would look into these alternatives.

J. Crawford thought that an annual workshop of this nature may be more useful than a newsletter.

W. Denner suggested bringing out an informative list similar to UNOLS (?) on several research programs involved in remote sensing of ice.

R. Ramseier thanked all the participants for their contributions to this successful workshop.

Next workshop of this nature will be at Langley Research Center, Hampton, Virginia, U.S.A. April 6-9, 1981.

2 SURVEILLANCE SATELLITE PROJECT WORKSHOP
ON
ACTIVE AND PASSIVE MICROWAVE MEASUREMENTS
OF
SEA ICE AND ICEBERGS

Toronto, Ontario, Canada

June 23-27, 1980

Prepared for

ICEX Science and Applications Working Group
National Aeronautics and Space Administration
Goddard Space Flight Center
Greenbelt, Maryland 20771

In Response to
Contract Number NAS5-25605 (MOD 2)

Prepared by

OAO Corporation
50/50 Powder Mill Road
Beltsville, Maryland 20705

The final Surveillance Satellite (SURSAT) Project Workshop on active and passive microwave measurements of sea ice and icebergs was called to order by Dr. Rene Ramseier at 9:00 a.m. on June 23, 1980.

Results from research projects were presented during the first two days of the workshop. The ordering of presentations generally followed the list in the pre-workshop mailing. Only the major results and conclusions which were presented will be discussed here.

R. Inkster said that the SURSAT airborne SAR project begin flying in July 1978. A total of 27,000 line-km were flown for experiments chosen by the SURSAT selection panel; 50% of the experiments were related to ice research. Of the data taken, 50% was of good quality and 85-95% was usable by the P.I. Evaluation of the data led to the conclusion that imaging radars can be quite useful in ice applications, performing functions such as distinguishing among ice types, making ice swath images and locating icebergs, all in real time. High resolution imaging radar is now available for non-military applications. Also, many PI's have now worked with the data and expertise in imaging radar has been built up in Canada's private sector.

R. Hawkins discussed results obtained by simultaneously observing profile signatures with both a microwave radiometer and a scatterometer. Several conclusions were drawn from this work. First, cross-polarized radars show more db separation in σ^0 than like-polarized radars, facilitating ice classification. Also, the ε and σ^0 of sea ice vary with temperature and conditions such as snow cover. Finally, and most importantly, simultaneous measurements of ε and σ^0 may be able to distinguish among ice classes where neither parameter could do so alone. This is a major point, which was reiterated througout the workshop. Complementary measurements from an active and passive sensor may yield much more information than was previously expected. There is a need for more investigations of combined active/passive systems and their uses. Discussion from the floor pointed out that Dr. Hawkins' results indicated that frequencies around C-band (5 GHz) have potential for ice classification and should be investigated. Also, the possibility of real-time classification using a minicomputer system should be pursued.

During the first afternoon and second morning several speakers discussed their observations. A consensus seemed to emerge from these observations that several characteristics are desirable in an ice-observing SAR. First, X-band or higher frequencies are most useful for making observations of ice, since they give tonal information related to ice type; L-band only responds to gross surface features. Texture is important to interpretation, and obtaining texture information requires the resolution of a SAR rather than a SLAR. Preferred observing depression angles are in the range 10° to 45° below horizontal. Topography dominates returns at far range (shallow depression angle); electromagnetic properties of the ice dominate imagery characteristics at near range (steep depression angles). One observer, R. Ketchum, noted that he had found false images produced at far range, on the back side of objects, in L-band. It was not apparent whether this was a characteristic of L-band or of his particular data set; however, he noted that if this is a characteristic of L-band, then L-band is a poor choice for iceberg tracking.

J. Rossiter and R. Santos displayed 100 MHz impulse radar data taken on the ice island, T-3 in the Beaufort sea. The air-ice and ice-water interfaces were easily discernable. W. Weeks, using the NASA LeRC X-band SAR, found strong returns coming from lake ice with water under it and weak returns when the ice is frozen to the bottom. M. Kirby digitized X-band SAR data by scanning the film with a microdensitometer, and analyzed the data on a GE I-100 system in an effort to develop iceberg detection techniques. He found that the Gaussian normal distribution statistics assumed by the I-100 software packages were insufficient for obtaining iceberg information from pack ice data. R. Lowry, reporting on Project Berg Map, stated that the data gathered indicates that populations of icebergs are distributed exponentially with size. He also noted that at the depression angles used by satellites, water is brighter in X-band than icebergs, and wipes out the signature of the bergs.

Several scientists from NASA LaRC showed results of aircraft measurements of ice taken with active and passive microwave sensors during the Arctic Ice Ridge Experiment. NASA LaRC is very interested in combined active/passive techniques and will produce a compilation of the data that they have taken by the fall. The instruments used were a nadir-viewing C-band step-frequency microwave radiometer (SFMR), and a 13.9 GHz scatterometer. The results showed the scatterometer response to first-year and multi-year ice and the effects of ridging. The SFMR distinguished between first-year and multi-year ice, observing a 5^{0} difference in brightness temperature between the two at 5.5 GHz. A similar Danish experiment, described by N. Skou, yielded similar results. The instrumentation included an X-band scatterometer and a radiometer with bandpasses at 5, 17 and 34 GHz. The largest radiometric variations occurred at 5 GHz and the smallest at 34 GHz, where the brightness temperature was uniformly high. Discussion of these results showed great interest in pursuing further research into the uses of C-band sensors.

Presentations of results continued into the third day. L. Arsenault presented results of a Seasat SAR optical ice data survey, which showed ice motions of 4 km/day between 8 and 24 August, 1978, and ice concentrations of about .4 near Banks Island. The survey found a cigar-shaped brightly emitting feature in 15 of the 50 passes examined. The feature was 3 km long x ½ km wide, and was not easily discernable in colocated SLAR data. The SAR that saw the feature was L-band with a high incidence angle; the SLAR that missed it was X-band with a low incidence angle. R. Ramseier said that Seasat SAR optical data analysis is being done very carefully and moving along slowly, and that there are not yet any conclusive digital results.

B. Mercer discussed the use of shipborne and airborne radars to provide an early warning system for oil drilling operations. Industry requirements are for a daily 25 x 40 km image centered on a drilling site and having a resolution better than 30 meters.

The remainder of the third day was dedicated to the "Quickie" session of brief reports on programs, meetings, new technology and systems. A listing of the speakers and their topics is included as an attachment.

During this session, several points were raised which pertain to the ICEX program. The Labrador Ice Dynamics Experiment (LIDEX) held a workshop March 6-8. Management and scientific panels were named to develop an experimental program. This process is presently occurring. Panels were established on the following topics: transportation; fisheries; ice conditions; meteorology; oceanography; modeling; remote sensing; and ocean engineering. Some cooperative work between LIDEX and ICEX might be possible.

C. Luther said that the time frame for MIZEX will be 1982-86, with the major emphasis in 1984-85. Participants will include NSF, NASA, NOAA, ONR, USGS, Canada, Denmark, Germany, England, Norway and Japan. Some MIZEX activities may be performed in conjunction with NORSEX. The primary area of concern for MIZEX will be the East Arctic Ocean (centered around Spitzbergen); however, the experiment cannot consider only one marginal ice zone, and so the Bering and Chukchi Seas and possibly the coasts of Labrador and the Antarctic will be of concern. The steering committee will meet in Bergen, Norway in October. Also, MIZEX really requires a microwave spacecraft to use in its observational program. R. Moore noted that the U.S.S.R. presently has 3 oceanographic spacecraft all with passive microwave systems and possibly one with an active microwave system.

W. Campbell noted that there is a growing international voice for an oceans and ice space radar. The French and Germans may fly their own in the mid-1980's. Canada has put forward a proposal to build a C-band SAR and is presently looking for a partner with whom to fly it; this will be discussed further later in this report. Dr. Campbell also said that at a recent meeting in Europe he discovered that only 5 days worth of Seasat SMMR data has been processed. The ICEX Workshop on Seasat SAR, SMMR, Scatterometer and Radar Altimeter Results for Sea Ice, to be held in the Winter/Spring 1981, will need simultaneous observations from all four sensors within the four selected zones - Point Barrow, Prudhoe Bay, Mackenzie Delta, and Banks Island. Dr. Campbell said that the Seasat scatterometer and altimeter data sets will be ready by the time of the ICEX Workshop, but that the SAR and SMMR data sets are in trouble. He said that he will soon write NASA headquarters asking for their help in assuring that the data sets will be processed. Dr. Campbell stressed that ICEX will consistently and regularly plead for the U.S. to work for an imaging space radar for sea ice observations and a satellite-borne laser for ice sheet observations. Of the five principal sensors called for in the ICEX Report these were the only sensors not presently planned for a specific forthcoming satellite.

The fourth and final day of the conference began with a discussion of NASA's future plans by F. Carsey, followed by a discussion of Canada's proposal to build a C-band SAR by E. Shaw of the Canada Centre for Remote Sensing (CCRS).

Dr. Carsey outlined NASA's timetable which includes NOSS and TOPEX (merged with GRAVSAT) in 1986. Three flights are planned for SIR in 1984-5 (-6?), 2 of which will be in a polar orbit. SIR will have a 30 km swath, 20-30 m resolution and a data turnaround ratio of 40 minutes of processing to one minute of data. NASA will fly a SLAR with 1 km resolution and 500 km swath to accompany SIR; a microwave sounder and a (28 channel?) IR sounder may also accompany SIR. A free-flying applications SAR is tentatively scheduled for 1989; however, the wide range of users and programs can probably not be served by just one SAR. NASA will have no aircraft radar between now and the end of 1982.

In the short term, Canada will make use of aircraft SAR. However, E. Shaw stated that CCRS has proposed that Canada budget $80 million for a satellite-borne SAR (also recognizing that they will also have to pay for a ground system as well). Canada is presently looking for a collaborator for this program. Candidates include the U.S., ESA, and Japan. The spacecraft would include instruments other than the SAR only if desired by Canada's collaborators. The first launch would be no earlier than 1987 and would be a demonstration, not an operational system. Current intent is to build a C-band (5.3 GHz) radar (or an L-band if the C-band SAR proves too difficult technically). The design and mission requirement studies will take 2 years; building the SAR will take 4 years. The demonstrational flight will occur from 1987 to 1990. Canada wishes to negotiate joint access to SAR and NOSS data with the U.S. A Canada-U.S. meeting will occur on July 10 in Ottawa, from which a joint mission requirements study will probably result. A Canadian decision on the CCRS proposal will be forthcoming by the fall.

Several points were raised during the discussion. First, a C-band radar may not be sufficient for agricultural purposes. NASA is presently planning to perform an intensified mission requirements study for SAR. Also, someone at MacDonald-Detweiler and UBC (Forestry Department) has coregistered a Landsat MSS image with a Seasat SAR image.

At this point, the workshop broke into panels to make recommendations for future experiment plans and programs. The four panels were:

a. Experiments - Active and Passive (L. Jones, C. Swift, co-chair)

b. Theory/Controlled Experiments (J. Rossiter, R. Moore, co-chair)

c. Industrial Requirements (B. Mercer, chair)

d. Programs (F. Carsey, H. Hengeveld, co-chair)

The results of the panel meeting were presented to the full group and are shown in the attachments, along with a 10-year plan developed by the experiments panel. More detailed viewgraphs of the panel recommendations will be typed up and mailed out to workshop participants very soon.

After presentation of the panel reports, the workshop was adjourned.

Attachment A

"Quickie" Session Speakers

Speaker	Topic
M. Warren (C-CORE)	Comparison of SAR-Impulse Data
G. Tang (SUNY at Buffalo)	Radar Image Processing Digital Techniques
S. Peteherych (AES)	AES Satellite Laboratory
V. Neralla (AES)	Winter Ice Experiment, Beaufort Sea
R. Inkster (INTERA)	WIEBS Site Specific Program
B. Mercer (Dome Petroleum)	Dome Program
R. Hawkins (CCRS)	Beaufort Sea Summer Program
J. Barnes (ERT)	U.S. Military Microwave Program
B. Jonasson (Petro-Canada)	Petro-Canada Program
J. Rossiter (C-CORE)	Ice Sounding Radar
H. Edel (OAS)	OAS Ice-Related Activities
H. Ramplee-Smith	Lasar Profilometer for Ridge Studies
J. Rossiter (C-CORE)	Over the Horizon Radar
W. Denner (NICOS)	LIDEX
C. Luther (ONR)	MIZEX
L. McNutt (PMEL)	Bering Sea Marginal Ice Zone
W. Campbell (USGS)	ICEX
R. Moore (U. of Kansas)	Venice Highlights, URSI Symposium

Attachment B

Workshop Panel Reports

1. Experiments - Active and Passive

   - Continue develope**m**nt of combined active/passive
   - Re-explore the 3-8 GHz band
     - Develop 5-6 GHz scatterometer
   - Encourage laboratory and on-site field experiments
   - Aircraft experiments in even years
   - Reduction of Seasat data
   - Develop remote sensing package for on-site field experiments and aircraft experiments
   - Utilize NASA C-130, 990 and aircraft of opportunity
   - Work into the NOSS validation plan

2. Theory/Controlled Experiments

   - Electromagnetic properties of ice and snow cover
   - Lab environemnt experiments
   - Field Experiments
   - Resolution Studies
   - Pattern recognition and processing

3. Industrial Requirements

- Industrial requirements should guide research efforts
- Industrial requirements must be defined
- Time scale of industrial requirements and reserch efforts should be linked
- All-weather capability is an operational necessity
- Industry requires shipborne remote sensing systems for hazard detection
- Industry requires airborne iceberg detection by SAR/SLAR and/or passive imagers.
- Operational use of SAR/SLAR should begin in certain areas (e.g. Beaufort Sea)
- Industry and research should fully analyze data and cooperate by exchanging data
- East coast of Canada is a priority area

4. Program Issues

- Timetables
- Interagency and industry collaboration
- Planned/needed program
- Research issues-programs
- Priorities

UNITED STATES
DEPARTMENT OF THE INTERIOR
GEOLOGICAL SURVEY

Ice Dynamics Project,USGS
Thompson Hall Room No.113
University of Puget Sound
Tacoma, Washington 98416

August 8, 1980

Dr. Ron Greenwood
Director, Environmental Observation Divison
NASA Headquarters EB-8
Washington, D.C. 20546

Dear Ron,

The purpose of this letter is twofold--to give you a brief update on progress and plans of the ICEX Scientific and Applications Working Group and to ask your advice and help on a data flow problem.

First, the ICEX update. The SAWG meeting held at Goddard from 23 through 25 April 1980 accomplished a great deal and was characterized by the normal ICEX ebullience and optimishm. You have probably seen the minutes of this meeting, but with your extraordinarily packed schedule I guess you may not have had time to read them. Perhaps, the most important event at the meeting was the timely creation of two subcommittees: the ICEX Research Analysis Facility Subcommittee, with Jay Zwally as the Acting Chairman; and the ICEX Data Platform Subcommittee with Jim Overland of NOAA-PMEL as Chairman. Both subcommittees have been hard at work and are meeting their schedules this summer.

The next meeting of importance to ICEX was the Surveillance Satellite Project Workshop on Active and Passive Microwave Measurements of Sea Ice and Icebergs held at the offices of the Atmospheric and Environmental Sciences (AES) in Toronto, Ontario, on June 23-27, 1980. Six members of the ICEX SAWG attended this excellent meeting. I enclose a copy of the minutes of this meeting prepared for ICEX by Frank Stone of OAO.

At both of these meetings the ICEX scientists discussed the ICEX Workshop we are planning to have in early 1981 on the analysis of the Seasat SAR, SMMR, Scatterometer, and Radar Altimeter date ensemble for sea ice. The need for such a workshop is clearly and universally recognized. The analysis of much of the aircraft data of active and passive microwave observations of sea ice is proceeding excellently--the recent SURSAT meeting mentioned above, the recent NORSEX workshop in Bern in June, the forthcoming NORSEX workshop in Bergen in September, and the forthcoming URSI Symposium on Signature Problems in Microwave Remote Sensing of the Surface of the Earth at the University of Kansas in January 1981 (which will be combined with an ICEX SAWG meeting) have given or will soon give much valuable results of aircraft observations. All ice scientists involved agree that following these meetings the time is ripe to finally do a joint analysis of the simultaneous Seasat active and passive microwave data of sea ice. It behooves us to recall at this moment that this analysis of the full Seasat microwave data ensemble for sea ice was clearly stated as an important objective f~~our~~ive years ago by the Seasat SAR and SMMR teams. Many members of the ICEX SAWG have spent a considerable part of those five years assiduously working toward this goal. The Seasat sea ice data ensemble is a unique and very important data set that must be analyzed.

Ron, here is where I earnestly request your help. The ICEX SAWG wishes to have this Seasat Sea Ice Microwave Workshop in April or May 1981. We have selected four areas of the Beaufort Sea-Pt Barrow, Prudhoe Bay, MacKenzie Delta, and Banks Island--where we feel we must analyze simultaneous Seasat SAR, SMMR, Scatterometer, and Radar Altimeter data. During many recent telephone conversations I have had with scientists at NASA Goddard, Langley, and JPL the following has emerged:

1) the Scatterometer data will be ready for the ICEX-Seasat meeting.

2) the Altimeter data will be ready for it also.

3) there is some doubt that a sufficient number of SAR images of the four selected areas will be digitally processed by the time of the meeting.

4) none of the Seasat SMMR data of the Beaufort Sea has been processed and it seems that JPL has no plans to process any of it.

The problems with the Seasat SAR and SMMR data processing are, as you are no doubt aware, complex, inter-related, and unfortunate. The problems are NASA ones, therefore the solution must be a NASA solution. We in ICEX are deeply indebted to you for your sustained interest and great help in our work, so we come to you now, once again, as friends seeking your aid.

Best wishes,

Bill

William J. Campbell
Chairman, ICEX SAWG

xc: Shelby Tilford, NASA HQ	Stan Wilson, NASA HQ	Jay Zwally, NASA GSFC
Bob Schiffer, "	Frank Carsey "	

ACKNOWLEDGEMENTS

The SURSAT workshop on Active and Massive Microwave Measurements of Sea ice and Icebergs was hosted by the Central Services Directorate, Atmospheric Environment Service.

The workshop could not have taken place without the efforts of the authors, session and panel chairpersons.

In addition, we would like to recognize the efforts of Henry Hengeveld who helped organize the workshops and Karen Laidlaw who helped extensively with the preparation of these proceedings.

4. EDITORIAL NOTE

The papers presented in Section 5 of these proceedings represent for the most part results and analyses of projects listed at the previous SURSAT ice workshop in May of 1979. Some of these papers, which are being reproduced as received, have been or are being published in other proceedings or journals, or as separate agency reports. They have been included here to provide a compilation of reports as complete as possible for easy access by the participants of SURSAT and other interested people.

A total of 22 papers are included. Some are extended abstracts of presentations made at the workshop while others were separate reports. The papers have been organized into several different subject areas:

a. sea ice classification based on active and passive microwave systems;
b. radar parameters vs. ice parameters;
c. microwave signatures of ice morphological features;
d. digital processing techniques and their evaluation;
e. operational considerations and demonstrations;
f. impulse radar for ice thickness;
g. future experiments and sensors.

The order of these proceedings follow the above guidelines. The proceedings are followed by Section 6 written by Rene O. Ramseier which provides a review and summary of the SURSAT ice experiment. Section 7 includes the recent agreement signed by NASA and DEM&R on a bilateral mission requirement definition study for a Radar Satellite (RadarSat).

It is hoped that these proceedings will serve as a useful reference for the state-of-the-art in microwave remote sensing of sea ice as well as provide insight into future directions and priorities, in support of NOSS and RadarSat.

SECTION 5.1

SINGLE AND MULTIPLE PARAMETER MICROWAVE SIGNATURES OF SEA ICE

Hawkins, R.K., C.E. Livingstone, A.L. Gray, K. Okamoto, L. Drapier
Arsenault, D. Pearson and T.L. Wilkinson

SINGLE AND MULTIPLE PARAMETER MICROWAVE SIGNATURES OF SEA ICE

R.K. Hawkins, C.E. Livingstone, and A.L. Gray,
Canada Centre for Remote Sensing, Ottawa

K. Okamoto,
Radio Research Laboratories, Tokyo

L. Drapier Arsenault,
Cold Regions Remote Sensing, Stittsville

D. Pearson,
Intera Environmental Consultants Ltd., Ottawa

T.L. Wilkinson,
University of Waterloo, Waterloo

ABSTRACT

Simultaneous 13.3 GHz dual-polarized fanbeam scatterometer data, 19.35 GHz horizontally polarized profiling radiometer data and nadir looking aerial photography with corresponding X- and L-band SAR (Synthetic Aperture Radar) imagery were collected with the CCRS Convair-580 in March 1979 in the Beaufort Sea and in the Eastern Arctic in April 1979. This data set was analysed to compile statistics on 11 WMO (World Meteorological Organisation) classes of sea ice, ranging from calm open water to multi-year ice and ice island.

The microwave signatures for each sea-ice class are presented in terms of the dependence on incidence angle and polarization of the backscattering coefficient as well as their emissivity and brightness temperature, at an incidence angle of 45°. Some class signatures were obtained at several temperatures which included the early stages of melting. These effects distort the microwave signatures, as is discussed for four ice classes.

The problem of sea-ice classification using quantitative microwave measurements is examined and it is shown that simultaneous emissivity and backscattering coefficient measurements using a fixed incidence angle can yield a unique sea-ice classification for certain instrument parameters.

INTRODUCTION

Much research effort has been directed towards the classification of sea ice using both passive (radiometric) and active (scatterometric, SLAR, and SAR) remotely sensed microwave data. Historically, individual studies have been based on single sensors (either active or passive) at a large number of frequencies in the range 400 MHz to 94 GHz and the bulk of the experimental data has been obtained in the Beaufort Sea under cold ($<-20^{o}$ C) conditions.

Rouse (1969) used 13.3 GHz, VV[1] polarized airborne fanbeam scatterometer data to show that the angular (θ) variation of the backscattering coefficient σ^{o}_{vv} defined a unique signature for open water, smooth first-year (FY) ice, rough FY ice and multi-year (MY) ice. Wilheit et al. (1972) reported that 'new' and 'old' ice had distinctive emissivities at eight frequencies over the range of 10.7 GHz to 58.8 GHz. Gloerson et al. (1973) showed that FY ice and MY ice had distinctive emissivities at 19.4 GHz. Meeks et al. (1974) reported that 37 GHz, dual-polarized radiometers at three incidence angles gave distinctive signatures for open water, FY ice, second-year (SY) ice, MY ice, and refrozen melt ponds. Parashar et al. (1977) extended the work of Rouse at 13.3 GHz by testing a Bayesian classifier based on the complete angular dependence of σ^{o}_{vv}. Seven ice thickness intervals corresponding to water, nilas, grey, grey-white ice, smooth FY, rough FY and MY were used as classes. The full set could be classified to 60% accuracy and a coarse subset of water and thin ice, FY ice and MY ice could be classified to better than 90% accuracy. In addition to the 13.3 GHz data , four-polarization (VV,HH,VH, and HV), 400 MHz scatterometer data were tested and found to yield 75% classification accuracy for the subset.

Gray et al. (1977a) extended the backscattering coefficient - angle data set to include younger ice forms found near the east coast of Canada in cold conditions, using a dual-polarized 13.3 GHz fanbeam scatterometer. The cross-polarized signatures, $\sigma^{o}_{vh}(\theta)$, were found to yield better ice type discrimination than $\sigma^{o}_{vv}(\theta)$. Gray et al. (1977b) reported dual-polarized 13.3 GHz fanbeam scatterometer signatures for older ice types in the Beaufort Sea and again found that cross-polarized $\sigma^{o}_{hv}(\theta)$ provided superior ice class discrimination. They also obtained joint scatterometer and 37 GHz radiometer data and noted that for some ice classes, the two instruments appeared to yield complimentary data.

---

[1] For the active sensors, polarization notation is such that the first letter (H or V) is the transmitter polarization and the second letter (H or V) is the receiver polarization.

Onstott et al. (1979) used a multi-frequency, dual-polarized ground based scatterometer to determine signatures for FY, MY, lake, and ridge ice at 1.5 GHz and 8 to 18 GHz. Again cross-polarized backscattering coefficients were found to yield superior ice signature separation.

Troy et al. (1980) have shown that multi-frequency radiometer measurements are capable of resolving 'new' ice, 'young' ice, FY ice, MY ice and open water provided that the frequency spread is sufficiently great.

The present paper extends these works to a wider range of sea-ice classes and surface conditions. We give a new sea-ice classification scheme based on simultaneous, dual-polarized backscattering coefficients and radiometer measurements at a single incidence angle.

EXPERIMENT

During the SURSAT Sea-Ice Experiment, the CCRS Convair-580 gathered nadir-looking, wide angle aerial photography, 19.4 GHz (1.55 cm), H-polarized radiometer measurements at an incidence angle of 45°, and 13.3 GHz (2.25 cm), HV and HH- polarized fanbeam scatterometer measurements over the range of incidence angles from 0 to ±60° in a series of flight lines. Flight lines in the Beaufort Sea during March, 1979 under cold (-27 to -34° C) conditions included mainly FY and MY ice with small segments of young ice. Data from FY and younger ice forms under melting conditions (-2° C) and freezing conditions (-5° C), warmer than those experienced in the Beaufort Sea, were also collected during a mission to the Eastern Arctic in April, 1979. In addition to this profiling sensor data, overlapping microwave imagery was taken using the ERIM X/L multipolarization SAR. The imagery was optically processed to 3 m resolution.

The CCRS, CW fanbeam (3° across track and ±60° along track) scatterometer is described by Gray and Chan, 1979 and usual procedures were employed to translate the Doppler profile of the receiver signal into backscattering coefficients as a function of incidence angle and polarization $\sigma^o_{hh}(\theta)$ and $\sigma^o_{hv}(\theta)$. The 19.4 GHz Dicke radiometer[2] used in this experiment has a fixed pyramidal horn antenna which points 45° forward along the aircraft track. The beam width is approximately 5.5° and only

H-polarized radiation is recorded. Radiometer readings were converted to brightness temperatures (T_B) and estimations of surface emissivity, ε, were made using the relation (Wilheit et al., 1972):

$$\varepsilon = \frac{T_B - T_{SKY}}{T_{SURF} - T_{SKY}} \tag{1}$$

In this relation, T_{SKY} is the radiometric temperature of the atmosphere at 19.4 GHz, and T_{SURF} is the physical temperature of the surface footprint under study.

σ^o_{hh}, σ^o_{hv}, and ε time histories were constructed along each flight line and were related to a linear mosaic of the aerial photography. Figure 1 shows a segment of this photomosaic with corresponding backscattering coefficients and brightness temperature along a flight line in the Beaufort Sea. A strong delineation[3] is seen in the scatterometer $\sigma^o_{hv}(\theta)$ curves between the FY ice before the ridge at B and the SY ice beyond this ridge.

In general, interpretation of ice photography (____, 1978) allowed a complete identification of segments of the flight history into ice events. Extraction of time boundaries, derived from cross-comparison with the profiling sensor time histories, provided a means of indexing and accessing data stored on computer.

A data base of microwave brightness temperature and backscattering coefficients for events from each flight line was constructed and further indexed by their WMO ice class or subclass. Figure 1 shows events 172 and 173, two examples of data from this data base. This system provided a means to study each ice class over a large region of the Arctic and develop a staticistical basis for their microwave properties.

Ground truthing of the data consisted primarily of photo interpretation; however, some ground-based studies accompanied the airborne measurements. In the Beaufort Sea,

---

[2] We are indebted to NASA Langley Research Centre, particularly Dr W.L. Jones, for the loan of the radiometer, its outfitting and calibration.

---

[3] Note that the response time of the radiometer is much greater than the scatterometer, mainly due to its larger footprint.

several physical parameters (ambient, surface and internal ice temperatures; surface roughness features; ice thickness; salinity and internal structure etc.) were studied at several locations on and near the experimental flight lines as part of the SURSAT ground truth program (SURSAT ground truth report, 1980; and Rossiter et al., 1979). Ground truthing was limited by rotten ice conditions in the eastern Arctic, as reported by Gray et al. (1979).

RESULTS AND DISCUSSION

Table 1 is a listing of the ice classes and subclasses which were studied in the experiment, together with the total number of sensor footprints (samples) and events which formed the basis for the set. The location of the event and approximate ambient temperature is also indicated since the mechanical and thermal history are important factors in determining the physical properties which control its microwave emissivity and backscattering coefficient.

From Table 1, it is clear that all of the old ice forms (SY, MY and Ice Island) were found in the Beaufort Sea under cold conditions ($< -30^\circ$ C). Most of the region to region overlap (and the most common class studied) was FY ice. Grey and grey-white ice were also studied under several temperatures and regions but these classes were sufficiently rare that only tentative conclusions may be drawn from the results processed so far. The very young ice forms (frazil, nilas, grease) and water were found in large enough sections in the eastern Arctic only, under near melting conditions.

Table 2 is a statistical summary of data from the complete analysis of the Active-Passive Experiment giving σ^o_{hh} and σ^o_{hv} for 6 look angles with T_B and ε estimates for the ice classes presented in Table 1[4]. The standard deviations given with each class are by sample and therefore favour the larger events. In general, the standard deviation between events is greater than the standard deviation within an event. The ice thickness data included in Table 2 is typical of the associated ice type (Dunbar, 1969) but were not measured in the experiment; the implication is that by remotely sensing the class to which an ice target belongs, its physical properties can be inferred for reconnaissance and navigation purposes.

---

[4] It should be noted that the scattering coefficient results implicitly include an estimation of the 2-way antenna pattern of the scatterometer. This function is known to better than 2 dB accuracy over most of the angular range, but a greater uncertainty exists between 45 and 60°. An improved estimation of the antenna pattern is now under review. An accurate knowledge of the antenna pattern however, is not important in comparing the backscattering coefficients at the same incidence angle since their dB separation is independent of the antenna pattern.

Ice Classification by Microwave Emissivity at 19.4 GHz

Figure 2 shows the relation between microwave emissivity, ε, of various ice classes as a function of ice thickness using the thickness estimates from Table 2. Differences in emissivity may be attributed to variations in surface layer properties (as deep as one skin depth) rather than ice thickness (Troy *et al.*, 1980). Emissivity increases as the ice thickness increases and reaches a maximum for medium FY ice. Similar results have been reported by Troy *et al.*, 1980. When the ice becomes thicker than medium FY ice, emissivity decreases with increasing ice thickness. These two tendencies are shown in Figure 2 by straight lines and data from different flight lines are shown by different symbols. It is clear from the figure that ice thickness (or type) cannot be uniquely determined from microwave radiometer data alone, when only one frequency and look angle is employed.

The majority of the ice younger than FY in this experiment, at the left side of Figure 2, is rather smooth and is close to the melting point, with the exception of a few grey and grey-white samples from the Beaufort Sea. The increase of emissivity with the increase of ice thickness (or age) may be explained by the change of the complex dielectric constant of the surface ice as controlled by the brine volume fraction. The ice on the right hand side of Figure 2, however, is described as old, rather rough and very cold (around -30° C in the Beaufort Sea) and is less saline, which results in low imaginary dielectric constants and larger values for skin depth. Therefore, not only the radiation from the surface, but also from the interior volume must be considered. Volume scattering effects from interior vacancies in old ice may be important in explaining the associated decrease in emissivity.

Backscattering Coefficient Sea-Ice Signatures

Inherent difficulty also exists with the classification by radar backscattering along. Figure 3 illustrates this difficulty, combining both σ^{o}_{hh} and σ^{o}_{hv} at an incidence angle of 45°. The outlined data envelopes represent the boundaries of event statistics from four flight lines. The central section of the figure is a tangle of overlapping ice classes and only when temperature and surface condition factors are considered, can this diagram be usefully interpreted. By separating the data by flight line as discussed below, this diagram is simplified considerably.

In the case of the 30803 and 30603 lines, which were under cold (-30° C) ambient temperatures in the Beaufort Sea, except for a few grey and grey-white samples, the separation of FY smooth, FY rough, SY and MY ice is clear. The separation of the average MY rough and FY smooth ice is 12.7 dB for σ^o_{hh} and 17.4 dB for σ^o_{hv}. It appears for ice classification, a cross-polarized radar channel will produce more contrast than the equivalent like-polarized channel for these cold ambient temperatures. The absolute scale of the cross-polarized scattering coefficients is, however, about 5 to 10 dB lower than the corresponding like-polarized scattering coefficients and would force the requirement for a higher transmitter power to maintain the same signal-to-noise ratio.

The larger contrasts measured in the cross-polarized channel, between MY rough and FY smooth, can be considered (Gray et al., 1977b) to be partially related to the different electrical and structural properties of MY and FY ice. The larger skin depth of MY ice implies that a significant contribution from volume scattering is included in the backscattering coefficient and large anisotropic, subsurface inhomogeneities, such as drained brine pockets and brine channels in MY ice, could lead to the observed depolarization. Because of the much smaller microwave skin depth in FY ice, mainly surface characteristics become important for this class.

FY smooth and grey-white ice are mechanically and electrically similar and differ mainly in their thicknesses. This may account for their partially overlapping microwave signatures.

Rough FY ice can be distinguished from smooth FY ice by a higher average scattering coefficient and by its greater radar texture represented in Figure 3 by a larger event envelope and in Table 2 by the larger standard deviation. A similar observation may be made for MY ice forms and are less pronounced. The contrast between rough and smooth ice, whether FY or MY, is greater with cross-polarization than like-polarization. The argument here is again that inhomogeneity and anisotropy are responsible for the depolarization effect and the advantage of a cross-polarized radar both in terms of dB separation and radar texture in discriminating these classes, is clear.

Grey, grey-white and nilas ice are much more variable ice forms and are apparently much more sensitive to the ambient temperature.

For melting ice (-2^{o} C) in the Davis Strait 032501 line, FY, grey-white, and nilas are indistinguishable and grey ice is about 3 dB apart from these groups which form part the central section of Figure 3. Most of this ice would have a thin water film over the surface which complicates the signature. Water and grease ice are, however, very much different from other ice classes. Wave-broken FY ice overlaps the rough FY area, presumably because of the increased surface area and effective roughness.

For the Frobisher Bay line, which is under freezing conditions (ambient temperature of -5^{o}), both like- and cross-polarized backscattering coefficients increase for ice classes in the order of dark nilas, light nilas, FY, grey-white, and grey ice. These classes are separable within one standard deviation. No apparent advantage is seen with either polarization in this line, but like-polarization is more desirable than cross-polarization when the signal-to-noise ratio is considered.

With the combination of the like- and cross-polarized scattering coefficients, it is difficult to classify FY, and younger ice forms in melting conditions; and even under cold ambient temperatures, the discrimination between MY ice and ice island is difficult with data from only one angle.

Backscattering Coefficient and Emissivity Sea-Ice Signatures

By combining both active and passive microwave measurements, some of the signature overlap represented in Figure 3 may be removed. Figure 4 shows the event envelope boundaries of each ice class using ε and σ^{o}_{hh} at 45^{o} as space variables. In almost every case, this combination helps to clarify the ice class, increasing the separation between adjacent types. FY, grey-white and nilas in the Davis Strait 32501 line, which were indistinguishable using σ^{o}_{hh} and σ^{o}_{hv} data, are clearly separated by their differences in emissivity. Ice island T_3 is now very easily separable from MY when emissivity is included. Because the emissivities of nilas, young ice and MY ice are almost the same, it was difficult to separate them on the basis of emissivity alone as indicated in the discussion of Figure 2. They become separable by their difference in backscattering coefficients as shown in Figure 4. This may be partially the result of the change of wavelength which alters the effective depth within the ice layer which gives rise to the microwave emission; but it is also indicative of the fact that ice radiometric emission is an integral over the bistatic scattering from ice (Peake, 1959), while the radar cross section represents only a small part of the integral. As such, they may be highly correlated properties but are nevertheless independent.

Grease, frazil, and water are well separated in this σ^{o}_{hh} vs ϵ diagram from the rigid ice forms. At 45° incidence, water shows a large separation in Figure 3 but the radar cross section of water is highly dependent on incident angle and at ~20° is easily confused with ice on the basis of backscattering coefficient alone (cf. Table 2). In addition to this strong angular dependence, the sea state affects the water return. Two differing sea states are represented in the examples of water and 'frazil' (in this case, a very loose mixture of water and ice spicules) from the two flight lines (Figures 4 and 5) accounting for their differences. Ambiguities, arising from the sea state and incidence angle effects, are easily removed by the addition of emissivity.

Temperature dependence of Sea-Ice Signatures

It should be noted that the microwave signatures of the sea-ice classes are influenced by the ice temperature and that part of the variation seen in Figures 2,3, and 4 is the result of differing thermal histories represented in each flight line. Figure 5 shows the relationship between backscattering coefficients and ambient temperature for four sea-ice classes, using data from three different experimental studies. In the usual range of temperatures occurring in the Arctic throughout the year, it can be seen that backscatter may vary, for a given ice class, by as much as 10 dB increasing with temperature for FY and younger (thinner) classes and decreasing for MY ice. This temperature dependence of the microwave signatures of sea ice complicates the interpretation of SAR imagery, but is manageable since the temperature varies slowly with time and location.

Emissivity may be seen from Table 2 to decrease montonically with ice temperature for each ice class for which data was taken at more than one temperature. (FY smooth ice from the Beaufort Sea and Frobisher Bay missions, show equal emissivity within the limits of their statistics.)

More work is required to establish the complete dependence of microwave signatures on temperature and on inherent morphological and electrical changes which accompany the seasonal variation with temperature.

Three-dimensional Signatures of Sea Ice

Each of Figures 3,4, and 5 are planar projections of a 3 or 4-dimensional space, which can be used to describe the microwave properties of sea ice. Figure 6 conceptually shows 3 dimensions of the 4-dimensional space; combining σ^0_{hh}, ϵ, and the depolarization ratio $\sigma^0_{hv}/\sigma^0_{hh}$ all at 45° incidence to span the space. In this representation, ellipsoids are used to represent the volume occupied by each sea-ice class. The projections to other co-ordinate planes are presented as the shaded areas on the base and far side of the box. Figure 6 illustrates the utility of combining several microwave parameters to separate ice classes and shows that automated classification schemes based on a combination of several parameters have a realistic potential for high success rates. Livingstone *et al.* (1980a) further explore several automated classification schemes based on such microwave signatures.

Dependence of Sea-Ice Signatures on Incidence Angle

The incidence angle has been confined to 45° in the figures and discussion of microwave signatures presented above. In this section, incidence angle is briefly considered explicitly, but the conclusions drawn above remain valid retardless of incidence angle except where already noted.

As a general conclusion it can be seen from close examination of Table 2, or a display of the data over the complete incidence angle range (see Livingstone *et al.*, 1980b), that the cross-polarized returns are less dependent on incidence angle than like-polarized returns and that classification with cross-polarized data is equally good at all incidence angles in the range measured in our experiment. The like-polarized backscattering coefficients in general show increasing separation between classes with increasing incidence angle and larger incidence angles are therefore prefered. A decided advantage for cross-polarized radar measurements at larger incidence angles is achieved for the detection of ice features (icebergs, and ridges) has been noted by Pearson *et al.* (1980). The advantage of large incidence angles and cross-polarization for ice classification and feature detection must however, be weighed against the degradation in signal-to-noise ratio which accompanies them as has been noted previously.

SUMMARY

This work has confirmed and extended previous results on the microwave properties of sea ice and suggests that its operational classification may be achieved by a limited sensor compliment, consisting of both passive and active microwave instruments at a fixed incidence angle. The addition of a remote surface temperature monitor, for example a precision radiation thermometer operating in the infrared regime, would be helpful but, is not mandatory.

More research is required into the temperature and seasonal variation of the microwave signatures of sea ice to establish the general validity of the the suggested classification scheme. Livingstone et al. (1980a) have successfully tested its feasibility for the cold conditions and ice classes encountered in the Beaufort Sea deployment.

REFERENCES

---------- (1978) Man Ice, (Manual of Standard Procedures and Practices for Ice Reconnaissance), Atmospheric Environment Service, Environment Canada, Ottawa, 60 p.

Dunbar, M. (1969) "A glossary of ice terms (WMO Terminology)" Ice Seminar, Special Volume 10, The Canadian Institute of Mining and Metallurgy, pp. 105-110.

Gloersen, P., W. Nordberg, T.J. Schmugge, T.T. Wilheit (1973) "Microwave signatures of first-year and multiyear sea ice." J. Geophysical Research 78, pp. 3564-3572.

Gray, A.L., K.K. Chan (1979) "A system study of the CCRS 13.3 GHz scatterometer and the design of a simple, optimized digital data processing scheme." CCRS internal report under review., 64 p.

-----------, J. Cihlar, S. Parashar, R. Worsfold (1977a) "Scatterometer results from shorefast and floating sea ice." Proc. 11th Int. Symp. Remote Sensing Envir., Ann Arbor Mich., pp. 645-657.

-----------, R.O. Ramseier, W.J. Campbell (1977b) "Scatterometer and SLAR results obtained over arctic sea-ice and their relevance to the problem of arctic ice reconnaissance." Proc. 4th Can. Symp. Remote Sensing, pp. 424-443.

Livingstone, C.E., K. Okamoto, R.K. Hawkins, T.L. Wilkinson, S. Young, L. Drapier Arsenault, D. Pearson, A.L. Gray (1980a) "Classification of Beaufort Sea ice using active and passive microwave sensors." Proceedings of COSPAR/SCOR/IUCRM Symposium on Oceanography from Space, Venice, Italy, 6p.

-----------, R.K. Hawkins, K. Okamoto, L. Drapier Arsenault, D. Pearson, T.L. Wilkinson, A.L. Gray (1980b) "The CCRS/SURSAT Active-Passive Experiment 1978-1980 - The microwave signatures of sea-ice types and features and their implication for remote sensing." CCRS Report (in preparation).

Meeks, D.C., G.A. Poe, R.O. Ramseier (1974) "A study of microwave emission properties of sea ice - AIDJEX 1972." Final Report 1786FR-1, Aerojet Electrosystems Co., Azusa, California, 140 p.

Onstott, R.G., R.K. Moore, W.F. Weeks (1979) "Surface-based scatterometer results of arctic sea ice." IEEE Trans. GE-17, pp. 78-85.

Peake, W.H. (1959) "Interaction of electromagnetic waves with some natural surfaces." IRE Transactions on Antenna and Propagation, pp. S324-S329.

Pearson, D., C.E. Livingstone, R.K. Hawkins, A.L. Gray, L. Drapier Arsenault, T.L. Wilkinson, K. Okamoto (1980) "Radar detection of sea-ice ridges and icebergs in frozen oceans at incidence angles from 8 to 55 ." Proceedings of the Six Canadian Symp. Remote Sensing, Halifax, 8p.

Parashar, S.K., R.M. Haralick, R.K. Moore, A.W. Biggs (1977) "Radar scatterometer discrimination of sea ice types." IEEE GE-15, No. 2, pp. 83-87.

Ramseier, R.O. (1980) SURSAT Final Report (in preparation).

Rossiter, J.R., K.A. Butt (1979) "Remote estimation of the properties of sea ice, Beaufort Sea field report - March 1979." C-C-CORE publication No. 79-9, 40 p.

Rouse, J.W., Jr (1969) "Arctic ice type identification by radar." Proc.IEEE 57, pp. 605-611.

Troy, B.E., J.P. Hollinger, R.M. Lerner and M.M. Wisler (1980) "Measurement of the microwave properties of sea ice at 90 GHz and lower frequencies." J. Geophysical Research 00 in press, 31 p.

Vant, M.R. (1976) "A combined empirical and theoretical study of the dielectric properties of sea ice over the frequency range 100 MHz to 40 GHz", Ph.D Thesis, Carleton University, 462 p.

Wilheit, T., W. Nordberg, J. Blinn, W. Campbell, A. Edgerton (1972) "Aircraft measurements of microwave emission from arctic sea ice." Remote Sensing Env. 2, pp. 129-139.

Table 1. WMO ICE CLASSES AND SUBCLASSES STUDIED

WMO CLASS AND SUBCLASSES	AMBIENT TEMPERATURE (C)	LOCATION	NUMBER OF EVENTS	NUMBER OF SAMPLES
Water	-5	Frobisher Bay	3	199
Grease	-5	Frobisher Bay	1	9
Dark Nilas	-5	Frobisher Bay	5	161
Light Nilas	-5	Frobisher Bay	4	191
	-2	Davis Strait	2	45
Grey	-28	Beaufort Sea	2	22
	-5	Frobisher Bay	3	103
	-2	Davis Strait	3	58
Grey-white	-28	Beaufort Sea	2	94
	-5	Frobisher Bay	1	10
	-2	Davis Strait	3	82
FY Smooth	-28	Beaufort Sea	9	357
	-5	Frobisher Bay	8	418
	-2	Davis Strait	19	1161
FY Rough	-28	Beaufort Sea	10	515
FY Wave-broken	-2	Davis Strait	4	339
SY Smooth	-28	Beaufort Sea	3	32
SY Rough	-28	Beaufort Sea	2	49
MY Smooth	-28	Beaufort Sea	17	659
MY Rough	-28	Beaufort Sea	18	671
Ice Island	-28	Beaufort Sea	1	140

Table 2. Microwave Signatures of Sea-Ice From the CCRS Active-Passive Experiment, 1979

CLASS (thickness)	T (°C)	T_B (K)	ε	σ°_{hh} (dB)						σ°_{hv} (dB)					
				8°	15°	25°	35°	45°	55°	8°	15°	25°	35°	45°	55°
Water (0 cm)	0	107 ±3	0.35 ±.01	13.6 ±1.5	2.4 ±1.6	-15.3 ±1.3	-28.6 ±0.9	-35.3 ±1.1		-7.8 ±1.5	-22.1 ±1.5	-35.4 ±0.9	-44.0 ±1.2	-45.6 ±1.6	
Grease	-2	135 ±4	0.46 ±0.02	-21.7 ±1.8	-30.6 ±0.7	-40.2 ±0.6	-40.9 ±0.6	-40.4 ±0.4		-39.2 ±0.7	-43.3 ±0.5	-45.3 ±0.4	-47.7 ±0.5	-46.1 ±0.5	
Dark Nilas (>5 cm)	-5	214 ±7	0.79 ±0.03	-5.5 ±3.4	-9.8 ±2.8	-14.6 ±2.5	-18.8 ±2.4	-24.4 ±2.3	-25.7 ±2.2	-24.9 ±2.9	-29.9 ±2.5	-31.4 ±2.4	-33.5 ±2.3	-34.7 ±2.2	-33 ±2
Light Nilas (5-10 cm)	-5	216 ±5	0.79 ±0.02	3.1 ±2.5	-2.4 ±2.0	-8.1 ±1.6	-12.9 ±1.6	-18.9 ±1.5	-20.1 ±1.8	-17.1 ±2.3	-23.2 ±1.7	-25.3 ±1.5	-27.8 ±1.5	-29.5 ±1.4	-28.8 ±1
	-2	191 ±4	0.69 ±0.02	0.9 ±1.8	-2.4 ±1.5	-7.0 ±1.2	-12.6 ±1.2	-18.9 ±1.5	-22.1 ±1.8	-18.7 ±1.7	-21.9 ±1.7	-21.8 ±1.6	-24.7 ±1.4	-25.2 ±1.3	-25 ±1.0
Grey (10-15cm)	-30	223 ±3	0.91 ±0.02	2.4 ±2.3	1.2 ±2.1	-2.5 ±2.0	-6.9 ±1.6	-11.7 ±1.5	-12.4 ±1.9	-19.7 ±1.6	-22.1 ±2.6	-22.8 ±3.1	-25.4 ± 2.9	-25.8 ±2.8	-25 ±2
	-5	213 ±11	0.78 ±0.05	7.3 ±1.0	2.9 ±0.7	-2.2 ±1.0	-6.9 ±1.2	-12.4 ±1.4	-13.9 ±1.3	-12.5 ±0.7	-16.6 ±1.1	-18.0 ±1.6	-20.6 ±1.6	-21.9 ±1.7	-22.3 ±0.9
	-2	214 ±6	0.78 ±0.02	6.3 ±1.3	2.7 ±1.0	-2.4 ±0.9	-8.4 ±0.9	-15.0 ±0.7	-18.2 ±1.0	-13.2 ± 1.0	-16.9 ±0.6	-17.2 ±0.8	-20.6 ±0.9	-22.1 ±0.6	-24 ±0.9
Grey-White (15-30cm)	-30	230 ±3	0.94 ±0.01	-6.0 ±2.9	-8.9 ±2.7	-11.7 ±2.6	-15.5 ±2.3	-19.7 ±2.1	-19.9 ±1.9	-23.1 ±2.2	-26.0 ±2.7	-25.6 ±2.7	-27.6 ±2.5	-28.0 ±2.5	-27 ±2
	-5	253 ±2	0.94 ±.01	3.1 ±0.6	0.2 ±0.4	-4.2 ±0.5	-9.8 ±0.6	-14.8 ±0.5	-16.0 ±0.6	-17.0 ±0.9	-19.1 ±0.5	-19.4 ±0.6	-22.4 ±0.7	-23.4 ±1.1	-23.5 ±0.9
	-2	205 ±6	0.74 ±0.02	7.2 ±1.4	1.1 ±2.2	-6.4 ±2.5	-13.0 ±2.5	-19.2 ±2.5	-19.1 ±1.1	-13.5 ±1.4	-19.9 ±2.0	-21.4 ±2.1	-25.1 ±2.2	-25.9 ±2.0	-25 ±0.
FY Smooth	-30	226 ±4	0.92 ±0.02	-3.2 ±1.8	-7.1 ±1.6	-11.0 ±1.4	-14.6 ±1.5	-18.9 ±1.4	-19.2 ±1.4	-21.2 ±1.7	-25.4 ±2.0	-25.6 ±2.0	-27.7 ±2.0	-28.1 ±1.8	-27. ±1
(30-200cm)	-5	255 ±5	0.95 ±0.02	-0.5 ±1.8	-3.0 ±2.0	-6.8 ±2.0	-11.4 ±2.3	-16.4 ±2.0	-17.3 ±2.1	-20.2 ±2.5	-22.5 ±2.2	-22.6 ±2.2	-25.1 ±2.3	-26.0 ±2.0	-25.8 ±2
	-2	240 ±9	0.88 ±0.03	3.3 ±2.1	-2.3 ±1.6	-8.2 ±1.9	-13.8 ±2.0	-19.6 ±2.1	-21.4 ±5.1	-17.1 ±1.6	-22.6 ±1.4	-23.3 ±1.8	-26.6 ±2.0	-27.6 ±2.0	-27. ±6.3
FY Rough (30-200cm)	-30	227 ±3	0.93 ±0.02	-1.8 ±1.53	-5.8 ±1.6	-9.2 ±2.0	-12.6 ±2.2	-16.7 ±2.3	-17.7 ±2.2	-19.1 ±2.2	-22.5 ±3.1	-22.5 ±3.3	-24.4 ±3.3	-25.0 ±3.3	-25. ±3.
FY Wavebroken	-2	230 ±9	0.84 ±0.04	3.7 ±0.9	-0.3 ±1.0	-4.7 ±1.4	-9.3 ±1.6	-14.3 ±1.7	-15.6 ±2.0	-15.9 ±1.0	-19.3 ±1.2	-19.5 ±1.3	-22.5 ±1.4	-23.3 ±1.4	-24 ±1.
SY (>200cm)	-30	208 ±5	0.85 ±0.02	0.9 ±1.3	-1.2 ±1.7	-2.7 ±2.1	-5.2 ±2.3	-9.2 ±2.2	-9.5 ±2.2	-12.4 ±2.6	-12.9 ±2.9	-12.4 ±3.0	-14.2 ±3.0	-15.0 ±2.9	-14.9 ±2.8
MY Smooth (>200cm)	-30	192 ±6	0.77 ±0.03	3.5 ±1.1	1.6 ±0.9	0.0 ±1.0	-2.8 ±1.1	-6.8 ±1.1	-7.4 ±1.2	-8.8 ±1.6	-9.0 ±1.7	-8.5 ±1.6	-10.5 ±1.6	-11.5 ±1.6	-11 ±1.
MY Rough (>200cm)	-30	191 ±8	0.77 ±0.04	3.6 ±1.3	1.9 ±1.1	0.5 ±1.2	-2.2 ±1.2	-6.2 ±1.1	-6.5 ±1.6	-8.2 ±1.8	-8.2 ±1.9	-7.7 ±1.8	-9.8 ±1.8	-10.7 ±1.7	-10 ±2.
T_3 (>3000cm)	-30	163 ±5	0.65 ±0.02	5.2 ±0.7	3.6 ±1.0	2.0 ±1.1	-1.5 ±1.1	-5.0 ±1.2	-5.2 ±1.0	-6.3 ±1.7	-5.9 ±1.9	-5.6 ±1.8	-8.0 ±1.8	-8.6 ±1.6	-8.9 ±1.5

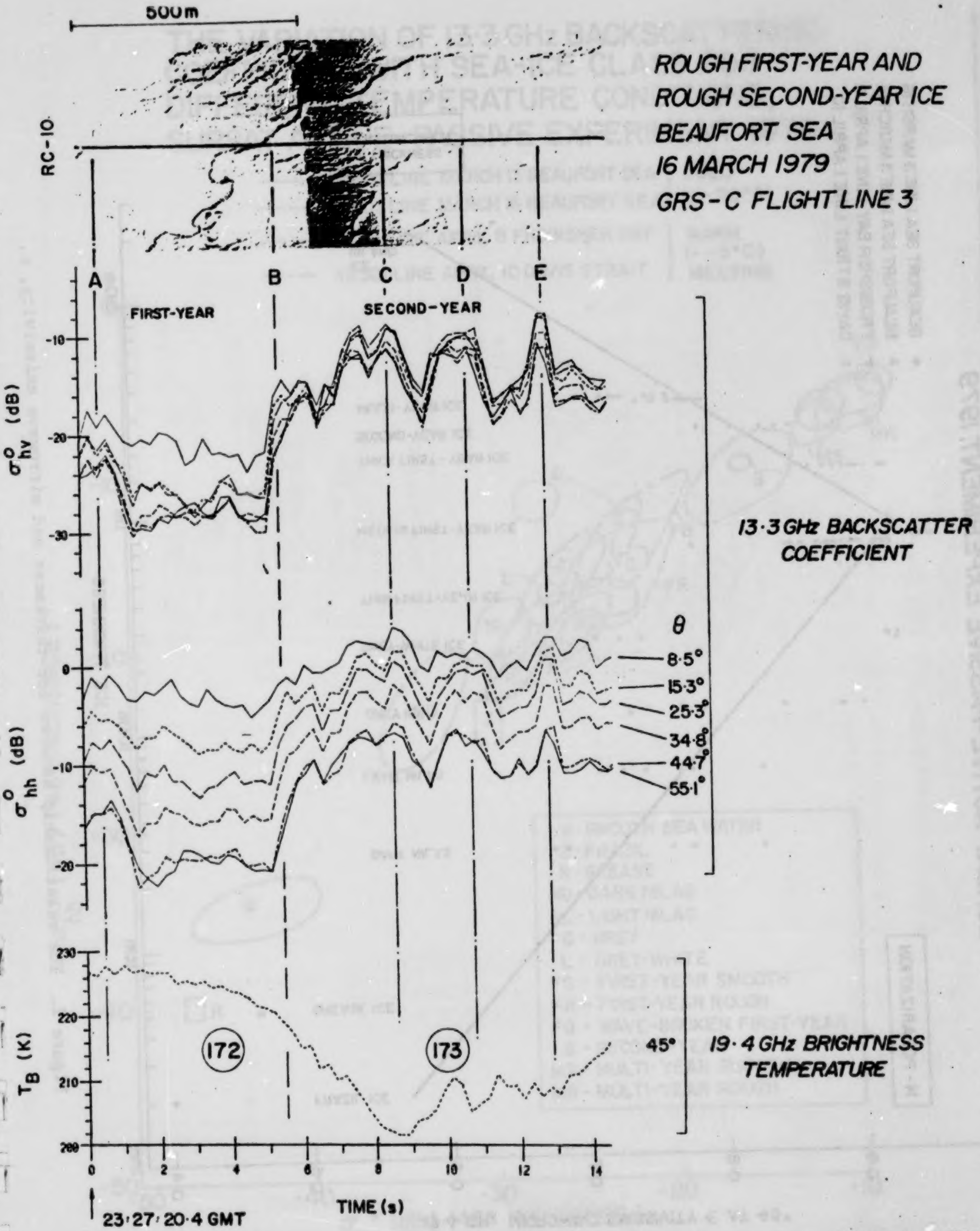

Figure 1. Simultaneous observations of sea ice by like- and cross-polarized microwave backscattering, σ^o_{hh}, σ^o_{hv}, for different incidence angles; and brightness temperature T_B, at 45° incidence angle along the flight line shown in the RC-10 image. The transition is shown from rough FY to rough SY ice, in the Beaufort Sea.

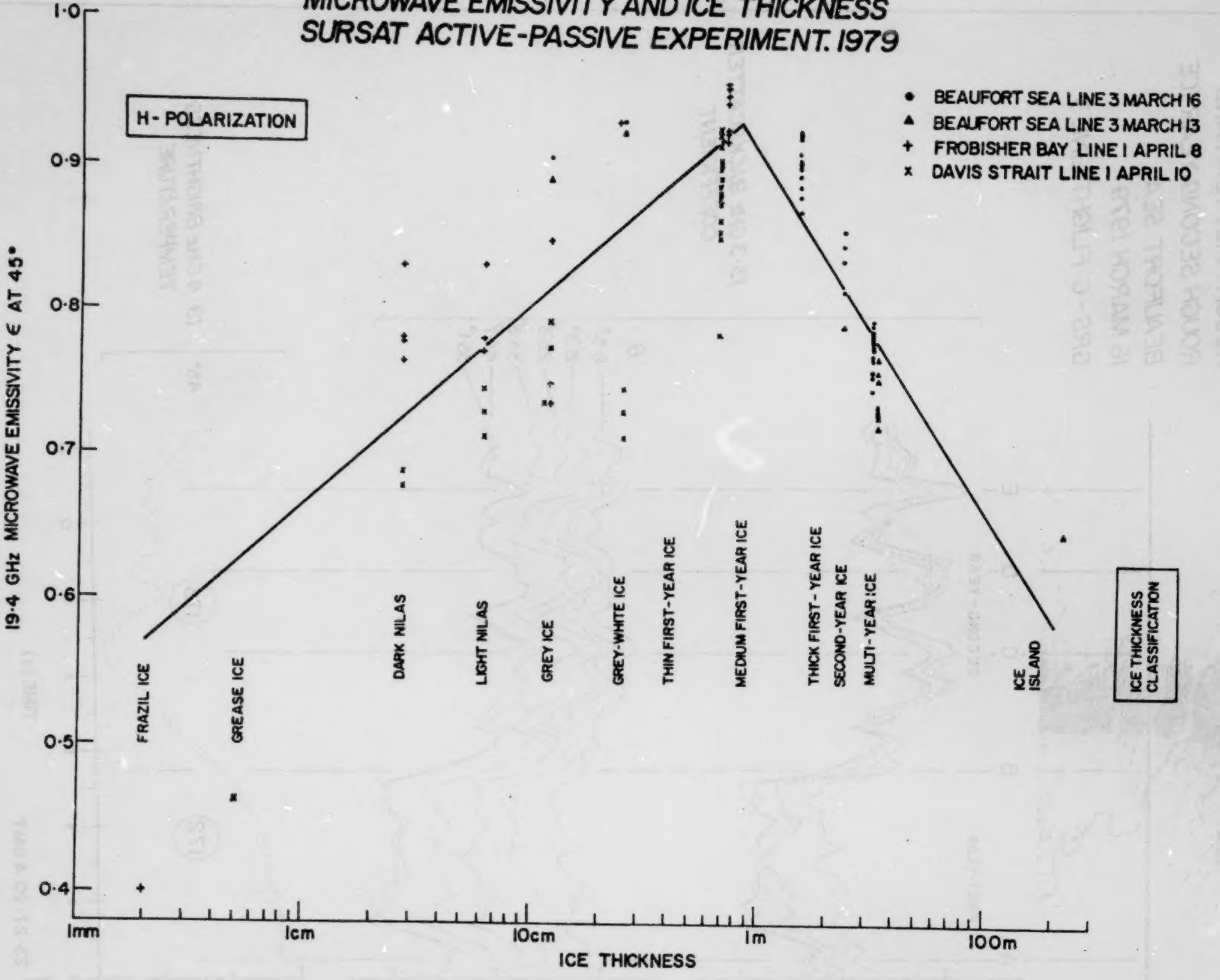

Figure 2. The relationship between ice thickness and microwave emissivity, ε.

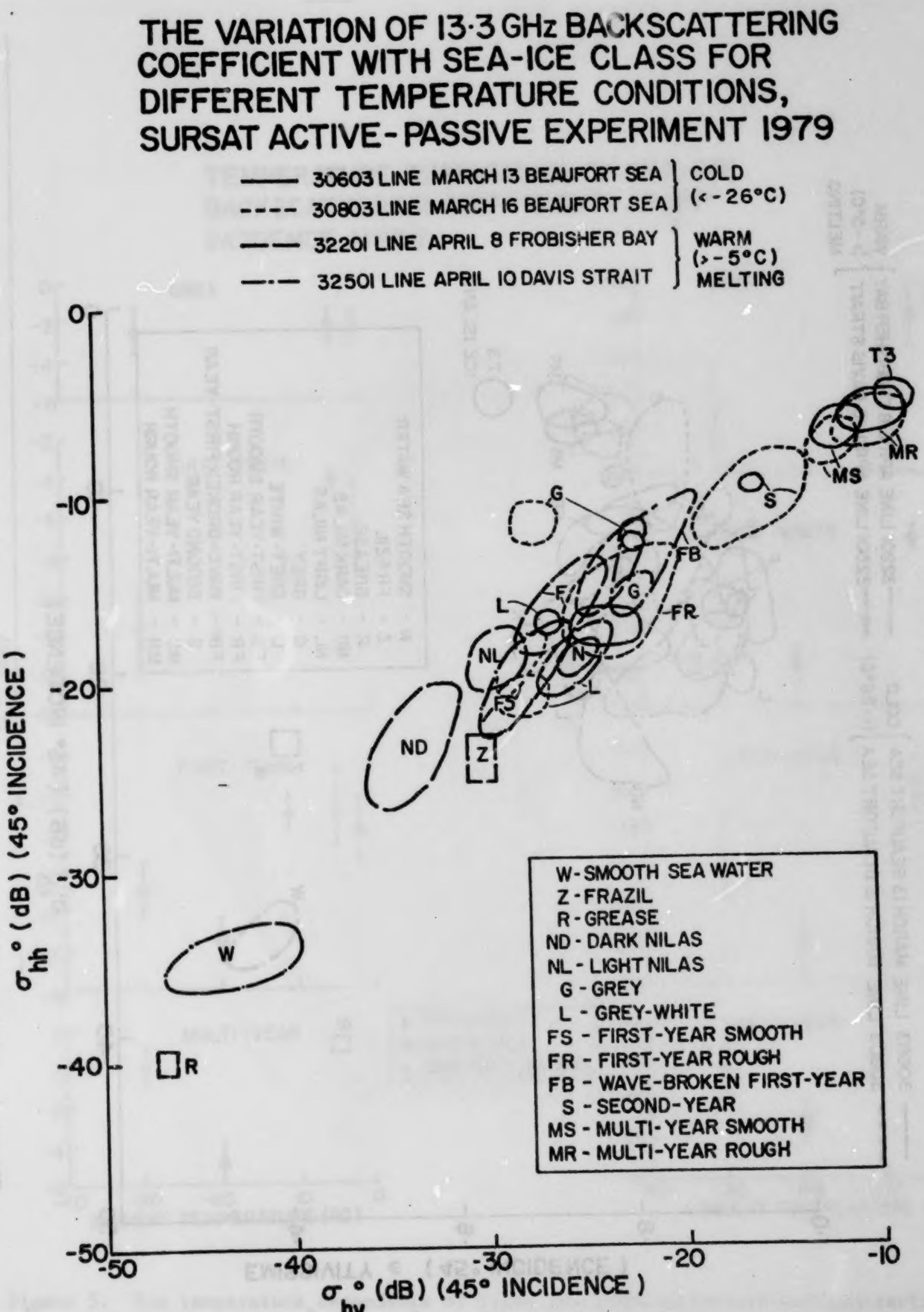

Figure 3. Classification of various sea-ice types by like- and cross-polarized backscattering coefficients, σ^{o}_{hh} and σ^{o}_{hv}, at an incidence angle of 45°. Data from four flight lines are included with associated ambient temperature.

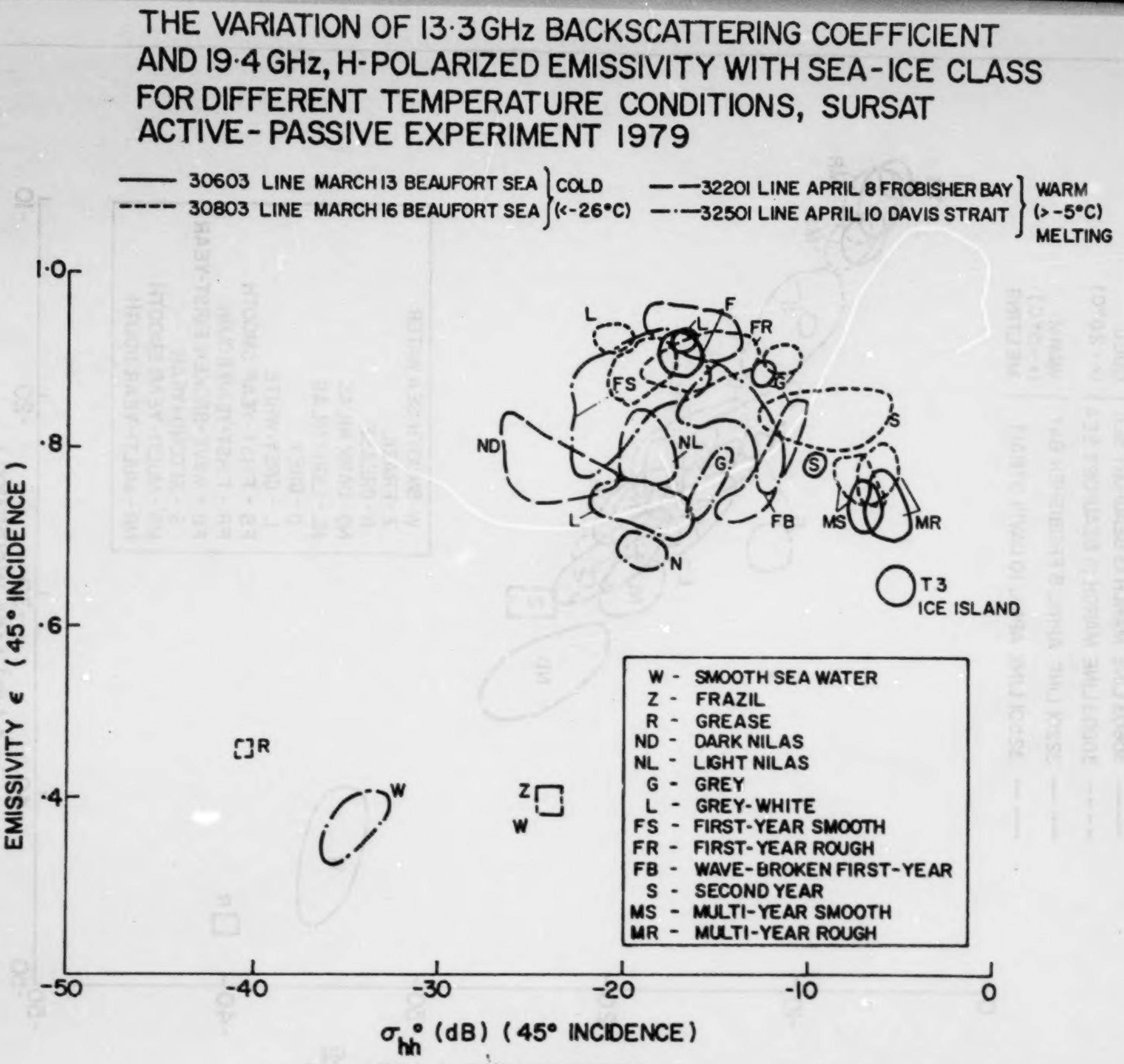

Figure 4. Classification of various sea ice types by like-polarized backscattering coefficient, σ^o_{hh}, and microwave emissivity, ε, at an incidence angle of 45°. Ambient temperature is indicated by the differing line types used to envelope the data from each class.

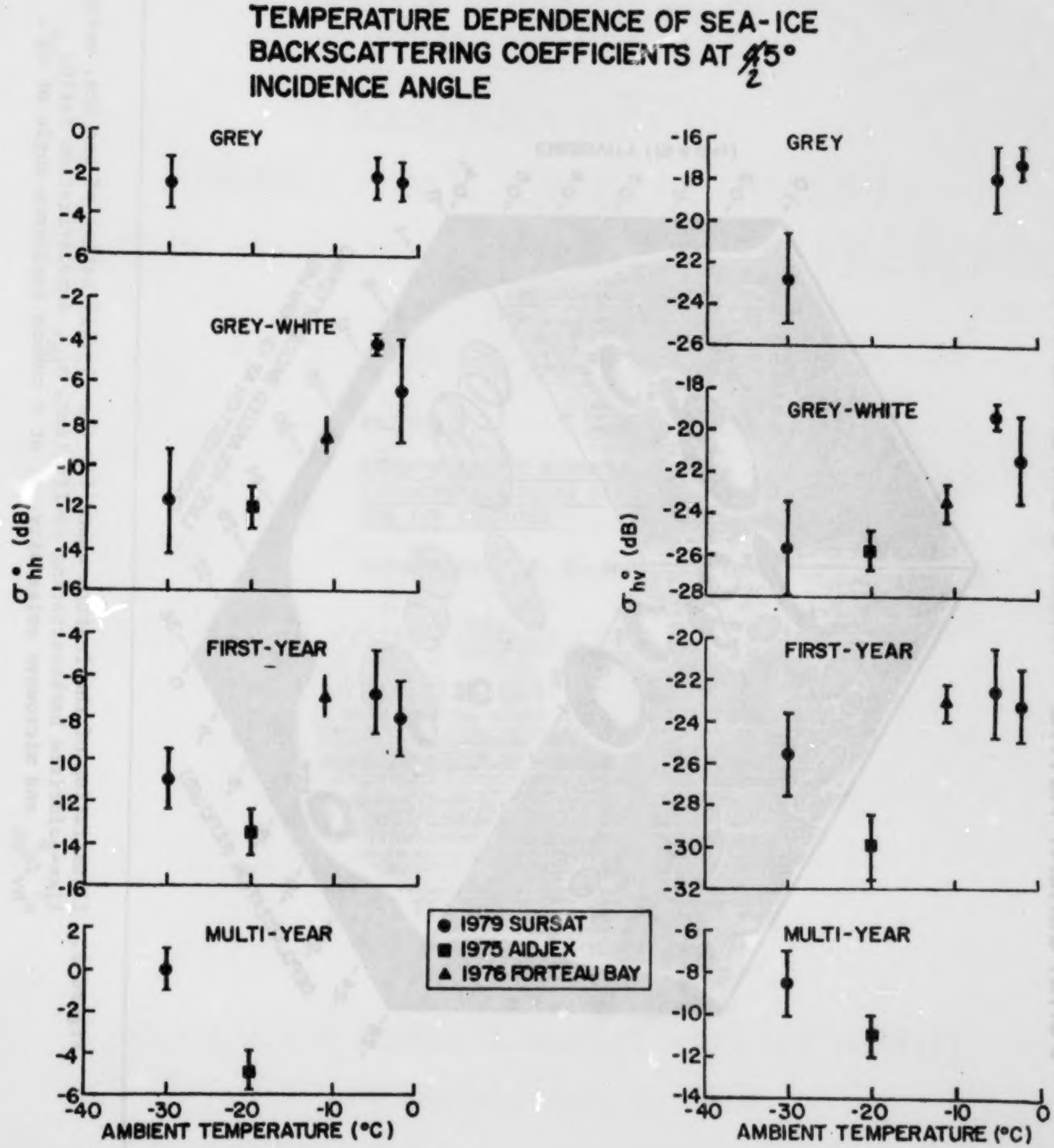

Figure 5. The temperature dependence of like- and cross-polarized backscattering coefficients, σ^o_{hh} and σ^o_{hv}, for various classes of sea ice, at an incidence angle of ~~4~~25°.

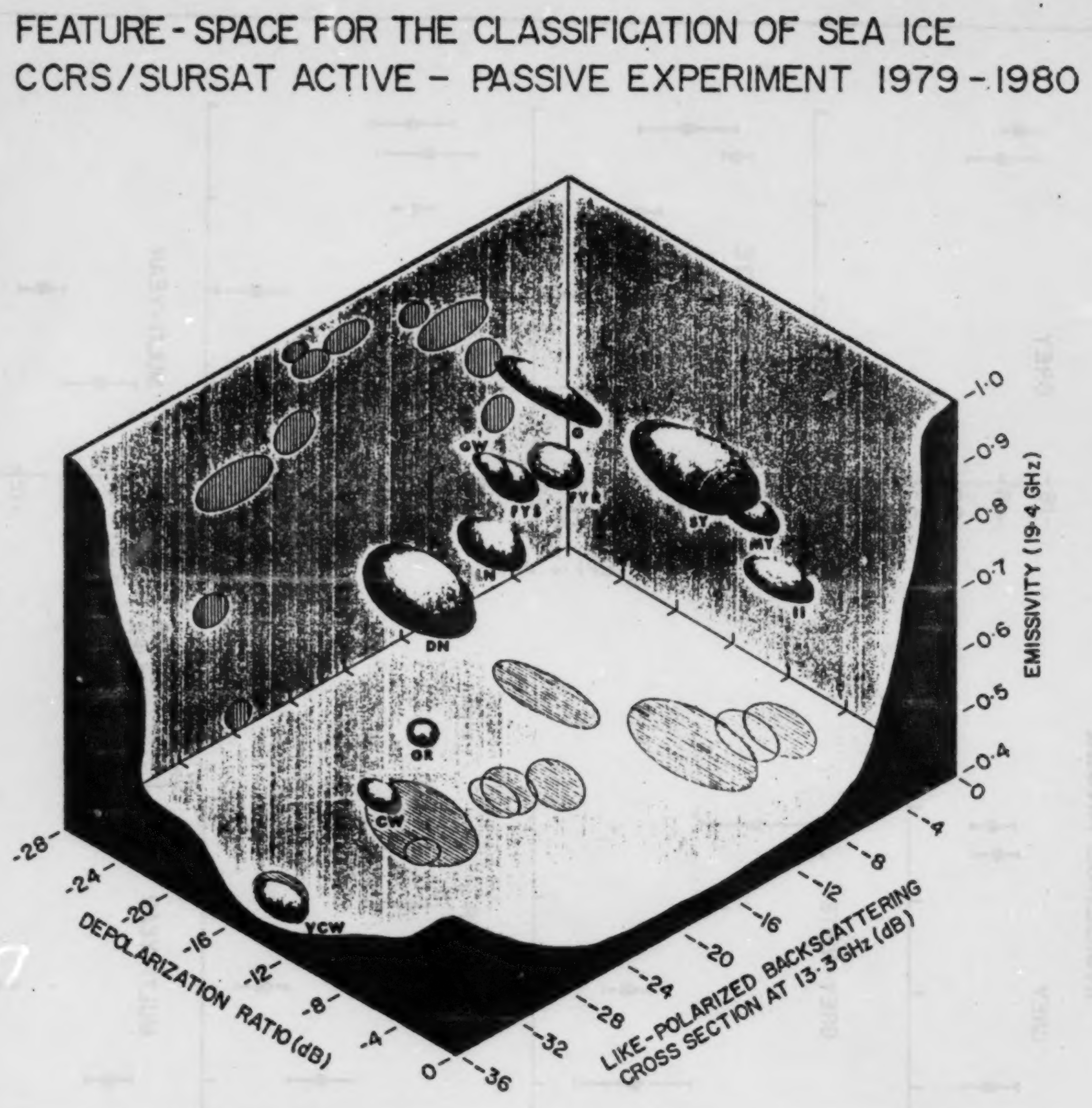
FEATURE - SPACE FOR THE CLASSIFICATION OF SEA ICE
CCRS/SURSAT ACTIVE - PASSIVE EXPERIMENT 1979 - 1980

GW
G
FYS
FYL
SY
MY
II
LN
DN
GR
CW
YCW
EMISSIVITY (19·4 GHz)
-1·0
-0·9
-0·8
-0·7
-0·6
-0·5
-0·4
0
-4
-8
-12
-16
-20
-24
-28
-32
-36
LIKE-POLARIZED BACKSCATTERING CROSS SECTION AT 13·3 GHz (dB)
-28
-24
-20
-16
-12
-8
-4
0
DEPOLARIZATION RATIO (dB)

Figure 6. Illustration of the feature-space for the classification of sea ice, using like-polarized backscattering coefficient, σ^{o}_{hh}, depolarization ratio, $\sigma^{o}_{hv}/\sigma^{o}_{hh}$ and microwave emissivity, ε, at a common incidence angle of 45°.

SECTION 5.2

EASTERN ARCTIC SURSAT SAR ICE EXPERIMENT: RADAR SIGNATURES OF SEA ICE FEATURES

Ketchum Jr., R. D. and L. D. Farmer

NORDA TECHNICAL NOTE 68

EASTERN ARCTIC
SURSAT SAR ICE EXPERIMENT:
RADAR SIGNATURES OF SEA ICE FEATURES

R.D. Ketchum, Jr. and L. Dennis Farmer

Oceanography Division
Ocean Science and Technology Laboratory

August 1980

NAVAL OCEAN RESEARCH AND DEVELOPMENT ACTIVITY
NSTL Station, Mississippi 39529

ABSTRACT

Evaluation of X- and L-band steep angle synthetic aperture radar (SAR) sea ice imagery taken in Baffin Bay and Davis Strait in April 1979 has shown that description and discrimination of first-season ice types can be difficult because of ambiguous radar returns. Ambiguous returns seen on X-band radar imagery are attributed to snow cover. The data have indicated that changes in snow properties due to melting and refreezing cause development of a highly reflective medium to the 3 cm X-band radar. The 25 cm L-band radar is not noticeably affected by the observed phenomena, thus correlation of coincident X- and L-band imagery often resolves interpretation ambiguities on the X-band imagery caused by the snow effects.

The data suggest that L-band radar energy often penetrates the ice and that subsurface returns are received. These returns also produce ambiguities in interpretation. Apparent smooth surfaces do not show this effect, but rough surfaces which have widely different roughness densities may produce apparently equal backscatter of L-band radar.

Ice ridge identification and discrimination was often poor due to the obscuring effects of background clutter associated with the above-suggested backscattering phenomena. Small ridge sizes versus system resolution and steep angles of incidence also reduce ridge identification capabilities.

Some icebergs produced time-delayed L-band signals, indicating internal reflections within the iceberg. Iceberg/water interface reflections rather than volume scattering are indicated. L-band radar cannot be depended upon for iceberg identification, since icebergs may be only partially imaged or not imaged at all by this frequency.

Table of Contents

Page

Abstract i

Introduction 1

Ice Conditions 2

SAR Data 2

South Baffin Bay Data 3

East Baffin Bay Data 7

North Baffin Bay Data 10

Discussion and Conclusions 13

Bibliography 14

INTRODUCTION

The Ice Experiment Plan of the Canadian Surveillance Satellite (SURSAT) Project was conducted during the winter and spring of 1979. This cooperative effort between Canada, the United States, and Denmark consisted of planned operational phases in four different geographic areas: the Gulf of St. Lawrence, the Beaufort Sea, the Eastern Arctic, and the Grand Banks. The Grand Banks phase was cancelled due to required aircraft and ship repairs.

The primary objective of the SURSAT Ice Experiment was to evaluate and to develop interpretation capabilities for dual-frequency, dual-polarized synthetic aperture radar (SAR) imagery of sea ice features and conditions. SURSAT and subsequent efforts will lead to an operational SAR that can be used to provide reports of ice conditions in real-time, to support ice forecasting, and also to serve as a system to support studies of sea ice dynamics.

This report discusses the collection and the analysis of data collected in April 1979 during the SURSAT Project Phase 3, which was conducted over ice-covered waters in the eastern Arctic. During this phase, the U.S. Navy's BIRDSEYE RP-3A aircraft, under the technical direction of the Naval Ocean Research and Development Activity (NORDA), flew jointly with the Canadian SAR-equipped aircraft to collect complementary data to aid in evaluation of the SAR data. The RP-3A aircraft was equipped with a Wild RC-8 cartographic camera, infrared line scanner, laser surface profiler, and PRT-5. The 9-inch (24 cm) photography obtained with the RC-8 camera provided the most useful data for cross-correlation and evaluation of the SAR imagery. The SAR system (INTERA Environmental Consultants, Ltd., 1978) was flown in a CONVAIR-580, owned by the Canada Centre for Remote Sensing. The Airborne SAR Project was managed by INTERA Environmental Consultants, Ltd., Ottawa, Canada.

Flight tracks were preselected by the SURSAT ice experiment team. Both aircraft were equipped with LTN-51 inertial navigation systems. The Navy RP-3A flight originally planned to fly 3.35 nautical miles to the starboard side of the Canadian CONVAIR-580 track in order to obtain the required coincident ice coverage. This procedure was not completely successful due to navigational errors. However, coincident coverage was obtained over areas having typically different ice conditions, thus providing adequate information for a useful evaluation of the four-channel SAR imagery.

Joint flights of the CONVAIR-580 and RP-3A aircraft were made during 8-13 April. The CONVAIR-580, with SAR system, flew at altitudes of 5200 and 5500 meters for optimum SAR coverage. The RP-3A flew at altitudes of 300 to 1500 meters to obtain photographic resolution more amenable to detailed interpretation of ice conditions and features. Low clouds (less than 150 meters) prevented RP-3A data collection on the 8 and 9 April tracks. Coincident data from the two aircraft were obtained on the 10, 11, and 12 April tracks. Areas of coincident SAR and RP-3A photographic data are shown in Figure 1. The 12 April CONVAIR-580 SAR track was flown on 13 April by the RP-3A aircraft. Ice deformation, which occurred during the approximate 24 hour period between these flights, is evident when comparing the coincident imagery.

GENERAL ICE CONDITIONS

The formation of ice in Baffin Bay generally begins in October. The early thin ice forms are easily broken into fragments of brash ice and ice cakes by wind and wave action. The fragments consolidate and both the deformational and consolidation processes may occur again and again. This interaction results in an icefield consisting of various sizes and shapes of ice fragments. Eventually, as the freezing process continues, a more stable consolidated ice cover is formed that has sufficient thickness to withstand wind and wave forces which easily deformed the ice earlier. In terms of surface roughness this ice cover will have a high density, but low relief. The fields of ice increase in size and extend southward into Davis Strait and over the Labrador Sea along the Canadian coast as the season progresses. The seaward edge of the ice, continually under the influence of sea and swell action, will remain broken and may be easily dispersed by winds and currents.

Deformation within the ice field continues throughout the season. The majority of newly formed ice in the fractures is deformed into ridges by shear stress and compression. Some areas, however, remain undisturbed and retain relatively smooth surfaces. Networks of pressure ridges and hummocks which form throughout the season are present in the ice. Ridges in this region are usually less than a meter high.

First-year ice and younger stages of ice development are the dominant sea ice types found in the eastern Canadian arctic region. Multi-year ice is not common in this area, although occasionally it is present. The multi-year floes have drifted into Baffin Bay from the Canadian Archipelago and Nares Strait. Icebergs, bergy bits, and growlers, derived primarily from Greenland glaciers, are common.

Air temperatures and the ice/snow surface temperatures in some of the experimental areas were above freezing prior to and during the experiment. Early surface melt conditions prevailed, producing slush or very wet snow, and some melt puddles.

SAR DATA

The SAR imagery is not calibrated, thus all inferences to radar backscatter are based on image gray tone differences, which may change from image to image. Many factors contribute to the relative backscatter (or gray tones) seen on the image from the time of system data collection through optical processing and, finally, during photographic processing procedures.

All four SAR channels were examined during this analysis. The imagery obtained from the cross-polarized channels was generally of poor quality, evidently lacking the dynamic range seen in the like-polarized channels. Minor differences noted between some frequency like- and cross-polarized imagery did not add to the quality of interpretation. With one exception (Figure 14), cross-polarized images are not illustrated.

Interpretation of the SAR imagery depended primarily on cross-correlation with the RP-3A 9-inch (24-cm) photography, and the accumulated experience and knowledge of the image analysts. The only ground truth information available was from a few on-site observations obtained by the Danes in the Danish Experimental area southwest of Disko Island.

Once cross-correlations with photography have been made, interpretation of the SAR imagery is dependent on the interpretation of the sea ice photography. At times, this process becomes somewhat speculative, particularly in snow-covered areas or when key features affecting the radar return are not evident on the photograph. Additionally, it appears that some radar returns are not from the observed surface, but are from subsurface boundaries and/or volume scattering. Clearly, the history of the ice formation, deformation, decay, and current weather conditions determine the ice and snow surface and subsurface properties, including the distribution of dielectric properties. These factors, in turn, control the radar backscatter for a given set of radar equipment parameters. One very important question is: How transient are the properties of a given section of ice or snow relative to fluctuating weather conditions (i.e., changing air temperature, precipitation, blown snow, etc.)? The interpretations formulated during this analysis are presented with the understanding that, in future SAR experiments when ground truth is available, they can be either further developed or disproved.

SOUTHERN BAFFIN BAY DATA

This portion of the SURSAT experiment, initiated and planned by the Technical University of Denmark, was flown on 10 April 1979 over two predetermined crossing lines, one oriented north-south, one oriented east-west, located over ice fields southwest of Disko Island (see Figure 1). The experimental area included ice from the ice edge inward. Many small, thin cakes and floes derived from wave and swell broken floes dominated the area in the vicinity of the ice edge. Farther in from the edge, larger floes were dominant; some were a consolidation of small floes, others appeared to have developed under stable conditions and were more homogeneous in appearance and thickness. The majority of the sea ice was very thin first-year ice or young ice. Nilas was present and the presence of snow on the nilas surface indicated a recent snowfall. Nilas will not maintain a snow cover for long periods, especially with air temperatures (around -1°C) which existed during the experiment. The snow appeared thickest over the northwestern portion of the experimental area. Surface air temperatures the day before the flights were reported to be as high as + 4°C. Surface temperatures for snow, ice, and water during the flight were nearly isothermal, as indicated by the airborne radiation thermometer (PRT-5), averaging between 0°C and - 1°C. Evidence of earlier melting was observed. Helicopter landings and observations on two separate floes by Scott Polar Research Institute investigators on the morning of the experiment revealed a very wet snow about 10 cm deep, which covered ice about 20 cm thick. Ice conditions were too unstable for continued ground truth observations.

Analysis of the SAR imagery has strongly indicated that wet snow significantly increases X-band radar backscatter, but does not noticeably affect L-band radar backscatter. The processes of refreezing and recrystallization of moist snow could account for development of metamorphosed snow with the properties necessary to produce X-band radar return due to volume scattering.

Examples are shown in Figure 2, which displays X- and L-band SAR imagery from the east-west line, and Figures 3 and 4 which show some coincident photography taken from a 300-meter altitude at far range on the SAR imagery. The areas A and B in Figures 2 and 3 are areas of thin dark gray ice. Area A is covered with slush (saturated snow) that formed from recently deposited snow and displays either no or low X-band radar backscatter. Area B retains a great deal of snow cover which is in a state of deterioration. In both areas the ice surface is smooth. Area B gives a much brighter X-band radar return. The difference appears to be in the slush cover and melting snow cover. The far range portion of the L-band image shown does not display any information. However, areas A and B both appear as no return areas on earlier generation film strips. The rafted area between A and B provides some L-band return.

Figure 4 shows an area C of thin, smooth, snow-covered ice. Adjacent to area C is an area D of consolidated, snow-covered, smaller forms of different ages (breccia). The snow here is also undergoing melt. The X-band SAR imagery displays similar returns from the wet, snow-covered, smooth, thin ice C and from the breccia D. Although not readily apparent on the L-band image shown here, the rough-surfaced breccia D is giving a significant return, while the smooth, wet, snow-covered ice C is a no return area. These differences in the X- and L-band radar returns are critical to interpreting imagery taken during this equipment. The apparent high scattering cross-section of wet snow for X-band radar produces many ambiguous images. The L-band radar image, apparently unaffected by the wet snow, can be used to resolve the ambiguities, as one can see by comparing the upper portions of the X- and L-band radar images in Figure 2. Some of the brightest return areas on the X-band image appear dark on the L-band image. These areas are interpreted to be snow-covered thin ice that is similar to those areas of snow-covered thin ice shown on the photographs in Figures 3 and 4. Some areas in Figure 2 give returns on both channels. These areas are interpreted to be breccias or consolidated small forms similar to area D in Figure 4. Areas that are dark on both channels are inferred to be areas of open water or very thin ice without a snow cover. It is speculated that some of the variations in the gray tone pattern from the breccias on X-band radar may represent either structural variations in a recrystallized snow cover or variations in snow moisture content.

Areas of consolidated small ice forms and closely packed small ice forms are not well-discriminated by backscatter characteristics on either X- or L-band imagery, particularly at near range where image distortion is great and system resolution capabilities are reduced. The presence and distribution of small open or newly frozen areas may allow inference of unconsolidated conditions. SAR images illustrated in Figure 5 show a mixture of consolidated and closely packed small ice floes and cakes. A preponderance of both scattered thin ice (nilas) and open water areas exists over portions of this zone. The presence of consolidated forms of any significant size is unlikely in these areas. However, areas similar to that of A, although a nilas is evident, could be weakly consolidated and may include the nilas. The photographs in Figures 6 and 7 provide visual examples of ice conditions in this area. In comparing these photographs with the coincident SAR imagery, it is readily apparent that backscatter cannot be used to discriminate very closely packed small ice forms from consolidated small forms. In addition, only the snow-free areas of nilas, which appear as low backscatter targets, can be discriminated as nilas on the X-band SAR image. The snow-covered dark gray ice has an X-band image tone and texture similar to the closely packed and consolidated thicker ice. L-band imagery better delineates all nilas-covered areas, since snow that is present apparently does not produce L-band backscatter. Note the apparent smaller size on the X-band radar image of the nilas-covered area at B (Figures 5 and 6). The snow cover around the periphery of this nilas-covered area produces X-band backscatter; thus, we see an apparent size difference of this target on the two channels. Another example of this difference is seen at A in Figure 5.

The open water area at C in Figure 5 provides no return signal on X-band imagery, but gives a return on L-band imagery. A similar phenomenon is shown on the radar image at D. This open water area is shown on the photograph in Figure 7. (The belt of small ice forms in the open water area moved there about one hour after the SAR imagery was collected.) In the L-band image in Figure 5 the open water area cannot be discriminated from the surrounding consolidated and very closely packed ice forms. This unusually high L-band return from open water was most common on the northern portion of the north-south line.

The photography indicated a recent snowfall, and it has been inferred from the photographic data that the snowfall was heavier in the northwestern portion of the experimental area. It is speculated that in areas of heavy snowfall, a fresh water-sea water mixture, which formed in the upper layer, provided scattering boundaries for L-band radar signals. Another interesting example of this anomalous L-band radar return is shown in Figure 8, which portrays ice conditions near the north end of the north-south line. Snow cover in this area, visible on the photographs shown in Figures 9 and 10, appears heavier than near the southern end of the line. Open water areas identified at A, B, C, and D (Figure 8) show no return on X-band imagery, but provide a good return on L-band imagery. The open water areas could be erroneously interpreted as ice cover on the L-band imagery. A photograph of Area A is shown in Figure 9. Several photographs of these areas of apparent open water, which produced high intensity L-band returns, were over-developed to see whether any ice could be detected. The results were negative.

The radar images shown in Figure 11 were taken along the southern portion of the north-south line. A number of no return open water areas are apparent on the X-band radar image. These areas also appear as no return areas on the L-band image, suggesting that a mixed water surface layer does not exist in this area or is not sufficient to produce L-band backscattering. Radar incidence angles are similar to those farther north where L-band backscatter was received from open water. The photographs in Figures 12 and 13 show some of the open water areas which appear at steep incidence angles on the SAR imagery (Figure 11). The surrounding ice does not have as much snow cover as observed on the ice farther north, i.e., less snowfall.

The examples already shown indicate that X-band radar backscatter is related to both ice surface roughness and snow conditions, whereas L-band radar returns are primarily related to the geometric shape and roughness of the ice surface (with the exception of the anomalous high returns from open water). The simultaneous use of both radars enables a more accurate evaluation of ice conditions, since L-band radar often can be used to resolve ambiguities encountered on X-band imagery that are related to the high backscatter caused by a wet snow cover.

In some situations, the high X-band return related to snow can enhance interpretation of ice conditions; examples are shown on the 30 km long sections in Figure 14. These images were taken near the western end of the east-west line. The composition of some of the consolidated ice forms and their distribution is better depicted by the X-band imagery because of the high contrast between the ice fragments and the matrix ice which comprise the floes. For example, recent fragmentation of the thin first-year ice floes seen near the center of the strip is clearly indicated on the X-band images. This fragmentation is not discernable on the L-band image. The angular shapes (i.e. non-rounded edges of discrete fragments) of the fragments in the floes indicate that little deformation has occurred since the breaking apart of the original floe. Therefore, brash and block ice, which would normally present a rough ice surface geometry, are scarce in the matrix ice between the angular fragments, thus reducing the possibility of radar backscatter. As a result, there is little contrast between the matrix ice and the fragments on the L-band imagery. However, the X-band imagery shows a large backscatter difference between the matrix ice and the fragments. The high backscatter from the thin matrix ice is largely attributed to the snow cover. The left portion of the radar sections displays many floes composed of consolidated small, rounded forms of thin first-year ice. Again, small forms are better detected on the X-band imagery because of the difference in backscatter. The slightly better X-band radar resolution is also a factor. The deformed zones between the floes produce high returns with both radars, probably because of the brash and block ice which resulted from floe collisions. Snow in these zones enhances X-band return. The high returns from these deformed zones aid in the delineation of the floes. Many other areas in Figure 14 that display light tones on the X-band imagery, but dark tones on L-band, are areas of snow-covered thin ice. This difference is shown at several nilas-covered sites near the center and left portion of the strips.

The first-year ice and younger ice types dominating the area shown on the right portion of the radar images in Figure 14 do not appear to be weakly cemented consolidations of swell-fragmented ice as do the floes on the left portion of the images. The long linear character of many of the ridges in this zone supports this conclusion. Long, straight ridges in weakly cemented fragments of ice are uncommon. The imagery suggests that wave and swell action have played an important role in the deformation processes of the ice shown on the left end of the image strips, but not in the ice shown on the right end of the strips.

Generally, areas in this region showing low or no radar return on all three channels can be interpreted as areas of open water or thin ice with little or no snow cover. Areas which produce a substantial radar return on all channels have rough surface structure related to deformation. More tonal texture is usually apparent on the X-band image because of the shorter wavelength and slightly better resolution. High return X-band images with coincident low return L-band images are often related to snow-covered thin ice. The surface of this ice is generally smooth and the ice can be a thin first-year type. In areas having low X-band return but high L-band return, penetration by the L-band signal is suspected with subsequent subsurface returns (Ketchum, 1978).

Some differences can be noted between the X_{HH} and X_{HV} imagery. It cannot always be determined if the differences in apparent backscatter are real or are due to variations in data processing techniques or dynamic range. For example, at areas marked A on the right end of the image strips in Figure 14, it appears that higher intensity returns were received on X_{HH} than on X_{HV}. In some cases the returns are more similar between L_{HH} and X_{HV} than between X_{HH} and X_{HV} (i.e., some areas having low L_{HH} returns also have low X_{HV} returns, but provide significant X_{HH} returns). These areas have been interpreted as smooth areas of first-year ice and evidently do not have the surface properties necessary for depolarization of the X-band signal. A more obvious distinction between the X_{HH} and X_{HV} imagery on the right end of the strips in Figure 14 is the greater clarity of the pressure ridge pattern on the X_{HV}. Background clutter reduces the ability to distinguish the ridges on the X_{HH} imagery. For the same reason, ridge identification is generally better on the L_{HH} than on the X_{HH} imagery.

In Figure 14 a number of icebergs, most of which are small, are tentatively identified because of their bright returns and shapes. However, all icebergs are not identified on all three channels and the quality of interpretation may vary with channels. The object at B is clearly shown by the X_{HH} radar, but is obscure on the X_{HV} radar and is not apparent on the L-band radar. There is some question as to whether this is an iceberg. The icebergs at C are identified on all three channels. The L-band image has no return areas within the icebergs. The largest iceberg on the imagery is shown at D. It is clearly depicted on the X-band channels, but again only a partial image is apparent on the L-band image. The distance between the two bright images, which are believed to represent the iceberg on L-band, is greater than the apparent length of the iceberg on the X-band imagery. The indication is that internal scattering of the L-band signal within the iceberg has caused a time delay, thus producing a false image which makes the iceberg appear either to be longer or as two icebergs.

EAST BAFFIN BAY DATA

Coincident SAR and photographic data collection was minimal. On 11 April, during the flight over Baffin Bay along the West Greenland coast (see Figure 1) from Sondrestrom AB to Thule AB, coincident data from the two aircraft were obtained at the beginning portions of passes 1 and 3. The ice conditions along pass 1 were very similar to ice conditions discussed above. Northward of pass 1, ice conditions changed from the breccia types and the fragmented conditions to more consolidated forms with an increase in ridging and in the number of icebergs. Surface temperatures along the northward run decreased progressively from -1.0°C to -8.0°C. It remains evident that snow conditions were still playing a dominant role in producing X-band radar backscatter, a backscatter which does much to reduce the ability to accurately interpret the sea ice conditions. As before, the use of the coincident L-band imagery resolves many of the ambiguities. Figure 15 shows a section of radar imagery taken at the beginning of Pass 3 on 11 April. Some coincident photography is shown in Figure 16. Some areas which are relatively smooth, but have a substantial snow cover, are marked A in Figures 15 and 16. These areas produce relatively low returns on the L-band image, but relatively high returns on the X-band image. The high X-band return precludes discrimination of the more heavily ridged and hummocked areas on the X-band image, such as the ones marked B in Figures 15 and 16. The rough area B can be identified and delineated on the L-band image.

The iceberg at C in Figures 15 and 16 appears to provide a radar shadow on X-and L-band images. The shadow area is more distinct on the L-band imagery. The L-band imagery displays two bright images immediately below the iceberg. These images are believed to be time-delayed returns from the iceberg. Many icebergs exhibited this condition on the L-band imagery. Part of the radar shadow probably represents a period of no radar return during which the radar signals were "captured" within the iceberg. Lack of an anomalous signal in the space between the iceberg image and the false image seems to preclude consideration of volume scattering within the iceberg. This effect and the apparent high strength of the false image signals indicate multiple ice/water interface reflections within the iceberg and a focusing of energy on a reflective interface, which subsequently directed the signal back to the radar antenna. The approximate location of the false images on the terrain is shown on the photography in Figure 16. Other icebergs in Figure 15 also show false signals on the L-band imagery. The iceberg at D looks very similar on both the X- and L-band images, indicating that L-band returns, in this case, are directly from the iceberg as with X-band. However, a small image below the L-band iceberg image could represent a time-delayed signal. The iceberg at E is well-displayed on the X-band imagery, but on L-band imagery the area of the iceberg is represented by a shape similar to that shown on X-band, but has no backscatter with the exception of the small return area near the center. The iceberg at F is easily delineated on the X-band imagery, but on L-band imagery it is represented by five bright distinct scattered returns with little or no return between them. Even though the returns from the surrounding ice in the lower portion of the L-band imagery are suppressed, the iceberg returns appear to have saturated the radar. These returns are probably reinforced.

No correlative photographic data were obtained northward of the beginning portion of Pass 3 during the flight to Thule AB, Greenland, but earlier correlations have given interpretive clues when using coincident X- and L-band imagery in this area. To amplify, it has been hypothesized (Ketchum, 1977) that the development of the radar backscattering surface may be generated by the accumulation of environmental heat at the snow-ice interface. Salt or brine from within the ice migrates to this warmer zone and increases the salinity, thereby increasing the dielectric constant. Sufficiently high temperatures in this zone, due to trapped heat, cause metamorphosis of the ice and snow at their boundary and development of a recrystallized zone which is rough to X-band radar. The resulting combination of a radar rough surface and increased dielectric constant produces the radar backscattering surface. The amount of heat which accumulates at the snow-ice interface is primarily a function of ice thickness, snow thickness and density, air temperatures, and time.

Because of high return on the X-band image much of the thin ice bordering the new fracture is believed to have been recently snow-covered (Figure 17). Southerly winds, thought to be responsible for the most recent opening of the fracture, could have caused snow drifting onto the thin ice. Recent precipitation of snow may have occurred. The presence of thin ice on the fracture is identified on L-band imagery only at the steeper angles of incidence. Areas interpreted to be mainly brash and block stand out clearly on L-band imagery. These areas are also high return areas on the X-band imagery, but are not as easily delineated due to background clutter. The wakes of brash and block associated with the differential motion of the sea ice and icebergs are also identified because of their high return on both channels. A false image is identified in association with the uppermost iceberg on the L-band image. As in Figure 15, some of the iceberg returns are very strong, indicating signal reinforcement.

Some backscatter variations observed on the X-band image in areas which show little return on the L-band image are believed to be due to variations in snow-ice interface development related to snow depth, ice thickness, and air temperatures. Minor variations in ice surface roughness may also be responsible for backscatter differences. However, a homogeneous gray tone indicates a very high density of scatterers, which tends to indicate an interface reflection.

Much of the ice cover shown on the radar images in Figure 18 is interpreted to be of fast ice origin. Both X- and L-band images display this ice with homogeneous high returns, which are attributed to a high density surface roughness related to the consolidation of many small fragments that formed during early growth of the fast ice. Ice fragmentation due to wave action is not uncommon because generally these areas are not protected by adjacent offshore ice fields during the early growth period of fast ice. The fast ice fragments are more pronounced and better delineated in the X-band image because the surrounding sea ice presents a much more variegated gray tone than in the L-band image, thus presenting more contrast in the pattern. The large areas of nilas adjacent to the fast ice fragments probably resulted from openings formed by differential motion of the thicker, heavier fast ice fragments and the surrounding drifting sea ice. Dark gray tones on the high return nilas in the lower portion of the X-band image appear to be flooded areas. Flooding would remove snow cover believed responsible for the high backscatter. The pattern orientation and extent of the indicated flooding could be related to the southerly winds which prevailed during this time. The dark lineations seen on the fast ice fragments are interpreted as thick ice frozen in the fractures which occurred while the ice was in its original shorefast location. The wider fracture is probably an old shear zone and the narrower fractures intersecting the shear zone may be tension fractures which developed during the shearing action. Friction caused by sea ice drifting adjacent to the fast ice zone was probably responsible for formation of the indicated shear zone. The initial orientation of the shear zone would then have closely paralleled the edge of the fast ice. Many icebergs are present in the lower left portion of the Figure 18 images. A false image is identified on the L-band image.

The X- and L-band radar image strips shown in Figures 19 and 20, respectively, were taken during a flight westward along the Greenland coast from Cape Melville to Cape York and beyond. Numerous icebergs, most rather small, are shown locked in the shorefast ice between Cape Melville and Cape York. The large concentration of icebergs immediately west of Cape Melville and east of Cape York indicate that this area is a primary source of icebergs in Baffin Bay. Icebergs are also seen in the drifting ice located west of Cape York. The sea ice adjacent to many of the icebergs exhibits low or no radar return. Low radar return areas are also present on the sea ice along the coastline. No coincident photographic data are available to aid in identifying the nature of these low radar return areas. However, it is believed that the low return signatures may be related to the action of very strong winds from the Greenland ice cap and the resulting surface flooding. It is speculated that the flooding is directly related to the forces of the strong winds on the icebergs and sea ice surface.

Fracturing of the sea ice around the sea level bases of the icebergs and along the coastlines, due to wind forces, would provide the necessary openings for flooding. Snow removal and smoothing of the ice surface would result from the flooding process. Flooding is also present along cracks running between some of the icebergs in a direction normal to the strong winds. These cracks are probably related to the wind stress on the icebergs.

A dominant east-southeasterly wind over this area is indicated by snow drift pattern identified in association with the icebergs in the drift ice west of Cape York in the X-band imagery (Figure 19). The great length of the snow drifts suggests very strong winds. The shape and orientation of the low return areas in association with the icebergs and the coastline also suggest east-southeasterly winds. Although we do not have sufficient information to determine the processes involved, it appears fairly evident that very strong winds have played a significant role in the apparent fracturing and flooding process.

Many of the icebergs shown in the Figure 20 L-band imagery produced false images or images which represented time-delayed return signals. These icebergs generally showed less return than the same icebergs on the X-band imagery. In some cases lack of any backscatter indicates that all the radar energy has been lost through internal iceberg reflections.

Internal reflections are suggested by many low or no return areas shown on the L-band imagery of the ice-covered land masses in Figure 20. Many of these areas of reduced return on the L-band imagery and good returns on the X-band imagery (Figure 19) are interpreted to be glaciers or inland ice sheets. Further comparison of the coincident X- and L-band imagery may allow some determination of glacial ice distribution.

NORTH BAFFIN BAY DATA

Although the majority of ice in North Baffin Bay is first-year ice, it is comprised of various thicknesses, which are in different stages of development, and have experienced different degrees of deformation. Relative age identification, using aerial photography, is based primarily on visible surface roughness. The season's earliest ice formations may undergo considerable sea and swell action and other deformational activity before any semblance of stability is established in the ice cover as it grows thicker. Because of this more pronounced deformation in the early stages of ice growth, the surface layers may be comprised of many broken pieces which have been consolidated. The underlying layer of ice probably represents a more normal, homogeneous growth. This condition would suggest the presence of a rough boundary between an upper layer of deformed ice and a lower layer of undeformed ice, a boundary which could act as a reflective interface if reached by microwave energy.

The 27 km long sections of coincident X_{HH} and L_{HH} SAR imagery in Figure 21, as with earlier dual frequency illustrations, show considerable backscatter variation in a single channel and significant backscatter variations from the same ice features on different channels. It has been stated that snow cover strongly affects backscatter and the backscatter variations seen in the X-band imagery. The L-band radar is not as strongly affected by snow cover, hence the frequent large variation in the display of the same ice features as imaged by the two channels. It is hypothesized that the variable X-band radar backscatter is due to the presence of moisture in the snow, the development of a reflective snow-ice interface (due to interactive processes dependent on various balances of ice thickness, snow depth and density, and air temperature), and the residual effects of melted, then refrozen, snow cover on a relatively thin ice surface. Examples of all these phenomena and their effects on X-band radar backscatter may be present in the Figure 21 radar image.

The radar imagery in Figure 21, which is correlated with the photograph in Figure 22, shows examples of radar backscatter; some of which can and some of which cannot be correlated with the variable surface roughness properties visible on the photography. The thinnest areas of first-year ice, some of which have been labeled A, have a thin snow cover over an apparently smooth ice surface with minor relief in the form of ridging and rafting. On the X-band imagery, these areas cannot be readily distinguished from the areas labeled B which are areas of thicker first-year ice with ridging and consolidated fragments and an apparent deeper snow cover. However, since the backscatter from these visibly different areas of surface roughness is very similar, the primary backscatter is believed to be related to a weakly developed snow ice interface on both ice types, not to the deformational features.

The L-band radar appears unaffected by a snow-ice interface development on the thin, smooth first-year ice areas A and displays low or no radar return. The thicker, rougher first-year ice areas B show a higher return than that displayed on the X-band imagery. This comparison suggests penetration and subsurface backscatter of the L-band radar signals. The interface of a two-layer ice cover suggested earlier (consolidated pieces of deformed ice in the upper layer overlying a more normal homogeneous lower layer) may be the reflective boundary for this suggested subsurface return. Areas labeled C have extremely rough surfaces (high density of rubble and ridges) and provide returns at both radar wavelengths. On the L-band imagery these high return areas cannot be readily distinguished from the high-return B areas, again suggesting that visible surface roughness does not play the primary backscattering role with the L-band radar. The high X-band returns from the C areas seem to be more closely related to surface roughness, but again a snow-ice interface development within the heavily deformed areas could make an important contribution to the backscattering. The ice conditions shown by the photograph in Figure 22 probably closely represent ice conditions throughout the left portion of the radar strips shown in Figure 21. It is clear that the smooth, thin, first-year ice areas can be readily identified only on the L-band imagery, and that identification of the extremely rough areas can be done with more confidence, although subjectively, using the X-band imagery.

The center portion of the SAR images shown in Figure 21 has a less intricate pattern of gray tones than the imagery shown on the left and right ends of the radar sections. This difference is greater on the X-band imagery because of the greater X-band radar sensitivity to surface conditions, particularly the suggested snow effects and snow-ice interface conditions. The center portion of the imagery does not depict much ridging, but the homogeneous high X-band returns, which indicate a high density of backscatterers (as would be expected from a reflective snow-ice interface) do much to obscure or mask returns from the ridges which are present. On the L-band imagery there is also a high, homogeneous return that may obscure ridge identification. The small size of many of the ridges and steep antenna angles may be factors here, too. The high L-band returns, which are homogeneous throughout this area, are attributed to subsurface reflections. It is apparent that reflective properties not discernible on the photography (Figure 23) are responsible for much of the radar return imaged by both X-band and L-band and that the masking effect of these "anomalous" returns reduces the ability to accurately interpret the sea ice conditions, particularly with respect to surface topography. As with the coincident SAR imagery and photography shown in Figures 21 and 22, respectively, areas identified as thin, smooth first-year ice A and rougher, thicker first-year ice B appear to be similar on the X-band imagery, but different on the L-band imagery. On X-band imagery, areas of greater surface roughness C provide the highest radar return, but on L-band imagery the extremely rough areas C cannot be easily distinguished from much less rough first-year ice B because of the similar returns. The thin, smooth, first-year ice at A is easily distinguishable on the L-band imagery by the low contrasting returns. The thin ice-covered fracture shown by the coincident SAR imagery and photography in Figures 21 and 23, respectively, gives a high X-band, but low L-band radar return. The 5000-foot altitude photography, which was taken about 24 hours after the SAR imagery, does not readily reveal a snow cover on the thin ice, but close examination of the photography reveals areas of flooding associated with recent rafting. The flooding has left darker surface areas on the photography and low radar return areas on the X-band imagery. It is evident that flooding has removed a portion of the surface material, probably snow cover or some residue from a former snow cover, and that this material had the properties necessary to produce X-band radar backscatter.

Ridge detection on the data examined during the analysis has been difficult in many areas. Many ridges do not produce discernible radar returns. This may, in part, be due to small ridge size in terms of the radar resolution and steep antenna angles; however, background clutter obscuring ridge detection seems to be the principal reason. It is evident, when comparing the photograph in Figure 24 with the SAR images in Figure 21, that the most outstanding high return features on the X-band imagery are snow-covered, thin-ice-filled narrow fractures. These areas, some of which are labeled A, Figure 21, are often found in association with and parallel to, or within a ridged area. These areas may be accidently overlooked visually because of snow cover. The relatively large ridge at B in Figure 21, is delineated on both channels. Portions of this ridge are relatively new, as affirmed by the lack of snow drifts. Recent flooding adjacent to the ridge, with associated snow and ice changes as well as the recently frozen snow-covered fracture parallel to this ridge, probably accounts for the radar return. Delineation of ridges on the right end of the radar section in Figure 21 is generally better than for the rest of this section; reduced background clutter is one reason. Discrimination of ridges from narrow ice-covered fractures could be difficult. The often sinuous nature of ridges, as compared to fractures, may sometimes be the best clue for interpretation. The newly opened fractures, depicted on the photography, were not present about 24 hours earlier when the SAR imagery was taken. The new fracturing, along the lines of the earlier fracturing, may have been underway. It seems implicit in this SAR imagery, as with the SAR imagery farther south, that in some way changes in snow properties have a profound effect on X-band radar backscatter.

CONCLUSIONS AND DISCUSSION

This analysis has clearly indicated the usefulness of dual-frequency SAR imagery to increase the objectivity of sea ice imagery interpretation, particularly in the marginal seas or areas which have large concentrations of relatively thin ice, a high incidence of snow, and large fluctuations in air temperatures. Combinations of these factors seem to contribute to changes in snow properties and to the development of a snow-ice interface, both of which appear to play important roles in X-band radar return. These observed phenomena produce many ambiguities in interpretation of X-band radar imagery; but coincident L-band radar imagery, which is not noticeably affected by these phenomena, can often be used to resolve these ambiguities.

Penetration of sea ice by the long wavelength L-band radar is not uncommon and subsurface returns are suspected. Hence, L-band radar as well as X-band radar imagery may, at times, be a poor indicator of ice surface topography when the masking effect of background clutter dominates the scene. In general, discrimination of various stages of growth and deformation of first-year ice was often very subjective with the X- and L-band radar imagery used during this analysis. Ice pressure ridge identification and discrimination were often poor and sometimes could not be carried out. Both deficiencies have been largely attributed to background clutter (snow and snow-ice interface backscattering with X-band, and subsurface backscattering with L-band).

Small ice ridge sizes versus the system resolution and the steep antenna angle also may be reasons for not discerning more ridges. The false images or time delayed L-band signals from icebergs were seen for the first time in this analysis. This prima facie evidence demonstrates that icebergs are penetrated by L-band radar. The illustrated variations of this effect (and lack of it) suggest that the internal structure and composition of icebergs vary considerably. Based on the evidence presented in this analysis, it is suggested that a comparative evaluation of coincident X- and L-band radar imagery of glaciated areas may lead to some assessment of glacial ice distribution over land masses.

BIBLIOGRAPHY

INTERA Environmental Consultants, Ltd. (1978). SAR 580 Production System. INTERA Report ASP-78-8, Aug.

Janza, Frank J., ed. (1975). Manual of Remote Sensing, V. I., Theory, Instruments and Techniques. American Society of Photogrammetry.

Ketchum, R.D., Jr. (1977). An Evaluation of Side Looking Radar Imagery of Sea Ice Features and Conditions in the Lincoln Sea, Nares Strait, and Baffin Bay. NORDA Technical Note 7.

Ketchum, R.D., Jr. (1978). An Evaluation of ERIM X-L Band Airborne Synthetic Aperture Radar Imagery of Sea Ice. NORDA Technical Note 28.

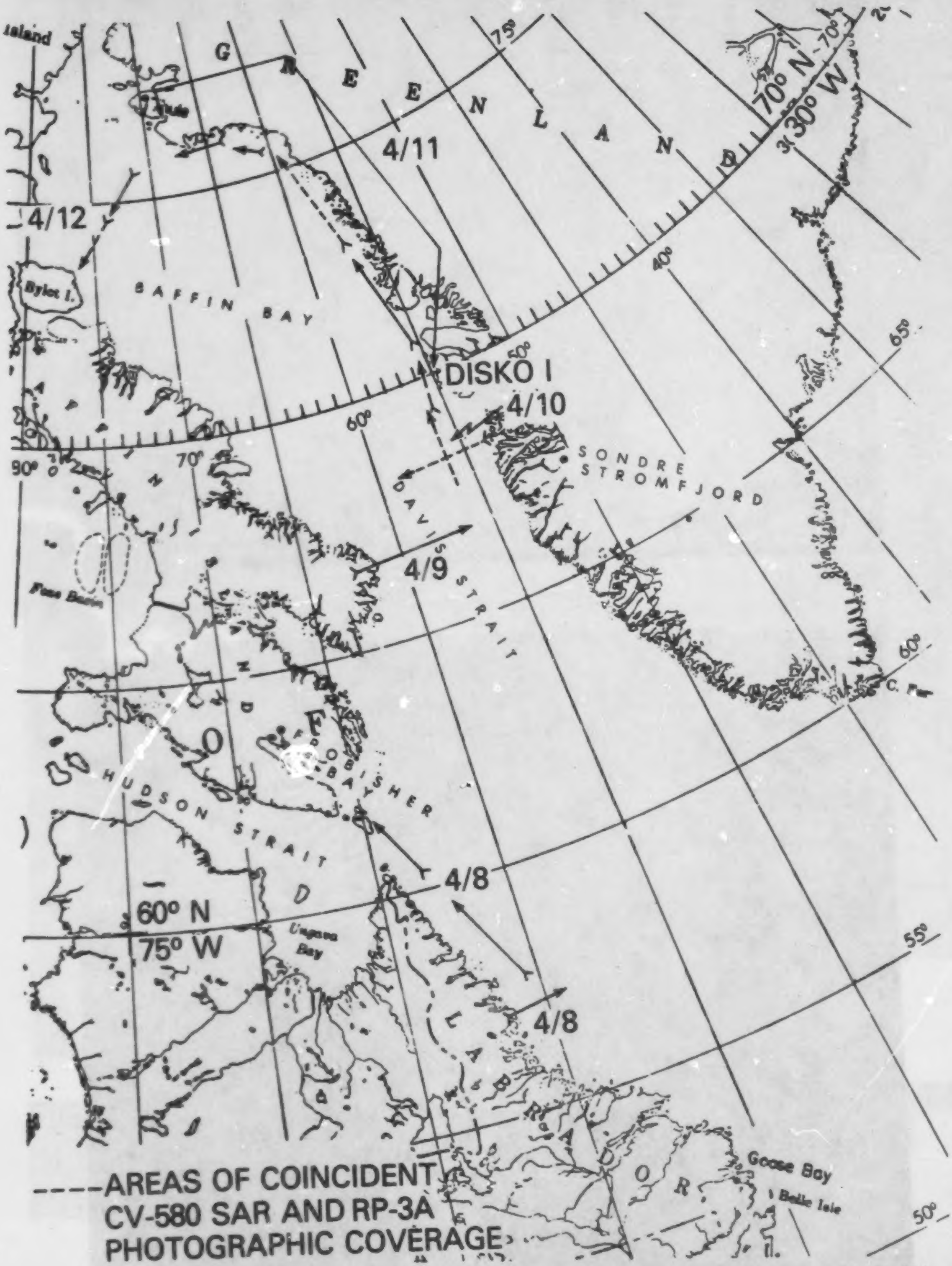
Island
Thule
G R E E N L A N D
75°
70° N
30° W
4/11
4/12
Bylot I.
BAFFIN BAY
DISKO I
4/10
40°
65°
60°
70°
90°
SONDRE STROMFJORD
DAVIS STRAIT
4/9
Foxe Basin
FROBISHER BAY
HUDSON STRAIT
4/8
60° N
75° W
Ungava Bay
4/8
LABRADOR
55°
C. Far
Goose Bay
Belle Isle
50°
----AREAS OF COINCIDENT CV-580 SAR AND RP-3A PHOTOGRAPHIC COVERAGE

FIGURE 1. SURSAT CV-580 AND RP-3A FLIGHT TRACKS IN EASTERN ARCTIC,APRIL/1979

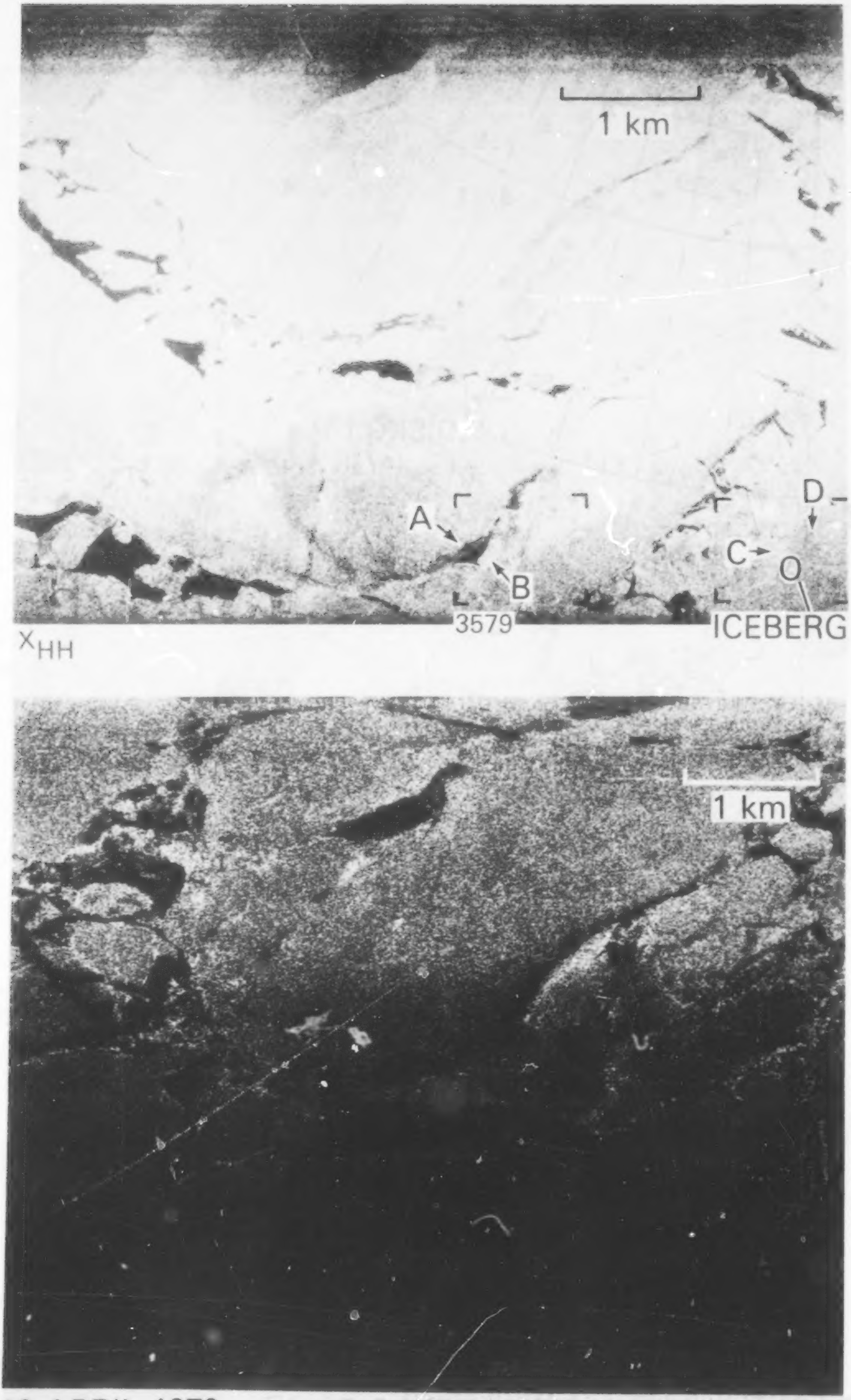
1 km
A
B
C
D
3575
3579
ICEBERG
1 km

X_{HH}

10 APRIL 1979

L_{HH}

FIGURE 2.3 COINCIDENT XHH AND LHH SEA ICE SAR IMAGES TAKEN IN DAVIS STRAIGHT 10 APRIL 1979

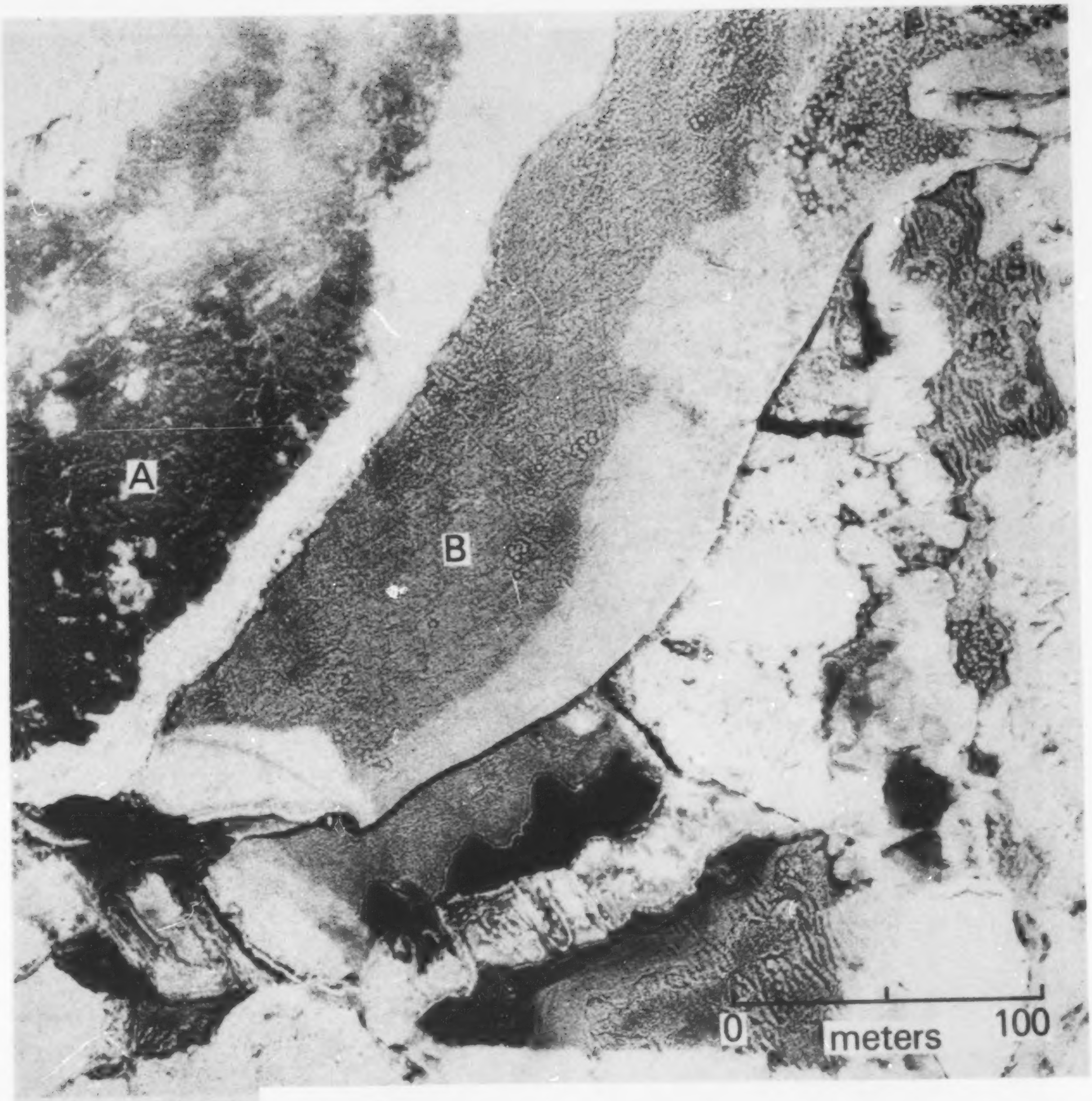

FRAME 3579
10 APRIL 1979

FIGURE 3 AERIAL PHOTOGRAPH (305 M ALTITUDE) TAKEN IN DAVIS STRAIT, 10 APRIL 1979. CORRELATES WITH FIGURE 2 SAR IMAGERY.

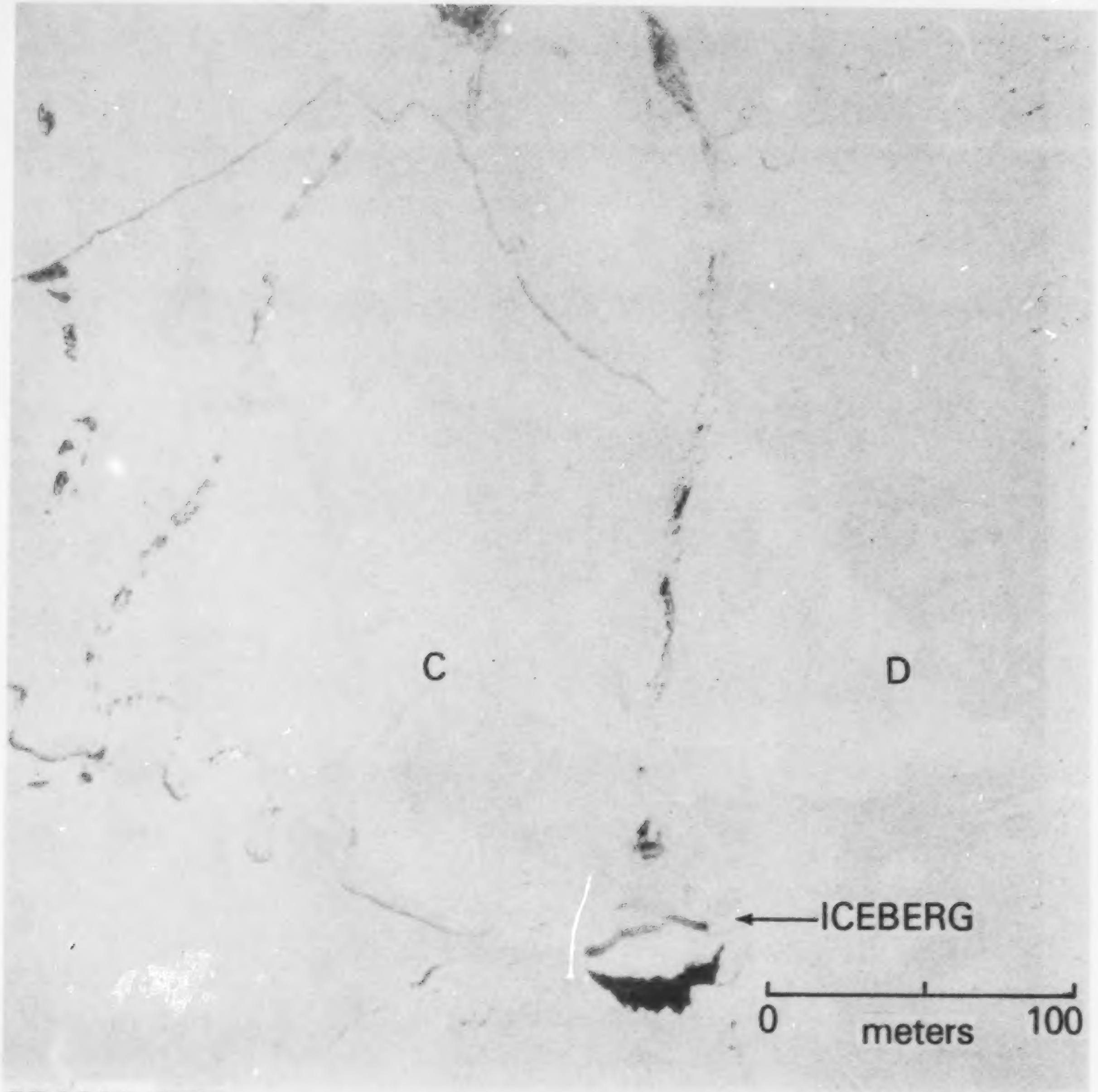
C
D
ICEBERG
0
meters
100

FRAME 3575
10 APRIL 1979

FIGURE 4 AERIAL PHOTOGRAPH (305M ALTITUDE) TAKEN IN DAVIS STRAIT, 10 APRIL 1979. CORRELATES WITH FIGURE 2 SAR IMAGERY.

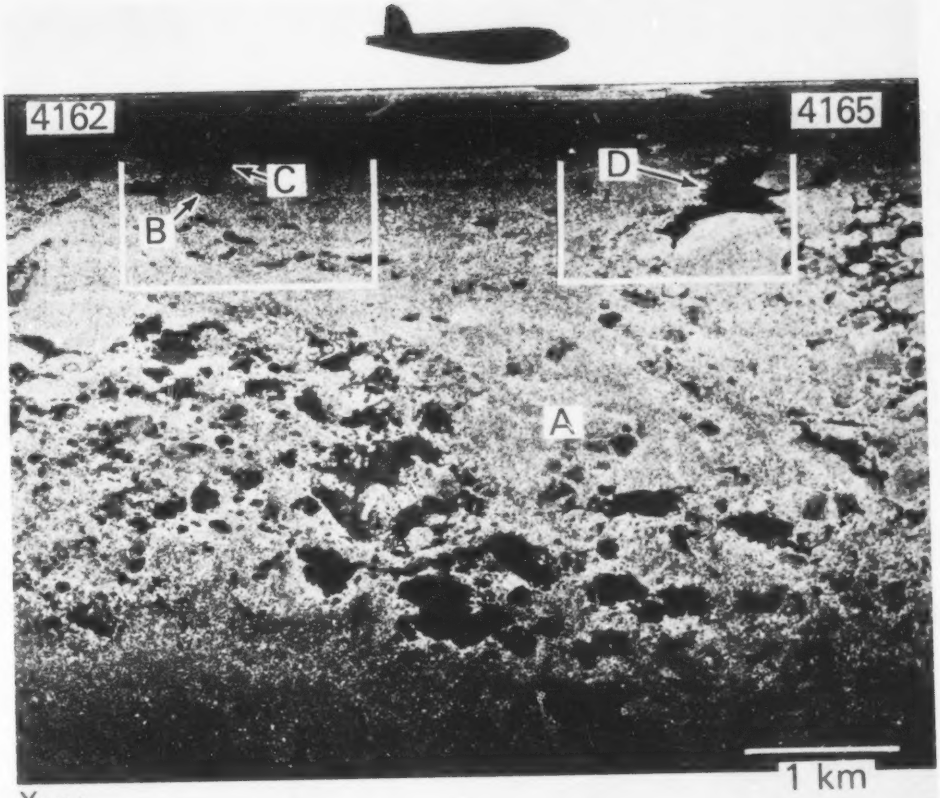
4162
4165
C
B
D
A
1 km

X_{HH}

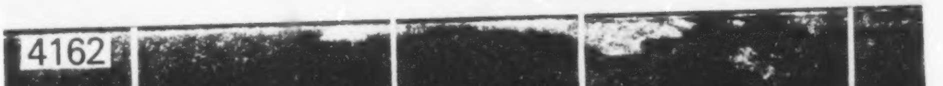
4162
C
B
D
4165
A
1 km

10 APRIL 1979

L_{HH}

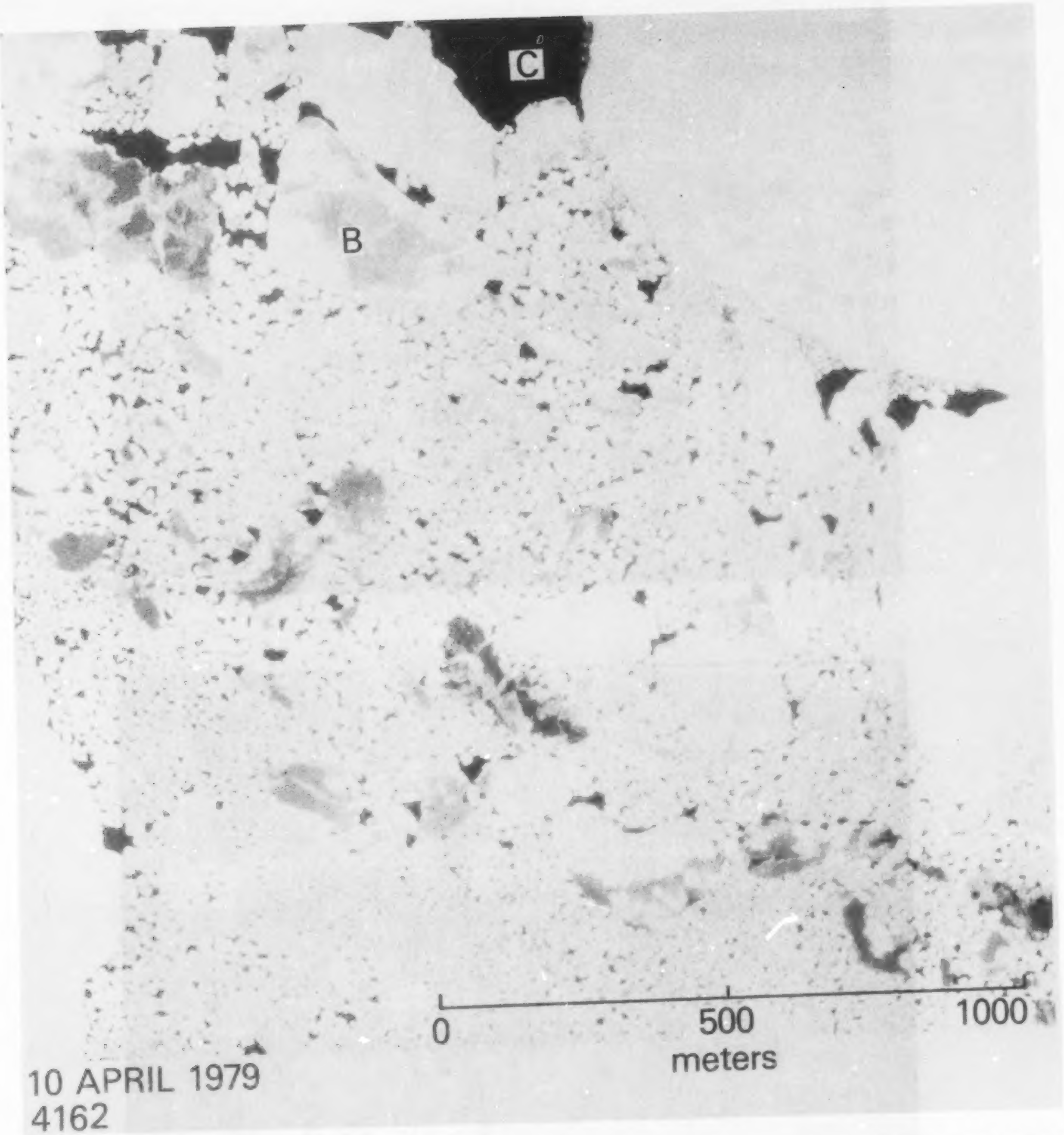
C
B
0
500
1000
meters
10 APRIL 1979
4162

FIGURE 6 AERIAL PHOTOGRAPH (1524M ALTITUDE) TAKEN IN DAVIS STRAIT, 10 APRIL 1979. CORRELATES WITH FIGURE 5 SAR IMAGERY.

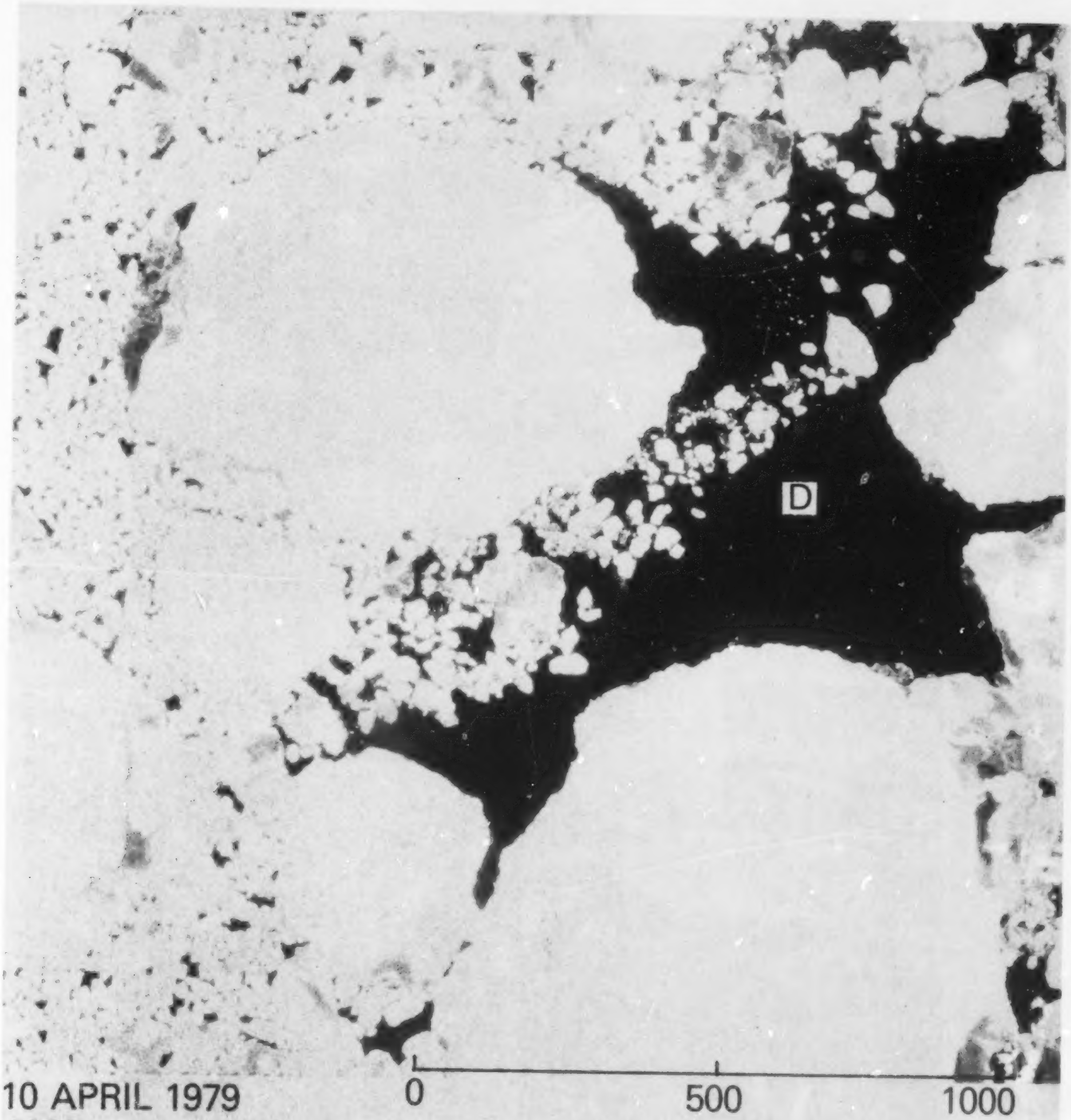
D
10 APRIL 1979
4165
0
500
1000
meters

FIGURE 7 AERIAL PHOTOGRAPH (1524M ALTITUDE) TAKEN IN DAVIS STRAIT, 10 APRIL 1979. CORRELATES WITH FIGURE 5 SAR IMAGERY.

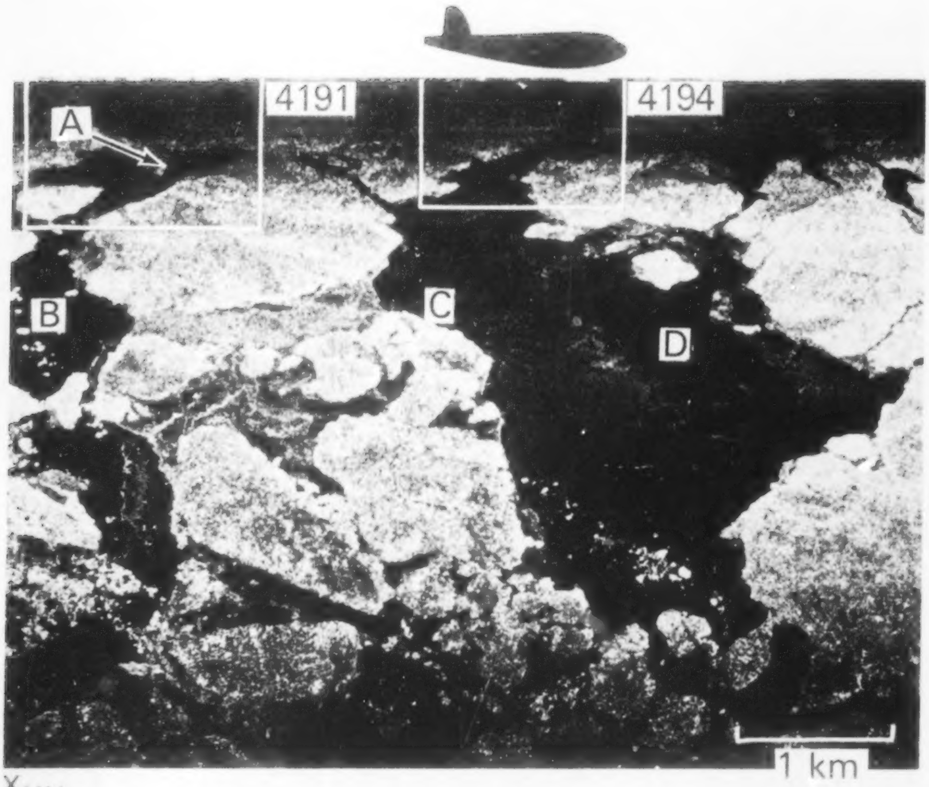
A
4191
4194
B
C
D
1 km

X_{HH}

A
4191
4194
B
C
D
1 km

10 APRIL 1979

L_{HH}

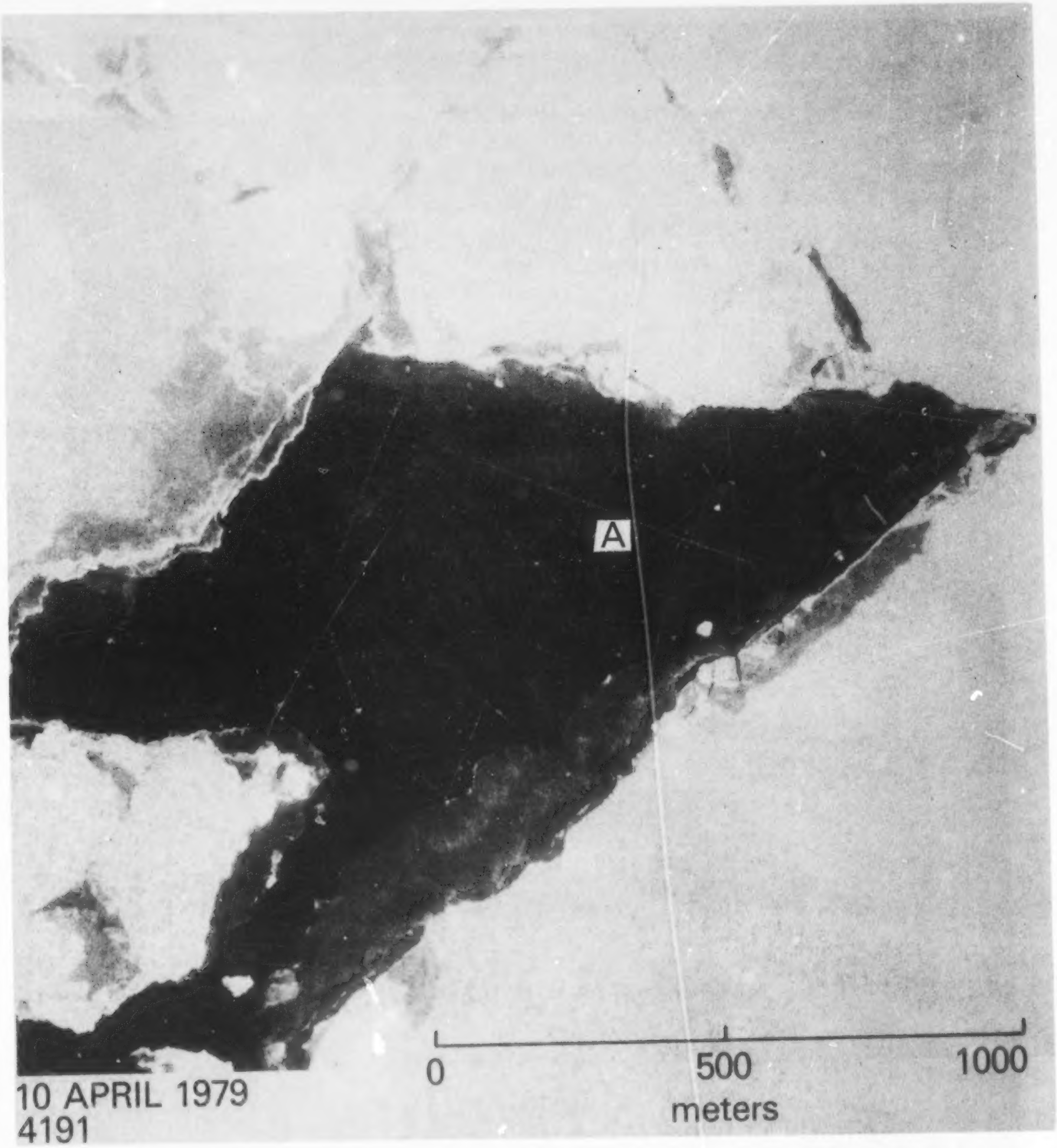
A
0
500
1000
meters
10 APRIL 1979
4191

FIGURE 9 AERIAL PHOTOGRAPH (1524M ALTITUDE) TAKEN IN DAVIS STRAIT, 10 APRIL 1979. CORRELATES WITH FIGURE 8 SAR IMAGERY.

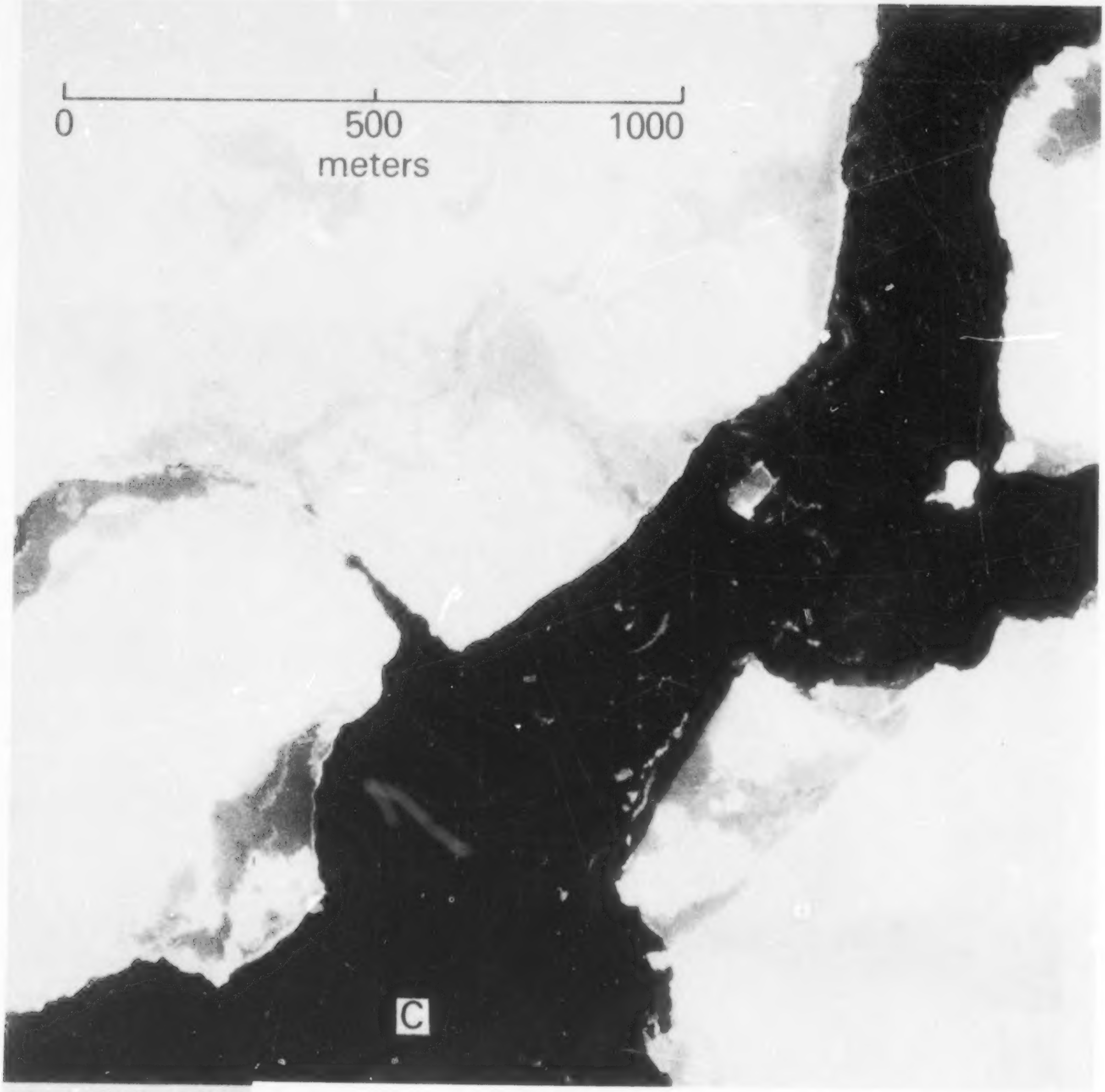
0
500
1000
meters
C

10 APRIL 1979
4194

FIGURE 10 AERIAL PHOTOGRAPH (1524M ALTITUDE) TAKEN IN DAVIS STRAIT, 10 APRIL 1979. CORRELATES WITH FIGURE 8 SAR IMAGERY.

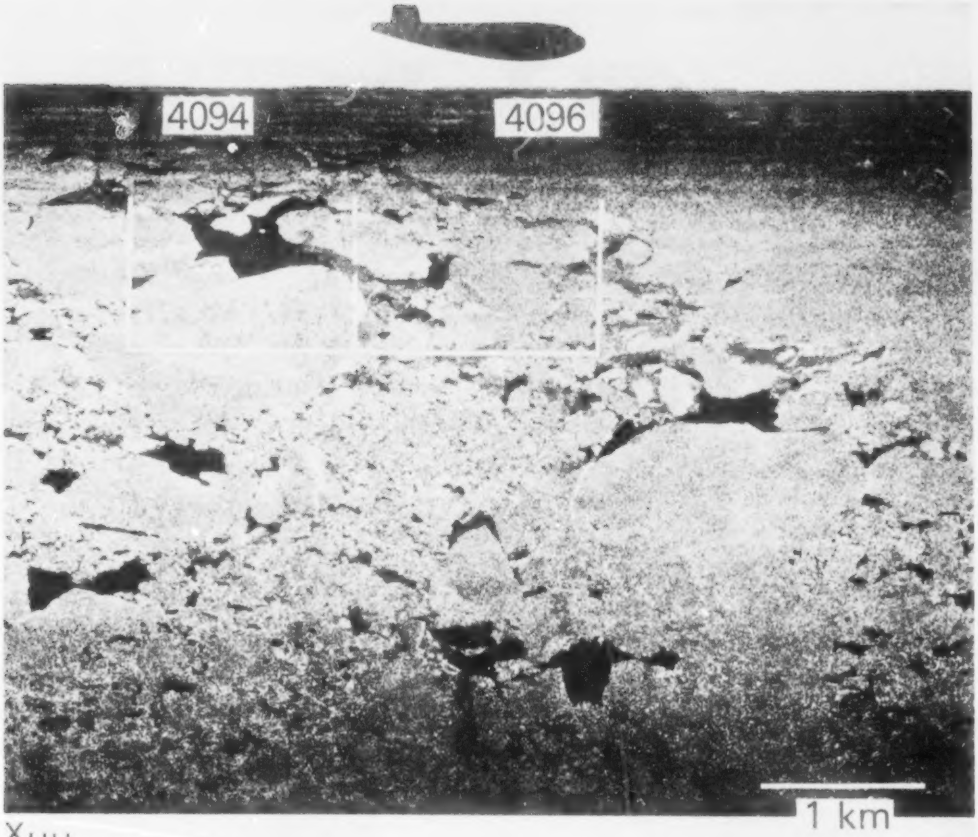
4094
4096
1 km

X_{HH}

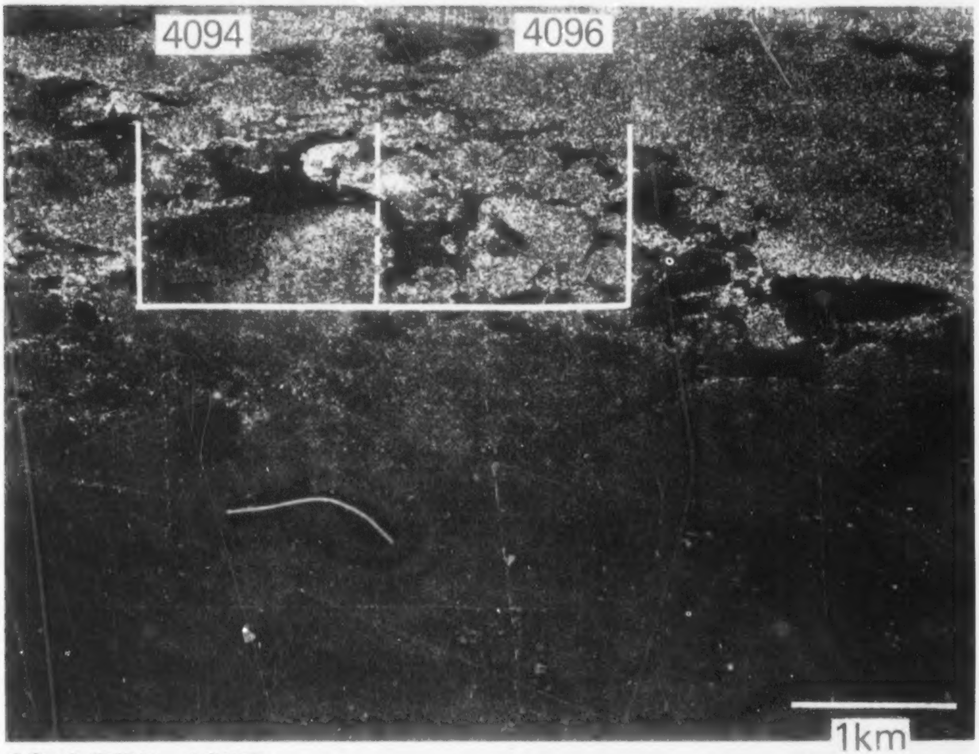
4094
4096
1km

10 APRIL 1979

L_{HH}

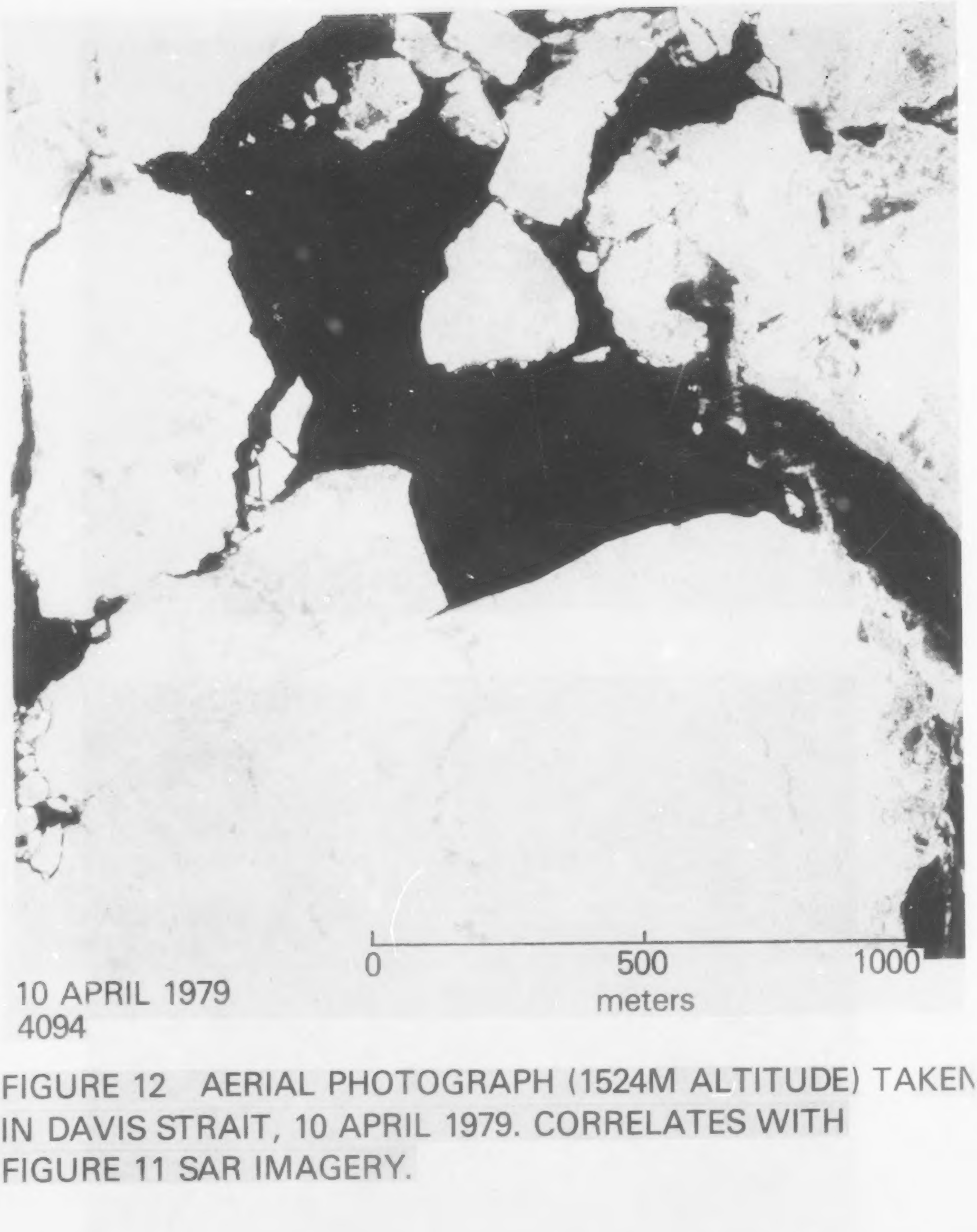
0
500
1000
meters
10 APRIL 1979
4094

FIGURE 12 AERIAL PHOTOGRAPH (1524M ALTITUDE) TAKEN IN DAVIS STRAIT, 10 APRIL 1979. CORRELATES WITH FIGURE 11 SAR IMAGERY.

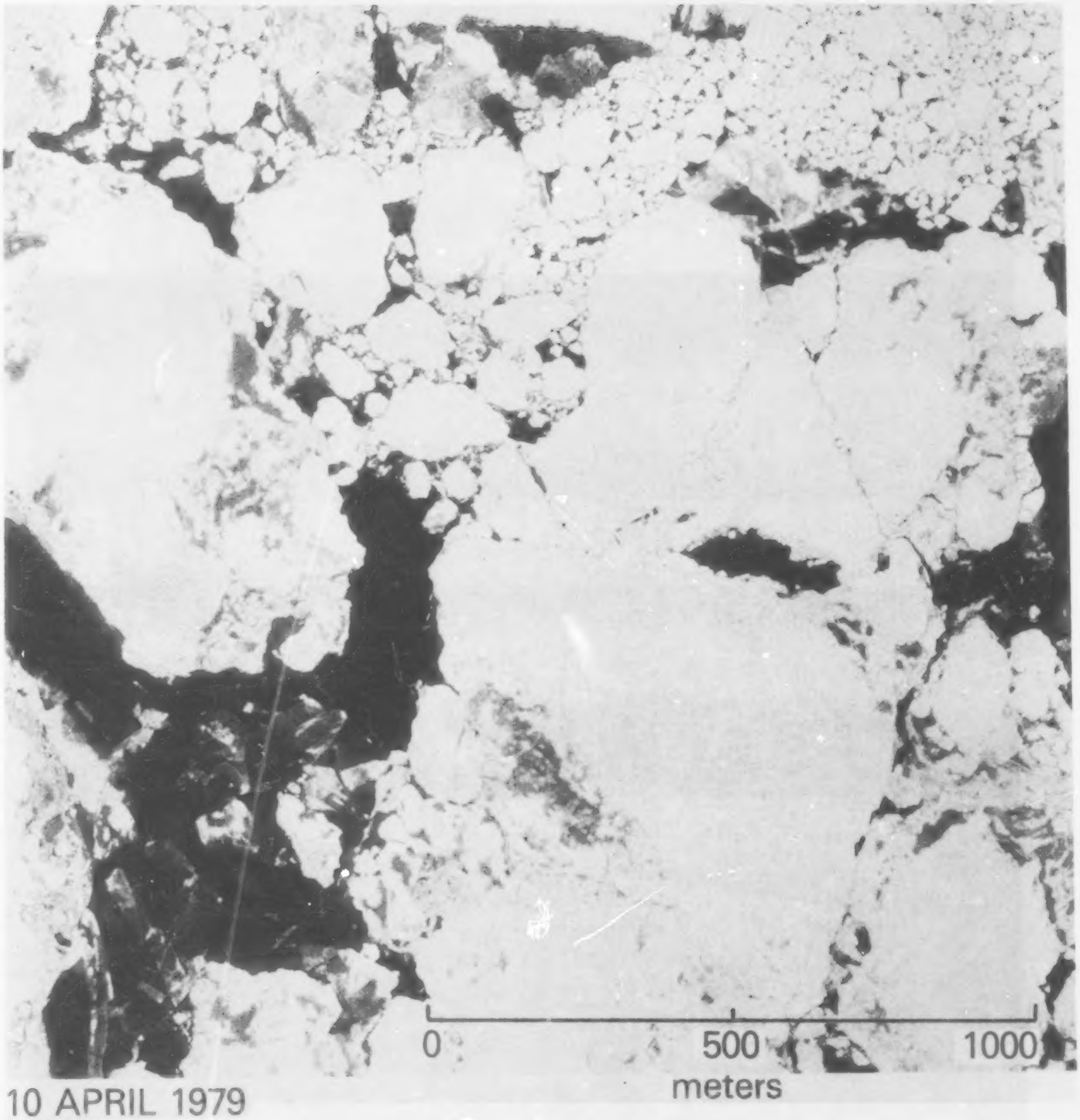
0
500
1000
meters

10 APRIL 1979
4096

FIGURE 13 AERIAL PHOTOGRAPH (1524M ALTITUDE) TAKEN IN DAVIS STRAIT, 10 APRIL 1979. CORRELATES WITH FIGURE 11 SAR IMAGERY.

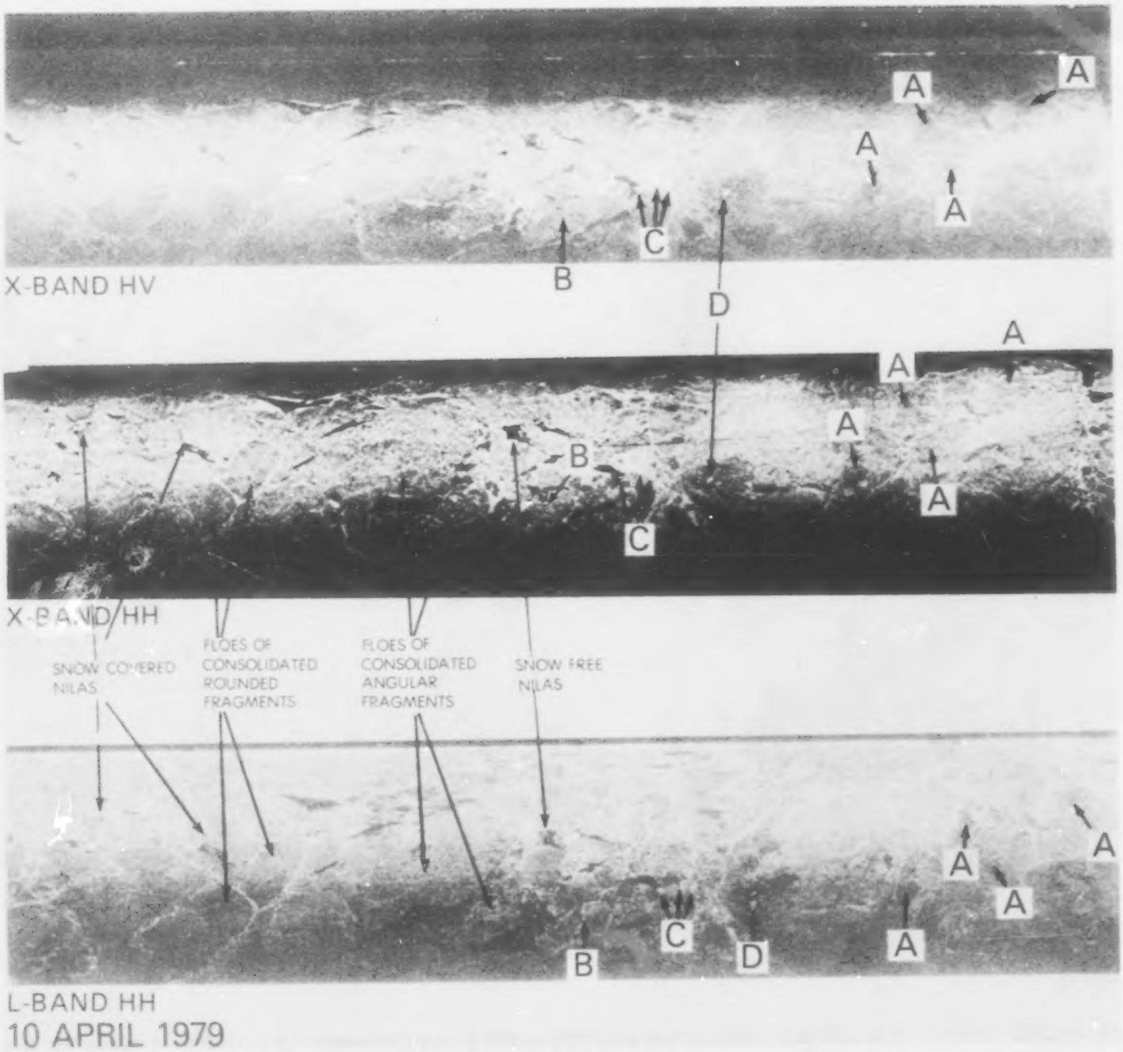
A
A
A
A
C
B
X-BAND HV
D
A
A
A
B
A
C
X-BAND HH
SNOW COVERED NILAS
FLOES OF CONSOLIDATED ROUNDED FRAGMENTS
FLOES OF CONSOLIDATED ANGULAR FRAGMENTS
SNOW FREE NILAS
A
A
A
C
B
D
A
L-BAND HH
10 APRIL 1979

FIGURE 14 COINCIDENT X_{HH} AND L_{HH} SEA ICE SAR IMAGERY TAKEN IN DAVIS STRAIT, 10 APRIL 1979.

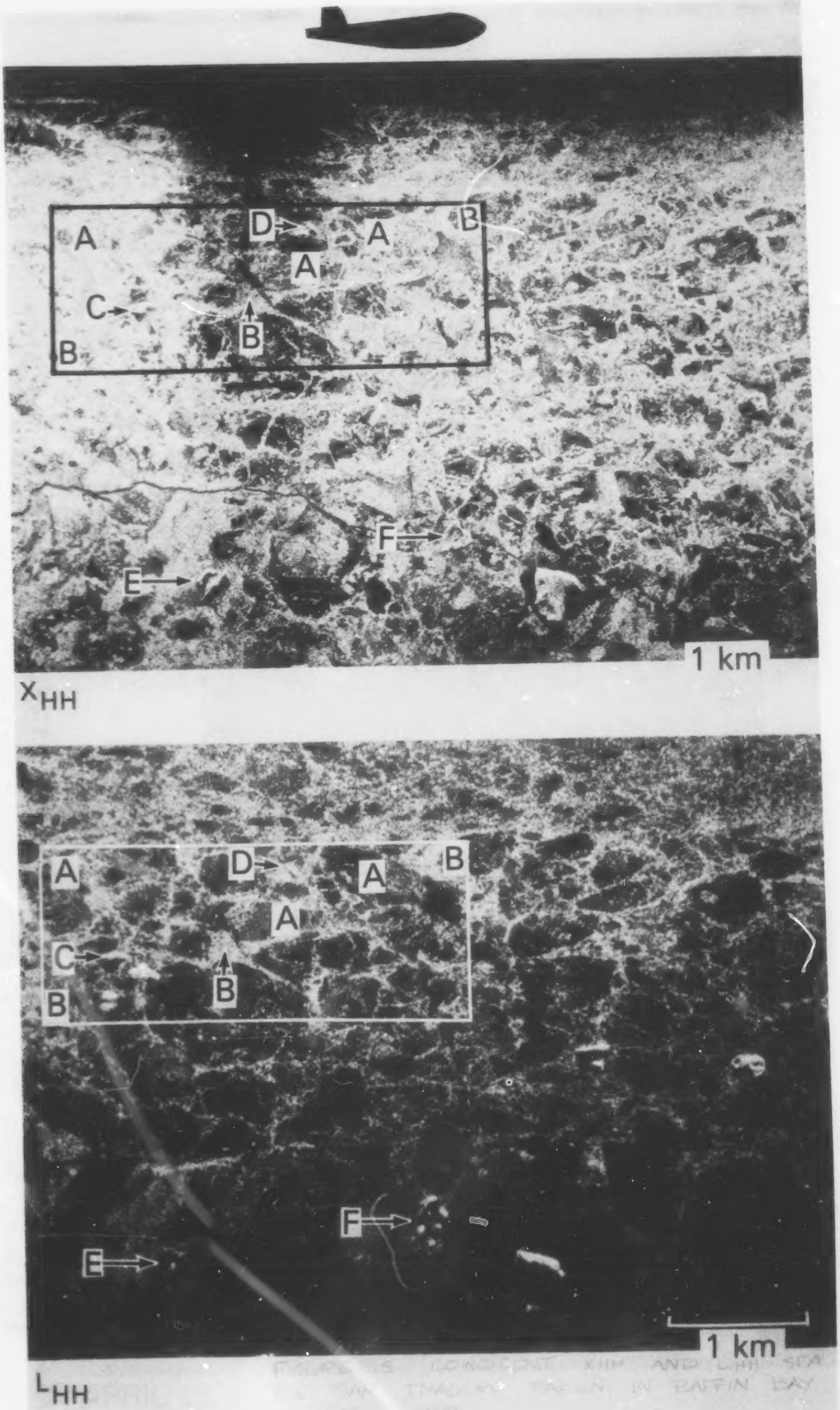
A
D
A
B
A
C
B
B
E
F
1 km
X_{HH}
A
D
B
A
A
C
B
B
F
E
1 km
L_{HH}

FIGURE 15 COINCIDENT XHH AND LHH SEA ICE SAR IMAGERY TAKEN IN BAFFIN BAY APRIL [illegible]

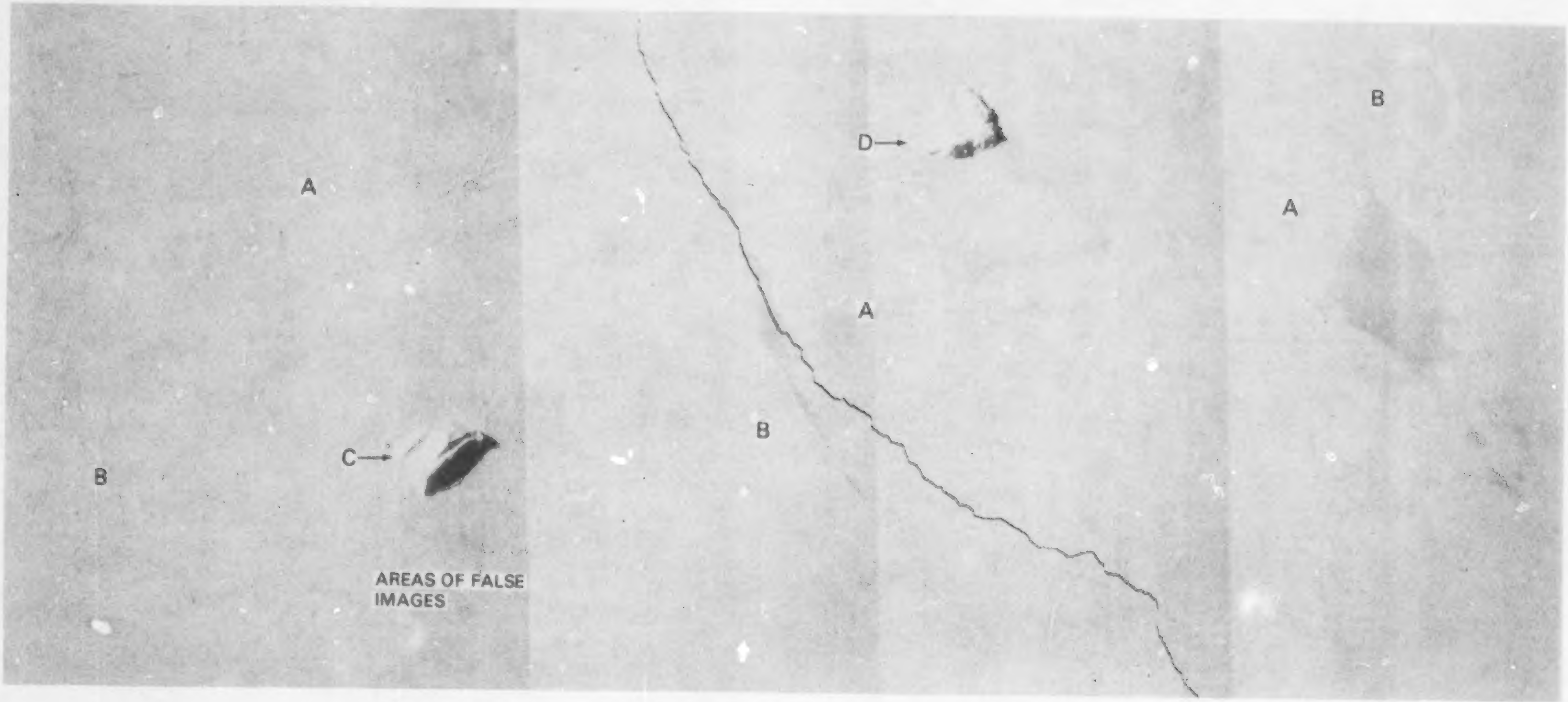
A
B
C→
AREAS OF FALSE IMAGES
D→
A
B
B
A

FRAME 4833-4836
11 APRIL 1979

0
meters
500

FIGURE 16 AERIAL PHOTOGRAPHY (1524M ALTITUDE) TAKEN IN BAFFIN BAY, 11 APRIL 1979. CORRELATES WITH FIGURE 15 SAR IMAGERY.

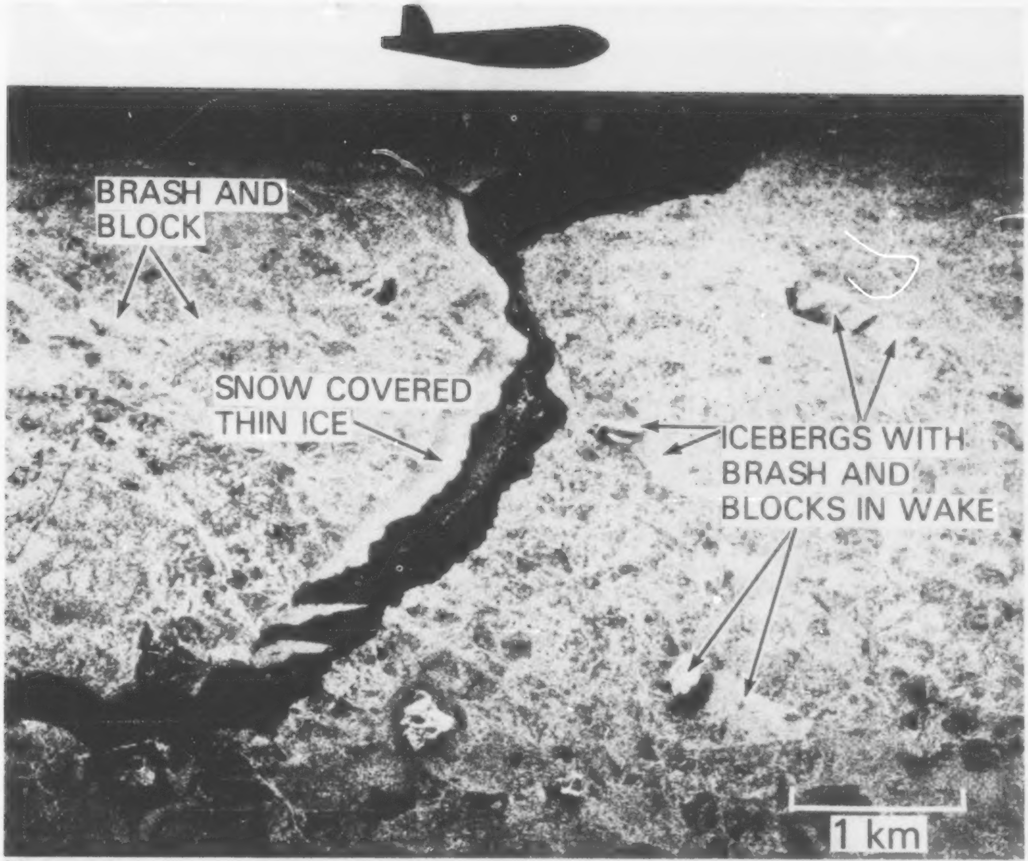
BRASH AND BLOCK
SNOW COVERED THIN ICE
ICEBERGS WITH BRASH AND BLOCKS IN WAKE
1 km

X_{HH}

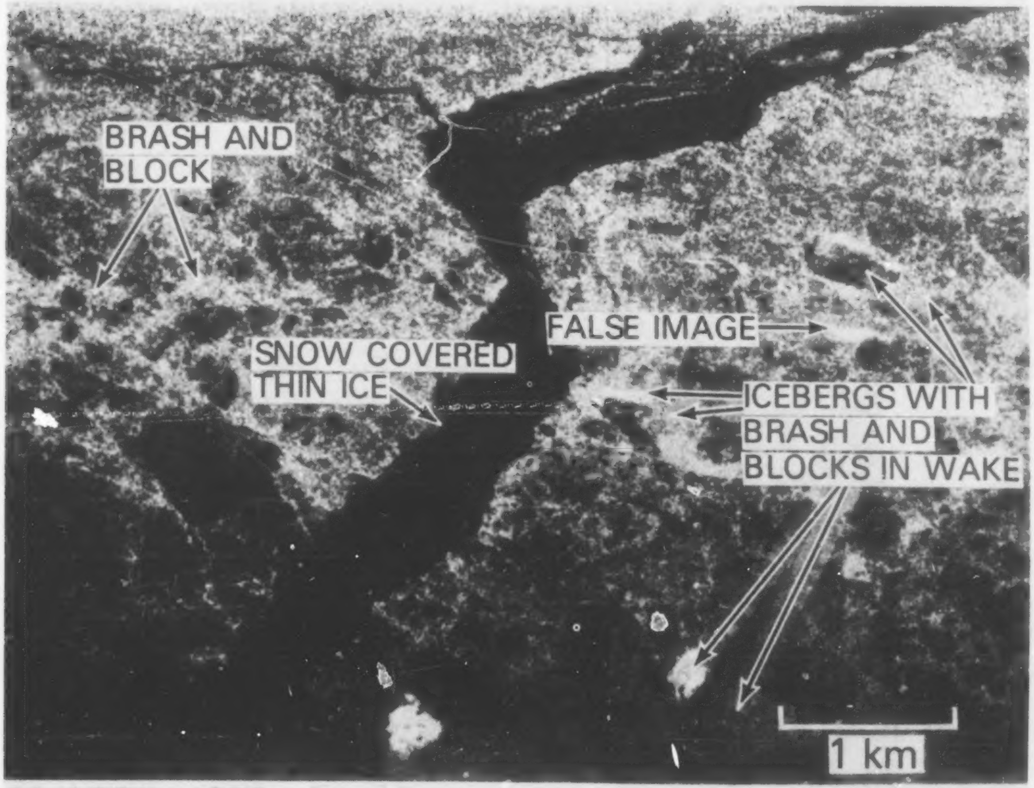
BRASH AND BLOCK
FALSE IMAGE
SNOW COVERED THIN ICE
ICEBERGS WITH BRASH AND BLOCKS IN WAKE
1 km

11 APRIL 1979

L_{HH}

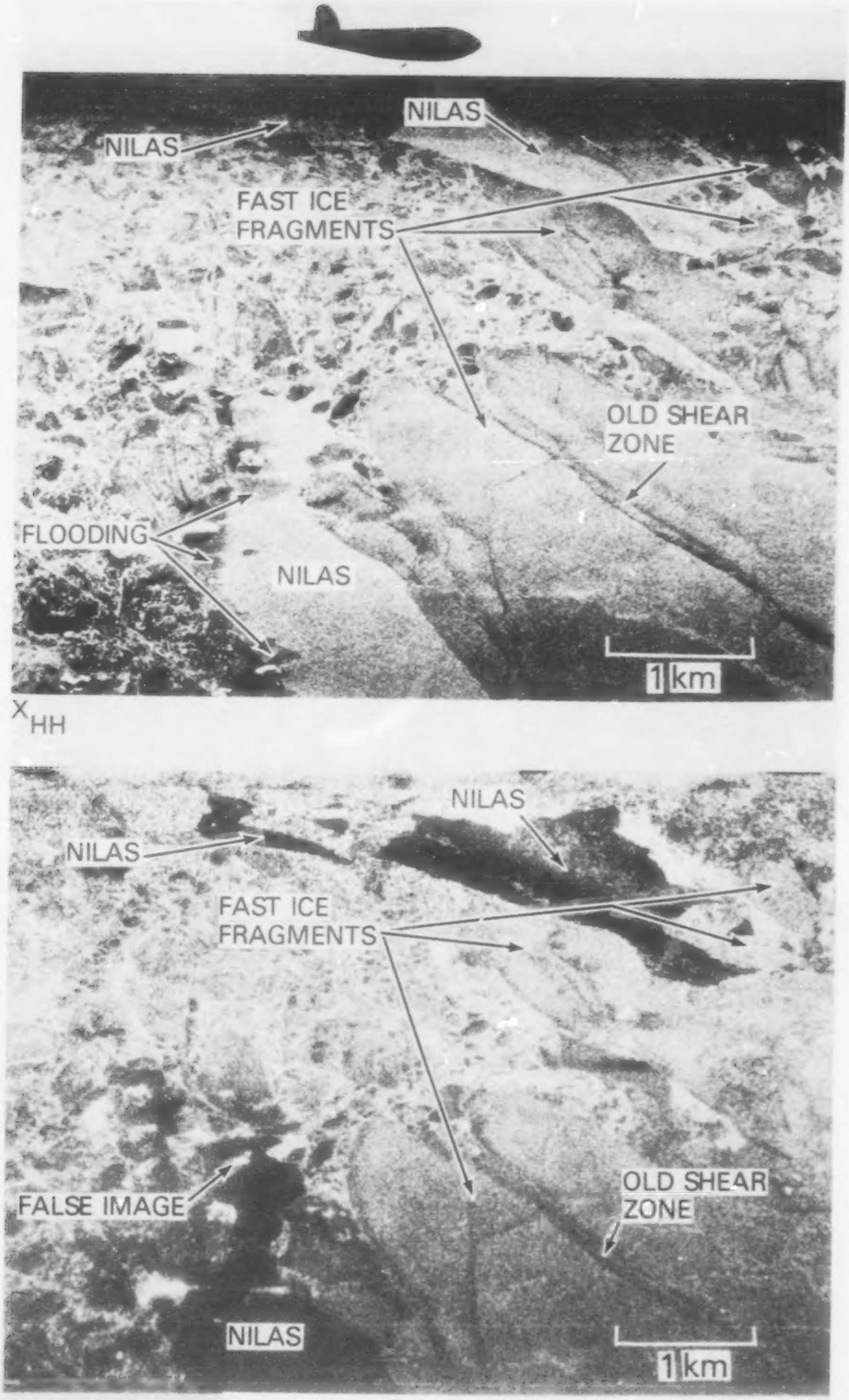
NILAS
NILAS
FAST ICE FRAGMENTS
OLD SHEAR ZONE
FLOODING
NILAS
1 km
X_{HH}
NILAS
NILAS
FAST ICE FRAGMENTS
FALSE IMAGE
OLD SHEAR ZONE
NILAS
1 km

11 APRIL 1979
L_{HH}

FIGURE 18 COINCIDENT X_{HH} AND L_{HH} SEA ICE SAR IMAGERY TAKEN IN BAFFIN BAY, 11 APRIL 1979.

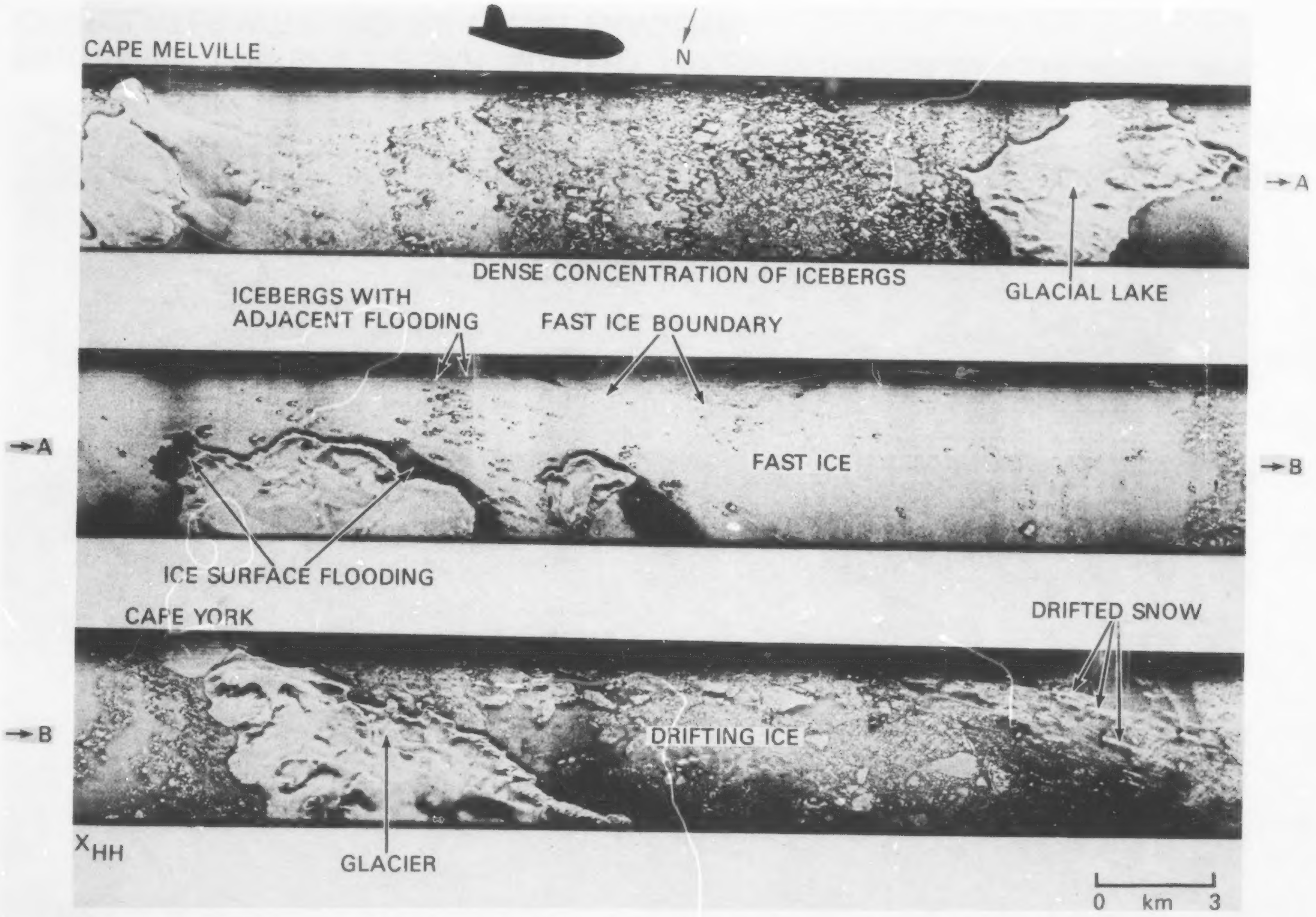
CAPE MELVILLE
N
→ A
DENSE CONCENTRATION OF ICEBERGS
GLACIAL LAKE
ICEBERGS WITH ADJACENT FLOODING
FAST ICE BOUNDARY
→ A
FAST ICE
→ B
ICE SURFACE FLOODING
CAPE YORK
DRIFTED SNOW
→ B
DRIFTING ICE
X_{HH}
GLACIER
0 km 3

FIGURE 19 X_{HH} SEA ICE SAR IMAGERY TAKEN IN BAFFIN BAY, 11 APRIL 1979. CORRELATES WITH FIGURE 20 SAR IMAGERY.

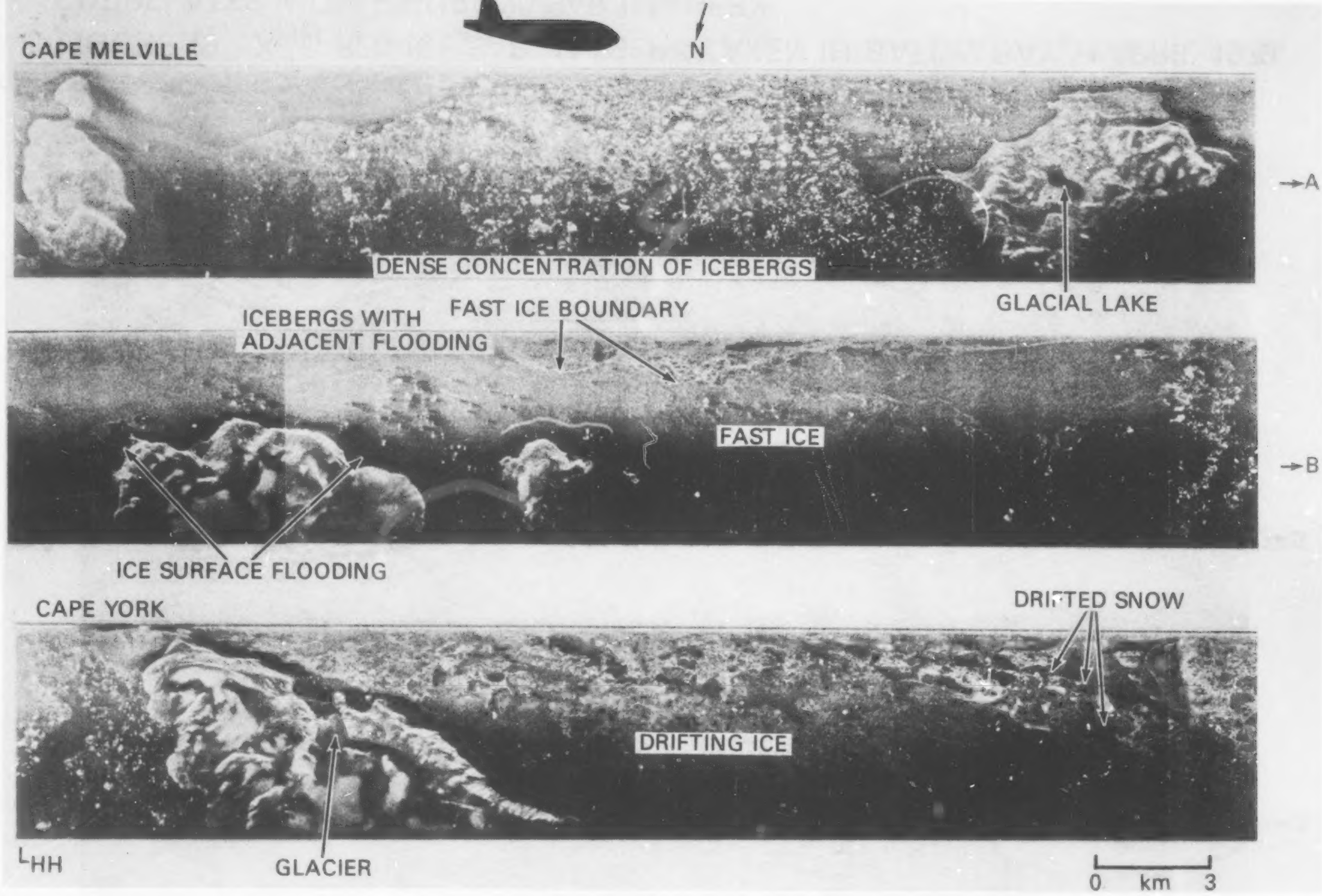
CAPE MELVILLE
N
→A
DENSE CONCENTRATION OF ICEBERGS
GLACIAL LAKE
ICEBERGS WITH
ADJACENT FLOODING
FAST ICE BOUNDARY
FAST ICE
→B
ICE SURFACE FLOODING
CAPE YORK
DRIFTED SNOW
DRIFTING ICE
LHH
GLACIER
0 km 3

FIGURE 20 L_{HH} SEA ICE SAR IMAGERY TAKEN IN BAFFIN BAY, 11 APRIL 1979. CORRELATES WITH FIGURE 19 SAR IMAGERY.

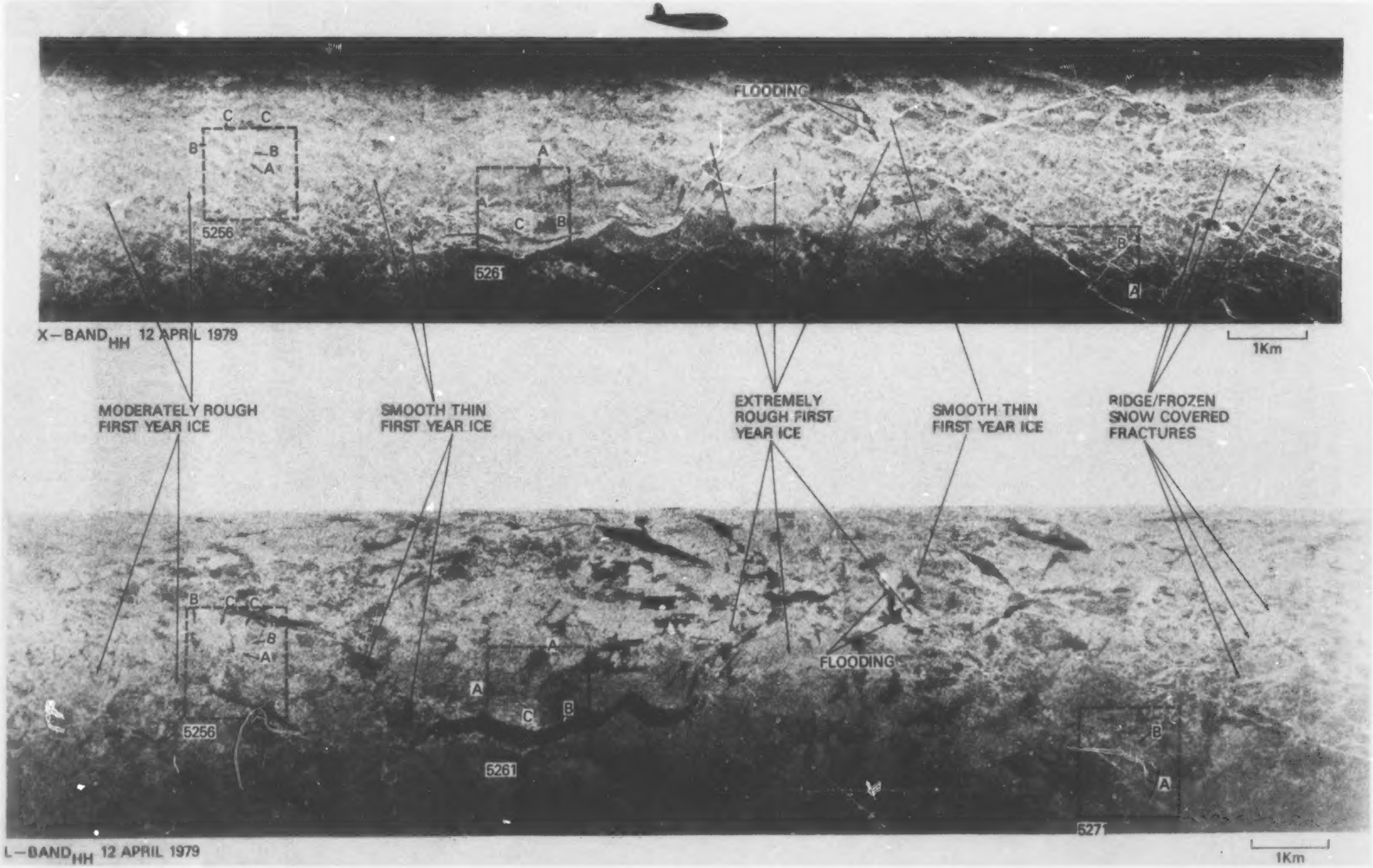
FLOODING
5256
B
C
C
B
A
A
C
B
5261
B
A
X–BAND$_{HH}$ 12 APRIL 1979
1Km
MODERATELY ROUGH FIRST YEAR ICE
SMOOTH THIN FIRST YEAR ICE
EXTREMELY ROUGH FIRST YEAR ICE
SMOOTH THIN FIRST YEAR ICE
RIDGE/FROZEN SNOW COVERED FRACTURES
B
C
C
B
A
A
A
C
B
5256
5261
FLOODING
B
A
5271
L–BAND$_{HH}$ 12 APRIL 1979
1Km

FIGURE 21 COINCIDENT X_{HH} AND L_{HH} SEA ICE SAR IMAGERY TAKEN IN BAFFIN BAY, 12 APRIL 1979.

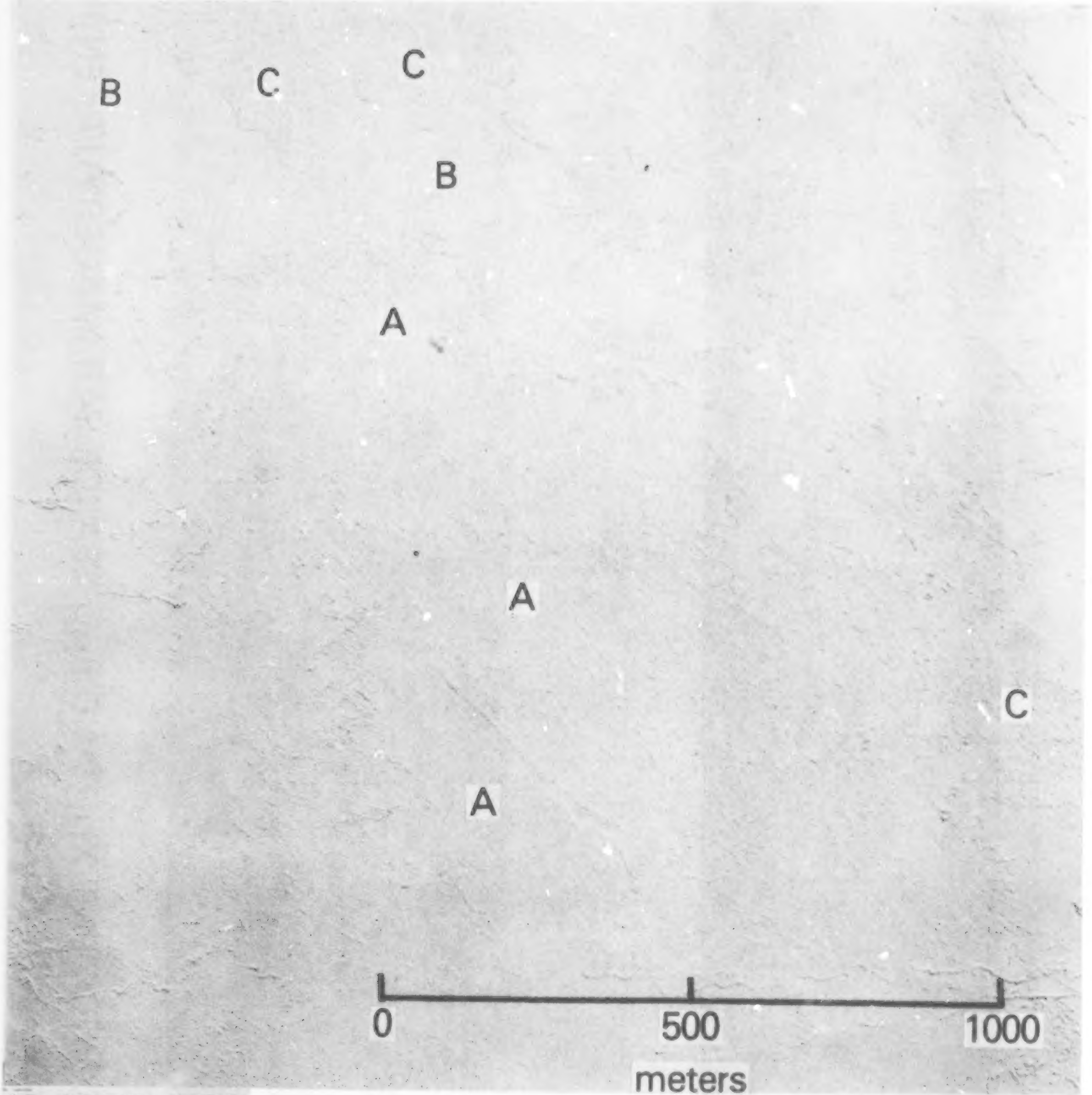
B
C
C
B
A
A
C
A
0
500
1000
meters

13 APRIL 1979
FRAME 5256

FIGURE 22 AERIAL PHOTOGRAPH (1524M ALTITUDE) TAKEN IN BAFFIN BAY, 13 APRIL 1979. CORRELATES WITH FIGURE 21 SAR IMAGERY.

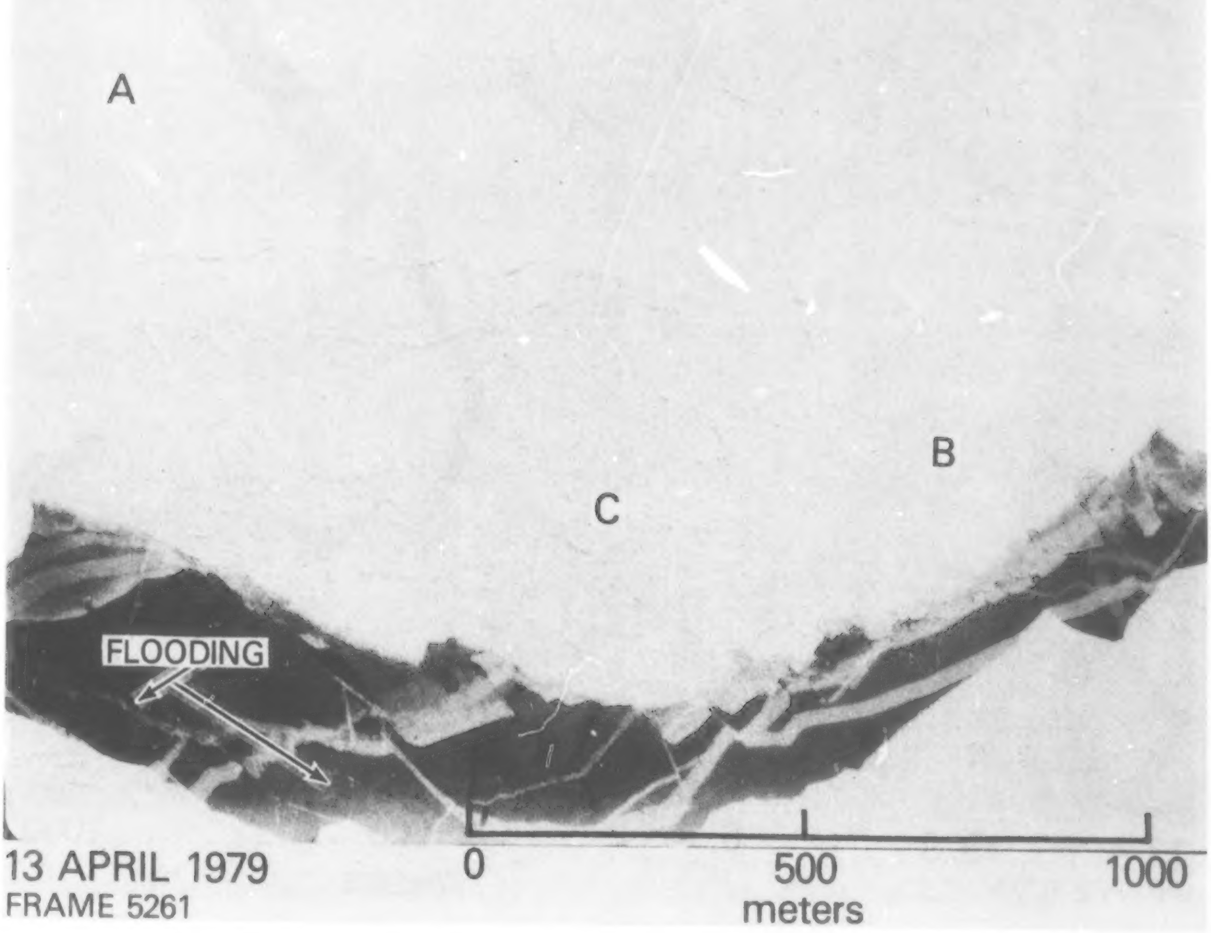
A
A
B
C
FLOODING
13 APRIL 1979
FRAME 5261
0
500
1000
meters

FIGURE 23 AERIAL PHOTOGRAPHY (1524M ALTITUDE) TAKEN IN BAFFIN BAY, 13 APRIL 1979. CORRELATES WITH FIGURE 21 SAR IMAGERY.

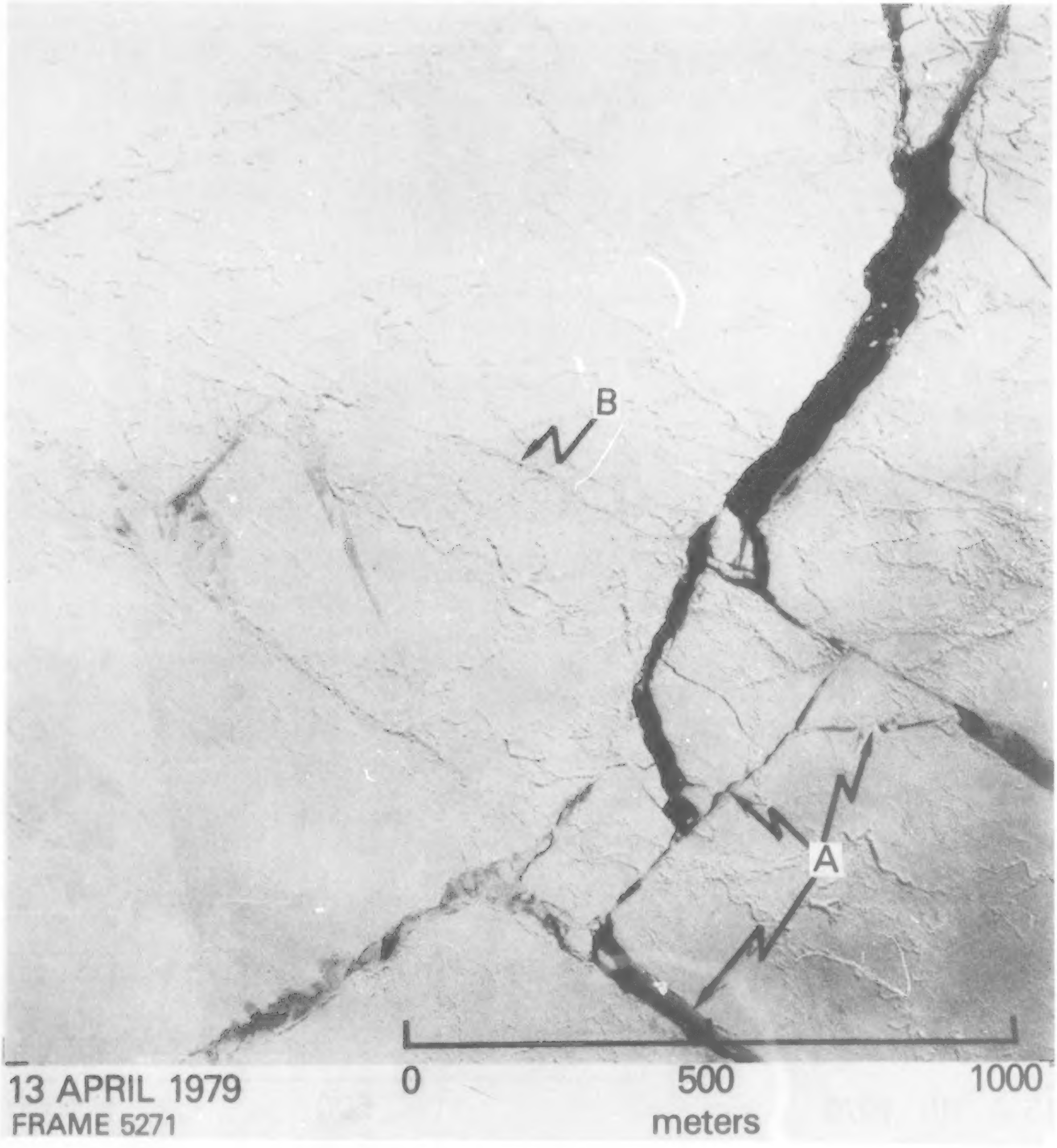
B
A
13 APRIL 1979
FRAME 5271
0
500
1000
meters

FIGURE 24 AERIAL PHOTOGRAPHY (1524M ALTITUDE) TAKEN IN BAFFIN BAY, 13 APRIL 1979. CORRELATES WITH FIGURE 21 SAR IMAGERY.

SECTION 5.3

INTERMEDIATE RESULTS OF THE RADAR BACKSCATTER STUDY OF SEA ICE IN THE BEAUFORT SEA

C.V. Delker, R.G. Onstott and R.K. Moore

INTERMEDIATE RESULTS OF THE RADAR BACKSCATTER STUDY OF SEA ICE IN THE BEAUFORT SEA

C.V. Delker
R.G. Onstott
R.K. Moore, Principal Investigator

Remote Sensing Laboratory
Center for Research, Inc.
The University of Kansas
Lawrence, Kansas 66045

RSL Technical Report
RSL TR 331-15

March 1980

Supported by:

OFFICE OF NAVAL RESEARCH
Department of the Navy
800 N. Quincy Street
Arlington, Virginia 22217

CONTRACT N00014-76-C-1105

ACKNOWLEDGEMENTS

The University of Kansas team of experimenters would especially like to express their thanks to Dr. René O. Ramseier, Ice Experiment Coordinator, for his cooperation and assistance throughout all phases of this measurement program.

We also wish to thank the Polar Continental Shelf Project for base camp privileges at Tuktoyaktuk and logistic support of our experimental efforts. We would especially like to acknowledge the assistance of Barry Hough, camp director.

We would like to acknowledge the expertise of Jim Hodges, pilot of the Okanagan Bell 205 helicopter, and Rich Tennant, engineer. Their valuable assistance in the successful completion of our program and their comic relief were most appreciated.

We also must acknowledge the cooperation we received from all the experimenters who worked at Tuktoyaktuk.

We would like to acknowledge the support of this research by the Office of Naval Research, Contract N00014-76-C-1105.

ABSTRACT

As a part of the Beaufort Sea segment of the Surveillance Satellite Project (SURSAT), a team of investigators from the University of Kansas conducted experiments to obtain quantitative measurements of radar backscatter from sea ice during the month of March 1979. Thick first-year sea ice, thin first-year sea ice, and an inland fresh water lake were studied using a surface-based FM-CW scatterometer that swept from 1.1 - 1.9 GHz and 8.5 - 17.5 GHz with angles of incidence (from vertical) of 10° to 75° and various linear polarizations. Measurements of thick first-year sea ice, thin first-year sea ice, brackish sea ice, and an inland fresh-water lake were also made using a helicopter-borne FM-CW scatterometer that swept from 8.5 - 17.5 GHz with incidence angles of 20° to 60° and VV polarization only.

The 1.1 - 1.9 GHz measurements show that lake ice can be distinguished from thick and thin first-year sea ice. The radar cross-sections of thick and thin first-year sea ice are not significantly different for incidence angles less than 45°. The 8.5 - 17.5 GHz measurements indicate that lake ice can be distinguished from the other types in all cases. Thick and thin first-year sea ice are separated by a 2 - 4 dB difference for incidence angles greater than 40°.

The effect of snow cover on the return from lake ice was also investigated with dramatic results. Returns from bare-surface lake ice were found to be 10 - 12 dB lower than the returns from snow-covered lake ice. This indicates that volume scatter in the snow may be the major contributor to lake ice backscatter when snow is present.

TABLE OF CONTENTS

Page

ACKNOWLEDGEMENTS i

ABSTRACT ii

1.0 INTRODUCTION. 1

2.0 SYSTEM DESCRIPTION. 4

2.1 TRAMAS 4

2.2 HELOSCAT 8

3.0 TRAMAS RESULTS. 11

3.1 L-Band Results 11

3.2 Ku-X-Band Results. 11

4.0 HELOSCAT RESULTS. 30

5.0 FREQUENCY RESPONSE. 35

6.0 CONCLUSIONS 39

REFERENCES 40

LIST OF TABLES

Page

Table 1: SUMMARY OF BACKSCATTER MEASUREMENTS. 2

Table 2: NOMINAL SYSTEM SPECIFICATIONS (TRAMAS) 6

Table 3: NOMINAL SYSTEM SPECIFICATIONS FOR HELI-BORNE SYSTEM (HELOSCAT). 9

LIST OF FIGURES

Number	Figure Description	Page
2.1	Block Diagram of HELOSCAT and TRAMAS System.	5
2.2	TRAMAS System in Operation at an Ice Site.	7
2.3	HELOSCAT System Installed on Bell 205 Helicopter	10
3.1	Average Scattering Coefficient of Thick First-Year, Thin First-Year, and Lake Ice at 1.5 GHz (March 1979). .	12
3.2	Average Scattering Coefficient of Thick First-Year and Thin First-Year Ice at 1.5 GHz (March 1979).	13
3.3	Average Scattering Coefficient of Thick First-Year, Thin First-Year, and Lake Ice at 9 GHz (March 1979). . .	14
3.4	Average Scattering Coefficient of Thick First-Year, Thin First-Year, and Lake Ice at 9 GHz (March 1979). . .	15
3.5	Average Scattering Coefficient of Thick First-Year, Thin First-Year, and Lake Ice at 9 GHz (March 1979). . .	16
3.6	Average Scattering Coefficient of Thick First-Year, Thin First-Year, and Lake Ice at 13 GHz (March 1979) . .	17
3.7	Average Scattering Coefficient of Thick First-Year, Thin First-Year, and Lake Ice at 13 GHz (March 1979) . .	18
3.8	Average Scattering Coefficient of Thick First-Year, Thin First-Year, and Lake Ice at 13 GHz (March 1979) . .	19
3.9	Average Scattering Coefficient of Thick First-Year, Thin First-Year, and Lake Ice at 17 GHz (March 1979) . .	20
3.10	Average Scattering Coefficient of Thick First-Year, Thin First-Year, and Lake Ice at 17 GHz (march 1979) . .	21
3.11	Average Scattering Coefficient of Thick First-Year, Thin First-Year, and Lake Ice at 17 GHz (March 1979) . .	22
3.12	Scattering Coefficient of Lake Ice with Bare, Normal, Rough, and Very Rough Snow Cover Conditions at 9 GHz (March 1979)	25
3.13	Scattering Coefficient of Lake Ice with Bare, Normal, Rough, and Very Rough Snow Cover Conditions at 9 GHz (March 1979)	26

LIST OF FIGURES (continued)

Number | Figure Description | Page

3.14 Scattering Coefficient of Lake Ice with Bare, Normal, Rough, and Very Rough Snow Cover at 17 GHz (March 1979) 27

3.15 Scattering Coefficient of Lake Ice with Bare, Normal, Rough, and Very Rough Snow Cover Conditions at 17 GHz (March 1979) 28

3.16 Difference Between Radar Cross-Section of Thin First-Year and Thick First-Year Sea Ice at 1.5, 9.0, 13.0, and 17.0 GHz with Vertical Polarization (TRAMAS, March 1979) 29

3.17 Difference Between Radar Cross-Section of Thick First-Year Sea Ice and Lake Ice at 1.5, 9.0, 13.0 and 17.0 GHz with Vertical Polarization (TRAMAS, March 1979) . . . 29

4.1 Average Scattering Coefficient of Thick First-Year, Thin First-Year, Brackish, and Lake Ice at 9 GHz (March 1979) 31

4.2 Average Scattering Coefficient of Thick First-Year, Thin First-Year, Brackish, and Lake Ice at 13 GHz (March 1979) 32

4.3 Average Scattering Coefficient of Thick First-Year, Thin First-Year, Brackish, and Lake ice at 17 GHz (March 1979) 33

4.4 Difference Between Radar Cross-Section of Thin First-Year and Thick First-Year Sea Ice at 9.0, 13.0, and 17.0 GHz with Vertical Polarization (HELOSCAT, March 1979) 34

4.5 Difference Between Radar Cross-Section of Thick First-Year and Lake Ice at 9.0, 13.0, and 17.0 GHz with Vertical Polarization (HELOSCAT, march 1979) 34

5.1 Scattering Coefficient Frequency Response of Thick First-Year, Thin First-Year, and Lake Ice (March 1979) 36

5.2 Scattering Coefficient Frequency Response of Thick First-Year, Thin First-Year, Brackish, and Lake Ice (March 1979) 37

1.0 INTRODUCTION

During the month of March 1979, a research team from the University of Kansas Remote Sensing Laboratories conducted experiments designed to investigate the radar backscatter properties of sea ice. This investigation was a part of the Beaufort Sea segment of the Surveillance Satellite Project (SURSAT) which occurred off the Canadian coast near Tuktoyaktuk, N.W.T., Canada. The Polar Continental Shelf Project facilities located at Tuktoyaktuk served as a base of operations for these experiments.

The experiments performed by the K.U. team may be divided into two parts. Part one utilized the surface-based Transportable Microwave Active Spectrometer (TRAMAS) system [1,2]. Measurements of thick first-year sea ice, thin first-year sea ice, and an inland fresh water lake were obtained during this portion of the experiment. Part two of the experiment utilized the helicopter-borne scatterometer (HELOSCAT) system [3]. Backscatter measurements from thick first-year sea ice, thin first-year sea ice, brackish sea ice, and the inland fresh-water lake were obtained with this system. A summary of the measurements obtained with each system is presented in Table 1.

The L-band measurements obtained with the TRAMAS system indicate that it is possible to distinguish lake ice from thick and thin first-year sea ice at all incidence angles for this frequency. Thick and thin first-year sea ice are separated by 1-2 dB for incidence angles greater than 45°. The results of the Ku-X-band measurements from both the TRAMAS and HELOSCAT systems indicate that lake ice can be distinguished from the other types in all cases. The TRAMAS results indicate that thick and thin first-year sea ice are separated by 2-4 dB for incidence angles greater than 40° while

TABLE 1

SUMMARY OF BACKSCATTER MEASUREMENTS

Sensor	Date	Site Number	Ice Type	Number of Looks
TRAMAS	3/13	T1	Lake	2
	3/14	T2	TFY	3
	3/15	T3	TFY	4
	3/16	T4	Young	3
	3/21	T5	Lake	5
HELOSCAT	3/31	H1	Lake	10
	4/1	H2	Lake	10
	4/1	H3	Brackish	13
	4/1	H4	TFY	10
	4/1	H5	TFY	10
	4/1	H6	TFY	10
	4/1	H7	Young	15
	4/1	H8	Brackish	14

the HELOSCAT results show a 2-6 dB difference. The brackish sea ice observed with the HELOSCAT system resulted in trends that were very similar to those obtained from thick first-year sea ice.

An experiment that was done to determine the effects of snow on the backscatter return from lake ice provided some dramatic results. The return from the bare lake-ice surface was found to be 10-12 dB lower than the returns from snow-covered lake ice. This would seem to indicate that volume scatter from the snow may be the major contributor to backscatter from lake ice when snow is present on the surface.

2.0 SYSTEM DESCRIPTION

Measurements of radar backscatter from sea ice were obtained using two systems -- the surface-based TRAMAS system and the helicopter-mounted version, HELOSCAT. Both systems are frequency-modulated continuous-wave (FM-CW) scatterometers. A system block diagram is shown in Figure 2.1. Only the Ku-X-Band antennas and electronics are used in the HELOSCAT system.

2.1 TRAMAS

The Transportable Microwave Active Spectrometer (TRAMAS) system is a four antenna FM-CW scatterometer mounted on a portable surface-based structure. The L-band radar is swept from 1.1 to 1.9 GHz for VV and VH polarizations (H = horizontal, V = vertical; the first letter identifies transmitted polarization and the second identifies received polarization). The Ku-X-Band radar is swept from 8.5 to 17.5 GHz with HH, HV, VH, and VV polarizations. These radars operate at a fixed range from the ice surface with selectable angles of incidence of 10° to 75°. Table 2 details nominal system specifications for both radars and Figure 2.2 shows the assembled system during operation.

Calibration of the scatterometer is achieved by frequently passing the signal through a delay line of known attenuation and by less frequently observing a standard radar target of known cross-section.

This system was designed to be disassembled and moved from site to site using a small aircraft, helicopter, or snowmobile and sled. A Bell model 206 helicopter provided for experiment and program support by the Canadian Polar Continental Shelf Project (P.C.S.P.) was used to sling the structure from site to site during this experiment.

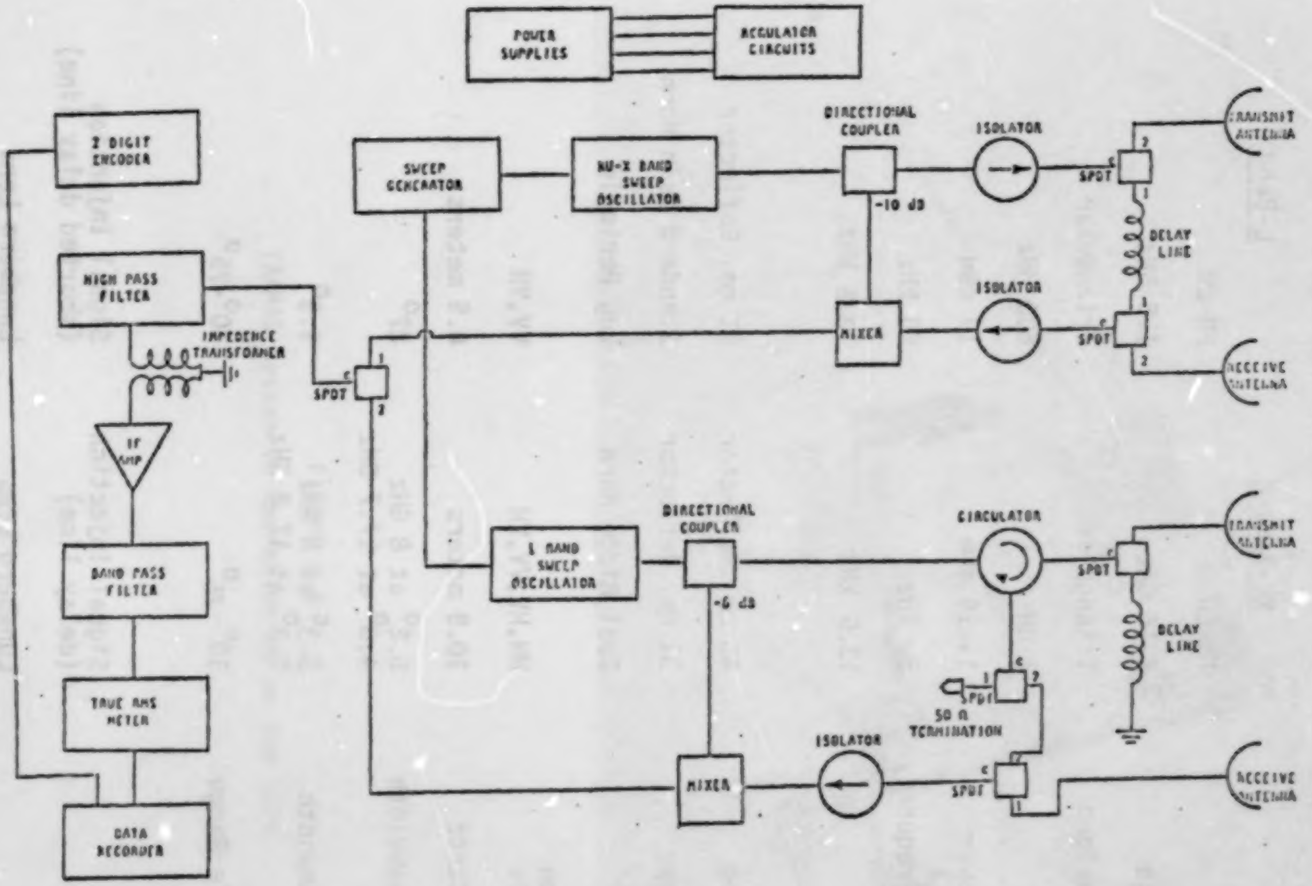
POWER SUPPLIES
REGULATOR CIRCUITS
2 DIGIT ENCODER
SWEEP GENERATOR
KU-X BAND SWEEP OSCILLATOR
DIRECTIONAL COUPLER
-10 dB
ISOLATOR
SPDT
TRANSMIT ANTENNA
DELAY LINE
ISOLATOR
RECEIVE ANTENNA
HIGH PASS FILTER
IMPEDENCE TRANSFORMER
MIXER
IF AMP
BAND PASS FILTER
TRUE RMS METER
DATA RECORDER
L BAND SWEEP OSCILLATOR
DIRECTIONAL COUPLER
-6 dB
CIRCULATOR
TRANSMIT ANTENNA
DELAY LINE
50 Ω TERMINATION
ISOLATOR
MIXER
RECEIVE ANTENNA

FIGURE 2.1

Block Diagram of HELOSCAT and TRAMAS System

TABLE 2

NOMINAL SYSTEM SPECIFICATIONS (TRAMAS)

	Ku-X-Band	L-Band
Type	FM-CW	FM-CW
Frequency Range	8-18 GHz	1.5 GHz
Modulating Waveform	Triangular	Triangular
FM Sweep: Δf	1 GHz	800 MHz
Transmitter Power	14-19 dBm	19 dBm
Intermediate Frequency	50 kHz	50 kHz
IF Bandwidth	13.5 kHz	13.5 kHz
Antennas		
Receive Type	46 cm. Reflector	91 cm. Reflector
Transmit Type	31 cm. Reflector	Standard Gain Horn
Feeds	Dual Ridge Horn	Log Periodic
Polarization Capabilities	HH,HV,VV,VH	VV,VH
Target Distance	10.9 meters	6.5 meters
Transmit Beamwidth	8.2° at 8 GHz 4.0° at 17.7 GHz	27°
Receive Beamwidth	5.3° at 8 GHz 2.3° at 17.8 GHz	9.5°
Incidence Angle Range	10°- 75°	10°-75°
Calibration:		
Internal	Signal Injection (delay line)	Signal Injection (shorted delay line)
External	Luneberg Lens Reflector	Luneberg Lens Reflector
Operating Temperature Range	-50° C to +50°C	-50°C to +50°C

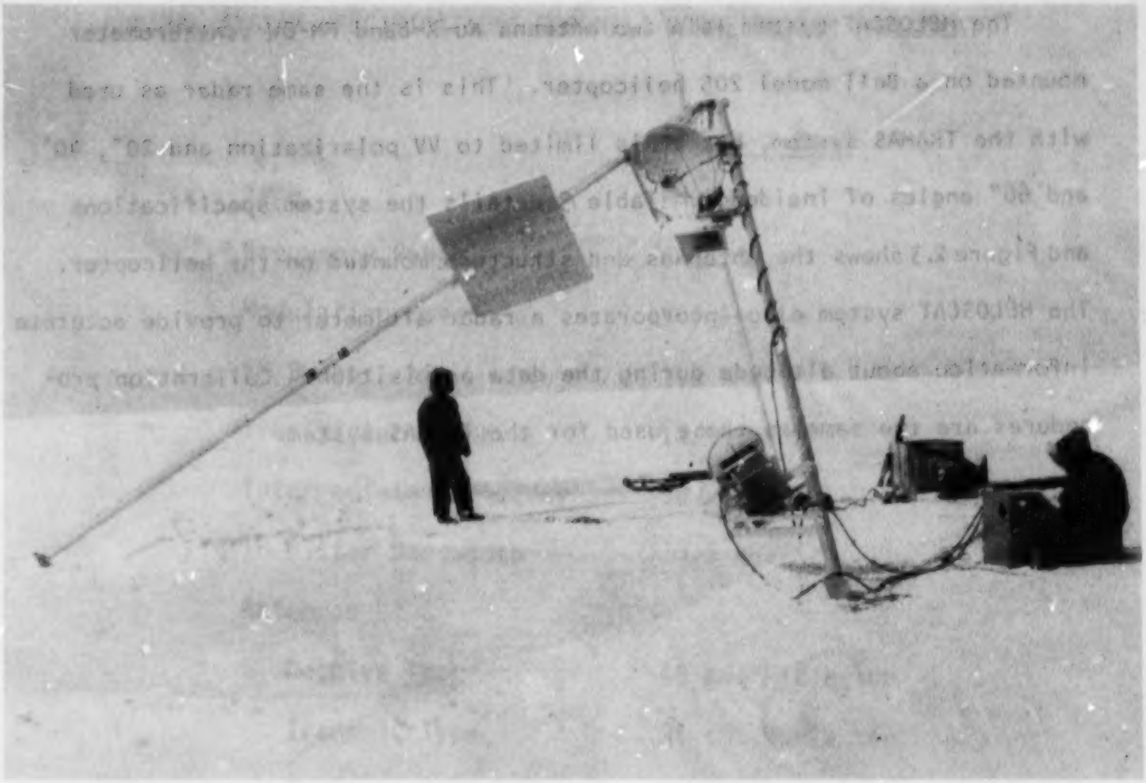

FIGURE 2.2

TRAMAS System in Operation at an Ice Site

2.2 HELOSCAT

The HELOSCAT system is a two antenna Ku-X-Band FM-CW scatterometer mounted on a Bell model 205 helicopter. This is the same radar as used with the TRAMAS system, but it is limited to VV polarization and 20°, 40° and 60° angles of incidence. Table 3 details the system specifications and Figure 2.3 shows the antennas and structure mounted on the helicopter. The HELOSCAT system also incorporates a radar altimeter to provide accurate information about altitude during the data acquisition. Calibration procedures are the same as those used for the TRAMAS system.

TABLE 3

NOMINAL SYSTEM SPECIFICATIONS FOR HELI-BORNE SYSTEM (HELOSCAT)

	Ku-X-Band
Type	FM-CW
Frequency Range	8-18 GHz
Modulating Waveform	Triangular
FM Sweep: Δf	1.0 GHz
Transmitter Power	14-19 dBm
Intermediate Frequency	50 kHz
IF Filter Bandwidth	13.5 kHz
Antennas	
Receive Type	46 cm. Reflector
Transmit Type	31 cm. Reflector
Feeds	Dual Ridge Horn
Polarization Capabilities	VV
Transmit Beamwidth	8.2^{o} at 8.0 GHz 4.0^{o} at 17.7 GHz
Receive Beamwidth	5.3^{o} at 8.0 GHz 2.3^{o} at 17.8 GHz
Incidence Angles Available	20^{o},40^{o}, and 60^{o}
Calibration:	
Internal	Signal Injection (delay line)
External	Luneberg Lens Reflector
Operating Temperature Range	-50^{o} C to $+50^{o}$ C

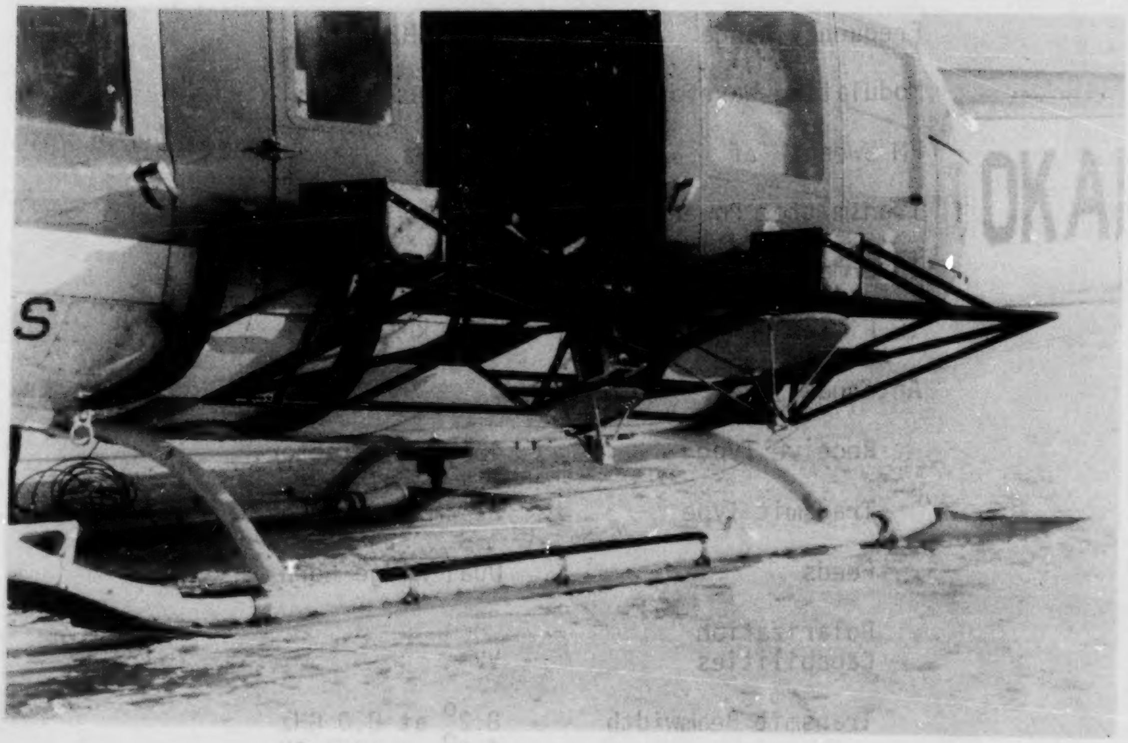

FIGURE 2.3

HELOSCAT System Installed on Bell 205 Helicopter

3.0 TRAMAS RESULTS

During the TRAMAS phase of the experiment three different types of ice were investigated. Included were fresh-water lake ice, thick first-year sea ice, and thin first-year sea ice. The lake was located a short distance from the P.C.S.P. buildings and was frozen to the bottom. It served as a convenient location for the initial setup and testing of the equipment before moving offshore to the pack ice sites. The thick first-year sea ice investigations were conducted on an undeformed expanse of ice designated as Site A by the experimenters. The thin first-year sea ice was located a few miles to the north of Site A on a refrozen lead.

3.1 L-Band Results

The average scattering coefficients obtained with the L-Band radar are shown on the graphs of Figures 3.1 and 3.2. These graphs indicate that it is possible to discriminate between lake ice and thick or thin first-year sea ice with VV polarization, particularly for angles of incidence between 20° and 60°. No lake-ice data were available for VH polarization at this frequency. Thick and thin first-year sea ice are very similar for VV polarization with thin slightly below thick at incidence angles greater than 40°. Cross-polarization (VH) provides good discrimination of thin and thick first-year sea ice (3-4 dB) for incidence angles greater than 40°.

3.2 Ku-X-Band Results

Scattering coefficient trends of thick first-year sea ice, thin first-year sea ice, and freshwater lake ice at 9, 13, and 17 GHz are shown in Figures 3.3 through 3.11. Discrimination between these three ice types may be possible for all frequencies in the 8-18 GHz region with the

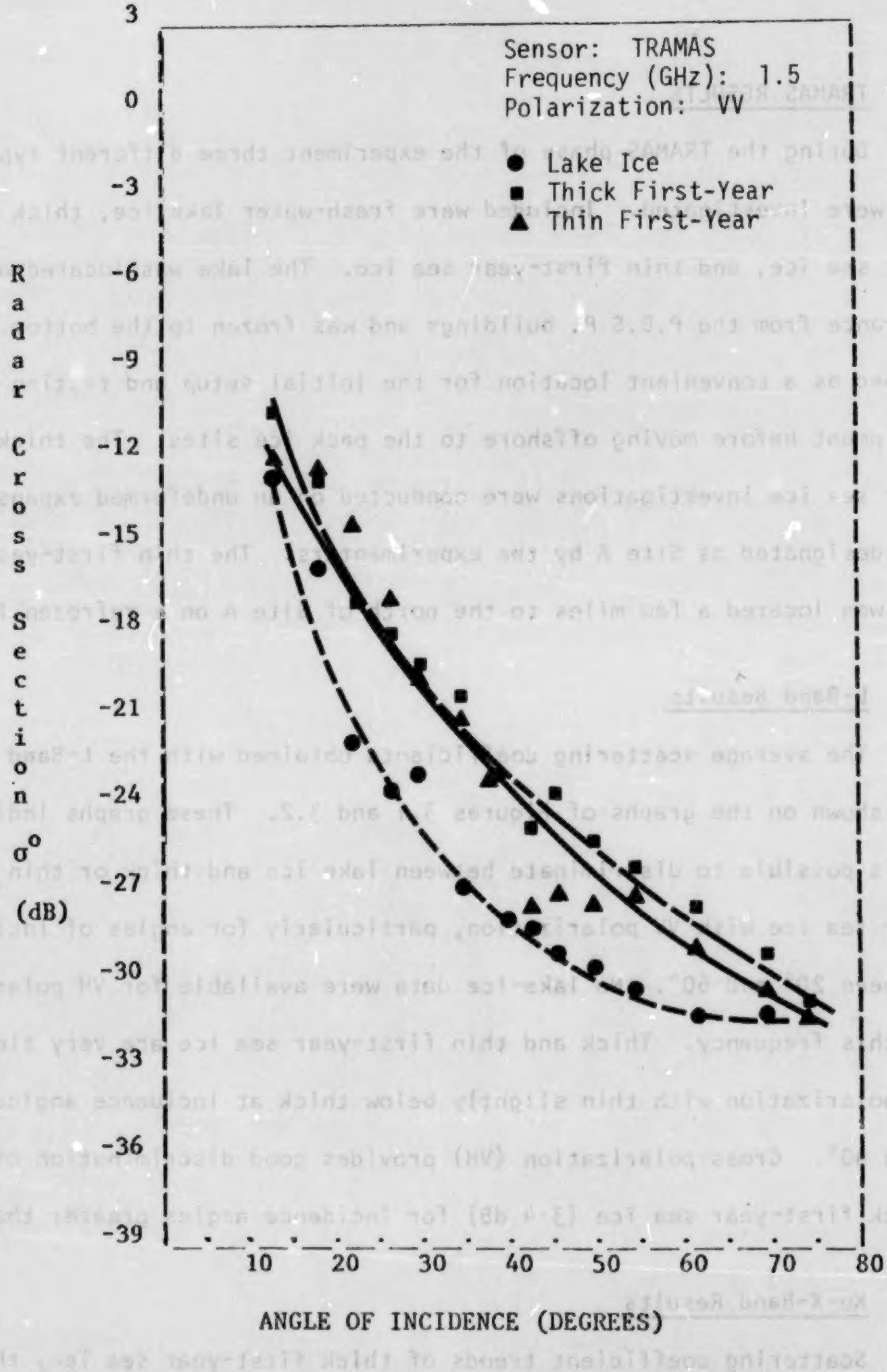

Figure 3.1. Average scattering coefficient of Thick First-Year, Thin First-Year, and Lake Ice at 1.5 GHz. (March 1979)

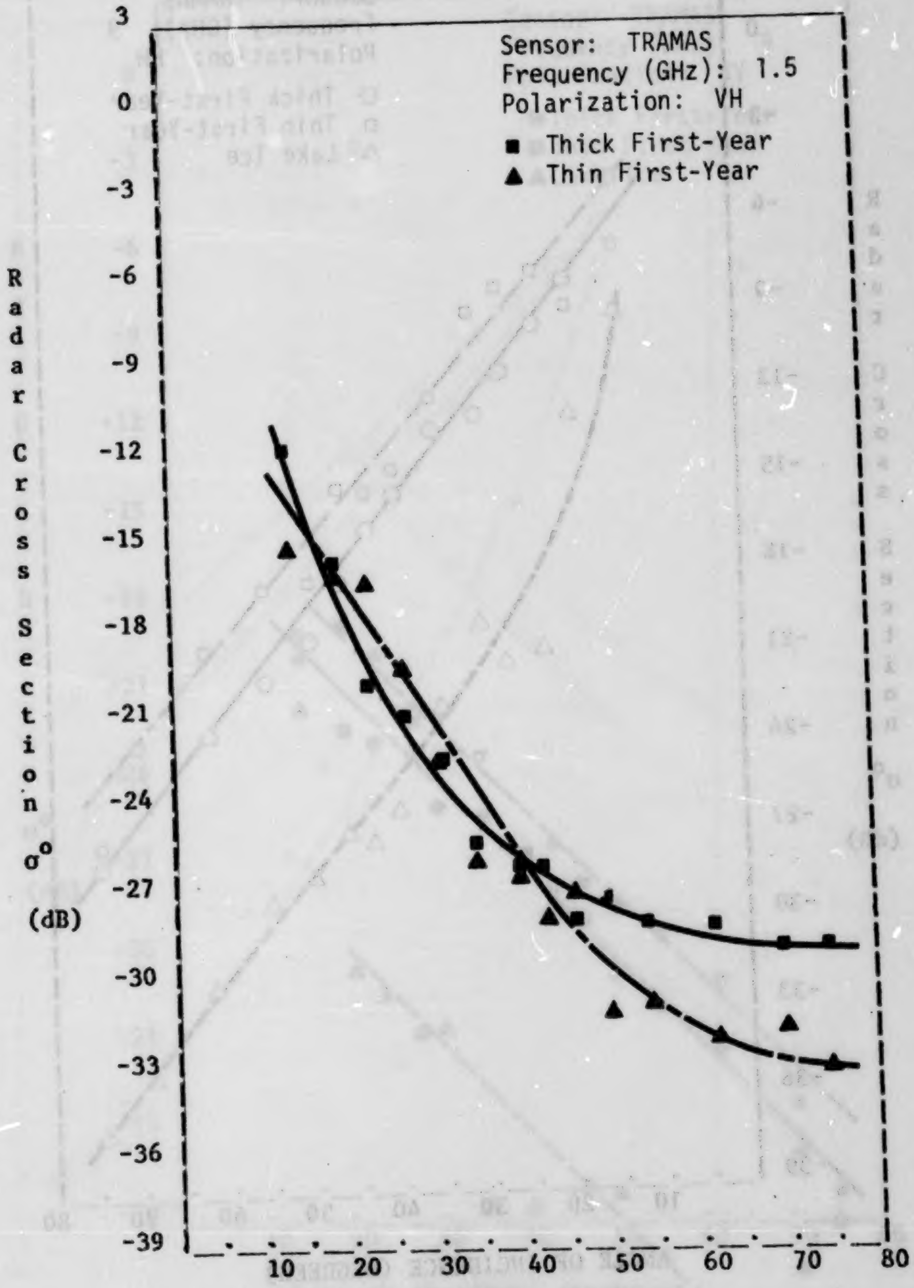

Figure 3.2. Average scattering coefficient of Thick First-Year and Thin First-Year Ice at 1.5 GHz. (March 1979)

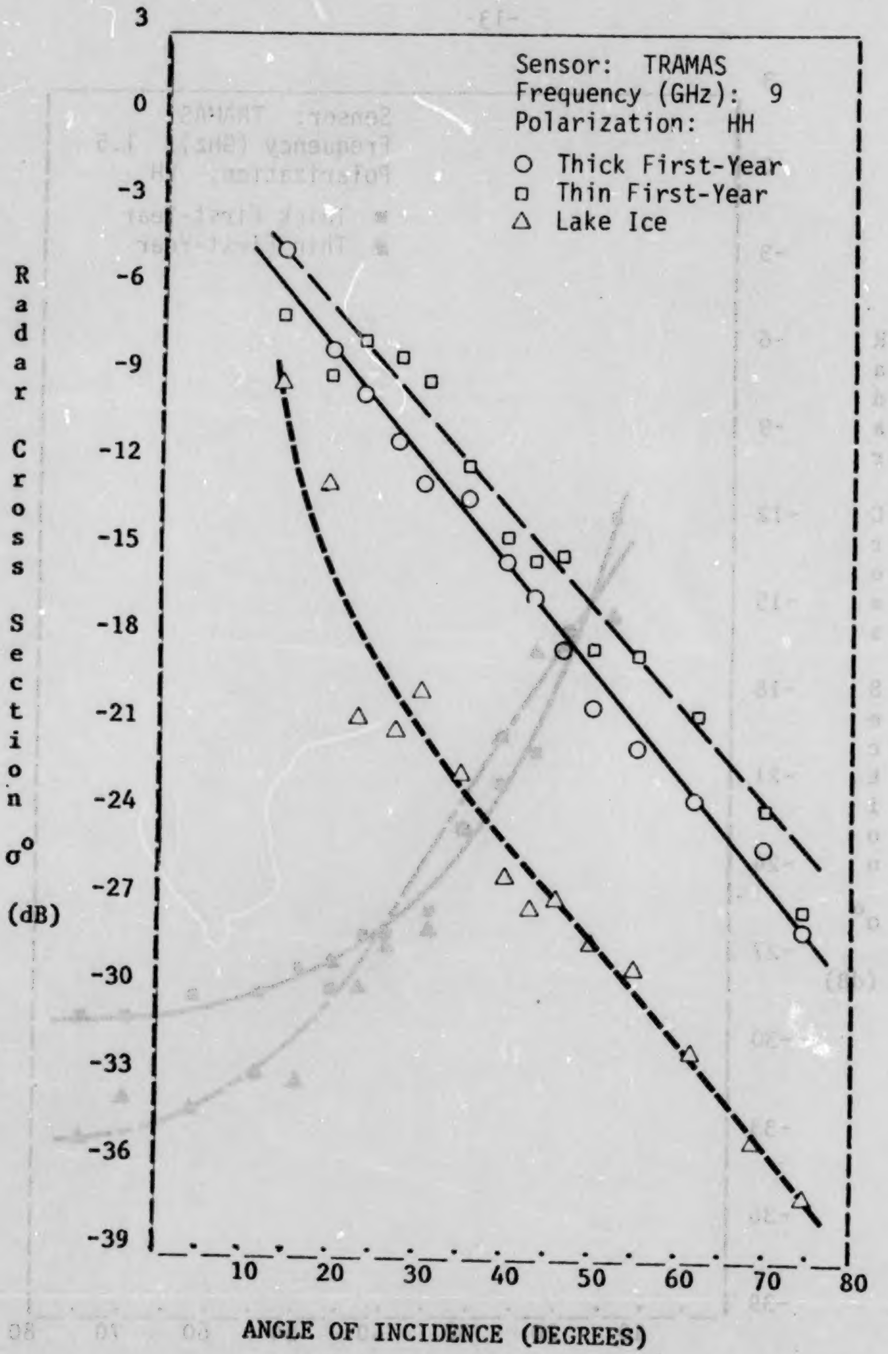

Figure 3.3. Average scattering coefficient of Thick First-Year, Thin First-Year, and Lake Ice at 9 GHz. (March 1979)

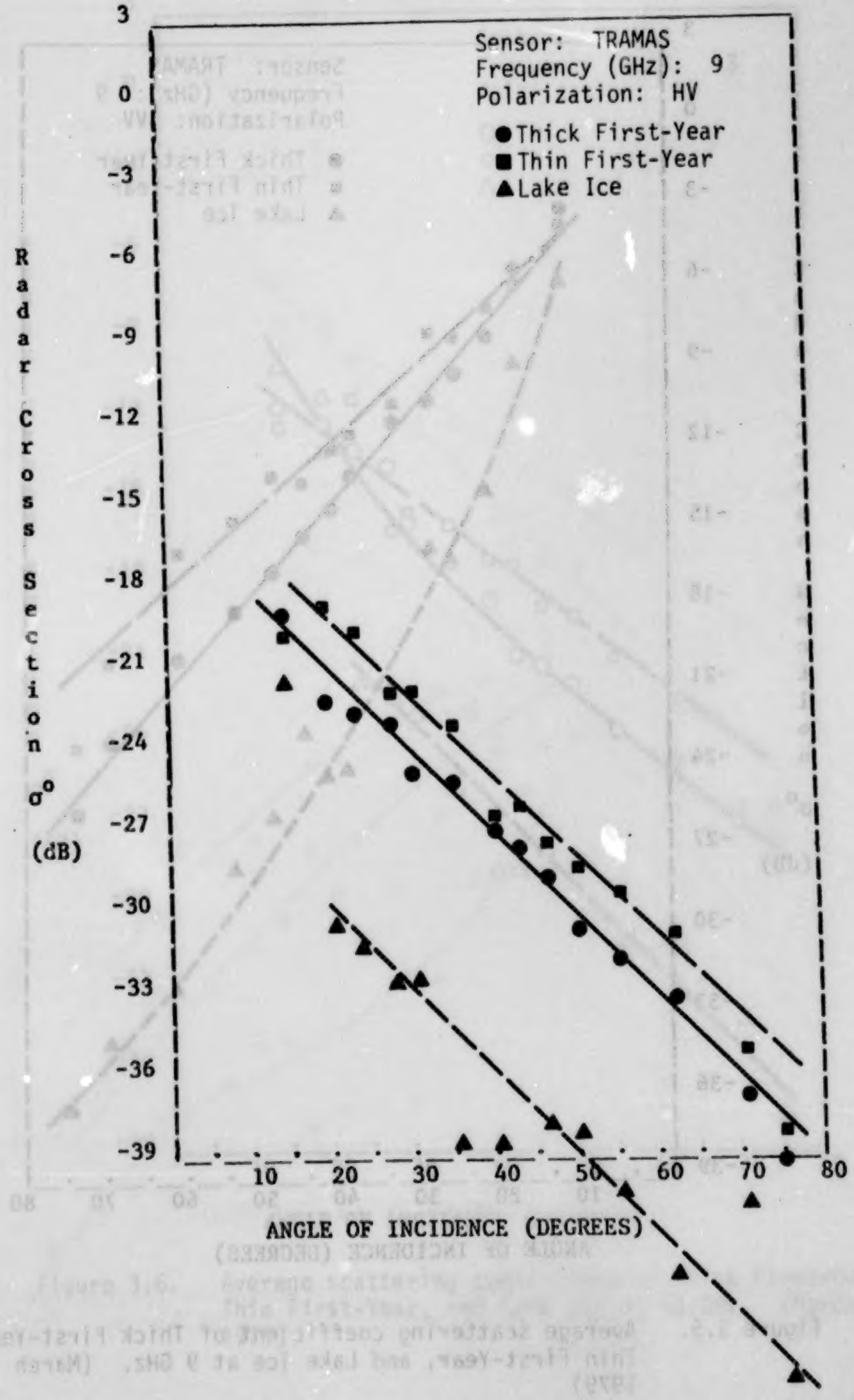

Figure 3.4. Average scattering coefficient of Thick First-Year, Thin First-Year, and Lake Ice at 9 GHz. (March 1979)

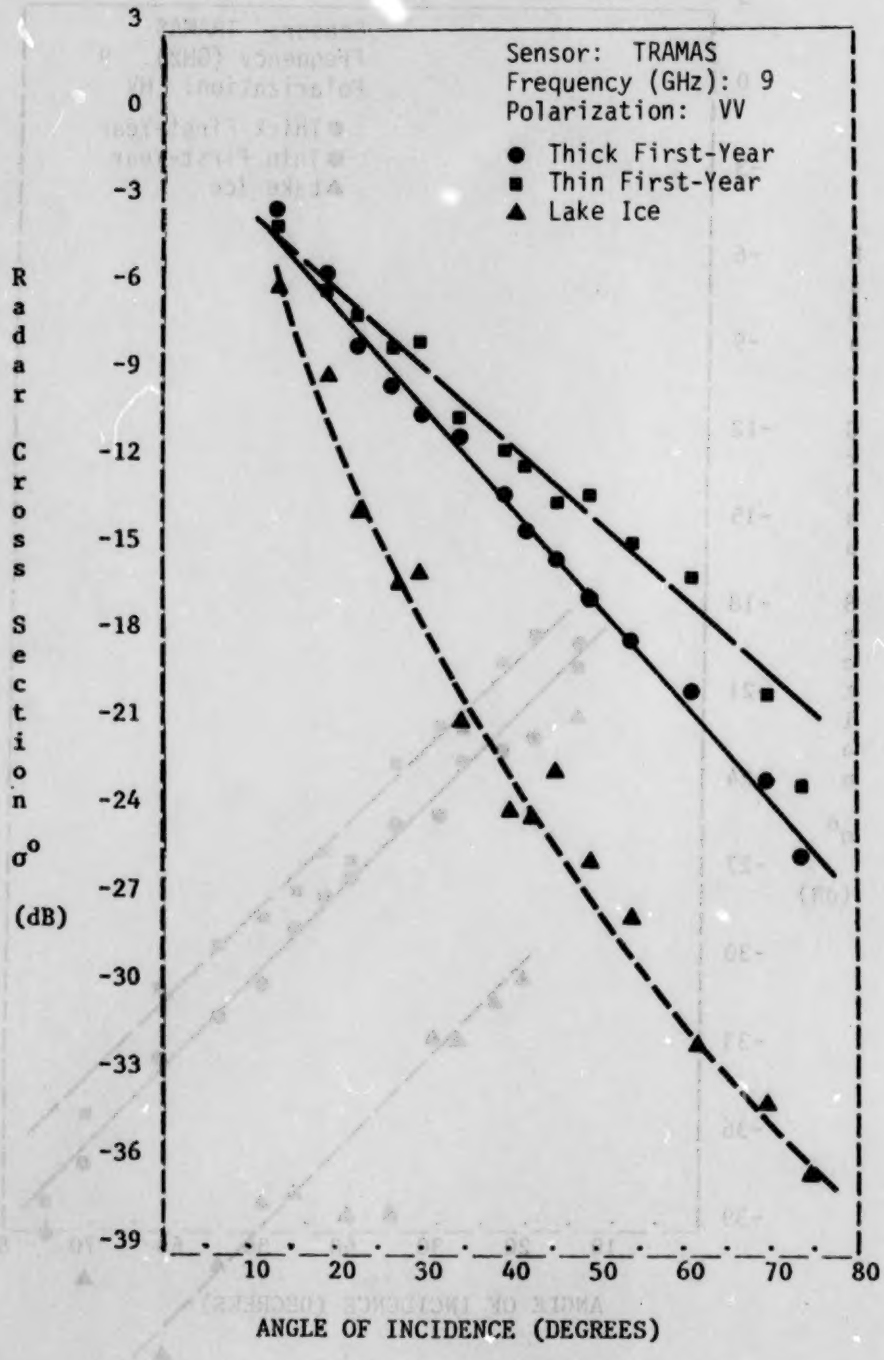

Figure 3.5. Average scattering coefficient of Thick First-Year, Thin First-Year, and Lake Ice at 9 GHz. (March 1979)

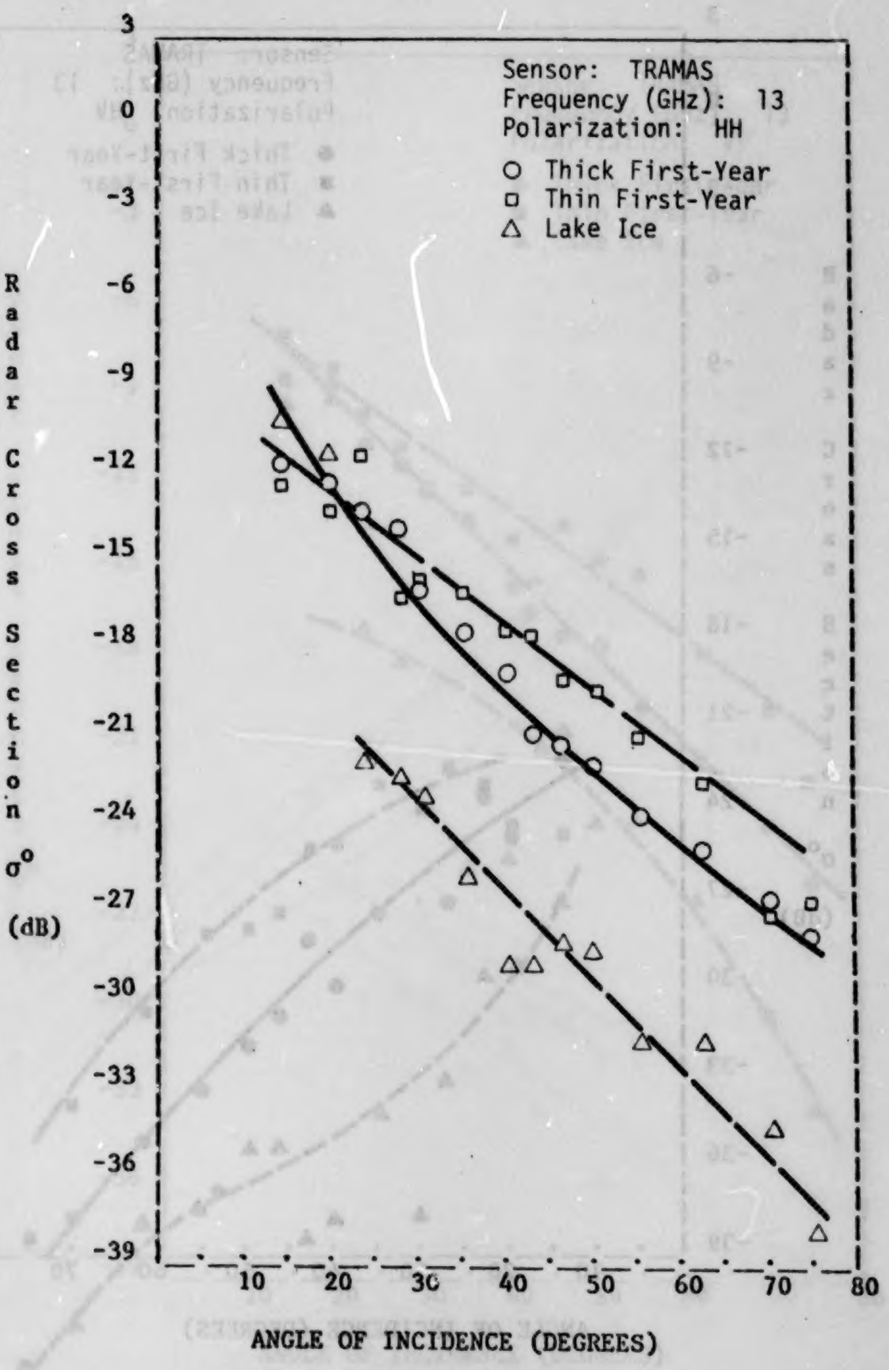

Figure 3.6. Average scattering coefficient of Thick First-Year, Thin First-Year, and Lake Ice at 13 GHz. (March 1979)

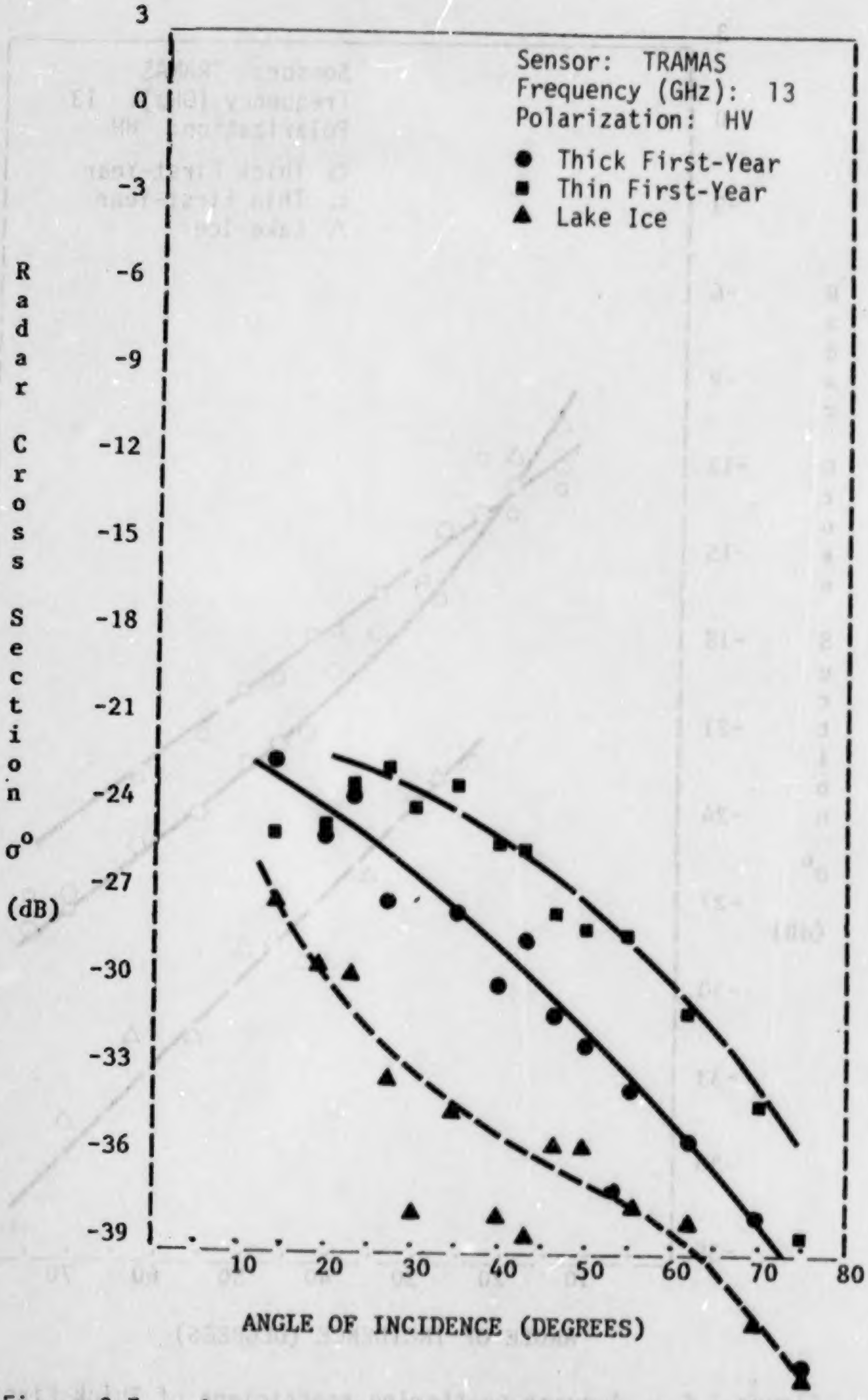

Figure 3.7. Average scattering coefficient of Thick First-Year, Thin First-Year, and Lake Ice at 13 GHz. (March 1979)

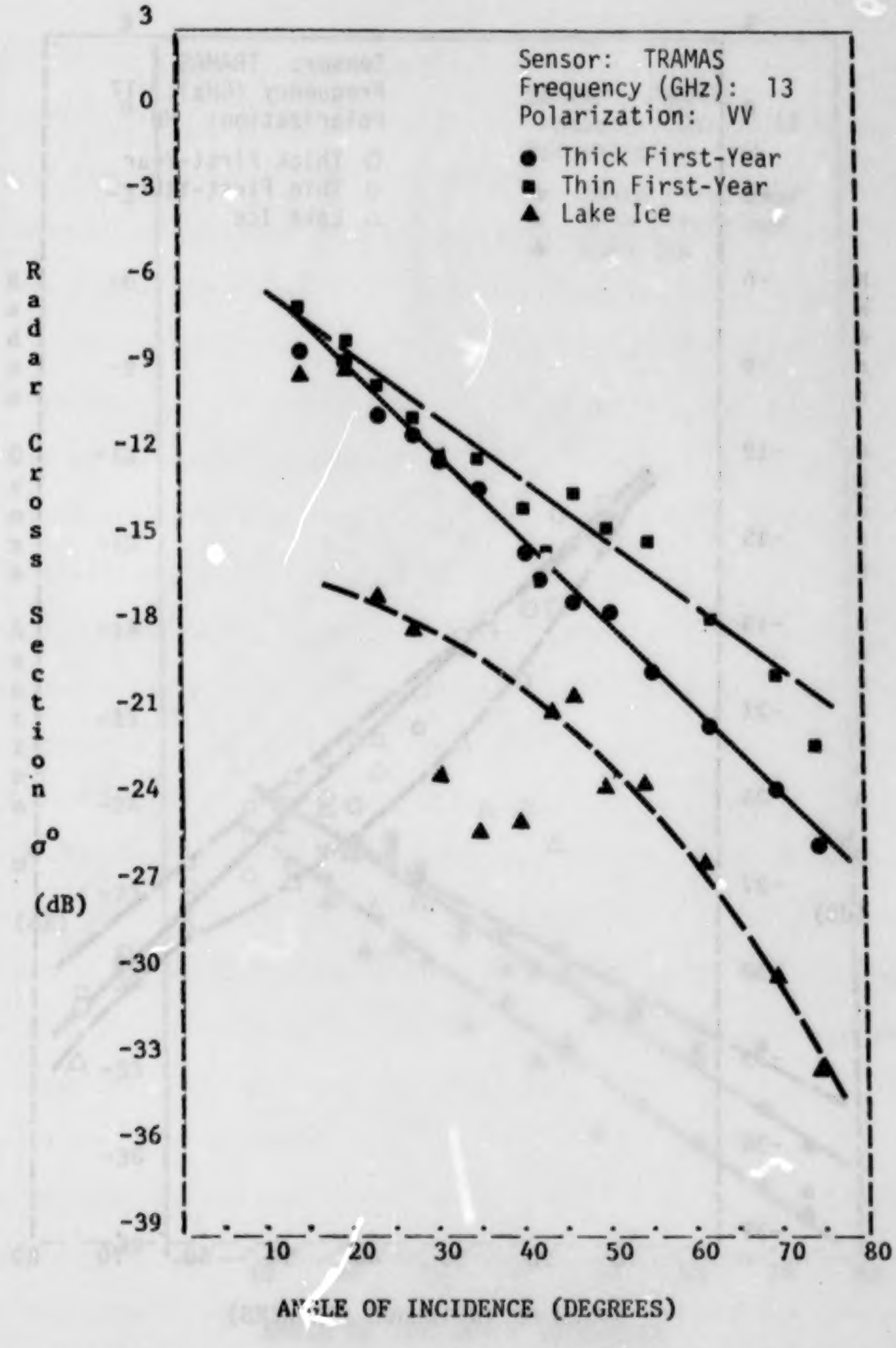

Figure 3.8. Average scattering coefficient of Thick First-Year, Thin First-Year, and Lake Ice at 13 GHz. (March 1979)

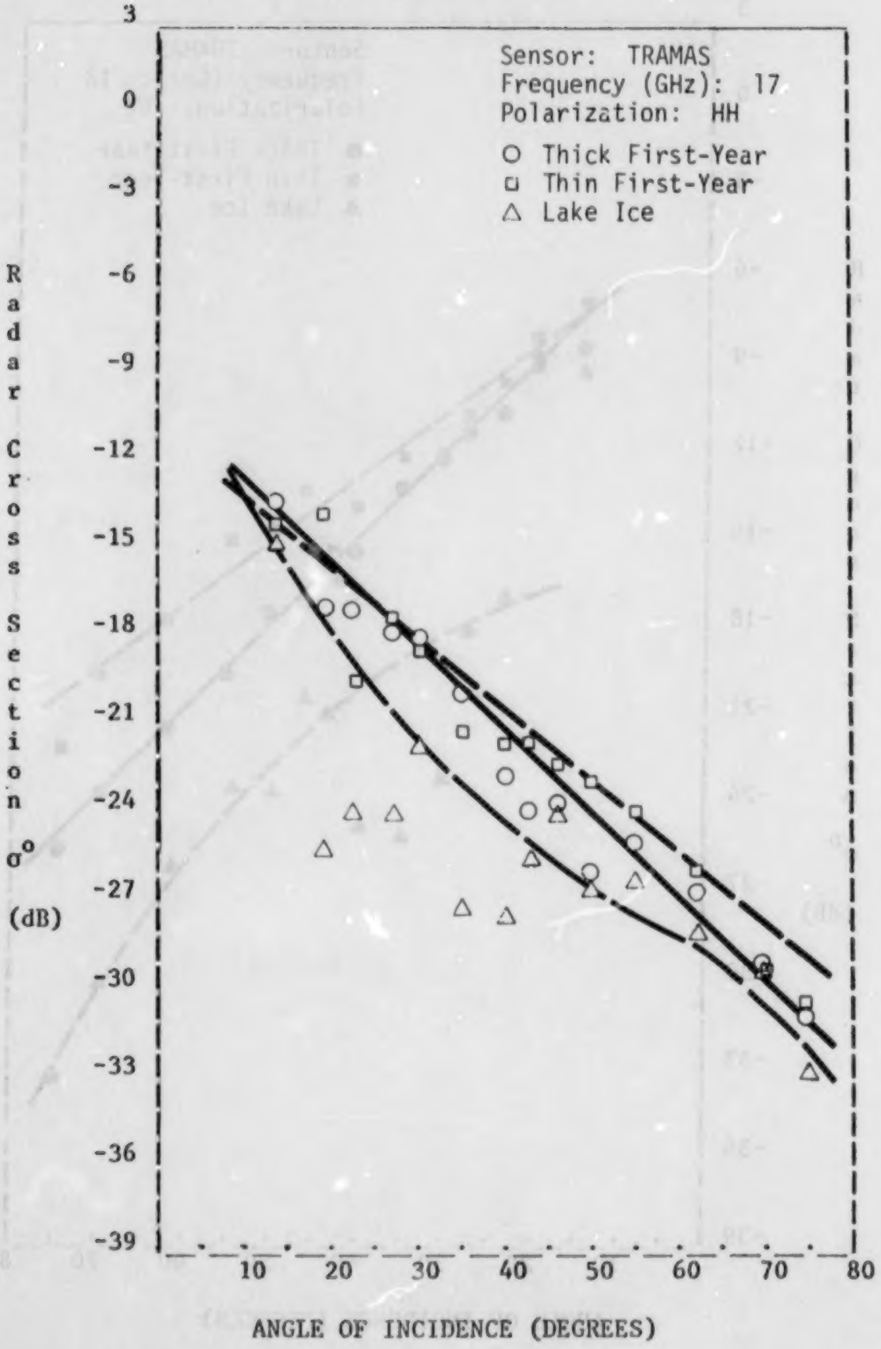

Figure 3.9. Average scattering coefficient of Thick First-Year, Thin First-Year, and Lake Ice at 17 GHz. (March 1979)

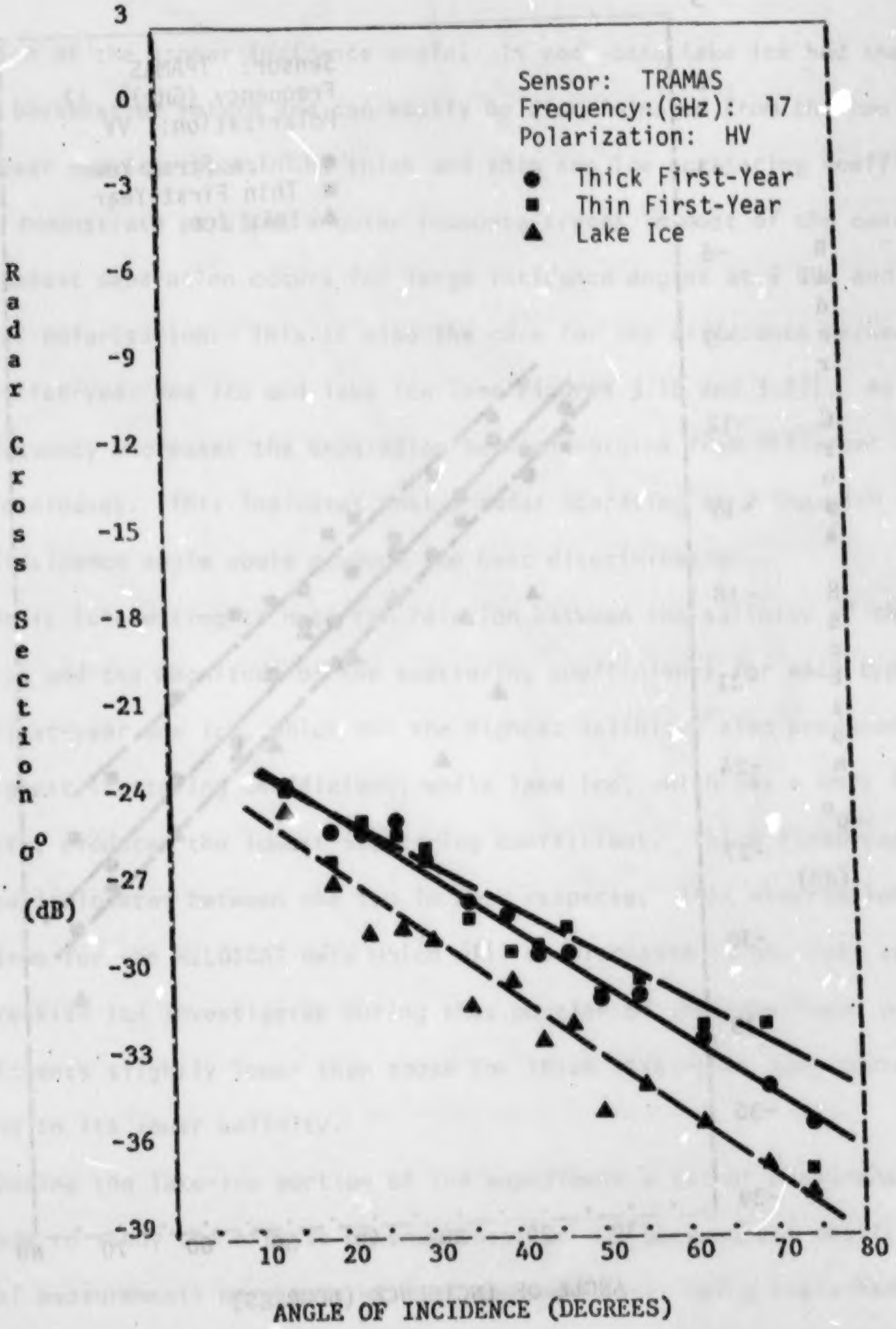

Figure 3.10. Average scattering coefficient of Thick First-Year, Thin First-Year, and Lake Ice at 17 GHz. (March 1979)

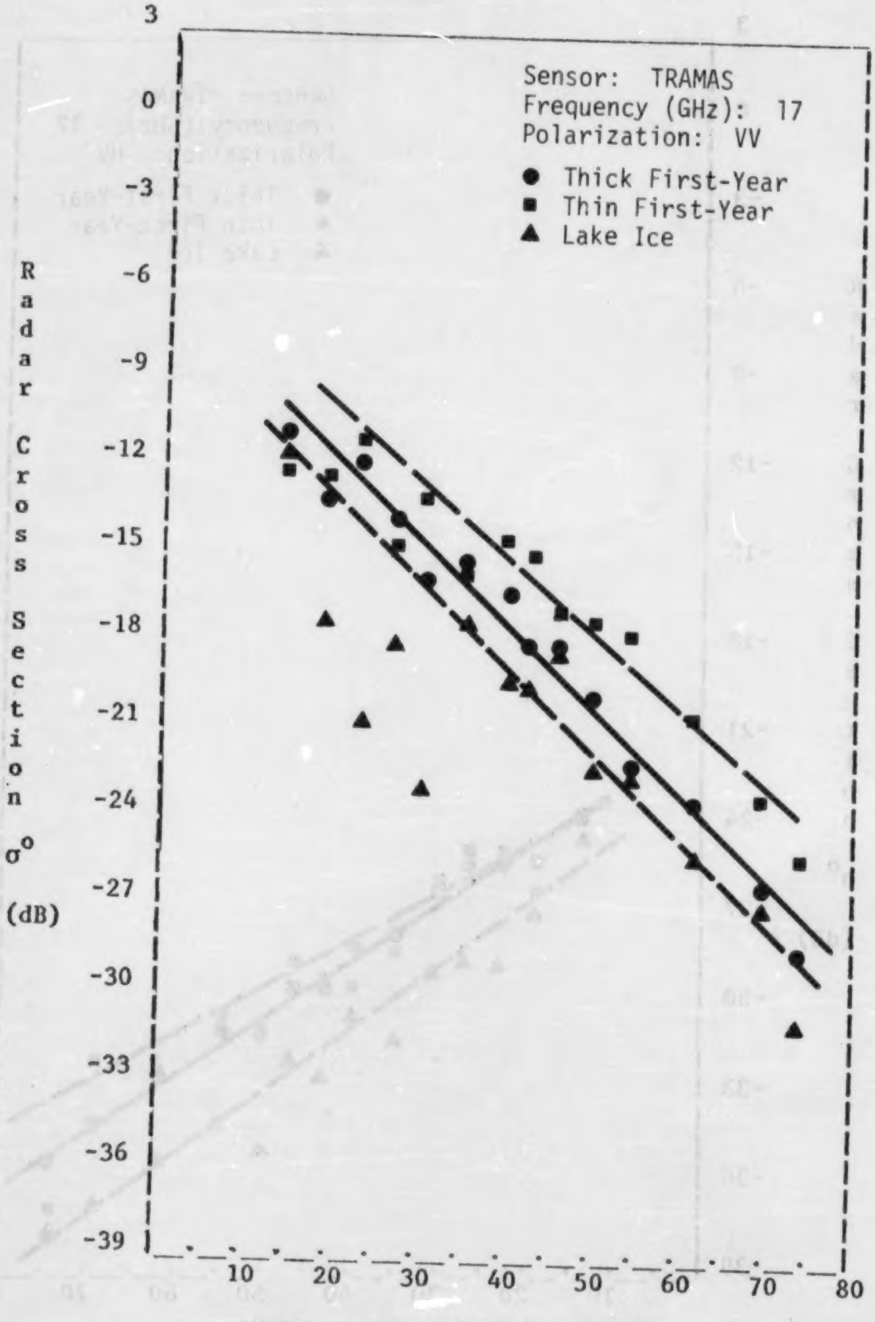

Figure 3.11. Average scattering coefficient of Thick First-Year, Thin First-Year, and Lake Ice at 17 GHz. (March 1979)

selection of the proper incidence angle. In each case lake ice had the lowest backscatter return and can easily be discriminated from the two first-year sea ice types. The thick and thin sea ice scattering coefficients demonstrate parallel angular response trends in most of the cases. The greatest separation occurs for large incidence angles at 9 GHz and vertical polarization. This is also the case for the difference between thick first-year sea ice and lake ice (see Figures 3.16 and 3.17). As the frequency increases the separation between returns from different ice types decreases. This indicates that a radar operating at 9 GHz with a large incidence angle would produce the best discrimination.

It is interesting to note the relation between the salinity of the ice type and the magnitude of the scattering coefficients for each type. Thin first-year sea ice, which has the highest salinity, also produced the highest scattering coefficient; while lake ice, which has a very low salinity, produced the lowest scattering coefficient. Thick first-year sea ice is located between the two in both respects. This observation is also true for the HELOSCAT data which will be discussed in the next section. The brackish ice investigated during that portion of the experiment produced coefficients slightly lower than those for thick first-year ice, corresponding to its lower salinity.

During the lake-ice portion of the experiment a set of measurements was made to study the effects of snow cover on the backscatter coefficient. Initial measurements were made without the snow cover being disturbed by the experimenters. Old snowmobile tracks and small surface features caused by the wind were characteristic of this hard-packed snow cover. In contrast to this natural 4 cm snow cover, the surface was artificially roughened with grooves 4 cm deep and 3 cm wide spaced 6 inches apart in a grid fashion. The snow was then completely removed from the target area.

The results of this process are illustrated in Figures 3.12 through 3.15. The horizontally polarized scatter was affected more by the roughening than the vertically polarized scatter. The orientation of the horizontal component of the radar signal with the grooves may be responsible for this dominant backscatter feature for HH polarization. The angular responses at vertical polarization for the natural and roughened cases were similar.

In all cases the scattering coefficient for the bare-surface lake ice was dramatically lower than the snow-covered-lake responses. The difference averaged 8 dB or greater. These results indicate that evan at these very cold temperatures snow plays a very important role in the backscatter from lake ice and that this must be taken into account when extracting information from imagery of frozen lakes. Snow surface roughness also has been shown to have an effect on backscatter and should be accounted for.

The difference between thick first-year and thin first-year sea ice and between thick first-year sea ice and lake ice is plotted versus angle of incidence for 1.5, 9, 13, and 17 GHz in Figures 3.16 and 3.17. There is little ability to discriminate thick from thin ice with 1.5 GHz. All of the other frequencies indicate similar ability to discriminate between thick and thin first-year sea ice with the greatest difference occuring for angles of incidence greater than 40°. Figure 3.17 shows that all of the frequencies have the ability to discriminate thick first-year sea ice from lake ice for almost all angles of incidence. The 9.0 GHz frequency has a significantly larger difference (2-4 dB) for incidence angles greater than 40°.

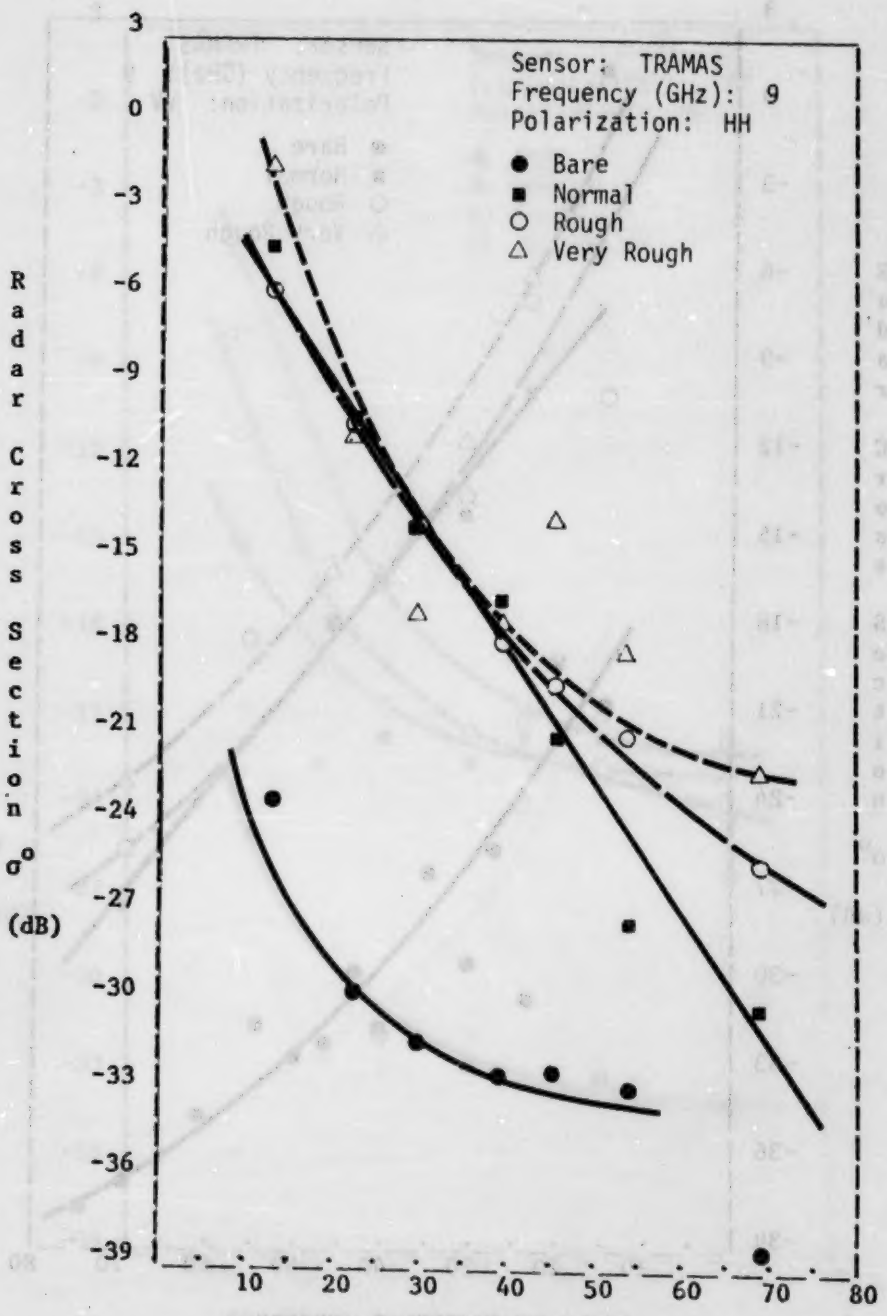

Figure 3.12. Scattering coefficient of Lake Ice with Bare, Normal, Rough, and Very Rough snow cover conditions at 9 GHz. (March 1979)

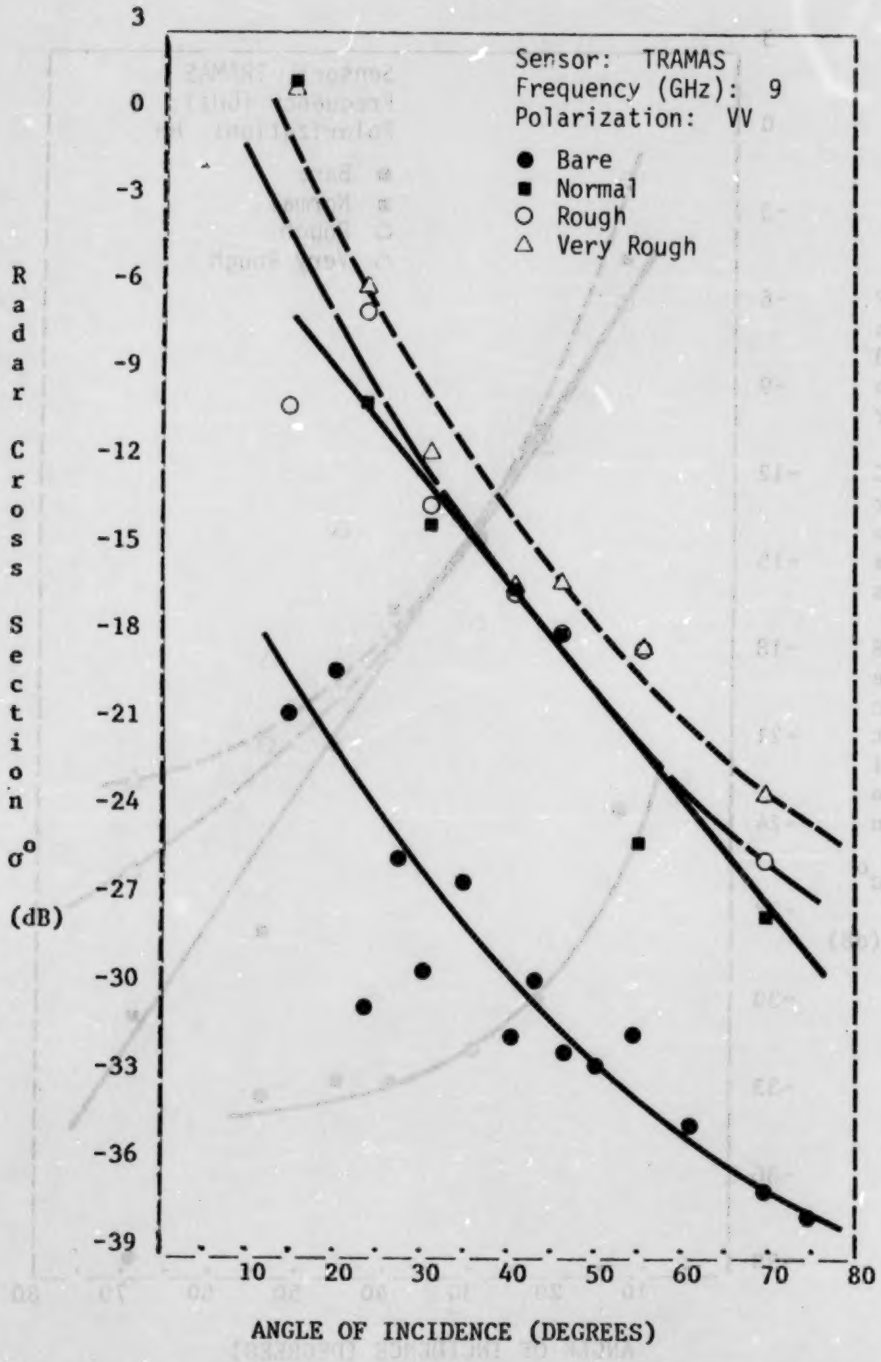

Figure 3.13. Scattering coefficient of Lake Ice with Bare, Normal, Rough, and Very Rough snow cover conditions at 9 GHz. (March 1979)

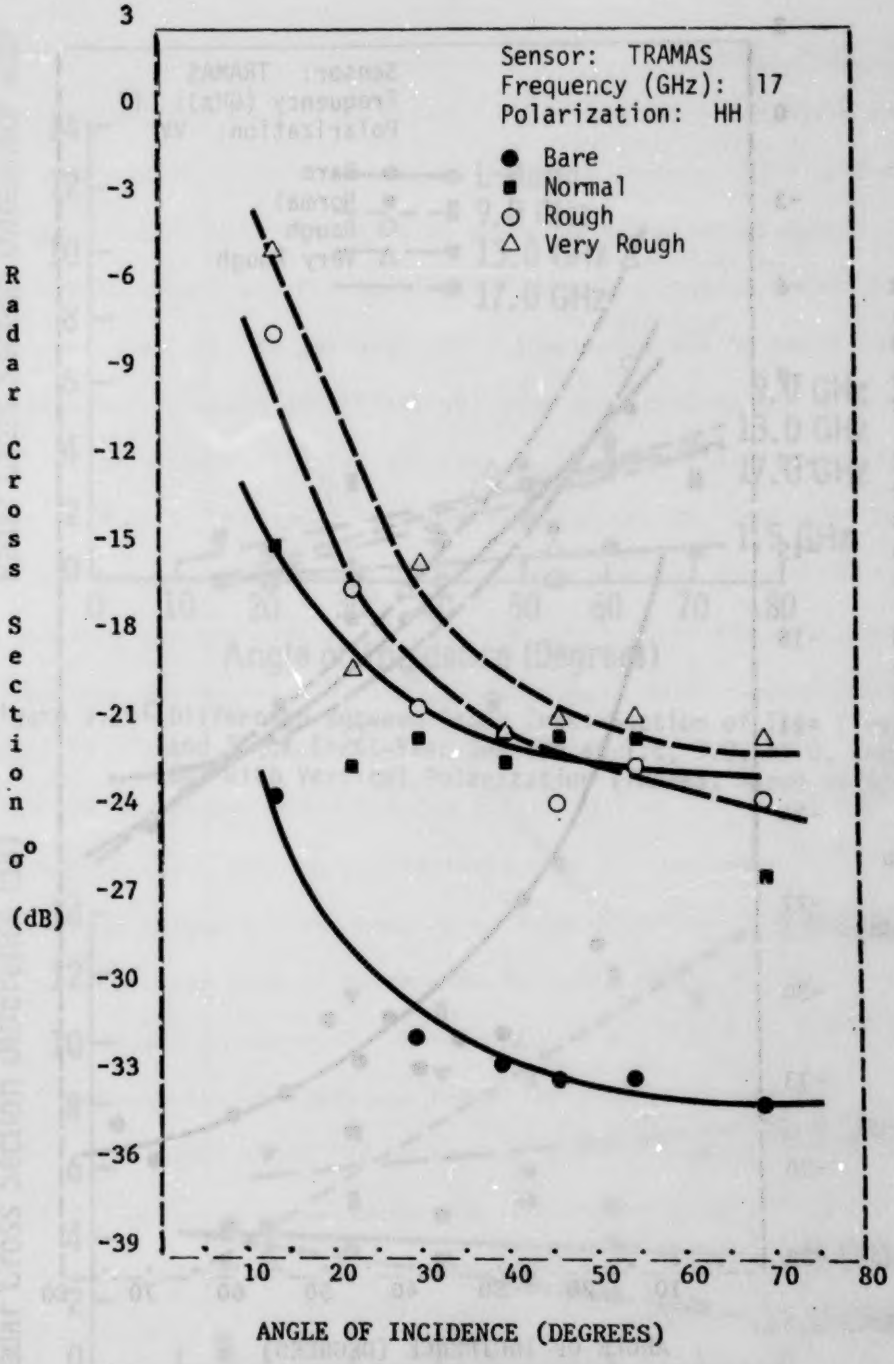

Figure 3.14. Scattering coefficient of Lake Ice with Bare, Normal, Rough, and Very Rough snow cover at 17 GHz. (March 1979)

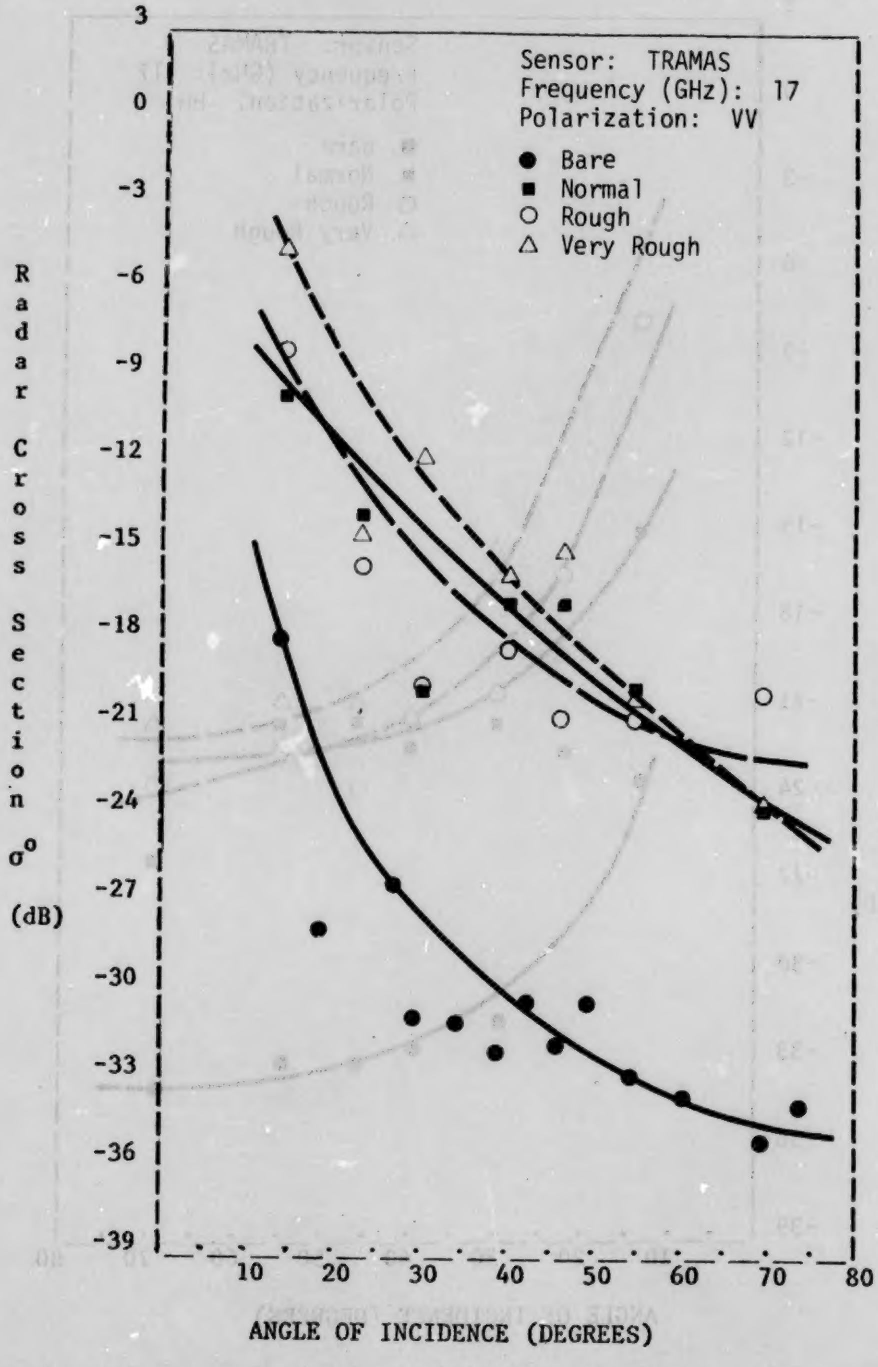

Figure 3.15. Scattering coefficient of Lake Ice with Bare, Normal, Rough, and Very Rough snow cover conditions at 17 GHz. (March 1979)

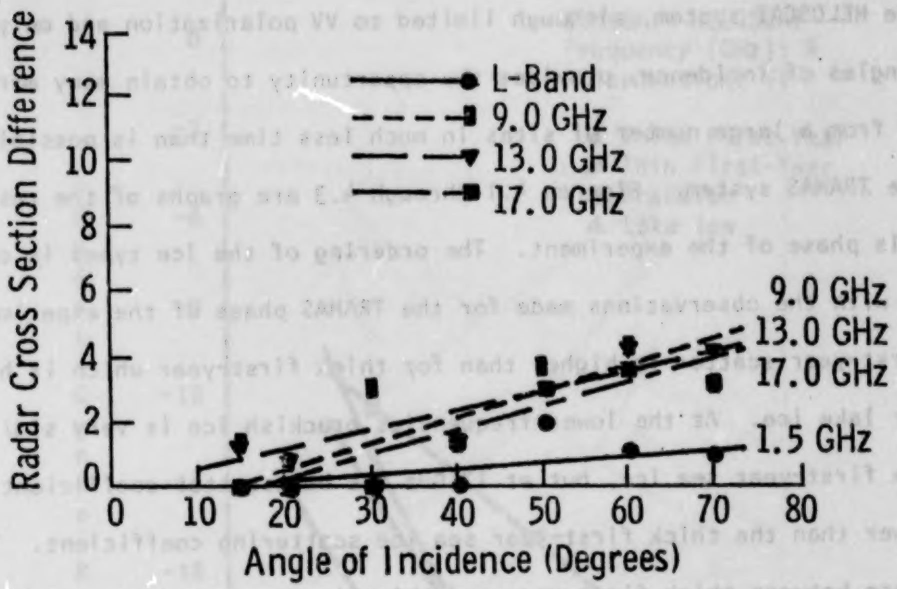

Figure 3.16 Difference Between Radar Cross-Section of Thin First-Year and Thick First-Year Sea Ice at 1.5, 9.0, 13.0, and 17.0 GHz with Vertical Polarization (TRAMAS, March 1979)

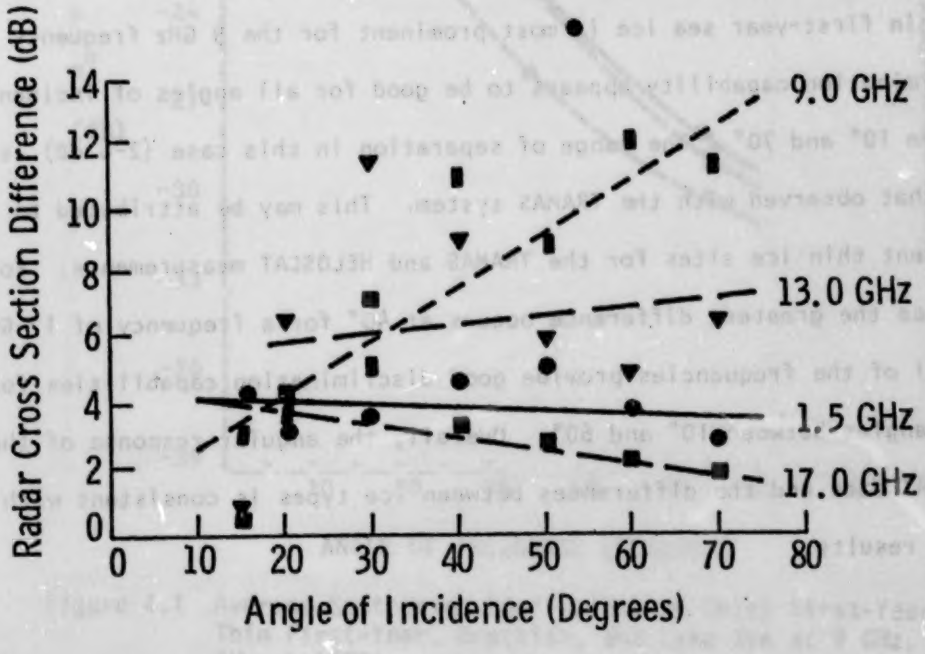

Figure 3.17 Difference Between Radar Cross-Section of Thick First-Year Sea Ice and Lake Ice at 1.5, 9.0, 13.0, and 17.0 GHz with Vertical Polarization (TRAMAS, March 1979)

4.0 HELOSCAT RESULTS

The HELOSCAT system, although limited to VV polarization and only three angles of incidence, provides the opportunity to obtain many more samples from a large number of sites in much less time than is possible with the TRAMAS system. Figures 4.1 through 4.3 are graphs of the results from this phase of the experiment. The ordering of the ice types is consistent with the observations made for the TRAMAS phase of the experiment. Thin first-year scatter is higher than for thick first-year which is higher than for lake ice. At the lower frequencies brackish ice is very similar to thick first-year sea ice, but at 17 GHz the backscatter coefficient is 3 dB lower than the thick first-year sea ice scattering coefficient. The difference between thick first-year and thin first-year sea ice and between thick first-year sea ice and lake ice is plotted versus angle of incidence for 9, 13, and 17 GHz in Figures 4.4 and 4.5. The separation between thick and thin first-year sea ice is most prominent for the 9 GHz frequency and discrimination capability appears to be good for all angles of incidence between 10° and 70°. The range of separation in this case (2-6 dB) is larger than that observed with the TRAMAS system. This may be attributed to using different thin ice sites for the TRAMAS and HELOSCAT measurements. For lake ice the greatest difference occurs at 40° for a frequency of 17 GHz but all of the frequencies provide good discrimination capabilities for incidence angles between 10° and 60°. Overall, the angular response of the HELOSCAT data and the differences between ice types is consistent with the TRAMAS results.

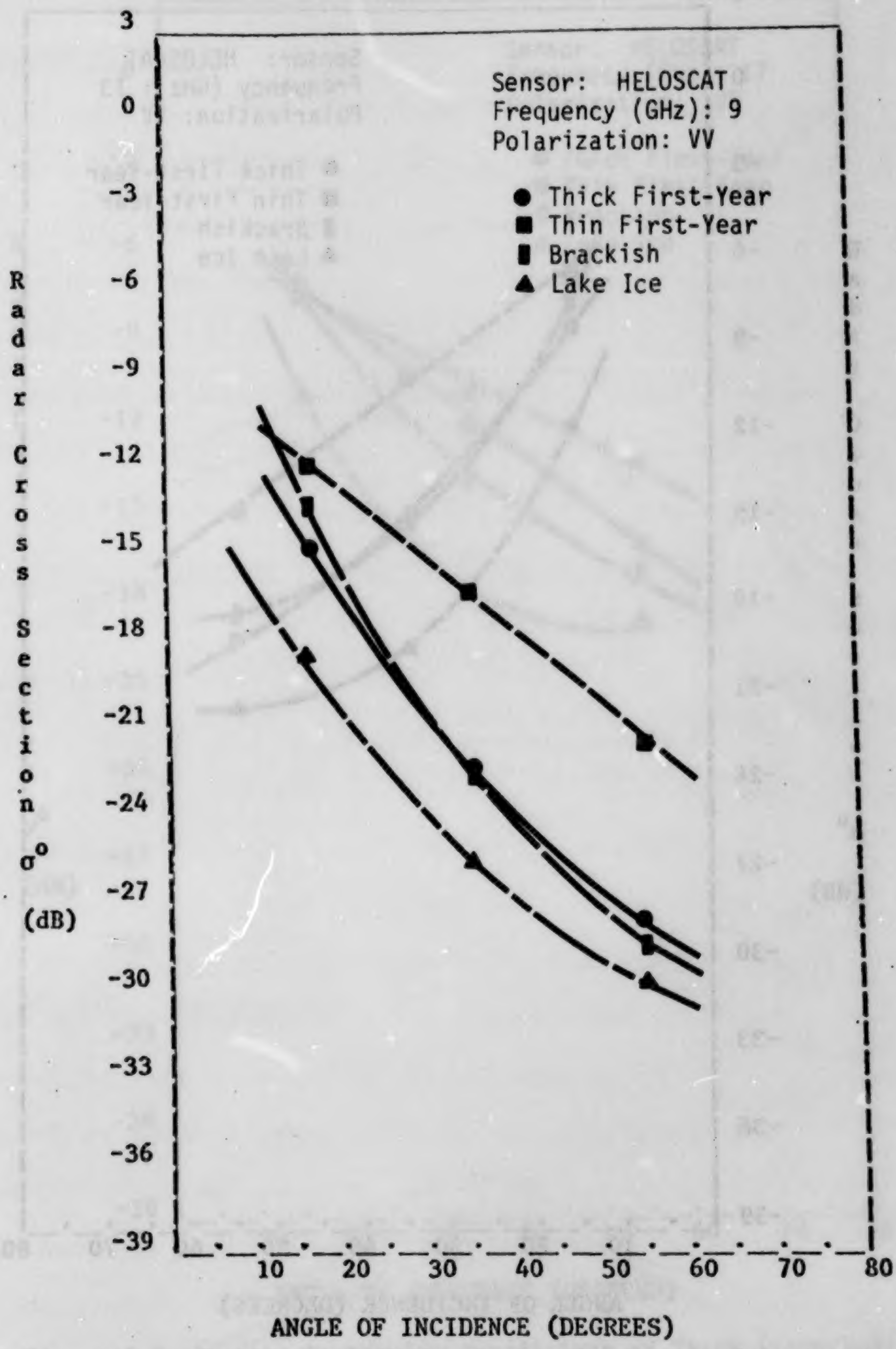

Figure 4.1 Average Scattering Coefficient of Thick First-Year, Thin First-Year, Brackish, and Lake Ice at 9 GHz. (March 1979)

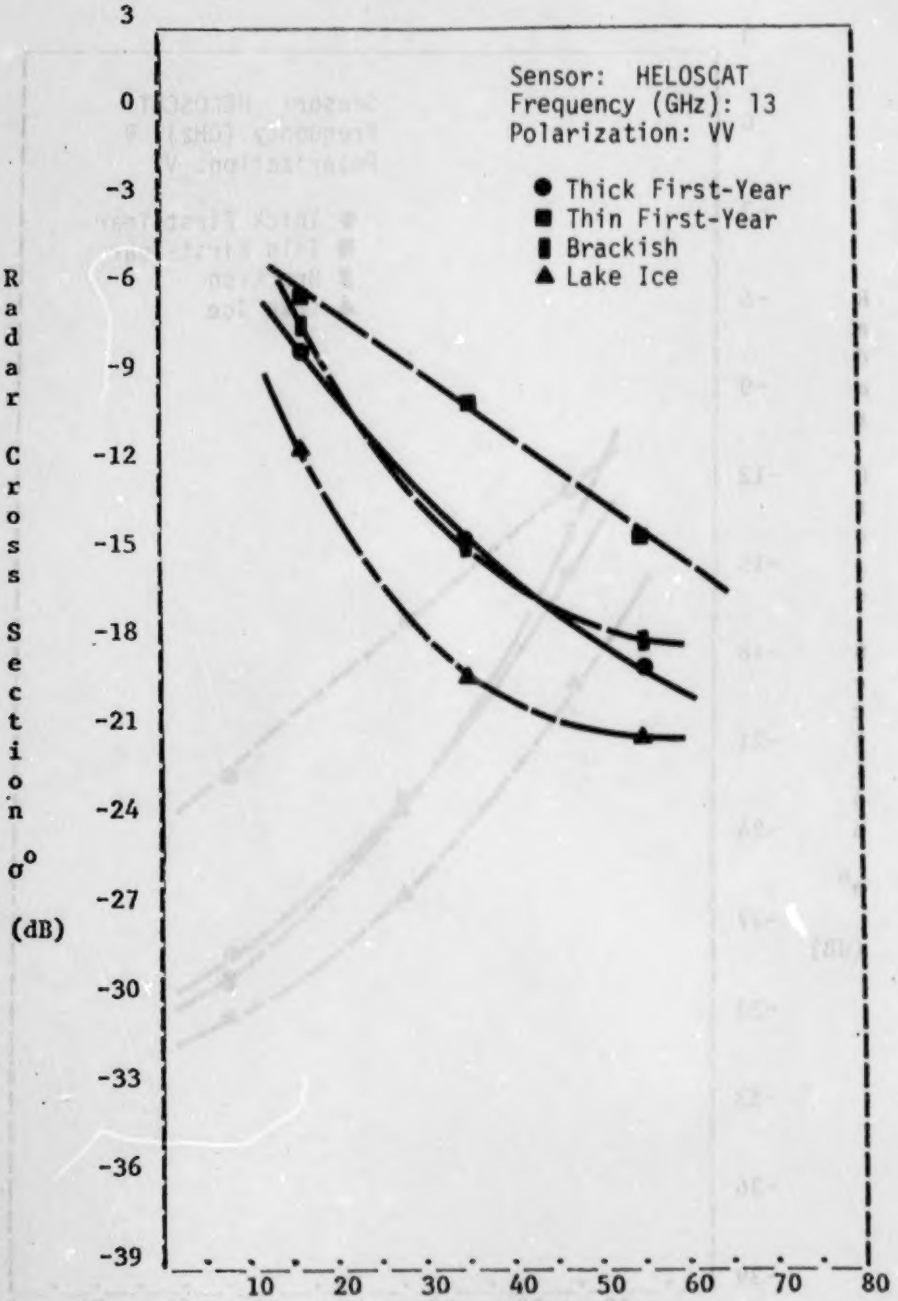

Figure 4.2 Average Scattering Coefficient of Thick First-Year, Thin First-Year, Brackish, and Lake Ice at 13 GHz. (March 1979)

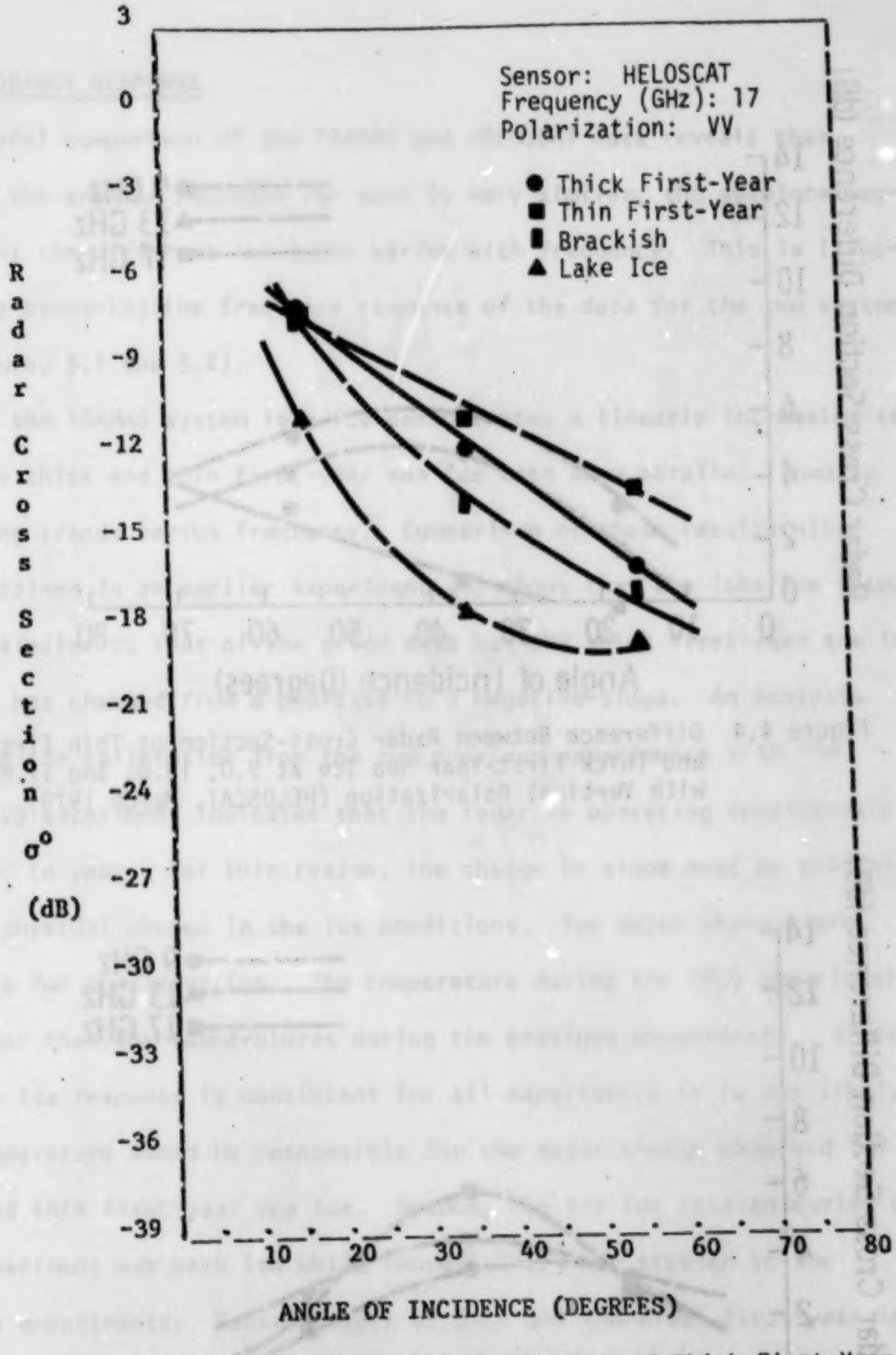

Figure 4.3 Average Scattering Coefficient of Thick First-Year, Thin First-Year, Brackish, and Lake Ice at 17 GHz. (March 1979).

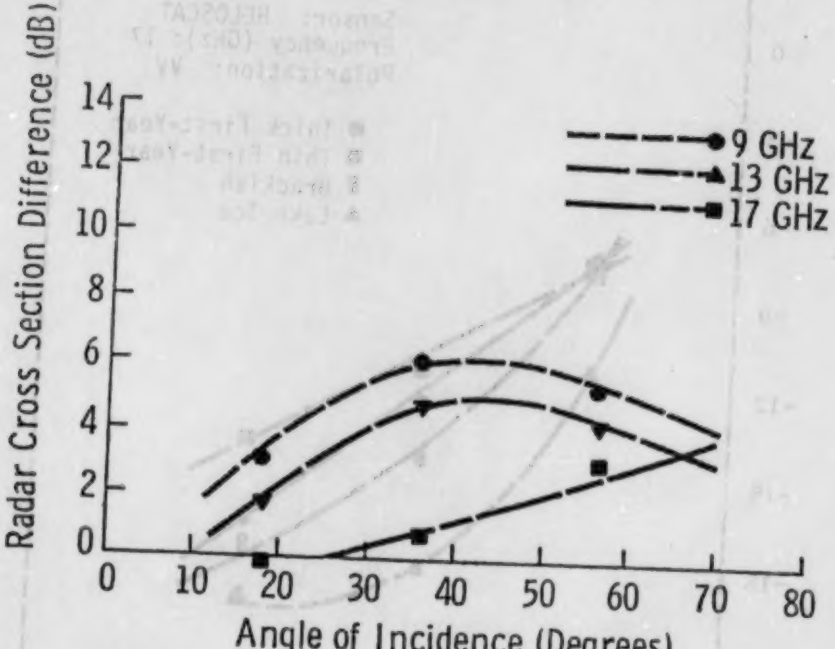

Figure 4.4 Difference Between Radar Cross-Section of Thin First-Year and Thick First-Year Sea Ice at 9.0, 13.0, and 17.0 GHz with Vertical Polarization (HELOSCAT, March 1979)

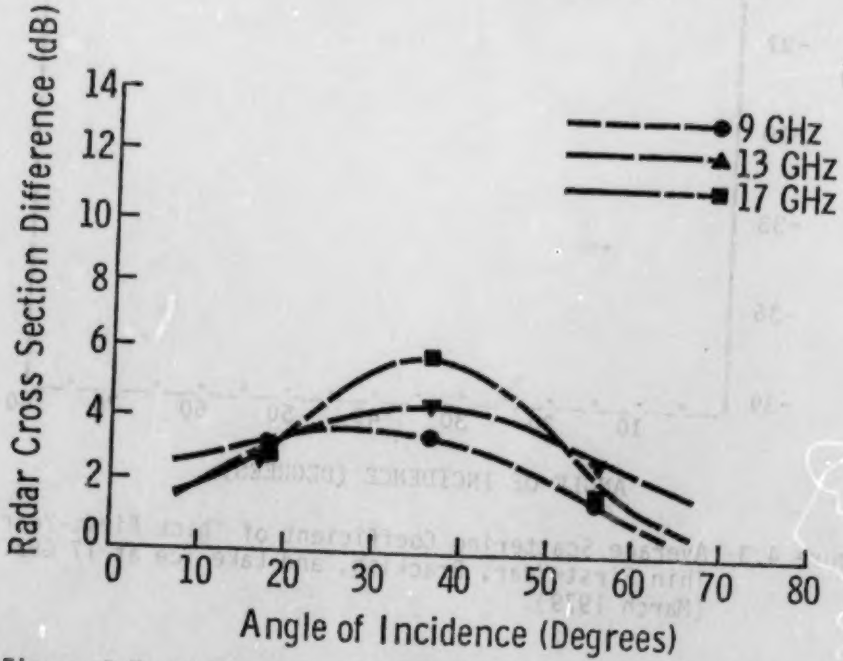

Figure 4.5 Difference Between Radar Cross-Section of Thick First-Year and Lake Ice at 9.0, 13.0, and 17.0 GHz with Vertical Polarization (HELOSCAT, March 1979)

5.0 FREQUENCY RESPONSE

Careful comparison of the TRAMAS and HELOSCAT data reveals that, although the angular response for each is very similar, the absolute magnitude for the different ice types varies with frequency. This is illustrated by comparing the frequency response of the data for the two systems (see Figures 5.1 and 5.2).

For the TRAMAS system lake ice demonstrates a linearly increasing trend while the thick and thin first-year sea ice both show parallel linearly decreasing trends versus frequency. Comparison of these results with those obtained in an earlier experiment [4] shows that the lake ice response is very similar to that of the prior data but the thick first-year sea ice response has changed from a positive to a negative slope. An analysis comparing the calibration from the two previous experiments with the March 1979 experiment indicates that the radar is operating consistently from year to year. For this reason, the change in slope must be related to some physical change in the ice conditions. Two major changes are available for consideration. The temperature during the 1979 experiment was much lower than the temperatures during the previous experiments. Since the lake ice response is consistent for all experiments it is not likely that temperature would be responsible for the major change observed for thick and thin first-year sea ice. Second, the sea ice studied during the 1979 experiment was pack ice while shorefast ice was studied in the previous experiments. Radar imagery of pack and shorefast first-year ice types indicates that there is a difference in the radar backscatter from the two and this may account for the different response.

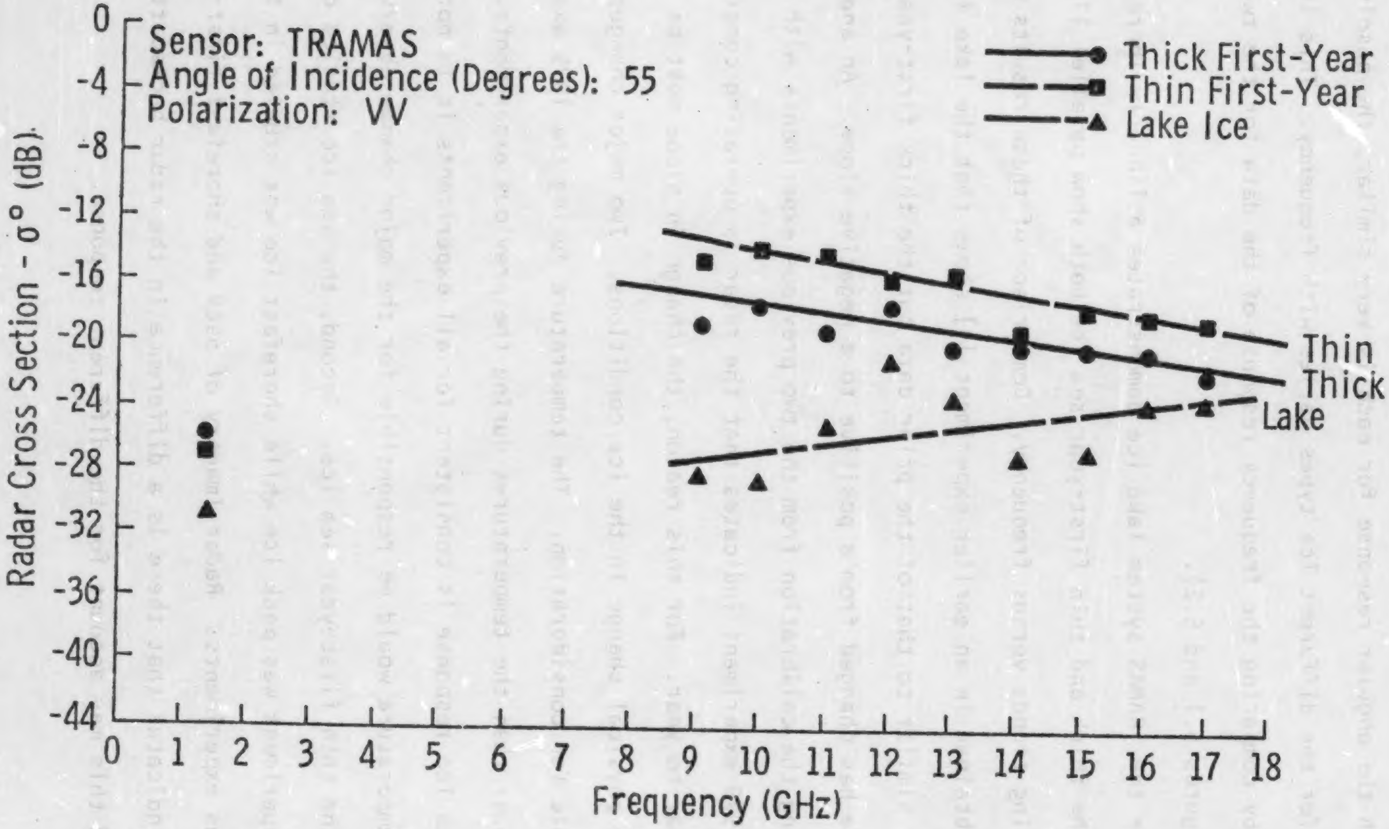

Figure 5.1 Scattering Coefficient Frequency Response of Thick First-Year, Thin First-Year, and Lake Ice (March 1979).

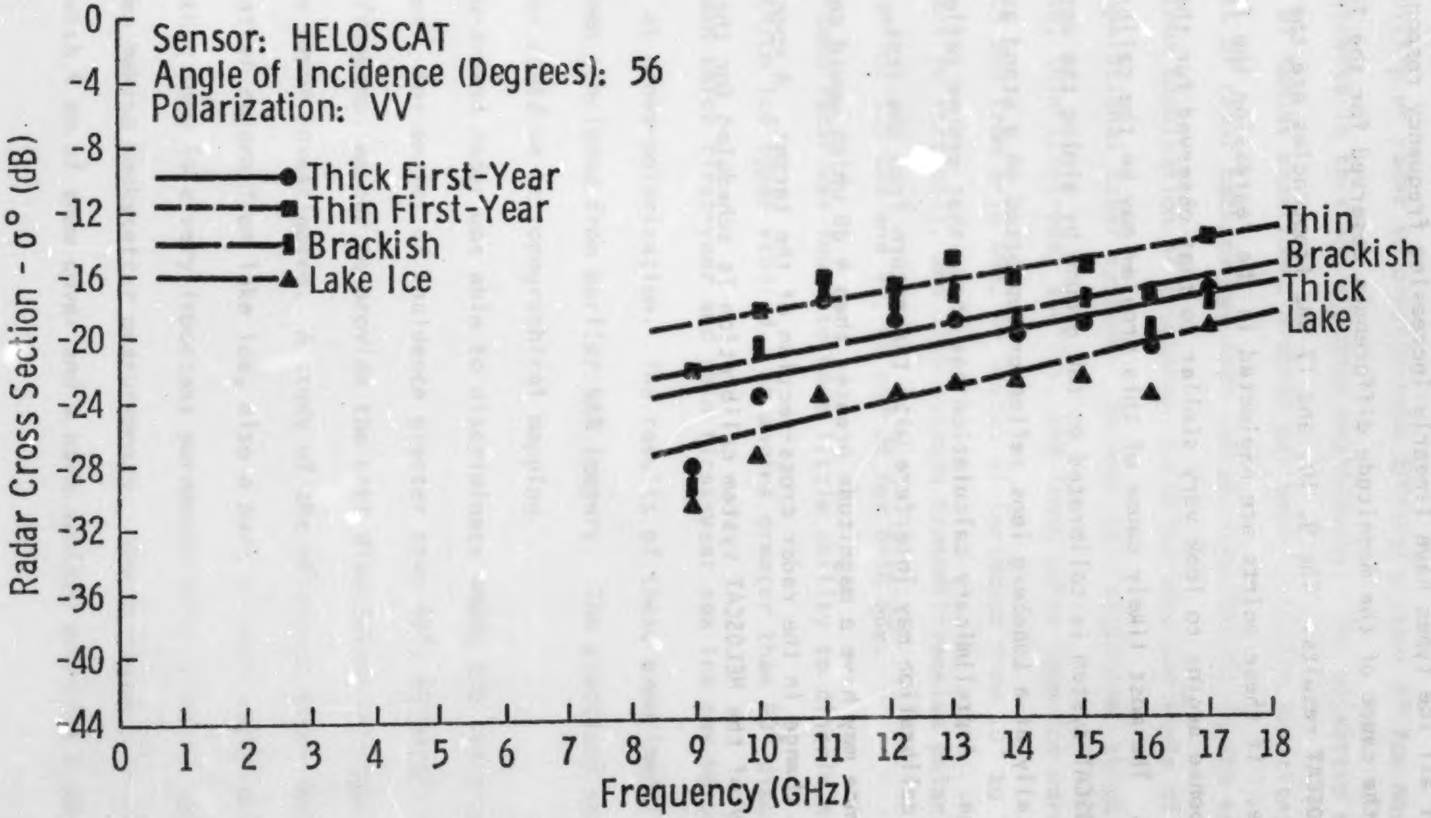

Figure 5.2 Scattering Coefficient Frequency Response of Thick First-Year, Thin First-Year, Brackish, and Lake Ice. (March 1979).

Linear regressions of the HELOSCAT data versus frequency indicate that all ice types have linearly increasing frequency responses. This is the cause of the magnitude differences observed for the TRAMAS and HELOSCAT results. The 9, 10, and 17 GHz frequencies are the most troublesome. If these points are neglected in the regression the frequency response begins to look very similar to that observed for the TRAMAS system. The most likely cause of this problem may be the calibration. The HELOSCAT system is calibrated on the ground by aiming the antennas horizontally at a Luneberg lens reflector supported on a stand at some fixed range. A preliminary calculation has shown that ground reflections during the calibration may interfere with the return from the lens. This interference may have a magnitude greater than 4 dB which would cause a significant change in the radar cross-section of the target. A more complete study of the HELOSCAT system calibration is scheduled for the near future.

6.0 CONCLUSIONS

The ability of radar to discriminate different types of ice has been well-demonstrated in this and previous experiments. The objective of the University of Kansas experiment program has been to obtain quantitative measurements of radar backscatter from ice which would help in the selection of the optimum combination of frequency, polarization, and angle of incidence for operational radar systems. To meet this objective, thick first-year sea ice, thin first-year sea ice, and fresh water lake ice were investigated at 1.5 and from 8-18 GHz, at angles of incidence from 10° to 75° (with respect to vertical), and with antenna transmit-receive polarizations of VV and VH for 1.5 GHz and VV, HV and HH for 8-18 GHz.

The L-band radar was found to have little ability to discriminate among the three ice types studied. At angles greater than 40° discrimination between thick first-year and thin first-year sea ice may be possible, especially at cross-polarization. The results of these experiments confirms what had been concluded from earlier SAR imagery. The practical use of L-band radar would be in topographical mapping.

The Ku-X-Band radar was able to discriminate among the ice types investigated. For angles of incidence greater than 40°, VV polarization and 9 GHz frequency appear to provide the best discrimination capability for all ice types investigated. A study of the effect of snow cover on the backscatter return from lake ice, also a part of this experiment, indicates that snow is a very important parameter which must be taken into account when making backscatter measurements. The difference in return from a surface with 4 cm of snow cover and a bare surface averaged 8 dB or more.

REFERENCES

[1] Onstott, R.G., R.A. Hand, J.S. Patel, R.K. Moore, "Transportable Microwave Active Spectrometer 'TRAMAS' or 'MAS JR.', Design Memo," Remote Sensing Laboratory, Technical Memorandum TM 331-4, University of Kansas Center for Research, Inc., Lawrence, Kansas, September 1978.

[2] Delker, C.V., R.G. Onstott, R.A. Hand, R.K. Moore, "Transportable Microwave Active Spectrometer "TRAMAS" -- Modifications Report I," Remote Sensing Laboratory, Technical Memorandum TM 331-5, University of Kansas Center for Research, Inc., Lawrence, Kansas, June 1979.

[3] Delker, C.V., J.S. Patel, R.G. Onstott, "Installation Procedures for HELOSCAT Scatterometer on Bell Model 205," Remote Sensing Laboratory, Technical Memorandum TM 331-12, University of Kansas Center for Research, Inc., Lawrence, Kansas, May 1979.

[4] Onstott, R.G., R.K. Moore, and W.F. Weeks, "Surface-Based Scatterometer Results of Arctic Sea Ice," IEEE Transactions on Geoscience Electronics, Vol. GE-17, No. 3, July 1979, pp. 78-85.

SECTION 5.4

MICROWAVE SIGNATURES OF SEA ICE IN THE MARGINAL ICE ZONE

Skou, N.

Microwave Signatures of Sea Ice

in the Marginal Ice Zone

N. Skou
Electromagnetics Institute
348 Technical University of Denmark
DK-2800 Lyngby, Denmark

1. Introduction

On 10 April 1979 five aircraft, a helicopter and the Danish vessel "Ingolf" participated in a very succesful Danish, Canadian, American and British remote sensing experiment. The initiative and planning for the West Greenland Sea Ice Experiment had been carried out by the Technical University of Denmark (TUD) in order to study and demonstrate the capabilities of different microwave remote sensors to provide information of the extent, type and thickness of sea ice, particularly to those concerned with shipping.

This experiment was unique in a number of ways: Firstly, it represented the first time that imagery from a high resolution, calibrated, multifrequency imaging radiometer could be compared with imagery from a high resolution dual frequency, dual polarized radar as well as visible, infra-red and profiling active and passive microwave sensors. Secondly, the majority of the experiments designed to study the capabilities of microwave sensors for ice mapping have been undertaken under different conditions and in different regions of the Arctic, e.g. in the Beaufort Sea during March and April. This experiment represents one of the few undertaken in the marginal ice zone under conditions typical of those which can be encountered by shipping along the west coast of Greenland. This is, of course, important to both Canada and Denmark as being the proposed route for the transport of natural resources, even liquified natural gas, out of the Canadian Arctic. To undertake such shipping safely and efficiently it will be necessary to support the activity with information which can be obtained only by all weather, microwave remote sensing.

Canada participated in the West Greenland Experiment by providing the CCRS (Canada Centre for Remote Sensing) Convair 580 which contains a sophisticated X/L band dual polarized synthetic aperture radar and other microwave sensors as well as cameras. Also the CCRS Falcon was flown and this aircraft obtained infrared imagery and RC-10 photography. The West Greenland Experiment thus became an element in the larger Canadian SURSAT project.

The radiometer imagery, which is the main subject for this paper, was obtained by the TUD multifrequency radiometer system being carried on board a C-130 from the Royal Danish Air Force.

A helicopter supported ground truth team contributed to the experiment.

Finally, a SLAR on a Danish Twin-Otter was operated and a NORDA P-3 obtained infra-red and optical imagery.

2. The Radiometer System

The radiometer system consists of three radiometers - at 5, 17 and 34 GHz - a multichannel antenna system and digital data processing and recording facilities, all designed for airborne use and developed and manufactured at the Electromagnetics Institute (Ref. 1 and 2).

The main characteristics of the system may be summarized as follows:

Radiometers

Type : Noise-injection with microwave front-end temperature stabilized to 40°C

Frequency :	5 GHz	17 GHz	34 GHz
Bandwidth :	500 MHz	1 GHz	1 GHz
Noise figure :	6.5 dB	5 dB	5 dB

Sensitivity : 0.95 K for 8 msec integration time (1.8 K for the 5 GHz radiometer)

Input range : 0 - 313 K

Antenna

Type : Offset parabolic reflector viewed by 3 vertical horns. The reflector scans around a vertical axis.

Angle of incidence on ground : 40.6°, 54.4° and 50° at 5, 17, and 34 GHz, respectively.

Polarization : Vertical

Scan angle : ± 25°

Scan speed : 0.48 Hz

Aperture : 1 m

Scan pattern : Sinousoidal

Swath width : Equal to altitude

Nominal altitude : 2 000 m

Nominal ground speed : 140 knots

During nominal conditions the foot-prints sizes are:

34 GHz : 47 × 73 m
17 GHz : 94 × 146 m
5 GHz : 320 × 496 m

and the minimum dwell time per foot-print is 16 msec requiring 8 msec sample rate.

Output

Type : Digital on 8 bit bus. Simultaneous values of radiometer data and antenna position available every 8 msec. Housekeeping and navigational data incorporated on the bus every 24 sec.

3. The Test Area

The cross-shaped test area was selected west of Egedesminde in the Davis Strait. The waypoints were:

WP 1 : 68.20N, 54W
WP 2 : 68.20N, 57W
WP 3 : 69.00N, 56W

The area overflown on April 10, 1979 was clearly in the marginal ice zone with the eastern part of the east-west track covering the water-ice boundary (and the southern part of the north-south leg coming close to it). The weather was very satisfactory with almost clear sky and the RC-10 mapping camera of the CCRS Falcon obtained high quality photography of the entire test area. From these images it has be deducted that generally the area just inside the ice-water boundary was covered with swell broken cake ice of average size appr. 5 - 10 m. The cakes were surrounded partly by open water partly by nilas (very thin, new ice which easily rafts under pressure). Further inside the pack, areas of cake ice were still found, the average size now being some 10 - 30 m in diameter and the percentage of open water rather small. But the dominant ice type here is larger, individual floes often surrounded by more or less rafted nilas.

The ground truth team attempted to land on several of the bigger floes in the area but it turned out that the ice were in a state of decay and were not able to support the helicopter. Some information about the ice was gathered however. The bigger ice floes were about 20 cm thick covered by a 10 cm dry snow layer. The surface temperature was measured to - 3°C and the salinity of the ice was some 20 °/oo.

The surface temperature of - 3°C yields an expected brightness temperature of 262 K. (The emissivity of first-year ice is 0.97).

4. Presentation of Data

Figure 1 shows an example of the radiometer imagery. The image covers an area close to the crossing point of the flight lines (68.20N, 56W). The radiometer imagery is presented in false colour and is produced on the rather simple colour display connected to the computer of the institute. Only 8 colours are possible which is far from being able to do the radiometer data justice regarding temperature range and resolution. But the image can be displayed (on the colour screen) subjected to different codings of brightness temperature to colour and useful information extracted. The imagery is presented with equal pixel size for all channels corredponding to the foot-print size of the 34 GHz radiometer (all 3 radiometers were sampled simultaneously). Recall that the swath width is 2 000 m.

The area imaged by the radiometer was also sensed by the SAR (Fig. 2), a mapping camera and an infra-red scanner (Fig. 3) as already mentioned in section 1.

5. Discussion of the Imagery

The first observation to be made from the radiometer image Figure 1 is that the 34 GHz channel indicates a very dense ice cover while the 5 GHz channel reveals a lot of structure.

The imagery chosen includes three very different ice types:

1) Large individual floes (A, B, C, D on Fig. 3a), roughly 20 cm thick and with a high radiometric temperature at all frequencies (typical first-year ice). These floes are easily picked out on the SAR image (Fig. 2) and they produce a rather substantial radar backscatter due to a rough surface.

2) Areas of swell broken cake ice (E, F). The average floe size is 10 - 30 m and the floes are very close together i.e. with little open water or thin ice in between. The radiometers still read high temperatures in all channels. These areas of cake ice are imaged by the SAR with exactly the same grey tone as the large individual ice floes have!

3) Quite extensive areas of nilas surrounding the large ice floes and the cake ice. Nilas is newly frozen ice, thin, and with a smooth surface giving low radar backscatter. The radiometric temperature at 5 GHz is much depressed as compared with 34 GHz.

To better analyse the radiometer data the results from the area in question have been reprocessed and are presented in Figure 1a with a better resolution of the upper end of the temperature scale.

The cake ice (E and F) signature at 34 GHz does now separate from the signature of solid ice through a depression of appr. 5 K. This indicates an average of 7 % open water in the areas E and F. The corresponding high reading in the 5 GHz channel implies that the cakes consist of rather thick first-year ice just like the solid floes A - D. It is interesting to note that the radiometer system is able to distinguish between cake ice and solid ice - a task in which the

SAR fails despite the fact that the individual cakes are rather large compared with the resolution of the radar (some 3 m).

Returning to the signature of the nilas one should especially note the area above G. The brightness temperatures as measured at the three frequencies are here:

34 GHz : 260 K
17 GHz : 240 K
5 GHz : 190 K

that is a depression of 70 K in the 5 GHz channel over en area with 100 % ice cover! Throughout the image different combinations of brightness temperatures of the nilas are found due to patches of open water and probably different ice thicknesses but a depression of some 50 K at 5 GHz are generally noted. A simple explanation to the depression of the longer wavelength channels over thin ice would emerge through an assumption of the skin depth in the ice being comparable to the ice thickness. Hence the low radiometric temperature of the underlaying water would cause a lowering of the measured brigthness temperatures - most pronounced at longer wavelengths. Such a mechanism is discussed by Tiuri et al. (Ref. 3 and 4). The following curves are from Ref. 3:

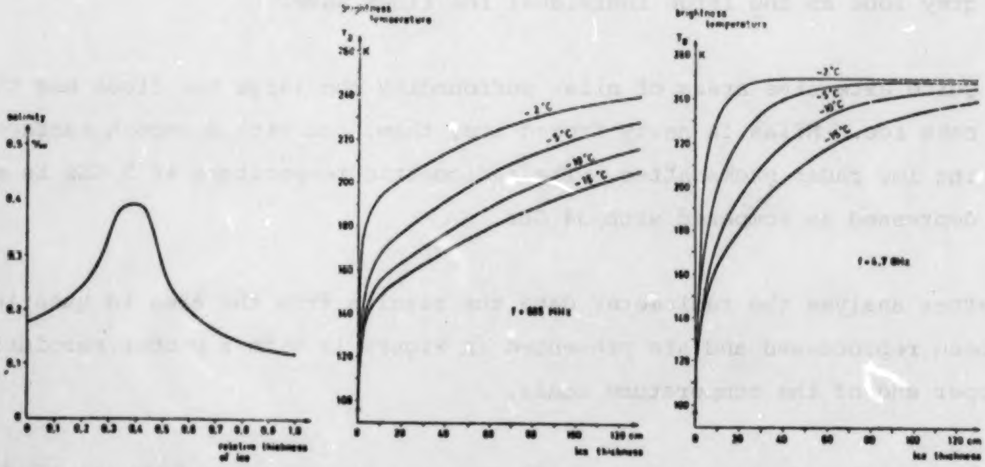

(a) (b) (c)

Normalized salinity profile (a) and calculated brightness temperatures of sea ice as a function of ice thickness at a frequency of 605 MHz (b) and 4.7 GHz (c).

It is seen that curves like these very nicely would explain the brightness temperatures at 5 GHz when measuring thin ice - but the salinities in question here are at least one order of magnitude greater than what is experienced by Tiuri in the Baltic Sea! Bogorodskii and Khoklov have carried out transmission measurements on newly formed ice at 10 GHz, salinity ∿ 27 ‰ (Ref. 5). The attenuations reported are as high as 15 dB per cm for 5 cm thick ice - enough to completely rule out any "looking through" the ice into the radiometrically colder water.

Based on Bogorodskii and Kholov's results the dielectric constant for thin ice have been calculated and extrapolated to the actual frequencies 5, 17 and 34 GHz, see Figure 4. This extrapolation is possible as one of B & K's conclusions is that ε for thin, initial forms of ice changes gradually from ε (water) to ε (first-year ice) with growing ice thickness. And the dielectric constant of sea water as a function of frequency is known. The nilas in question are known to have a thickness of some 5 cm (thinner ice is not able to raft). Hence the 5 cm ε's have been read from the curves Figure 4 and they have, together with ε (water) and the physical temperature of 270 K, served as input parameters to a computer programme which calculates the brightness temperature of a layer of ice on water as a function of thickness. The resulting curves are shown in Figure 5 and indicated on the curves are the asymptotic values for T_B. These are calculated by the same programme by entering $\varepsilon 2 = \varepsilon 3$ $(= \varepsilon(\text{ice}))$. It is seen that the brightness temperatures reach their final value very rapidly with increasing ice thickness and certainly at 5 cm thickness no depression of the 5 GHz channel due to underlaying water is present. The calculations do also show, however, that for new ice the brigthness temperatures at 5 GHz could be somewhat lower than at the higher frequencies solely due to differences in ε, hence reflection coefficient (230 K versus 250 K). But it must be emphasized that other mechanisms than reflection - first of all scattering - play important roles in producing brightness temperatures of ice. And the observed depression of 70 K in the 5 GHz channel is clearly not explainable by simple reflection coefficient differences.

But no matter which explanation to adopt for this problem the value of the correlation between thin ice and low 5 GHz brightness temperatures is clear: The 34 GHz channel outlines the areas covered with ice and gives the percentage of open water within the ice pack - irrespective of the ice type (we are here discussing areas without multiyear ice!). Simultaneous inspection of the 5 GHz data enables discrimination between solid ice and nilas.

6. Conclusions

Measurements with the imaging radiometer system have clearly demonstrated its capability to classify sea ice. Discrimination between first-year ice and multiyear ice has been known for some time but it has been shown that newly formed thin ice, nilas, can also be clearly recognised. Owing to the capability of measuring the percentage of open water in an ice pack, the radiometer system will distinguish between solid ice and cake ice (same ice type) - a task even a high resolution SAR fails to carry out.

Further data presentation and discussions can be found in Ref. 6 and 7.

7. References

1. N. Skou:
"Development of an Airborne Multifrequency Radiometer System",
Electromagnetics Institute, Technical University of Denmark, Lyngby,
Report R 203, December 1978.

2. N. Skou:
"Design of an Airborne Multifrequency Radiometer System",
Electromagnetics Institute, Lyngby, Denmark,
Report R 221, December 1979.

3. M. Tirui, M. Hallikainen, K. Kaski:
"Experiments on remote sensing of sea ice using a microwave radiometer",
Proc. URSI Meeting on microwave scattering and emission from Earth,
Berne, 1974.

4. M. Tiuri, M. Hallikainen, A. Lääperi:
"Microwave radiometer theory and measurements of sea ice characteristics",
Report S 89, Helsinki University of Technology, Finland, 1976.

5. V.V. Bogorodskii, G.P. Khoklov:
"Microwave refractive index and absorption of initial forms of the sea ice cover and newly formed ice",
Sov. Phys. Tech. Phys. Vol. 22(6), 1977, translated by American Inst. of Physics.

6. L. Gray, P. Gudmandsen, S. Overgaard, N. Skou, F. Søndergaard Pedersen:
"West Greenland Sea Ice Experiment. SURSAT Report No. 1",
Electromagnetics Institute, Lyngby, Denmark
Report R 219, November 1979.

7. N. Skou:
"Airborne Multifrequency Radiometry of Sea Ice",
Electromagnetics Institute, Lyngby, Denmark,
Report LD 42, March 1980.

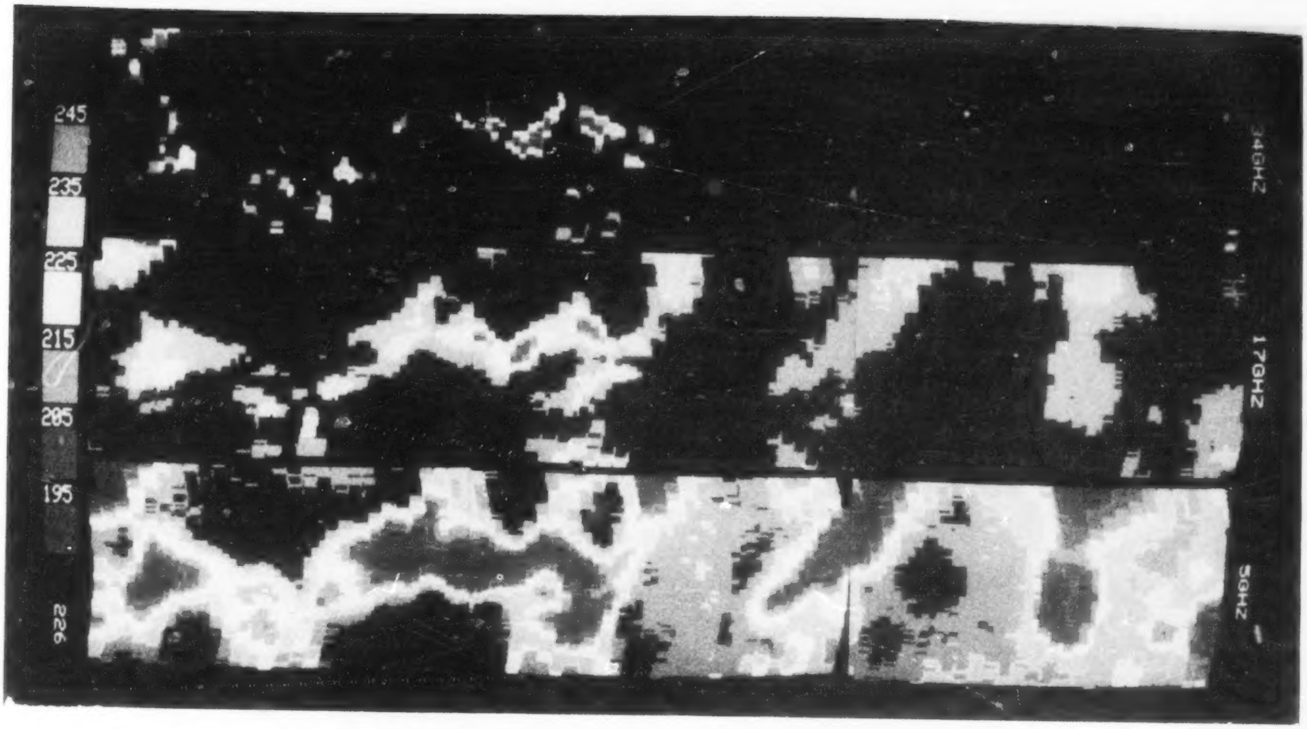
245
235
225
215
205
195
226
34GHZ
17GHZ
5GHZ

Figure (1). False colour radiometer image of the area indicated on Figure (3a). Note the brightness temperature to colour code translator on the left of the image.

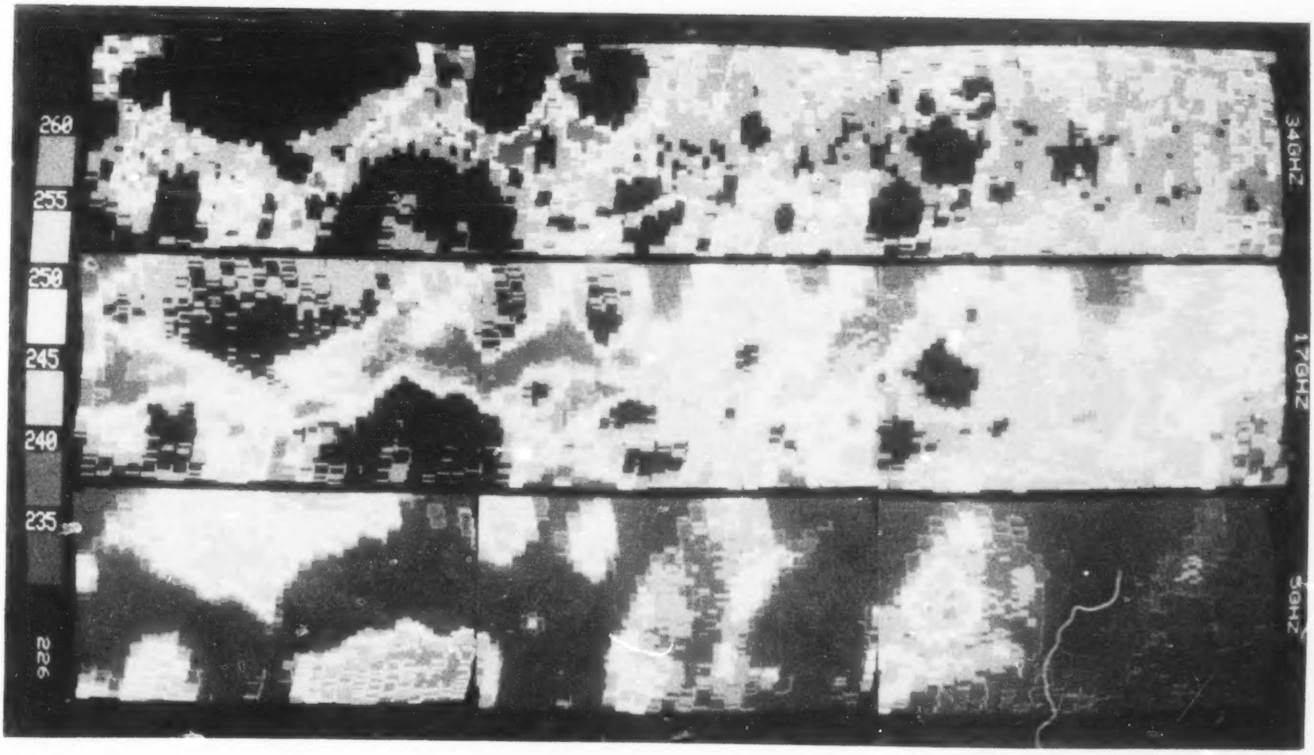
260
255
250
245
240
235
226
34GHZ
17GHZ
5GHZ

Figure (1a). Radiometer image reprocessed for better resolution of the upper end of the temperature scale.

SECTION 5.5

CLASSIFICATION OF BEAUFORT SEA ICE USING ACTIVE AND PASSIVE MICROWAVE SENSORS

Livingstone, C.E., R.K. Hawkins, A.L. Gray, K. Okamoto,
T.L. Wilkinson, S. Young, L. Drapier Arsenault, D. Pearson

CLASSIFICATION OF BEAUFORT SEA-ICE USING ACTIVE AND PASSIVE MICROWAVE SENSORS.

C.E. Livingstone, R.K. Hawkins, A.L. Gray
Canada Centre for Remote Sensing

K. Okamoto
Radio Research Laboratories, Tokyo, Japan

T.L. Wilkinson, S. Young
University of Waterloo

L. Drapier Arsenault
Cold Regions Remote Sensing

and

D. Pearson
Intera Environmental Consultants Ltd.

ABSTRACT

Results obtained by the Canada Centre for Remote Sensing (CCRS) show that simultaneous dual-polarized 13.3 GHz airborne scatterometer and 19.4 GHz H-polarized radiometer data may be used to uniquely classify sea-ice data into 11 WMO sea-ice classes under a variety of ambient temperature conditions found in the Beaufort Sea (March 1979), Frobisher Bay (April 1979) and Davis Strait (April 1979).

Two distinct feature spaces have been constructed for sea-ice classification: $\sigma^{\circ}_{hh}(\theta)$, $\sigma^{\circ}_{hv}(\theta)$, θ discriminates sea-ice classes in terms of the incidence angle variation of the backscattering coefficients; while $\sigma^{\circ}_{hh}(\theta_o)$, $\sigma^{\circ}_{hv}(\theta_o)$, $\varepsilon_h(\theta_1)$ relies on the complementary nature of emissivity and backscattering coefficients at fixed incidence angle.

In this paper, both feature spaces are assembled from data collected in the Beaufort Sea in March 1979 and are evaluated for ice type discrimination. A sea-ice classification algorithm is presented for the fixed incidence angle space, and a requirement for generalization of the feature spaces to four dimensions by the inclusion of ambient temperature is indicated.

The total CCRS results suggest that generalized feature spaces $\sigma^{\circ}_{hh}(\theta)$, $\sigma^{\circ}_{hv}(\theta)$, θ, T and $\sigma^{\circ}_{hh}(\theta_o)$, $\sigma^{\circ}_{hv}(\theta_o)$, $\varepsilon_h(\theta_o)$, T are valid for sea-ice classification over a very wide range of ambient temperature and ice surface conditions.

Introduction

As part of the Canadian SURSAT Sea-Ice Program (1978-1980), CCRS conducted an experiment in which sea-ice along a flight line was simultaneously measured by a 13.3 GHz HH and HV polarized airborne fan beam scatterometer, a 19.4 GHz H-polarized airborne pencil beam radiometer and an RC-10 mapping camera to determine which WMO sea-ice class (Dunbar, 1969) had distinctive backscattering coefficient (σ°_{hh} and σ°_{hv}) and emissivity ε_h signatures at these frequencies. Data was collected in the Beaufort Sea under late winter conditions (ambient temperatures -28° to -32°C) in March 1979, in Frobisher Bay under early spring conditions (ambient temperatures -28° to -32°C) in March 1979, in Frobisher Bay under early spring conditions (ambient temperatures -8°C to -5°C) in April, 1979 and in the Davis Strait ice margin zone under spring conditions (ambient temperatures -2°C to 0°C). The RC-10 photography (as augmented by SAR imagery where available) was used to classify the ice into WMO ice types. Data from regions measured by the radiometer and scatterometer which represented unique ice classes were identified, and used to partition the radiometer and scatterometer data into 'events'. Each event was thus a single ice class with a uniform thermal and mechanical history. The microwave brightness temperature was reduced to emissivity ε_h using ambient surface temperature estimates. Statistics of ε_h (at 45° incidence angle) and of σ°_{hh}, σ°_{hv} (at incidence angles from 0° to 60°) were computed for each event and all events of the same ice class and subclass were grouped for each experiment area. Class statistics were computed, compared to the event statistics, testing for position dependent trends, and those microwave signatures that were not separable by at least one standard deviation were regrouped into the associated major class.

All WMO classes and subclasses had distinct emissivity, backscattering coefficient signatures within the measured incidence angle range as reported in Hawkins et al. (1980). In addition, the rough and smooth subclasses of multi-year ice and second-year ice had marginally separable signatures under cold conditions. The microwave signatures of sea-ice were found to change with ambient temperature as reported in Hawkins et al. (1980) and Livingstone et al. (1980).

The remainder of this paper will concentrate on classification of sea-ice data from the Beaufort Sea under cold conditions. Sea-ice classification results from the other experiment regions are reported elsewhere (Livingstone et al., 1980).

Sea-Ice Classification by Backscattering Coefficient and Incidence Angle

Previous results of Parashar et al. (1977) and Gray et al. (1977a,b) showed that sea-ice under cold conditions could be classified into coarse ice classes using the angular dependance of σ°_{vv}. Parashar applied a Bayrian classifier to $\sigma_{vv}(\theta)$ data to demonstrate that seven ice types from water to multi-year ice could be discriminated with 67% accuracy and also that the coarser division; water, young ice, first-year ice and multi-year ice could be discriminated with at least 90% accuracy. Gray et al. (1977a,b) noted that for many ice types σ°_{vh} produced better class separation than σ°_{vv}. The CCRS Beaufort Sea data was assembled to form the feature space $\sigma^\circ_{hh}(\theta)$, $\sigma^\circ_{hv}(\theta)$, θ, where θ was the incidence angle. To test the sea-ice classification capabilities of this space, each event was expressed in the parametric form $\sigma^\circ_{hh}(\theta) \simeq A\ \theta \div B$, $\sigma^\circ_{hv}(\theta) \simeq C\ \theta \dagger D$ using best χ^2 straight line fits. The feature space was then represented by the two parameter planes A, B and C, D shown in Figures 1 and 2. The event clustering patterns in these planes indicate that neither $\sigma^\circ_{hh}(\theta)$ nor $\sigma^\circ_{hv}(\theta)$ is superior for sea-ice classification over the full range of ice types found in this data set. When both σ°_{hv} and σ°_{hh} combined, keeping track of the individual event mappings, only one point (2 coincident events) remains ambiguous (first-year rough ice/first-year smooth ice ambiguity). The event emissivities have been included in these figures as the data point grey scale and indicate the additional information provided by radiometric measurements.

Microwave results for sea-ice presented by Hawkins et al. (1980) show that all major sea-ice types found in the data (including young and new ice types) can be classified in the $\sigma^\circ_{hh}(\theta)$, $\sigma^\circ_{hv}(\theta)$, θ space with accuracies of 75% to 85% for ambient temperatures as warm as -5°C provided that the classification signatures used are matched to the temperature. The space classification potential begins to degrade for ambient temperatures in the -2°C to 0°C range.

Sea-Ice Classification by Backscattering Coefficient and Emissivity

An examination of the sea-ice signature data presented by Hawkins et al. (1980) show that the feature space defined by $\sigma^\circ_{hh}(\theta_0)$, $\sigma^\circ_{hv}(\theta_0)$, $\varepsilon_h(\theta_1)$ for fixed incidence angles θ_0 and θ_1 may have a greater classification potential than the $\sigma^\circ_{hh}(\theta)$, $\sigma^\circ_{hv}(\theta)$, θ space and is certainly simpler to implement. Table 1 shows the primary signature elements (excluding cross covariance terms) for the ice types found in the Beaufort Sea data set.

A "maximum a priori probability" (MAPP) classifier was constructed to test the fixed incidence angle space by selecting a training set of events from each ice class and subclass, decomposing these events to produce training vectors, and computing their class characteristic vector and covariance matrix. The scaled distance in this space between an "unknown" and the mean location for each class is computed (using the inverse of the class covariance matrices for scaling) and is weighted by the determinant of the class covariance. The unknown is assigned to the nearest class. Table 2 shows the classifier confusion matrix for a set of events of known ice type--not including the training set. Of the five major ice types found in this data set, grey-white ice has the lowest classification success rate (88%) as expected from Table 1. Ice islands are not shown in Table 2 but classification accuracies should be 95% as estimated from Table 1. The first-year ice subclasses can be resolved with sufficient accuracy to consider these as distinct classes . In general, upward classification errors are associated with ridges as suggested by Pearson et al., 1980.

When the ice classification potential of the $\sigma^{\circ}_{hh}(\theta_o)$, $\sigma^{\circ}_{hv}(\theta_o)$, $\varepsilon_h(\theta_1)$ space is examined for warmer conditions, it is found to remain unchanged down to ambient temperatures of 2° provided that the appropriate temperature dependent signatures are used (Livingstone et al., 1980).

In summary, for general application of microwave sea-ice classifiers two, four-dimensional feature spaces $\sigma^{\circ}_{hh}(\theta)$, $\sigma^{\circ}_{hv}(\theta)$, θ, T and $\sigma^{\circ}_{hh}(\theta_o)$, $\sigma^{\circ}_{hv}(\theta_o)$, $\varepsilon_h(\theta_1)$, T appear to be suitable. The detailed temperature dependence of σ°_{hh}, σ°_{hv}, ε_h is not known for most ice types (Hawkins et al. 1980) and further research is required in this area.

A preferred instrument package for operational implementation of this space would contain a sensor head composed of a dual polarized fixed incidence angle scatterometer bore sighted with a dual polarized fixed incidence angle radiometer on infrared radiation thermometer, and a small mini computer or a micro computor processor.

The optimum frequencies and incidence angles are not yet known.

References

(1) Parashar, S.K., R.M. Haralick, R.K. Moore, A.W. Biggs (1977) "Radar scatterometer discrimination of sea-ice types." IEEE GE-15, No. 2, pp. 83-87.

(2) Gray, A.L., J. Cihlar, S. Parashar, R. Worsfold (1977a) "Scatterometer results from shorefast and floating sea-ice." Proc. 11th Int. Symp. Remote Sensing Envir., Ann Arbor Mich., pp. 645-657.

(3) Gray, A.L., W.J. Ramseier, W.J. Campbell (1977b) "Scatterometer and SLAR results obtained over arctic sea-ice and their relevance to the problem of arctic ice reconnaissance." Proc. 4th Can. Symp. Remote Sensing, pp. 424-443.

(4) Hawkins, R.K., C.E. Livingstone, A.L. Gray, T.L. Wilkinson, K. Okamoto, L.D. Arsenault and D. Pearson. Single and Multiple Parameter Microwave Signatures of Sea-Ice. Presented at the 7th Canadian Symposium on Remote Sensing, Halifax, May 1980.

(5) Pearson, D., C.E. Livingstone, R.K. Hawkins, L.D. Arsenault, K. Okamoto, A.L. Gray and T.L. Wilkinson. Presented at the 7th Canadian Symposium on Remote Sensing, Halifax, May 1980.

(6) Livingstone, C.E., R.K. Hawkins, K. Okamoto, L.D. Arsenault, D. Pearson, T.L. Wilkinson and A.L. Gray. "The CCRS/SURSAT Active-Passive Experiment 1978-1980 - The microwave signatures of sea-ice types and features and their implication for remote sensing". Canada Centre for Remote Sensing report 1980. (in press)

Figure 1 A, B space cluster plot

Figure 2 c, d space cluster plot

Note:

Ambient temperature March 13, 1979 -32°C
Ambient temperature March 16, 1979 -28°C

Symbol Key: T_3 - Ice Island T_3, M - multi-year ice, S - second year ice,
FR - first-year rough ice, FS - first-year smooth ice,
L - Grey-white ice, G - grey ice.

Table 1. Sea-ice signatures at 45° incidence angle as measured with a 13.3 GHz fan beam scatterometer and a 19.4 GHz H-polarized radiometer in the Beaufort Sea, March 1979. Ambient temperature $-28^{\circ}C$ to $-32^{\circ}C$. $DR_{hv} = (\sigma_{hv}/\sigma_{hh})$ in dB.

T_B is the brightness temperature, and M and S indicate mean and standard deviation.

Ice Type / Parameter	Ice Island		Multi-year				Second-year				First-year				Grey-White		Grey	
			rough		smooth		rough		smooth		rough		smooth					
Statistic	M	SD	M	SD	M	SD	M	SD	M	SD	M	SD	M	SD	M	SD	M	SD
TB (K)	163	5.3	191	7.8	192	6.0	210	4.6	205	5.3	227	3.3	225	4.0	230	3.0	223	3.4
ε_h	.646	.023	.768	.035	.774	.027	.853	.020	.833	.024	.929	.015	.922	.018	.942	.013	.911	.016
σ°_{hh} (dB)	-5.0	1.2	-6.2	1.1	-6.8	1.1	-9.2	2.5	-9.3	1.8	-16.7	2.3	-18.8	1.4	-19.7	2.1	-11.7	1.5
σ°_{hv} (dB)	-8.6	1.6	-10.7	1.7	-11.5	1.6	-14.8	3.3	-15.3	2.1	-25.0	3.3	-28.1	1.8	-28.0	2.5	-25.8	2.8
DR_{hv} (dB)	-3.6	0.7	-4.4	1.1	-4.6	1.0	-5.6	1.0	-5.9	0.6	-8.3	1.3	-9.2	0.8	-8.3	1.4	-14.1	3.1

TABLE 2. CONFUSION MATRIX FOR THE MAPP SEA-ICE CLASSIFICATION FOR NON-TRAINING SET SAMPLES OF CLASSIFIED ICE.

TRUE CLASS \ ASSIGNED CLASS	MULTI-YEAR		SECOND-YEAR		FIRST-YEAR		GREY-WHITE	GREY	ACCURACY SUBCLASS	ACCURACY CLASS
	ROUGH	SMOOTH	ROUGH	SMOOTH	ROUGH	SMOOTH				
MULTI-YEAR										
ROUGH	184	4	4	10	0	0	0	0	91%	93%
SMOOTH	97	186	4	11	0	0	0	0	62%	95%
SECOND-YEAR										
ROUGH	3	0	41	5	0	0	0	0	84%	94%
SMOOTH	0	0	9	20	0	0	0	0	69%	>96%
FIRST-YEAR										
ROUGH	0	0	0	9	84	11	0	0	81%	91%
SMOOTH	0	0	0	0	9	35	0	0	80%	>97%
GREY-WHITE	0	0	0	0	3	5	60	0	88%	95%
GREY	0	0	0	0	0	0	0	15	>93%	>93%

ICE ISLANDS WERE NOT INCLUDED IN THE CLASSIFIER TEST RUN BUT SIGNATURE SEPARABILITY ESTIMATES PLACE CLASSIFIER ACCURACY AT >95%

SECTION 5.6

WEST GREENLAND SEA ICE EXPERIMENT SURSAT REPORT NO.1

Gray, L., P. Gudmansen, S. Overgaard, N. Skou, F. Søndergaard Pedersen

West Greenland Sea Ice Experiment

SURSAT Report No. 1

by

L. Gray, P. Gudmandsen, S. Overgaard
N. Skou, F. Søndergaard Pedersen

R 219 November 1979

1g/90

List of contents

	Acknowledgements	Page 0
1.	Introduction	– 1
2.	Aircraft and sensors	– 3
2.1	CCRS Convair 580	– 3
2.2	US Naval Ocean Research and Development Activity (NORDA) P-3	– 5
2.3	CCRS Falcon	– 6
2.4	Royal Danish Air Force (RDAF) C-130	– 6
2.5	Twin Otter	– 6
3.	Surface measurements	– 7
4.	Test Areas and Figures	– 9
5.	Discussion of the results	– 13
5.1	TUD Real Aperture Radar	– 13
5.2	Synthetic Aperture Radar	– 14
5.3	Comments on the relative merits of SAR and SLAR for ice reconnaissance	– 15
5.4	The Detection of Icebergs with SAR or SLAR	– 16
5.5	13.3 GHz Scatterometer Results	– 17
5.6	19.4 GHz (H, 45°) Profiling Radiometer Results	– 20
5.7	Imaging Radiometer Results	– 21
6.	Conclusions and Recommendations	– 24
7.	References	– 27

Acknowledgements

We would like to thank the scientists and personnel from the following agencies for their valuable contributions to the success of the West Greenland Sea Ice Experiment.

Danish Meteorological Institute, Greenland Ice Services (for providing the Twin Otter Aircraft).

Royal Danish Air Force, Luftgruppe Vest (for providing the C-130 aircraft).

Island Command Greenland (for the participation of the Frigate "Ingolf").

National Aeronautics and Space Administration, Langley Research Center, Hampton, Virginia (for providing the 19.4 GHz radiometer).

Canada Centre for Remote Sensing, Ottawa, Canada (for providing the Convair 580 and Falcon and for the processing of the 13.3 GHz scatterometer and the 19.4 GHz radiometer data).

Intera Environmental Consultants, Ottawa and Calgary, (for the management of the Convair 580 component of the SURSAT project and for providing the sensor operators for both CCRS aircraft).

Innotech Aviation Ltd., Ottawa and Montreal (for providing the air crews for both the CCRS aircraft).

Environmental Research Institute of Michigan (for providing, under contract to Intera, operator and maintanance support for the X/L SAR and for processing the imagery).

Scott Polar Institute, Cambridge, England (for participation in the Surface truth programme).

Naval Ocean Research and Development Activity, Mississippi (for participating in the experiment with the P-3 aircraft and for providing a copy of all their results).

United States Air Force, Søndrestrøm Air Base (for providing the services of the base for the participating agencies).

1. Introduction

On 10 April 1979 five aircraft a helicopter and the Danish vessel "Ingolf" participated in a very successful Danish, Canadian, American and British remote sensing experiment. The initiative and planning for the West Greenland Sea Ice Experiment had been carried out by the Technical University of Denmark in order to study and demonstrate the capabilities of different microwave remote sensors to provide information of the extent, type and thickness of sea ice, particularly to those concerned with shipping.

This experiment was unique in a number of ways: Firstly, it represented the first time that imagery from a high resolution, calibrated, multifrequency imaging radiometer could be compared with imagery from a high resolution dual frequency, dual polarized radar as well as visible, infra-red and profiling active and passive microwave sensors. Secondly, the majority of the experiments designed to study the capabilities of microwave sensors for ice mapping have been undertaken under different conditions and in different regions of the Arctic, e.g. in the Beaufort Sea during March and April. This experiment represents one of the few undertaken in the marginal ice zone under conditions typical of those which can be encountered by shipping along the west coast of Greenland. This is, of course, important to both Canada and Denmark as being the proposed route for the transport of natural resources, even liquified natural gas, out of the Canadian Arctic. To undertake such shipping safely and efficiently it will be necessary to support the activity with information which can be obtained only by all weather, microwave remote sensing. Further, it is planned to obtain and study imagery from four satellites; LANDSAT, NIMBUS-7, TIROS-N and METEOR. The data obtained by the aircraft, helicopter and ship provides the kind of information necessary to evaluate the new sensors on the satellites, e.g. the scanning multichannel microwave radiometer (SMMR) on board NIMBUS-7. Satellite images can also provide a perspective and view which helps with the analysis of the low altitude data. Unfortunately, no satellite data has been made available to date.

Canada participated in the West Greenland Experiment by providing the CCRS (Canada Centre for Remote Sensing) Convair 580 which contains a sophisticated X/L band dual polarized synthetic aperture radar and other microwave sensors and cameras. The West Greenland Experiment then became an element in the larger Canadian SURSAT project. The main objective of the SURSAT project was to evaluate in detail microwave remote sensing systems in order to recommend to the Canadian Government which elements of Canadian surveillance and remote sensing needs could be accommodated by suitably equipped aircraft and which elements could be accommodated by suitably equipped satellites.

A P-3 aircraft belonging to the US Naval Ocean Research and Development Activity (NORDA) also participated in the West Greenland experiment and data are being exchanged between the US and Danish scientists. Unfortunately, the NORDA data were received too late to be included in this report. British researchers involved in ice flexure studies using a Sikorski S-61 helicopter, also provided some useful ground truth information.

The experiment date was selected based on the following considerations: sea ice maps of Davis Strait for the last ten years showed an average maximum extent to the latitude of Holsteinborg (67^{O}N, 54^{O}W) to occur in the beginning of April. An experiment area west of Holsteinborg gives a minimum distance from the shore and from the airport in Søndre Strømfjord (67^{O}N, 50.5^{O}W). LANDSAT would cover the area west of Holsteinborg in the period 9-13 April and, finally, the scanning microwave radiometer on NIMBUS-7 is only operated on even Julian days, 10 April being the 110th Julian day.

Two alternate flight line patterns were proposed in the original Experiment plan(Gudmandsen and Overgaard, 1979) depending on the ice conditions at the time of the Experiment. The patterns were estimated to be well within the ice cover at its maximum extent in Davis Strait in the beginning of April. However, 1979 was an exceptionally light ice year and the day prior to the flight a decision, contrary to that originally planned, was made to move the Experiment site more to the north and west. The experiment area and the cross pattern of the N-S and E-W. SLAR swaths are shown in Figure 1.

The data acquisition flights took place almost simultaneously, as planned, with the various aircraft operating at different altitudes. The weather was fairly good although the cloud ceiling was as low as 1000 m over parts of the experiment area. Temperatures at the ice surface were just below freezing and it was clear, from the ground truth reports, that the ice had undergone significant melting and decay.

The various aircraft and their sensor complements are described in the following section. Details of the surface measurements and ice condition are given in section three and examples of coincident sensor coverage are described in section four. Discussion of the results and conclusions are given in section five and six. A great deal of valuable data were obtained in this experiment and it warrants careful analysis. Because much of the data have only been received recently in Denmark this report represents an initial, interim report.

2. Aircraft and sensors

2.1 CCRS Convair 580

The Convair 580 aircraft is a twin engine turbo-prop, owned and equipped by the Canada Centre for Remote Sensing with a synthetic aperture radar, a scatterometer, a profiling radiometer, a mapping camera and a side-looking 35 mm camara. A summary of the specifications of these sensors is given below. Two LTN-51 inertial navigation units are used, one for navigation and SAR motion compensation and the other is interfaced to and recorded by a digital data acquisition system used for the other aircraft sensors.

(a) The X/L Synthetic Aperture Radar (SAR)

Frequencies:	1.2 and 9.3 GHz
Antennas:	dual linear polarization for each frequency
Average power:	5 Watts (X-band) and 25 Watts (L-band)
Slant range:	5.4 km
Ground range:	Dependent on altitude, approx. 9.4 km at 18 000 feet
PRF:	Approx. 3.4 kHz transmit
Resolution:	Approx. 3 m
Altitude:	18 000 feet (5 500 m) in this experiment
Incidence* angles:	0° at near edge of the imaged swath decreasing rapidly at first and equal to approximately 58° at the far edge of the swath. Because of the image distortion due to the slant range presentation and because of

---

* The term incidence angle is used in this report to describe the radar look angle with respect to the vertical. The depression angle is 90° minus the incidence angle and this term is also used in the discussion of some of the SLAR results for convenience and clarity.

the antenna pattern effects, it is normally difficult to interpret the imagery for incidence angles less than approximately 20°.

Output: The SAR signal film is processed optically onto 70 mm transparency film. Consequently, for any flight line four images are obtained corresponding to a like and cross polarized channel for each frequency.

(b) The Ku-band Scatterometer

Frequency: 13.3 GHz

Antennas: Two linearly polarized transmit and two similar receive antennas

Average Power: 2 Watts

Resolution: Approximately 20 metres at an altitude of 1 500 feet

Incidence angle: 8° to 55° (35° to 82° depression angle)

Output: Normalized backscattering coefficients as a function of incidence angle for a contiguous sequence of ground footprints directly beneath the aircraft.

(c) The K-band Radiometer

This system belongs to the NASA Langley Research Centre (LaRC) and was loaned to CCRS as part of a co-operative study on the active and passive signatures of sea ice.

Frequency: 19.4 GHz

Bandwidth: 500 MHz

Integration time: Approx. 0.4 sec

Incidence angle: 45°

Antenna: H-polarized microwave horn, beamwidth approximately 5°

Resolution: Approx. 80 m at 1 400 feet

Calibration: The system is basically a Dicke radiometer with two reference temperatures and eight thermistors which are used to measure the physical temperature of the antenna and various sections of the waveguide receiver. Knowing the waveguide losses, the antenna brightness temperature is calculated. Unfortunately, the results obtained for a clear sky temperature, smooth water and sea ice results all appear to be about 30 K high indicating a change in calibration after shipment from NASA. The ordinate scale in the figures illustrating the radiometer results has not been corrected for this error. In the text of the report 30 K has been subtracted from the experimental results in order to give brightness temperature values consistent with other work. The relative measurements appear to be quite accurate.

(c) RC-10 Mapping Camera
Lens: 3.45 inch super wide angle lens
Film: 2402 black and white film
Output: 9 x 9 inch negatives with, in this experiment, 20% overlap between frames.

(d) Olympus OM-2 35 mm Camara
Film: Kodacolour colour negative film
Lens: Normal 50 mm lens

2.2 US Naval Ocean Research and Development Activity (NORDA) P-3

This aircraft is a four-engined long range turbo-prop equipped with the following sensors and an LTN-51 Navigation System.

(a) RC-8 Mapping Camara
Lens: 6.00 inch focal length
Film: 2402 black and white film
Output: 9 x 9 inch negatives with 20% overlap at 5 000 feet altitude.

(b) AN/AAR-35 Infra-red Line Scanner

This is the military designation for a Reconofax IV scanner operating in the thermal infra-red region between 8 and 14 microns.

(c) Spectra Physics Laser Profilometer

This system profiles the surface of the ice beneath the aircraft. The accuracy apparently depends on the medium being profiled and, at best, is approximately 6 inches.

2.3 CCRS Falcon

The Falcon is a twin engined executive jet modified for remote sensing and equipped with the following sensors:

(a) Daedalus dual channel infra-red (8-14 µ) and ultra-violet line scanner.
(b) Wild RC-10 Camera
Lens: 3.46 inch super wide angle lens
Film: 2402 black and white film.

2.4 Royal Danish Air Force (RDAF) C-130

This long range four engined transport aircraft is normally used for fisheries patrol and was used in this experiment as a platform for the imaging radiometer. The scanning antenna for the radiometer is mounted on a cargo pallet and during data acquisition, this pallet is fixed to the ramp and the antenna views out the open door. Navigation data is obtained from the aircraft's inertial navigation system.

Both the radiometer system and colour images made from a TV screen are described in a report by Skou (1979). A summary of the radiometer specifications of this system is given below and it is described in more detail by Skou (1978).

Frequencies: 5., 7 and 34 GHz
Bandwidths: 0.5, 1.0 and 1.0 GHz respectively
Antenna: 1 m scanning parabolic reflector viewed by three horns
Incidence angle: 50°
Scan angle: ±25°
Polarization: Vertical
Resolution: at 2 000 metres altitude
5 GHz: 320 x 496 m
17 GHz: 94 x 146 m
34 GHz: 47 x 72 m
Swath width: 2 000 m

2.5 Twin Otter

This aircraft is used for ice reconnaissance off the coast of Greenland by the Ice Patrol of the Danish Meteorological Institute, It is equipped with an Omega navigation system which is interfaced with the SLAR data annotation system. The specifications for the SLAR system and the images acquired on the 10th April 1979 are given in the report by Søndergaard (1979). The SLAR specifications are summarized below.

Frequency: 9.4 GHz
Resolution: Range 10 m or 100 m
Azimuth 30 m/naut. mile
Antenna: Dual horizontal polarization system which can be used to map the left or right of ground track.
Output: 6 inch dry silver paper (uv paper in present experiment)
Swath width: 20 naut. miles
Navigation infor. Latitude and longitude from the OMEGA system are printed on the film
Altitude: 5 000 feet (10th April)
Incidence angles: 82^{o} at 5 naut. mile (8^{o} depression angle)
85^{o} at 10 naut. mile (5^{o} depression angle)
88^{o} at 20 naut. mile (2^{o} depression angle).

3. Surface measurements

As part of the experiment it was planned to carry out detailed measurements of three sets of parameters particularly at the cross over region of the N-S and E-W flight lines. These were:

(1) Parameters related to the physical properties of the sea ice
(2) Measurements of the floe flexure and heave response to the swell propagating through the floe.
(3) Measurements of meteorological parameters.

The ground truth party was based in Egedesminde on the west Coast of Greenland close to the experiment area.

During the helicopter flight to the test area on 10 April in the morning it became apparent that the ice was in a decayed condition. Three landings were made, two times on the same floe and the third time on a floe further to the west. These floes are marked as X and Y on the SLAR image shown in Figure 5. Samples of the firn and ice were collected from the two floes and the surface temperature was measured on the second floe. On one touch down water came through small holes in the ice. It was clear that the ice was too rotten to carry out the detailed floe measurements and the original ground truth plan was abandoned. On the flight back to Egedesminde samples of firn and ice were collected from fast ice between some small islands south of Egedesminde.

Both floes examined consisted of approximately 10 cm of snow on top of approximately 20 cm of ice as shown in Figure 2. The top of the snow layer was dry but the snow-ice interface was wet. Two samples, the upper one and two in Table 1, were taken from the first floe (X in Figure 5). Sample one was taken from the upper 5 cms of snow and sample two was taken from the upper 5 cm of ice. Five samples were taken from the second floe (Y in Figure 5), two in the snow layer, one from the snow-ice interface and two in the ice. The two floes were quite similar in snow cover and ice thickness. The positions of the samples are shown approximately by the two profiles in Figure 2. The temperature measurement on the second floe was an average from the upper 5 cm of snow as shown diagrammatically in Figure 2. These results together with two measurements from shore-fast ice are summarized in Table 1. The salinity values were calculated from conductance values corrected to 25°C using the standard relation *

$$S(^{o}/oo) = -0 \cdot 08996 + 28 \cdot 2972R + 12 \cdot 80832R^2 - 10 \cdot 67869R^3 + 5 \cdot 98624R^4 - 1 \cdot 32311R^5$$

where R is the ratio of the sample conductivity to the conductivity of sea water (49.71 mS at 25°C) at a temperature of 25°C.

The pH values and the salinities of the ice samples indicate that the ice is melting and had been penetrated with sea water. The results for the firn layer show low salinities and neutral pH values, but the sample of the snow-ice interface (No. 3, floe Y) shows the presence of sea water. The measured temperature of the surface layer of floe Y was -2.9°C. The fast ice samples showed a lower salinity and a slightly acid pH value for the snow layer.

---

* International Oceanographical Tables, Vol. 1, 1971, National Institute of Oceanography of Great Britain and UNESCO.

Table 1

Sample	Position	pH	Conductivity at 25°C	Salinity
1	68°17'N	7.1	1.21 mS	0.61 °/oo
2	56°12'W	7.9	32.25 mS	21.65 °/oo
1		7.1	0.319 mS	0.09 °/oo
2	68°13'N	7.0	0.389 mS	0.13 °/oo
3	56°37'W	8.0	26.75 mS	17.62 °/oo
4	(floe Y)	8.1	28.75 mS	19.08 °/oo
5		8.0	33.84 mS	22.83 °/oo
1 (snow)	68°30'N	6.8	0.244 mS	0.04 °/oo
2 (ice)	52°57'W (fast ice)	8.0	27.55 mS	18.20 °/oo

4. Test Areas and Figures

The cross over region of the N-S and E-W lines has been selected as the primary test site for this report because the degree of overlap between the various flight lines of the different aircraft is greatest in this region. Further, many of the ice conditions and types encountered in the total experiment area can be observed close to the cross-over region.

Figure 3a is a photo mosaic made from five frames of the RC-10 photography acquired by the Falcon on the N-S line. This area has been imaged completely by the SAR and partially by the imaging radiometer, the line drawn along Figure 3a delineates the upper edge of the radiometer image. The large floe, labelled A, is approximately 2.2 x 2.8 km in size and appears to be typical of the first-year floes in the region, consequently the snow and ice conditions described in section 3 probably existed also on floe A. Adjacent to the north-eastern (lower right) edge of floe A is an area of rafted nilas, this is thin ice about 5 cm in thickness which bends easily and rafts under pressure. In the northern (right hand) part of Figure 3a the ice has been broken into small ice floes and ice cakes 10-30 m in diameter by the action of waves and swell. This condition is very common close to the edge of the pack ice in the marginal ice zone. Closer to the ice-water boundary at the east end of the east-west line the average size of the ice cakes decreases to approximately 5-10 m. There is some nilas present among the small ice floes and cakes in Figure 3a together with a small percentage of open water.

Figure 3b illustrates the thermal infra-red imagery acquired simultaneously to Figure 3a by the Falcon. The air temperature was below freezing by a few degrees as the top of the snow is clearly colder (whiter) than open water or new ice. The snow temperature measured from one of the larger floes was -2.9°C. The infra-red imagery does not show any thermal contrast between open water and nilas which has not been rafted.

Figure 4 is an X-band, HH-polarized SAR image which includes the same scene as Figures 3a and b. This image was obtained by the Convair on its high altitude N-S pass over the cross over region. The nadir line is on the top of the image and the depression angles are marked on the left. Because of antenna side lobe effects and image compression due to the slant range presentation it is difficult to interpret the X-band imagery for depression angles greater than 70° (equivalent to incidence angles less than 20°). It should be noted that the apparent brightness of the image of the large floe A is the same as the small broken floes and ice cakes further to the north (right) in the image. Further, the texture (the variability both spatially and radiometrically of the image brightness on a scale somewhat larger than that of the radar resolution) is very similar for the two regions. It is probable that at some stage in the history of the large floes that ice cakes, brash ice, etc. became frozen together to form a much larger floe. This may be part of the reason why the two regions in the SAR image have similar brightness and texture.

Figure 6 is a SLAR image of the cross over region of the N-S and E-W lines. In this image north is to the top of the image and the white lines form a grid pattern with a 5 nautical mile separation between lines. The ice floes on which the helicopter landed are marked as X and Y and the limits of the N-S and E-W SAR swaths are also marked.

Figure 6 is a composite image of the three frequencies of the imaging radiometers. The top image is the 34 GHz channel, the middle image is the 17 GHz channel and the lower image is the 5 GHz channel. Figure 6 is actually a mosaic of three colour photographs of a seven-colour TV-display. It should be emphasized that the sampling rate is the same for all three frequencies and was selected so as not to undersample the 34 GHz data. Consequently, the 5 GHz channel is oversampled and the apparent "resolution" in the outline of the different colours is somewhat misleading. North is to the right in Figure 6 and the area imaged is very similar to that illustrated in Figure 3. The outline of floe A can be seen in either the 5 or 17 GHz images in the middle of the left one third of the images. The dark blue in the 5 GHz image corresponds quite well to the outline of the nilas in Figure 3a. The differences between the three frequencies are discussed more fully in the next section, but in this presentation the red colour on the 34 GHz image is indicative of essentially 10/10 ice cover, while the red on the 5 GHz image delineates the thicker, snow covered ice. There is a relatively small difference (about 10 K) between the 5 GHz (V, 50°) brightness temperature of the large floe 'A' and that of the wave broken ice cakes and small floes. However, the nilas is colder radiometrically, at 5 GHz, by approximately 50 K. It can also be seen that the difference between the 5 and 34 GHz brightness temperature for the thinner ice can be as much as 50 K. In Figure 6 the limited seven-colour TV-presentation does not do justice to the radiometric resolution of the radiometer. Further, the choice of 10 K steps for the colour presentation while displaying fairly well the range of the 5 GHz results, does not illustrate adequately the radiometric or spatial resolution of the 34 GHz channel.

Figure 7a illustrates part of a photo mosaic of the Convair low altitude (400 m) E-W pass close to the cross-over region. Regions 1, 2 and 3 in Figure 7a correspond respectively to open water (possibly with some grease ice), a snow covered first-year ice floe (the floe immediately underneath the upper X in Figure 4) and nilas. The approximate width of the scatterometer beam (at nadir) is shown by the dotted black lines on the photograph. The radiometer beam width is approximately twice this size. Figure 7b is a comparison of the 13.3 GHz HH backscatter at an incidence angle of 38°(fore) with the H polarized 19.4 GHz brightness temperature at an incidence angle of 45° (fore). Note that the 19.4 GHz (H. 45°) brightness temperature and the 13.3 GHz (HH, 38°) backscatter are not given in absolute terms, the brightness temperature can be estimated by subtracting 30 K from the ordinate scale and the relative backscatter can be estimated by using the fact that one small division is equivalent to 2.5 dB. Because the incidence angles are not equal the scatterometer "sees" a feature approximately one second after the radiometer. The open water in Figure 7a exhibits very low backscatter and it appears that no capillary waves were formed on the surface of the water due to the very low wind speed and, possibly, the presence of grease ice. The 19.4 GHz (H, 45°) brightness temperature for region 1 is approximately 130 K. The high brightness temperature (about 240 K) for the first-year floe (2) adjacent to the open water is typical of some of the larger floes. Adjacent to this floe is an area of rafted nilas (3) which is colder radiometrically by approximately 50-60 K but which shows a comparable value for the 38° backscatter. More complete scatterometer results for the aft beam are illustrated in Figure 7c. In this plot each trace represents one of six incidence angles, these are given on the right hand side of Figure 7c. The similarity in backscatter between the larger floe (2) and the rafted nilas (3) can be seen. Only the open water can be immediately observed as an area with significantly different backscatter. It should be remembered, however, that the scale on these plots is much larger than is normally presented as black to white on a SAR image (possibly 15-18 dB). In fact, the areas of nilas do normally appear darker in the SAR imagery than the first-year floes, unless there is a large degree of rafting.

Figures 8a, b and c show another example of the combined radiometer and scatterometer results. Region 1 is a snow covered first-year ice floe and region 2 is grey ice with much less snow cover. The 19.4 GHz (H, 45°) brightness temperature of the grey ice is significantly lower than that of the first-year ice, however, the 13.3 GHz (HH, 38°) backscatter is approximately the same. By inspection of Figure 8c, however it can be seen that the near nadir backscatter, particularly the 8° trace, shows an increase in backscatter by 8-10 dB for the grey ice in comparison to the snow covered first-year ice.

Figure 9 summarizes the angular variation in 13.3 GHz (HH) backscatter for some of the ice conditions observed in the E-W line. The curves have been obtained by averaging sections of the plots such as in Figures 7c and 8c. Currently, work is underway at CCRS and NASA LaRC to try to improve the absolute calibration of the CCRS scatterometer. Preliminary results of this work indicate that the results given in Figure 9 may be a few dB too large, however, the relative values are reliable. The backscatter curves for the open water and the swell broken ice cakes (very close pack) were estimated from the results obtained at the east end of the E-W line. The two curves for first-year ice floes show some of the variability in backscatter from ice floes that appeared visually similar. In Figure 9 the backscattering curve for the grey ice was estimated from region 2 in Figure 8a.

Figures 10a and b illustrate SLAR images of an area of the swell broken ice cakes close to the ice-water boundary at the east end of the E-W line. Figure 10a was obtained when the Twin Otter was flying east and Figure 10B was obtained when the aircraft was flying west. Consequently, the aircraft track is to the left in Figure 10a and to the right in Figure 10B. Figures 11a and b are tracings of the bright targets from the original imagery of this region and interpreted as being icebergs. Some comments on the detectability of icebergs as a function of incidence or depression angle are included in the section 5.1.

5. Discussion of the results

5.1 TUD Real Aperture Radar

This radar is under evaluation by the ice reconnaissance group of the Greenland Ice Services. The SLAR system has shown that it can map ice-water boundaries and identify the edges and shapes of larger floes. In general this system has performed quite adequately in estimating ice extent and ice concentration. In this experiment, areas of smooth new ice or open water could often be distinguished in the ice pack. The sea ice imagery obtained previously (Skou and Søndergaard, 1979) with the TUD SLAR mounted on an RDAF C-130 demonstrates the capability of this system over different ice conditions from the current experiment. Further, improvements in the imagery due to the more stable platform (C-130 in comparison to the Twin Otter) can be seen.

Despite the limitations of the SLAR some useful, previously unobserved results were obtained related to the detectability of icebergs in a sea ice background. Figures 10a and b, as described in section 4, show approximately the same ice region close to and including part of the edge of the pack ice. The ice water boundary is visible on the lower right of each image. The aircraft flew in the opposite direction for each image and, therefore, the depression angles are reversed. Figures 11a and b are tracings of the approximate positions of the icebergs. In both images it can be seen that no icebergs are detected with a depression angle greater than approximately 6° - 8° despite the fact that the other image, particularly Figure 11b, shows that icebergs were present in the imaged swath. It is interesting to note that icebergs can still be detected at far range (approx. 20 naut. miles) although the system noise is now comparable to the sea ice backscatter signal and the azimuth resolution is approximately 600 m which is undoubtedly larger than most of the icebergs detected. Consequently, the SLAR imagery has demonstrated the importance of depression angle in the detection and tracking of icebergs in a sea ice background. Further discussion of the detectability of icebergs with SAR and SLAR is given in section 5.4.

5.2 Synthetic Aperture Radar

Only the X(HH) channel imagery has been studied, further work on the total data set will include a more detailed comparative study of the four channels Much more detailed information can be gained from the SAR than from the SLAR because of the higher spatial and radiometric resolution. However, it should be remembered that the SAR is a high resolution (approx. 3 m) research and development radar which images a much smaller swath (5.4 km in slant range) than the TUD SLAR.

The ice-water boundary can be seen clearly in the X(HH) SAR image shown in Figure 4. The small ice floes and ice cakes (approx. 5-10 m) making up the edge of the pack could not be individually resolved by the SAR. The average size of the swell broken fragments increased with distance from the eastern edge of the pack, however, even much larger ice floes were not individually resolved unless surrounded by open water or nilas. The average X-band image brightness and texture from the wave and swell broken ice cakes and small floes was comparable to that obtained from the much larger snow covered, first-year ice floes. This may be related to the origin of the larger floes in that they may have formed through the freezing together of ice cakes and small floes. New ice (nilas) adjacent to the larger floes was normally darker in image tone than the first-year ice but brighter than open water. This observation depends, of course, on the wind speed as well as the extent of the rafting of the thin ice. The nilas may have formed during the nights immediately preceeding the experiment. The scatterometer data indicated that capillary waves were not present on some of the small leads, consequently there would be essentially no backscatter from such a surface. The ship "Ingolf" reported no wind, however, the scatterometer data for the open water adjacent to the ice edge showed that there was sufficient wind (a few knots) to excite capillary waves.

On some of the imagery brash ice adjacent to the larger floes was brighter in tone than the floes themselves. As long as the adjacent ice is slightly brighter or darker it is normally possible, through the good spatial resolution of the SAR to delineate individual ice floes a few hundred metres across. The ability to differentiate two regions on a SAR image depends, of course, on the difference in average brightness, the size of the regions and the texture of the image making up the two regions.

5.3 Comments on the relative merits of SAR and SLAR for ice reconnaissance

At present it appears that only real aperture side-looking radars are used operationally for civilian ice and coastal reconnaissance: (US and Canada; APS 94 D, USSR; "Toros" system, Denmark; TUD SLAR, Sweden; Ericsson SLAR). While it is clear that synthetic aperture radars could be used for these purposes it is not clear that the additional complexity, cost and processing problems are justified in terms of additional information. From a comparison of the data from the TUD SLAR and the Canadian eastern Arctic X-L SAR data the following points are pertinent.

(a) The high spatial resolution of the SAR does not appear to be necessary in terms of estimating ice extent.

(b) The high spatial resolution possible with a SAR in comparison to a SLAR will be helpful in identifying and estimating the percentage of different ice types in an ice cover. For example, a SAR may allow the detection of relatively small multiyear ice floes (Ketchum, 1977) which would be impossible with a SLAR system. Further, the high spatial resolution of a SAR may allow the observation of image patterns indicative of ice type and thickness e.g. rafting and ridging patterns.

(c) Normally, ice concentration can be estimated using a SLAR. It is possible, however, that the value for the ice concentration for a very loose pack situation would be an overestimate if the average floe size were smaller than the system resolution. Careful inspection of the imagery will usually reveal this situation (Skou and Søndergaard, 1979).

(d) While either a SAR or SLAR operating at low depression angles will be reasonably successful in mapping large icebergs in open water or pack ice it is probable that a SAR will be required to detect smaller icebergs and bergy bits in sea ice. It is not known at present how successful this will be.

(e) With good engineering it is possible, with SAR techniques to not only improve the resolution at far range but also the signal to noise ratio. Signal fall off at far range is a problem with most SLAR's.

More experience and evaluation with both types of imagery in different conditions is necessary before more detailed comparisons can be made.

5.4 The Detection of Icebergs with SAR or SLAR

It has already been shown (section 5.1) that the SLAR can detect icebergs in sea ice better with smaller depression angles (less than about 8°) than at larger values. Inspection of the SAR imagery shows that the detection of icebergs is possible at larger depression angles, however, there is often a small contrast between the iceberg and the surrounding ice.

A comparison with other work is useful: It has been observed by Ketchum (1977) that icebergs in sea ice can be difficult to detect with a SAR. This was true despite the fact that the sophisticated US military X-band SAR used in the mission had a resolution many times smaller than the icebergs observed on the aerial photography but which were difficult to identify on the SAR imagery. The example shown in Ketchum's (1977) report was observed in Kennedy Channel and it demonstrates that the iceberg radar signature can be less bright than small multiyear floes in the region close to the iceberg. Ketchum's observation indicates that the detection of icebergs cannot be achieved by high resolution alone. From the radar shadow information and the nature of the sea ice imagery it is clear that Ketchum's SAR imagery was obtained from relatively high altitude and that the depression angles were not less than 10° for any of the imagery. As part of the SURSAT Convair 580 Canadian eastern Arctic Sortie, imagery was collected along the west coast of Greenland in areas where there were many icebergs. By comparison with visual imagery it has been shown (Kirby and Lowry, 1979) that particularly the X-band data could be used to detect the larger icebergs in a sea ice background. Other work still in progress has shown, however, that icebergs in the size range from 10 m to 100 m are much more difficult to detect reliably from high resolution steep mode SAR imagery. The detection of the larger icebergs depended on the ability of the interpreter to see and recognize the target outline as being characteristic of an iceberg rather than these being a high backscatter contrast between the iceberg and the sea ice.

From a simple consideration of the shape and size of icebergs and the fact that the backscatter from the surrounding sea ice will fall off with decreasing depression angle θ one would expect that the contrast (or "signal to clutter radio") to increase with decreasing depression angle for angles less than approximately ten degrees (Rawson et. al. 1977, Gray et. al. 1979). The inverse sin θ angular dependence of the Rayleigh roughness criterion reinforces the belief that at small depression angles ($\theta < 5^{\circ}$) the bright regions in a SAR or SLAR image will correspond more with the larger features (e.g. ridges, icebergs, bergy bits) than would be the case at larger depression angles ($\theta > 10^{\circ}$). This effect has been observed previously in a study of X-band SLAR and scatterometer results from Beaufort Sea ice (Gray et al. 1977a). Recently an experiment with the SAR on the Convair 580 has been undertaken in Melville Bay in an attempt to resolve this question.

5.5 13.3 GHz Scatterometer Results

Because SAR and SLAR imagery is normally not calibrated it is impossible to do more than compare relative brightness along one piece of imagery. Even relative brightness may be misleading in terms of relative backscatter unless one is certain of the system and processing gain adjustments, films used etc. It is only with a calibrated system, such as scatterometer, that one can make a quantitative comparison of the backscatter between one area and another or between one flight and another. If backscatter was a good indicator of ice type it is possible that future imaging systems could incorporate some measure of absolute calibration * and, possibly, automated classification. It is clear, however, from previous scatterometer work (Gray et al., 1977b), steep mode SAR imagery (Ketchum 1977 and 1978) and small depression angle SLAR imagery (Dunbar and Weeks, 1975) that in areas in the marginal ice zone the backscatter at one incidence or depression angle is not a unique indicator of ice type. In the Beaufort Sea, however, in winter or spring the 10-18 GHz backscatter at

---

* A calibration system is being implemented on the X-L SAR.

depression angles greater than 10° does appear normally to allow a differentiation between old and first-year ice types (Parashar et al. 1975, Gray et al. 1977a, and Onstott et al. 1978). Interpretation of sea ice imagery depends, in general but particularly in the marginal ice zone, on an appreciation of the pattern of image brightness as well as the brightness itself.

The scatterometer measurements as a function of incidence angle are important for three reasons:

(a) To help establish an understanding of the backscatter phenomena itself and its relation to ice properties.
(b) To provide the magnitude and dynamic range numbers necessary for the design of satellite ice mapping radars.
(c) To measure the signal to clutter ratio of targets as a function of incidence angle; again this information is useful for the design of satellite SAR systems.

Only the like polarized HH scatterometer data has been analysed for this report. A more complete statistical analysis of this and the other SURSAT Arctic sea ice data, together with a cross correlation of the scatterometer data with the 19.4 GHz (H, 45°) radiometer data will be performed with CCRS and NASA Langley Research Center.

The largest values for the backscatter coefficient at the larger incidence angles (>40°) were observed for the ice at the ice-water boundary at the east end of the E-W line. This was the very close pack, swell broken ice cakes which were typically 5-10 m in diameter. The average backscatter decreased slightly (by approx. 2-4 dB) for the larger ice cakes and floes further to the west: Figure 9 includes the backscatter curve for the swell broken ice cakes and for two of the larger floes close to the cross over region. The two scattering curves were selected to illustrate the fact that there was some variation between different floes. It was observed in some cases that those floes which had a lower than average backscatter at larger incidence angles often had larger than average values for angles close to nadir. Further, the ice floes with high backscatter close to nadir (incidence angle = 8°) often exhibited lower values for the 19.4 GHz (H, 45°) brightness temperature. For example, the 19.4 GHz (H, 45°) brightness temperature of floe 2 in Figure 9 was approximately 30 K lower than that of floe 1 in Figure 9. The backscatter curve for the grey ice (region 2 in Figure 8) also shows a higher value for the near nadir (8°) backscatter than the first-year ice. The 19.4 GHz (H, 45°) brightness temperature of this ice is lower by approximately 40-60 K when compared to the first-year ice. The possible explanations for the changes in brightness temperature and backscatter are discussed more fully in the following sections, however, one possible explanation for the high near nadir backscatter and low emissivity for the almost snow free grey ice is that the upper ice surface was quite wet and, therefore, represented a more reflective surface. The complications arising from the snow on the first-year ice are not understood as yet.

The backscatter curve for the open water was obtained by averaging some of the data at the east end of the E-W line. While the ship "Ingolf" reported no winds the scatterometer data shows that there was sufficient breeze to excite small capillary waves. The backscatter from open water will, of course, be much higher in strong winds (see eg. Jones et al., 1977) and therefore at small incidence angles, such as will be used by satellite SAR's, there will not be the usual SAR image interpretation key that open water will appear dark (low backscatter) in comparison to sea ice.

It is interesting to note that the average 13.3 GHz (HH, 45°) backscatter data obtained for multiyear ice in the Beaufort Sea was larger than that for any of the ice conditions observed in the E-W flight line. Also, some of the first-year ice forms observed in the Beaufort Sea are comparable to eg. floe 1 in Figure 9. More comparative work, including the statistics of the backscatter for particular ice types, is being completed, however, our work to date shows that very different first-year ice conditions and thicknesses can have comparable average backscatter. The analysis of the recent series of SURSAT experiments in the Beaufort Sea, in the eastern Canadian Arctic and off Greenland may determine the extent to which the corollary of this statement is true, i.e. what is the variability of the backscatter of first-year ice which is approximately the same thickness but which has different degrees of surface roughness. It appears that the effect of snow is not understood as yet.

5.6 19.4 GHz (H, 45°) Profiling Radiometer Results

The brightness temperature at 19.4 GHz showed significant variations dependent on the ice conditions. The largest values for the brightness temperature, about 240-250 K, were observed for some of the larger snow covered ice floes, while the lowest brightness temperatures were observed for open water (about 120 K). Intermediate temperatures were observed when there was some open water in the radiometer footprint, for the thinner ice conditions or even in some cases for some of the snow covered first-year ice floes. The variations observed for different ice conditions were larger than those observed during the CV-580 flights with the same installation in the Beaufort Sea during March 1979.

The mechanism leading to the decrease in the 19.4 GHz (H, 45°) brightness temperature for some of the larger first-year ice floes and for the grey ice is not clear. However, we suspect that it is due to a variation in the surface emissivity more related to changes in the surface relative dielectric constant than to surface roughness changes. For a smooth surface the emissivity is one minus the reflectivity and this is governed by the relative dielectric constant through the Fresnel reflection equations (see e.g. Shanda, 1976). A wet surface will have a much higher relative dielectric constant and hence be more reflective for horizontally polarized radiation than a dry surface. Consequently, it is possible that the physical change responsible for the decrease in the brightness temperature over some of the ice conditions is due to the degree of wetness of the upper ice surface. This explanation is consistent with the higher near nadir scatterometer results for the sea ice which also exhibited the lower brightness temperatures.

The observation that the 19.4 GHz (H, 45°) brightness temperatures can vary over a relatively wide range raises the question of the accuracy with which it is possible to estimate ice concentration in the marginal ice zone from low resolution NIMBUS-5 19.4 GHz (H) imagery. The estimation of ice concentration using NIMBUS-5 data has been discussed by Zwally and Gloersen, 1977 and Gloersen et al. 1973, 1978, and used, with success, in the polar regions. However, low brightness temperature regions observed for August in the middle of the Arctic Ocean have been explained on the basis of a low ice concentration (Gloersen et al. 1978). Our results indicate that the explanation for the low brightness temperature may involve the state, particularly wetness, of the sea ice surface. The NIMBUS-5 observations were made in the Arctic Ocean at a time when most of all of the snow on the ice will have melted. However, it should be emphasized that the ice observed in this work is quite different from that in the Arctic Ocean and our results do not disprove the low concentration explanation for the August imagery. Further radiometric work under melting conditions would be useful to help resolve this uncertainty.

The reduction in 19.4 GHz (H, 45°) brightness temperature for the thinner ice may arise if the skin depth is comparable to or greater than the ice thickness and, consequently, the brightness temperature is less than that it would otherwise have been. This mechanism and the use of low frequency radiometers for estimating ice thickness has been discussed by Tiuri et al. (1974, 1978). Recent X-band (10 GHz) results (Bogorodski and Khoklov, 1977a) obtained from thin ice have shown that the attenuation values per unit length and the refractive index are significantly larger than those values obtained for samples obtained from much thicker first-year sea ice (see e.g. Vant, 1976, Bogorodski and Khoklov 1977b). For 4 cm thick ice Bogorodski and and Khoklov 1977a give an attenuation of about 15 dB per cm. This corresponds to a skin depth of approximately 0.6 cm, i.e. much smaller than the ice thickness. At 19.4 GHz one would expect the skin depth of 4 cm sea ice to be even smaller and, consequently, there would be effectively no reduction in the brightness temperature due to the ice-water interface. If the attenuation values were one to two dB per cm, which seems unlikely but which puts the results in the same region as those obtained for much thicker ice, then there would be a measurable decrease in the 19.4 GHz (H, 45°) brightness temperature. Because of the relatively large changes in 19.4 GHz (H, 45°) brightness temperature for the thin ice types and because of Bogorodski's results we feel that the low brightness temperatures for nilas arise from the ice properties (complex dielectric constant and surface roughness) rather than being directly related to ice thickness. The argument is essentially the same as that used for a wet ice surface, i.e. the relative dielectric constant is large (as shown by Bogorodski) and hence the surface is more reflective and less emissive.

5.7 Imaging Radiometer Results

Although a detailed analysis of the imaging radiometer data has yet to be performed, three results are apparent from a preliminary examination of the measured brightness temperatures.

(a) The 5 GHz (V, 50°) brightness temperatures are normally lower than either the 17 or 34 GHz (V, 50°) values. On average the 17 GHz results are marginally lower than the 34 GHz results.

(b) The 5 GHz brightness temperature drops significantly for thin ice (nilas) in comparison to the snow covered first-year ice. A smaller effect was observed for the 17 Ghz results and very little effect was observed for the 34 GHz results.

(c) By comparing the 19.4 GHz (H, 45°) profiling radiometer data with the 17 GHz (V, 50°) imaging channel it appears that the changes in brightness temperature between different ice conditions are larger for the H - than for the V-polarized data. Despite the poorer absolute calibration of the H-polarized 19.4 GHz data it is also clear that the brightness temperature for the thinner ice is lower for the H-polarized system then for the V-polarized system.

It is well known that the surface emissivity of some materials can be modelled, at least to a first approximation, by assuming a smooth surface and by calculating the Fresnel reflection coefficient and hence emissivity, from a knowledge of the dielectric properties. Such an approach predicts immediately that vertically polarized brightness temperatures will, for most angles of incidence, be higher than horizontally polarized radiation and that the vertical component will go through a maximum at some angle normally referred to as the Brewster angle. For rough surfaces, on the other hand, where surface and , possibly, subsurface scattering are important one would expect the brightness temperature to be less dependent on the angle of incidence and microwave polarization. The results of the current experiment and the results given by Campbell et al., 1977 seem to indicate that the emissivity of new and young ice depends to some extent on the reflective properties of the surface (and hence the average dielectric constant).

The reduction in the 5 GHz (V, 50°) brightness temperature for the thin ice in relation to the thicker ice may involve the mechanism described by Tiuri and already discussed in relation to the 19.4 GHz results. Tiuri et al., 1978 have quoted the results that at 4.7 Ghz the brightness temperature of 8 cm thick ice at -3°C is reduced by approximately 30 K in relation to thick ice.

However, it should be remembered that the Gulf of Bothnia sea ice modelled and studied by Tiuri has a salinity approximately an order of magnitude lower than Beaufort Sea or West Greenland sea ice. The change in 5 GHz (V, 50°) brightness temperature between nilas and the first-year ice in this experiment was approximately 40-50 K. Consequently, this mechanism does not appear to explain completely the large differences observed.

The problem remains; why are the differences in brightness temperature between first-year and nilas significantly larger for the 5 GHz channel than for the 34 GHz channel. The obvious solution is to examine the effect of ice thickness. However, as we have seen above this may not be the complete explanation. Another possibility is related to the fact that the dielectric constant of the brine solution of the composite sea ice system (crystalline ice and brine solution in the brine inclusions) is significantly larger at 5 GHz than at 34 GHz. Bogorodski and Khoklov (1977b) quote values of 9.15 and 56.83 respectively for ϵ_r (37 GHz) and ϵ_r (3.5 GHz) for sea water with a salinity of 40 ($^{\circ}/oo$) at 0°. Consequently, if we are to assume that the larger attenuation values for thin ice in relation to thicker first-year ice (Bogorodski and Khoklov, 1977a) are due to a larger brine volume then this implies that the change in average dielectric constant between thin and thick ice will be larger at 5 GHz than at 34 GHz. Therefore, one would expect a larger change in brightness temperature at 5 GHz than at 34 GHz. Surface roughness may, of course, also be significant in that the same surface will appear to be smoother at 5 GHz than at 34 GHz. More experiments including an evaluation of the effect of snow, will be required to understand sea ice brightness temperatures as a function of frequency and ice conditions.

Irrespective of the mechanism producing the reduced brightness temperatures from thin ice the value of the data is clear. By combining 34 GHz and 5 GHz results much more information on the ice type distribution can be obtained; the 34 GHz results provide relatively good resolution and good ice-water contrast and the 5 GHz data provides an indication of the distribution and concentration of the thin ice. The multifrequency radiometer may be able to estimate the extent of wave broken ice cakes and small floes. Unless there is a large swell running through the ice the SAR does not appear to be able to readily indentify this situation. However, by studying the 34 GHz results which indicate about 90-95 % ice cover) and the 5 GHz results (which indicates that the ice is not thin ice) one might be able to deduce that the individual floe size was small and that, given the right meteorological conditions, the ice could disperse readily. More analysis and further experiments are required to explore all the possibilities for multifrequency radiometry, however, the potential for useful information is clear.

6. Conclusions and Recommendations

Relatively simple SLAR systems can be used to estimate ice extent and concentration. It is recommended that continued evaluation of SLAR systems be carried out in an operational environment (as is being done by Canada and Denmark) in order to understand better the shortcomings and limitations of these systems. Only through a good understanding of the limitations of the currently available data in relation to user requirements can useful improvements in sensor design and performance be made. The SLAR results have shown that the detection of icebergs in sea ice should use low depression angles (less than about 8°) to try to increase the iceberg-sea ice contrast. Further experiments using a SAR at low depression angles are required to study iceberg size versus detectability and to examine the problem of differentiating ice ridges with small icebergs.

Although much is now known about the improved capabilities of a SAR in relation to a SLAR for ice reconnaissance we need to know more. For example, SAR can be better in discriminating different ice conditions and types but is the reliability good enough for operational use? Can a SAR system be used for detecting bergy bits and icebergs at small depression angles and, again, would the reliability be adequate for operational use? The potential use of satellite SAR's at steep incidence angles raises questions of the reliability of ice-water discrimination. What are the satellite SAR parameters which will optimize the information content of the imagery? Many other problems exist not only in the interpretation of the imagery but also in the engineering implementation of a wide swath SAR on an aircraft or satellite and in the data processing and data and information transmission. Consequently, it is important that continued research be carried out with flexible SAR systems in multisensor experiments under as many ice conditions as possible.

From the scatterometer data it has been shown that the backscatter from the decaying, rather thin first-year ice in this experiment is not significantly different from the range of values observed for much thicker first-year ice in the Beaufort Sea. This confirms that in the marginal ice zone, the greytone of the imagery from a calibrated imaging radar operating at 2-3 cm wavelength could not be used alone to infer ice type or condition. By comparing the E-W line 13.3 GHz (HH, 45°-60°) scatterometer results with March Beaufort Sea results it is apparent that none of the ice observed had values for the backscatter as large as the multiyear ice in the Beaufort Sea. Further comparative work is in progress.

The radiometer imagery shows the value of multifrequency passive microwave data in differentiating ice types and, possibly, ice conditions even in the marginal ice zone. It is particularly important to know if, or to what extent multifrequency radiometry can be used to sense ice surface condition because often visual observations cannot due to the snow cover. If the snow cover is dry the radiometers, even the shorter wavelength channel, will be sensing the ice properties at and near the ice surface. Consequently, historical multifrequency radiometer imagery may be very important in estimating ice condition even when visual observations are possible. Although none of the aircraft involved in routine ice reconnaissance collect microwave radiometer data it is suggested that information from a multifrequency radiometer system (possibly 5 GHz and 34 GHz) could complement and improve the usefulness of the other aircraft sensors particularly, of course, in the poor weather situation. It appears that a 34 GHz imaging radiometer alone would be of much less value than a 34 GHz system combined with a low frequency channel.

The following work is being completed in connection with the West Greenland Sea Ice experiment. This analysis may modify and extend our conclusions.

(1) Study of the Norda P-3 data in relation to the other data and imagery.
(2) Study of all four channels of the X-L SAR. To date only the X(HH) imagery has been studied in detail.
(3) Further comparison and statistical study of the scattering coefficient and brightness temperature distributions from the Convair 580 profiling sensors (with CCRS and NASA LaRC) and from the multifrequency radiometer on the RDAF C-130.

Future remote sensing experiments should investigate the low 19.4 GHz (H, 45°) brightness temperatures observed for some ice conditions. Preferably this should be a combined active-passive experiment involving, if possible, nadir looking scatterometer measurements to estimate the reflectivity of the sea ice surface. Such an experiment has important implications concerning the interpretations of the observed low brightness temperatures from August NIMBUS-5 data for the middle of the Arctic Ocean and for the estimation of ice concentration in the marginal ice zone. Considerations are also being given now, at TUD, to adding an L-band (profiling) channel and a dual polarization capability to the imaging radiometer system for future experiments.

Bogorodski, V.V. and Khoklov G.P., 1977a, "Microwave Refractive Index and Absorption of initial forms of the sea ice cover and newly formed ice", Sov. Phys. Tech. Phys. Vol. 22(6). Translated by the American Institute of Physics.

Bogorodski, V.V. and Khoklov G.P., 1977b, "Anisotropy of the microwave dielectric constant and absorption coefficient of Arctic drift ice", Sov. Phys. Tech. Phys. Vol. 22(6). Translated by the American Institute of Physics.

Campbell, W.J., Ramseier R.O., Weaver R.J. and Weeks W.F., 1977, "Skylab Floating Ice Experiment", Fisheries and Environment Canada, Miscellaneous Special Publication 34, Ottawa.

Dunbar, M. and Weeks, W.F., 1975. "The interpretation of Young ice forms in the Gulf of St. Lawrence using Radar and IR imagery", DREO Report 711.

Gloersen, P., Campbell, W.J., Zwally, H.J., Chang, T.C., Wilheit, T.T., Hall, D.K., and Ramseier R.O., 1978. "Time dependence of sea ice concentration and multiyear ice fraction in the Arctic Basin", Boundary Layer Meteorology Vol. 13, pp. 339-359.

Gloersen, P., Nordberg, W., Schmugge, T.J., Wilheit, T.T. and Campbell, W.J., 1973, "Microwave Signatures of First-Year and Multiyear Sea Ice", J. Geophys. Res., Vol. 78, pp. 3564-3572.

Gray, A.L., Ramseier, R.O., and Campbell, W.J., 1977. "Scatterometer and SLAR Results obtained over Arctic Sea Ice and their Relevance to the Problems of Arctic Ice Resonnaissance", Proc. Fourth Chandian Symposium on Remote Sensing, pp. 424-444.

Gray, A.L., Cihlar, J., Parashar, S. and Worsfold, R. "Scatterometer Results from Shorefast and Floating Sea Ice", 1977, Proc. Eleventh International Symposium on Remote Sensing of Environment, Ann Arbor, Michigan, pp. 645-657.

Gray, A.L., Hawkins, R.K., Livingstone, C.E., Lowry, R., Larson, R. and Rawson, R., 1979. Proc. Thirteenth International Symposium on Remote Sensing of Environment, Ann Arbor, Michigan.

Gudmandsen, P. and Overgaard, S., 1979. "Operations at Greenland West Coast Experiments". Technical University of Denmark report No. IR 158.

Jones, W.L., Schroeder, L.C., and Mitchell, J.L., 1977. "Aircraft Measurements of the Microwave Scattering Signature of the Ocean", IEEE J. Ant. and Prop. Vol. AP-25, pp. 52-61.

Ketchum, R.D., 1977."An evaluation of side-looking radar imagery of sea ice features and conditions in the Lincoln Sea, Nares Strait and Baffin Bay". NORDA Technical Note 7.

Ketchum, R.D., 1978. "An evaluation of ERIM X-L band airborne synthetic aperture radar imagery of sea ice", NORDA Technical Note 28.

Kirby, M. and Lowry, R, 1979. "Iceberg Detectability problems using SAR and SLAR systems", to be published.

Onstott, R.G., Moore, R.K.and Weeks, W.F., 1978. "Surface Based Scatterometer Results of Arctic Sea Ice", presented at the WMO Workshop on Remote Sensing of Sea Ice, Washington, 16-20 October.

Parashar, S.K., Biggs, A.W., Fung, A.K. and Moore, R.K., 1974. "Investigations of Radar Discrimination of Sea Ice", Proc. Ninth International Symposium on Remote Sensing of Environment, pp. 323-332.

Rawson, R., Larsen, R., Shuchman, R. and Worsfold, R., 1977. "The capability of SAR systems for iceberg detection", Proc. of the First International Conference on Iceberg Utilization", Ames, Iowa.

Schanda, E, 1976. "Remote Sensing for Environmental Sciences" ed. E. Schanda, Springer-Verlag.

Skou, N., 1978. "Development of an Airborne Multifrequency Radiometer System", Technical University of Denmark, Report R 203.

Skou, N., 1979. "Radiometer Imagery from the SURSAT experiment on April 10th, 1979. Technical University of Denmark, Report No. IR 177.

Skou, N. and Søndergaard, F., 1979. "Radiometer Signatures and SLAR Imagery of Sea Ice in Greenland, Results from July 1977 and November 1978". Technical University of Denmark, Report No. R 216.

Søndergaard, F., 1979. "X-band SLAR images from the SURSAT ice experiment on April 10th, 1979". Technical University of Denmark, Report, No. IR 170.

Tiuri, M., Hallikainen, M. and Kaski, K., 1974. "Experiments on remote sensing of sea ice using a microwave radiometer". Proc. URSI meeting on Microwave Scattering and Emission from the Earth, Berne.

Tiuri, M., Hallikainen, M. and Lääperi, A., 1976. "Microwave Radiometer Theory and Measurements of Sea Ice Characteristics", Report S 89, Helsinki University of Technology, Finland.

Zwally, H.J. and Gloersen, P., 1977, "Passive Microwave Images of the Polar Regions and Research Applications", Polar Record, Vol. 18, No. 116, pp. 431-450.

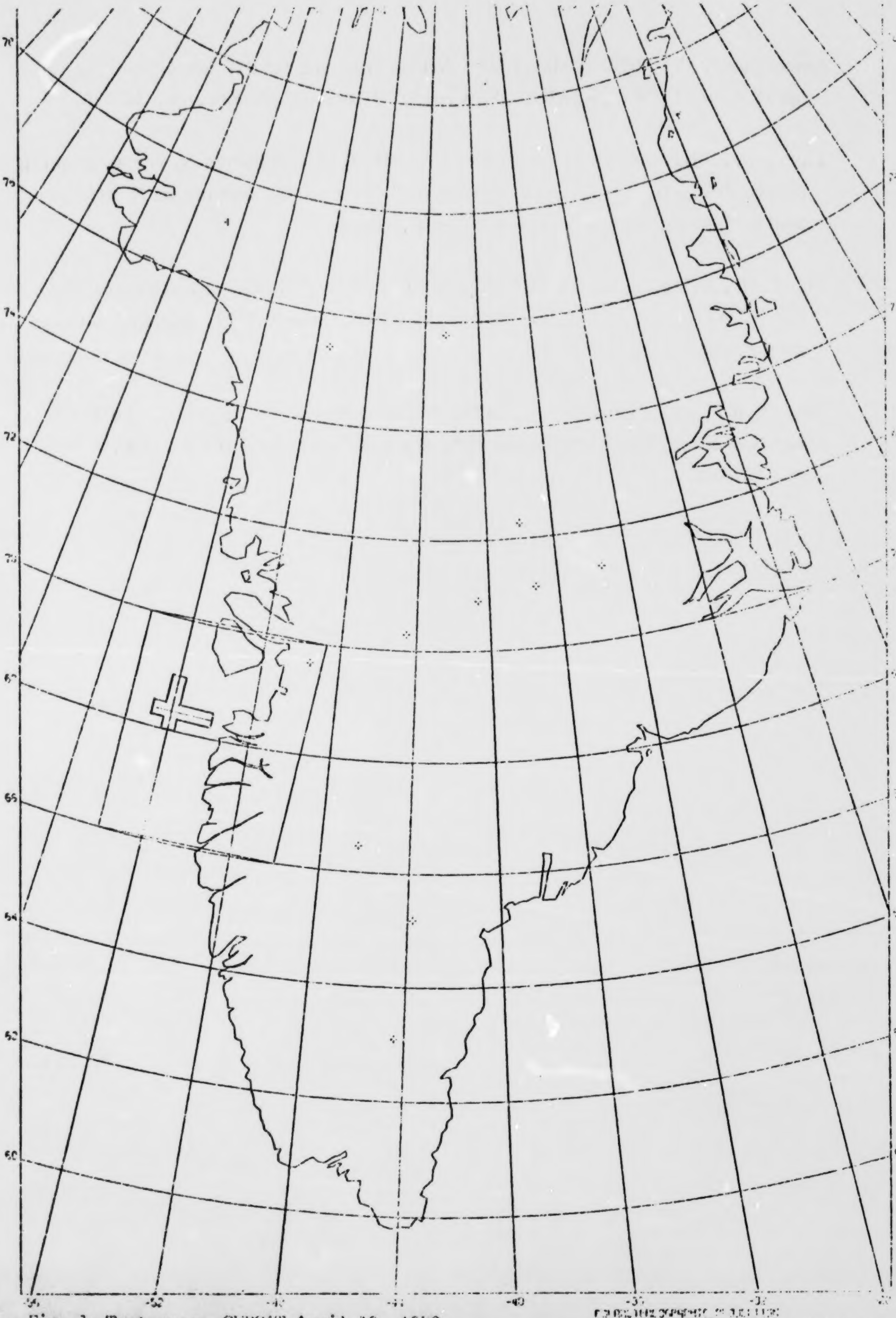

Fig. 1. Test area, SURSAT April 10, 1979.

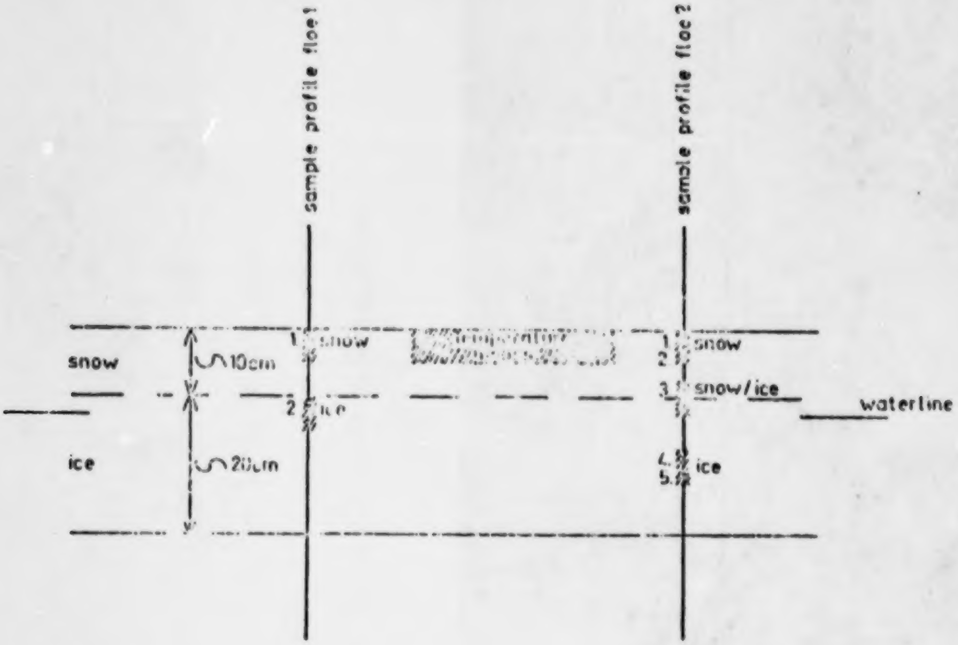
sample profile floe 1
sample profile floe 2
snow
ice
∽10cm
∽20cm
1 snow
2 ice
1 snow
2
3 snow/ice
4
5 ice
waterline

Figure 2

An illustration of the snow and ice thickness on the two first year ice floes from which samples were taken. The positions and numbers for both the snow and ice samples are shown on the profiles 1 and 2 which were obtained from floes X and Y in Figure 5.

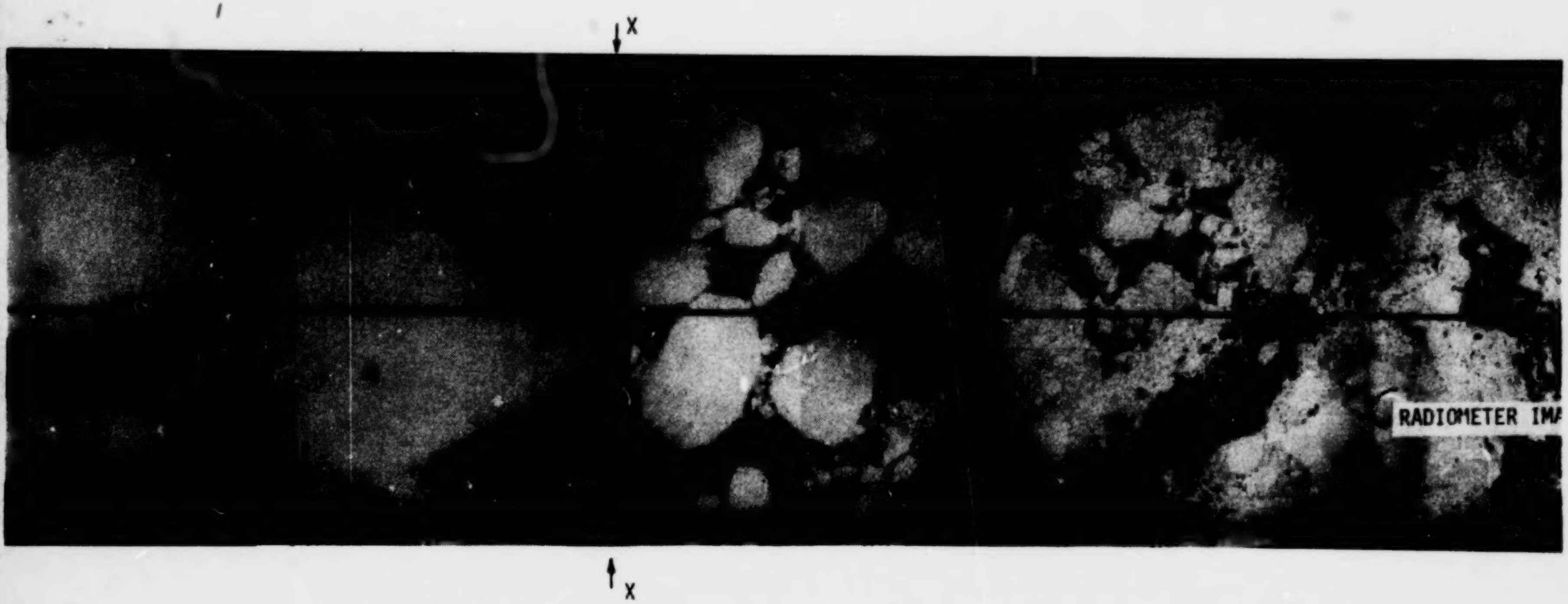

Figure (3a). Photo mosaic of five RC-10 frames imaged also by the SAR and the 3 frequency radiometer.

Figure (3b). Infra-red image of the same area as Figure (3a). North is to the right of the picture.

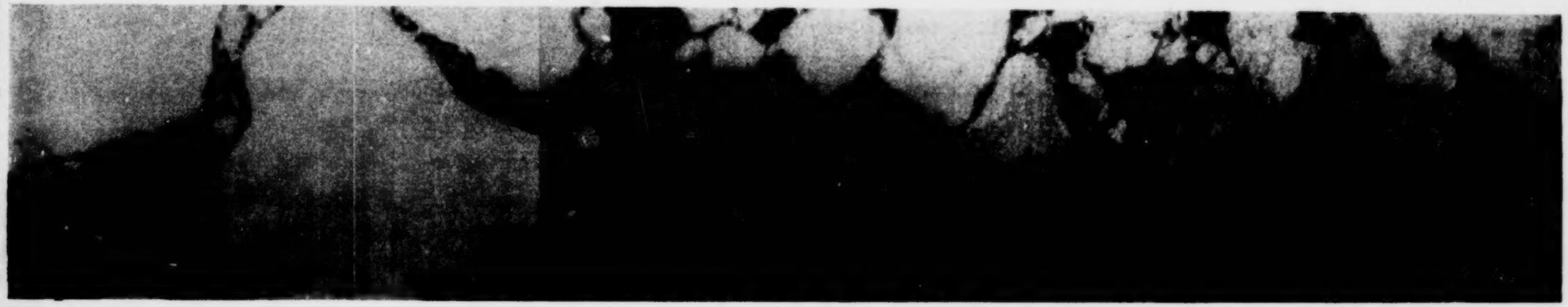

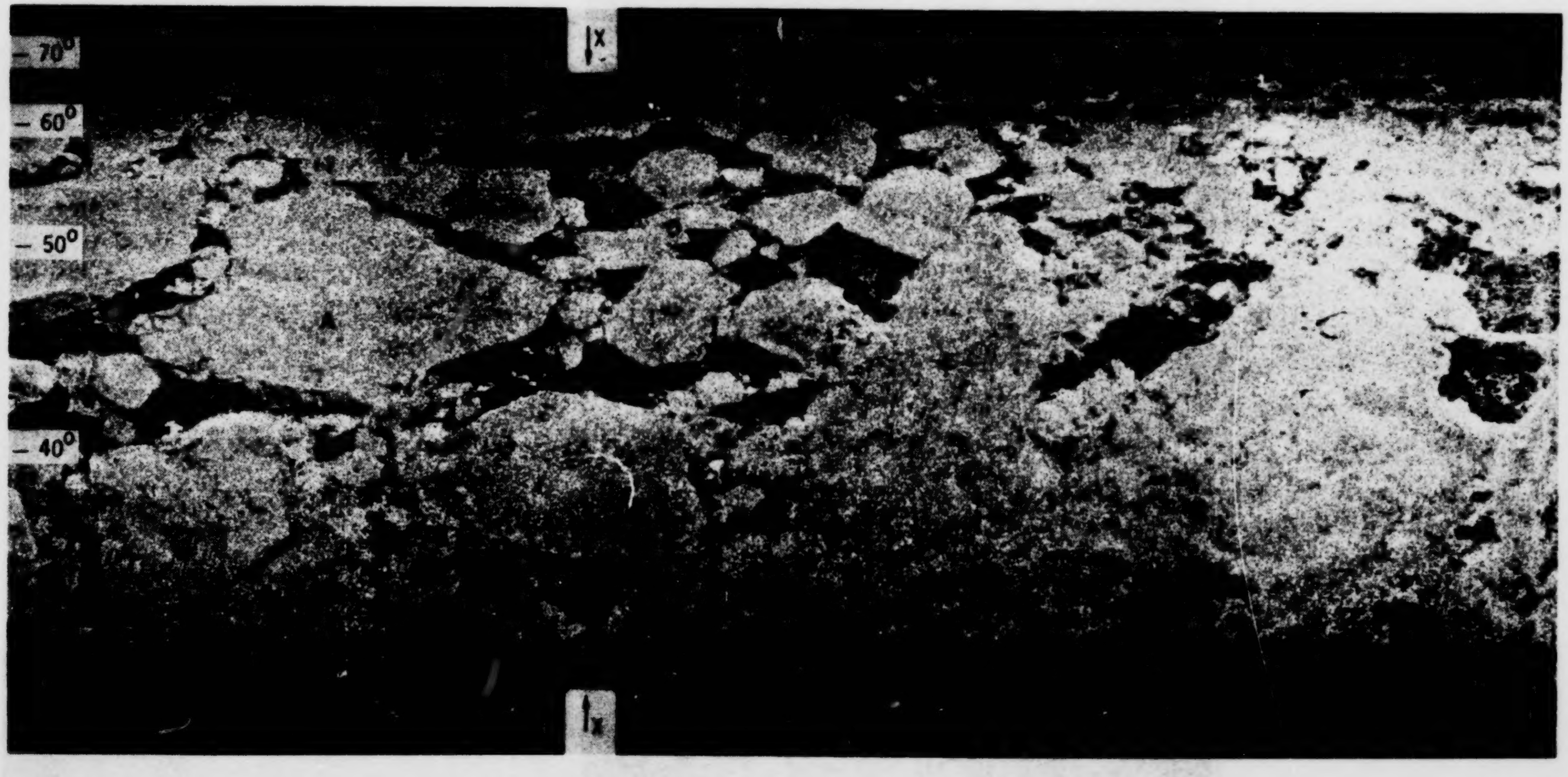

Figure (4). X-band HH SAR image encompassing the same area as Figures (3a) and (3b). Depression angles on the left of the image.

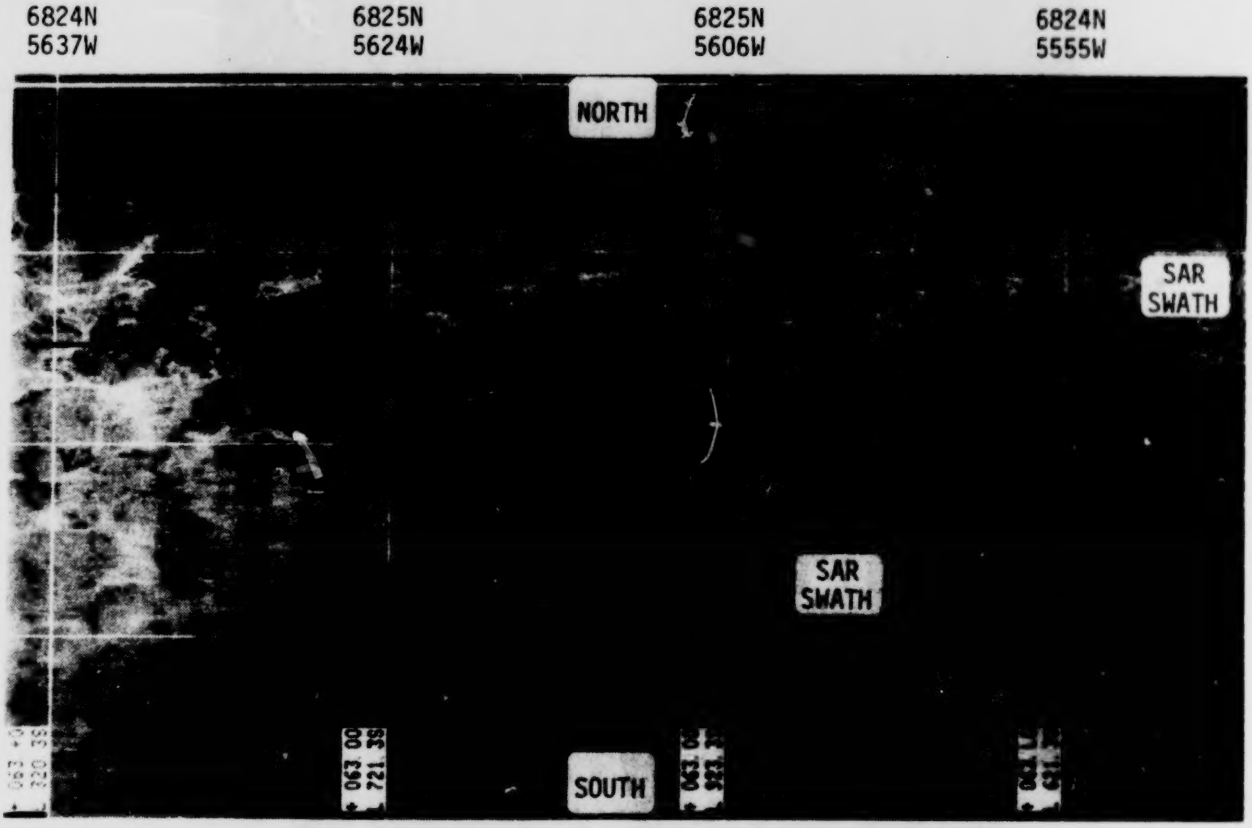
6824N
5637W
6825N
5624W
6825N
5606W
6824N
5555W
NORTH
SAR
SWATH
SAR
SWATH
SOUTH
063 00
721 3S

Figure (5). SLAR image of the cross over region of the E-W and N-S flight lines. The floes which were ground truthed, marked X and Y, are indicated on the image as well as the approximate SAR swathes on the CV-580 N-S and E-W SAR flights.

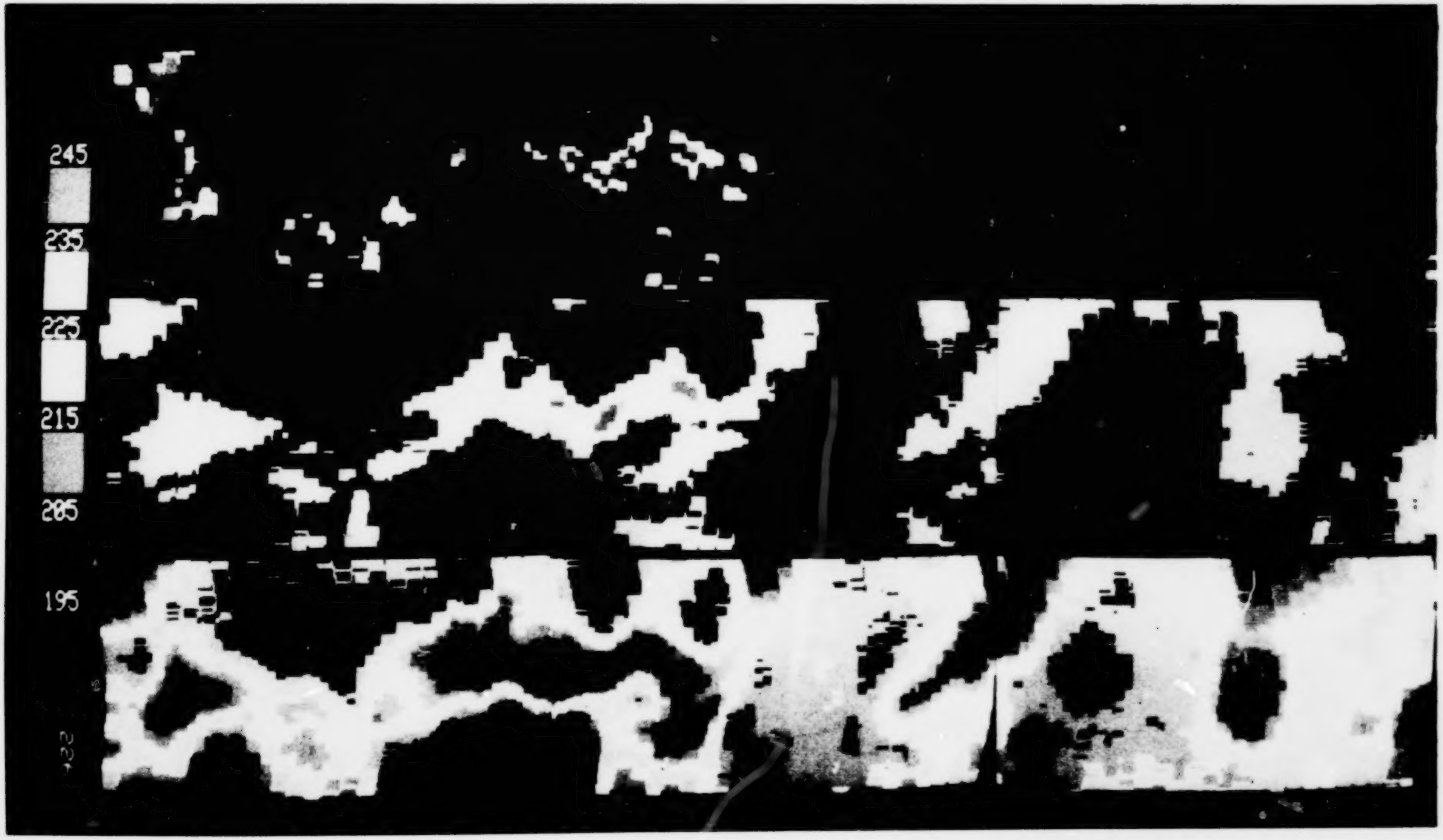
245
235
225
215
205
195
224

Figure (6). False colour radiometer image of the area indicated on Figure (3a). Note brightness temperature to colour code translator on the left of the image.

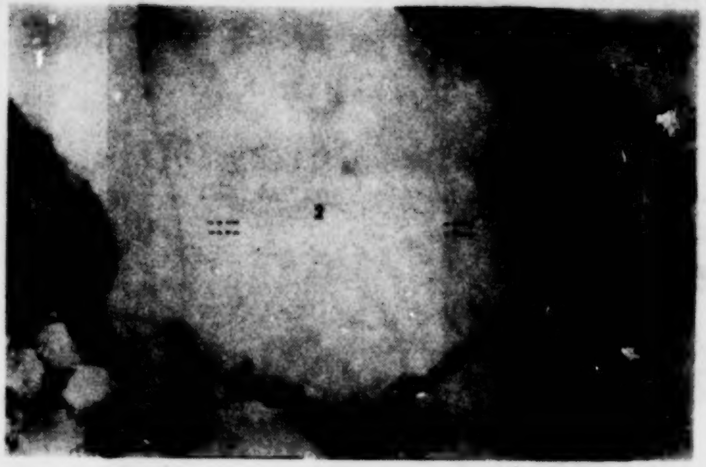

Figure (7a).

Photo mosaic for part of Convair 580 low altitude E-W line.

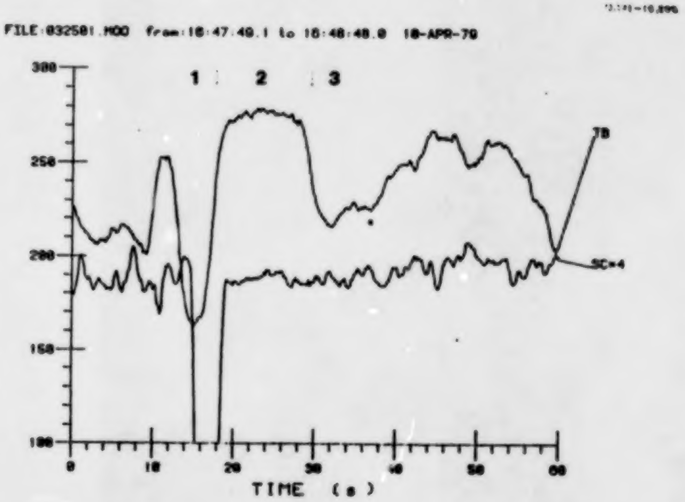

Figure (7b).

Comparison of relative radiometer profile (TB) at 45° incidence angle with relative backscatter at 37° (fore beam) for a profile which includes regions 1, 2 and 3 in Figure (7a). One small division corresponds to 10° K and 2.5 dB.

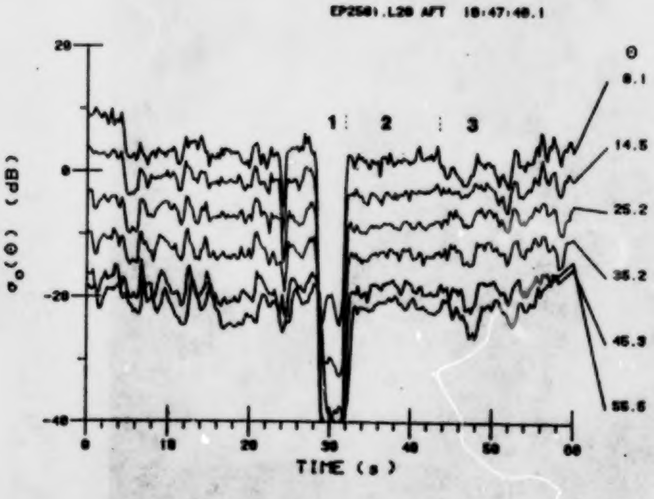

Figure (7c).

Six angle scatterometer results for aft beam. The incidence angles to the vertical are marked on the right hand side.

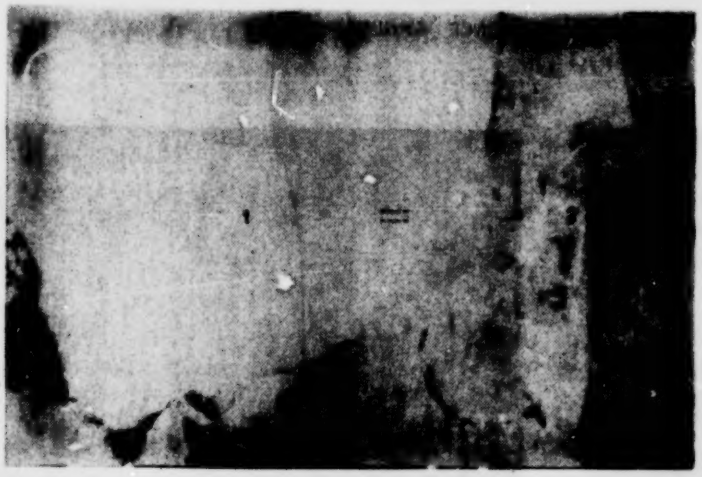

Figure (8a).

Photo mosaic for part of Convair 580 low altitude E-W line.

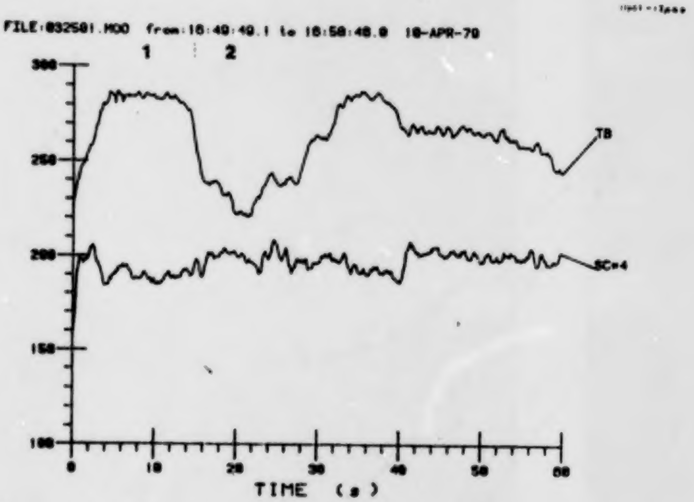

Figure (8b).

Comparison of relative radiometer profile (TB) at 45° incidence angle with relative backscatter at 37° (fore beam) for a profile which includes regions 1 and 2 in Figure (8a).

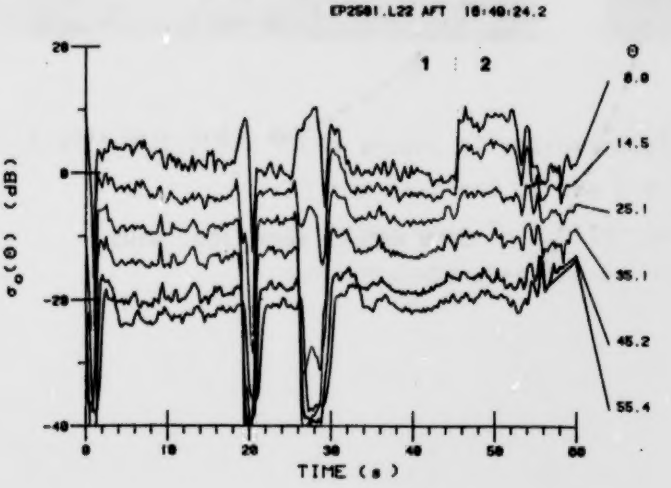

Figure (8c).

Six angle scatterometer results for aft beam. The incidence angles to the vertical are marked on the right hand side.

BACKSCATTERING COEFFICIENT VERSUS INCIDENCE ANGLE FOR DIFFERENT ICE CONDITIONS ALONG E/W LINE

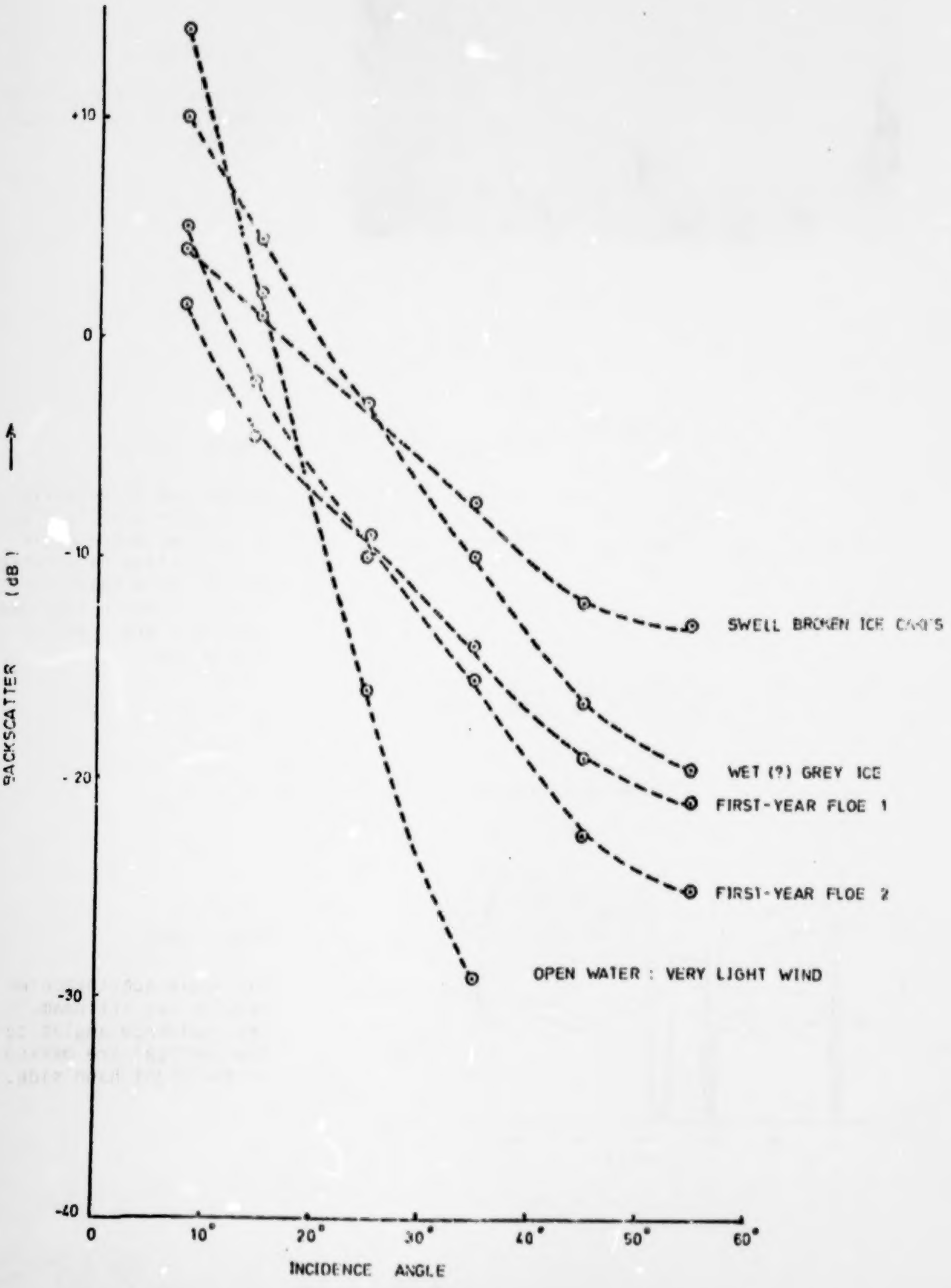

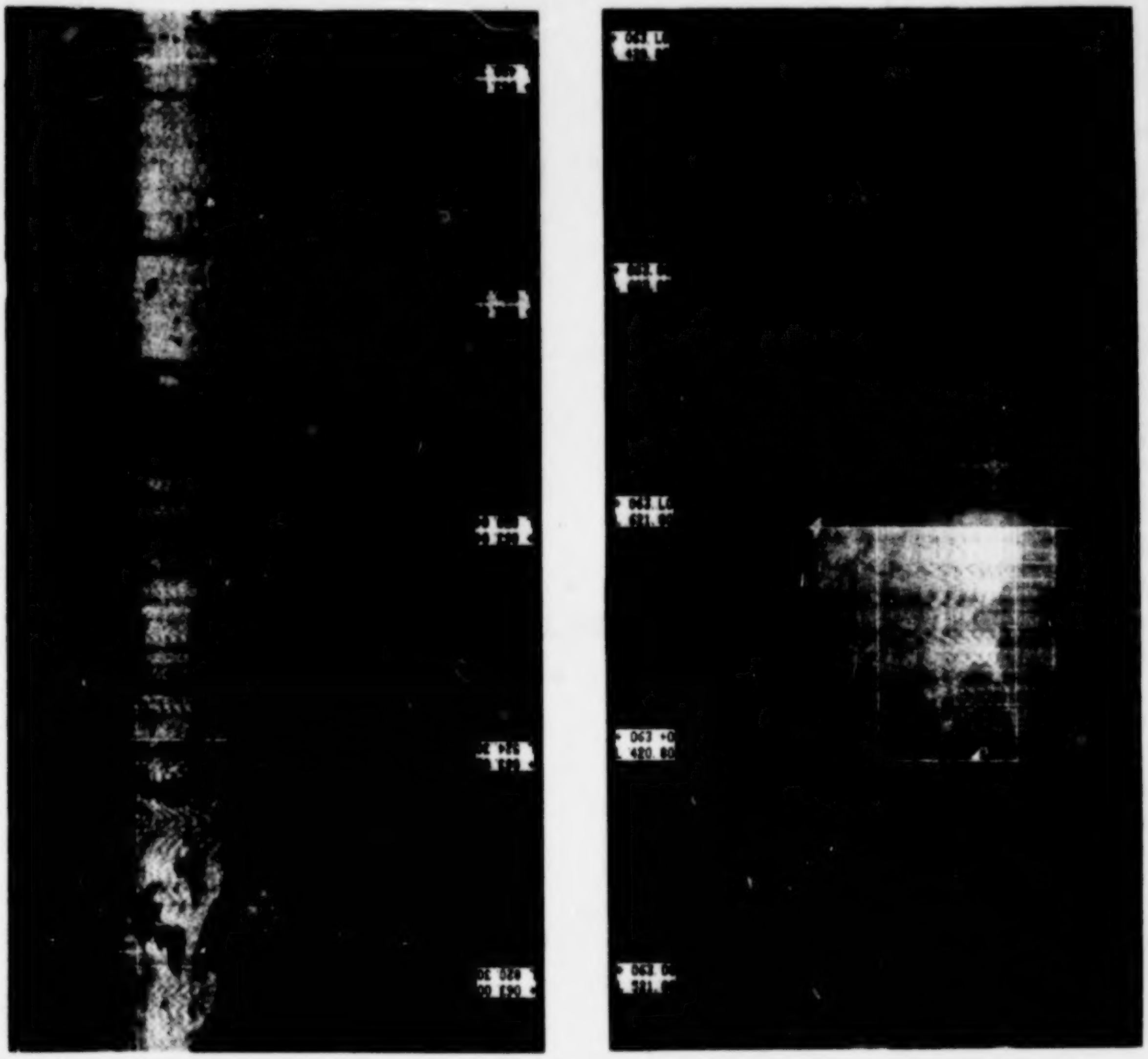

(a) (b)

Figure (10a and b). SLAR images of approximately the same region of pack ice at the east end of the E-W line. Figure (10a) was obtained when Twin Otter was flying east and Figure (10b) was obtained when the aircraft was flying west.

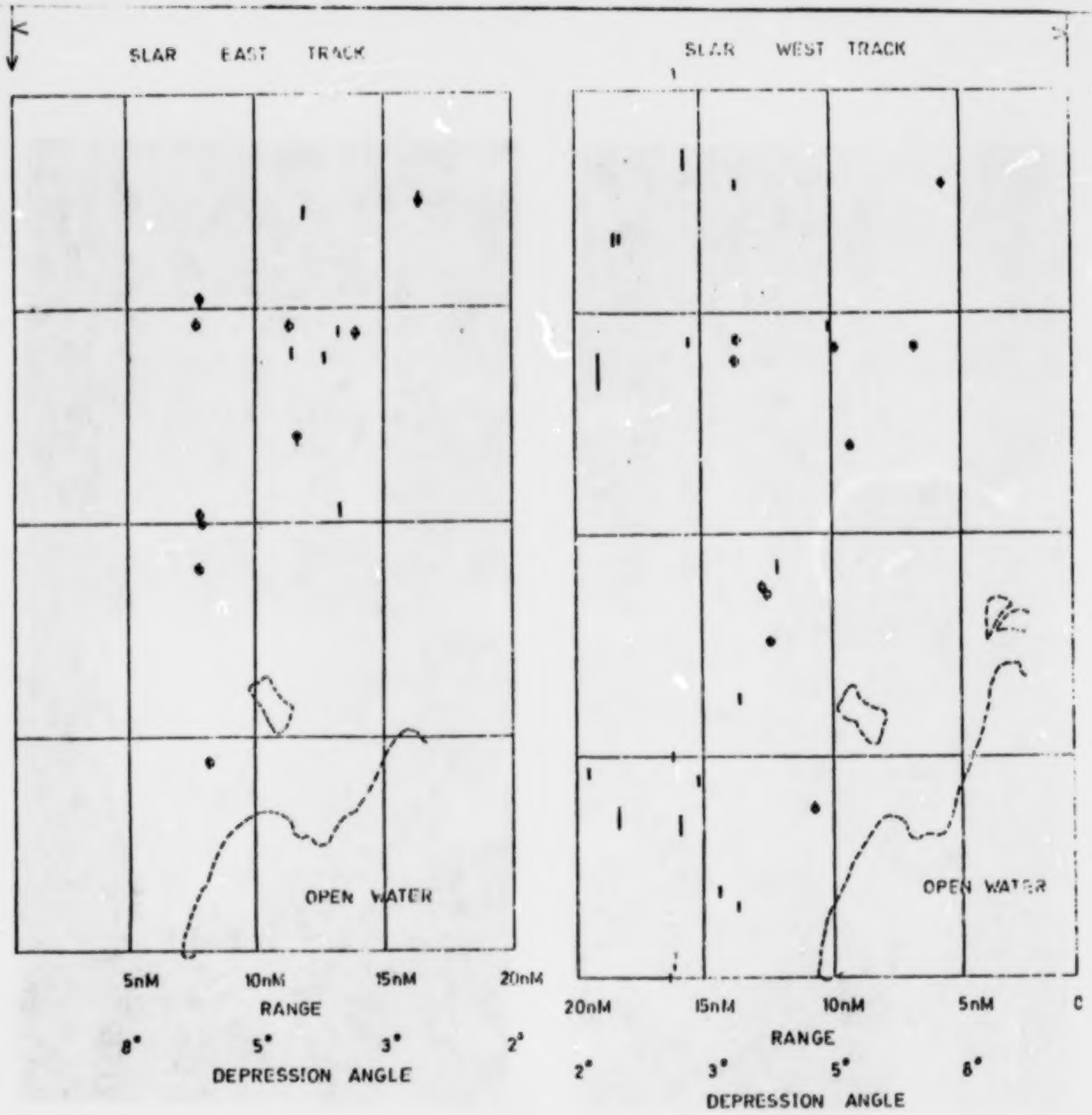
SLAR EAST TRACK
OPEN WATER
5nM
10nM
15nM
20nM
RANGE
8°
5°
3°
2°
DEPRESSION ANGLE
SLAR WEST TRACK
OPEN WATER
20nM
15nM
10nM
5nM
C
RANGE
2°
3°
5°
8°
DEPRESSION ANGLE

(a)

(b)

Figure (11a and b). Diagrams showing the bright targets traced from Figure (10a and b) and interpreted as icebergs. Those targets marked with circles appear on both images. It can be seen that there are a number of targets in (11b) which are not apparent in (11a).

SECTION 5.7

DEPRESSION ANGLE STUDY, SURSAT REPORT NO.2

Gray, L.

Depression Angle Study,
SURSAT Report No. 2

L. Gray[*]

R 223 February 1980

---

[*] On leave from the Canada Centre for Remote Sensing, Ottawa, Canada

fd 75

CONTENTS

Page

1. INTRODUCTION 2
2. RESULTS AND DISCUSSION 3
    2.1 Summary of data used for this report 3
    2.2 Detection of icebergs in open water 3
    2.3 Detection of icebergs in sea ice 5
    2.4 Detection of ships 6
    2.5 Discrimination of ships and icebergs 6
    2.6 Sea ice mapping 9
3. RECOMMENDATIONS 12
    3.1 Real time processing 12
    3.2 Aircraft Research and Development for ice work 13
    3.3 Satellite Research and Development for Ice work 14
    3.4 Use of Marine Type Radars 14

ACKNOWLEDGEMENTS 15

REFERENCES 16

FIGURES

1. INTRODUCTION

Off shore oil or gas production will not be feasible without weather and hazard information which should include repetitive mapping and tracking of icebergs and sea ice as well as meteorological and sea state information. The safety and efficiency of shipping in the Arctic, off the Canadian east coast and off Greenland depends also on timely weather and sea ice information. Imaging radar systems are now viewed, correctly, as an essential element in providing this information. Whether in fact a particular radar can adequately fulfil its desired function depends upon the parameters which describe the radar. This SURSAT report is concerned with the influence of one such radar parameter, the depression angle, on the usefulness of the radar imagery for civilian, coastal, ocean and sea ice reconnaissance.

The objectives of the SURSAT experiment (#79) were twofold:

a) To measure the contrast or signal to clutter ratio (SCR) of "targets", particularly ships and icebergs in the ocean as a function of depression angle.

b) To examine the relative merits of steep (satellite, $> 10^{0}$) versus shallow (aircraft, $< 5^{0}$) depression* angle radar imagery for sea ice mapping.

To a large extent both objectives have been met and some results have already been published and submitted to SURSAT as an interim report (Gray et al, 1979a). Further relevant work is described in this report although detailed illustrations and statistical analysis (where possible) will be reserved for future work. Results and conclusions related to the radar detection and mapping of icebergs, ships and sea ice from both aircraft and satellite are included in section 2 and recommendations, relevant particularly to Canadian remote sensing needs, are made in section 3. Danish needs for coastal and sea ice reconnaissance around Greenland are quite similar to Canadian requirements in the eastern Canadian Arctic.

---

* Measured with respect to the horizontal.

2. RESULTS AND DISCUSSION

2.1 Summary of data used for this report

Useful data relevant to this project were obtained from the following SURSAT SAR-580 missions:

a) The Arctic Marine Oilspill Program (AMOP) mission to Scott Inlet, Baffin Island, September 1978.

b) Beaufort Sea mission, March 1979.

c) Eastern Arctic mission, April 1979.

Data from the X/L SAR, the Ku band scatterometer and from the two cameras (RC-10 and Olympus 35 mm) on board the Convair 580 have been used to provide the primary data set for this experiment. Some examination of the radar imagery from the X band SLAR (modified APS-94D) on the NASA LeRC C-131, the X band SLAR/SAR (CRC modified APS-94D) on the AES Electra, the X band SLAR (Technical University of Denmark) and the SEASAT SAR has also contributed to the results given in the following sections.

2.2 Detection of icebergs in open water

Some of the results summarized in this section have already been published in Gray et al, 1979a. In this work, the iceberg signal to sea clutter ratio was modelled as a function of wind speed using the 13.3 GHz scatterometer data obtained from two icebergs and from the open ocean backscatter data of Jones et al, 1977. Scatterometer iceberg data obtained from the SAR-580 eastern Arctic sortie (acquired subsequent to the earlier work) have shown that the iceberg backscatter signature assumed earlier was reasonably representative of medium to large (> 100 m horizontal extent) icebergs. All the scatterometer data has been processed to a resolution of approximately 20 x 20 m. Future work will look at the statistics of iceberg radar returns.

The result of this work has been the demonstration that the SCR of icebergs in the open ocean will be relatively small (positive or negative) for steep, satellite radar depression angles in the range $60^\circ - 75^\circ$ ($15^\circ - 30^\circ$, incidence angle). The SCR values are sufficiently small that it is predictable that a moderate resolution spaceborne SAR (resolution 20 - 50 m, depression angle $60^\circ - 75^\circ$) will not be able to reliably detect icebergs in the opean ocean.

A further result, based on an examination of X/L radar imagery of the same group of icebergs on successive days, has been the demonstration that low depression angles and HH polarization appear to offer the best SCR for aircraft SAR operation. Clearly, the aircraft geometry (i.e. the possibility of small depression angles) is much superior for the radar detection of targets in the ocean.

It appears, given the current proposals for civilian spaceborne SAR systems, that the reliable detection and tracking of icebergs in the ocean will not be possible from space in the near future. The European Space Agency (ESA) Coastal Ocean Monitoring Satellite System (COMSS) SAR has been planned with a depression angle of 70° and (approximately) a 4 look resolution of 20 x 20 m. Simply decreasing the depression angle to improve SCR for targets in the ocean would reduce the swath width and lead to excessively noisy imagery for all other ocean applications. Increasing the transmitted power by a factor of approximately seven would allow the depression angle to be decreased by about 15°*. Further, even with a depression angle of 55° and a 20 m resolution, the performance for iceberg detection, particularly for those less than approximately 100 m long, in high winds and sea states could be marginal.

A satellite SAR system has also been included as part of the ICEX proposal (Ice and Climate Experiment, Report of the Science and Applications Working Group, NASA, Goddard Space Flight Center). The proposed SAR differs from the ESA COMSS SAR in a number of ways. The frequency band is X instead of C, two antennas are used to achieve a swath of 360 km (instead of 100 km), the resolution is 100 m (instead of 20 m), and the depression angles are lower (near range 63°, far range 41° as opposed to approx. 70°). The degree of incoherent averaging is equivalent to approximately 6 looks. Because of the decreased depression angle, this system may be superior to the COMSS system for the detection of targets in the open ocean, however, relatively large values of the SCR will still be required because the target size is comparable to or even smaller than the resolution cell. A better evaluation must await a better statistical description of the variability of ocean SAR returns and a better understanding of the statistics of the backscatter of icebergs. However, it is felt that, at present, it is unlikely that such a radar could detect and track smaller icebergs in a sufficiently reliable manner to be of value for operational use.

---

* The increase in transmitted power depends strongly on the model used to describe the angular change in average terrain backscatter. In order to take advantage of the increased contrasts at the lower depression angles for an ocean SAR scene containing open water, it is appropriate to use the backscatter curve for open water. This was done in estimating the factor of seven above. For land applications a much smaller factor would be required.

2.3 Detection of icebergs in sea ice

The detection of icebergs in sea ice has been studied and discussed in reports by Ketchum, 1977, Rawson et al, 1977, Kirby and Lowry, 1979 and Gray et al, 1979b. It is apparent from this work that the average contrast or SCR between the icebergs and the surrounding sea ice can often be quite small when relatively large depression angles are employed by the radar. For large icebergs (> 150 m) and high resolution (e.g. the 3 m resolution of the X/L SAR) the detectability improves because of the greater probability that some iceberg pixels will have significantly brighter returns than average, and because outline and shape information helps significantly in the identification process. However, it is clear from the available imagery that a satellite radar with a moderate resolution (~ 20 m) will not reliably detect 20 - 100 m icebergs in sea ice. Even the X/L SAR with a resolution of 3 m was not particularly successful in detecting smaller icebergs (10 - 100 m) off the coast of Greenland.

Gray et al, 1979b have shown, on the basis of imagery obtained from the TUD SLAR, that the signal to clutter ratio increases significantly for depression angles less than approximately eight degrees. The reason for the increasing SCR was assigned to a greater depression angle dependence of the backscatter of the sea ice in comparison with that of icebergs. However, it has been reported (Kirby and Lowry, 1979) that when SLAR systems are used (at small depression angles), it is possible to confuse radar returns from icebergs with those from sea ice ridges. Further research into this problem with higher resolution SAR systems at low depression angles ($< 10^\circ$) is desirable.

Consequently, the detection and tracking of smaller (10 - 100 m) icebergs in sea ice cannot be carried out with foreseen satellite SAR systems. Only by using low depression angles ($< 10^\circ$) and relatively high resolution will it be possible to achieve a performance adequate for operational requirements.

2.4 Detection of ships

Similar considerations, and rather similar conclusions, apply to the detection of ships in the ocean as well as to the detection of icebergs. The work of Gedney and his co-workers at NASA Lewis Research Center (Gedney,1978, Marthaler and Heighway,1978) and the scatterometer results in Gray et al, 1979a have shown that ships normally represent brighter targets than icebergs of a comparable size. However, the use of steep look angles will still not lead to reliable ship detection in all sea states and wind speeds. For example, the ship "Oceanographer" participating in GOASEX was not observed in the SEASAT SAR imagery but was observed in the X/L SAR imagery taken with the Convair 580. The wind speed was relatively low (~ 5 m/sec) during the acquisition of this data. In low sea states and wind speeds, the detection of ships will be possible with a SEASAT type SAR, however, the range of ship sizes, look angles with respect to the ship's axis and wind speeds for which detection is (say) 90% possible is not known. The change in ocean surface roughness associated with ship wakes is usually detectable by radar (even at 70° depression angle) but often there is the requirement to detect and classify stationary targets.

2.5 Discrimination of ships and icebergs

Four possible ways are discussed in which it may be possible to discriminate ships and icebergs using aircraft radar systems and measurements:

a) By using a high resolution imaging system it may be possible to discriminate on the basis of the shape of the pattern of bright returns and the shape and size of the radar shadows (if they are visible).

b) On average, as discussed in section 2.4, it appears that ship returns are larger than iceberg returns. Consequently, if one had a high resolution system (to estimate size) the strength of the returns per pixel may aid in the discrimination process.

c) Ships in motion have characteristic wakes which obviously icebergs do not and which are often visible on radar images. Ship wakes have been observed on SEASAT imagery even when the ship return was not significantly above the average sea clutter background.

d) If the radar (i.e. search radar) views the target for some time, then the fluctuations in the intensity of the backscattered returns (target fading or scintillation) may be characteristically different for ships and icebergs. These four possibilities are now discussed:

From an examination of high resolution (3 m) airborne SAR imagery of ships (Liskow et al, 1977) and icebergs (Gray et al, 1979a) in the open ocean, it is clear that the shape of the pattern of bright returns is not a reliable indicator of whether the target is a ship or iceberg. The motion of both the sea surface and of the ship, complicates the 'focussing' process for synthetic aperture systems so that often the bright regions on the image do not have a one to one correspondence with the position of those regions in the scene which had the highest backscatter. For icebergs in open water, the shape of the bright image pattern often corresponds to the shape of the near edge of the iceberg and sometimes also of any large regions of the iceberg approximately normal to the radar beam. If surrounded by sea ice, the shape of the larger icebergs (> 150 m) can sometimes be estimated reasonably well. Also, the radar shadow, due to the iceberg, is often visible when it is surrounded by sea ice. However, small signal suppression complicates the possible observation of shadows when the iceberg is surrounded by open ocean and, in no cases known to the author, has the unique identification of radar shadows been possible from SAR imagery of icebergs in the open ocean. Shadows have been observed, however, on SLAR imagery of icebergs (e.g. Skou and Sondergaard, 1979). Consequently, ship and iceberg discrimination, based on shape and size, may be possible and useful particularly when the target is surrounded by sea ice but in many instances, particularly in the open ocean, it is believed that this method, on its own, will be unreliable.

More work is required to study the variability of radar signatures of icebergs and ships. However, while it is probably true that, on average, ships will be brighter targets than an equivalent sized iceberg, the backscatter distribution functions probably overlap. Further, in order to classify an isolated target in an open ocean background, some measure of radar absolute calibration would be required. As this is difficult to implement within approximatly a factor of two to three in power (3 - 5 dB) it may not be feasible to operationally use the backscatter magnitude to help classify a particular bright target as a ship or iceberg.

The third classifier, the identification of ship wakes undoubtedly works (see e.g. Skou and Sondergaard, 1979) but depends on a significant ship motion to create the wake. It is possible that by combining the information from these three techniques that identification can be made in many cases.

The fourth option, that of studying fading patterns of the bright targets on a search radar display may* work in a situation where ships are being sought out in a sea clutter background which included icebergs, bergy bits and individual sea ice floes.

The explanation for the different fading patterns is probably related to the following considerations of the surface nature of icebergs and ships. Icebergs are composed of glacier ice which has been weathered such that the surface often has an appearance somewhat like a pebble-dashed wall with the 'bumps' having a size of the order of centimeters. It appears therefore, from their appearance and from sun glint patterns, that icebergs have a two scale roughness; i.e. the relatively small scale surface undulations superimposed on the large scale random and often spectacular shape of the iceberg. Further, the relatively low dielectric constant of the fresh water ice means that an iceberg with a dry surface will reflect approximately one tenth the power of a metal object of the same shape. Consequently, it appears reasonable to assume that icebergs at X-band represent a target which has a relatively large number of, in comparison with metal, quite inefficient scattering centres. This assumes that the surface of the iceberg is not wet. Ships appear to behave rather differently as scatterers of microwave radiation because the basic material is very reflective. Further, there exist large surfaces which even at X band are smooth and often the geometry of the target satisfies the conditions for two and even three plane corner reflection.

---

* It has been reported (Sondergaard, private communication) that search radar operators of the Royal Danish Air Force routinely use fading to help with target identification on their work during fisheries

Having established the different nature of the surfaces of icebergs and ships, it remains to discuss why the fading of the signal should be different in the two cases. Fading or target scintillation takes different forms in different situations, and with the different variables (space, time and frequency). In this situation we are concerned with the time variation in received signal magnitude related to the varying geometry of the target and the search radar. The fluctuations caused by the changing interference between the many scattering centres in the icebergs (principally those facets normal to the radar beam) will have a relatively short correlation time and the observable changes in target brightness will, it is believed, be related to the much slower change in average target cross section as the radar look angle changes. This time scale will be on the order of seconds or tens of seconds.

It is hypothesized that the important difference between icebergs and ships is that the probability distribution function describing ship radar cross sections will be broader than that for icebergs. In particular, the tail of the distribution, i.e. the relative probability of larger cross sections will be larger for ships than for icebergs. This reflects the fact that there will probably be a smaller number of scattering centres contributing to the total ship signal and that the power reflected from some of these will be much higher than from the rest. The conditions for good corner reflector geometry (which will include the sea surface as well as the ship's hull and superstructure) will persist for times of seconds or fractions of seconds and would, normally, be visible to the radar operator. Consequently, it would be expected (and apparently observed by Danish radar operators) that ship returns will fluctuate over a wider dynamic range than the returns from icebergs on a time scale observable by the radar operator.

2.6 Sea ice mapping

Sufficient experiments have been performed with different SLAR and SAR systems from different geographic areas to say that the all weather mapping of sea ice can be done extremely well using airborne imaging radars. The examples of SEASAT SAR imagery now available, support the anticipated conclusion that satellite microwave imagery should also have a tremendous potential for all weather, day-night sea ice reconnaissance. It should be emphasized, however, that research has shown that the radar parameters are important and do affect the information content and usefulness of the final radar image.

Research using X band SLAR and Ku band scatterometer data (Gray et al, 1977a), has demonstrated the importance of the radar depression angle in the interpretation of sea ice imagery. The use of small depression angles (< 5°) emphasizes the large scale roughness (particularly sea ice ridging) while, with larger values of the depression angle (> 10°) the effects of smaller scale surface and, possibly, subsurface roughness and dielectric constant inhomogeneities are apparent on the imagery. Figure 1 a and b illustrate the same ice scene imaged by the SAR-580 at different depression angles and confirm the earlier findings. With radar depression angles greater than (5° - 10°) multiyear ice in the Beaufort Sea (winter and spring conditions) normally appears brighter in X band image tone than first year ice, even though the surface topography on a scale of feet or metres may not be significantly rougher. Further, at these depression angles the contrast between multiyear and first-year ice types is significantly enhanced with cross-polarized in comparison with like polarized data implying also a significant backscatter component arising from small scale surface and subsurface roughness.

Sea ice scatterometer results (Rouse 1969, Parashar 1977, Gray et al 1977, Onstott et al 1978) can also be used to show that there will normally be an inversion in the relative backscatter between sea ice and open water in the depression angle range of 60° - 75°. Airborne SLAR's and SAR's do not generate good imagery in this angular range, however, with the steep mode of the X/L SAR on the CCRS SAR 580, the imagery in this angular range is sometimes acceptable in terms of examining relative backscatter. One example of contrast inversion was observed in the imagery obtained on a target of opportunity basis on a flight across Baffin Bay en route from Thule to Frobisher Bay on September 14th, 1978. At the time the imagery was acquired there was a low concentration of ice floes (open pack situation) in the centre of Baffin Bay. Figure 2 a and b show the like polarized HH X and L band images obtained at this time. With careful examination it can be seen that the contrast between the ice floes and the open water inverts in both images. For the depression angle range less than approximately 60°, the ice floes are brighter than the open water but close to nadir the ice floes are dark with respect to the open water. It is possible that if SEASAT imagery of this region had been obtained, there might have been sufficient detail and changes in image texture to recognize the presence of ice even though the average water and ice backscatter would have been comparable at the SEASAT depression angle. There is no question, however, that the recognition of the presence and estimation of the concentration of the sea ice would be more readily accomplished with depression angles less than approximately 60°. This angle will vary with the ice conditions and wind speed but will normally be in the range 50° - 60°. A further example of this situation is given in the two SEASAT images presented by Sondergaard (1979) acquired on the 16th August and 19th August 1978 of the same area of the east Greenland coast. An ice map obtained from a Danish ice reconnaissance flight on the 25th August showed the presence of sea ice in the region south of Scoresby. Ice is visible in this region in the imagery of the 16th, at which time the wind speed was light (5-10 knots) but no ice is visible on the SEASAT image of the 19th August when the wind speed was much stronger (approx. 30 knots). It is possible that the ice visible on the 16th had moved out of the imaged area by the 19th, but considering the ice chart of the 25th, it is considered unlikely that there was no ice in the imaged swath on the 19th August.

The problem of identifying an open ice pack situation and estimating the concentration in a relatively high wind situation appears to be a problem for ice reconnaissance from space using SAR's like the SEASAT SAR or the proposed ESA COMSS SAR. The outer region of the proposed ICEX SAR should have a depression angle sufficiently small (63° - 41°) that this problem will be alleviated.

Normally when interpreting imagery of distributed targets, only a small contrast is required to easily distinguish between large regions. Further, one would expect that there would be sufficient detail (e.g. ridging and edge detail) in any ice-water scene containing extended ice water boundaries to clearly differentiate between the ice and water, irrespective of the relative backscatter.

As an example, SEASAT imagery acquired on August 20th and optically processed by the Defense Research Establishment, Ottawa, shows part of the large shore lead in the Southern Beaufort Sea, the ice edge and part of the Arctic pack ice. Despite the fact that the average backscatter and texture of the water and sea ice are very similar, it is possible to identify the larger floes at the edge of the ice pack and the imagery could be easily used to map the extent of sea ice.

3. RECOMMENDATIONS

3.1 Real time processing

The most significant problem now facing the remote sensing community advocating, correctly, the use of spaceborne SAR for sea ice reconnaissance are the problems associated with transmitting the resulting information to where it is needed in the time frame within which the information is valuable. These problems are severe for the usually envisaged situation of a wideband microwave data link transmitting unprocessed SAR data to an expensive, sophisticated ground station, processing the imagery to a resolution of typically 20-100 m and thirdly, retransmitting the imagery (preferable) or interpreted, low bandwidth, image (less desirable) to the Arctic operation or ship requiring the information. While the feasibility of these operations may have been demonstrated separately, to carry out all three tasks, particularly the third, within six hours (Gedney and Schertler, 1978) of data acquisition is an extremely difficult task. The complexity of the problem can be appreciated by study of the Advanced Information Transmission System (AITS) proposed for ICEX. Consequently, it is recommended that feasibility studies examine the design of real time, low resolution, on board SAR processors and systems for the transmission of this imagery in a form which could be received by relatively simple ground stations. It is possible that such receivers could be installed on ships e.g. ice breakers.

A design for the real time processor could be envisaged in the following manner: The radar range returns could be compressed - presummed using digital filtering techniques such that the slant range resolution was reduced by a factor of, for example, 16 to approximately 256 range bins. Subsequent azimuth processing could be done using relatively straightforward multilook, unfocussed processing. This could be done in a way similar to that described by Sondergaard (1977), using digital filtering. An azimuthal resolution of 200-500 m could be achieved for most satellite geometries without any correlation of the output of the digital filters (i.e. without 'focussing' the SAR returns). Assuming earth rotation and spacecraft yaw effects were removed for the middle of the swath by e.g. a clutter lock loop which tuned the reference phase signal, then range walk problems become insignificant and disappear within the resolution to which the imagery is being processed. Image distortion is not viewed as a serious problem for real time users and could be handled by an interpreter using plastic overlays. The output from such a multilook processor would be a low noise, low speckle image which, it is believed, would be very valuable for ship navigation purposes, for which the key information is the ice extent, mapping of ice boundaries and ice concentration. The existence of low resolution, real time microwave data, which could be transmitted by land line could improve the operation of Ice Forecasting Central. It is not suggested that the real time processor and associated low date rate telemetry replace the high bandwidth transmission of raw SAR data, clearly this would still be needed for other applications.

It has been shown in this work that some of the potential applications of a spaceborne SAR (e.g. the detection and tracking of icebergs and ships) will, in fact, be difficult to achieve even with 20 m resolution. Other applications e.g. the detailed information on ice ridging and ice type classification will also require fairly high resolution and would normally not be easily interpretable from the low resolution real time output. In this case the best way of satisfying user needs would be to estabilsh a receiving, processing and transmitting station in the Arctic, close to the operation. For example, a receiving station on the Tuktoyaktuk peninsula could supply the necessary information for an ice breaker involved in resupply to a winter Beaufort Sea drilling operation. While this would be very expensive, it might be the most reliable way of getting the satellite information to a position where it could be used.

3.2. Aircraft Research and Development for ice work

Continued research is required into the problems of interpreting and using steep, satellite type SAR data of sea ice, particularly summer season imagery. The SAR-580, with its complement of microwave sensors, is the ideal tool for this work provided that it is recognized that only a very small fraction of the imaged swath represents (e.g. 70°) satellite type look angle imagery.

3.3 Satellite Research and Development for Ice Work

As well as study of the real time processor discussed in section 3.1, it is recommended that further R and D is desirable to study large antenna structures (to improve swath width) and space qualified, high power transmitters to allow for operation at depression angles less than 60°. Such satellites may require shuttle launches.

3.4 Use of Marine Type Radars

It is recommended that continuing efforts be put into the use of marine type radars from shore (mountains or cliffs close to shore) or from drill platforms to monitor sea ice drift, icebergs and bergy bits. It is possible that a network of marine type radars suitably situated (e.g. adjacent to the NW passage, west coast of Greenland, etc.) could provide very valuable information to shipping. Such a system has been used by Japan to monitor sea ice off the north coast of Japan, for a number of years (Tabata, 1975). It would seem that the installation of such radars on drill platforms (as high as possible) would be essential in the waters off the Labrador coast, Davis Straits, etc.

ACKNOWLEDGEMENTS

The help of Dr. Livingstone and Dr. R. Hawkins of the Canada Centre for Remote Sensing, in the early stages of this work, was invaluable. Discussions with Professor P. Gudmandsen and F. Sondergaard of the Technical University of Denmark, and Dr. R.K. Raney, CCRS, have been extremely helpful in the preparation of this report.

REFERENCES

Gedney, R.D., "Iceberg Detection and Tracking by Imaging Radar," Presentation for Workshop on Remote Sensing of Sea Ice, Calgary, Alberta, 1977.

Gedney, R.D. and Shertler, R.J., "Microwave Systems for Monitoring Sea Ice,"
W.M.O Workshop on Remote Sensing of Sea Ice, Washington DC, Oct. 1978.

Gray, A.L., Hawkins, R.K., Livingstone, C.E., Lowry, R., Larson, R and Rawson, R., "The Influence of Depression Angle on Microwave Radar Returns on 'Targets' in an Ocean Background,"
Proc. 13th Int. Symposium on Remote Sensing of Environment, Ann Arbor, 1979.

Gray, A.L., Ramseier, R.D. and Campbell, W.J.,"Scatterometer and SLAR Results obtained over Arctic SEa Ice and their Relevance to the Problems of Arctic Ice Reconnaissance,"
Proc. Fourth Canadian Symposium on Remote Sensing, pp 424-444, 1977.

Gray, A.L., Gudmandsen, P., Overgaard, S., Skou, N. and Sondergaard, F., "West Greenland Sea Ice Experiment SURSAT Report No. 1,"
Technical University of Denmark, Report No. R 219, 1979.

Gray, A.L., Cihlar, J., Parashar, S. and Worsfold, R., "Scatterometer Results from Shorefast and Floating Sea Ice,"
Proc. Eleventh Int. Symposium on Remote Sensing of Enviroment, pp 645-657, 1977.

Jones, W.L., Schroeder, L.C. and Mitchell, J.L., "Aircraft Measurements of the Microwave Scattering Signature of the Ocean,"
IEEE J. Ant. and Prop., Vol. AP-25, pp 52-61, 1977.

Ketchum, R.D., "An Evaluation of Side-Looking Radar Imagery of Sea Ice Features and Conditions in the Lincoln Sea, Nares Strait and Baffin Bay,"
NORDA Technical Note 7, 1977.

Kirby, M. and Lowry, R., "Iceberg Detectability problems using SAR and SLAR systems,"
to be published.

Liskow, C., Klooster, A., Rawson, R., Shuckmann, R. and Wagner, H., "Analysis of Georges Bank Radar Imagery,"
ERIM report 120, 800-6-F, 1977.

Marthaler, J.G. and Heighway, J.E., "Radar Image Processing of Real Aperture SLAR Data for the Detection and Identification of Icebergs and Ship Targets,"
Proc. of the Sixth Canadian Symposium on Remote Sensing, Victoria B.C., 1978.

Onstott, R.G., Moore, R.K. and Weeks, W.F., "Surface Based Scatterometer Results of Arctic Sea Ice,"
Presentation at WMO Workshop on the Remote Sensing of Sea Ice, Washington, Oct. 1978.

Parashar, S.K., Haralick, R.M., Moore, R.K. and Biggs, A.W., "Radar Scatterometer Discrimination of Sea Ice Types,"
IEEE Trans. Geo. Elect. GE-15, No. 2, 1977.

Rawson, R., Larson, R., Shuchmann, R. and Worsfold, R., The Capability of SAR Systems for Iceberg Detection,"
Proc. of the First International Conference on Iceberg Utilization, Ames, Iowa, 1977.

Rouse, R.W., "Arctic Ice Type Identification by Radar,"
Proc. IEEE, Vol. 57, pp 605-611, 1969.

Skou, N. and Sondergaard, F., "Radiometer Signatures and SLAR Imagery of Sea Ice in Greenland, Results from July 1977 and November 1978."

Sondergaard, F., "SAR Imagery of Sea Ice," presentation to the SEASAT SAR Processor Workshop No. 2, Frascati, Italy, 1979.

Tabata, T., "Sea Ice Reconnaissance by Radar," J. Glaciology, Vol. 15, No. 73, pp 215-223, 1975.

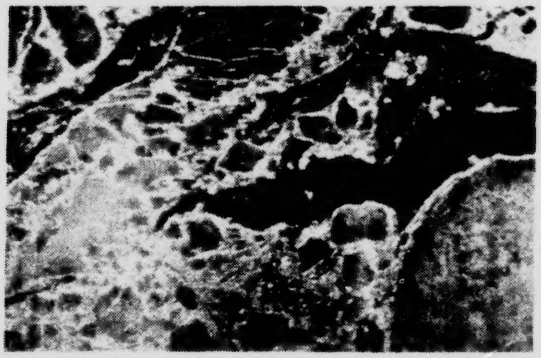

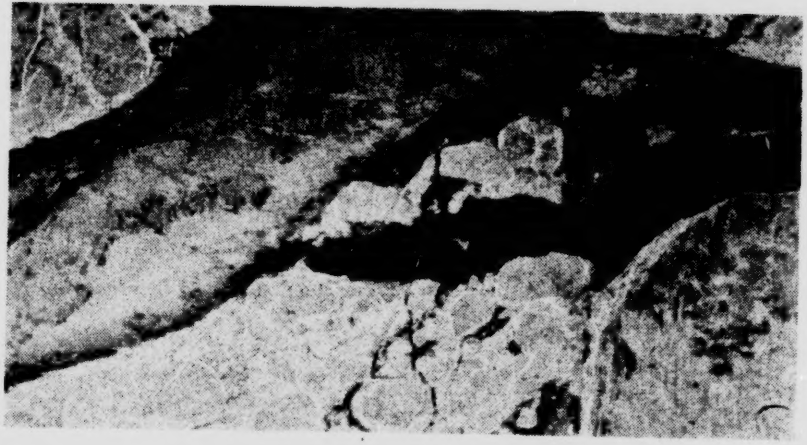

Figure 1a and b

Comparison of two X(HH) images of the same sea ice scene imaged on the 12th March 1979 (upper) and the 16th March (lower) by the X/L SAR. The depression angle for the top of the upper image is approximately 4° while the depression angle of the lower image is greater then 30°. The scene includes a corner of ice island T3 (lower right), some multiyear floes (to the left of T3 and upper left) and first year ice (adjacent to the top of T3). The increased sensitivity to ice ridging and large scale roughness at the lower depression angles can be seen in the upper image.

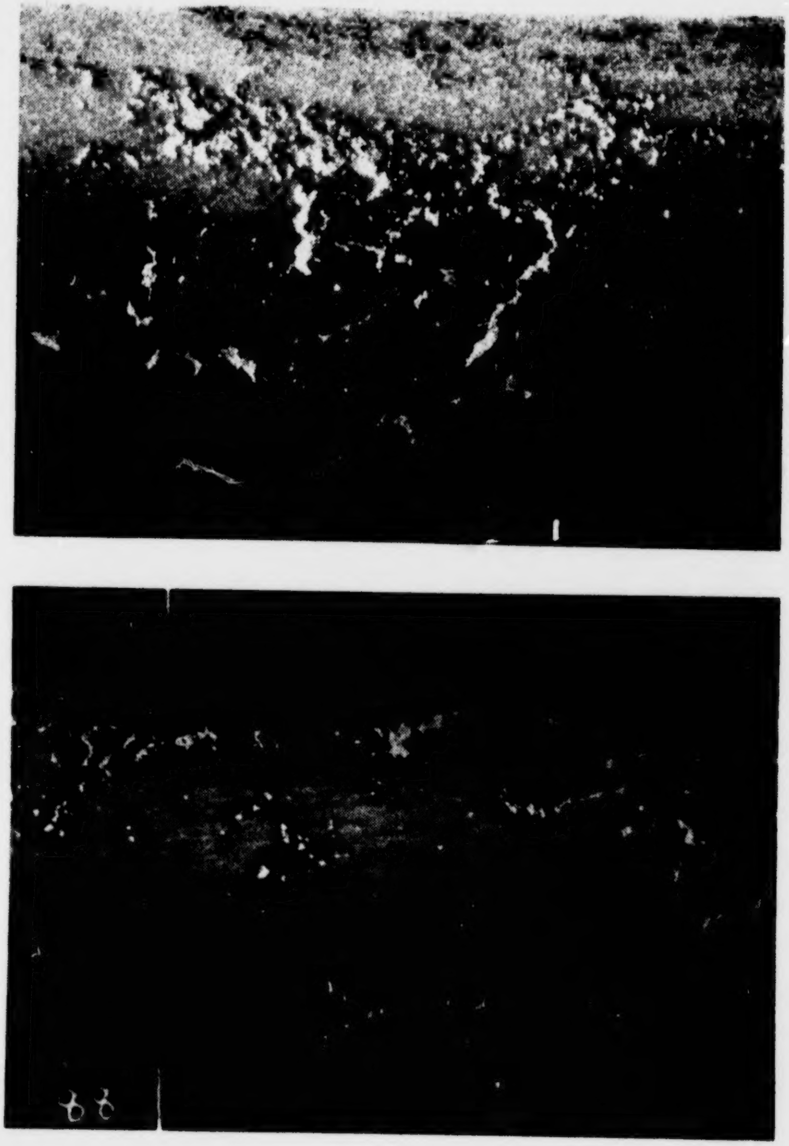

Figure 2a and b

L(HH) (upper) and X(HH) (lower) images of ice floes in Baffin Bay acquired on Sept. 14th 1978. Contrast reversal between the ice floes can be observed at the near nadir (upper) edge of the two images. For angles very close to nadir the ice is darker (lower backscatter) than the water while for depression angles less than 60° the ice is brighter than the open water.

SECTION 5.8

QUALITATIVE COMPARISON OF SLAR AND SAR DATA SETS

Hengeveld, H.G.

SURSAT ICE EXPERIMENT

PROJECT #4

QUALITATIVE COMPARISON OF SLAR & SAR DATA SETS

H.G. HENGEVELD, ATMOSPHERIC ENVIRONMENT SERVICE

INTRODUCTION

Data reliability, accuracy and timeliness, are essential elements in the effective ice information support of marine activities in northern waters. Hence, active microwave sensors, particularly side looking radars, have become vital tools in operational ice reconnaissance programs. However, despite several years of operational use of these sensors as well as extensive investigation into their usage by the research community, many unresolved questions still remain with respect to radar parameters required for an optimized operational sensor package for ice reconnaissance platforms. Radar variables which must be considered in such a design include spatial resolution, incidence angles, number of looks, tendencies of data availability, and extent of spatial coverage.

During the SURSAT ice experiments held in the Beaufort Sea in March, 1979, extensive active microwave data sets were collected over winter Beaufort Sea ice pack in conjunction with surface ice measurements. The microwave data sets include near-coincident coverage of the experiment area with both the multi-channel Synthetic Aperture Radar (SAR), mounted on the CCRS Convair-580 aircraft, and the X-band Motorola APS-94D Side Looking Airborne Radar (SLAR) on the NASA C-131 aircraft. These data proved useful for a qualitative evaluation of the effect of incidence angle and spatial resolution on the nature and quality of microwave imagery.

EFFECT OF INCIDENCE ANGLES

Figure 1 illustrates the typical range of incidence angles encountered in SLAR imagery recorded on operational ice reconnaissance missions. (These missions must respond to requirements for wide areal coverage as well as multi-sensor data collection capability.) As indicated in the figure, 80% of typical reconnaissance coverage is provided at high incidence angles between 80° and 89°. These angles are similar to those which marine vessels must cope with in the use of their radars for ice hazard detection. A good knowledge of the characteristics of microwave imagery at these angles is therefore essential. To date, although considerable research has been undertaken on microwave properties of sea ice through scatterometry experiments, very little work has been undertaken at high incidence angles. However, the SAR data sets collected during the SURSAT experiments included one short run portraying ice imagery at high incidence angles (Pass 3 on March 12, 1979, over ice surrounding ice island T-3). In addition, passes 1 and 2 of the same flight provided SAR coverage at intermediate incidence angles (up to 80°).

.../2

In order to determine the validity of comparing data from SAR passes 1 and 2 with corresponding SLAR data of high incidence angles, a preliminary evaluation of the effect of incidence angle on SAR imagery was first undertaken. Passes 2 and 3 of the March 12 SAR imagery flight over ice island T-3 were recorded at flight altitudes of 3800 m and 430 m respectively. Therefore, as illustrated in Figure 2, the two images provide repeat coverage of the same ice cover at similar resolutions but differing incidence angles. Careful examination of these images (see Figures 3 and 4) provides the following results:

Incidence Angles ~ 55°. Most ice floes show detailed texture influenced by surface electromagnetic properties. Multi-year floes show clear indications of hummocks and small-scale irregularities. First-year ice shows low smooth returns between ridges, while returns from young ice show higher textured returns due to extensive rafting and other possible surface characteristics. Recent leads, presumably covered with new ice, stand out clearly in the young ice due to their smooth, very low returns. Ridges in general are clearly identifiable, but some of the weathered ridges across the multi-year floes are difficult to distinguish from the background textured surface returns.

Incidence Angles ~ 75°. Similar to those at 55°, although contrast between ridge returns and textured surfaces is increased. Weathered ridges are still difficult to identify.

Incidence Angles ~ 80°. Smooth young ice now shows minimal returns, while returns from rafted young ice and the multi-year ice show a decreased textured return. Returns from ridges and rafts, including weathered ridges, are becoming accentuated.

Incidence Angles ~ 85°. MY floes show only coarse, subdued returns. Weathered ridges barely noticeable at 75° now show strong linear responses. Young ice in general shows a considerably reduced return, although rafts are prominent.

Incidence Angles ~ 87-88°. Very coarse, strongly contrasting speckle from large MY floes, while FY and young ice show minimal returns. Ridges and rafts are very prominent on all ice types.

The above observations indicate a distinct change in the characteristics of the imagery between 80° and 85° incidence angles. At angles less than 80°, ice surface texture is dominant and an important clue in identification of the ice type. Topography appears subdued and in some instances lost in the background noise. However, above 85°, the ice surfaces provide minimal returns and topographical features dominate the imagery, resulting in sharply contrasting signatures.

.../3

These conclusions are similar to those reached by L. Gray in his recent study of depression angle effects.[1]

COMPARISON OF SAR AND SLAR IMAGERY

As a result of the preceding discussion, it can be assumed that valid comparison of SAR/SLAR images at non-similar incidence angles cannot be conclusive, particularly if one of the images is recorded at angles above 80°. As illustrated in Figure 2, the only portion of the Beaufort Sea SURSAT radar imagery set that can be effectively used for such a comparison is that of SAR imagery pass 3 on March 12 and the corresponding SLAR imagery flown on March 12 and 18. These data are, however, of particular importance since their angles of incidence lie in the high range of such great interest to operational airborne and shipboard radar detection systems.

Portions of the two images which were thus compared are illustrated in Figure 5, showing radar returns of a large, multi-year floe near ice island T-3. This floe was imaged at 87° on the SAR imagery and 86° in the SLAR. Corresponding resolutions were 1.5 m x 2.1 m and 30 m x 140 m, respectively. Comparison of the images resulted in the following observations:

1. Multi-Year Ice. The SAR image shows prominent returns from a network of ridges contrasting starkly with the background floe surface. The surface of the floe also reveals a coarse, sharply contrasting speckle, assumed to be attributable to weathered hummocks and other isolated topographic features. A faint background signal return from smoother ice areas is still evident at 86°, but has completely disappeared by about 87.5°. The corresponding SLAR imagery shows a similar ridging network, revealing all ridges visible on the SAR image, but showing considerably less detail of the ridge size and shape, and in one or two cases, resulting in the merging of two ridges in close proximity to each other into one broad linear return. The coarse speckle apparent on the SAR image is present on the SLAR image but appears very smudged. There is no background return evident for the smoother surfaces of the floe.

2. First-Year and Younger Ice. Smooth areas of these ice types show no significant return on the SAR image, although rafts show prominently. Heavily rafted areas appear similar in tone and contrast to MY ice, but shapes of returns are distinctly different from those of MY ridges. The heavy rafting is also visible on the SLAR image but again lacks crispness. Isolated rafts found on SAR images are generally not evident on the SLAR. The younger ice is, however, easily distinguished from the adjacent

multi-year.

3. Rubble. The SAR image provides considerable detail on ice structure within broken-up rubble areas. Where small, intact floes within the rubble frequently resulted in only a slightly mottled strong return area on the SLAR image due to its inability to resolve such detail, they could be distinctly identified as separate identities on the SAR. Smallest, clearly resolvable floe sizes were 100 m and 20 m respectively, the latter presumed to be significantly affected by degradation in resolution during photographic reproduction. In general, the main difference observed between the two images, as expected, was that of topographic detail. However, despite the lack of crispness of topographic information on the SLAR image, the basic information on ice types and their boundaries, the extent of deformation and surface roughness, general floe structure, and lead size and orientation is apparent in both images. The implication is that the additional detail of information observed on the SAR image is useful, but not essential to the extraction of basic ice information required by marine users. Unfortunately, the data set analyzed provides for only one isolated case study and cannot be considered conclusive without acquisition and analysis of similar data sets over differing ice conditions, geographic location, and seasons.

CONCLUSIONS AND RECOMMENDATIONS

On the basis of a rather limited and qualitative study of a coincident SAR and SLAR data set, the following tentative conclusions are provided:

- that incidence angle is a critical factor in the nature of active microwave imagery, resulting in negligible effect of surface e.m. properties beyond angles of 80°.
- that, in the 85-88° incidence angle range, SAR imagery provides much better crispness and detail to returns from ice surface topography than does SLAR.
- that, for this case study, basic ice information required for operational strategic support of marine activities are equally available from SAR and SLAR images despite the large differences in spatial resolution.

Recommendations are as follows:

- Because of the significance of imagery at high incidence angles to operational reconnaissance programs throughout the 1980s, as well as to marine vessels relying on radar for hazard detection, extensive research should be undertaken in scatterometry measurements of sea ice at the 80-90° incidence angle range.
- Coincident SAR and SLAR image data sets at high incidence angles should be obtained and analyzed for a variety of ice conditions at various geographic locations and seasons.

.../5

- Digital analysis of SAR imagery of sea ice, recorded at high incidence angles and processed at varying data rates, should be undertaken to further evaluate the effect of resolution at these angles.

REFERENCE

1. Gray, L, "Depression Angle Study", SURSAT Report, Technical University of Denmarks, February, 1980.

FIGURES

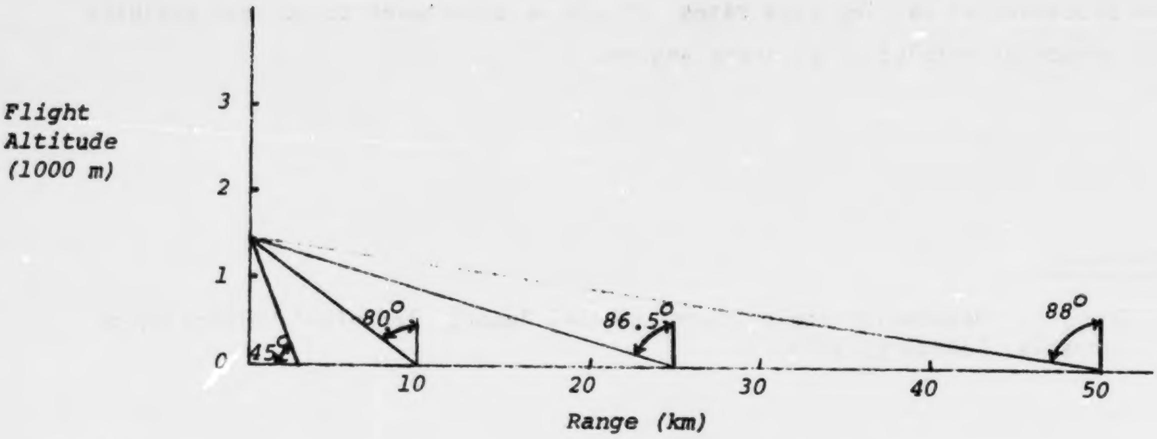
Flight Altitude (1000 m)
3
2
1
0
45°
80°
86.5°
88°
10
20
30
40
50
Range (km)

Figure 1. Typical incidence angles used in operational ice reconnaissance activities identical to those used on the March 12, 1979 SLAR flight.

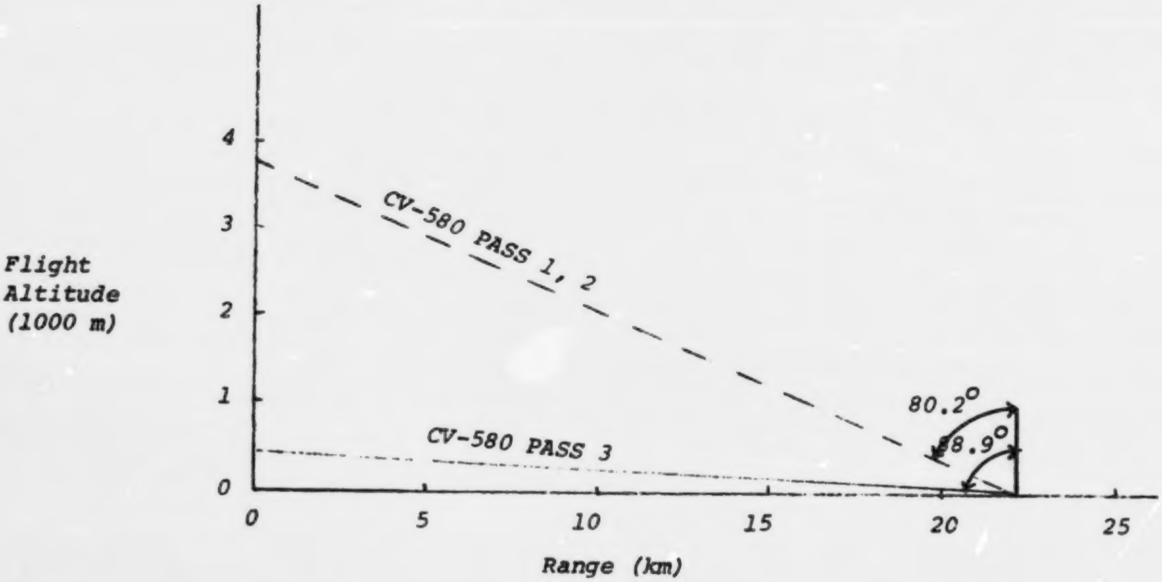
Flight Altitude (1000 m)
4
3
2
1
0
CV-580 PASS 1, 2
CV-580 PASS 3
80.2°
88.9°
0
5
10
15
20
25
Range (km)

Figure 2. Comparison of incidence angles on March 12, 1979 SAR flights

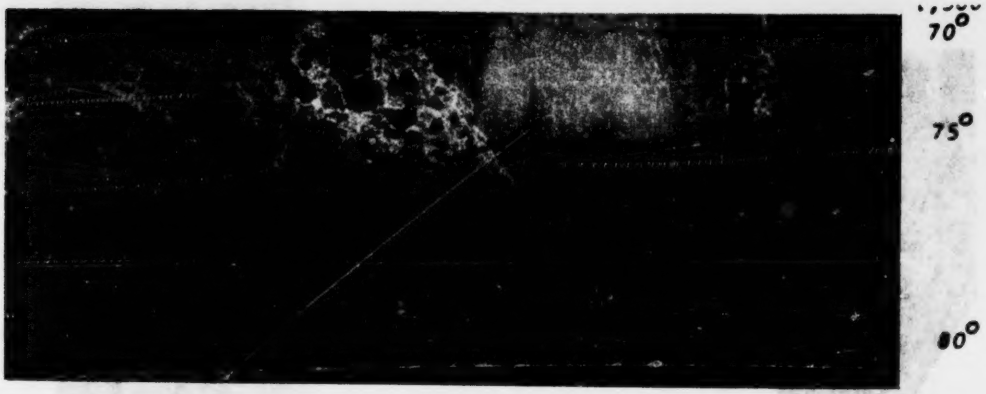

Figure 3. Far range portion of SAR imagery over T-3 collected on Pass 2 of March 12, 1979 flight. Incidence angles vary from 70° to 80°+.

80°
85°
86°
87°
88°

Figure 4. Far range portion of Pass 3 of March 12, 1979 SAR flight, showing SAR imagery over incidence angles 80° to 88°.

5a

5b

Figure 5. Comparison of images of large MY floe at similar high incidence angles, as collected on SLAR (5a) at 30 m x 140 m resolution and SAR (5b) at 1.5 m x 2.1 m. The line shown on each image represents the 86° incidence angle position.

SECTION 5.9

X-BAND SAR IMAGE RESPONSE FROM FIRST-YEAR ICE OFF NEWFOUNDLAND

Wedler, E. and J.R. Rossiter

Edward Wedler
Air, Earth and Oceans Ltd.
Surveillance Systems
P.O.Box 54
Oshawa, Ontario, Canada. L1H 7K8

James R. Rossiter *
Centre for Cold Ocean Resources Engineering
Memorial University of Newfoundland
St. Johns, Newfoundland, Canada. A1B 3X5

X-BAND SAR IMAGE RESPONSE FROM FIRST YEAR ICE OFF NEWFOUNDLAND

Poster Paper:

URSI Commission F Symposium
Lawrence, Kansas, U.S.A.
January 5-8, 1981

* now with: Huntec ('70) Ltd.
25 Howden Road
Scarborough, Ontario, Canada. M1R 5A6

ACKNOWLEDGMENTS

Acknowledgement is given to the Ice Branch of the Atmospheric Environment Service of Canada for its support and review of the work involved in this report. Specific credit is given to René Ramseier, Henry Hengeveld and David Lapp.

Acknowledgement is also given to C-CORE, St. Johns, Newfoundland, for allowing access to the SAR '77 field data reports and field notes, the photography and the impulse radar records.

Edward Wedler
Air, Earth and Oceans Ltd.
P.O.Box 54
Oshawa, Ontario, Canada. L1H 7K8

James R. Rossiter *
Centre for Cold Ocean Resources Engineering
Memorial University of Newfoundland
St. John's, Newfoundland, Canada. A1B 3X5

X-BAND SAR IMAGE RESPONSE FROM FIRST YEAR ICE OFF NEWFOUNDLAND

Dual-polarized (HH and HV) X-band (3.2 cm, 9.3 GHz) Synthetic Aperture Radar (SAR) data at an incidence angle between 66-77 degrees were acquired on March 15, 1977, over first year sea ice near Twillingate, Newfoundland. Three distinct ice zones within an area of 7.6 sq. km were visually delineated on both polarizations of the imagery according to tone and texture.

Surface measurements covering all three zones included over 75 ice core salinity and density profiles, over 300 augered ice thickness measurements, temperature and crystal structure measurements, and an impulse radar profile at 400 MHz centre-frequency. Ice and meteorological observations were made for several weeks prior to the SAR overflight.

Each of the physical properties measured was analysed using statistical techniques to evaluate its contribution to the tonal differences between the three zones. This analysis was performed for each of the upper four 7.6 cm thick layers within the ice. Although it was found that total ice thickness variations correlated with the ice zones seen on the imagery it is doubtful that X-band SAR sensed ice thickness directly. Using the statistical results as a guide, it appears that the X-band response was both largely from ice beneath a relatively low salinity (approximately 2.4 parts per thousand) surficial layer that had refrozen from melted snow and from the surface roughness of the ice cover.

INTRODUCTION

Interpretation of airborne radar imagery over ice is an ongoing activity of the Atmospheric Environment Service of Canada. Relating the nature and condition of the ice to the observed tone and texture as seen on radar imagery is important to comprehensive operational interpretations. Extensive preliminary investigations over many different ice types and conditions are required to fully utilize interpretations made from future surveillance satellites having a Synthetic Aperture Radar (SAR) capability. Using data collected during SAR '77 (Larson, et al, 1977; Worsfold, et al, 1977; Wedler, et al, 1977a and 1977b; and Hengeveld, 1977) and data collected in a concurrent C-CORE program near Twillingate (Lau and Rossiter, 1978; and Rossiter, et al, 1977) this paper attempts to identify and understand more closely those first year sea ice properties affecting the X-band SAR image response.

X-band like- and cross-polarized synthetic aperture radar (SAR) data having 3 m X 5 m resolution were acquired at 2,750 m (9,000 ft.) ASL over first year sea ice near Twillingate, Newfoundland, on March 15, 1977 (Larson, et al, 1977) (Figure 1). The SAR imagery was obtained as part of a program conducted by C-CORE, the Centre for Cold Ocean Resources Engineering, St. John's, Newfoundland, Canada (C-CORE, 1979).

---

* now with: Huntec ('70) Ltd.
25 Howden Road, Scarborough, Ontario
Canada. M1R 5A6

Preliminary observations of the X-band SAR imagery indicated tonal variations that were possibly related to ice surface roughness and ice thickness variations (Wedler, et al, 1978).

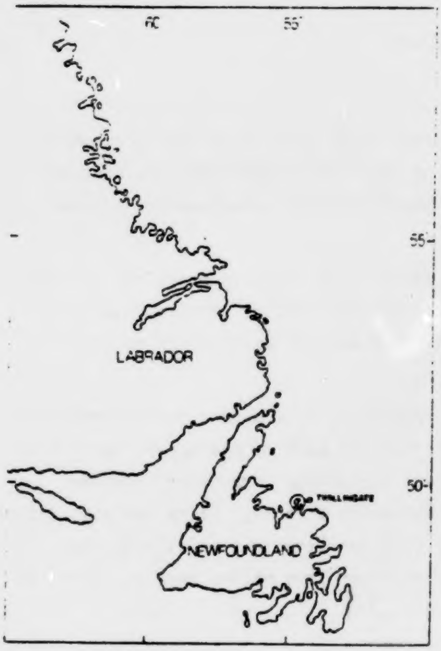

Figure 1 Study site, Twillingate, Newfoundland.

BACKGROUND

SAR image tones and textures are a result of the radar system and properties of the illuminated target. These system and target properties include: wavelength, polarization, look angle, look direction, aspect angle, surface and subsurface roughness, resonant particles, and dielectric discontinuities. Since each of these factors can singly or collectively affect the SAR image, a knowledge of the radar system and the microwave properties of the target is important in the comprehensive interpretation of image tone and texture.

Radar backscatter from sea ice is a measure for determining SAR image tone and texture. The sea ice properties contributing directly or indirectly to the radar backscatter include: dielectric interfaces such as air-ice, air-water and ice-water; irregularities within the ice volume such as air bubbles and brine channels; surface roughness; layering within the skin depth; salinity; and temperature. Previous radar studies over sea ice indicate that ice age, ice drift, surface topography, fractures, pressure ridges (Johnson and Farmer, 1971), and the stages of ice development (Ketchum and Tooma, 1973) affect radar image tone and texture. Rouse (1968) lists physical ice properties that determine ice structure and that may affect the radar image, namely: salinity of the original sea water, ice temperature, pressure, porosity, speed of ice formation, age, and other factors concerned with the history of the ice. Elachi, et al, 1976, concluded in a study of radar return from freshwater ice that ice observations of particular SAR image tonal interest include: ice thickness and composition, ice structure and bubble content, and surface and subsurface roughness. Weeks, et al, 1978, extended the above possibilities to include: thermal contrasts and ice thickness differences.

DELINEATION OF ICE ZONES ON THE SAR FILM

Three distinct ice zones were visually delineated on the X-band SAR film over ice near Twillingate. These zones are seen equally well on both cross- and like-polarized SAR film (Figures 2 and 3) and for passes at two different azimuth angles. Twenty random samples of SAR negative film were obtained in each Zone using a 1 mm diameter aperture on a MacBeth densitometer (60 m diameter equivalent ground resolution). A normal distribution was assumed for each Zone, since each appeared tonally uniform.

A student-t test of the SAR film densities indicates that the ice Zones are statistically separable at the 0.01 significance level, based on greytone alone (Table 1). Since film density in the mid-tone region can be considered directly proportional to the radar return signal in most cases (C. Liskow, personal communication), Zone C then has the highest amount of backscatter, while Zone B has the lowest backscatter. The variance in film density is approximately the same for all zones, indicating similar backscatter variance for all zones. Although this data set is limited, it appears that image greytone (backscatter) variations may be slightly larger in the ice zones on X-HV imagery than on the corresponding X-HH imagery. Livingstone, et al, 1979, observed that the variance of the depolarization rates over sea ice, at 45 degrees incidence angle, may be related to the surface roughness and variability of the snow depth.

X-HH IMAGE

ZONE	$\bar{x}$	σ	T-VALUE	DEGREES OF FREEDOM	SIGNIFICANCE LEVEL 0.05	SIGNIFICANCE LEVEL 0.02
A	0.473	0.025	4.326	38	•	•
B	0.437	0.027				
A	0.473	0.025	9.306	38	•	•
C	0.547	0.025				
B	0.437	0.027	13.321	38	•	•
C	0.547	0.025				

X-HV IMAGE

ZONE	$\bar{x}$	σ	T-VALUE	DEGREES OF FREEDOM	SIGNIFICANCE LEVEL 0.05	SIGNIFICANCE LEVEL 0.02
A	0.447	0.022	2.360	38	•	
B	0.432	0.018				
A	0.447	0.022	13.425	38	•	•
C	0.547	0.025				
B	0.432	0.018	16.933	38	•	•
C	0.547	0.025				

• indicates statistical separation (Hypothesis : $u_0=u_1$)

Table 1 Relationships between ice zones based on SAR negative film densities.

The study site was composed solely of bare, fast ice at the time of the SAR overflight, with isolated traces of old, crystalline snow. Zone A appears uniformly dark grey on the imagery, indicating a history of ice formation under relatively calm conditions. A smooth surface and uniform ice thickness (Table 2) supports this history of formation. Zone B appears, visually, equally grey in tone but contains some parallel east-west linears. Imbedded and slightly rafted smooth ice pans (Wedler, et al, 1978a) provide evidence of an unsettled history of formation. Zone B was probably formed under calm conditions, like Zone A, but because of its vulnerability to the open bay it became swell-broken during an earlier storm, 5 weeks prior to the SAR overflight. Ice thickness variations in Zone B are greater than in Zone A. Since Zone A and Zone B are not separable based on ice thickness, however, indications are that both zones were formed simultaneously. Zone C appears lightest in tone. It also appears uniform in texture. Variations in ice thickness (Table 2) and observations from ground photos taken in Zone C (Figure 4) indicate a homogeneously-rough surface, suggesting a zone with an unsettled history of formation. Zone C was almost exclusively formed from pack ice brought in by the strong northerly winds during the earlier storm. The pack subsequently consolidated to Zone B, extending the existing fast ice.

Ice Thickness (cm)	Zone	Zone	Student t-value	Degrees of Freedom	Significance Level 0.05	Significance Level 0.01
	A	B				
$\bar{x}$	48.2	51.3	1.267	96		
σ	6.7	16.8				
	B	C				
$\bar{x}$	51.3	82.8	5.224	102	•	•
σ	16.8	37.7				
	A	C				
$\bar{x}$	48.2	82.8	6.608	110	•	•
σ	6.7	37.7				

• indicates statistical separation (Hypothesis: $\mu_0=\mu_1$)

Table 2 Relationships between ice zones based on ice thicknesses obtained from augering.

A heavy precipitation of snow (230 mm) fell on all three zones during the earlier storm over a period of about 4 days, 5 weeks prior to the SAR overflight. The snow melted within a few days after the storm (Worsfold, et al, 1977). This freshwater source froze to become part of the surficial ice layer, resulting in fairly low salinities in the upper layers of ice (Table 3).

FIELD DATA COLLECTION

Prior to data collection over the ice a sampling grid

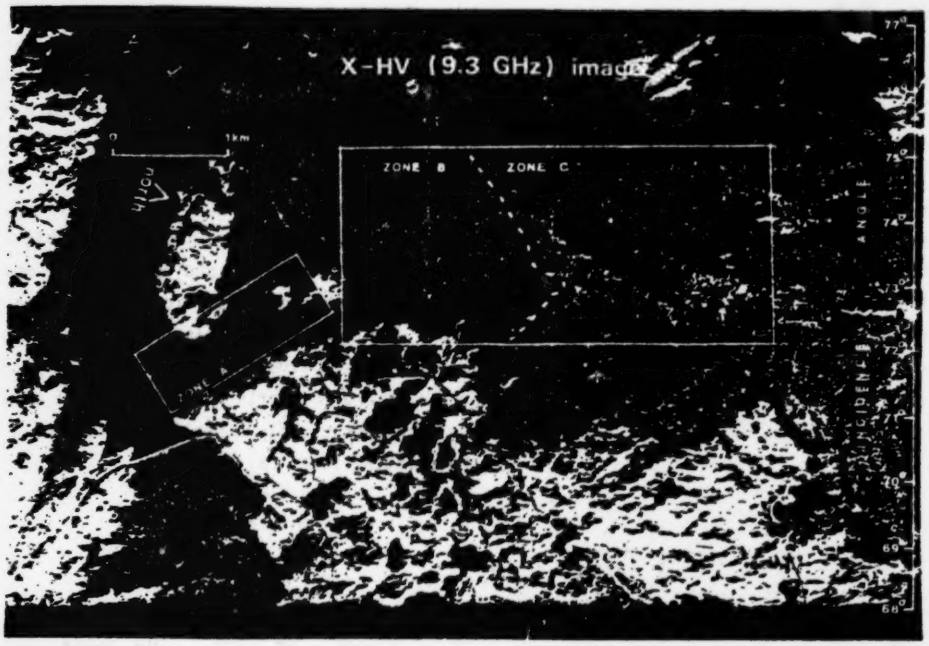
X-HV (9.3 GHz) image
0
1km
NORTH
ZONE B
ZONE C
ZONE A
INCIDENCE ANGLE
77°
75°
74°
73°
72°
71°
70°
69°
68°

Figure 2 SAR X-HV Imagery taken from an altitude of 2,750 m (9,000 ft.) on March 15, 1977, near Twillingate, Newfoundland. Angles of Incidence are shown. Very bright areas are land.

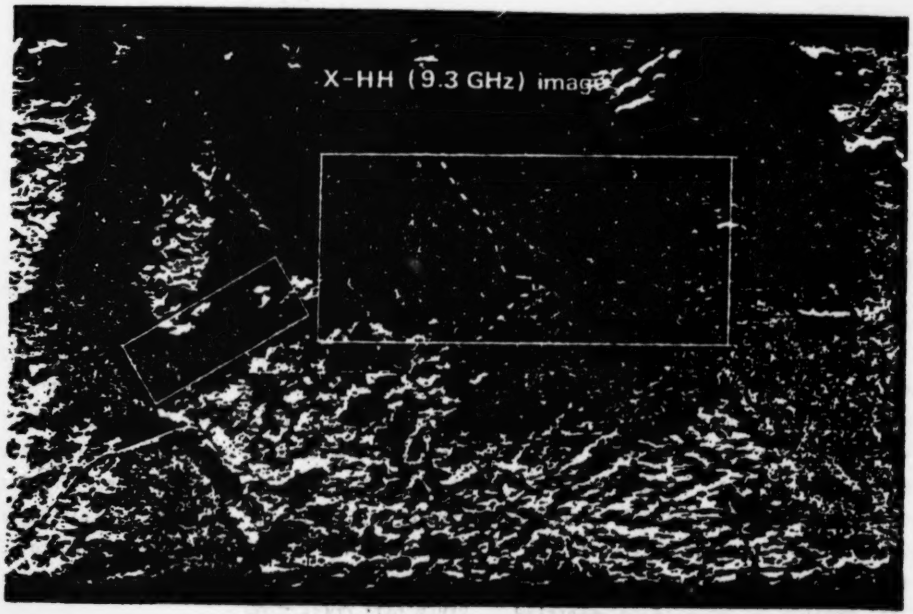
X-HH (9.3 GHz) image

Figure 3 SAR X-HV Imagery taken from an altitude of 2,750 m (9,000 ft.) on March 15, 1977, near Twillingate, Newfoundland.

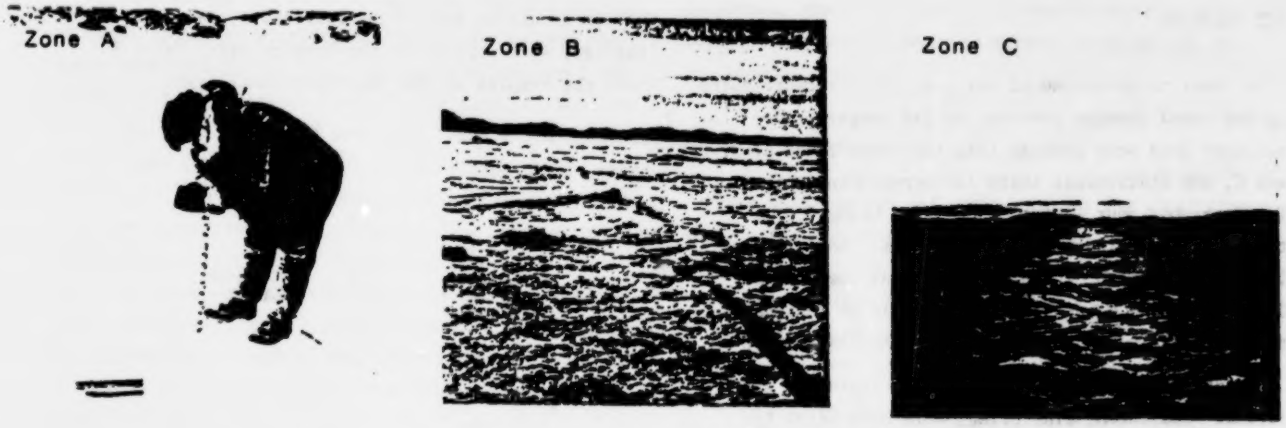

Figure 4 Twillingate ice zones as seen from ground photos.

was precision-surveyed over the study area using an engineer's transit and chain. X- and L-band reflectors were placed at three different locations to assist the accurate reconstruction of the grid onto the SAR imagery. Since the appearance of the study site on the radar imagery was unknown during field operations ice thickness measurements and ice core locations were randomly selected (see Figure 7). Two or more cores were obtained at each location, at a different time and position. After reconstructing the sampling grid on the SAR imagery it was found that 11 core locations fell within Zone A, 10 core locations fell within Zone B, and 9 core locations fell within Zone C. Ice thicknesses were measured (± 1 cm) from 300 augered 1½ inch (4.8 cm) diameter holes over a period of 35 days prior to the SAR overflight. Ice salinities and densities were measured (± 0.01 gm.cm^{-3} and ± 0.1 ppt., respectively) from 83 ice cores over a period of 22 days prior to the SAR overflight. Each ice core, 15 cm in diameter, was divided along the length of the core into 7.6 cm sections. Each 7.6 cm section was then divided into two across the core face - one half for salinity measurements and the other half for density measurements. Salinity was determined using a YSI Model 33 S-C-T electrical conductance salinometer and density was determined using a weigh scale, kerosene and Archimedes principle. Tables of salinity and density and further details on measurement procedures used can be found in Wedler, et al, 1977a and 1977b, and in Lau and Rossiter (1978).

Layer		Zone		
		A	B	C
1	$\bar{x}$	2.4	2.6	3.1
	σ	2.4	2.0	3.3
2	$\bar{x}$	2.7	3.8	2.7
	σ	2.5	2.1	1.1
3	$\bar{x}$	2.9	3.5	3.1
	σ	1.7	0.8	1.8
4	$\bar{x}$	4.2	3.3	3.7
	σ	2.6	1.4	0.6

LAYERS	ZONES	F-VALUE HOTELLING T-TEST	DEGREES OF FREEDOM	SIGNIFICANCE LEVEL 0.05	0.01
1,2	A,B	1.5585	2,53		
	A,C	0.3739	2,48		
	B,C	2.2434	2,38		
1,3	A,B	1.2115	2,53		
	A,C	0.4173	2,46		
	B,C	1.0759	2,38		
2,3	A,B	2.4783	2,53		
	A,C	0.0900	2,48		
	B,C	2.6532	2,38		
2,4	A,B	3.5990	2,53		
	A,C	0.3113	2,48		
	B,C	2.4559	2,38		
3,4	A,B	2.3462	2,53		
	A,C	0.3559	2,48		
	B,C	2.0114	2,38		

* indicates statistical separation (Hypothesis: $u_0=u_1$)

Table 3 Two-dimensional relationships between all Zones and Layers based on Salinity (ppt.)

For 33 days prior to the SAR overflight wet- and dry-bulb air temperature, wind speed and direction, precipitation type and amount, air pressure and cloud cover were observed and measured. This data and the procedures used can be found in Worsfold, et al, 1977.

ICE SALINITY

In order to determine if sea ice salinity contributed to the tonal changes seen on the SAR imagery, the salinity data were grouped into the three zones A, B, and C, and statistical tests for separation applied. The uppermost four layers, each layer being 7.6 cm thick, were considered in the analysis. Should a statistical separation of the data occur at the 0.05 or 0.01 significance level, salinity would be considered to have contributed to the tones on the SAR imagery.

One-dimensional and two-dimensional tests for statistical separation, clustering, were made using the student-t and Hotelling's-T^2 tests respectively, as described in Timm (1976). The Hotelling's-T^2 tests take into account the different number of data values from each zone. In applying the tests here the mean and standard deviation used were based on the sample data. The data were too few in number to test for population distribution. Table 3 shows the results of the two-dimensional tests. Column 1 (Layers) indicates the core layers being compared. Column 2 (Zones) indicates the Zones being compared. Columns 3, 4, and 5 indicate the results of the statistical tests. The F-value is determined from the Hotelling's-T^2 test of the data. Together with the degrees of freedom the F-value is used to determine the level of statistical separation.

It can be seen from Table 3 that there exists no layer-zone combination that is statistically separable at the 0.05 or 0.01 significance levels. The analysis indicates that factors other than salinity are responsible for the tonal changes over ice as seen on the X-band SAR imagery. Figure 5 illustrates the lack of zone-layer separation in the upper two ice layers.

Rouse (1968) has suggested that the salinity of the ice does contribute to the intensity differences noted in radar imagery. The data collected at Twillingate, however, indicated no contributions from low salinity fast ice to the SAR image tonal changes.

ICE DENSITY

Since salinity did not contribute to the tonal changes seen on the SAR imagery, it was decided to determine if sea ice density contributed to the tonal changes. Similar groupings and statistical tests, described earlier, were applied to the density data. Table 4 shows the results of the two-dimensional tests.

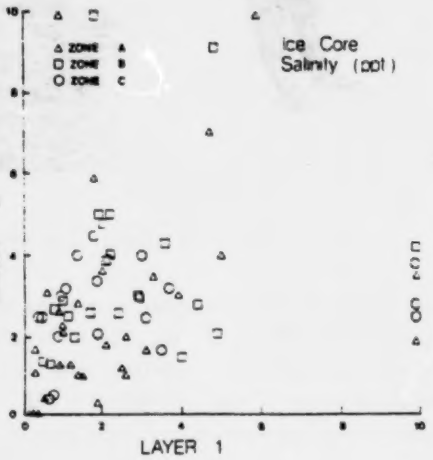

Figure 5 Relationship between Layer 1 (0-7.6 cm) and Layer 2 (7.6-15.2 cm) in Zones A, B, and C based on salinity (ppt.).

Layer		Zone A	Zone B	Zone C
1	X	0.873	0.874	0.867
	σ	0.013	0.016	0.016
2	X	0.859	0.884	0.885
	σ	0.025	0.022	0.019
3	X	0.885	0.892	0.890
	σ	0.028	0.017	0.019
4	X	0.894	0.895	0.888
	σ	0.027	0.020	0.019

LAYERS	ZONES	F-VALUE HOTELLING T-TEST	DEGREES OF FREEDOM	SIGNIFICANCE LEVEL 0.05	SIGNIFICANCE LEVEL 0.01
1,2	A,B	8.5780	2,53	*	
	A,C	12.5076	2,48	*	*
	B,C	1.2819	2,38		
1,3	A,B	0.9447	2,53		
	A,C	1.5937	2,48		
	B,C	0.9442	2,39		
2,3	A,B	7.6698	2,53	*	
	A,C	7.9326	2,48	*	
	B,C	0.1670	2,39		
2,4	A,B	7.6495	2,53	*	
	A,C	8.6485	2,48	*	
	B,C	0.6682	2,38		
3,4	A,B	0.7876	2,53		
	A,C	1.2277	2,48		
	B,C	0.6295	2,38		

* indicates statistical separation (Hypothesis: $u_0=u_1$)

Table 4 Two-dimensional relationships between all Zones and Layers based on Sea Ice Density ($gm.cm^{-3}$).

Contrary to the ice salinity results, the ice density analysis indicated statistical separation between zone-layer combinations, at the 0.05 significance level and at the 0.01 significance level in one case. It was seen that Zone A was separable from both Zones B and C, while Zones B and C were statistically indistinguishable from each other. The student-t test, furthermore, indicated that the zonal separation of Zone A from Zones B and C occurred primarily in the second ice layer (7.6-15.2 cm). All zones were statistically similar in the uppermost layer (0-7.6 cm). Figure 6 graphically illustrates the separation of Zone A from Zones B and C, primarily in the second layer, and the similarity between Zones B and C.

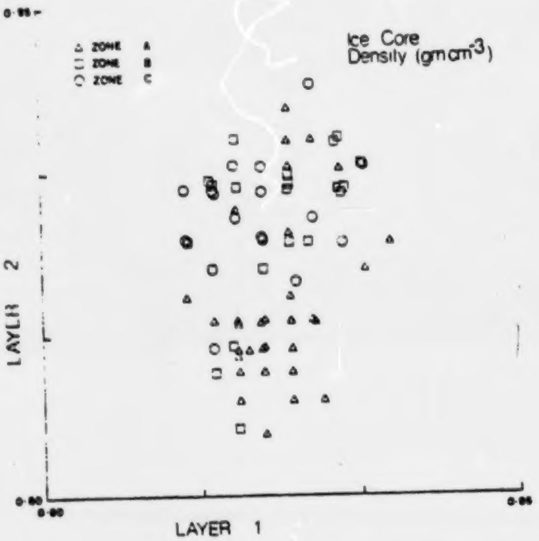

Figure 6 Relationship between Layer 1 (0-7.6 cm) and Layer 2 (7.6-15.2 cm) in Zones A, B, and C based on density (gm.cm^{-3}).

The SAR image (Figure 2) and SAR film density (ie. grey tone) analysis (Table 1), however, shows Zones B and C as distinct. The separation of Zones B and C as seen on the SAR imagery, then, must be due to factors other than density differences while the separation of Zone A from both Zones B and C may be due to density differences. The fact that Zone A is distinct in density at the second ice layer, at the 0.01 significance level, indicates possible X-band signal penetration beyond the top surficial layer of low salinity ice. Skin depth estimates, described later, indicate a possible penetration of X-band signals to between 5-15 cm, ie. to the second layer.

SURFACE ROUGHNESS

Since salinity did not contribute to the tonal changes seen on the SAR imagery and since sea ice density was not responsible for the tonal change between Zones B and C but possibly between Zone A and Zones B and C, it was decided to investigate the role of surface roughness on the tonal changes.

No direct surface roughness measurements were made in the study area. Indirect measures of surface roughness were obtained, however, from impulse radar profiles and ground-based photography.

Three surface roughness zones were reported in the field data notes (Wedler, et al, 1977a and 1977b). These zones were based on visual surface-based observations. Zone A appeared to have had the smoothest surface. Zone B had a relatively smooth surface but contained very smooth, tilted and imbedded blocks of ice. Zone C ice appeared distinctly roughest. Figure 4 illustrates the visual disinction between each surface.

An airborne impulse radar profile near the surveyed 'control line' was flown on March 16, 1977, one day after the SAR overflight. Figure 7 illustrates the approximate location of the impulse radar profile data within Zone B, while Figure 8 illustrates the character of the profile data. Centre-frequency of the impulse radar was 80 MHz and the antenna was slung approximately 3 m below a low-flying helicopter. Flying height was 6 to 10 m above the ice (to the antenna) and airspeed was approximately 20 m.s^{-1} (40 knots). The long period variations seen in Figure 8 are due to helicopter altitude variations, and not to ice surface relief.

The distance scale indicated is for travel time of the signal in the air. No echoes from the ice-water interface were detected at either 80 or 400 MHz centre-frequencies. The second echo is a reverberation from the bottom of the aircraft to the ice and back.

The character of the ice surface echo in Zone B changes near survey station 20+00, shown in Figure 8, from a smooth strong reflection in the South, to a irregular weaker reflection in the North. This change in character

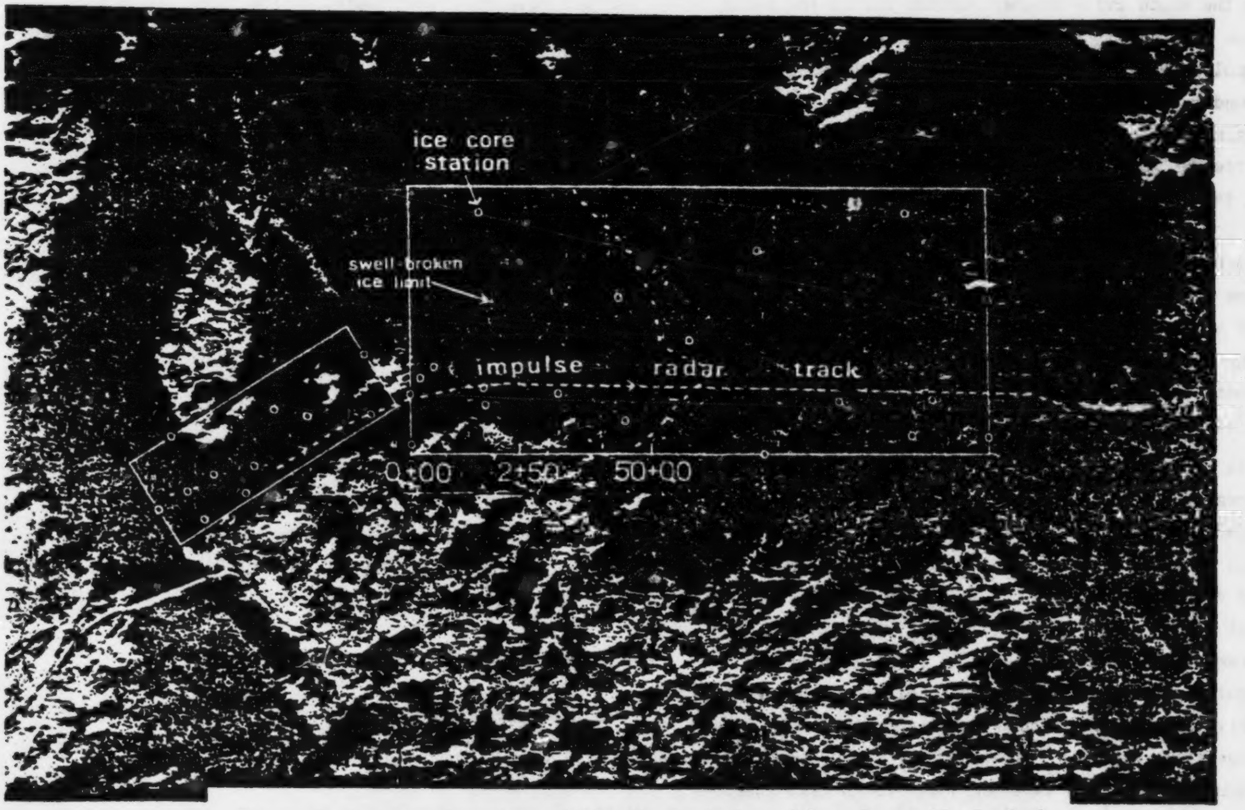
ice core station
swell-broken ice limit
impulse radar track
0+00
2+50
50+00

Figure 7 Ice core locations within the Study Area (shown by small circles) and the location of the Impulse Radar Track (shown by dashed line). Stations along the Impulse Radar Track are related to the Stations along the profile shown in Figure 8

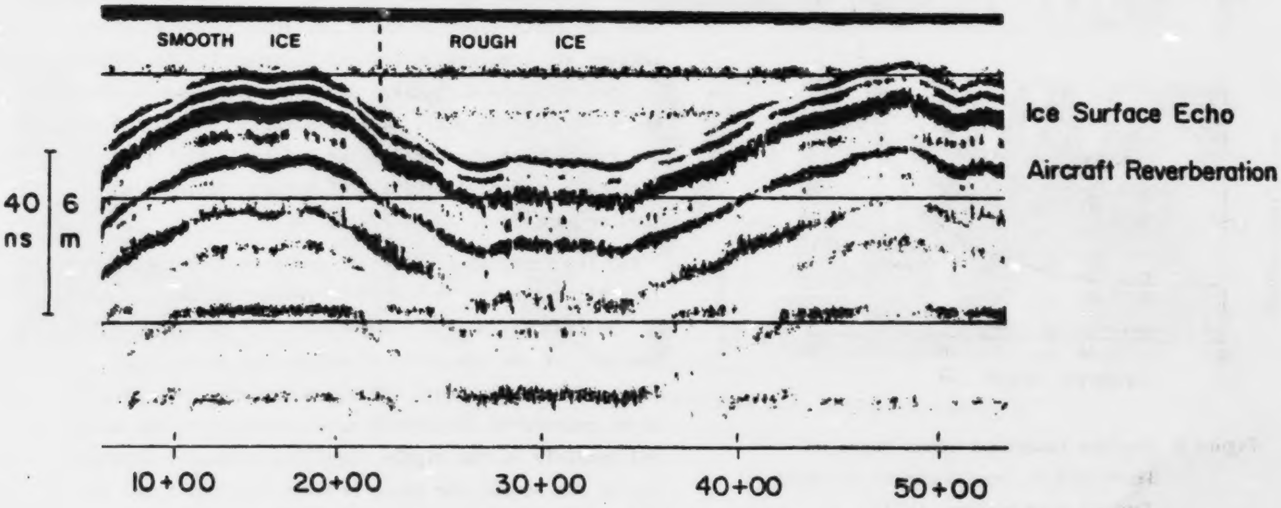

Figure 8 Impulse Radar Profile within Zone B. Smooth Ice is in the South part of Zone B and Rough Ice is in the North part of Zone B.

indicates that Zone B contains a smooth surface ice in the South and a rougher surface ice in the North. A look at Figure 7 indicates that the change in the impulse radar signal occurs at the swell-broken ice boundary. The roughness indicated in Figure 8 is on the scale of 1-5 m or less horizontally and a few centimetres or less vertically. Although not shown in Figure 8, the impulse radar profile seen North of station 20+00 in Zone B is similar throughout Zone C, indicating no visible distinction between the swell-broken area in Zone B and the consolidated pack ice in Zone C. Also not shown in Figure 8 is the impulse radar profile in Zone A. The profile in Zone A is identical to the strong smooth reflection in the non-swell-broken area of Zone B (station 0+00 to 20+00).

In the case of Twillingate ice roughness, all zones appear visually separable on the ground-based photography. Impulse radar data however distinguishes the ice into two roughness zones, the separation between smooth and rough occurring at the swell-broken limit of the fast ice in Zone B. The X-band SAR imagery indicated three distinct tonal zones. The resolution of the impulse radar data is unable to distinguish the more subtle changes in roughness that the SAR might. Radar image tones based on Peake and Oliver roughness criteria (Figure 9) indicate that SAR image tones will change from dark to light with corresponding changes in RMS roughness between ½ cm to 3 cm, near 75 degrees incidence angle.

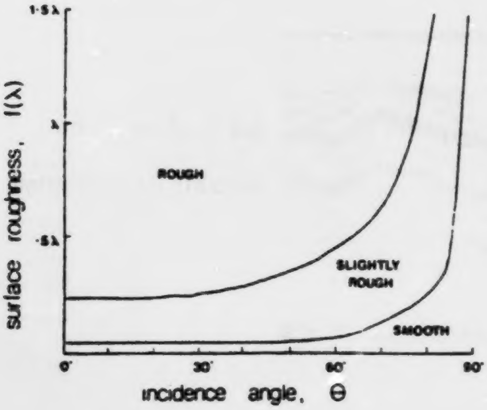

Figure 9 Surface roughness zones based on Peake and Oliver Roughness criteria (curves from Wedler, 1977).

Based on the available roughness data it is seen that surface roughness contributed to the tonal changes between Zone A and Zone C, and between the unbroken and swell-broken ice areas of Zone B. The resolution of the data, however, did not allow an explanation for the three tonal changes between the zones as seen on the SAR imagery.

Rouse (1969) described a technique to estimate surface roughness by fitting 2.25 cm (13.3 GHz) radar scatterometer data to backscatter theory based on Kirchhoff-Huygens Principle, giving a "roughness factor". Data beyond 30 degrees incidence angle was not used because of the general lack of this Principle for incidence angles far from verticle. Since the incidence angle for Twillingate ice was far from vertical, about 75 degrees, an estimation of roughness was not possible. Unknown antenna beam pattern characteristics and unknown signal-to-film transfer functions also made quantitative attempts at surface roughness estimates beset with difficulty.

ICE CRYSTALLOGRAPHY

As described earlier, highly significant zonal separation based on sea ice density was found between Zone A and Zones B and C at the second ice layer (7.6-15.2 cm). Although it is questionable how definitive the crystal structures are in terms of interpreting the Twillingate ice from the SAR imagery there do appear to be differences between the surficial layer and the underlying ice (Figure 10). Ice crystals were photographed and examined from ice cores taken in the study area. Detailed observations are reported in Lau and Rossiter (1978). Other crystal sections also taken near this site show differences between the small, polycrystalline (1 mm to 3 mm) ice crystals of the upper layer and the larger (1 cm) vertically-oriented crystals of the underlying ice (Lau and Rossiter, 1978, Figure 16).

Too few vertical ice crystal sections were taken for generalizations to be made with respect to the effect of ice crystals on the SAR imagery. The distinction, however, of the ice crystals within the radar skin depth, described later, and the underlying ice appears to be related to the precipitation history of the site, and possibly to the highly significant density separation at the second ice layer between the Zone A and the

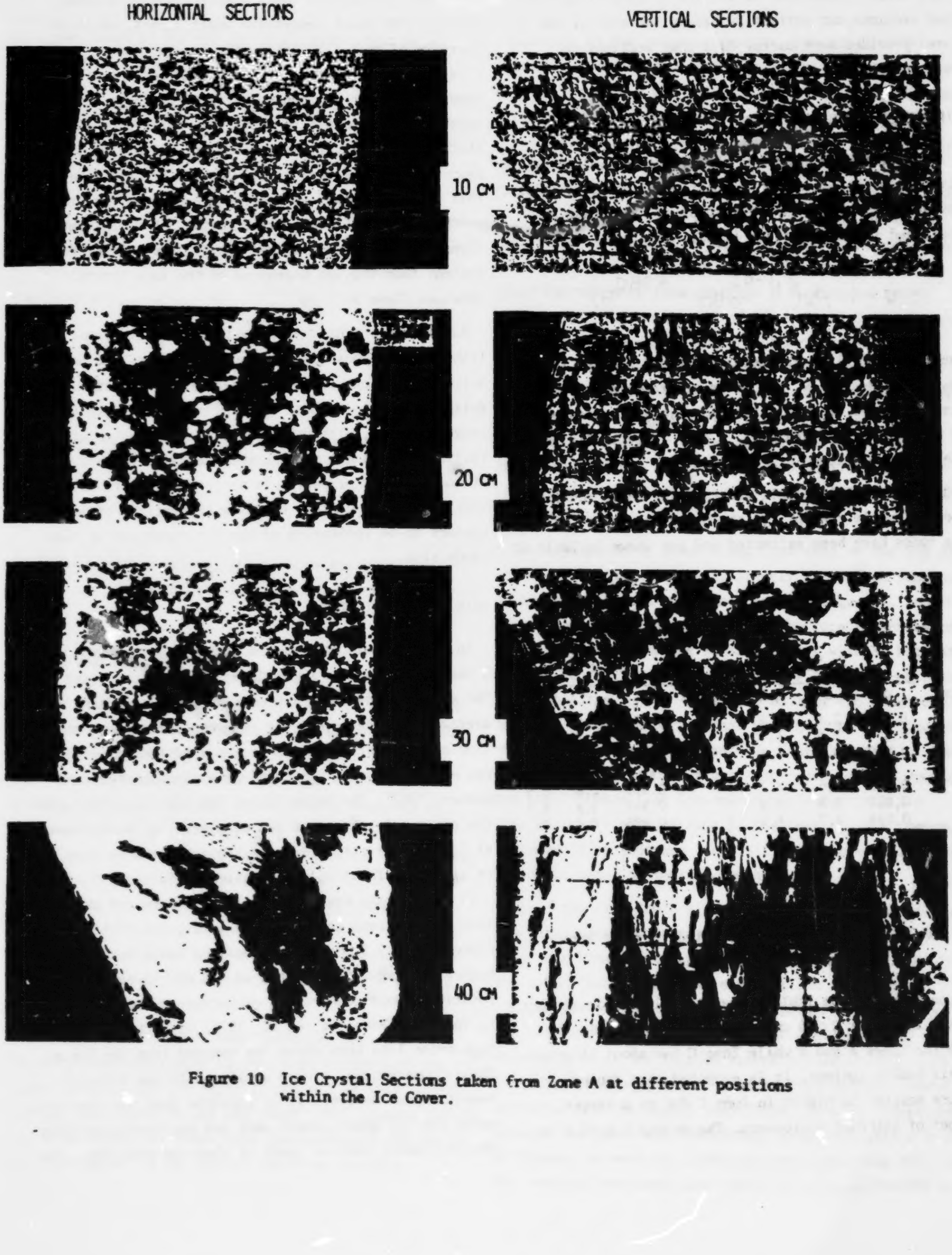
HORIZONTAL SECTIONS
VERTICAL SECTIONS
10 CM
20 CM
30 CM
40 CM

Figure 10 Ice Crystal Sections taken from Zone A at different positions within the Ice Cover.

other zones. Inspection of the ice crystals indicated that sections cut vertically (along the axis of the core) provided more useful data than sections cut horizontally.

AIR BUBBLE CONTENT

A theoretical estimate of the fractional volume of air bubbles in sea ice as a function of density, salinity and temperature can be made using relationships described in Schwerdtfeger (1963), namely,

$$U = 1 - \rho_s \left(\frac{(1-\sigma)}{0.917} + \frac{4.98\sigma}{\theta} \right)$$

where, ρ_s and σ is the density and salinity of the sea ice respectively, and θ is the temperature of the ice. Densities of pure water and pure ice are assumed to be 0.999 $g.cm^{-3}$ and 0.917 $g.cm^{-3}$ respectfully, for the above relationship.

Using the SAR '77 field data and the above equation the air bubble content in the upper two layers of the ice zones have been estimated and are shown in Table 5.

		-2 °C			-4 °C		
Layer	Zone	ρ_s	σ	% B	ρ_s	σ	% B
1	A	0.873	2.4	5.5	0.873	2.4	5.3
	B	0.874	2.6	5.5	0.874	2.6	5.2
	C	0.867	3.1	6.4	0.867	3.1	6.1
2	A	0.859	2.6	7.2	0.859	2.6	6.9
	B	0.884	3.8	4.8	0.884	3.8	4.4
	C	0.885	2.7	4.3	0.885	2.7	4.1

Table 5 Theoretically estimated percent bubble content in the ice zones.

It can be seen from Table 5 that the air bubble content within the upper 0-7.6 cm layer is approximately the same for Zones A and B while Zone C has about 1% greater air bubble content. It is expected that X-band volume scatter is higher in Zone C due to a larger number of internal scatterers. The second 7.6-15.2 cm ice layer indicates a lower bubble content in Zones B and C from their respective upper layers, while an increase of over 1.5% air bubble content occurs in Zone A in the second layer. The air bubble content of the second layer, in all zones, differ from their respective upper layers from 0.6 to 2.0%. This difference indicates that the upper layer had a different history of formation from the second layer. Also indicated by this data is that the ice exposed to lateral pressure of the strong northerly winds 5 weeks prior to the SAR overflight (Zones B and C at the second layer), had a lower bubble content than the ice unexposed to the same lateral pressure (Zone A).

Bubble content has been found to be an important contributor to reponse in the thermal infrared and passive microwave regions of the electromagnetic spectrum. It is felt that bubble content also contributes to the SAR image response, although the ice data collected at Twillingate did not allow a more detailed investigation of this sea ice property. It is interesting to note that the bubble content based on theoretical estimates appears to be indicative of the ice formation at this study site.

SKIN DEPTH ESTIMATES

An estimate was made of the probable attenuation of the X-band signal in the upper layers of the ice, based on the measured physical properties of the ice. Using the average salinity values and the temperature near the time of the overflight, an estimate of the brine volume was made using the formula given by Frankenstein and Garner (1967). The brine volume was then inserted into the empirical regression fit of electrical measurements at 7.5 GHz for first year sea ice presented by Vant, et al, 1978. The results are given in Table 6.

It is expected that the tabulated values are the minimum attenuations (or maximum skin depths) that could be expected. At 9.3 GHz the attenuation would be somewhat higher (perhaps 20-30%) than at 7.5 GHz. Second, the relatively poor penetration of impulse radar signals in the area (Rossiter, et al, 1977) was attributed to the high brine loss when cores are removed from the ice at these temperatures, giving artificially low salinity measurements. However, it is possible that the measurements for the upper layers were not exessively in error. The conclusion that we reach is that the skin depth for the upper layer of the ice in this region could be as large as 5-15 cm even at X-band.

ZONE	AVERAGE SALINITY (ppt)	TEMP. (°C)	BRINE VOLUME (ppt)	ATTENUATION (dB/m)	SKIN DEPTH (cm)
A	2.4	-2	79	93	9
		-4	41	55	16
B	2.6	-2	85	99	9
		-4	44	52	15
C	3.1	-2	101	114	8
		-4	52	65	13

Notes : Attenuation calculated at 7.5 GHz (see text).
Distance of attenuation is 1/e or 8.68 dB.

Table 6 Brine volume, attenuation and skin depth calculations for the upper ice layer.

SUMMARY AND CONCLUSIONS

Three ice zones (denoted as A, B, and C) were visually delineated on dual-polarized (HH and HV) X-band SAR imagery which was acquired over first year, fast sea ice near Twillingate, Newfoundland, on March 15, 1977, based on tone and texture. Densitometric analysis of the negative strip film supported the visual delineation. The zones were statistically separable to the 0.01 significance level based on image tone. Since mid-tone returns are approximately directly proportional to signal backscatter, greatest backscatter was received from the consolidated pack ice (Zone C) and the least backscatter was received from smooth and very smooth, though swell-broken, fast ice.

Although other studies have indicated that sea ice salinity does contribute to the tonal differences on radar imagery, the low salinity sea ice at Twillingate did not contribute to the SAR image tonal changes within the study site. All zones were statistically similar in all four upper 7.6 cm layers, based on salinity.

Contrary to the salinity results, sea ice density indicated significant separation of the ice zones - but only in the second ice layer (7.6-15.2 cm). The separation occurred between Zone A and Zones B and C. Zones B and C were statistically similar to each other in this second layer. All zones were statistically similar in the upper, surficial layer, probably since the surficial in all zones was formed primarily from over 200 mm of melted and refrozen snow. While two zones are separable in the second layer, based on sea ice density, the SAR image and the grey tone analysis indicate that three zones exist. The separation of Zones B and C as seen on the SAR film are due to factors other than sea ice density. Zone A appears different from Zones B and C on the SAR film possibly due to density differences at the second ice layer. This would suggest that the X-band skin depth penetrates to the second ice layer. Skin depth calculations based on measured physical ice properties indicate possible signal penetration to between 5-15 cm.

The separation of Zones B and C as seen on the SAR film could only be provided qualitatively by surface roughness differences as seen on ground-based photography. Zone A also appeared distinct in terms of surface roughness on the photography. Impulse radar profiles with 80 MHz and 400 MHz centre-frequencies and having lower ground resolution than the X-band SAR indicated only two roughness zones. A strong, smooth signal was received over smooth, unbroken fast ice (Zone A and the Southerly part of Zone B). A weaker, irregular signal was received over smooth but swell-broken fast ice and consolidated pack ice (the Northerly part of Zone B, and Zone C). The limited roughness data indicate that all zones were qualitatively separable based on surface roughness.

Since the skin depth signal penetration calculations indicated possible penetration to the second ice layer it is not known, using the Twillingate data set, whether the X-band response was solely from the roughness at the ice surface or from the roughness possibly defined by the ice interface between the surficial and underlying ice. Observations of the limited number of ice crystal sections and calculations of theoretical percent bubble content estimates and the highly significant density differences between the upper and underlying layers indicate a marked difference between the surficial and underlying ice. Too few vertical sections were taken for generalizations to be made with respect to the effect of ice crystals and percent bubble content on the SAR imagery, although these sea ice properties appeared to be indicative of the history of ice formation in the study area and of the interface formed between the surficial and underlying ice layers. Extended geographical coverage and extended quantitative field data, particularly with respect to roughness and vertical crystal sections would have provided a more difinitive assessment of the relative contribution of the various sea ice properties on the X-band SAR imagery tone and texture.

Literature relating the physical characteristics and the larger-scale properties of sea ice to the microwave backscatter is at present limited and fragmented. Increased activity in ice-covered and ice-frequented waters will require an improvement of more rapid field data observation and measurement techniques and a more timely dissemination of SAR data to the field crews in order to increase the understanding and orderly establishment of relationships between SAR image response and sea ice properties.

REFERENCES

Anderson, V.H., 1966
" High Altitude Side-Looking Radar Images of Sea Ice in the Arctic "
In: Proceedings of the 4th. International Symposium on Remote Sensing of the Environment, Ann Arbor, Michigan.

Bradie, R.A., 1967
" SLAR Imagery for Sea Ice Studies "
Photogrammetria Engineering
Volume 33 No. 7, pp. 763-766

C-CORE, 1979
" Project SAR '77 Summary Report "
Contract Report, December 1979
C-CORE Publication No. 79-15

Elachi, C., M.L.Bryan, and W.F.Weeks, 1976
" Imaging Radar Observations of Frozen Arctic Lakes "
Remote Sensing of the Environment
Volume 5, pp. 169-175

Frankenstein, G., and R. Garner, 1967
" Equations for Determining the Brine Volume of Sea Ice from -5 C to -22 C "
Journal of Glaciology, Vol. 6, pp. 943-944

Hengeveld, H.G., 1977
" Airborne Remotely Sensed Data Collected by the Atmospheric Environment Service over Radar Target Areas "
Project SAR '77 Field Data Report No. 10
C-CORE Publication No. 77-39, 37 pp.

Johnson, J.D., and L.D. Farmer 1971
" Use of Side Looking Airborne Radar for Sea Ice Identification "
Journal of Geophysical Research
Volume 76 No. 9, pp. 2138-2155

Ketchum, R.D., and S.J. Tooma, Jr., 1973
" Analysis and Interpretation of Airborne Multifrequency Side Looking Radar Sea Ice Imagery "
Journal of Geophysical Research
Volume 78 No. 3, pp. 520-538

Larson, R., C. Liskow, R. Rawson, R. Schuchman, and F. Smith, 1977
" Areas Imaged During Project SAR'77 using the ERIM Four Channel Radar"
C-CORE Publication No. 77-30, 55 pp.

Lau, G., and J. R. Rossiter, 1978
" Physical Properties of Fast Ice near Twillingate, Newfoundland, February-March 1977"
C-CORE Publication No. 78-1, 95 pp.

Livingstone, C., L. Gray, R. Hawkins, L. Arsenault, D. Pearson, and L. Jones, 1980
" Statistics of Scattering Coefficients for Varying Types of Ice over Specific Sites"
Airborne Project Component of the Canadian SURSAT Program, Intera Report ASP-80-1

Rossiter, J.R., P. Langhorne, T. Ridings and A. Allan, 1977
" Study of Sea Ice Using Impulse Radar"
Proceedings of the Fourth International Conference on Port and Ocean Engineering under Arctic Conditions, St. Johns, Newfoundland, Sept. 26-30, 1977, pp. 556-567

Rouse, J. W., Jr., 1968
" Arctic Ice Type Identification by Radar"
The University of Cansas Centre for Research, Inc., Technical Report No. 121-1, 30 pp.

Rouse, J.W., Jr., 1968
" Radar Scatterometer Measurements of Sea Ice"
Earth Resources Aircraft Program Status Review,
Houston
N71-16178/NASA Manned Spacecraft Centre, Houston
Texas, A&M University

Schwerdtfeger, P, 1963
" The Thermal Properties of Sea Ice"
Journal of Glaciology,
Vo. 4, No. 36, pp. 789-807

Timm, N.H., 1976,
" Multivariate Analysis with Applications in Education and Psychology"
Brooks/Cole Publishing Co.
Monterey, California

Vant, M.R., R. Ramseier, and V. Makios, 1978
" The Complex Dielectric Constant of Sea Ice
Frequencies in the Range 0.1 - 40 GHz. "
Journal of Applied Physics
Vol. 49, pp. 1264-1280

Wedler, E., 1977
" Spectral Terrain Analysis by Airborne Remote
Sensing"
M.A.Sc. Thesis (unpublished)
University of Toronto, Toronto

Wedler, E., R.D. Worsfold, B. Roberts, and R. Miller,
1977a
" Ice Characterization, Twillingate, Newfoundland,
February-March, 1977"
Project SAR'77 Field Data Report No. 3
C-CORE Publication No. 77-40, 97 pp.

Wedler, E., and R.D. Worsfold, 1977b
" Additional Ground Truth Measurements, Twillingate,
Newfoundland, February-March, 1977"
Project SAR'77 Field Data Reprot No. 4
C-CORE Publication No. 77-33, 37 pp.

Wedler, E., S. Parashar, and R.D. Worsfold, 1978
" Preliminary Radar Analysis, Twillingate, Newfoundland, February-March 1977"
Project SAR'77 Field Data Report No. 11

Weeks, W.F., A.G. Fountain, M.L. Bryan, and C. Elachi,
1978
" Differences in Radar Return from Ice-Covered North
Slope Lakes"
Journal of Geophysical Research
Vol. 83, No. C8, pp. 4069-4073

Worsfold, R.D., E. Wedler, R. Miller, and B. Roberts,
1977
" Meteorological Ground Truthing, Twillingate,
Newfoundland, February-March 1977"
Project SAR'77 Field Data Report No. 2
C-CORE Publication No. 77-31

AEOSS Publication No. 81-01

SECTION 5.10

THE IMPLICATIONS OF MELTPONDS TO THE REMOTE SENSING OF SEA ICE

Kirby, M.E., R.O. Ramseier, D.E. Pearson and R.G. Dixon

Presented at the Sixth Canadian Symposium on Remote Sensing; May, 1980; Halifax, N.S.

THE IMPLICATIONS OF MELT PONDS TO THE REMOTE SENSING OF SEA ICE

M.E. KIRBY*, R.O. RAMSEIER**, D.E. PEARSON*, R.G. DIXON*

*INTERA Environmental Consultants Ltd.
2841 Riverside Dr., Suite 204
Ottawa, Ontario

**Atmospheric Environment Service
Ice Branch
4905 Dufferin St.
Downsview, Ontario

1. INTRODUCTION

In recent years numerous researchers and agencies alike have focussed attention on topics such as ice types, ice concentrations and dynamics, pressure ridges and icebergs with a particular emphasis on the implications that these features present for exploration activities. However, from a remote sensing point of view melt pond morphology and dynamics have received very little consideration.

Melt ponds can be very dynamic during the heavy melt periods in the summer months and generally fall into two categories: shallow or surface ponds and ponds which interconnect with the ocean. The interconnecting ponds are particularly important for both transportation and wildlife reasons, but with cross-purposes. From a transportation point of view it may be desirable to direct a vessel through ice that has interconnecting ponds with the ocean since such ponds often represent weak points in the ice and could result in easier passage. On the other hand these same ponds allow seals to penetrate through the ice to the surface and serve an important role in their seasonal migrations. However, shipping through these melt regions could have serious ecological effects on a local seal population. Therefore the identification and distribution of melt ponds in ice, for either transportation or wildlife purposes, will be an important application for remote sensing data sets.

2. ACTIVE MICROWAVE IMAGING

Recent remote sensing experiments and operational programs have demonstrated the utility of microwave techniques for ice applications. However, the identification of melt ponds becomes particularly difficult with active microwave sensors over different ice types. For example melt ponds on multi-year (MY) ice generally have low salinity levels and are therefore relatively transparent to active microwave energy in the commonly used X band wavelengths. Ketchum (1977) has shown that frozen melt ponds on MY ice are characterized by their low radar returns with the radar energy penetrating the fresh water ice and being attenuated by the underlying MY ice. On the other hand melt ponds on first year (FY) or younger ice are typically high in salinity and therefore form a sharp dielectric boundary near the surface which is generally impenetrable with microwave sensors. The authors have found that vast areas of FY ice along the Northwest Passage which had a melt pond coverage from 45% to 77% of the total ice area appeared as uniform smooth regions on the SLAR imagery with no indication of melt ponding. Had coincident air photos not been taken along with the SLAR imagery, an interpreter would probably have identified a continuous FY ice cover without the presence of melt ponds. It should be noted that the SLAR ice imagery was X band like-polarized data that was collected at shallow depression angles.

3. PASSIVE MICROWAVE IMAGING

Over the past decade the application and utility of passive microwave techniques have proven to contribute valuable information to the further understanding of sea ice dynamics (Zwally and Gloersen, 1977; Campbell et al, 1978; Gloersen et al, 1978). However, the effects that melt ponds have on the brightness temperatures (T_B) of sea ice at the 1.55 cm wavelengths have proven to be quite variable and therefore subject to possible misinterpretations. For example, sea water has a brightness temperature of about 120 K (Zwally and Gloersen, 1978) while high concentrations of FY ice have brightness temperatures of about 235-240 K and MY ice generally has a T_B less than 232K (Zwally and Gloersen; 1978). However, as melting progresses the minimum T_B of moist sea ice is 230 K which is also the signature of dry MY ice just below melt point (Gloersen et al, 1978). This could make the distinction between FY and MY ice difficult. In addition, T_B lower than 230 K can be caused by either large regions of open water in the pack ice or by extensive areas of surface melt ponds (Gloersen, et al, 1978). Refrozen melt ponds (2-3 cm of skin) have also caused a drop of about 20 K in the brightness temperatures (Gloersen, et al, 1978) from the norm and could result in some confusion.

For the sake of illustration, Gloersen, et al, (1978) found that passive microwave data from an aircraft over the AIDJEX camp resulted in low T_B values in August of 1975 which indicated that some 20% of the total experiment site was comprised of open water. At the sametime ESMR-5 data was collected over the same site from the Nimbus-5 satellite and yielded T_B values which indicated that about 30% of the area was open water. The discrepancy was attributed to a decrease in sea ice microwave emissivity as a result of increased amounts of free water in the surface layer and open melt ponds. It is worth noting that the T_B of ice-free melt ponds is about 130 K, which is the same as the T_B for open water (Gloersen, et al, 1978).

4. DENSITY SLICING OF PHOTOGRAPHIC PRODUCTS

Weather permitting, one of the most useful methods for collecting melt pond information is black and white photography. The optical properties of the melt ponds are particularly suited for photographic techniques where return from the various melt pond depths are sufficiently strong to be imprinted on the film in the form of varying densities. Langleben (1971) found that a linear, negative correlation existed between albedo and the degree of puddling, indicating that as the percentage of melt ponds increased the amount of energy reflected from the ice surface decreased due to absorption and attenuation in the melt ponds. As in most natural situations the absorption and attenuation of visible wavelengths increases with the depth of water. Therefore it is possible to not only extract melt pond coverage statistics from air photos, but also to obtain melt pond depth information as a function of film density.

In the figures that follow, melt pond information extraction methods from 70 mm photos and analog density slicing are presented. Figure 1 shows a portion of a July photography of a melt pond region in FY ice along the Parry Channel. The melt ponds in the centre of the photo appear to interconnect with the ocean. Figure 2 depicts the results of the level slicing analysis for an enlarged section from the 70 mm photo. The darkest parts of Figure 2 represent the unmelted surfaces of the ice. These features have been blacked-out in order to provide the greatest contrast with the melt pond densities. The melt pond propers contain some 8 to 10 density levels which could be related to the pond depths. The lightest portion of Figure 2 represents a region which likely interconnects with the ocean.

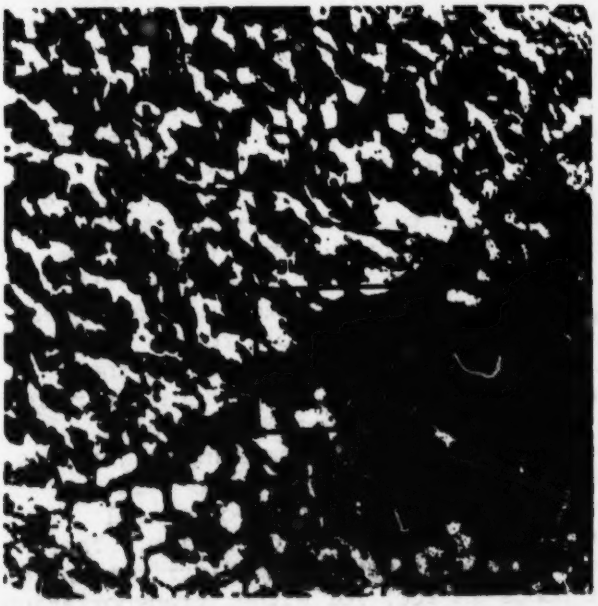

FIGURE 1

70 MM BLACK & WHITE IMAGE OF MELT PONDS

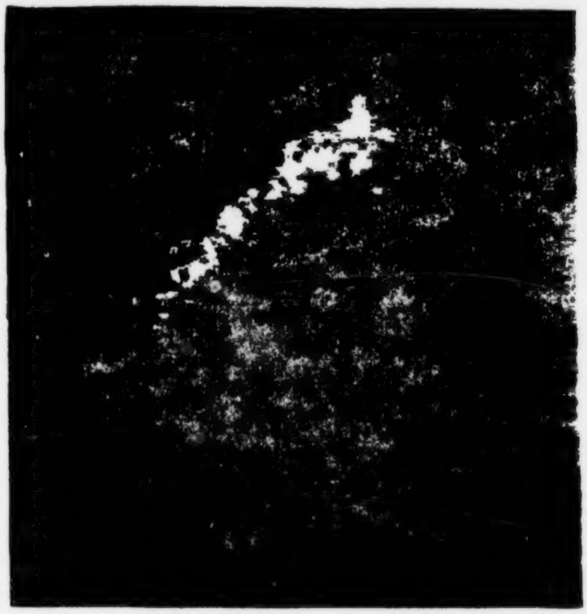

FIGURE 2

DENSITY SLICE OF ENLARGED PORTION OF 70 MM IMAGE

Relative melt pond concentrations for a selected number of images were calculated using density slicing methods. Melt ponds were found to cover from 45% to 77% of the total ice area studied, with interconnecting ponds forming no more than 3% of the total ice area. Although limited data sets were investigated in this study, they did serve to show that density slicing is a quick and accurate method for determining melt pond areas and melt pond types.

5. DISCUSSION

The above discussion has demonstrated that melt ponds can cover large proportions of sea ice surfaces but that the identification of the ponds by a single active or passive microwave system can be a difficult task. With the emerging importance of melt ponds for Arctic transportation and wildlife purposes, and with the continued dependence on microwave remote sensing data sets, further research is required for a complete understanding of melt pond morphology and dynamics throughout the Arctic. This future research should involve a complement of both passive and active microwave sensors for a comprehensive evaluation of their relative utility for melt pond identification studies.

6. REFERENCES

Campbell, W.J., et al, 1978: Microwave Remote Sensing of Sea Ice in the AIDJEX Main Experiment; Boundary-Layer Meteorology, v. 13, p. 309-337.

Gloersen, P., et al, 1978: Time-Dependence of Sea-Ice Concentration and Multi-year Ice Fraction in the Arctic Basin; Boundary-Layer Meterology, v. 13, p. 339-359.

Ketchum, R.D., 1977: An Evaluation of Side Looking Radar Imagery of Sea Ice Features and Conditions in the Lincoln Sea, Nares Strait, and Baffin Bay; NORDA Technical Note 7.

Langleben, M.P., 1971: Albedo of Melting Sea Ice in The Southern Beaufort Sea; Journal of Glaciology, v. 10, no. 48, p. 101-104.

Zwally, H.J. and P. Gloersen, 1977: Passive Microwave Images of the Polar Regions and Research Applications; Polar Record, v. 18, no. 116, p. 431-450.

SECTION 5.11

RIDGE HEIGHT MEASUREMENTS WITH SAR

Inkster, D.R., R.T. Lowry

RIDGE HEIGHT MEASUREMENT WITH SAR

by: D.R. Inkster and R.T. Lowry,
Intera Environmental Consultants Ltd., Ottawa, Ontario

ABSTRACT

Forty ice ridges in the vicinity of T3 were identified on XHH SAR imagery, and on low altitude photography. Ridge heights were estimated, using the lengths of shadows cast on the photography, and were compared to the widths of the ridges as seen in steep- and shallow-angle radar imagery. The results indicate that both multi-year and first year ridges are more detectable at shallow depression angles (from 6° to 20°), than at steep angles (from 40° to nadir). For a given height, a multi-year ridge is more detectable than a first year ridge. For instance, viewed at shallow angles, a 1-m-high, first year ridge typically had an apparent width of about 10 m on the SAR imagery, while a comparable multi-year ridge had an apparent width of 16 m. Finally, more directional dependence of ridge signatures was seen for first year ridges than for multi-year ridges. Young ridges, viewed broadside, had wider signatures than similar ridges viewed "end-on". The widths of multi-year ridge signatures were less dependent on viewing angle.

A simple scattering model for ridges was developed to explain the results. Ridges were assumed to be triangular in cross-section, with ridges of different heights being geometrically similar. When reasonable angles of repose for ridges were assumed, the model predictions of ridge heights were consistent with the observed heights.

These results suggest that ridge heights can be estimated rather rapidly to within a factor of 2 to 3, over large areas, using high-resolution SAR. More work is planned, using a larger data set, including laser profiles, to relate SAR ridge height distributions to heights obtained using conventional techniques.

INTRODUCTION

Ice ridges are important features for several reasons. Ridges and their associated keels are serious hazards for shipping in ice-infested waters, and ridge height and spacing distributions are key inputs for design studies of ice-breakers, and other carriers proposed for the Arctic. Ridges are also hazards for stationary drill ships or rigs, and the early detection and monitoring of these features are required for ice management systems. Models of sea-ice dynamics also require ridge information. Changes in ridging intensity not only identify "active" areas, but reflect changes in rheology which are important in the modelling process.

A great deal of work has been reported on physical characteristics of ridges; on their height, width and spacing distributions, on their mechanical and dynamical properties, and on relationships between ridges and keels. Most of these studies have used data collected during on-ice surveys, using sonar or laser profiling techniques, impulse radar, or aerial photography alone. Statistical properties have been investigated, primarily with laser, sonar, and photographic methods (e.g., see Lowry and Wadhams, 1979). The stereo-photographic techniques have the advantage of allowing large area surveys rather than profiles, but are very expensive and time consuming.

Following the collection of the first high-resolution SAR imagery of sea ice during the SURSAT Project, when it became apparent that SAR could detect and map ridges, it was decided to quantify this mapping ability. The SAR offers the ability to collect imagery of sea ice, regardless of weather conditions, which is a definite advantage over photography and other visual techniques. Further, the digitally processed and recorded data that SAR produces lend themselves to image-processing techniques. This work is the first step toward developing a simple relationship between radar signatures of ridges and the heights of those ridges.

DATA SET

The data used here were collected during the SURSAT Airborne SAR Project. The Canada Centre for Remote Sensing Convair 580, equipped with the four-channel X-L SAR, formerly operated by the Environmental Research Institute of Michigan, flew several missions over the Beaufort Sea during March 1978. A recent description of the radar and aircraft can be found in Inkster et al. (1978). X-band imagery (polarization HH) at a resolution of about 2 m, was collected at steep angles (nadir to 40°) on March 16th, and at shallow angles (6° to 20°) on March 18th. This imagery was optically processed and printed at a scale of 1:40 000. Black and white aerial photography was collected at the test site on March 16th, at a scale of 1:6000.

The area studied was about 10 by 50 km in size at the southern limit of the permanent pack. It contained multi-year floes; a variety of younger ice forms, some heavily ridged; and probably, some open leads.

ANALYSIS

A total of 81 ridges was selected on the photography. Linear ridges of approximately constant height and shape were sought, rather than rubble piles or irregular ridges. Ridges of varying orientation in respect of the flight line, were picked to study the effect of viewing angle.

The maximum height of a ridge was calculated by measuring the maximum shadow length within a short stretch of the feature, and converting this length to a height, using sun-angle tables and simple geometry. This calculation requires that the shadow be cast on a flat surface, and the results may be somewhat in error because of this assumption. The orientation of the ridge was measured with a protractor, and the results tabulated.

Next, the same ridges were identified on both steep- and shallow-angle SAR imagery. The ridges appear as very bright, linear features, at least 5 to 10 dB brighter than their surroundings. The apparent width of a particular ridge was easy to measure, as the reflectivity gradient at the edge of the ridge appeared very steep. Hence, the apparent width was defined as the maximum width of the saturated portion of the signature, as measured with a calibrated glass.

The measured apparent width of the ridge depends, not only upon the steepness of the reflectivity gradient, but also on processing parameters and photographic printing parameters. To investigate these effects, a portion of the SAR imagery was digitized at the output plane of the hybrid optical-digital correlator, described by Rawson et al. (1975). This digital imagery allowed a precise measurement of apparent ridge width at various locations on the ridge shoulder. As well, because the dynamic range inherent in the digital imagery is about 37 dB, compared to less than 20 dB on the optical data, it was possible to measure the reflectivity of even the very bright ridges. These reflectivities were correlated with ridge heights.

RESULTS

In general, it was noted that the shallow-depression-angle XHH imagery was well suited to distinguishing ridges. First year features that were very subtle, due to drifted snow, were easily detected by the SAR. In fact, at least one ridge was seen in the SAR imagery which could not be identified at all in the photography: this ridge may have been formed in the two-day period between the SAR flight and the photo flight.

The specific relationships between ridge heights and apparent widths are illustrated in Figure 1. Figure 1a, for example, is a scattergram, showing the relationship between ridge width and height for first year ridges viewed at shallow depression angles. Ignoring, for the moment, the "digital" data set and the "model" curve, each entry on the graph represents the height and apparent width of particular ridge. The observations have been made according to azimuth angle between the radar viewing direction and the ridge direction. Ridges viewed "end-on" (azimuth angle < 45°) are shown with the symbol "X", while those viewed broadside (azimuth angle > 45°) are shown with the symbol "O".

The line labelled "Analogue" is the least-squares best fit to the data, and the linear correlation coefficient is 0.51. Notably, many of the data points represent ridges less than 1 m in height. This indicates the sensitivity of the SAR to small targets. There is some evidence of directional dependence in Figure 1. Those ridges viewed "end-on" tend to fall above the best-fit line; that is, ridges viewed "end-on" tend to appear narrower for a given ridge height than those viewed broadside.

Figure 1b shows the same relationship for multi-year ridges. Multi-year ridges as high as 5 m were observed, with apparent widths of 32 m. It appears that, for a given height, multi-year ridges are wider than first year ridges. Further, no striking directional dependence is seen in this figure.

Figures 1c and 1d are comparable to Figures 1a and 1b, except that they are constructed, using steep-angle SAR imagery. Fewer data points are seen here, as some of the smaller ridges measured on the shallow-angle imagery were not detectable on those prints. The poor quality of the steep data for ridge detection is also demonstrated in the fact that even large ridges have relatively narrow widths in both Figures 1c and 1d. Finally, there does not appear to be much directional dependence of ridge signatures in either of these "steep" data figures.

Returning to Figure 1a, a second set of points and a best-fit line, labelled "Digital", can be seen. The points are from the digital data set previously described. The apparent width of these ridges was defined as the width at the highest reflectivity portion of the ridge, in fact, at a point where the reflectivity was 20 dB more than that of the undeformed ice. As a result, the ridges appear to be narrower for a given height than those in the analogue data set, where widths were measured at a lower reflectivity threshold. The linear correlation coefficient in this case is 0.73.

Figure 2 illustrates the relationship between ridge reflectivity and height, as determined from the digital data set, described by Pearson et al. (1980). There appears to be only a weak relationship between the parameter "relative $\bar{\sigma}_0$" and height for these ridges. Relative $\bar{\sigma}_0$ was obtained by averaging the digital reflectivity values over a small area, near the highest reflectivity portion of the ridge signature. Since reflectivity gradients can be rather steep, the averaged value is very dependent on the size of the area over which averaging is done. Hence, the scattering in Figure 2 may be due to uncertainties in the analysis technique, rather than to lack of a relationship between reflectivity and height. In any case, since a better technique for defining average reflectivity would be difficult to implement, it is not likely that reflectivity, taken alone, will be a good measure of ridge height.

A RIDGE SCATTERING MODEL

The results shown in Figures 1a through 1d can be summarized as follows:

1. Ridges viewed at shallow angles appear wider than those viewed at steep angles; and
2. Multi-year ridges (at least those viewed at shallow angles) appear wider than first year ridges.

These observations can be explained by means of a simple model. The ridges are modelled as being approximately triangular in cross-section, with large and small ridges being geometrically similar. The assumption is that first year ridges of all heights have the same angle of repose. It is also assumed that the bright ridge signature seen on the SAR imagery represents scattering only from the portion of the ridge facing the radar. With these assumptions, and an understanding of the viewing geometry of the radar, it is possible to generate model curves relating apparent ridge width to height, for any given angle of repose.

The geometry of the situation is illustrated in Figure 3. Here, "W" is the ridge half-width, "h" is the ridge height, and "α" is the angle of repose. If "θ" represents the radar depression angle, then "W_S" is the "apparent ridge width" seen by the SAR. The relationship between "W_S" and α is shown.

The parameter which remains to be specified, before model curves relating apparent ridge width and height can be generated, is , the angle of repose. There are few reported values of this parameter in the existing literature. Lowry and Wadhams (1979) suggest that varies between 5° and 20°, with smaller values being observed for multi-year ridges. According to Kirby (INTERA), his laser profile studies in the Canadian Arctic suggest a mean angle of repose for first year ridges of 4°, with multi-year ridges being more gently sloped. Pearson (INTERA) used aerial photography to measure heights and widths of 26 first year ridges in the Beaufort. He found a mean angle of repose of 9°, with a standard deviation of 2°.

All the results above are dependent upon season, location, and measurement technique. For the purposes of the present model, assumptions have been made which are consistent with the general trends indicated above, as follows:

first year ridges	$\alpha \approx 10^\circ$
multi-year ridges	$\alpha \approx 5^\circ$

The model has been compared with the data shown in Figure 1, with results shown in Table 1.

Table 1. Summary of model results.

	k (slope)	
	observed	modelled
FY shallow	.09	.18
(digital)	(.18)	
FY steep	.14	.27
MY shallow	.14	.09
MY steep	.17	.12

ridge height = k x ridge width + constant

In Table 1, k represents the slope of both the observed and modelled width-height relationships. It is clear that the model predicts that ridges viewed at shallow angles appear wider than those viewed at steep angles, consistent with the observations. Further, the difference between the analogue and digital data sets in the FY shallow case shows that the slope of this relationship is dependent upon where, on the reflectivity gradient, the width measurement is made. In other words, the angle of repose required to make the model fit the data depends upon how "apparent ridge" is defined in the data. It is likely that, if ridge width were defined differently for the multi-year ridges, they would appear wider than first year ridges, as the model predicts.

In summary, the model can be tuned to fit the data, by varying the angle-of-repose parameter, or the definition of ridge width. In fact, in forcing a good fit, it is not necessary to use unreasonable values for α , at least according to the few measurements reported by others. The model, however, should be considered only as a rough description of the complex scattering mechanisms involved when a high-resolution radar images ice ridges.

CONCLUSIONS

The results of this work are encouraging because they show a correlation between an important ice parameter and a simply defined characteristic of SAR imagery; between ridge height and apparent ridge width. The simple model developed here helps to explain this relationship. It is expected that the technique can be used to obtain estimates of ridging intensities over large areas, quickly and simply. The parameter, apparent ridge width, can be extracted from SAR imagery through automated image-processing techniques, and related to ridge height distributions using the relationship described here.

Obtaining ridge heights with SAR imagery has some disadvantages which will be investigated in the future. First, it is clear that the absolute value of the ridge heights determined with this technique will not be as accurate as those measured on the surface, or those obtained with laser profiles. The distribution of data points in Figure 1 suggests that ridge heights might be estimated with uncertainty of plus or minus 1 m. This accuracy is being more carefully defined by analysis of many more ridges imaged under differing conditions. Second, the relationship between apparent ridge width and ridge height is probably influenced by such factors as season, ice thickness, snow cover, ice type and the dynamic situation in which ridges are formed. These influences are being investigated currently, with data collected during the summer and fall of 1980.

ACKNOWLEDGEMENTS

The authors wish to acknowledge the support of the SURSAT Project, especially the Ice Group, led by Dr. Rene Ramseier, which funded the collection of these data. The Polar Continental Shelf project helped make data collection possible by supplying field logistic support and helicopter time for the SURSAT investigators during March 1978.

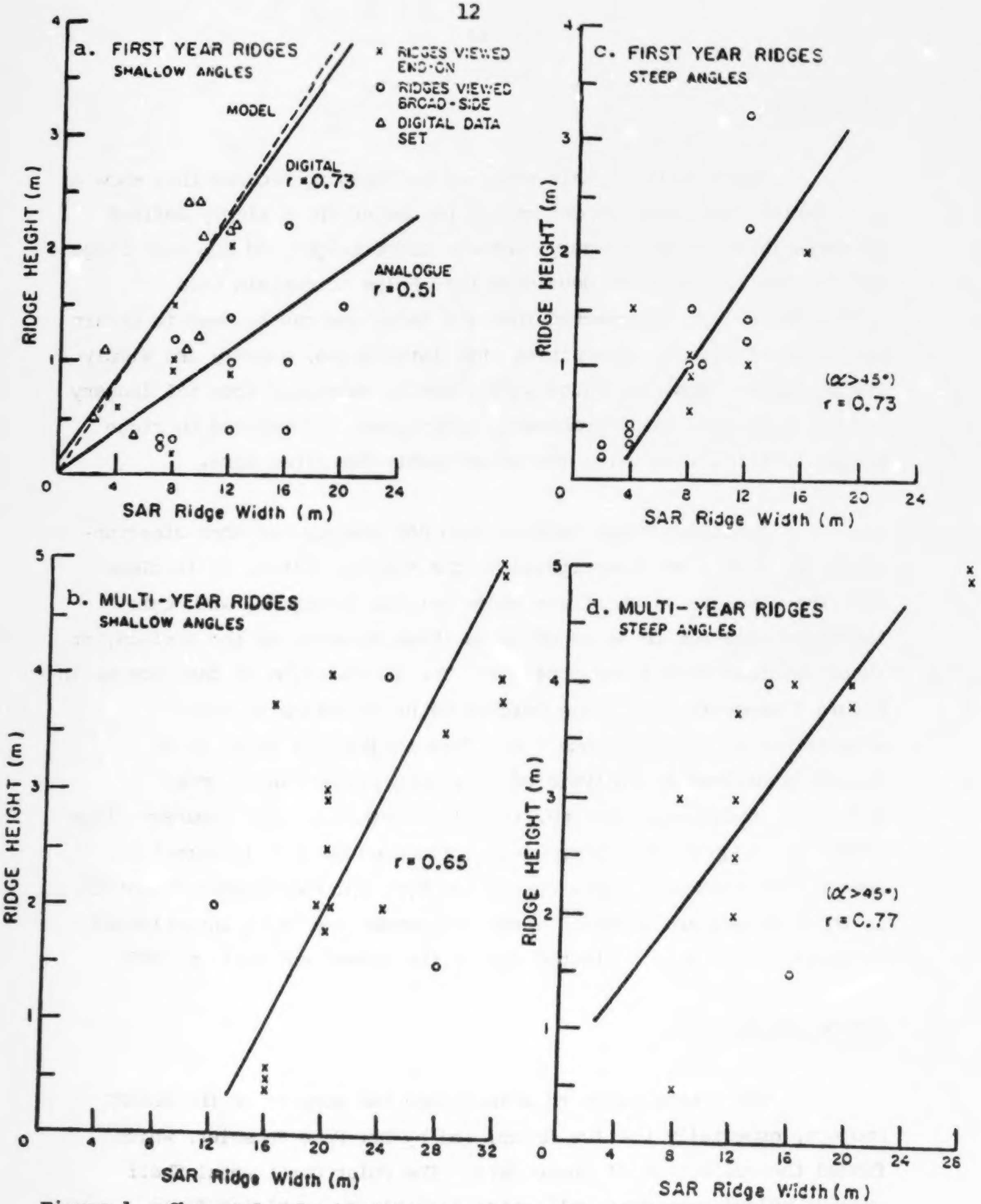

Figure 1. Observed relationships between apparent ridge width and ridge height for first year and multi-year ridges, viewed at steep and shallow angles.

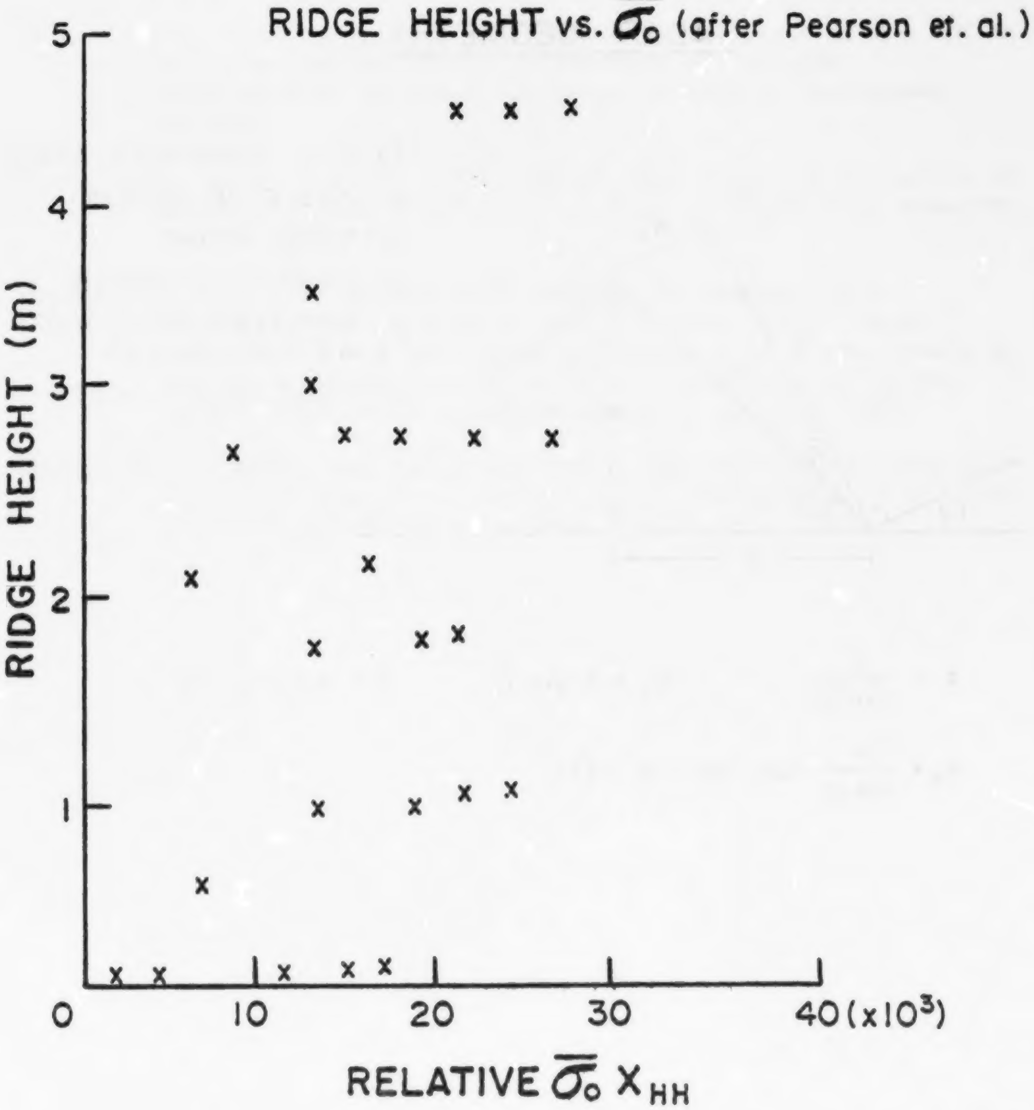

Figure 2. Relative ridge reflectivity as a function of ridge height for 25 ridges.

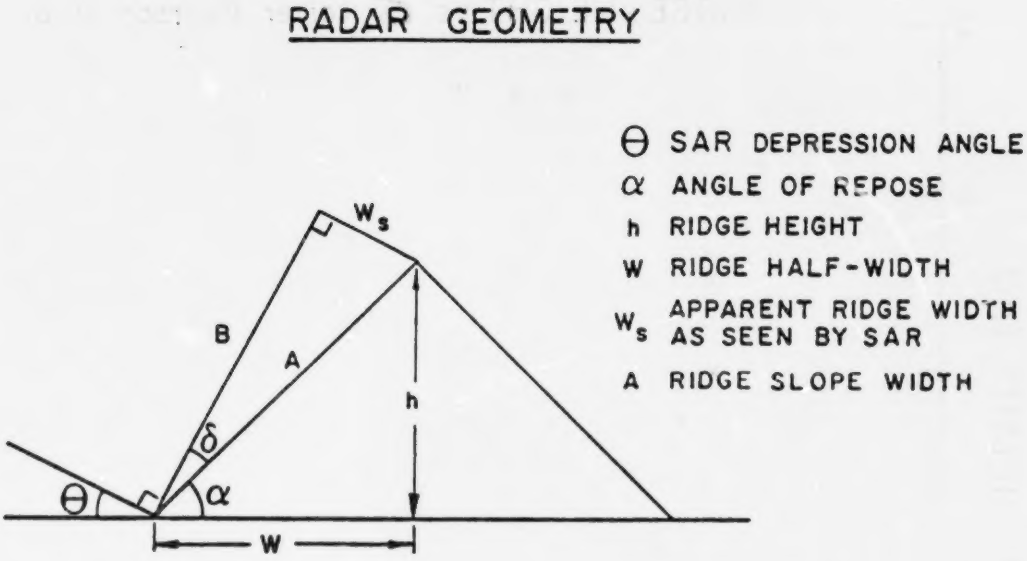
RADAR GEOMETRY
Θ SAR DEPRESSION ANGLE
α ANGLE OF REPOSE
h RIDGE HEIGHT
W RIDGE HALF-WIDTH
W_s APPARENT RIDGE WIDTH AS SEEN BY SAR
A RIDGE SLOPE WIDTH
W_s
B
A
h
δ
Θ
α
W

$$A = \frac{h}{\sin\alpha} \qquad W_s = A\sin\delta \qquad \delta = 90 - \alpha - \Theta$$

$$W_s = \frac{h}{\sin\alpha}\sin(90 - \alpha - \Theta)$$

Figure 3. Radar viewing geometry appropriate for a model ridge of height "h" and half-width "W".

REFERENCES

Inkster, D.R., R.K. Raney, and R.F. Rawson. 1979. State of the art in airborne imaging radar. Proceedings of the 13th International Symposium of Remote Sensing of Environment. 361-381.

Lowry, R.T., and P. Wadhams. 1979. On the statistical distribution of pressure ridges in sea ice. Journal of Geophysical Research 84(C5): 2487-2494.

Pearson, D., C.E. Livingstone, R.K. Hawkins, K. Okamoto, L.D. Arsenault, T.L. Wilkinson, and A.L. Gray. 1980. Radar detection of sea ice ridges and icebergs in frozen oceans at incidence angles from 8° to 55°. Proceedings of the 6th Canadian Symposium on Remote Sensing. Halifax, 1980.

Rawson, R., F. Smith, and R. Larsen. 1975. The ERIM simultaneous X- and L-band dual polarization radar. Proceedings of the IEEE International Radar Conference. Washington, 1975.

SECTION 5.12

RADAR DETECTION OF SEA ICE RIDGES AND ICEBERGS IN FROZEN OCEANS AT INCIDENCE ANGLES FROM 0° TO 90°

Pearson, D., C.E. Livingstone, R.K. Hawkins, A.L. Gray, L. Drapier
Arsenault, T.L. Wilkinson, K. Okamoto

RADAR DETECTION OF SEA-ICE RIDGES AND ICEBERGS IN FROZEN OCEANS AT INCIDENCE ANGLES FROM 0° TO 90°

D. Pearson
Intera Environmental Consultants Ltd.

C.E. Livingstone, R.K. Hawkins and A.L. Gray
Canada Centre for Remote Sensing

L. Drapier Arsenault
Cold Regions Remote Sensing

T.L. Wilkinson
University of Waterloo

and

K. Okamoto
Radio Research Laboratories, Tokyo, Japan

ABSTRACT

Dual-polarized 13.3 GHz scatterometer data and X-Band SAR data, collected in the Beaufort Sea and in the eastern Arctic, during the SURSAT sea-ice experiment deployments in March 1979 and April 1979 respectively, have been analyzed to determine the radar contrasts (signal to sea-ice clutter) between sea-ice ridges and the surrounding sea ice in the Beaufort Sea and between icebergs and the surrounding sea ice in the eastern Arctic. The effects of radar resolution cell size on ridge detectability were examined using aerial photography to estimate ridge dimensions.

Over the incidence angle range observed, the contrast between ridges and the surrounding sea-ice is nearly independent of incidence angle for all ice types. Cross-polarized radars produce larger ridge contrasts than like-polarized radars, with the largest contrasts and greatest polarization dependence being observed for rough first-year ridges in smooth first-year ice and the smallest contrasts and least polarization dependence being observed for multi-year ridges in multi-year ice.

The contrast between icebergs and the first-year ice background is nearly independent of incidence angle over the observed range.

Cross polarized radars enhance iceberg detectability but synthetic aperture radars operated at satellite incidence angles are found to be unsuitable for iceberg detection.

INTRODUCTION

The extension of the Arctic shipping season to include shipping through frozen oceans requires that all-weather remote sensing techniques be developed to identify and map hazardous ice conditions along shipping routes. All-weather sea-ice surveillance over wide regions will necessitate the use of both satellite and airborne microwave sensors (imaging radars and radiometers) for routine monitoring of the northern environment.

In this paper, airborne scatterometer and synthetic aperture radar (SAR) data acquired during the SURSAT experiment sea-ice program (March/April 1979) are examined to determine the radar signatures of sea-ice ridges and icebergs in frozen oceans and to estimate the detectability of these targets by satellite imaging radars.

The ice ridge data reported here were collected by the CCRS Convair 580 under late winter conditions in the Beaufort Sea shear zone and polar pack. The iceberg data were collected under early spring conditions in the Davis Strait ice marginal zone and along the northern Greenland coast. Some relevant work is reported by Gray et al. (1979), Lowry et al. (1979) and Parashar et al. (1980).

EXPERIMENT DESCRIPTION

The data set used in this study consists of:

(a) 13.3 GHz dual-polarized fan beam scatterometer data
(b) a nadir looking, wide angle RC10 aerial survey camera providing black and white photography
(c) dual-polarized X/L band SAR data.

To optimize the scatterometer spatial resolution, both the scatterometer data and the photography were recorded during low altitude flight lines (1,500 ft). The SAR data was collected at higher altitude (20,000 ft. for steep depression angle SAR, 3,000 ft. for shallow depression angle SAR). Where possible, overlapping scatterometer and SAR lines were flown during the same sortie to ensure that the scatterometer and SAR data sets referred to identical ice conditions.

A photo mosaic was used to identify and measure those ice features seen by the scatterometer. Only those targets fully illuminated by the scatterometer beam, which occupied at least one scatterometer footprint (18m x 18m), were used for first order analysis. However, some ridges with along track dimensions less than 18m were also selected to examine the effect of sensor resolution cell size on scattering cross section measurements. A few shallow depression SAR scenes were digitized to 3m square resolution cells to study this effect further and to determine the relationship between the ridge dimensions (size and shape) and the corresponding brightness intensity on the SAR image.

To determine ice ridge and iceberg back-scattering cross sections and target to background contrast ratios, segments of the scatterometer time history containing a ridge or berg along with a representative sample of the background ice were extracted from the data set. The targets were characterized by their peak back-scattering cross sections and the background ice by its mean back-scattering cross section over the incidence angle range 0° to 60°.

Within the Beaufort Sea experiment area only first-year and multi-year ridges were sufficiently common to discuss in detail. Since the majority of ridges traversed by the profiling sensor had widths less than 18m, an adequate statistical ensemble could not be created and thus the sea-ice ridges are presented as discrete events.

Similarly, for the iceberg study in the Eastern Arctic, the number of bergs traversed by the scatterometer was too small to permit a statistical treatment of the data. Consequently the iceberg data set is also presented as discrete events.

Pressure Ridge Results

Typical examples of the data sets associated with first-year sea-ice ridges in first-year ice and multi-year ice are shown in Figures 1a, b, c and 2a, b, c, respectively.

The ridge in Figure 1a (803.R45) is relatively young, contains little drifted snow and is composed of large blocks of ice. The ridge is 20m wide and 1.9m high at the point crossed by the profiling sensor. The surrounding ice has undergone moderate deformation, as is seen from the number of recent and older (snow drifted) ridges present in the area. The scatterometer signatures in Figures 1b and 1c are typical of rough first-year ice.

The ridge in Figure 2a (803.R01) is a large multi-year ridge situated within a multi-year floe. The ridge width is estimated to be 20m and the height to be 4.8m. The scatterometer signatures shown in Figures 2b and 2c are typical of multi-year ice.

The scatterometer signatures of eight first-year ridges meeting the data selection criteria show:

(a) the peak like-polarized, first-year ridge back-scatter had a maximum value of +6 dB and a minimum value of -2 dB at 8° incidence angle; a maximum value of -4 dB and a minimum value of -15 dB at 55° incidence angle; and an increase in slope (with incidence angle) beyond 25°,

(b) the peak first-year, cross-polarized ridge back-scatter has a maximum value of -4 dB and a minimum value of -17 dB at 8° incidence angle; a maximum value of -7.5 dB and a minimum value of -22 dB at 55° incidence angle; and an increase in slope (with incidence angle) beyond 25°.

A study of the corresponding photography reveals that the ridges which have the largest back-scattering cross sections (both σ°_{hh} and σ°_{hv}) are topographically very rough events whose immediate background consists of relatively smooth ice. One of these, 803.R44, is a large first-year ridge bordering a multi-year floe.

Figures 3a and 3b summarize the incidence angle dependence of the ridge to background ice radar contrast ratios (signal to clutter ratios) for σ°_{hh} and σ°_{hv} respectively. In Figure 3a it is seen that the like-polarized contrast ratio increases with incidence angle between 8° and 25° and then changes very little with incidence angle between 25° and 55°. This effect is most pronounced for ridges with large contrast ratios. A similar effect is seen in Figure 3b with the contrast increase occurring between 8° and 15° incidence angle and very little further change in contrast up to 55°.

Figure 3b also suggests a grouping of the first-year ridges into three classes with the largest contrast class corresponding to the large ridges in locally smooth backgrounds mentioned previously. The cross-polarized ridge to background contrasts are enhanced, up to 5 dB, over the like-polarized contrasts, even though the absolute cross-polarized cross sections are approximately 10 dB smaller than the absolute like-polarized cross sections.

An evaluation of the scatterometer signature for the six multi-year ridges meeting the data selection criteria revealed that:

(a) the peak, multi-year, like-polarized ridge back-scatter had a maximum value of 8 dB and a minimum value of 4 dB at an incidence angle of 8°; a maximum value of -1 dB and a minimum value of -6 dB at an incidence angle of 55° and varies with incidence angle in a manner similar to the background ice,

(b) the peak, multi-year, cross-polarized ridge back-scatter had a maximum value of -1.5 dB and a minimum value of -10 dB at an incidence angle of 55° and varies with incidence angle in a manner similar to the background ice.

An examination of the corresponding photography did not reveal any apparent correlation between visible ridge features and the back-scattering cross sections. Figures 4a and 4b summarize the incidence angle of the ridge to background ice contrast ratio. These figures indicate that over the scatterometer range of incidence angles (0-60°), multi-year ridge to multi-year ice contrasts are nearly independent of incidence angle. The figures also show that the contrast ratios for the cross-polarized component are enhanced approximately 2 dB with respect to the absolute cross-polarized cross sections. Because σ°_{hv} is approximately 10 dB smaller than σ°_{hh}, a substantially greater transmitter power is required to maintain the same signal-to-noise ratio and take advantage of the increase contrast with σ°_{hv}.

A comparison of Figures 4a and b with 3a and b indicates that both the range of variation and the maximum value of ridge contrast ratios are much smaller for multi-year ridges in multi-year ice than for first-year ridges in first-year ice. Also, in most instances, both σ°_{hh} and σ°_{hv}, for multi-year ridges are larger than σ°_{hh} and σ°_{hv} for first-year ridges. This study has revealed, however, that very bright first-year ridges may have signatures similar to multi-year ice.

Non Beam-Filling Ridge Results

In order to determine the effect of resolution cell on pressure ridge detectability, numerous ridges with along track dimensions less than one scatterometer footprint (18m) were analyzed. An empirical linear mixing formula was developed to scale ridge σ°_{hh} and σ°_{hv} by the ratio of the scatterometer footprint to the ridge width. This simple approximation proved satisfactory for all ridges wider than 9m but was unreliable below this width. Failure of the empirical scaling formula is associated with the dominance of other ice features in the same footprint. A similar analysis with the digitized SAR results suggested that pressure ridges become indistinguishable from the background clutter when resolution cells are 3-5 times the width of a ridge, dependent upon the radar texture of the background ice.

Ridge Detectability from SAR

On March 16 and March 18, high resolution (∿3m) SAR coverage of the Beaufort N/S photo line was obtained, in the steep and shallow depression modes respectively. Ridges on the SAR imagery were visible as bright, narrow linear features and were especially visible within a smooth, first-year ice background as noted previously. Small ridges within multi-year floes were the most difficult to identify because of the pronounced radar texture of multi-year ice (Livingstone *et al.* 1980).

The X-band radar channels proved superior to the L-band channels for pressure ridge studies and the cross-polarized component of the X-band radar yielded better local contrast than the like-polarized component. Nevertheless, the like-polarized component does provide excellent tonal contrast within young ice forms (nilas, dark grey, etc.). Such contrasts are indicative of ice age and thus allow the age of ridges present within these ice forms to be inferred.

An examination of the same ice features in both steep and shallow depression modes revealed a significant reduction of surface ice texture and an enhancement of all large scale topographic features at shallow (∿10°) depression angles.

Increasing ridge-to-ice contrast and decreasing background ice texture may be seen in the range direction of shallow depression SAR imagery, illustrating these effects. This data set suggests that the most suitable angles for ridge detection lie between depression angles of 5° and 20° (incidence angles of 70-85°).

DIGITAL SAR RESULTS

A digital analysis of 26 ridges, imaged by the SAR at shallow depression angles (∿6°) and processed at ERIM using the optical digital hybrid processor, revealed little correlation between beam-filling pressure ridge dimensions (height or width) and ridge brightness (the magnitude of σ°_{hh} and σ°_{hv}, as shown in Figures 5, 6 and 7. A more extensive study incorporating a larger ridge sample population is currently in progress and will be reported at the SURSAT Sea Ice Workshop, Toronto, June 1980 (Lowry and Pearson 1980).

Preliminary results suggest that factors other than the physical dimensions of pressure ridges are important contributers to ridge brightness on the SAR image. It has been suggested (Livingstone *et al.* 1980) that the microstructure (wave length scale: surface roughness, salinity, crystal structure, air and brine inclusions) of the deformed ice and the local mean incidence angle (as weighted by block fracture patterns and orientations) primarily determine ridge back-scattering cross sections.

Figure 8 is an example of a numeric map used to generate the results shown in Figures 5, 6 and 7. This map shows a first-year ridge, 3.9m high by 11.5m wide, within a background of first-year ice. The numeric values in Figure 8 are relative SAR image intensities digitized to 3m resolution and scaled to produce 256 grey levels, from the smoothest first-year ice to the roughest ice in the scene, with the brightest target having an intensity value of 255 (indicating saturation). The image of the deformed ice comprising the ridge has a pronounced texture and an average intensity value of 130. In contrast, the undeformed background ice has little texture and an average intensity value of 46. In terms of average contrast this ridge is 10 dB brighter than the background ice.

ICEBERG STUDY

As mentioned in the introductory section, iceberg data for this experiment was collected from two Eastern Arctic regions in April, 1979.

The north Greenland coast bergs were located in Melville Bay and were embedded in smooth, land fast first-year ice. The surface ambient temperature was below -2°C. The iceberg data set consists of dual-polarized scatterometer data (σ°_{hh}, σ°_{hv}) and RC10 photography.

The Davis Strait ice-marginal zone bergs were located south west of Disko Island, along a N/S line approximately parallel to the Greenland coast, and were surrounded by broken first-year floes and ice cakes. The surface ambient temperature in this region was between -2°C and 0°C.

For this data set X-and L-band SAR imagery are available to augment the scatterometer data and the RC10 photography.

Scatterometer Results

The iceberg to background ice contrasts shown in Figure 9, for seven beam filling icebergs, indicates a wide variation in back-scattering coefficients from berg to berg which appears to be related to the iceberg surface topographies. The lowest σ°_{hh} contrasts seen in the data set correspond to domed bergs, which, having undergone extensive weathering, reflect microwave radiation away from the receiving antenna. The highest σ°_{hh} contrasts seen in the data set were found for blocky and tabular bergs where the multiple facets act as corner reflectors to incoming microwave energy.

As was noted in the ridge study, the cross-polarized iceberg to background contrast was enhanced 2 to 4 dB above the like-polarized contrast. A further analysis of Figure 9 also reveals iceberg contrast ratios to be nearly independent of incidence angle over the scatterometer range 15° to 60°. The berg to background ratios seen in Figure 9 are in general agreement with those reported by Parashar et al. (1980). However, as others have reported (Gray et al. 1979, Parashar et al. 1980), an increase in berg to ice contrast is expected beyond the range of incidence angles recorded by the scatterometer.

When the angular dependences of the σ_{hh} and σ_{hv} contrasts are examined in detail, substantial differences are found from berg to berg for the same variable and from angle to angle for the same berg. The detailed contrast structure appears to be related to the iceberg surface morphology but the data set is too small to quantify the relationship.

It must be noted that although Figure 9 provides target to background contrasts for large icebergs visible in the scatterometer data, many small, but beamfilling bergs visible in the photography were crossed by the scatterometer track but showed no radar contrast. In particular, iceberg detection proved very difficult in a broken, first-year ice background at radar incidence angles in the 0° to 60° range.

On numerous occasions, the scatterometer recorded a region of low backscatter along one edge of an iceberg, as seen in Figures 10a,b,c. Within this region, back-scattering coeficients were 5 to 10 dB lower than those of the surrounding first-year ice. These features, in combination with pressure cracks near the icebergs, are interpreted to be evidence of recent motion of the bergs in the pack ice. The regions of depressed back-scattering coefficients are felt to be regions of younger ice. For the iceberg shown in Figure 10a, the microwave signature of the depressed back-scatter region suggests that this region is grey-white ice and that the ambient temperature is between -5°C and -15°C (Hawkins et al. 1980).

SAR Results

Although numerous icebergs were visible on RC 10 imagery from the Eastern Arctic, only five bergs were also distinguishable in the scatterometer data; these were found on the southern Davis Strait photo time. Of these five icebergs, only two were positively identified in the steep depression angle SAR imagery, the others being indistinguishable from the surrounding ice floes. Both detectable bergs were larger than 200m in the along-track dimension and were viewed at incidence angles of approximately 50°. Those icebergs not detected by the SAR ranged in size from 25 m to 125 m in the along-track dimension and were also viewed at incidence angles of 50°.

CONCLUSIONS

From the discussion in the previous sections, it is seen that incidence angles in excess of 60° are preferred for the detection of sea-ice features in a sea-ice background and that radars operating in the viable satellite SAR incidence angle range (16° to 45°) may be suitable for sea-ice ridge detection but are not suitable for iceberg detection. As has been noted by other investigators (Parashar et al. 1980), X-band SAR is more suitable for ice feature discrimination than L-band SAR and the cross-polarized SAR channels produce the best local feature enhancement.

The scatterometer results indicate that both first-year and multi-year ridges are distinguishable from their respective backgrounds and that first-year and multi-year ridges are usually separable from each other. However, the pronounced texture of multi-year ice reduces the ridge to background contrast and may occasionally obscure a ridge. The resolution cell size of the radar was seen to limit ridge detectability, with most ridges being lost in the background clutter when the resolution cells were 3 to 5 times the along track dimension of the ridge.

A digital analysis of 26 ice ridges extracted from the SAR data revealed little correlation between pressure ridge dimensions (height or width) and ridge brightness. This poor correlation suggests that ridge brightness in SAR imagery is more dependent on the microstructure (wavelength scale) surface roughness, crystal structure, brine and air inclusions and salinity of the deformed ice and on the local mean incidence angle (Livingstone et al. 1980) than on the large scale structure directly.

Although the iceberg data set was small, it was clearly evident that iceberg detection in a sea-ice background was a more difficult problem than ridge detection. Iceberg back-scattering coefficients were highly variable and were dependent on berg type, orientation and weathering. No quantitative relationships could be derived between iceberg surface morphology and the back-scattering coefficients.

Over the incidence angle range 0° to 60°, iceberg detectability was found to be poor, especially for bergs in a broken first-year ice background. No icebergs with along-track dimensions less than 5 resolution cells could be recognized in the scatterometer results.

Those icebergs which were either marginally detectable or undetectable in the SAR imagery, ranged in size from 25m to 126m in the along-track direction and were viewed at an incidence angle near 50°. From the scatterometer results the radar returns from these icebergs were only 3 dB brighter than the broken ice background. Since a 10 to 15 dB iceberg contrast is required for a 90% identification accuracy(Gray et al. 1979), many icebergs and bergy bits larger than the resolution cell of a SAR will not be detected in a steep depression angle SAR image.

REFERENCES

(1) Gray,A.L., R.K.Hawkins,C.E. Livingstone, R.Lowry, R.Larson and R.Rawson "The Influence of Incidence Angle on Microwave Radar Returns of 'Targets' in an Ocean Background", Proc. 13th Int. Symp. on Remote Sensing of the Environment, Ann Arbor Michigan 1979, pp 1815-1837

(2) Hawkins,R.K., C.E.Livingstone, A. L.Gray, K. Okamoto, L.Drapier Arsenault, D.Pearson and T.L. Wilkinson "Single and Multiple Parameter Microwave Signatures of Sea Ice", Presented at the 6th Canadian Symposium of Remote Sensing, Halifax, May 1980

(3) Livingstone,C.E., R.K.Hawkins, K.Okamoto, L.Drapier Arsenault, T.L.Wilkinson, D.Pearson and A.L. Gray "The Microwave Signatures of Sea-Ice Types and Features and their Implications for Remote Sensing", Canada Centre for Remote Sensing Report 1980 (in press)

(4) Lowry,R.T., D.R.Inkster and M.E. Kirby "Ice and Iceberg Studies using State-of-the-art Remote Sensing", Proc. 5th Int. Conf. on POAC, Trondheim, August 1979, pp

551-570

(5) Parashar,S., G.Stapleton, R. Worsfold and R.O'Neil "Potential of SAR in Detecting and Monitoring Icebergs", Cold Regions Science and Technology Symposium, Amsterdam, 1980, V1, pp 195-210

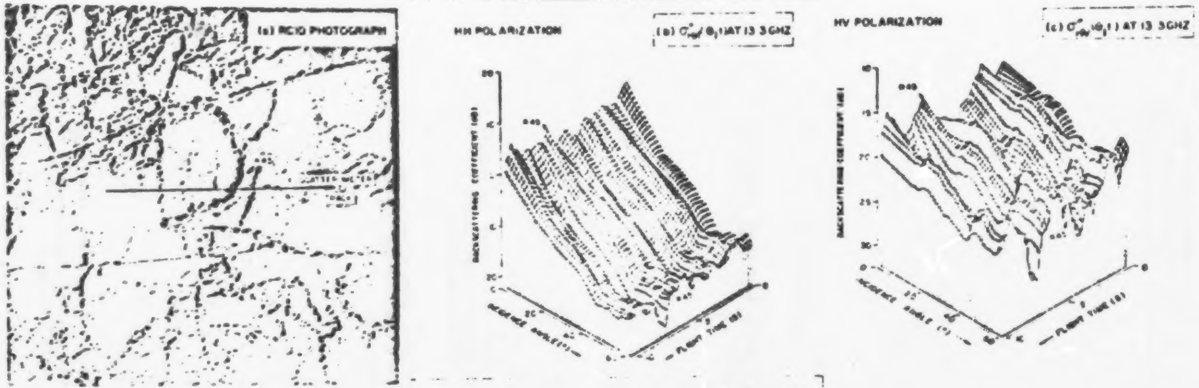

FIG.1 FIRST-YEAR RIDGE R45

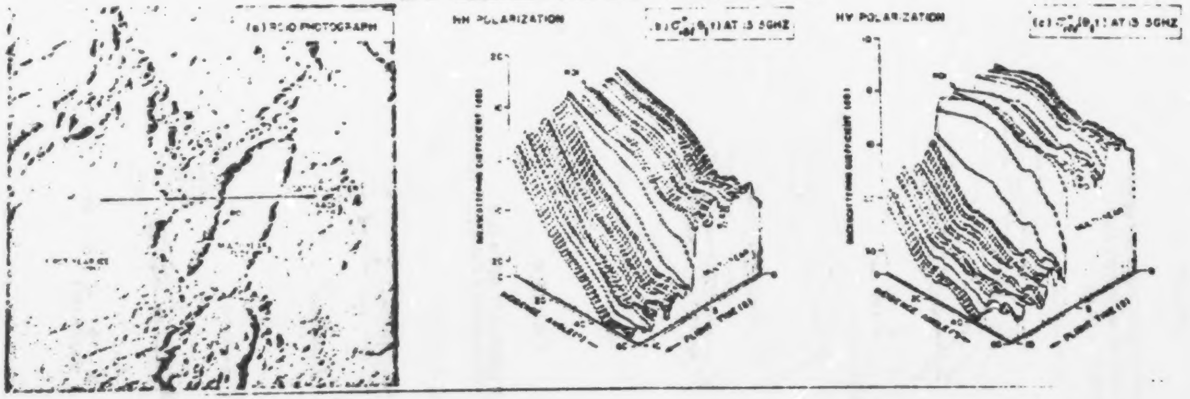

FIG.2 MULTI-YEAR RIDGE ROI

FIGURE 3

RADAR CONTRAST BETWEEN FIRST-YEAR RIDGES AND FIRST-YEAR ICE

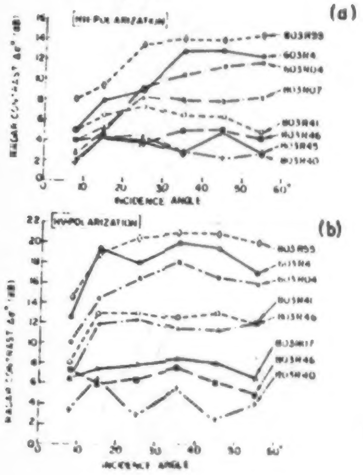

FIGURE 4

RADAR CONTRAST BETWEEN MULTI-YEAR RIDGES AND MULTI-YEAR ICE

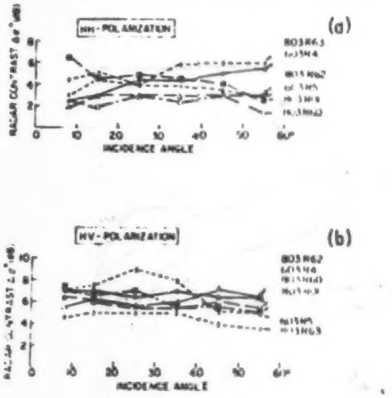

FIG 5 THE VARIATION OF RIDGE HEIGHT WITH RIDGE WIDTH THE DATA POINT NUMBER IS THE NUMBER OF EVENTS CORRESPONDING TO THAT POINT.

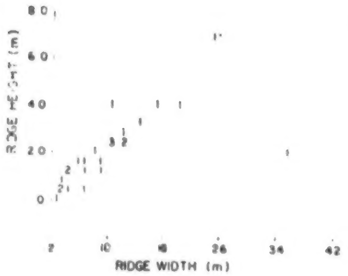

FIG 6. THE CORRELATION BETWEEN RIDGE WIDTH AND THE RELATIVE X BAND HH POLARIZED SAR IMAGE BRIGHTNESS

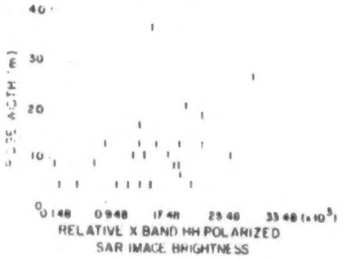

FIG 7 THE CORRELATION BETWEEN RIDGE HEIGHT AND X BAND HH POLARIZED SAR IMAGE BRIGHTNESS

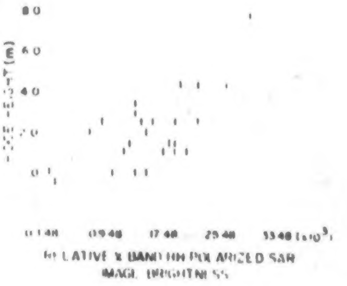

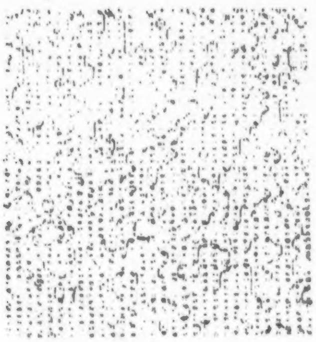

Figure 8. A Numeric Map of Digitized SAR Data Containing a First-year Ridge within a Background of First-year Ice. The image was optically processed and subsequently digitized, each operation to 3 m resolution. The brighter radar returns are represented by large numeric values and contour lines indicate 6 dB intervals.

FIGURE 9 RADAR CONTRAST BETWEEN ICEBERGS AND SMOOTH FIRST-YEAR ICE

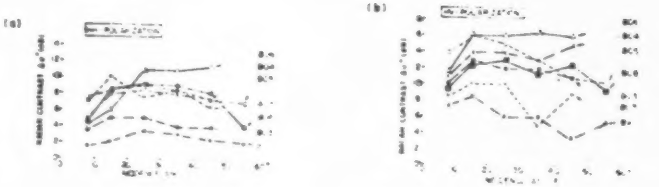

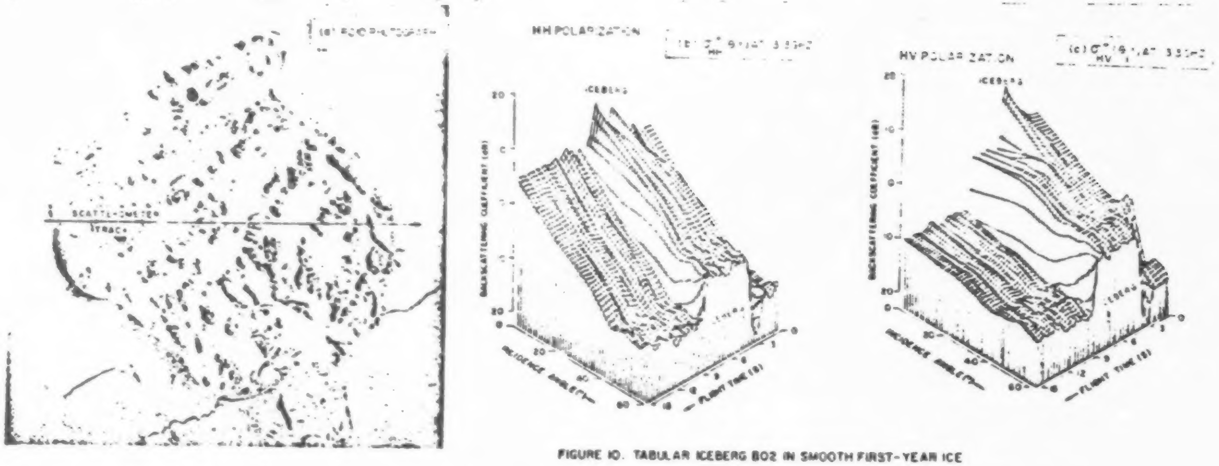

FIGURE 10. TABULAR ICEBERG BO2 IN SMOOTH FIRST-YEAR ICE

SECTION 5.13

ICEBERG DETECTABILITY PROBLEMS USING SAR AND SLAR SYSTEMS

Kirby, M.E. and R.T. Lowry

Paper presented at the 5th Annual W. T. Pecora Symposium: Satellite Hydrology,
Sioux Falls, South Dakota, June 10-15, 1979.

ICEBERG DETECTABILITY PROBLEMS USING SAR AND SLAR SYSTEMS

M.E. Kirby, R.T. Lowry

Intera Environmental Consultants Ltd.
Ottawa, Ontario

ABSTRACT

The application of synthetic aperture radar (SAR) and real aperture side-looking airborne radar (SLAR) systems for the identification of icebergs involves an understanding of the complicated interactions between the radar beams and the multi-faceted bergs. This paper summarizes the major problems that have been encountered in iceberg census research from selected portions of SLAR and SAR airborne experiments that were recently conducted. Since little radar iceberg data have been gathered from space satellites, the airborne systems offer attractive simulation possibilities. These systems have been used here to address such topics as iceberg detectability in relation to resolution, depression angle, sea clutter, and iceberg size and type.

KEY TERMS: Icebergs, Synthetic Aperture Radar (SAR), Side-looking Airborne Radar (SLAR).

ICEBERG DETECTABILITY PROBLEMS USING SLAR AND SAR SYSTEMS

M.E. Kirby, R.T. Lowry

Intera Environmental Consultants Ltd.
Ottawa, Ontario

1. INTRODUCTION

In recent years more and more attention has been directed towards resource activities into Canada's vast Arctic regions. Much of this activity has been specifically oriented toward iceberg census studies in Baffin Bay, Davis Strait and the North Atlantic. The impetus comes from increasing oil and gas exploration in these regions with the establishment of drilling sites and Arctic shipping routes. Icebergs pose a formidable threat to the ships and drilling rigs.

It is necessary that accurate iceberg census data be made available for the operators of Arctic drilling rigs and ships to safely conduct their production tasks. Remote sensing data sets seem well suited to show the geographical locations of icebergs at a given time and to provide valuable information regarding their type, size and spatial distributions. Given the climatic conditions that often persist in Canada's Eastern Arctic, the requirements for timely iceberg data necessitate the use of active systems that can operate independent of most weather states. SAR and SLAR systems are the technologies available today that can meet these objectives in the variable Arctic environment.

The application of these systems for accurate iceberg census work has proven to be a difficult task requiring a detailed understanding of iceberg and radar interactions. By investigating the difficulties of iceberg census work with airborne radars it is possible to evaluate the potential utility of a spaceborne SAR for the detection of icebergs. In this paper examples of iceberg data sets are presented as imaged from two airborne systems: the ERIM SAR and the Motorola AN/APS 94E SLAR.

2. ICEBERG TYPES AND SIZES

If it is assumed that the shape of the above-water portions of icebergs are generally random (Murray, 1968), then the categorization of icebergs by type and size does not seem feasible. However, for purposes of simplicity, most icebergs can be grouped into at least one of five iceberg types based on their dominant shape. The five major types of icebergs have been summarized by Murray (1968) and are listed in the following table.

Insert Table 1 →

In addition to the iceberg types listed in Table 1, there are other features composed of glacially derived ice but which are not referred to as bergs. These include ice islands, bergy bits and growlers. An ice island is a large piece of floating glacial ice about 5 m. above sea level having a thickness of 30-50 m. and an area from a few thousand square metres to 500 sq. km. or more (WMO, 1970). Ice islands occur much less often than icebergs. A bergy bit is a piece of glacial ice about the size of a small cottage showing between 1 and 5 m. above sea level and normally about 100 - 300 sq. m. in area (WMO, 1970). A growler is a piece of ice extending less than 1 m. above the sea surface and usually occupying an area of about 20 sq. m. (WMO, 1970). Bergy bits and growlers occur more commonly than icebergs. As last year's shipping season in the Arctic demonstrated, bergy bits, growlers and ridges proved to be a hazard to even ice strengthened vessels such as the icebreaker John A. MacDonald and the ore carrier MV Arctic, as well as two other drilling ships.

In addition to types, icebergs can be categorized by size. There are two ways to classify bergs by size: one which includes an estimate of the entire berg volume including the sum of the above-water and below-water portions, and the other which just considers the above water part of a berg. Since the remote sensing systems that are most commonly employed for census purposes can only image the above water sections of a berg, we refer to iceberg sizes by the latter scheme.

The table below summarizes the general iceberg classes by size as discussed by Murray (1968).

Insert T. 1 & 2. ->

3. DESCRIPTION OF RADAR SYSTEMS

Iceberg data from two systems were studied for this paper. The first was the ERIM four-channel SAR flown in the Canada Centre for Remote Sensing Convair-580, while the second system was a Motorola AN/APS 94E flown in the Atmospheric Environment Service Ice Patrol Electra aircraft. Following is a brief description of each system; more detailed summaries can be obtained from the cited references.

3.1 The SAR-580 System

The SAR-580 system (Inkster et al, 1979) is based on the ERIM four-channel SAR. This consists of two dual polarized radars, one operating at 1.2 GHz. (L-band) and one at 9.0 GHz. (X-band). Both radars are capable of transmitting either vertically or horizontally polarized radiation, and receiving both parallel and crossed polarizations. The radar has approximately two metres resolution at X-band and somewhat less at L-band. A swath width of 5.5 km. slant range is recorded for all four channels. The ground range is a function of depression angle and altitude. The depression angle of the main lobe of the antenna is manually adjustable. Typically the system is flown at either steep or shallow mode. In steep mode, the aircraft is flown at approximately 6,000 m. (20,000 ft.), with the antenna pointed at

45°. Data are recorded from the nadir return out to 5.5 km. slant range (approximately 10 km. ground range). In shallow mode the antenna is depressed 22° below the horizon and has a ground range offset from nadir of about 11 km. and a swath width of 6 km. Data from the real time digital processor is produced in real time and is used to monitor performance of both the radar and the navigation system.

The radar is installed on the Convair-580 of the Canada Centre for Remote Sensing. The aircraft has a complete set of radio, navigational and remote sensing gear. The prime navigation is supplied by an LTN-51 inertial navigation system (INS). The INS is located at the antenna and is the heart of a sophisticated motion compensation system. The autopilot control is derived from this system, and the aircraft is under this autopilot control during all imaging passes.

3.2 AN/APS 94E SLAR

In 1977 AES acquired a Motorola SLAR from the Department of Defense to assist in the Ice Branch reconnaissance activities. The SLAR is installed in an Electra long range aircraft with dual LTN-51 Inertial Navigation sets and Omega Global Navigation equipment (Ramplee-Smith, and Hengeveld, 1978).

The SLAR (Motorola, 1975) is composed of a tunable receiver-transmitter, a slotted array, yaw stabilized antenna, a signal processor and a real time processing unit. The system resolution is 0.45 degrees in azimuth (8 m. per km. of range) and 30 m. in range. Imagery can be generated at scales of 1:250 K., 1:500 K. or 1:1,000 K. on heat sensitive transparency film in a negative format that is 241 mm. wide, with a display resolution of 30 lines/mm. Mapping ranges can be set at 25,50 or 100 km. simultaneously on both sides of nadir with range delays from 0 through 60 km. in 10 km. increments. The receiver-transmitter pulses single channel X-band (9 GHz.) like-polarized radiation. The antenna has been positioned to optimize returns received at altitudes of about 5,000 ft. This radar has been employed for operational ice reconnaissance purposes for almost two years.

4. RADAR DETECTION OF ICEBERGS

The ability of an imaging radar to detect icebergs will be dependent on the signal level relative to the clutter level. Signal levels and clutter levels are determined by the system parameters such as resolution, depression angle, frequency and polarization, as well as the target parameters such as iceberg size, type, texture and background characteristics. The interactive effects of signal levels and clutter levels upon the detection of icebergs are discussed within this section.

For an accurate discussion of the detectability of an iceberg with a SAR or SLAR system one should treat each berg as a separate entity; this would be an impossible task. In the meantime we may generally discuss the detectability of bergs by type.

By definition tabular and blocky bergs should be more detectable because of their steep, precipitous sides which act as excellent corner reflectors for incoming radar beams.

Drydock and pinnacled bergs tend to be much more multi-faceted than other bergs and therefore should have a greater probability of detection. However, since the larger proportion of their sides tends to be vertically oriented, it stands to reason that they would be more detectable from shallow depression angles.

Finally, domed bergs are the most difficult to detect by virtue of their shape. Most domed bergs have well rounded and smooth features in all of the above-water dimensions. This makes them less detectable since much of the radar energy would be reflected off of the target berg at glancing angles away from the receiving antenna.

The above discussion assumes that the bergs of interest are all of a size that far exceeds the system resolution. For small bergs, bergy bits and growlers, size with respect to resolution plays a major role in their detectability.

The dielectric constant of iceberg ice is relatively low (approximately 3 at 10 GHz.) and being non-saline, would have a low loss tangent. It can therefore be argued that bergs are visible only because of Rayleigh type scattering from surface texture and facet reflections. Thus, for bergs that are large compared to the resolution cell, one would expect stable radar reflections. For bergs on the order of the resolution scale and smaller, much greater variability would be expected. The surface scattering comes from texture that has a scale on the order of the wavelength. It is reasonable to assume that longer wavelengths would see somewhat less texture, but may see more bulk effects and internal reflections. For example, impulse radars at 840 MHz have been used to examine internal reflections (Goodman et al, 1977). Gray et al (1979) have observed that the strength of surface reflections are directly related to roughness or texture. However, the signal to clutter ratio (SCR) could dominate the textural effects and thus make the identification of a berg difficult.

The clutter return in which bergs are located is highly variable for sea ice or open water which tend to demonstrate a non-uniformity of return (texture). Water returns range from almost nothing at low angles for calm seas, to +10 db or more at steep depression angles in rough seas. Further, waves, if they are resolved, show brightness with a high degree of texture. Strong, confusing returns can occur with high resolution systems (Jakeman and Pusey, 1977). Undeformed sea ice tends to have less variation with depression angle than water (Gray et al, 1977). However, most sea ice is normally deformed with ridges and rubble that usually produce strong reflections. The exception would be multi-year ice that has dielectric properties similar to glacial ice. Other spatial factors can be used to distinguish glacial ice and multi-year ice.

The two radar systems discussed in this paper represent two extremes with respect to the iceberg detection problem. The SAR-580 imagery is high resolution (3 x 3 m.), one look data, while the APS 94E imagery is lower resolution (30 x 100 m. approximately) and has several hundred looks with incoherent averaging. The effect of these quite different sets of radar parameters is illustrated in the following section.

5. PRESENTATION OF DATA SETS

Examples of icebergs imaged by the SAR and SLAR systems are presented in this section. It should be pointed out that there are no examples of coincident data between the two systems. The purpose served by these examples is to demonstrate the various detection problems described earlier.

5.1 SAR Iceberg Imagery

In April of 1979 a SAR sortie was flown in iceberg infested waters along the Greenland coast from Disko Island to Thule as part of the Canadian Surveillance Satellite Project (SURSAT). A number of SAR images with examples of various iceberg situations are presented in this section along with a brief discussion of the imagery.

The SAR data were collected in steep mode at depression angles from 30° to 90° (incidence angles from 0° to 60°). A 35 mm. side-looking camera was operated and provided an occasional simultaneous slide.

In the first set of examples (Figures 1-4) four-channel SAR data is presented showing icebergs in the fast ice adjacent to Cape York on the Greenland coast. The most obvious aspect about the four-channel comparison is the difference between the X and L band images. The icebergs in the X-band data sets are depicted in great detail while those in L-band are often barely visible. Even though there were no corresponding air photos or ground truth data sets, the authors feel that the different appearance of the images can be related to the surface texture characteristics of the bergs as well as the variations in penetration, absorption and scattering between the bands.

As the imagery shows there is less radar return from the bergs at L-band that at X. It could be hypothesized that the icebergs appear smoother in L-band because their surface texture characteristics more closely resemble the dimensions of the X-band wavelengths. In addition, the resolution for L-band is lower than X by a factor of about 2 which would then have a quantization effect on the L-band data and reduce the detail.

An additional factor affecting the differences between the two bands concerns their respective interactions with freshwater ice as a function of wavelength. It is commonly accepted that the L-band radiation will penetrate freshwater ice to a much greater extent than the X-band radiation. As a result it can be expected that the L-band radiation will be subjected to greater amounts of absorption and scattering within an iceberg, thus reducing the amount of radiation that could be returned to the antenna.

One further observation concerning the imagery in Figures 3 and 4, is that there is a significant difference in the fast ice background clutter between the X_{HH} and X_{HV} polarizations. In the X_{HV} imagery the background clutter has been suppressed in relation to the iceberg radar returns, while in the X_{HH} image there is a large degree of reflection from the background fast ice. At the same time the return from the icebergs in both images appears to be quite similar. This is in agreement with other published work which showed that the contrast between ice types is enhanced using the cross-polarized term (Gray et al, 1977) and that the iceberg returns show less polarization dependence (Gray et al, 1979). It is tempting to speculate that bergs reflect energy more by Rayleigh scattering and volume scattering and that the ice has 'facet'reflectors. However, no proof of this mechanism can be presented, at least for the moment.

For the next set of imagery (Figures 5-7) we were fortunate to have an oblique photo taken simultaneously with the SAR imagery. From Figure 5 a number of medium sized bergs are visible along with numerous small bergs and bergy bits. Except for the polynya in the centre of the photo (A) and the ridging at (B), the ice between the bergs appears to be quite uniform first year ice or younger. However, examination of the radar images reveals a much more complex situation.

In Figures 6 and 7 we have the X_{HH} and X_{HV} bands displayed for the same area as the oblique photo. Upon comparison of the images it is obvious that all of the bergs have been imaged and most of the bergy bits. The rough tabular berg at (C) and the cluster of bergs at (D) have all been accurately depicted in terms of their size, shape and type. However, the small bergs at (E) are just barely visible on both radar images and would be very difficult to identify without the aid of the oblique photo. From the photo we can see that the primary reflective surfaces of the two bergs at (E) are facing away from the incidence vector of the incoming radar radiation resulting in only a minimal amount of specular return. At the same time the smaller pieces of ice at (H) appear brighter than those at (E). This is an example of how iceberg orientation instead of size was the predominant variable affecting the detectability of the bergs.

Perhaps the most striking feature about the radar imagery, in Figure 6 especially, is the apparent variability within the ice that is not at all obvious in Figure 5. From Figure 5 the ice at (F) and (G) appear to be the same. However, as Figure 6 shows the ice at these locations is very different. At (F) there is a zone of deformed and consolidated first year ice, while at (G) we have younger and smoother first year ice. From a shipping point of view it would be more desirable to move through the younger and smoother ice. It would be difficult to chart such a course from just the visual information.

Figure 8 shows the impressive volume and variety of bergs that can result from one season of calving. In this image we see hundreds of bergs from the Gade glacier frozen into the fast ice. In the summer the fast ice will melt and all of the bergs will be allowed to float freely in the open water.

In Figure 9 a number of bergs are shown as they appeared in fast ice surrounded by Barcan shaped features. It is hypothesized that during the formation of the fast ice the bergs were surrounded by open water as a result of their differential "bobbing" with the tides. These water areas eventually froze into smooth fast ice regions. As the season progressed, snow and ice flowers gathered over the rougher ice beyond the smooth areas but were prevented from being captured and formed in the vicinity of the bergs because of the effects of the prevailing winds.

In Figure 10 another example of a complex ice situation is presented. The bergs near (A) have been frozen into a zone of young ice and exhibit trails that have been imaged by the radar. These trails are most likely composed of rough, frozen berg pieces and grease ice spread out and away from the bergs by the wind and then frozen into the new ice. It is unlikely that these trails would be apparent visually. On the other hand the bergs at (B) are part of a quite different environment of consolidated pack ice and do not exhibit the same trails.

The feature indicated by the arrow in Figure 10 is characteristic of the thermal cracks that occur as a result of the compressive forces from variations in a freeze/thaw cycle. These cracks are usually long and straight through a zone of homogeneous ice which leads the authors to conclude that the nearby pack ice is consolidated. Again it is not likely that such a small feature would visually be obvious. It would be most advantageous for a ship to locate and follow such a crack in the ice.

In the next sequence of images (Figures 11 and 12), a grounded berg (arrow) near Disko Island is presented. Extending beyond the berg is a lead (A) which has been formed as the pack ice moved past the stationery berg. The authors speculate that the berg was frozen into the pack ice at (B) until the berg became grounded in about 240 ft. of water. The pack ice has moved the distance from (B) to the berg since the grounding occurred. The sheer zone between the rough shore-fast ice and the pack ice is apparent along (C).

An additional feature of interest in Figures 11 and 12 is the area near (D). In the X_{HH} image the zone is barely visible, while in the X_{HV} image the feature has been enhanced. In most pack ice situations the opposite is usually true where such a feature should be more obvious in

X_{HH}. However, an exception will occur when ice has been thrown up to form a strong dihedral corner reflector. It is quite possible that the ice at (D) has been deformed in such a manner because of a shoal.

Up to this point we have presented numerous examples of icebergs in pack ice situations. In September of 1978 the SAR system was flown over a number bergs in open water near Scott Inlet in Baffin Bay. The next three images (Figures 13 to 15) are X_{HH} band examples of the icebergs flown with the radar in a very shallow mode (8° depression angle).

The bergs in Figure 13 (A, B and C) are surrounded by pack ice fragments. It is worth noting that much of the return from the brash ice appears to be at a similar level to the return from the bergs. It is the spatial information related to the two features which supplies the interpretive clues. There is almost no return from the ocean suggesting that there was very little wave action.

In Figure 14 we see some eight icebergs in high contrast to the background water. This image was generated on September 9. Two days later the area was flown again with the results shown in Figure 15. Upon comparison of the images it can be seen that most of the bergs were present in both images, thus suggesting that they were grounded. The only exception was the berg at (A) in Figure 14 which moved out of the area between September 9 and 11.

It has been clearly demonstrated from the above examples that very detailed iceberg information can be extracted from a high resolution SAR system. However, from a satellite viewpoint it would be unreasonable to expect that same type of high resolution imagery could be generated because of data transmission and recording limitations. The resolution of a satellite borne system would likely resemble that of the lower resolution SLAR.

5.2 SLAR Iceberg Imagery

Two examples of SLAR imagery are presented from which iceberg census work has been conducted. In the first example an iceberg tongue adjacent to Cape York in Greenland was imaged. Figure 16 was taken with a hand held 35 mm. camera at the same time as the SLAR image of that area which has been reproduced in Figure 17.

From Figure 16 it is apparent that there are a variety of bergs stuck within the shorefast ice. Most of the bergs are of the pinnacled type with a number of tabular bergs interspersed. The bergs are so densely packed in the far range that it is impossible to accurately count them. All of the nearly 400 bergs in the picture have been recently calved and thus have not had a chance to roll or become domed.

In order to gain some appreciation for the size of the bergs in Figure 16 some six icebergs were measured from an enlargement of the photo. The specific bergs measured have been identified on the image and their dimensions summarized in Table 3.

Insert
Table 3 ->

In the reproduction of the SLAR image (Figure 17) for the same region it is apparent that the identification of the icebergs is not as straight forward a process as compared to the visual interpretation. For example, the large bergs along the fast ice edge have been virtually lost within the return from the face of the first year fast ice which acted as an excellent corner reflector. Even the ridging behind berg (A) resulted in significantly high returns which obscured a number of larger bergs. The small bergs or bergy bits at (F) resulted in quite apparent returns in the SLAR data as well. The returns from berg clusters tended to overlap with one another and resulted in a single large return patch making an iceberg census difficult. As a result of the high returns from even the small ice features it was not possible to derive iceberg size and type information from SLAR data. This image is a good example of how large icebergs can become lost within the similarly high returns from small ice features such as ridges and the fast-ice edge at shallow depression angles (in excess of 40°).

In the second sequence of figures an example of a berg in an ice strip situation is presented. Figure 18 shows a view of the ice strip region with a small tabular berg (48 m. or 157 ft.) visible in the centre of the photo. Much of the pack ice contains pieces of ice that have edges which act as corner reflectors. This is quite obvious in the SLAR image of the same area (Figure 19) which shows large regions of high return from the ice strip regions. The return from the many small pieces of pack ice have completely obliterated the return from the berg which cannot be identified at all. If an interpreter was to work with the SLAR imagery alone for this area, numerous pieces of the pack ice could be mistakenly identified as icebergs.

The above figures are only representative of two isolated situations in which icebergs occur. However, they clearly demonstrate that iceberg census activities with SLAR data at shallow depression angles can be a difficult task. The primary problem is a lack of spatial resolution so that bright reflectors cannot be resolved. Compounding that problem is the limited dynamic range available on dry silver film so that bright targets all show up as 'white', i.e. saturate, and bloom.

6. CONCLUSIONS

In a pack ice situation with the SAR data, depression angle did not seem to be a limiting factor for iceberg detection since very few of the ice features appeared to exhibit the same high levels of radar return or spatial characteristics as the bergs. However, at incidence angles of less than 20° the ground resolution becomes poorer than the slant range resolution while the sea and sea ice could become brighter and thus make iceberg detection difficult.

At shallow depression angles, small features such as ridges appeared as bright as large bergs in the SLAR imagery, making berg detection difficult. The blooming of these features is due to the low dynamic range of the film (15 db). Gray et al (1977) have recommended that any display medium should have a dynamic range of at least 35 db to adequately show the variability regularly seen in ice.

It was not possible to classify icebergs according to size and type with the SLAR while it was possible with the SAR.

For iceberg identification purposes with SAR, the X-band data was far superior to L-band. This is related to the different scattering mechanisms that take place at different wavelengths and to the slightly degraded resolution of the L-band data.

The cross-polarized X-band imagery appeared superior to parallel polarization for iceberg detection because of a larger tonal separation between bergs and sea ice. However, higher transmitter power levels are required to achieve a given signal to noise ratio with cross polarizations and this factor may become important when designing spaceborne SARs. A spacecraft program would most likely involve multi-variate applications for the purpose of identifying ice types, ridges, etc. as well as icebergs. Even though the SCR is low for the X_{HH} imagery, the data for this study would indicate that parallel polarized imagery would best meet the objectives of a multi-variate ice program. This observation is based on a limited data set that did not include multi-year ice, special processing for data enhancement or digital analysis. Further research would have to be conducted to verify the comparative utility of the two X-band polarizations.

It is apparent from the data sets studied that the accurate identification of icebergs requires high resolution SAR data and even then is a complex and difficult task. It is unlikely that an operational spaceborne SAR will achieve 3 m. resolution. Therefore, it would be reasonable to suggest that a high resolution SAR from an airborne platform would be operated in a tactical mode to complement the data from a much lower resolution, strategic, spaceborne SAR.

Since the launching of a spaceborne imaging radar will probably not become a reality for another five or six years, additional iceberg research should be conducted with the existing SAR and SLAR systems. For example, the SAR data may be processed to simulate the resolutions and depression angles that could be expected from a spacecraft. In addition, pattern recognition techniques are being employed to evaluate the utility of automated methods for iceberg detection purposes.

ACKNOWLEDGEMENTS

The SAR imagery for this study was collected and made available through the Canadian Surveillance Satellite Project Office, while the SLAR data was generated by the Ice Branch of the Atmospheric Environment Service. The authors are grateful to Intertech Remote Sensing Ltd. for its support during this study.

TABLE 1

ICEBERG TYPES

Iceberg Type	Description
a) Pinnacled	Large central spire or pyramid of one or more spires dominating shape.
b) Domed	A smooth and solid berg that has been rounded from rolling in the water.
c) Drydock	Eroded such that a large U-shaped slot is formed, with twin columns or pinnacles. Slot extends into the water line or close to it.
d) Blocky	Steep precipitous sides with horizontal or flat top. A very solid berg with a length-height ratio less than 5:1.
e) Tabular	Horizontal or flat-topped berg formed by calving from an ice shelf.

TABLE 2

ICEBERG SIZES

Size	Description
a) All types but tabular:	
Small	Height less than 15 m.; length less than 60 m.
Medium	Height 15 m. - 45 m.; length 60 m. - 122 m.
Large	Height 45 m. - 77 m.; length 122 m. - 213 m.
Very Large	Height greater than 77 m.; length greater than 213 m.
b) Tabular bergs:	
Small	Height 15m ; length less than 91 m.
Medium	Height 6 - 15 m.; length 91 - 213 m.
Large	Height greater than 15 m.; length greater than 213 m.

TABLE 3

ICEBERG DIMENSIONS

Identifier	Length Along Base metres (feet)	Height at Highest Point metres (feet)
A	800 (2624)	40 (131)
B	200 (656)	40 (131)
C	180 (590)	80 (262)
D	273 (895)	109 (357)
E	325 (1,065)	65 (213)
F	36 (118)	9 (29)

REFERENCES

Goblot, René, 1978. Diverting Icebergs from Labrador Oil Rigs, Canadian Geographical Journal, June/July: 52-57.

Goodman, R.H., E. Outcalt, B.B. Narod, 1977. Radar Techniques in the Measurement of Floating Ice Thickness. Presented to the 4th Canadian Symposium on Remote Sensing, Quebec City, Quebec.

Gray, A.L., R.O. Ramseier, W.J. Campbell, 1977. Scatterometer and SLAR Results Obtained Over Arctic Sea Ice and Their Relevance to the Problems of Arctic Ice Reconnaissance. Presented to the 4th Canadian Symposium on Remote Sensing, Quebec City, Quebec.

Gray, A.L., et al, 1979. The Influence of Incidence Angle on Microwave Radar Returns of "Targets" in an Ocean Background. Presented to the 13th International Symposium on Remote Sensing of the Environment, Ann Arbor, Michigan.

Inkster, D.R., R.K. Raney and R.F. Rawson. State of the Art in Airborne Imaging Radar. Proceedings of the 13th International Symposium on Remote Sensing of the Environment, Ann Arbor, Michigan.

Jakeman, E. and P.N. Pusey, 1977. A model for Non-Rayleigh Sea Echo. IEEE Transactions on Aerospace and Electronic Systems.

Motorola Technical Brochure: AN/APS 94D Side-Looking Airborne Radar. Scottsdale, Arizona.

Murray, J.E., 1968. The Drift, Deterioration and Distribution of Icebergs in the North Atlantic. The Ice Seminar, CIM Special, Vol. 10: 3 - 18.

Ramplee-Smith, C. and H.G. Hengeveld, 1978. Side-Looking Radar for Ice Reconnaissance. Canadian Journal of Remote Sensing, Vol. 4, No. 1: 44 - 50.

World Meteorological Organization, 1970. Sea Ice Nomenclature. Secretariat of the WMO, Geneva, Switzerland: No. 259.TP.145.

FIGURE 1
L_{HH} SAR Image of Icebergs at Cape York, Greenland

FIGURE 2
L_{HV} SAR Image of Icebergs at Cape York, Greenland

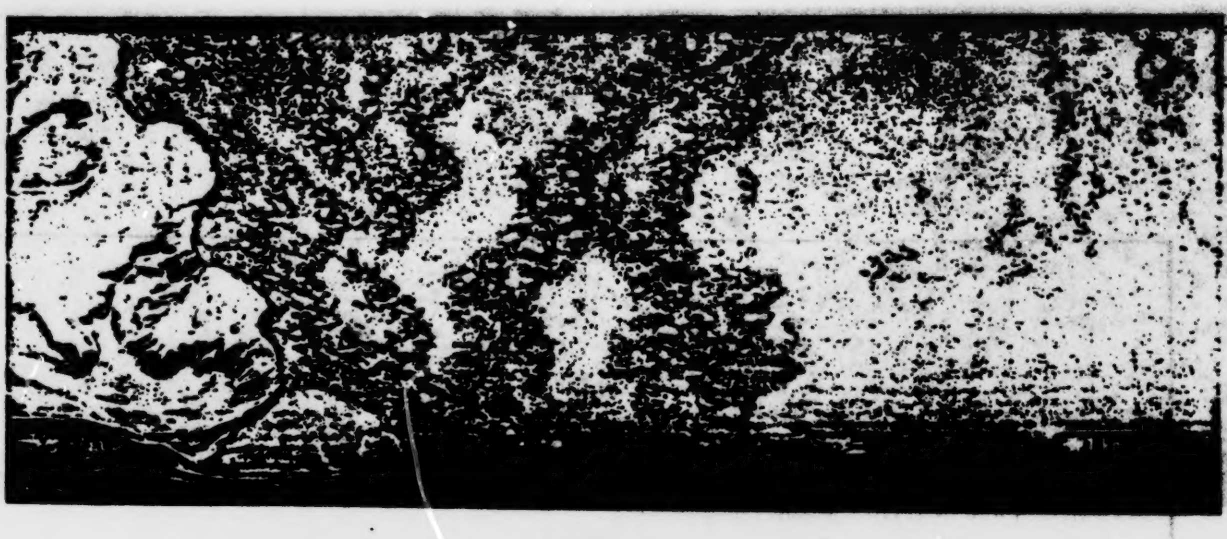

FIGURE 3

X_{HH} SAR Image of Icebergs at Cape York, Greenland

FIGURE 4

X_{HV} SAR Image of Icebergs at Cape York, Greenland

FIGURE 5
Photo of Icebergs and Ice along Greenland Coast

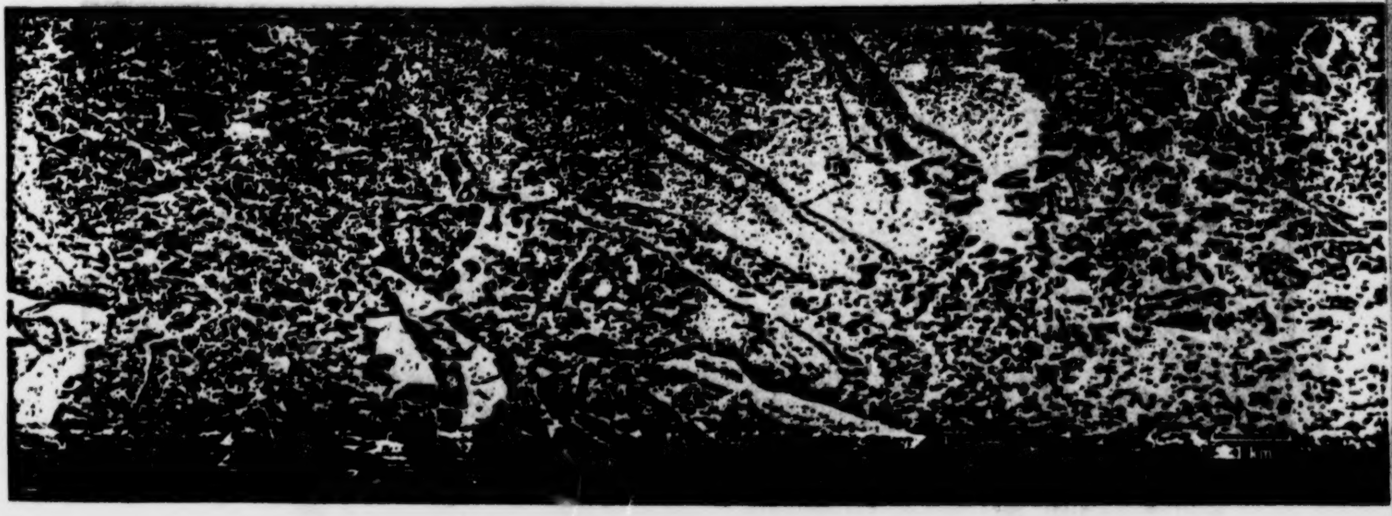

FIGURE 6
X_{HH} SAR Image of Icebergs and Ice along Greenland Coast

FIGURE 7
X_{HV} SAR Image of Icebergs and Ice along Greenland Coast

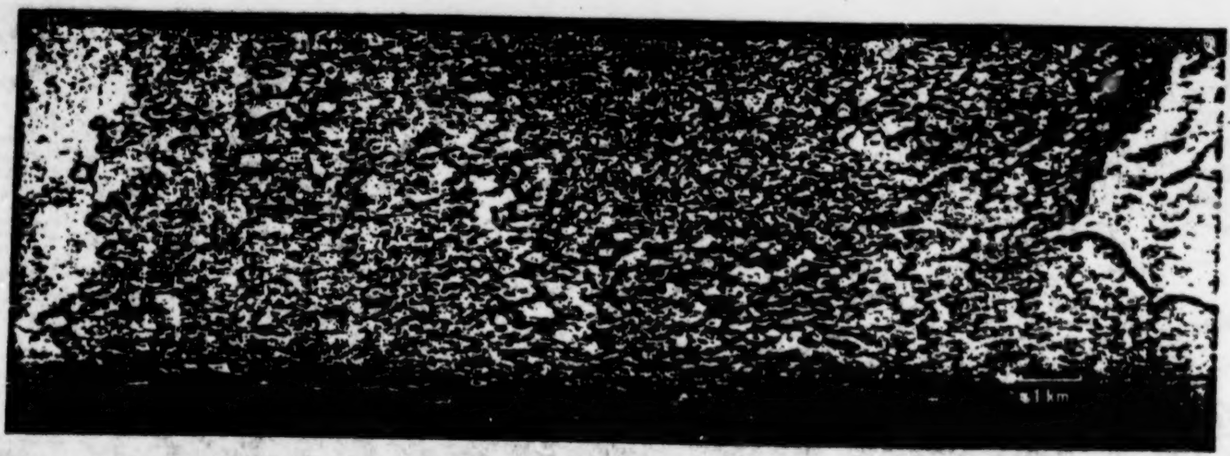

FIGURE 8
X_{HH} SAR Image of the Gade Glacier Calving Zone

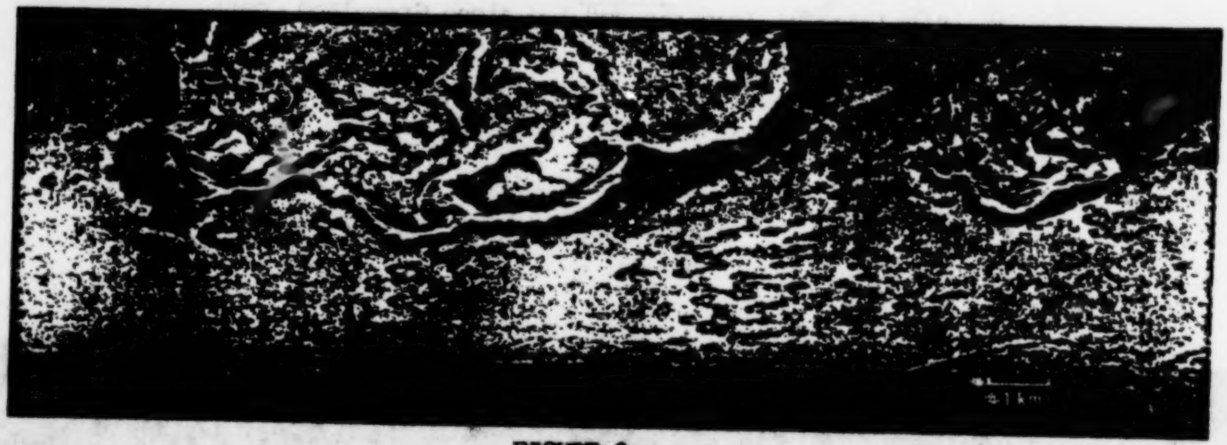

FIGURE 9
X_{HH} SAR Image of Icebergs in Fast Ice

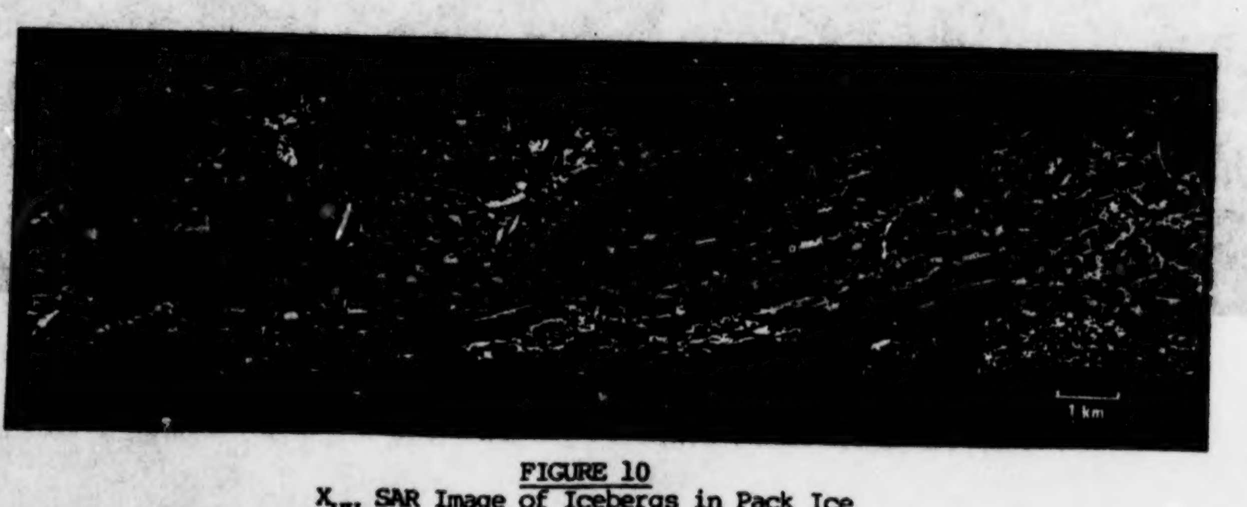

FIGURE 10
X_{HH} SAR Image of Icebergs in Pack Ice

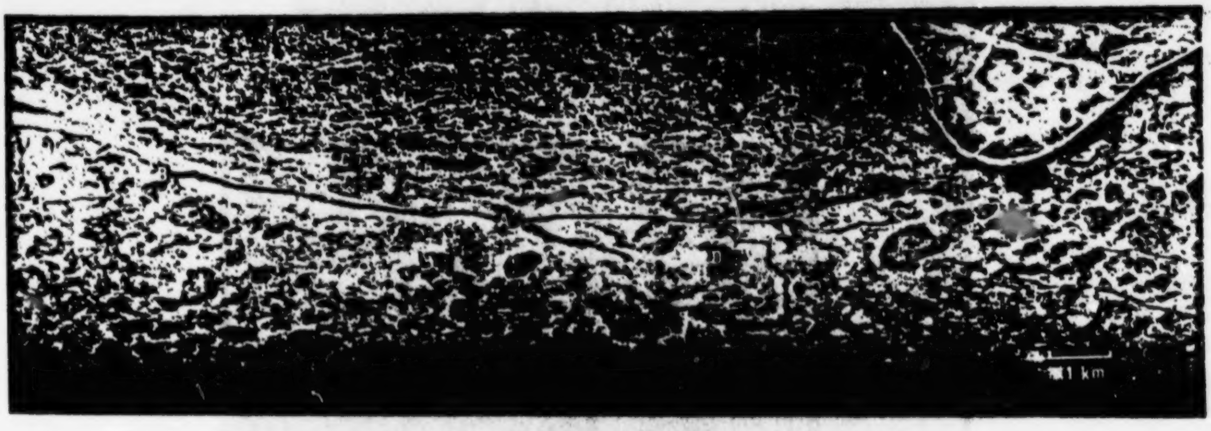

FIGURE 11
X_{HH} SAR Image of Grounded Iceberg near Disko Island, Greenland

FIGURE 12
X_{HV} SAR Image of Grounded Iceberg near Disko Island, Greenland

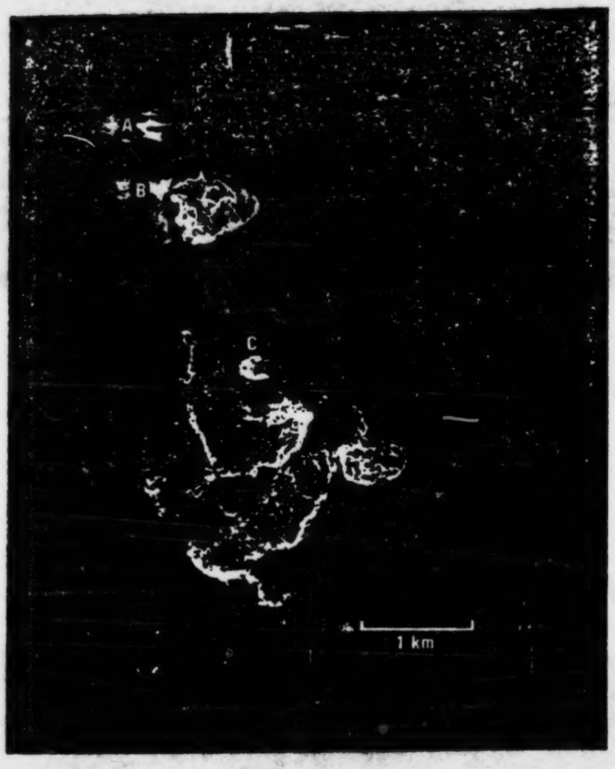

FIGURE 13
X_{HH} SAR Image of Icebergs and Brash Ice

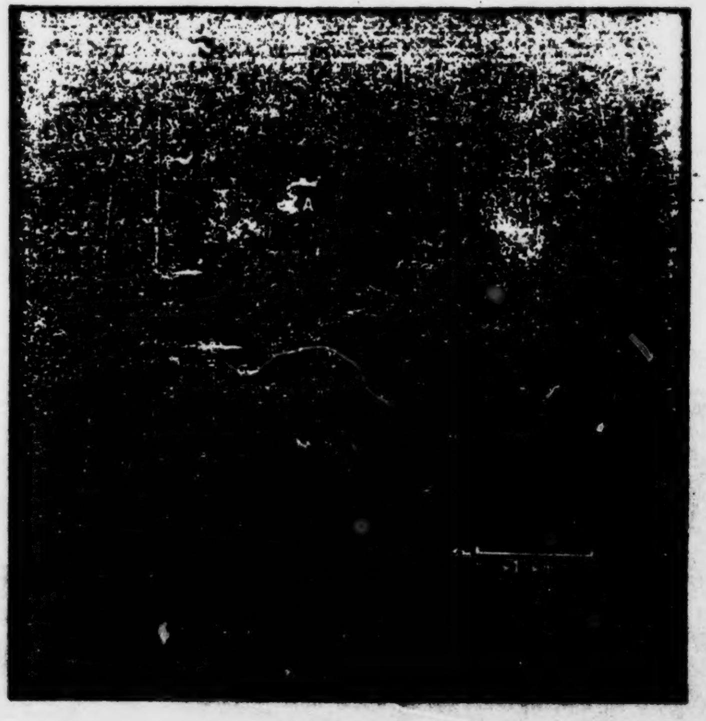

FIGURE 14
X_{HH} SAR Image of Icebergs in Baffin Bay: September 9, 1978

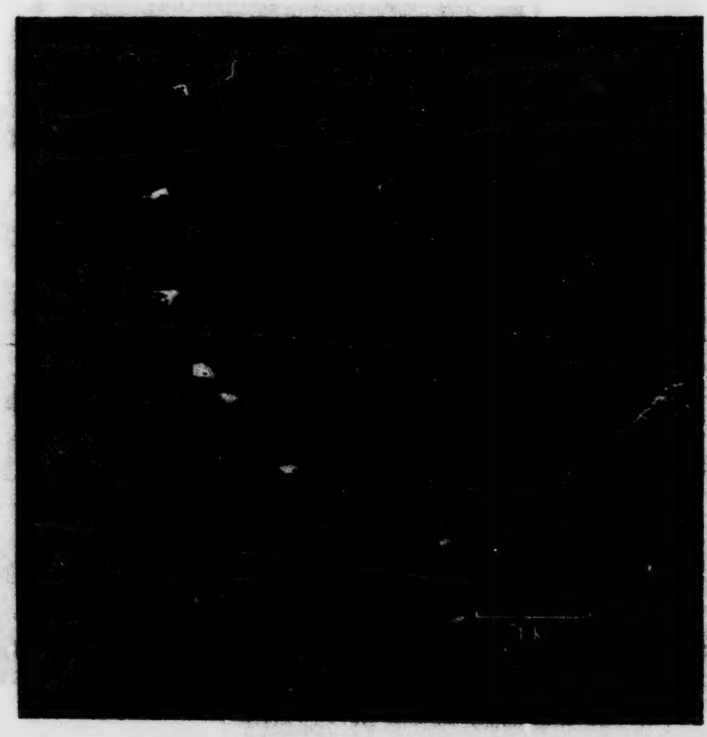

FIGURE 15
X_{HH} SAR Image of Icebergs in Baffin Bay: September 11, 1978

FIGURE 16
Photo of Iceberg Tongue at Cape York, Greenland

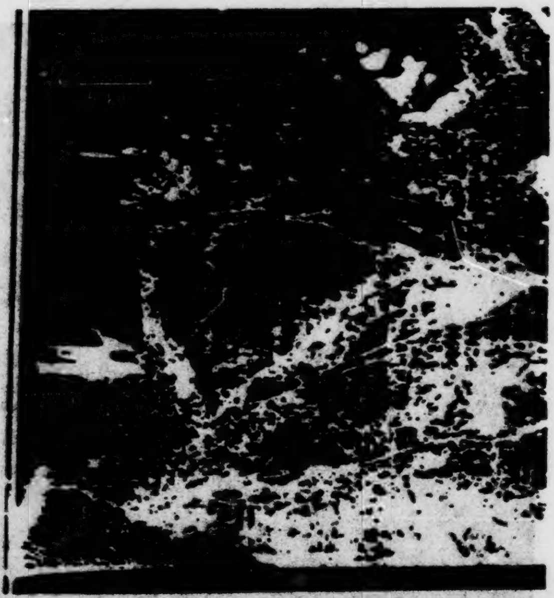

FIGURE 17
SLAR Image of Iceberg Tongue at Cape York, Greenland

FIGURE 18
Photo of Iceberg and Pack Ice in Baffin Bay

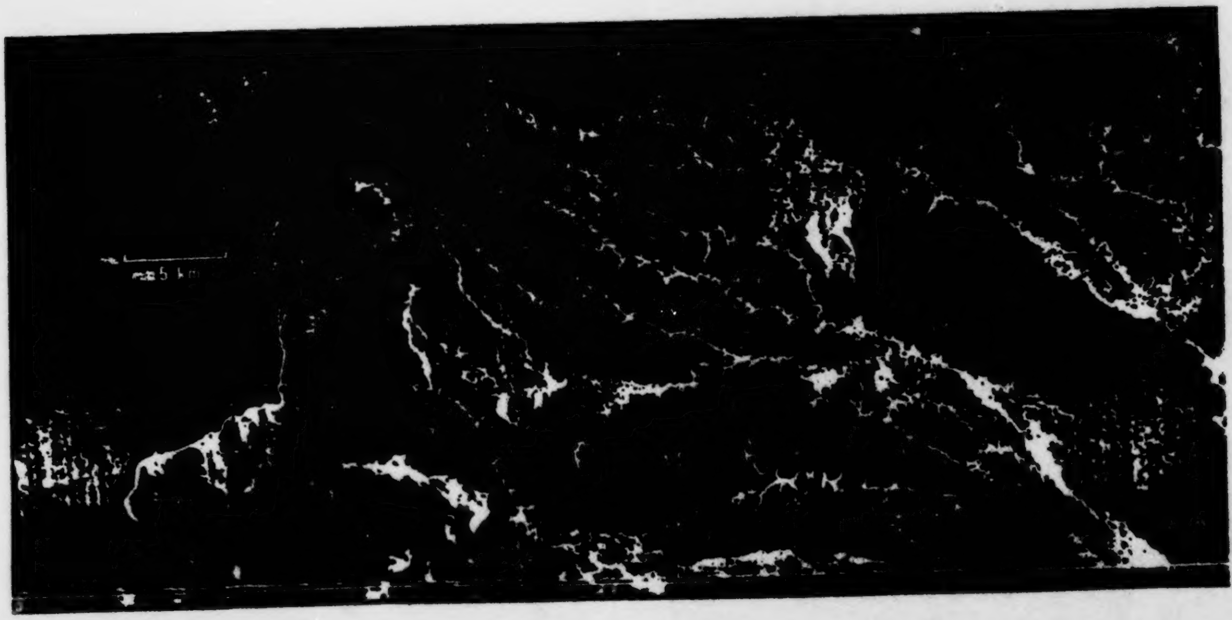

FIGURE 19
SLAR Image of Iceberg and Pack Ice in Baffin Bay

SECTION 5.14

DIGITAL IMAGE ANALYSIS OF SAR IMAGERY FOR THE DETECTION OF ICEBERGS

Kirby, M.E.

Presented at the Sixth Canadian Symposium on Remote Sensing; May, 1980; Halifax, N.S.

DIGITAL IMAGE ANALYSIS OF SAR IMAGERY FOR THE DETECTION OF ICEBERGS

M. E. KIRBY
INTERA Environmental Consultants Ltd.
2841 Riverside Drive
Ottawa, Ontario

ABSTRACT

In anticipation of fully operational drilling and shipping programs in iceberg infested waters, a number of state-of-the-art methods are being evaluated for their utility in support of these projects. For example, numerical models are being developed to predict the probabilities of iceberg encounters with drill rig platforms and ships.

The important factors in the prediction models are the initial detection of the icebergs followed by the processing of the resulting iceberg information as inputs to the prediction models. In order for the prediction models to adequately incorporate the iceberg information in a real-time forecast mode for operational use, suitable quantitative spatial data must be generated. One of the fastest means for creating quantitative iceberg files would involve the automated analysis of remote sensing data sets. However, years of iceberg census work in the Arctic has shown that reliable iceberg information is very difficult to obtain using conventional observation and remote sensing techniques. Reliance on active systems, such as synthetic aperture radars (SAR) has thus become increasingly important.

In the spring of 1979 extensive 4 channel SAR data sets over iceberg infested waters were obtained as part of the SURSAT program. Portions of this imagery were digitized and analyzed on the CCRS Image Analysis System in an effort to evaluate the utility of present image processing methods for isolating icebergs for future incorporation into iceberg prediction models.

INTRODUCTION

The hazard that icebergs pose for offshore drilling and shipping operations in Arctic waters has yet to be fully realized. However, the outcomes of such encounters are predictable. It is extremely important then that the probability of an iceberg encounter with a drill rig or tanker be minimized as much as possible. Numerical models are being developed in which the probabilities of iceberg encounters can be predicted with the hope of providing Arctic operators with sufficient forewarning to avoid such hazards.

From a modelling point of view it is extremely important that digital iceberg information be made available for prediction purposes in near-real time. The crucial first step involves the detection of the icebergs under a variety of weather conditions. Recent experience has shown that a high resolution synthetic aperture radar (SAR) system can provide this iceberg data. However, the problem of quickly extracting accurate iceberg information from large digital image arrays for input into the models precludes the use of a human interpreter for all tasks. Even though the contribution that an experienced interpreter can make to a project could not be duplicated by a machine, it will be necessary to employ analysis systems to handle the greater part of the data manipulations.

STUDY OBJECTIVES

The objective of this research was to evaluate present state-of-the-art image processing methods for the automated identification of icebergs from digital SAR data. The emphasis of the research was on the image processing techniques with very little discussion about the factors which affect the detectability of icebergs using SAR systems. The topic of iceberg detectability has been discussed in an earlier publication (Kirby and Lowry, 1979).

SAR DATA SET

The SAR imagery used in this study was collected along the Greenland Coast north of Disko Island on April 12, 1979 as part of the Canadian SURSAT program. The resulting imagery from the SAR-580 system was single look, high resolution (3 metre), four channel data. For a detailed description of the SAR-580 system refer to Inkster et al.,(1979).

The imagery was generated with the antenna in steep mode with depression angles of 90° at near range, 43° at mid range and 32° at far range.

At the time of the mission the temperatures were well below freezing and the sky conditions were clear and dry. In addition, the iceberg population was located in a region of active pack ice comprised of young, undeformed ice and heavily ridged first year ice types. The combination of these environmental conditions with the steep antenna mode expectedly resulted in imagery with a low signal to clutter ratio. Intuitively this would suggest that the automated identification of the icebergs would be difficult.

A portion of the SAR imagery was selected for this study which covered an area of approximately 70 sq. kms. The SAR image film was scanned on the CCRS microdensitometer at an aperture of 40 microns for creation of the digital arrays. Even though this approach resulted in a certain degree of data averaging or smoothing, the effect was not noticeable on the imagery. Lowry et al. (1978) have explained that digitizing the film product is limited by the fact that the original SAR data may have a dynamic range in excess of the film, resulting in saturation of the higher intensities.

Only the two X-band channels (like and cross-polarizations) were used since it has been demonstrated that the L-band imagery is inadequate for the detection of icebergs (Kirby and Lowry, 1979; Ketchum, 1980). In particular, the longer wavelength L-band radiation will penetrate freshwater ice to a much greater extent than the X-band radiation. As a result it can be expected that the L-band radiation will be subjected to greater amounts of attenuation within an iceberg, thus reducing the amount of energy that could be returned to the antenna.

The digital analysis was conducted on the CCRS Image Analysis System (CIAS) which is a modified General Electric Image 100 controlled by a PDP 11/70 with 256K words of core memory. The original system was initially designed to analyze four channel Landsat imagery. However, it has since been modified to include a variety of functions for the analysis of SAR and multi-spectral scanner imagery. The present emphasis of the system analysis statistics is on Gaussian data distributions where the variances are small compared to the mean. The assumption of normality in the highly variable radar data is somewhat inadequate since the radar imagery is often characterized by Rayleigh and exponential distributions where the variances and means are similar. A detailed summary of the CIAS has been presented by Goodenough (19[illegible]).

The raw X-band data for the analysis are presented in Figures 1 and 2 which are 16 grey level plots of the raw digital data. It can be seen from these images that a number of large bergs were present in the pack ice. The icebergs appear equally bright in both images; however, there is a dramatic difference between the radar return from the background pack ice from the two data sets.

The histograms of the distributions for the intensity levels from the raw data of the images are presented in Figure 3. The intensity intervals from 0 to 25 are presented along the abscissa, while the number of pixels in each intensity level are depicted on the ordinate axis. These histograms show that there is a large degree of high return intensities in the XHH imagery while the XHV data is a highly skewed distribution towards the lower intensities. The icebergs are characterized by very high and very low intensity values. A small proportion of the iceberg pixels occurred in the transition region between these two extremes.

IMAGE PROCESSING ANALYSIS

Brief explanations of the digital methods used in the research are presented in this section along with a discussion of the results that were obtained in the analysis. Much of the material describing the techniques has been taken from the unpublished CIAS memos.

Level Slicing - The simplest method for identifying a feature of interest in a digital array is to perform a level slice of the data. In a level slice only the pixels within a specified region in one dimensional histogram space are 'sliced' from the histogram. Level slicing assumes that the feature of interest occupies a unique region in the histogram and can therefore be identified by separating the appropriate intensity levels from the rest of the intensity distributions.

In this study a series of level slices was conducted for both X-band channels in an attempt to isolate the iceberg intensities. Figures 4 and 5 show the results of one level slice through both channels. The level slice regions have been identified on the histograms and then displayed in image form. It is apparent from the display of the level slices that many of the iceberg high intensities have been identified, but so have many of the background ice features, especially in the XHH channel. This shows that there is much overlap in intensity space between the icebergs and the surrounding ice features, and that it is not possible to solely isolate icebergs using this technique with the imagery in its present format. Other finely sliced data sets were generated with similar results, perhaps due to the limited dynamic range of the

Median Filtering - A common characteristic of radar imagery is the high degree of speckle within the data. When employing image processing techniques which involve single pixel classification algorithms, it is most desireable to reduce the radar speckle and maintain the information content. A useful method of reducing speckle is to apply a median filter to the imagery.

In a median filter a sliding window of 3 x 3 pixels moves across the image and replaces the pixel at the centre of the window with the median grey level. In Figure 6 we see the results of applying a median filter to a portion of the digital scene. The filtered data has lost much of the radar speckle while retaining image contrast. In addition, the filtered data has greater edge definition which is very important for image processing in the spatial domain.

Image Classification Procedures - The objective of the classification procedures is to make use of the multi-dimensional spectral distributions that exist in the images for the identification or separation of features of interest, such as icebergs. There are two basic approaches to the classification procedures: unsupervised and supervised techniques. In the unsupervised approach the user instructs the computer to classify an image into a specified number of classes using for example, a migrating means clustering algorithm. The advantage of this approach is that the user does not have to possess a detailed knowledge of the image data sets to perform the classification. The user merely specifies that the entire window be classified into N number of classes. The technique is also non-exclusionary in that all pixels within the image array are used to create the class clusters. On the other hand, the supervised methods using for example, an N-dimensional parallelepiped classifier, requires that the user be intimately familar with the imaged data. The user must determine the exact areas within an image that will be used to determine the signature files for each class prior to the classification. This is very time consuming and is often exclusionary from the point of view that significant pixels may be eliminated from the classification as a result of incomplete training sets. As we shall see, the supervised approach yielded large classification gaps.

Image Registration - Prior to the multi-dimensional classification of the digital data sets, the two X-band images had to be registered to one another. This process involved the selection of control points from features that were clearly identifiable in both bands. The sets of control points were then matched to one another using a geometric transformation. Following the final selection of the most appropriate transformation coefficients, the remaining pixels in the image array for the two bands were matched together and were then ready for classification.

In the case of radar imagery it is difficult to accurately select a set of control points that are common to more than one band because of the varying appearances of the features between the bands. With the iceberg imagery a total of 28 control points were initially selected. However, 8 of the points had to be rejected due to excessive residuals after transformation. A final set of 20 control points was used for the transformations. A simple linear Affine transformation yielded root mean square errors (rms) of 1.067 pixels in the azimuth dimension and 1.457 pixels in the range dimension. A non-linear Quadratic transformation of the same set of control points yielded rms errors of 0.856 pixels in the azimuth dimension and 1.267 pixels in the range dimension.

Unsupervised Classification: Migrating Means Clustering - With migrating means clustering the program attempts to find groupings or clusters within a given set of cells or vectors in N-dimensional feature space based on the number of clusters that the user specifies. A spectral cell contains a vector which is the cell coordinate in spectral space. The vector must be within the parallelepiped defined by the 1 dimensional upper and lower spectral limits. A set of cluster centres is then determined with the centres lying evenly distributed along the hyperdiagonal of the parallelepiped. Each cell is classified through its association with the cluster whose centre it is closest to in spectral space. When all cells have been classified the means for each cluster are computed. The means of the clusters are then compared to their cluster centres to see if the centres have converged. If the clusters have not converged, then the cluster centres are set equal to the means and the cluster process is repeated.

Figure 7 shows the results of a migrating means clustering of a segment from the original images. Two medium sized icebergs are barely visible in the centre of the image. As the figure shows a total of 7 classes were specified. It appears from this image that the highly specular nature of the raw SAR data significantly affected the clustering process and is unfortunately preserved in resulting classes. The icebergs have not been classified as unique features.

As a result of the statistics that have been created during the classification process, it is possible to display the results in a number of different ways for further evaluatio One such method involves a 2 dimensional (2-D) parallelepiped decision region plot which is a rectangle whose size and position are determined by the upper and lower bounds in the 2 features (bands) of the training sets. These plots may be used to depict class spectral space overlap. Figure 8 shows the 2-D parallelepiped plot for the unsupervised classification that was presented in Figure 7. It is quite apparent from Figure 8 that the brightest parts of the image (class 7) were classified differently than the low return regions (class 1). However, there is a significant amount of overlap between the remaining classes (2 to 6) which describe portions of the icebergs as well as the greater part of the background pack ice. This suggests that too many classes were initially specified for the classification.

The degree of overlap between the classes can be further evaluated by looking at the confusion and divergence matrices. A confusion matrix is a theoretical estimate of the probability of correct classification for each class. It explains the percent of the pixels in a class that were correctly classified, misclassified and unclassified. A divergence matrix describes how dissimilar two classes are from a chosen set of features from zero to infinity using the class sample means and the class covariance matrices (Goodenough, et al., 1978). Large divergence implies that the classes are far apart in feature space and should therefore be easy to distinguish.

Both the confusion and divergence matric suffer from one major limitation which must always be considered when interpreting the results. Ideally the matrices should be generated from the entire parallelepiped distributions of the pixels in each class. However, in actual practice the user must retrain within each class to generate truth files to be used in the creation of the matrices. It is quite likely then that only a portion of the pixels from each class would be selected for the truth files which may not be entirely representative of the parallelepiped bounds for the classes.

Tables 1 and 2 show the confusion and divergence matrices for the unsupervised results from Figure 7. The diagonal elements of the confusion matrix show the percentage of correct classification for the class. The off-diagonal elements give the percentage of classification error which was assigned to the class. The last row in the matrix gives the percentage of each class which was unclassified. The divergence matrix shows 0 value for each class in the diagonal as there can be no divergence between a class and itself.

The matrices show that most of the lower intensity returns (classes 1, 2 and 3) were usually classified correctly, while greater confusion occurred in the mid-class intensity values. One must be careful not to over interpret the meaning of correct classification. In this context it does not mean for example, that all icebergs in class 1 were 89% correctly classified, but rather that 89% of the pixels in the lower intensity regions as defined by the upper and lower bounds of the class parallelepiped were correctly assigned to that class. It just happens that a large percentage of class 1 is comprised of icebergs. However, there are other pixels that were also correctly classified in class 1 which do not describe icebergs.

Supervised Classification: N-D Parallelepiped - In this classification procedure a parallelpiped for each selected class is found by determining the minimum and maximum limits to the spectral intensities based on the user determined training data. Pixels are then classified by comparing their spectral signatures with these limits. In the event that the spectral signature of a pixel satisfied the limits for more than one class, a maximum likelihood decision rule then assigned the pixel to the class with the greatest likelihood of it belonging to a particular class. It should be noted that if a pixel intensity value has not been included in the training sets, then that intensity value would not be classified and would result in an classification gap.

The same window that was used in the unsupervised classification (Figure 7) was also selected for the supervised exercise. The author selected four separate classes for training: one class was defined as the higher intensity portions of the icebergs (class 1), the next was the lower intensity values in the iceberg shadows (class 2) and the remaining two classes (3 and 4) were what appeared to be low intensity and high intensity background ice regions. The results of the supervised classification are shown in Figure 9. It is apparent from this figure that much of the radar intensity data was not selected during training and that these gaps were significant enough to prevent any iceberg identification.

The 2 dimensional parallelepiped plot of the classes in Figure 10 shows that even though the lowest and highest intensity returns from the icebergs were separate, there was still a large degree of overlap with the intensities from the other background ice classes.

Tables 3 and 4 summarize the confusion and divergence matrices for the supervised classification results. These matrices are similar to those from the unsupervised case in that there was a larger degree of confusion in the low intensity class (2) and that the greatest divergence occurred between the extremes of the low and high intensities.

Analysis Combinations - The above discussion demonstrates some of the major image processing techniques that are available. However, there are combinations of these techniques which can further improve the analysis results.

Figure 11 shows the XHH and XHV display of the raw data for a large berg and its surrounding ice background. The radar speckle is quite apparent in both channels. The data was classified using both unsupervised and supervised techniques as before. The results of the classifications are shown in Figure 12 with similar effects to those presented in Figures 7 and 9. The unsupervised classification closely resembles the XHH raw data suggesting that this channel dominated the clustering process.

The results of the classification can be further smoothed by eliminating isolated pixels using the spatial information in the region around a pixel. This method is known as nearest neighbour theme filtering where the user can specify a 3 x 3 pixel filter or a 5 x 5 pixel filter in either a weak or strong mode. The strength of the filter is determined by a weighting function for the number of nearest neighbour pixels. It was found that a 3 x 3 filter, weak or strong, was not useful because it resulted in data gaps. Figure 13 depicts the nearest neighbour 5 x 5 strong filter effects for the unsupervised and supervised classification results. This figure shows that much of the radar speckle in the classes was significantly reduced and the edges enhanced. However, in the supervised results the classification gaps were enlarged.

Three medium sized icebergs are shown in Figure 14 with the unsupervised results in Figure 15 where the speckle is still apparent in the classification. Median filtering the raw data and then performing an unsupervised classification eliminated the class speckle as seen in Figure 16. Nearest neighbour filtering the classes from the raw data yielded similar effects to the median filtered data as seen in Figure 17 but with greater spectral variability. There were subtle effects between the weak and strong filters. From this comparison it appears that the median filter was more effective in reducing the speckle while maintaining the iceberg information.

CONCLUSIONS AND RECOMMENDATIONS

The following conclusions and recommendations have been reached as a result of an evaluation of state-of-the-art image processing methods for the automated identification of icebergs from one example of digital SAR imagery:

(a) Level slicing of the raw data was not suitable for isolating icebergs from the background pack ice, especially in the XHH band. Filtering or smoothing the imagery prior to slicing may improve the results.

(b) Median filtering significantly reduced radar speckle and improved the identification of the icebergs. Median filtering should be included as a standard function for the analysis of SAR imagery.

(c) Supervised classification methods resulted in significant data gaps and were found to be time consuming. Unsupervised techniques were quick and non-exclusionary in that all pixels were included in the clustering process with a minimal amount of effort.

(d) The 2-D parallelepiped plots were valuable in assessing the results of the classification procedures. However, the confusion and divergence matrices were not as useful as they could be since the generation of the truth files required retraining on the class data. For radar imagery that is highly variable (textured) in the feature domain, training on the classes was often impractical and resulted in incomplete statistics for the matrices.

(e) Nearest neighbour filtering of the classes reduced the speckle but not to the same degree as median filtering. A 5 x 5 strong filter was the preferred size and strength.

(f) None of the techniques that were used could isolate the icebergs from the background pack ice since the methods almost exclusively function in feature space where the distributions of the spectral intensities determine the classifications. Further research is required to explore the effectiveness of using statistics in the spatial domain which would combine feature space distributions with edge and shape detectors. For example, Haralick (1976) has explained how autocorrelation functions, digital transforms, edgeness, structural elements and spatial grey tone co-occurrence probabilities employ image texture to enhance feature recognition. The variable textured (speckle) nature of the radar data may be well suited for the application of spatial domain statistics.

(g) The problem of iceberg reidentification from one data set to the next has not been addressed from a digital recognition viewpoint. Reidentification remains an important problem for modelling purposes and requires significant attention for future research.

REFERENCES

1. HARALICK, R.M., 1976: Automatic Remote Sensor Image Processing, in Digital Picture Analysis, edited by A. Rosenfeld. Publisher: Springer-Vislag, Berlin, Heidelberg.

2. GOODENOUGH, D.G., 1977: The Canada Centre for Remote Sensing's Image Analysis System (CIAS), presented at the 4th Canadian Symposium on Remote Sensing; Quebec City, Quebec.

3. GOODENOUGH, D.G., P.M. NARENDRA, K.J. O'NEI, 1978: Feature Subset Selection in Remote Sensing; Cdn. J. Remote Sen., Vol. 4, No. 2, Pg. 143-148.

4. LOWRY, R.T., S. Shlien, D.G. Goodenough, 1978: A CCRS System for Synthetic Aperture Radar, presented at the 5th Canadian Symposium on Remote Sensing; Victoria, B.C.

5. INKSTER, D.R., et al., 1979: State of the Art in Airborne Imaging Radar, presented at the 13th International Symposium on Remote Sensing of the Environment; Ann Arbor, Michigan.

6. KETCHUM, R.D., 1980: Sea Ice and Iceberg Analyses of SAR Data; NORDA Technical Note.

7. KIRBY, M.E. and R.T. LOWRY, 1979: Iceberg Detectability Problems Using SAR and SLAR Systems, presented at the 5th Annual W.T. Pecora Symposium on Satellite Hydrology; Sioux Falls, South Dakota.

ACKNOWLEDGEMENTS

The author would like to express his appreciation to the SURSAT program office for its support during this research, and to thank the Canada Centre for Remote Sensing for the use of its facilities, as well as thank Mr. G. Fedosejevs for his assistance.

TABLE 1
CONFUSION MATRIX FROM UNSUPERVISED CLASSIFICATION

True Class Chosen Class	Class 1	Class 2	Class 3	Class 4	Class 5	Class 6	Class 7
Class 1	89	3	0	0	0	0	0
Class 2	2	80	0	6	0	0	0
Class 3	0	3	82	6	0	1	0
Class 4	0	7	5	79	3	0	0
Class 5	0	0	4	2	86	5	3
Class 6	0	0	4	0	7	87	6
Class 7	0	0	0	0	1	3	77
Unclassified	9	7	5	7	3	4	14

TABLE 2
DIVERGENCE MATRIX FROM UNSUPERVISED CLASSIFICATION

	Class 1	Class 2	Class 3	Class 4	Class 5	Class 6	Class 7
Class 1	0						
Class 2	14.41	0					
Class 3	27.24	12.95	0				
Class 4	44.44	9.32	9.39	0			
Class 5	92.45	39.96	14.41	14.91	0		
Class 6	88.69	54.13	14.36	28.59	9.45	0	
Class 7	90.00	55.22	33.21	36.23	19.39	16.08	0

TABLE 3
CONFUSION MATRIX FROM SUPERVISED CLASSIFICATION

True Class Chosen Class	Class 1	Class 2	Class 3	Class 4
Class 1	82	0	5	0
Class 2	0	73	0	7
Class 3	3	0	80	0
Class 4	0	13	0	82
Unclassified	15	14	15	11

TABLE 4
DIVERGENCE MATRIX FROM SUPERVISED CLASSIFICATION

	Class 1	Class 2	Class 3	Class 4
Class 1	0			
Class 2	131.11	0		
Class 3	13.22	53.89	0	
Class 4	64.82	7.21	16.90	0

90°
Depression
43°
Angles
32°

FIGURE 1

16 Grey Level Plot of Raw XHH Digital SAR Data

90°
Depression
43°
Angles
32°

FIGURE 2

16 Grey Level Plot of Raw XHV Digital SAR Data

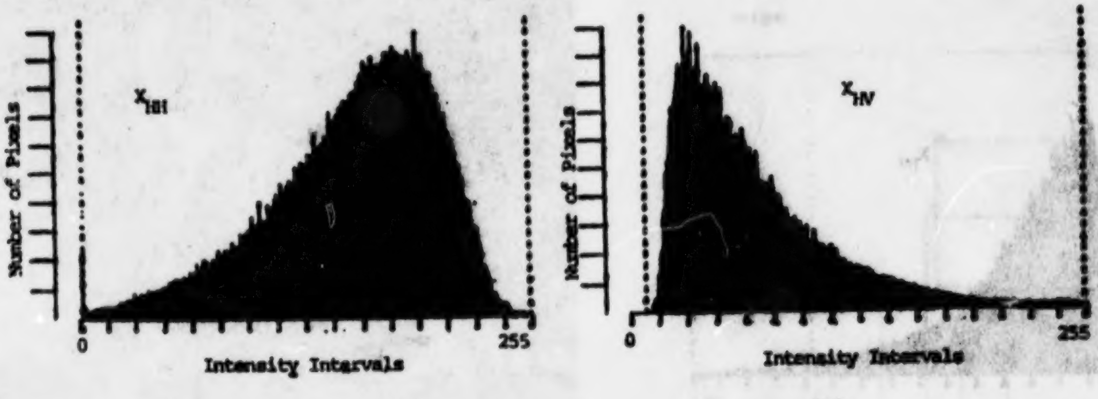

(a) (b)

FIGURE 3

Histogram Plots of Intensity Distributions: (a) XHH, (b) XHV

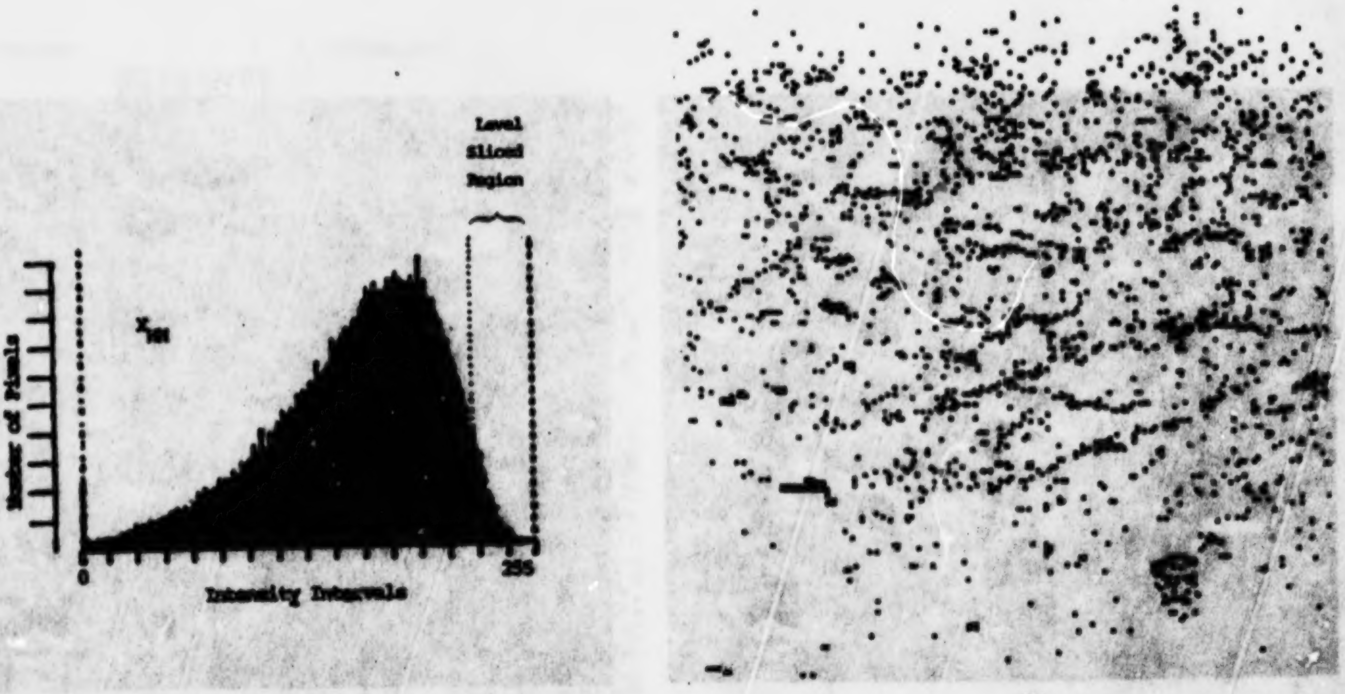

(a) (b)

FIGURE 4

Level Sliced Results of XHH Data: (a) Level Sliced Region, (b) Pictorial Display of Level Slice

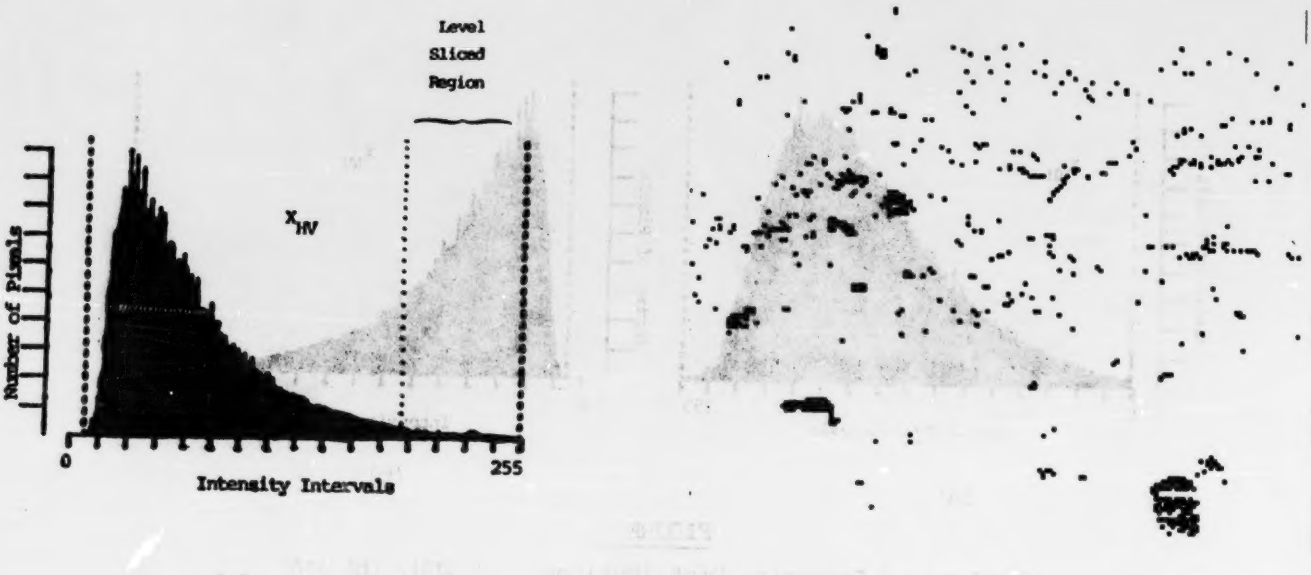

(a) (b)

FIGURE 5

Level Sliced Results of XHV Data: (a) Level Sliced Region, (b) Pictorial Display of Level Slice

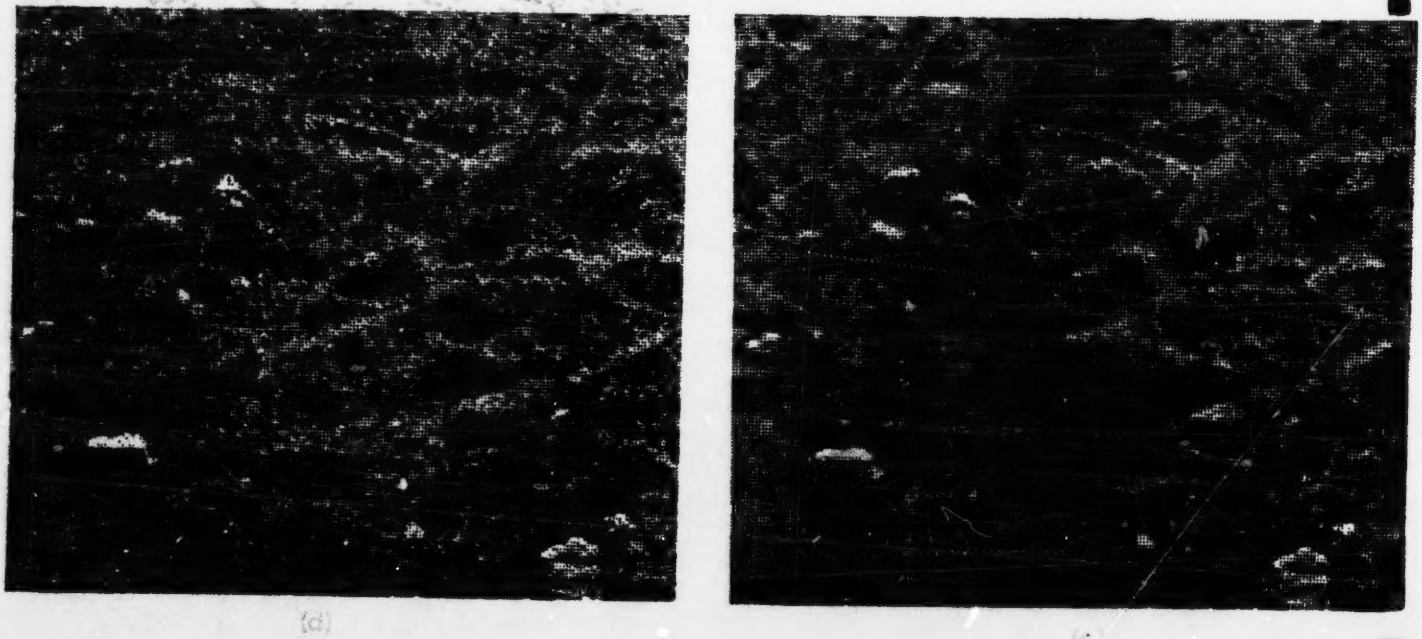

(a) (b)

FIGURE 6

Median Filtered XHH Data: (a) Raw XHH Data, (b) Filtered XHH Data

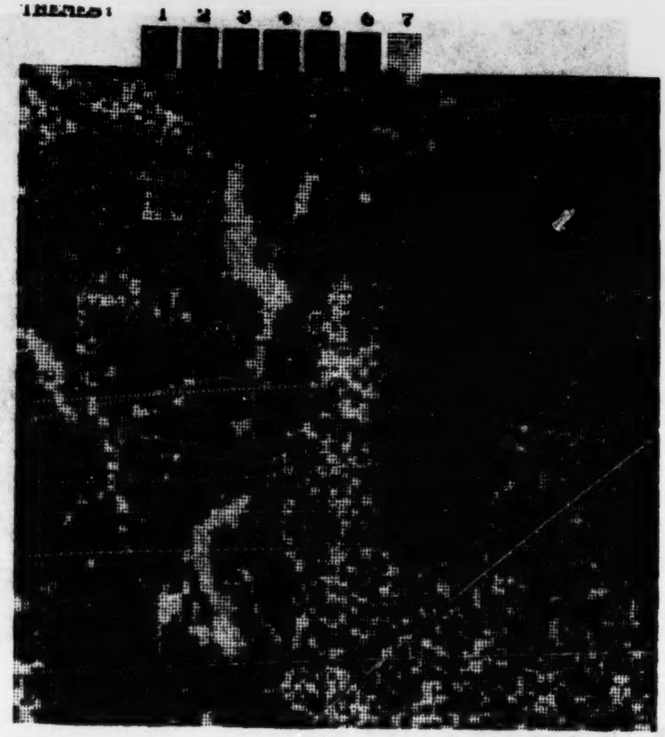
THEMES:
1
2
3
4
5
6
7

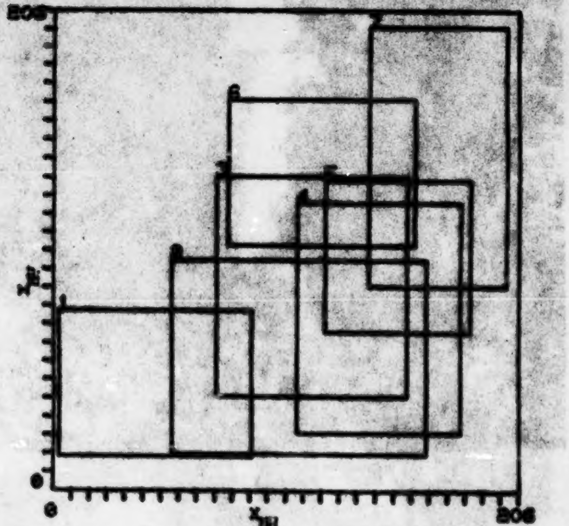

FIGURE 7

Unsupervised Classification Results with Seven Classes (Themes) Specified

FIGURE 8

2-D Parallelepiped Plot of Unsupervised Class (Theme) Overlap

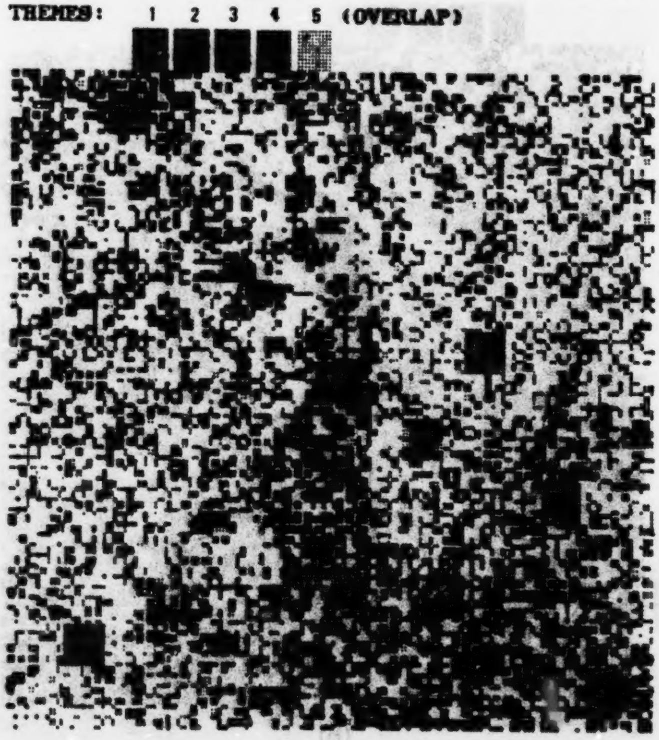
THEMES:
1
2
3
4
5
(OVERLAP)

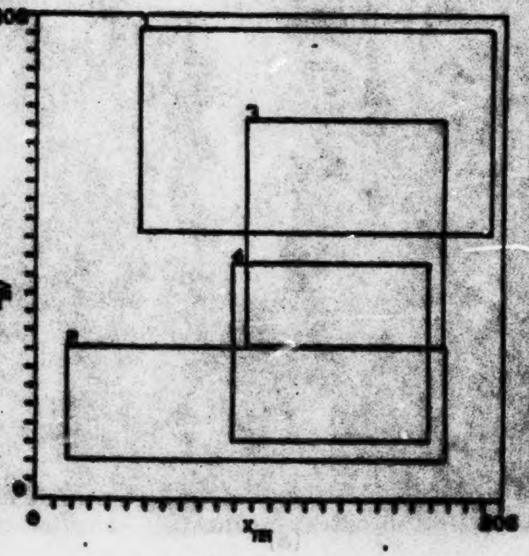

FIGURE 9

Supervised Classification Results with Four Classes (Themes) Specified. Class 5 Shows Class

FIGURE 10

2-D Parallelepiped Plot of Supervised Class (Theme) Overlap

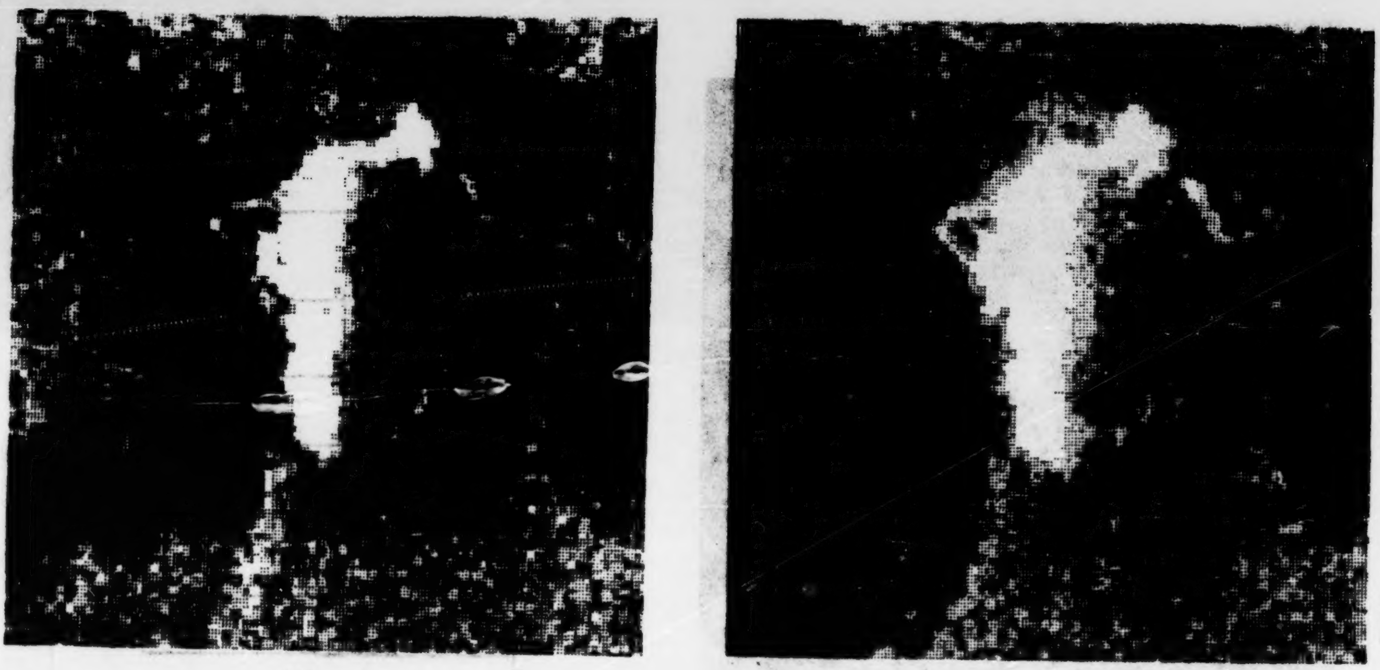

(a)

(b)

FIGURE 11

Raw Digital Data of a Large Iceberg: (a) XHH, (b) XHV

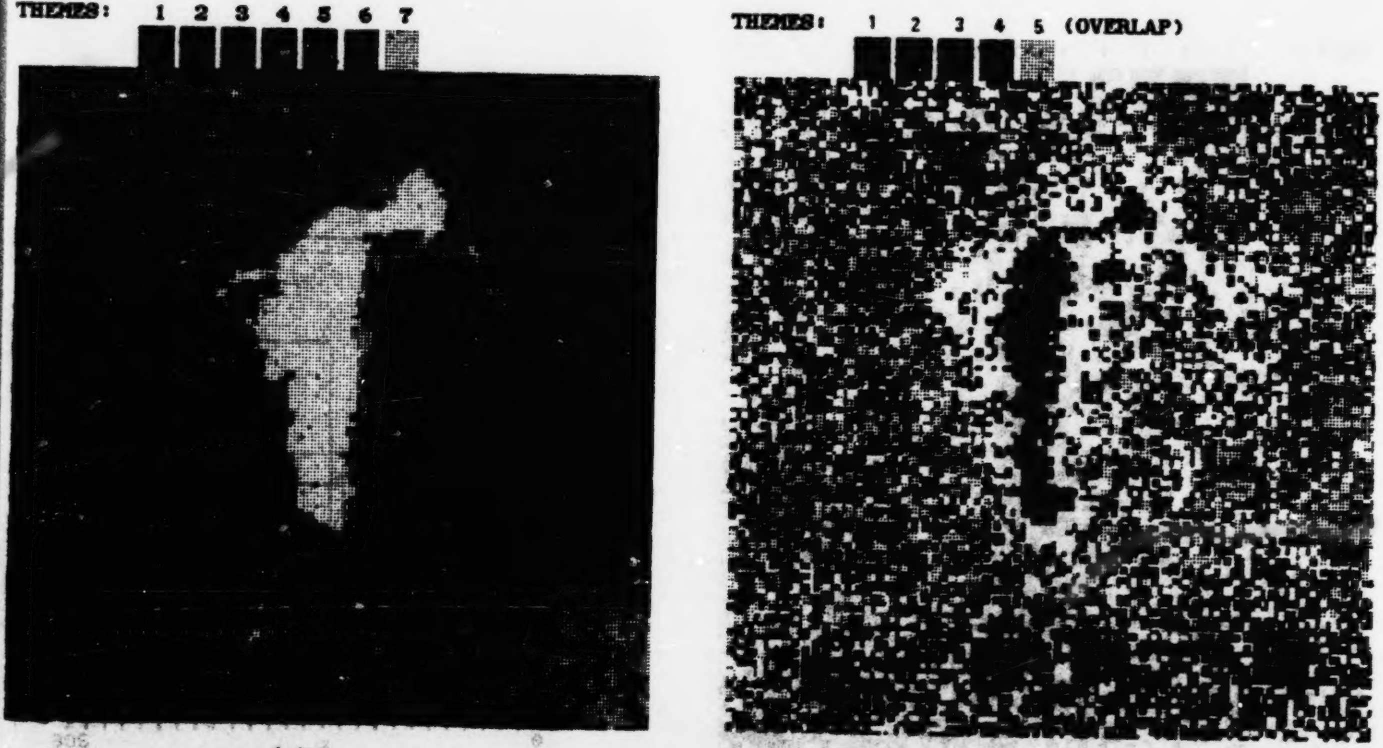
THEMES: 1 2 3 4 5 6 7
THEMES: 1 2 3 4 5 (OVERLAP)

(a)

(b)

FIGURE 12

Classification Results: (a) Unsupervised Classification, (b) Supervised Classification

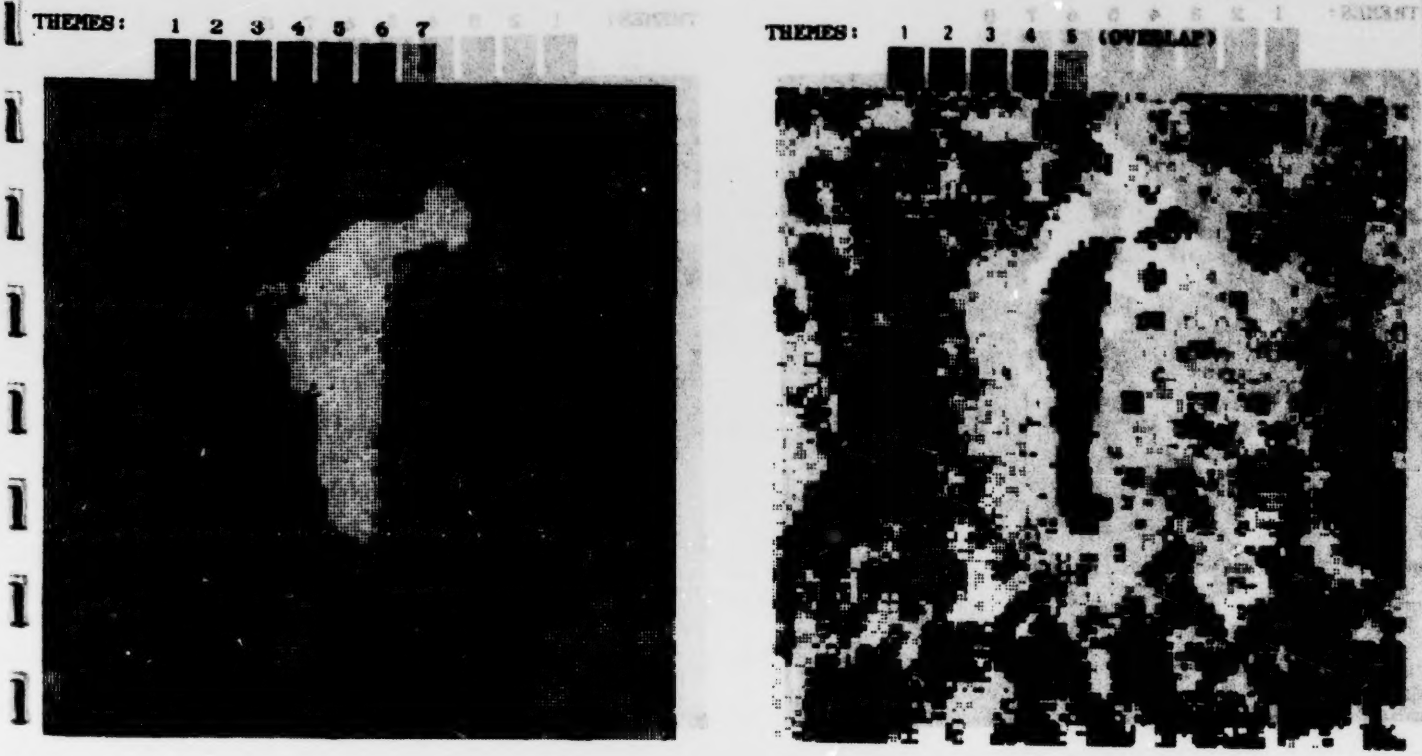
THEMES: 1 2 3 4 5 6 7
THEMES: 1 2 3 4 5 (OVERLAP)

(a)

(b)

FIGURE 13

Nearest Neighbour 5 x 5 Strong Theme Filter: (a) Filtered Unsupervised Data, (b) Filtered Supervised Data

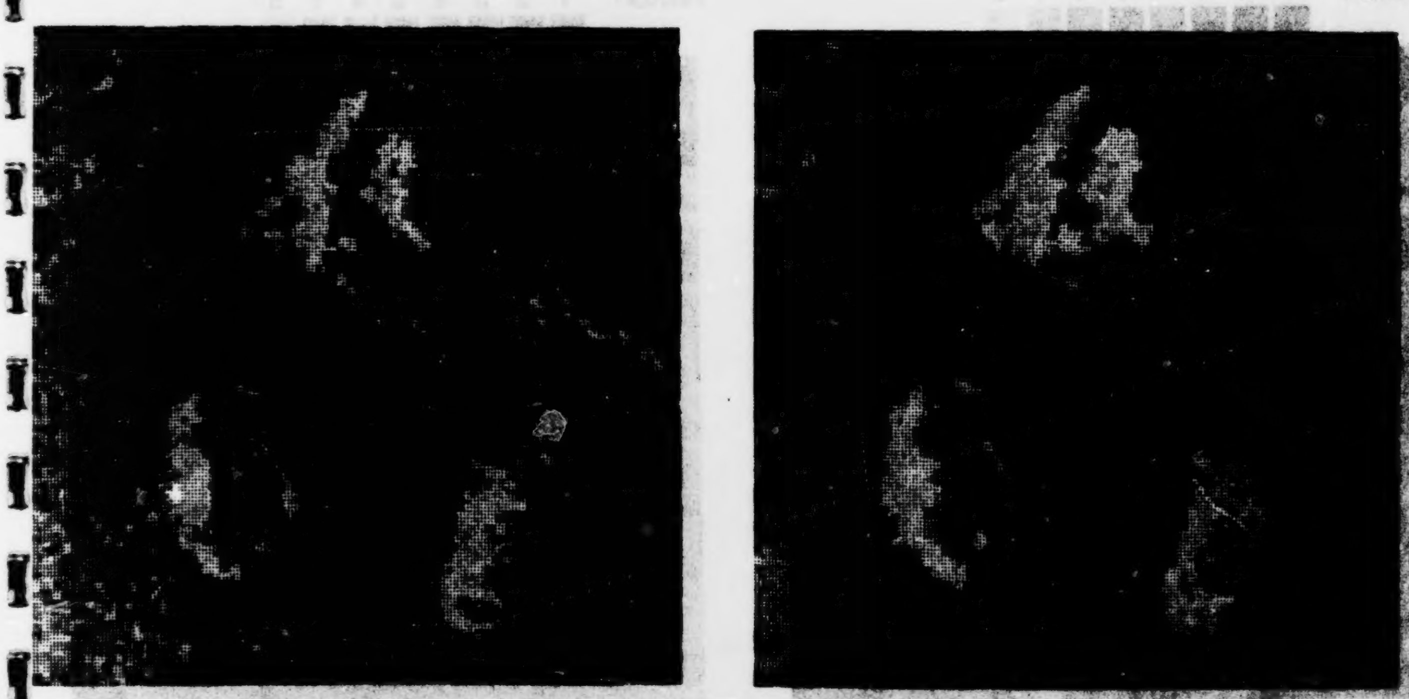

(a)

(b)

FIGURE 14

Raw Digital Data of Three Medium Icebergs: (a) XHH, (b) XHV

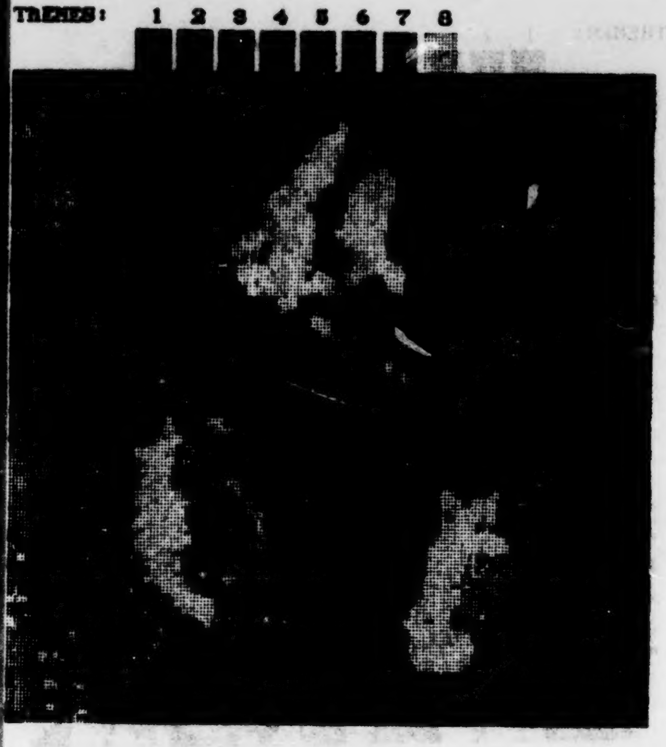
THEMES:
1 2 3 4 5 6 7 8

FIGURE 15

Unsupervised Classification Results of Raw Data

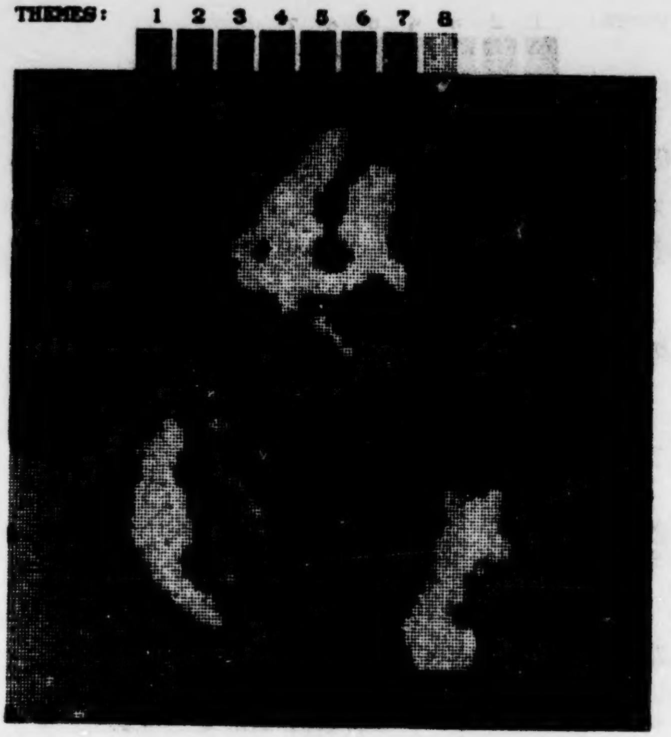
THEMES:
1 2 3 4 5 6 7 8

FIGURE 16

Unsupervised Classification Results of Median Filtered Data

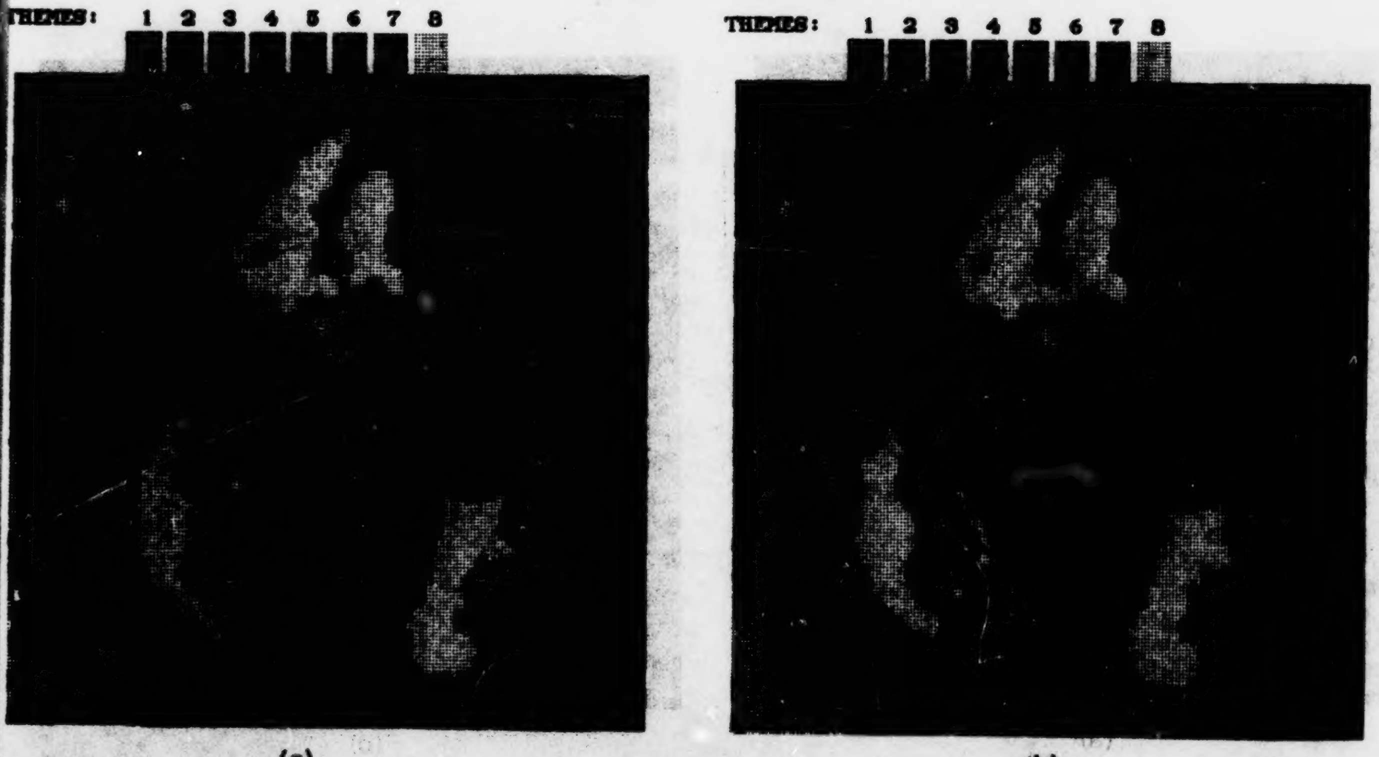
THEMES:
1 2 3 4 5 6 7 8
THEMES:
1 2 3 4 5 6 7 8

(a)

(b)

FIGURE 17

Nearest Neighbour Filtered Class Data After Unsupervised Classification:
(a) 5 x 5 Weak Filter, (b) 5 x 5 Strong Filter

SECTION 5.15

QUANTITATIVE ANALYSIS OF ICE RADAR IMAGES USING DIGITAL IMAGE PROCESSING TECHNIQUES

Tang, G.Y.

QUANTITATIVE ANALYSIS OF ICE RADAR IMAGES USING DIGITAL IMAGE PROCESSING TECHNIQUES

Gregory Y. Tang
Department of Electrical Engineering
State University of New York at Buffalo

Introduction

A number of investigations have been carried out to improve our understanding of the dynamics and thermodynamics of sea ice. These investigations have suggested the need for more quantitative information on the ice condition in order to successfully model ice transport and ice deformation. Several types of remote sensors have been used to gather such information. Among them are the SLAR and the SAR imaging devices. The advantage of radar imagery is its all-weather capability. It has been proven that these radar images do provide vital information for ice study and ice forecasting. As space technology progresses, new satellite-borne radar sensors can provide researchers with large numbers of ice radar images at fine resolutions. In the past, most radar images have been analyzed manually. Such manual processing involves the conversion of the digital signal received at the earth to a continuous tone photograph. An experienced interpreter then inspects the photograph and extracts information from it. Manual analysis such as this lacks both accruacy and speed. To cope with the disadvantages of manual analysis and the large amount of information returned by the satellite-borne and the aircraft-borne sensors, digital image anaylsis methods may be extremely useful in the rapid and quantitative interpretation of radar pictures.

The present research has a long-term goal of developing algorithms such that interpretation of these ice radar images can be done automatically by a computer. The short-term research goal is to use image processing techniques to identify statistical parameters for distinguishing different ice features on the radar image quantitatively. Statistical inference will be used to find such correlations. In this paper, the progress to date is reported.

Background of Radar Imaging

The acronym SLAR stands for side-looking airborne radar. Usually it refers to real aperture side-looking airborne radar. The acronym SAR represnts synthetic aperture radar. SAR usually refers to images obtained from synthetic aperture side-looking radar.

When a radar is directed sideways in a flying carrier, the direction of the flight path is referred to as the azimuth direction and the direction perpendicular to the azimuth is called the range direction. Two range directions commonly referred to are the slant range, R_S, and the ground range, R_G.

The basic principle of SLAR imaging is as follows: the airborne radar radiates through an antenna whose vertical pattern is chosen to illuminate a ground strip properly. This strip is parallel to the flight path. The antenna beam, usually narrow in the along-track (azimuthal) direction, is not rotated, but scans the ground as a result of the forward motion of the aircraft. The width of the strip covered by the radar beam is called the swath width, S_W. The SLAR system generates a two-dimensional image of the reflectivity distribution of the ground strip, with one-dimension proportional to the slant range and the second to the along-track coordinate position.

The slant range resolution of SLAR imagery is determined by the radar pulse width and the round trip time-delay. Therefore the slant range resolution is constant along the swath. The azimuthal resolution is determined by the along-track beam width, L, at range R_s. The along-track beam width, L, is approximately equal to the range R_s multiplied by the beam spread angle, β. The beam spread, β, is proportional to the ratio of the radar wave-length, λ, to the antenna aperture, D, in the azimuthal direction. Since there is a limit on the physical antenna aperture, D, the SLAR image has a limited azimuthal resolution.

The SAR system has the same geometry and operating principle as the SLAR system except that the antenna aperture, D, is not real, but is synthesized by suitably storing the received signal before processing the data. The SAR system can achieve an azimuthal resolution equal to the physical antenna aperture. This ability of the SAR system has made it possible to utilize satellite-borne imaging radar as in the case of SEASAT-1.

The gray tone of a radar image is proportional to the received power of the returned pulse. The received power depends on the backscatter coefficient, σ, of the target, the flight altitude, the depression angle, and the system parameters. The backscatter coefficient, σ, is dominant among these factors.

Progress in SLAR Image Analysis

Since little has been done on digital processing of ice radar images, most ice radar images available are in the form of a photograph. A negative of a SLAR image of Lake Erie was acquired. This SLAR image was digitized into an array of 4500 x 1900 elements with 256 gray scales for each element (courtesy of Optronics International, Inc., Chelmsford, Mass.). The digitized image was stored on a magnetic tape. A COMTAL image processing system was used to process the SLAR images. The COMTAL system can only display a picture matrix of size 256x256 elements. Hence, only a portion of the original SLAR image can be seen on the TV screen at one time. A program (call it PROG1) is written to select a portion of the original picture at a selected resolution. Figure 1 shows a portion of the original SLAR image. It is a lot more comfortable to look at the SLAR image on the TV monitor than using a magnifier to inspect the negative. Once the picture is displayed, another program (PROG2) is employed to display the intensity profile along any straight line segment defined by its endpoints. Cursors are used to select the endpoints. The straight line of Figure 1 is the line segment whose intensity profile is displayed as the histograph. This profile shows well the variation of return intensity of the different ice features.

A program (PROG3) has been written to calculate certain statistical measurements in the neighborhood of any given point selected by the cursor for a specified neighborhood size. In each neighborhood, five local statistical parameters (i.e., mean, variance, vertical gradient, horizontal gradient, and gradient) are calculated. These and some other relevant data are tabulated and printed by PROG3 as shown in Table I. Applying PROG3 to a portion of the SLAR image where the ice feature is known, we obtain a table such as I, where Class 1 is open water, Class 2 is an ice floe (considered relatively smooth), and Class 3 is an ice ridge. Observing Table II we can see that the local variance can discriminate between the open water and the ice floe, and the gradient and the variance can discriminate ice ridges from ice floes. However, Table II indicates that the discrimination based entirely on the local features, is subject to error. This type of error can be removed by using some a priori knowledge. Because only one SLAR image has been tested and only a few local measurements made, the data contained in Table IIare not considered to be conclusive. Rather, the findings to date demonstrate the feasibility and the potential for the successful use of computers to assist in ice image interpretation.

A program, PROG4, has been written to estimate the statistics of a given ice region. This region is assumed to correspond to an ice feature class. Using this program, an operator can use the cursor to select a number of points in the same region. For each selection, gray levels of pixels of a predefined neighborhood around that point are considered to form a multi-dimensional vector. Therefore, there is a vector corresponding to each selected pixel. These selected vectors provide a sample set for estimating the mean and the covariance matrix. Figures 2 and 3 show results from PROG4. Figure 3 deals with the application of PROG4 over open water regions. Comparison of the results indicates that the covariance matrices are not nearly the same.

The classification system (PROG3) when applied to selected regions of the SLAR image, will enable the estimation of the number of ice floes contained in the region, the size distribution of these floes, and the frequency of ridge formation along a specified azimuth direction. The obtainment of this type of quantitative information rapidly will be valuable in ascertaining the applicability of the continuum approximation in ice modeling and in the determination of the most appropriate grid size in the discretization of the governing equations. A program to accomplish the above (PROG5) is being developed. The uncertainty regarding the accuracy of the classification program has delayed the application of PROG5.

Summary

SEASAT-1 SAR images of the Beaufort Sea area have been obtained in digital format. These images are received stored on magnetic tapes. At present, these digital data on magnetic tapes are being deciphered and converted into suitable format for application of PROG1, PROG2, PROG3, PROG4, and PROG5. Hopefully, some conclusive results will then be obtained. Notice that all the radar images are beamed to the earth in digital format. It is therefore better to process the original digital picture rather than to digitize a photograph which has been converted from a digital image optically in the first place.

Several other programs are being developed. One will use Fisher's discriminant to find useful features to distinguish different ice types. Another is a Gaussian Classifier based on the estimation of PROG4 to do point by point classification. Still another will represent a segmented image by RAG (Region Adjacentcy Graph) such that some a priori knowledge can be applied to remove statistical ambiguity and classification errors.

The theme of this research is to apply digital image processing techniques to remotely-sensed ice radar images such that information extraction from these images can be done in a more quantitative and automatic manner. The first task, therefore, is to understand these images statistically. Several programs have been developed to do this. As more digitial images are processed, more conclusive results regarding the statistical properties of ice radar images will be obtained.

TABLE I

Sample Statistics from PROG3

IX	IY	IW	Class	Mean	Var.	V-GRAD	H-GRAD	GRAD
69	201	5	1	113.80	147.36	18.10	4.20	22.30
105	194	5	2	140.52	15.77	4.10	2.60	6.70
204	80	5	3	12.84	6.29	1.30	2.30	3.60
173	136	5	4	112.04	454.28	8.50	34.80	43.30
173	136	13	5	117.62	296.52	3.08	9.47	12.55
206	113	13	6	42.67	701.21	3.58	12.72	16.29
97	109	13	7	137.95	21.23	2.04	1.15	3.19

IX,IY = the center coordinate of each window

IW = the window size is IW x IW

Class = label

Mean = mean

V-GRAD = vertical gradient

H-GRAD = horizontal gradient

GRAD = gradient

TABLE II

Table Displaying Quantitative Properties of Ice Features. (PROG3)

IX	IY	IW	Class	Mean	Var.	V-GRAD	H-GRAD	GRAD
108	195	3	1	139.44	8.69	.33	3.67	4.00
169	177	3	1	138.58	10.08	1.00	2.00	5.00
209	201	3	1	138.56	14.47	.00	5.00	5.00
194	159	3	1	144.44	18.47	4.00	3.33	7.33
214	219	3	1	137.78	13.51	6.00	2.67	8.67
199	221	3	1	137.44	19.58	1.00	5.33	6.33
13	158	3	1	144.67	20.00	5.33	5.67	11.00
61	198	3	1	137.67	29.34	3.67	3.00	6.67
187	173	3	1	141.11	14.99	2.67	4.00	6.67
31	156	3	1	142.67	11.34	2.00	4.67	6.67
228	219	3	1	138.44	12.25	4.33	4.67	9.00
70	158	3	1	143.33	15.56	1.00	.00	1.00
109	126	3	2	133.33	27.34	.67	3.67	4.33
158	137	3	2	140.56	13.36	2.67	5.33	8.00
174	137	3	2	134.78	9.73	.67	.67	1.33
181	90	3	2	130.11	38.77	9.00	.33	9.33
220	110	3	2	138.44	92.69	1.33	7.33	8.67
146	103	3	2	133.44	30.69	4.00	6.67	10.67
35	90	3	2	137.56	36.48	2.67	5.67	8.33
47	108	3	2	135.44	34.02	2.67	6.33	9.00
178	109	3	2	123.00	157.11	5.67	2.33	8.00
72	115	3	3	129.44	94.47	14.33	12.33	26.67
191	125	3	3	124.89	364.55	24.67	31.33	56.00
230	112	3	3	122.44	350.02	21.00	22.33	43.33
63	109	3	3	111.89	517.21	19.67	46.00	65.67
33	106	3	3	69.33	933.11	2.67	39.00	41.67

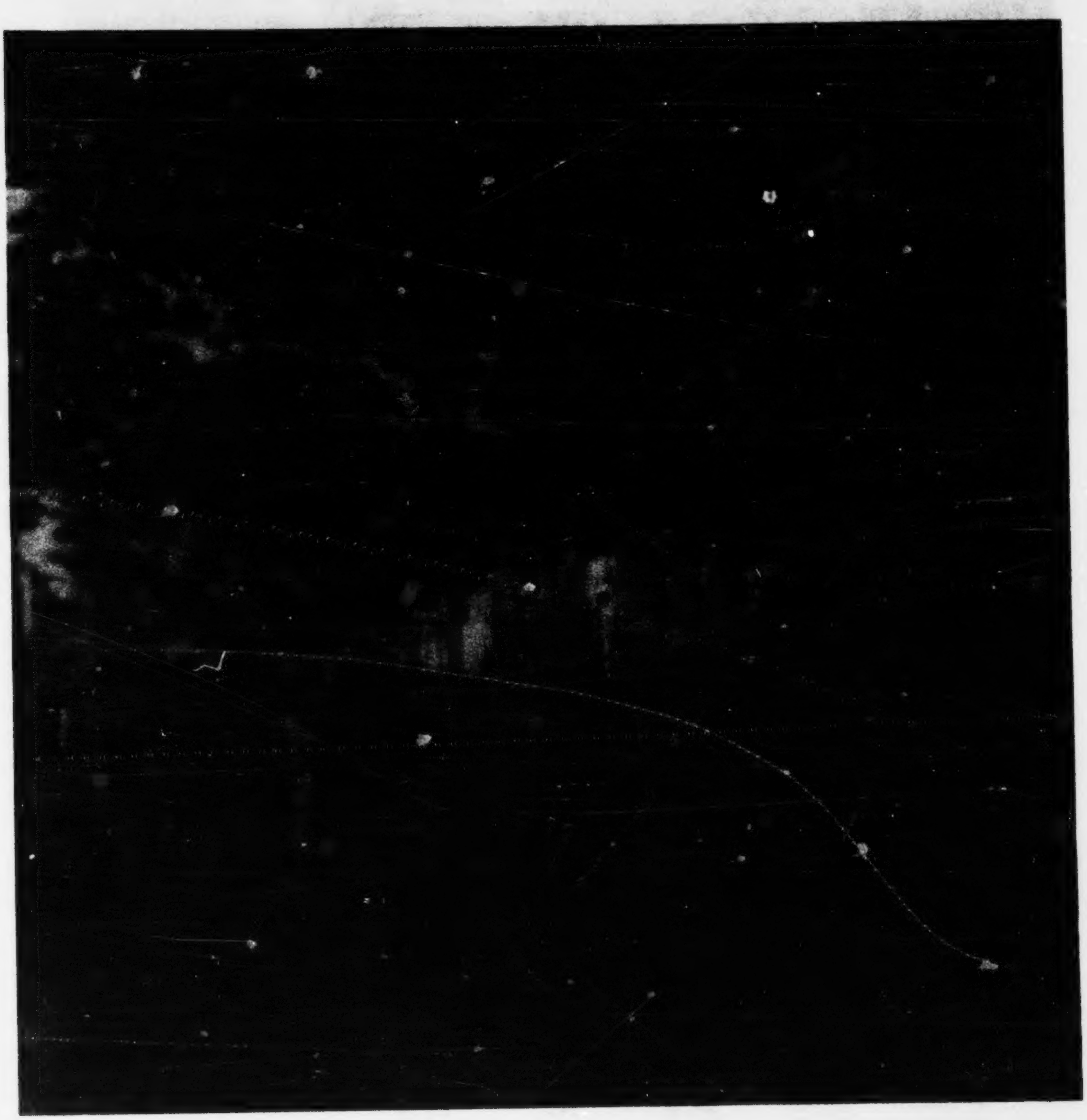

Figure 1. Photograph of TV Monitor: Lake Erie SLAR Image
(Line Segment Across Pack Ice Field)

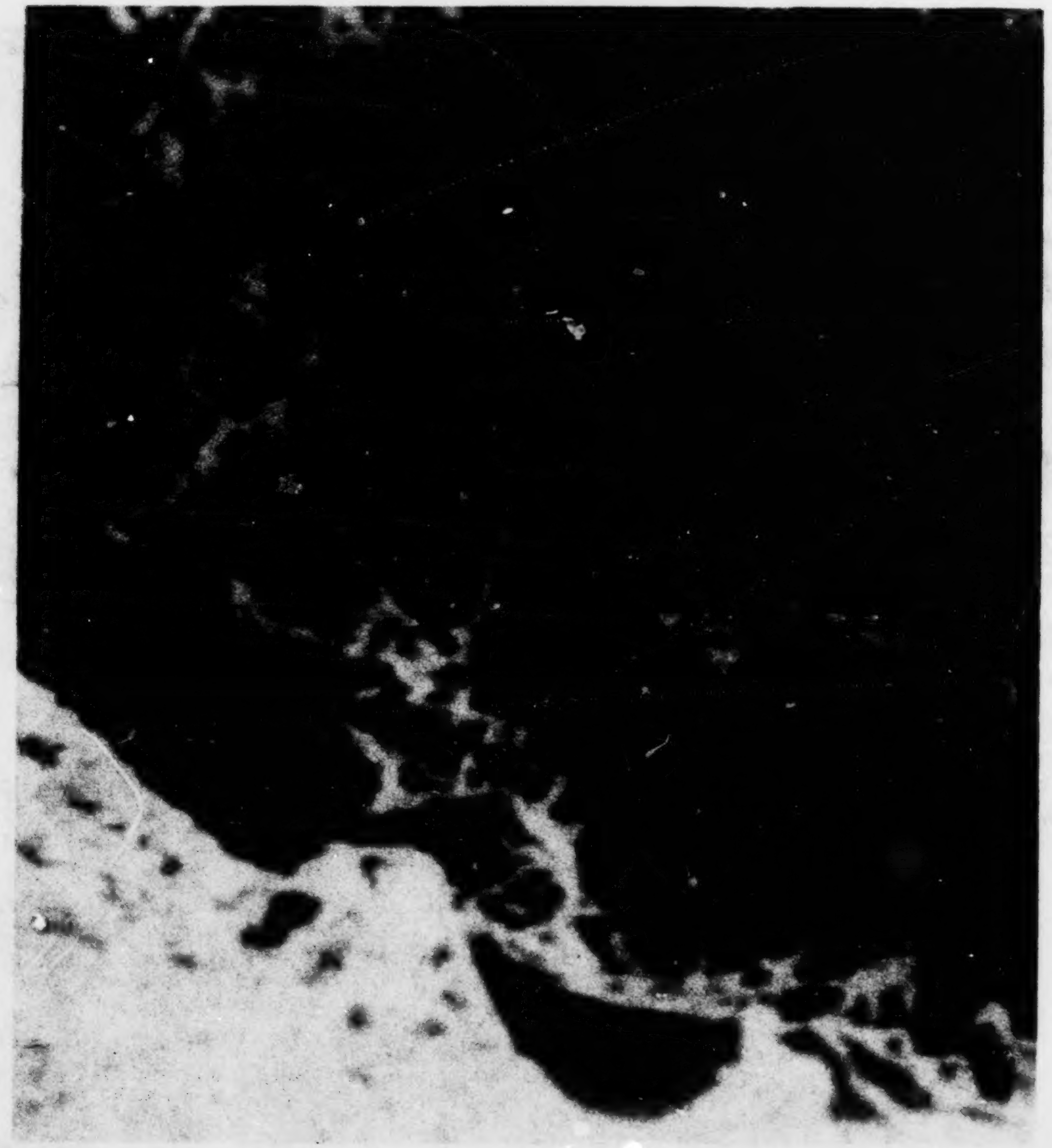

Mean	133.62	135.45	134.00	133.83	134.17
Covariance	52.72	21.00	13.21	8.39	21.55
	21.00	50.87	17.11	12.98	22.06
	13.21	17.11	29.65	11.45	16.79
	8.39	12.98	11.45	26.21	16.27
	21.55	22.06	16.79	16.27	51.80

Figure 2. Results from PROG4. The mean and covariance of ice surface reflection are estimated.

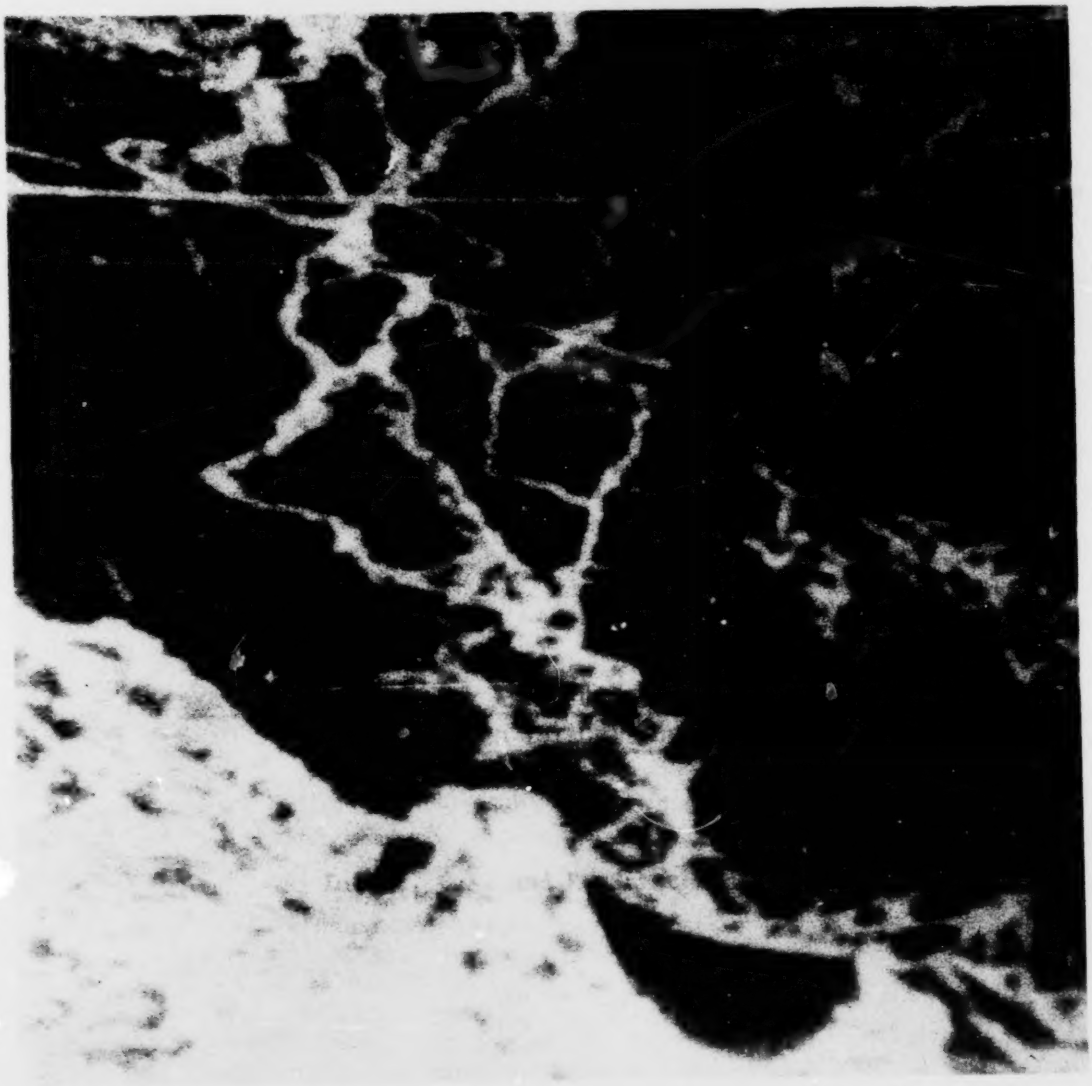

Mean	138.11	137.80	137.49	137.78	137.85
Covariance	33.02	6.97	11.56	6.13	12.01
	6.97	36.29	3.31	.70	3.87
	11.56	3.31	33.04	6.42	8.94
	6.13	.70	6.42	33.21	6.72
	12.01	3.87	8.94	6.72	37.86

Figure 3. Results from PROG4. The mean and covariance of water surface reflection are estimated.

SECTION 5.16

SEA ICE DETECTABILITY AS A FUNCTION OF RESOLUTION AND MIXED INTEGRATION

Luther, C.A. and R. Schuchmann

SEA ICE DETECTABILITY AS A FUNCTION OF RESOLUTION AND MIXED INTEGRATION

C. A. LUTHER[1] and ROBERT SHUCHMAN[2]

ABSTRACT

Numerous attempts have been made to define an appropriate resolution for Synthetic Aperture Radar (SAR) operations in polar regions. SEASAT SAR provided 25 m resolution believed adequate for both operational and research purposes, but high data rates and inordinate processing times rendered the SEASAT SAR less than an optimum tool for providing near real-time data for Arctic use. In an attempt to arrive at a resolution which would meet perhaps the minimum requirements of the operational and research communities, while permitting a wide (∿ 300 Km) swathwidth and a reasonably low systems data rate, a resolution of 100 m was speculated within the scientific community as being sufficient. This parameter was based mostly on intuition, with no scientific study to verify the adequacy of the poorer resolution to satisfy both operational and research requirements. In this paper, SAR imagery at various resolutions is analyzed in an attempt to determine the most appropriate SAR system resolution for meeting the requirements of both the operational and research communities in the Arctic. SAR data collected on Fletcher's Ice Island and other Beaufort Sea ice types was progressively degraded, starting with a nominal 3 m x 3 m resolution and continuing through several coarser resolutions down to a 100 m 4-look sample. The results provide an interesting and informative visual representation of sea ice characteristics at various resolutions from which decisions regarding resolution adequacy can be made.

INTRODUCTION

With the increase in importance of the Arctic as a result of the oil and other minerals found to be located there, considerable emphasis has been placed on Synthetic Aperture Radar as a means of providing all weather, day or night

---

[1] Office of Naval Research, Arlington, Virginia

[2] Environmental Research Institute of Michigan, Ann Arbor, Michigan

remotely sensed data of this vast, remote and harsh environment. Because the Synthetic Aperture Radar is unquestionably the best sensor for detecting sea ice characteristics and dynamics, efforts are being made to define optimum SAR system parameters for operation over polar regions. The Canadian Surveillance Satellite (SURSAT) Project, sponsored by the Canadian Government and participated in by Canada, Denmark and the United States, had as its primary objective the evaluation of Synthetic Aperture Radar for determination of ice characteristics and ice dynamics. This experiment was conducted during the Winter and Spring of 1979 in the Gulf of St. Lawrence, the Beaufort Sea, and around Baffin Bay in the Eastern Arctic. In addition to the Synthetic Aperture Radar which operated from a Convair 580 aircraft at both X and L-band, a wide complement of other remote sensing equipment, mostly active and passive microwave, in addition to laser profilometry and photography, was utilized in one of the most comprehensive sea ice remote sensing experiments to date.

This paper reports results of a brief study in which SAR data resulting from the SURSAT experiment in the Beaufort Sea in March 1979 was utilized to analyze the corresponding loss in data content as the SAR image resolution was successively degraded from 3 m to 100 m. The intent of this study is to provide some basis other than intuition upon which to base a decision regarding an adequate SAR system resolution for Arctic use.

BACKGROUND

SAR imagery of Ice Island T-3 and the surrounding area in the Beaufort Sea was utilized for this study since imagery of excellent quality was obtained of this area during the experiment, and since the island was surrounded by several different classes of ice ranging from what appeared to be very thin, first-year ice to multi-year ice, all of which could be analyzed at the various resolutions. T-3, depicted in outline form in Figure 1, is the first sizeable U.S. drifting station found in the Arctic ice pack. It is suspected as having

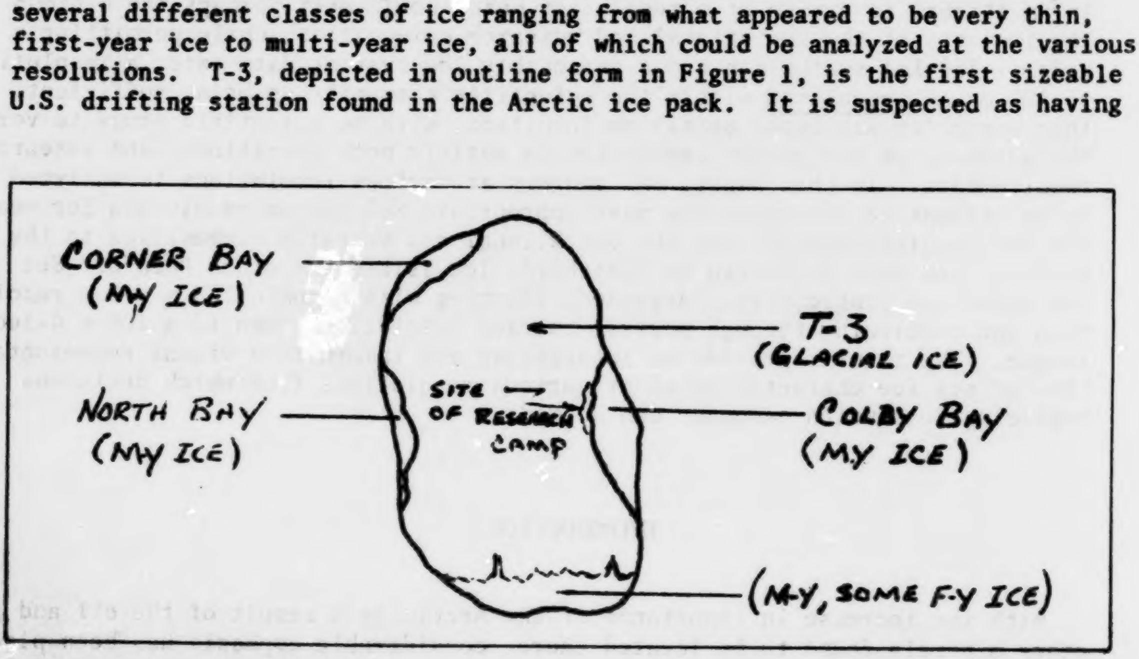

Fig. 1 - An outline of T-3, as lifted from an ERIM X-Band Radar Image of 12 March 1979.

been part of the vast glacial ice shelf areas of northern Ellesmere Island (Crary, 1960). The major surface features that characterize the T-3 ice is the ridge and trough system of rather uniform wavelength, with distances between ridges estimated at approximately 230 m. Depths of these troughs vary from less than a meter to 6 m (Crary, 1960). Although these ridges and troughs were not visible to the eye (conversations with Arne Hanson and Ken Butt), they are quite evident in the SAR image of T-3 shown in Figure 2. Hanson, who visited the island in early April 1979 reported T-3 covered with snow approximately 40 cm deep near the central part of the island, with somewhat less snow at the edges. The surface topography was found to be rather subdued, with some sastrugi. As depicted in Figure 1, immediately surrounding T-3 was multi-year ice in Colby Bay, Corner Bay and North Bay, and multi-year and possibly some first-year ice near the bottom edge.

The imagery of T-3 and the surrounding ice was taken by the ERIM SAR system flying in the wide swath mode (X-band, HH Polarization, 22 Km swath), and was processed to simulate various resolutions and number of coherent averages or looks (i.e., amount of mixed integration). The data was optically processed by the Environmental Research Institute of Michigan (ERIM), using a Precision Optical Processor (POP). The resolution was determined by limiting the aperture width in both range and azimuth at the frequency plane of the optical processor. An equation is used that relates range and azimuth resolution to frequency plane bandwidth knowing processor and radar system scale factors. The mixed integration was performed in the azimuth direction only using a multiplexing simulation method. This method superimposes cross section returns from various aspect angles (i.e., squints) to enhance the average target return and suppress adjacent clutter. The speeds of the output aerial image and the output recorder film are carefully adjusted to achieve the desired number of coherent looks utilized to create the final image.

Single coherent images are compared in this study with ones of equal resolution produced from both two and four images averaged together. The number of independent looks is a measure of the statistical image intensity fluctuations of homogeneous diffuse targets, where a diffuse target is a target comprising a number of resolution cells. If the individual resolution cells of a coherent imaging system are distinguishable, then diffuse objects will show a very pronounced speckle pattern with independent intensity variations equal to the corresponding mean intensity. By averaging independent images, these statistical fluctuations are smoothed. For specular targets, the signal-to-noise ratio (SNR) improvement is proportional to $\sqrt{N}$, where N is the number of independent coherent looks. Thus, the four-look imagery has an SNR improvement of a factor of two.

RESULTS

Presented in Figures 2-10 are X-band (HH) SAR images of T-3 and surrounding ice types processed as follows:

Figure No.	Resolution (m) Azimuth	 Slant Range	Number of Looks
2	2.1	3	1
3	8	8	1
4	25	8	4
5	25	70	1
6	50	70	2
7	50	70	1

Figure No.	Resolution (m)		Number of Looks
	Azimuth	Slant Range	
8	50	70	4
9	100	70	4
10	100	70	1

On each figure, an approximate scale is given along with the calculated near and far edge incident angles. The full 22 km swath is shown in each of nine figures. Note the large range of incident angles presented in the data. This is a function of the large swath width flown at aircraft altitudes (wide swath mode).

A visual examination of the figures appears to indicate that the lower portions of each image have higher resolution, i.e., more discernible features and boundaries between ice types. This can indeed be the case, for the ground range resolution does improve as the incident angle increases. Recall that ground range resolution (ρ_g) is related to slant range resolution (ρ_{SR}) by the following equation:

$$\rho_g = \rho_{SR}/\sin\psi$$

where ψ is the incident angle.

An additional consideration is necessary when examining each figure. The backscatter mechanism can and probably does change in the images as one goes from 0° incident angle to 80°. This data set may therefore additionally provide insight into the backscatter mechanism between the X-band radiation and the ice surface.

Figure 2 represents the finest resolution obtainable by the ERIM 580 system. This image is processed fully coherent (i.e., 1 look). The ice island T-3 is located in right quarter position of the figure. Various ice types including first year and multi-year ice can be observed around T-3. Note the appearance of the multi-year sea ice in Colby Bay and Corner Bay; and near the bottom edge of the island as opposed to the ridged and troughed surface of the T-3 glacial ice. Note also the multi-year floes surrounding the island, and the thin, young ice (black ice) apparent in what otherwise would be taken as open leads. First-year ice is also discernable amidst the multi-year floes.

Figures 3 and 4 are intended to simulate a SEASAT-A resolution ice image. Figure 3 uses the available azimuth (Doppler) bandwidth to produce 1 look data while Figure 4 uses the same bandwidth processed non-coherently to obtain 4 look data. Initial analysis indicates very little ice information appears to be lost when one goes from 2.1 x 3 m resolution (Fig. 2) to 8 m x 8 m resolution (Fig. 3) or to 25 x 8 m (4-look) resolution, (Fig. 4). All forms of ice evident in Figure 2 are still readily identifiable. Note also the difficulty in differentiating between the 8 meter resolution of Figure 3 and the 25 x 8 m (4-look) resolution of Figure 4.

Figures 5-10 represent various resolution configurations between 25 x 70 m and 100 x 70 m. Figure 5 has 25 m (1-look) azimuth resolution. Note the loss of a vast amount of detail in this image when contrasted with the SEASAT resolutions (Figs. 3 & 4). Specifically, the glacial ice of T-3 is no longer distinguishable from the surrounding multi-year ice (except perhaps by shape). Ridges and thin cracks are no longer discernable in the surrounding ice, although the thin, young-ice still stands out. Figures 6 and 9 represent alternative processings (2 and 4 look, respectively) of the bandwidth available in Figure 5. Some slight improvement in contrast is gained with the 2 look processing (Fig. 6) but some loss of sharpness begins to occur with the 4 look processing. Not much improvement in the ability to discern ice types appears to be gained with multiple look processing of these images, although ridges do tend to stand out slightly better.

Figure 7 is a single look image of 50 meter azimuth resolution. It is readily apparent that a significant amount of detail is lost at this resolution. With exception of the thin ice areas, no other distinction between ice types, including T-3 glacial ice, can be made. On the other hand, Figure 8, a 50 meter, 4 look azimuth and 70 m slant range image shows practically all of the ice types visible in Figures 3 and 4, albeit at some loss of detail. Figure 8 represents a compromise between the 25 m azimuth, one look resolution and the SEASAT simulated data. Recall that 4 look, 50 m resolution data can be processed to 12.5 m, one look data.

The 100 meter resolution, single look image of Figure 10 is only slightly worse than the 50 meter, single look image of Figure 7. Neither resolution is particularly useful except for showing the grossest type of ice detail. The 100 meter, 4 look image (Fig. 9) provides a noticable degree of improvement over both the single look, 50 m or 100 m resolution imagery, in terms of reduced speckle, contrast, and the ability to display gross ice types.

SUMMARY

By the process of degrading extremely fine (2.1 m x 3 m) resolution SAR imagery through progressively poorer resolutions while also varying the number of looks, a study of the probable resulting product was permitted. On the basis of this study, SAR systems designed for polar regions should have a resolution no worse than 50 m, 4 looks, unless the capability for providing extremely gross ice classification only, is satisfactory. To be a useful tool for both the Operational and Research communities, a resolution capability no worse than SEASAT 25 m, 4 looks is suggested.

RECOMMENDATIONS

It should be pointed out that this study was accomplished using optically processed data. Digitally processed imagery, in comparison, is normally much superior to optically processed imagery in terms of contrast, which is very important in the classification of ice types. A digitally processed image of sea ice at 25 meter resolution would provide more information than an optically processed image at the same resolution.

It follows then that a digitally processed image of sea ice at 100 meter resolution might possibly provide information in sufficient detail for ice type classification and determination of ice dynamics. It is therefore recommended that a study similar to the above be accomplished using digitally processed data, and the results of the two studies be compared before any final conclusions regarding SAR resolution adequacy are reached.

ACKNOWLEDGEMENTS

The data used in this study was processed at The Environmental Research Institute of Michigan by Messrs. James Marks, Alex Klosster, and Jack A Losee. Ms. Karla Amible assembled the radar mosaics.

Dr. Rene Ramseier of the Canadian Sursat Project Office, as well as Dr. Robert Inkster of Environmental Consultants, Ltd. (INTERA) are thanked for allowing use of the radar data for this analysis. Finally, Mr. Arne Hanson of the Polar Science Center; Dr. James Rossiter and Mr. Ken Butt of C-CORE, Memorial University of Newfoundland, provided useful inputs concerning ice conditions on and in the vicinity of T-3 during March-April 1979.

REFERENCES

Crary, A. P. 1960. Arctic Ice Island and Ice Shelf Studies, Part II Arctic. Vol. 13, No. 1, P. 32-50.

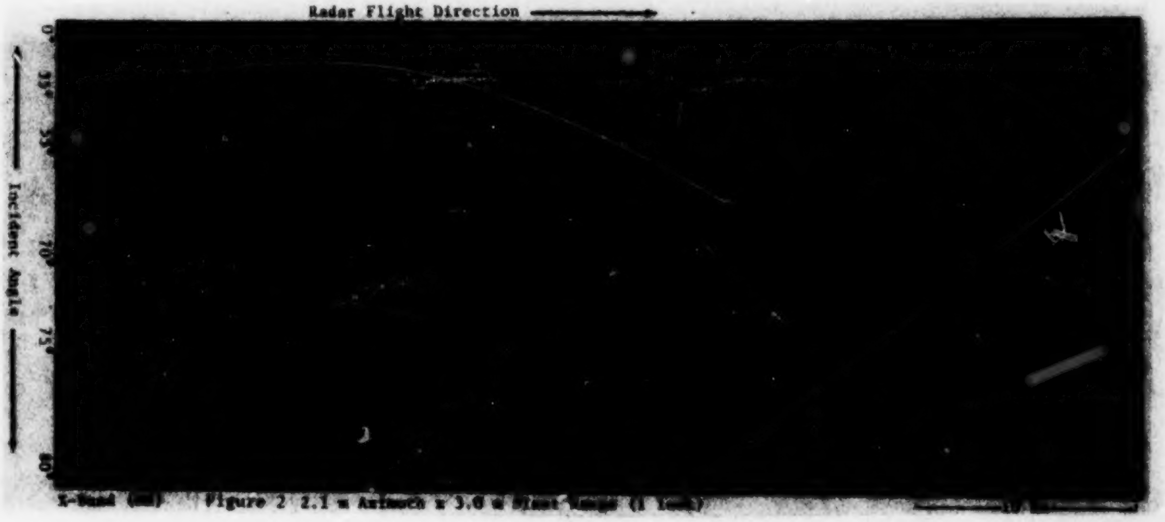
Radar Flight Direction
0°
35°
55°
70°
75°
80°
Incident Angle
X-Band (HH)
10 km

Figure 2 2.1 m Azimuth x 3.0 m Slant Range (1 look)

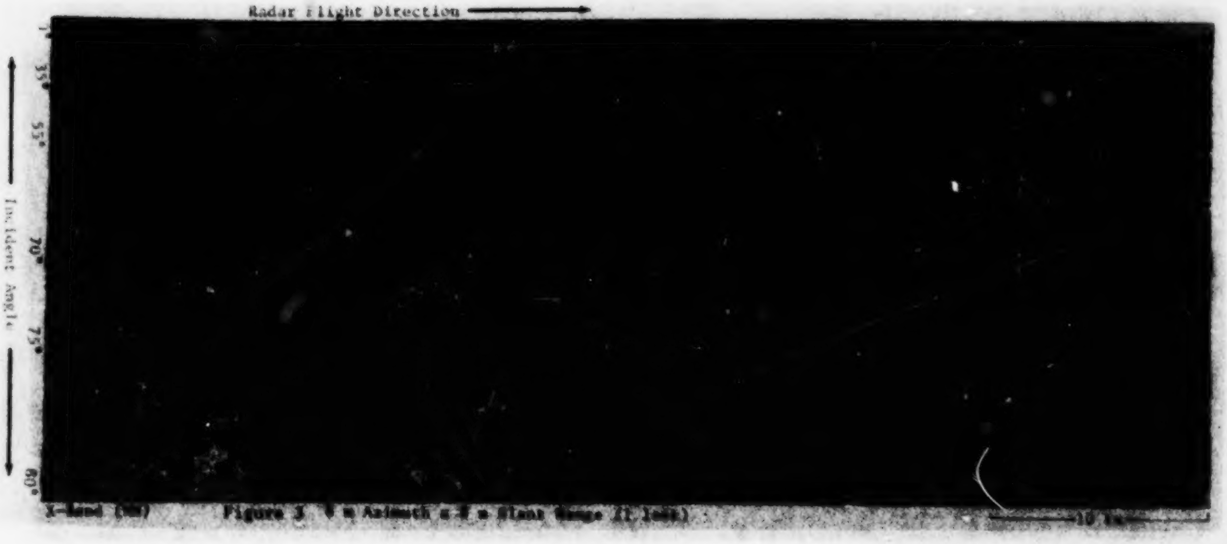
Radar Flight Direction
35°
55°
70°
75°
80°
Incident Angle
X-Band (HH)
10 km

Figure 3 [illegible] m Azimuth x [illegible] m Slant Range (1 look)

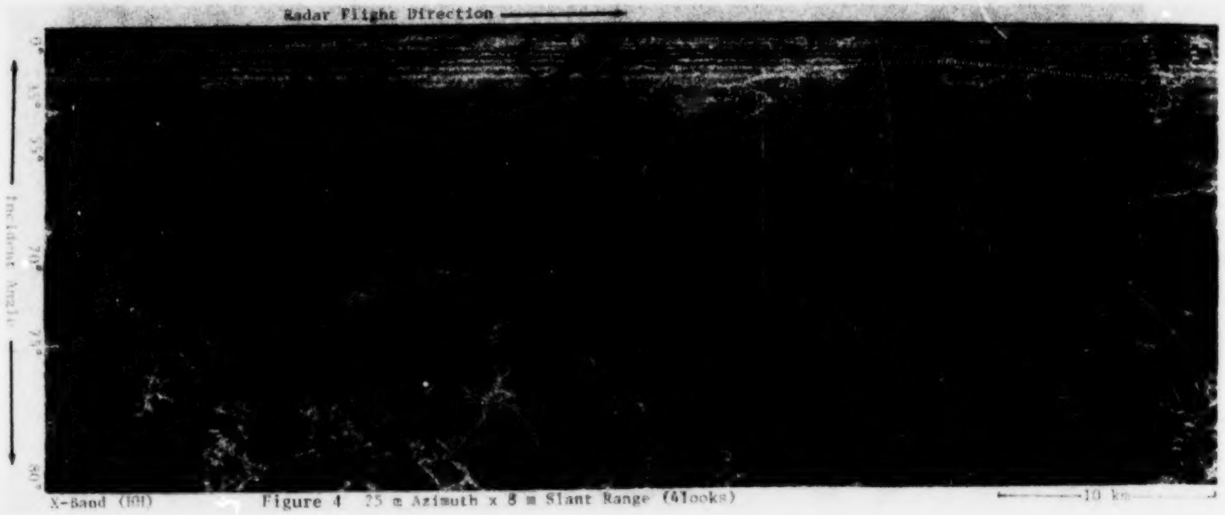
Radar Flight Direction
0°
35°
55°
Incident Angle
70°
75°
80°
10 km

X-Band (HH) Figure 4 25 m Azimuth x 8 m Slant Range (4looks)

Radar Flight Direction
0°
35°
55°
Incident Angle
70°
75°
80°
10 km

X-Band (HH) **Figure 5** 25 m Azimuth x 70 m Slant Range (1 look)

Radar Flight Direction
0°
35°
55°
Incident Angle
70°
75°
80°
X-Band (HH)
10 km

Figure 6 50 m Azimuth x 70 m Slant Range (2 looks)

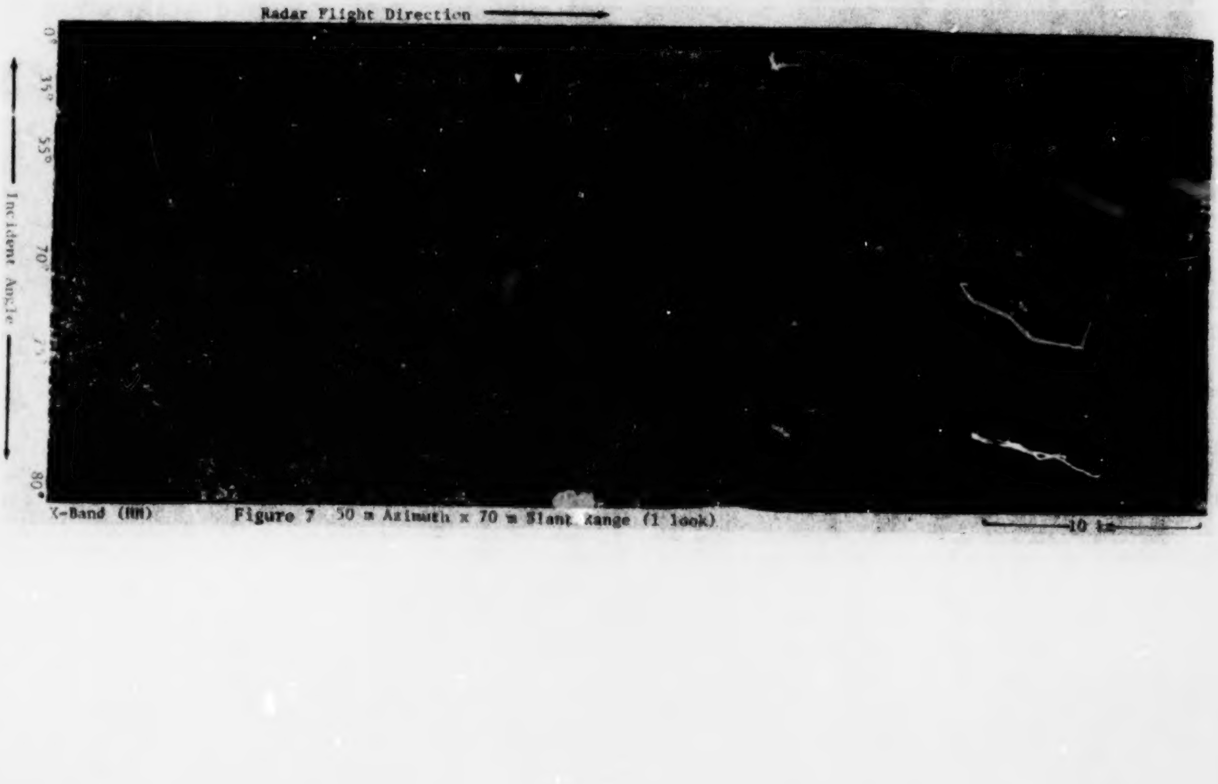
Radar Flight Direction
0°
35°
55°
Incident Angle
70°
75°
80°
X-Band (HH)
10 km

Figure 7 50 m Azimuth x 70 m Slant Range (1 look)

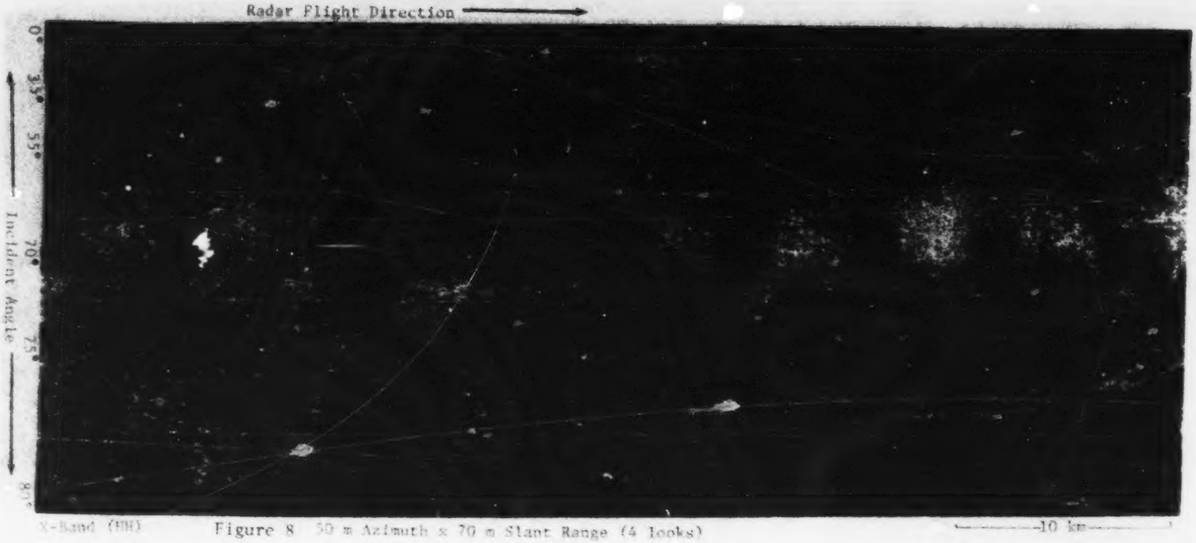
Radar Flight Direction
0°
35°
55°
70°
75°
80°
Incident Angle
X-Band (HH)
10 km

Figure 8 50 m Azimuth x 70 m Slant Range (4 looks)

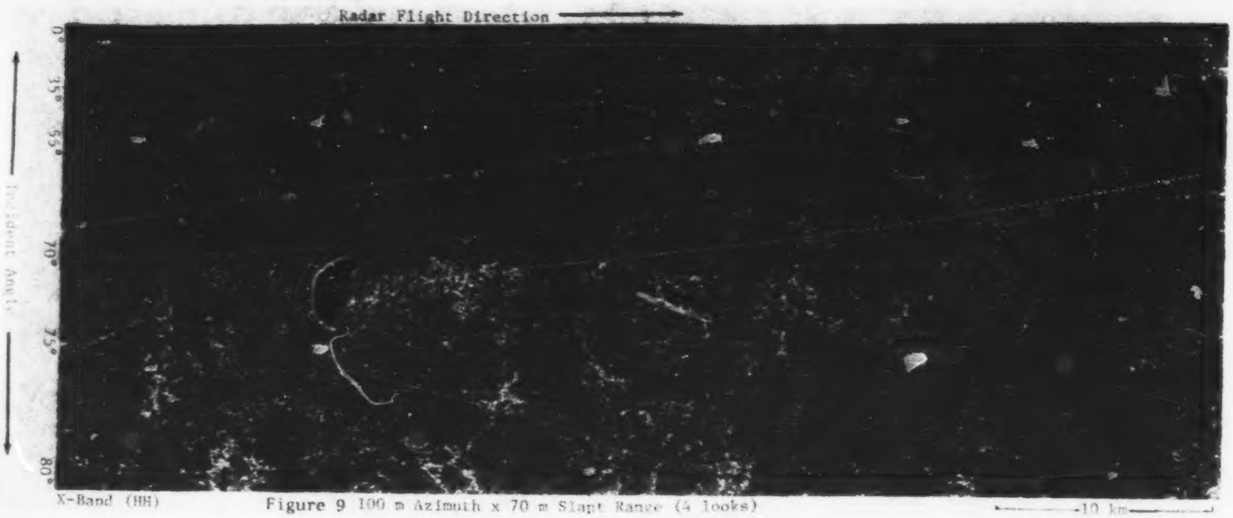
Radar Flight Direction
0°
35°
55°
70°
75°
80°
Incident Angle
X-Band (HH)
10 km

Figure 9 100 m Azimuth x 70 m Slant Range (4 looks)

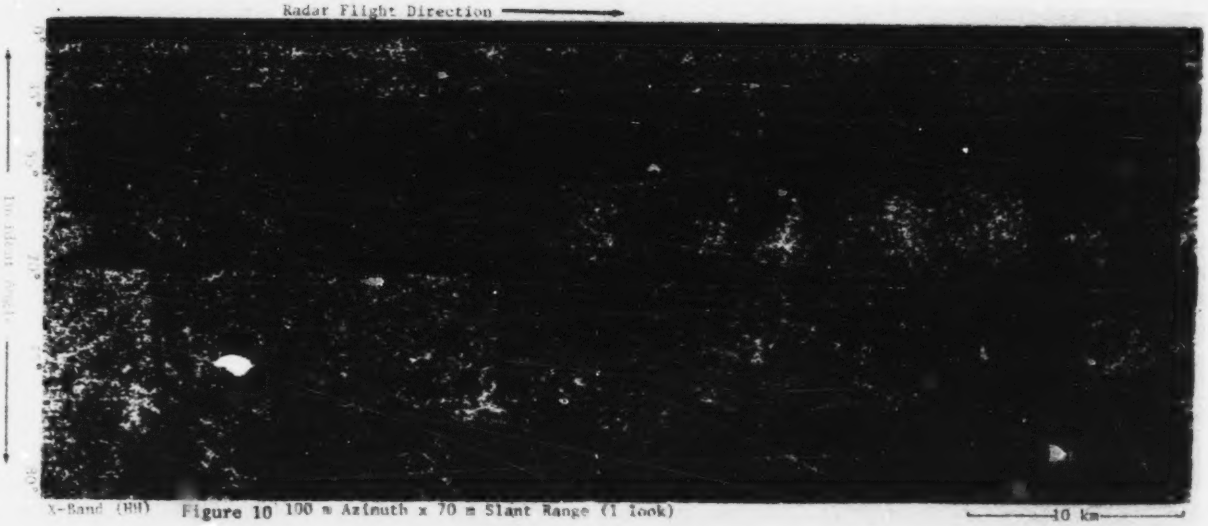
Radar Flight Direction
Incident Angle
70°
80°
X-Band (HH)
10 km

Figure 10 100 m Azimuth x 70 m Slant Range (1 look)

SECTION 5.17

OPTIMIZING IMAGING RADAR PARAMETERS FOR ICE RECONNAISSANCE

Lowry, R.T. and H.G. Hengeveld

OPTIMIZING IMAGING RADAR PARAMETERS
FOR ICE RECONNAISSANCE

R.T. Lowry, Intera Environmental Consultants Ltd., Ottawa, Ontario

H.G. Hengeveld, Atmospheric Environment Service, Downsview, Ontario

ABSTRACT

Imaging radar systems are fast becoming the mainstay of all Arctic sea ice reconnaissance systems. This is true in spite of all available radars having been designed for rather different purposes, and fabricated before the impact of modern digital hardware. Synthetic Aperture Radar (SAR), once considered too complicated for operational use, has been transformed by digital processor into a practical and reliable tool. In preparation for the development of future radars, the authors undertook a study aimed at defining the parameters needed for an ice reconnaissance radar. Using imagery generated under the SURSAT project, the authors have investigated the effects of resolution and incoherent averaging on image interpretability.

The investigations reported here included a study of the relationship between the utility of the image as a function of the data rate as well as the optimum way of presenting a given data rate the relationship between non-square pixels and interpretability was studied along with the relationship between incoherent averaging and image interpretability. It was found that product of range and azimuth resolution is the best measure of image quality up to distortions of 4:1. Incoherent averaging, and thereby reducing resolution, was found to have a small positive effect on image utility, for 3 or 4 looks. This result is very dependent on the means by which the incoherent averaging is implemented.

The study of image utility indicates that an equivalent to an 8m x 8m 1 look radar is the minimum acceptable system. Further work is needed to more precisely delineate the tradeoffs for other ice types and other displays. In particular, much more work is needed to specify exactly the effect of display limits.

1. INTRODUCTION

In the past 10 years, interest in microwave remote sensing has increased dramatically, with floating ice a leading application. Regular cloud cover and extended periods of 24 hour nights combined with the extra information in microwave imagery give it a large advantage over other reconnaissance systems. Prime among microwave systems is the imaging radar, and in particular the synthetic aperture radar (SAR). With modern digital techniques, real time processors make SAR the fast, reliable and real time sensor that is needed for both strategic and tactical support. It is to be expected that such systems will eventually replace the real aperture SLAR systems such as those used operationally in Canada and the USSR.

To prepare the way for the digital SAR designers, it is essential that guidelines be laid down that are relevant to the problem of ice reconnaissance. To this end, a study of SAR data collected during the SURSAT program (Inkster et al 1980a, VanKoughnett et al 1980) has been undertaken. Using SAR data from the SAR-580 operated in X-band wide swath mode (Inkster et al 1979) and processed on the ERIM tilted plane, tracking, optical correlator (Kozma et al 1972), images were prepared at numerous resolutions. These were then examined and ranked by trained ice observers, and studied in detail by a trained photo interpreter.

The image selected for analysis came from a Beaufort Sea flight line over the Ice Island T3 on March 12, 1979. At the time of the flight one of the authors was on the ice as part of the SURSAT ground truth team. The conditions were cold (-25°C) and many different types of ice were present in the scene including new ice, first year ice, second year ice, multi-year ice and an ice island. In addition to the SAR-580 data, RC-10 photography, radiometer, and scatterometer data were collected over the site (Livingstone et al 1980). At the same time, ASP 94-D SLAR imagery was being collected by the NASA Lewis C-130.

The radar parameter that was most extensively evaluated during these tests was the information rate. This is a complex function of both range and azimuth resolution, and degree of incoherent averaging, as well as many other aircraft and radar parameters. For our purpose however, a simplified version of the resolution volume concept devised by Moore (1979) was used. We define the information rate for an image as K;

$$K = \rho_a \rho_r / N$$

where

ρ_a = azimuth resolution

ρ_r = range resolution

N = number of incoherent looks

Readers not familiar with the concept of "incoherent looks" are referred to the Manual of Remote Sensing Chapter 9, where it is referred to as independent samples, and radar speckle is referred to as fading, terminology which comes from radar engineering.

The implication of the concept is that information content not resolution is the prime determinant of image utility. Thus, if the product of range and azimuth resolution is kept constant, the ratio may vary without affecting the information extractable from an image. Similarly, the number of looks may increase as resolution decreases and provided the K remains constant, image utility remains constant. Moore (1979) shows these concepts to have a rather broader range of applicability than might at first be supposed, but he does not examine the specifics of ice imagery. Other work (Inkster et al 1980b) suggests for a specific application there are fixed resolutions coarser than which, textural details needed for interpretation are lost. The impact of this concept on digital processor design, can be substantial.

Two separate experiments were run; one to evaluate the relationship between information content and K, and one to examine the relationship between images with a range of K values, and their utility for ice reconnaissance. The first part of the experiment used one trained photo interpreter and was broken into two separate parts; the effect of non-square pixels, and the effect of incoherent averaging. For the utility ratings a set of 10 highly experienced ice observers was used. They spent much less time on the imagery, but a quick analysis is their normal mode during operational ice reconnaissance missions. The imagery used was at approximately 1:200,000 scale.

It is extremely difficult to evolve a quantitative, transferable rating system for imagery. In these tests we used only relative ratings to define image interpretability. In no case did the interpreter know the parameters of the imagery under study. The photo interpreter, in addition to relative ratings, constructed a key of some 20 classes of features, on an overlay. Images with only very subtle differences in content could then be rated against these classes. All this work was done on 1:50,000 blowups.

In the text and figures for this paper the convention has been adopted to quote resolution in azimuth, then range and always in metres. Thus 2.1 x 3 m refers to 2.1m in azimuth and 3 m in range. The size of the resolution quoted refers to an effective bandwidth in the optical correlator. It is estimated to be accurate to within 5%. Checks were made on the imagery using a calibrated eyepiece to measure the size of the speckle. From this we are confident that the resolutions quoted are reasonable and correct.

2. NON SQUARE PIXELS

The data set selected for analysis was in the vicinity of Ice Island T3. It contained all the ice types occurring in the Beaufort Sea in March. Figure 1a shows a portion of the far range swath from that pass. On that image, thin young ice, thick first year ice, multi-year ice and T3 can all be distinguished. A degraded image was selected as datum; namely 10 x 10m. This permitted us to go to 2 x 50m resolution and still maintain K at 100 m^2. The 10 x 10m image is shown in figure 1b. The complete data set used in this part of the experiment is listed in Table 1.

Table 1: Data Set for Non-Square Pixel Study

ρ_a(m)	ρ_r(m)	N	K(m^2)
10	10	1	100
5	20	1	100
20	5	1	100
3	33.3	1	100
2	50	1	100

Figure 2 shows the same area as figure 1 but with non-square pixels. Figure 2a is 5m x 20m resolution (1:4) and figure 2b is 20m x 5m resolution (4:1). Only the very speckle shape shows any difference. Both images were rated equally and the interpreter could find no loss of information in either when compared to the datum. Larger distortions did reduce the quality of the imagery, not to mention making the observer uncomfortable. Figure 3a shows the 2m x 50m imagery (1:25). It is much less pleasant, and contains less information. Surprisingly however, only the finest of ridges in azimuth are lost. Ridges in range are, of course, much sharper. The 1:10 image was rated to somewhat better than the 1:25 but still poorer than the other three (i.e. 1:1, 1:4 and 4:1).

From this work we conclude that, provided the product of range and azimuth resolution remains constant, the ratio may vary up to a factor of 4, without serious degradation of image quality for general ice reconnaissance. This conclusion is specific to the conditions tested however, and care should be taken in extending it beyond our conditions.

3. INCOHERENT AVERAGING

Incoherent averaging, or multi-looking as it is also known, effectively reduces the spatial resolution of the sensor while at the same time, reducing the speckle (or coherent fading). There are several ways of implementing an incoherent average in an optical correlator. The effects are similar but not precisely the same for all methods. The easiest to implement is an averaging of output data in the image plane of the correlator (see for example figure 3b). This can be effected, in azimuth only, by having the image mistracked by the image film. This is analagous to low pass filtering the image in one dimension. A similar effect can be had by using sub-aperture processing. An attempt was made when preparing the data set to build in a test of the applicability of the two different techniques to the design of digital processors. The data set used is listed in Table 2.

Table 2: Data Set Used in the Incoherent Averaging Experiment

ρ_a(m)	ρ_r(m)	N	K(m^2)
10	10	1x1	100
14	14	2x1	98
17	17	3x1	96.3
20	20	4x1	100
25	25	6x1	104
40	40	16x1	100
35	35	12.25x1	100
35	35	3.5x3.5	100

An analysis was first conducted on the 40 x 40m, 16 look data, relating it to the datum. The results were as would be expected. The tonal characteristics of this imagery, exhibiting much less speckle, are more like those of photography. Therefore ice type classification based on tone was judged to be slightly superior than with the datum 10 x 10m image. Small ridges either disappeared or became discontinuous on the 40 x 40m data. On average the interpreter preferred the 16 look data visually but noted that the lower resolution resulted in some loss of information on the fine scale structure.

The second test performed was an evaluation of the two 35 x 35m data sets in an intercomparison (see Fgiures 4a and 4b). This was intended as a test of the validity of our results compared to other ways of generating multilook imagery. The 3.5 x 3.5 look data was generated using true sub-aperture processing. That is, an image was formed by incoherently adding (on the film) images made by sequentially exposing the film using different portions of the frequency spectrum of the image. This is implemented by placing a moving slit in the transform plane of the correlator. A larger fixed aperture determined the basic resolution (35m) and the size of the moving slit relative to this aperture determined the number of looks; hence the number 3.5. This procedure is always adopted for range multilooking. For azimuth multilooking this procedure is also applicable but a much simpler technique is available, namely azimuthal mistracking. If the film in the output image plane mistracks the moving image, then the image will be smeared. This smearing is equivalent to low pass filtering the image in the digital case. If the image being smeared is of high azimuth resolution (app. 2.8m in this case), the resultant image will have a lower resolution (35m) and increased incoherent averaging (12.25 looks).

The interpreter noted that the information content in the images appeared to be equal, but the images looked very different. Firstly, the 3.5 x 3.5 look image had a fuzzy appearance, but the highlights of the image appeared to be much brighter. Subtle tonal variations were lost on the 1 x 12.25 look images compared with the 3.5 x 3.5 look. However, over the complete set of features, a slight edge was given to the 1 x 12.25 look imagery. It is clear from the imagery that it is 'crisper' looking. We conclude that multilooking an image that has already been produced at full resolution, and with maximum sidelobe supression is preferrable to doing sub-aperture processing. The increased brightness response seen in the 3.5 x 3.5 look data is due to film reciprocity effects, and would not be noticed in a digital system.

The next test was to take the 2, 3, 4, 6, 12.25 and 16 look imagery and rank them in terms of which image was the most interpretable, against the set of targets chosen. The results indicate that of the 2, 3 and 4 look data, very little separates the imagery. The three look was rated first, the two look second and the four look third. The 6, 12 and 16 look were rated lower and in that order. The 6 look was beginning to show a loss of visibility for very fine structure which was increasingly noticeable at 12 and 16 looks.

The conclusions drawn from this study must be tempered with the conditions used. That is, the imagery was presented at constant 1:50,000 scale, was printed on photographic paper and the value of K was kept constant. The indication is that image interpretability is not adversely affected and may be slightly improved by a small amount of incoherent averaging. An optimum appears to be 3 ± 1 look, with amounts of 6 or more looks being noticeably poorer. At 12 looks serious loss of fine scale detail can be noted.

4. INFORMATION RATE AND IMAGE UTILITY

Having answers to the question of how the information should be presented is helpful, but the prime question to be asked was how much information is needed for ice reconnaissance. To this end, data generated by ERIM for the Office of Naval Research (Washington) and for the SURSAT Project were analyzed by a group of AES ice observers. The data set is tabulated in Table 3. A group of 10 experienced ice observers were asked to rate all the imagery in order of utility. They were also asked to give a qualitative rating to the imagery. The results of their ratings are given in Table 4.

In addition to rating the imagery in descending orders of perceived quality, the observers made notes and estimated the utility of the imagery for general ice reconnaissance. The top three images were all called 'good', that is they would be considered very adequate for drawing ice maps. The next 6 images were rated as useful but those with K values larger than 900 were rated as very poor or useless. It is interesting that the 30 x 30m image has a signal to noise ratio (S/N) some 22 db lower than the 2.1 x 3m image. This is due to the loss in coherent gain in the optical correlator. It is possible therefore that the 'useless' rating of the observers relates as much to the image as to the resolution. If high S/N data with larger numbers of pixels (greater swath width) were to be presented, a higher rating may result. Different but none-the-less useful information would be obtained, as with NOAA or Landsat imagery.

The three images rated 'good' by the ice observers all have K values above 100, and, from the detailed studies of the photo interpreter, this seems to be fundamental. That is, textural details and fine scale structure needed to make ice interpretations are lost a K=100. There were no observers calling K=100 better than K=64 although confusion exists both above and below. We therefore conclude that there is a dividing line below which any proposed system should not go. Because of the way in which our experiment was constructed it is not possible to precisely locate the optimum compromise value of K. We can however, say with some confidence that any airborne SAR for use in ice reconnaissance should have an information rate at least equivalent to that of 8 x 8m 1 look data (K=64).

Table 3: Data Set Used in the Interpretability Test

$\rho_a \rho_r$	N	K
2.1 x 3.0m	1 look	6.3
25 x 8m	4 look	50
8 x 8m	1 look	64
10 x 10m	1 look	100
15 x 15m	1 look	225
20 x 20m	1 look	400
24 x 25m	1 look	625
50 x 70m	4 look	875
30 x 30m	1 look	900
40 x 40m	1 look	1600
100 x 70m	4 look	1750
50 x 70m	2 look	1750
25 x 70m	1 look	1750
50 x 50m	1 look	2500
50 x 70m	1 look	3500
100 x 70m	1 look	7000

Table 4: Trained Ice Observers Ratings

	RATER/RATING											
$K = \rho_a \rho_r / N$	1	2	3	4	5	6	7	8	9	10	Mean Rating	Variance
6.3	16	14	16	16	15	16	16	15	14	16	15.4	.8
50	14	16	15	14	16	15	15	16	15	15	15.1	.7
64	15	15	14	15	14	14	14	14	16	14	14.5	.7
100	13	13	13	13	13	13	13	13	12	13	12.9	.3
225	12	12	12	12	12	12	12	11	13	12	12.0	.4
400	11	11	11	11	11	11	11	12	11	11	11.1	.3
625	10	10	10	10	9	9	9	10	10	9	9.6	.5
875	8	8	9	8	10	10	10	8	8	10	8.9	.9
900	9	9	8	9	5	8	8	9	9	8	8.2	1.2
1600	6	4	4	4	4	5	4	6	5	4	4.6	.8
1750	3	5	7	5	8	4	6	4	6	5	5.3	1.5
1750	7	7	6	6	7	6	7	7	4	7	6.4	1.0
1750	5	6	5	7	6	7	5	3	7	6	5.7	1.2
2500	2	1	1	3	2	2	2	1	2	2	1.8	.63
3500	1	3	3	2	3	3	3	5	3	3	2.7	1.0
7000	4	2	2	1	1	1	1	2	1	1	1.6	1.0

5. SUMMARY OF RESULTS

The objective of this experiment was to provide guidelines for the design of a digitally processed SAR specifically intended for ice reconnaissance. Due to the limits of our data we are only able to place boundaries on this design, and a frame work in which future work can be conducted. We have examined image utility as a function of data rate and find that a minimum of 8 x 8m, 1 look data will be required of any future radar system. For full flexibility, a better figure may well be required.

We have examined the effect of non-square pixels on image interpretability. We conclude that, provided the product of range and azimuth resolution remains constant, the ratio may vary by as much as 4:1 without serious impact on image utility.

We have also examined the effects of incoherent averaging or multi-looking. We conclude that reducing resolution to increase the incoherent averaging can have a small, positive effect on image utility. We found an optimum value would be 3 ± 1 look. Our tests were conducted using low pass image filtering. We know the effect of sub-aperture processing will be different and could in fact totally change our conclusions.

6. RECOMMENDATIONS FOR FUTURE WORK

Our study was conducted using optically processed data presented on photographics paper at a constant scale. This means we were displaying a different number of pixels in each case. Because displays tend to have a limit of approximately 2,000 points per unit, a display limited test should be run. The implications of such a test for digital design can be great. For example, let us consider a basic 4 x 4m system. The 2,000 point display would cover 2,000 x 4 = 8 km. However, if the display sweep rate could be increased, so that 2m azimuth resolution, 8m range resolution data could be presented, 16 km of data could be displayed with no apparent loss in quality. Similarly if 4 x 16m, 1 x 4 look data were to be presented, 32 km of data could be presented, again with no apparent loss of quality. It is not clear how the information an ice observer would be able to glean from such presentations would vary. However, it is clear that much more work needs to be done to specify exactly how the limited display will modify our results.

Our results were based on a specific form of incoherent average that is not optimum for digital processors. We feel therefore the results will vary somewhat for a digital processor but it is not obvious exactly how. More work is needed to clarify this point.

Our results were obtained using only one ice scene. Although the scene contained a large variety of ice types, it was not completely representative of the entire Arctic. In particular, any radar used in the Eastern Arctic must be capable of detecting rather small icebergs. Further work should be done to generalize these results to other data sets.

Lastly, we have not examined the effects of depression angle on our results. Any operational system is likely to be forced to fly lower than optimum due to other sensors on the aircraft. That means much of the image generated by a radar will be of very low depression angles. This will have implications for the frequency of the radar, and may well modify our results. This effect needs to be quantified as part of any system design.

In conclusion, we feel we have delimited the problem of designing a digitally processed ice reconnaissance radar. It is now necessary to develop a much tighter specification based on the interaction between image interpretability and hardware considerations.

ACKNOWLEDGEMENTS

We would like to thank the 10 AES ice observers who took the time from a busy schedule to study our imagery. We would also like to thank Mr. Peter Hunt (Intera, Calgary) who did the detailed interpretation upon which many of our conclusions rest. The data used in this experiment were in large part generated under the SURSAT project. However, key portions were provided by R.A. Shuchman (ERIM) and were generated under contract to the Office of Naval Research. We are also grateful to Alex Klooster of ERIM for his helpful comments.

REFERENCES

INKSTER, D.R., R.K. Raney and R.F. Rawson (1979): State of the Art in Airborne Imaging Radar. Proc. 13th International Symposium on Remote Sensing of Environment, Ann Arbor, Michigan, 1979, p. 361-381.

INKSTER, D.R., R.T. Lowry, N.A. Prout, R.K. Raney, K.P.B. Thomson (1980a): The Airborne SAR Project - Conclusions and Applications (In these proceedings).

INKSTER, D.R., R.T. Lowry and M.D. Thomson (1980b): Optimum Radar Resolution Studies for Land Use and Forestry Applications. Proceedings of the 14th International Symposium on Remote Sensing of the Environment, April 1980, San Jose, Costa Rica. (In Press).

KOZMA, A., E.N. Leith and N.G. Massey (1972): Tilted Plane Optical Processor. Applied Optics, Vol. 11, No. 8, August 1972, p. 1766.

MOORE, R.K. (1979): Tradeoff Between Picture Element Dimensions and Non-coherent Averaging in Side-Looking Airborne Radar. IEEE Trans. on Aerospace and Electronic Systems, Vol. AES-15, No. 5, p. 697-708.

VANKOUGHNETT, A.L., R.K. Raney, E.J. Langham (1980): The Surveillance Satellite Program and the Future of Microwave Remote Sensing. (In these proceedings).

Figure 1a 2.1 x 3 m 1 look

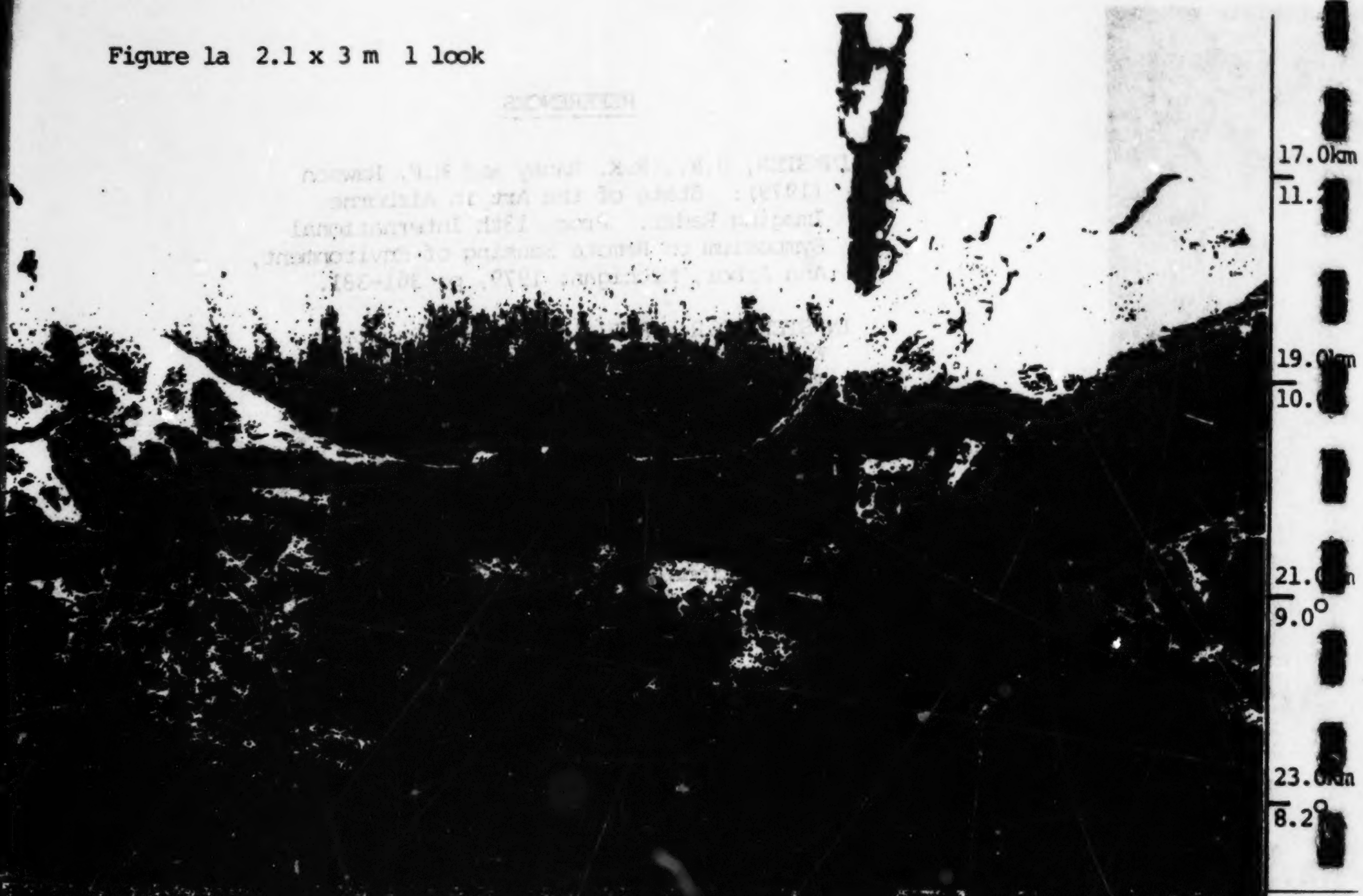
17.0km
11.2
19.0km
10.0
21.0km
9.0°
23.0km
8.2°

Figure 1b 10 x 10 m 1 look

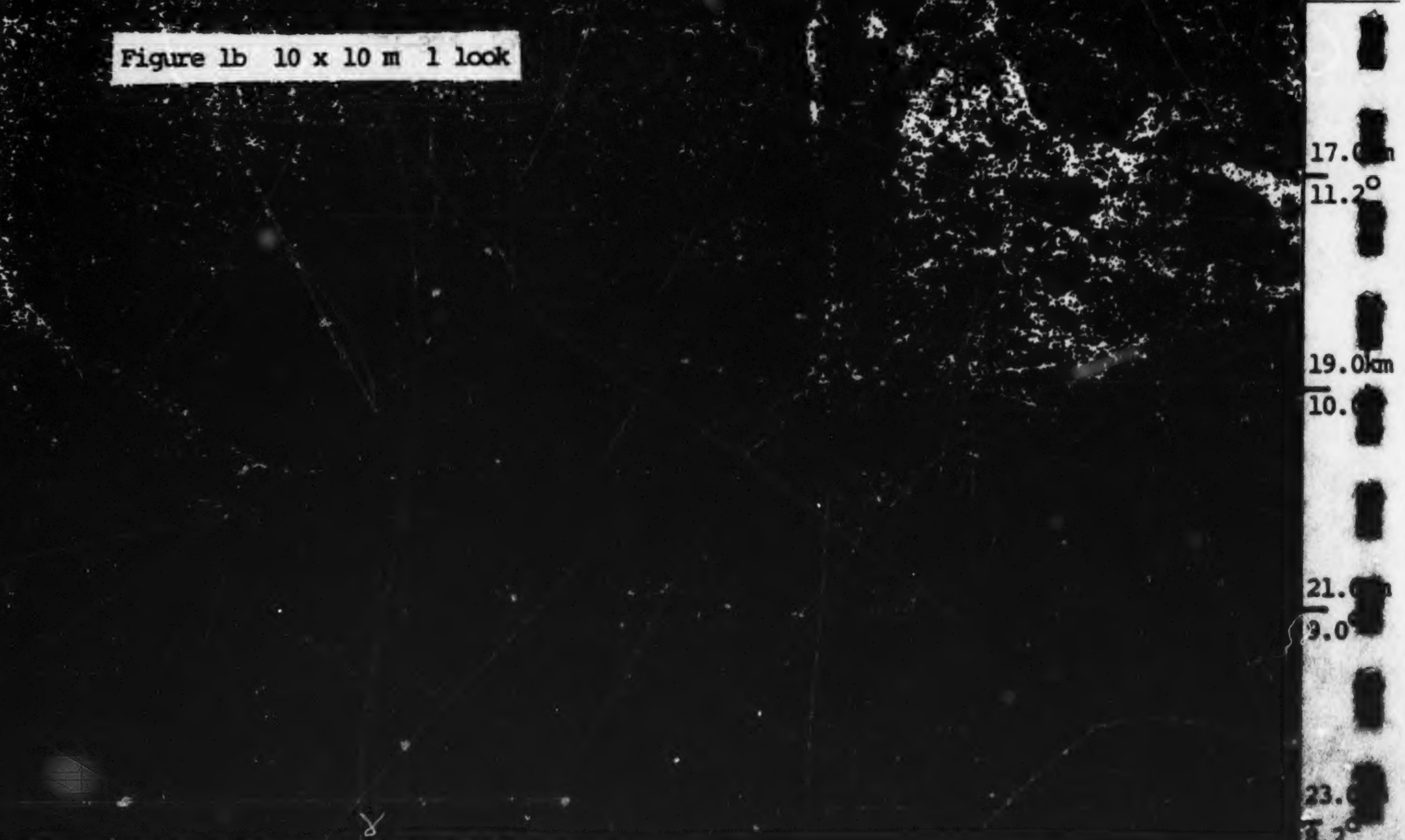
17.0km
11.2°
19.0km
10.0
21.0km
9.0°
23.0
8.2°

Figure 2a 20 x 5 m 1 look

17.0km
11.2°
19.0km
10.0°
21.0km
9.0°
23.0km
8.2°

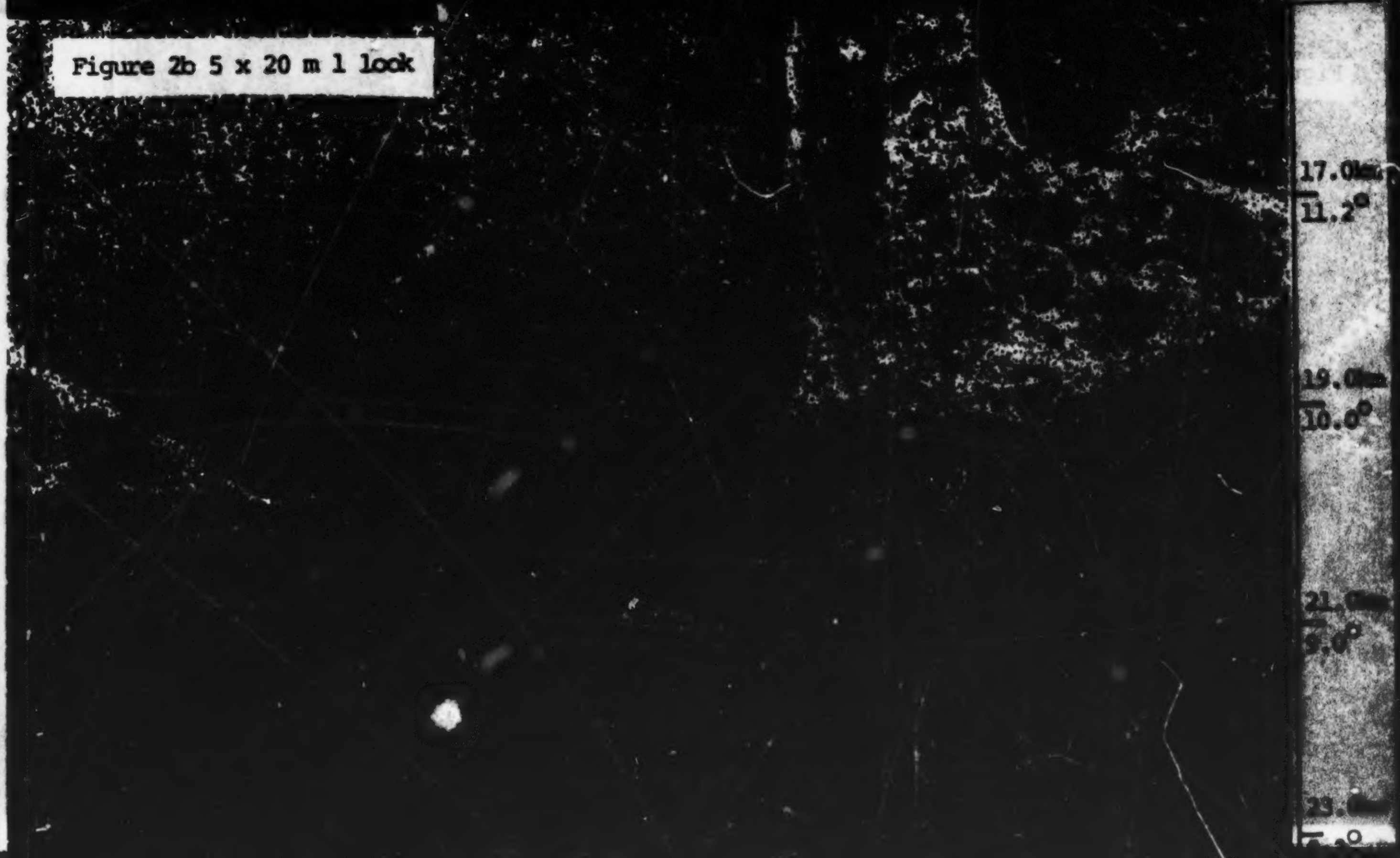

Figure 2b 5 x 20 m 1 look

17.0km
11.2°
19.0km
10.0°
21.0km
9.0°
23.

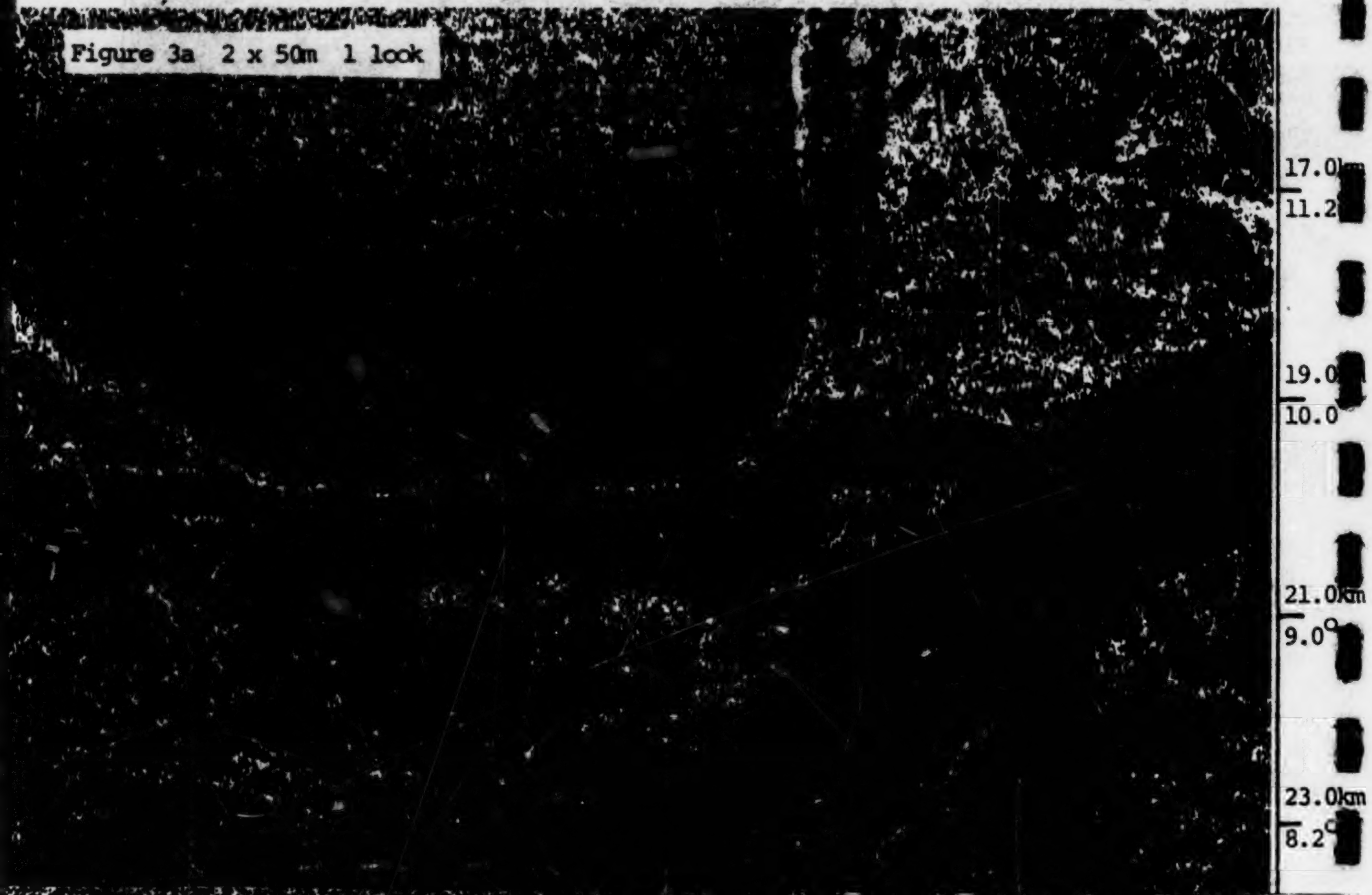
Figure 3a 2 x 50m 1 look

17.0km
11.2°
19.0km
10.0°
21.0km
9.0°
23.0km
8.2°

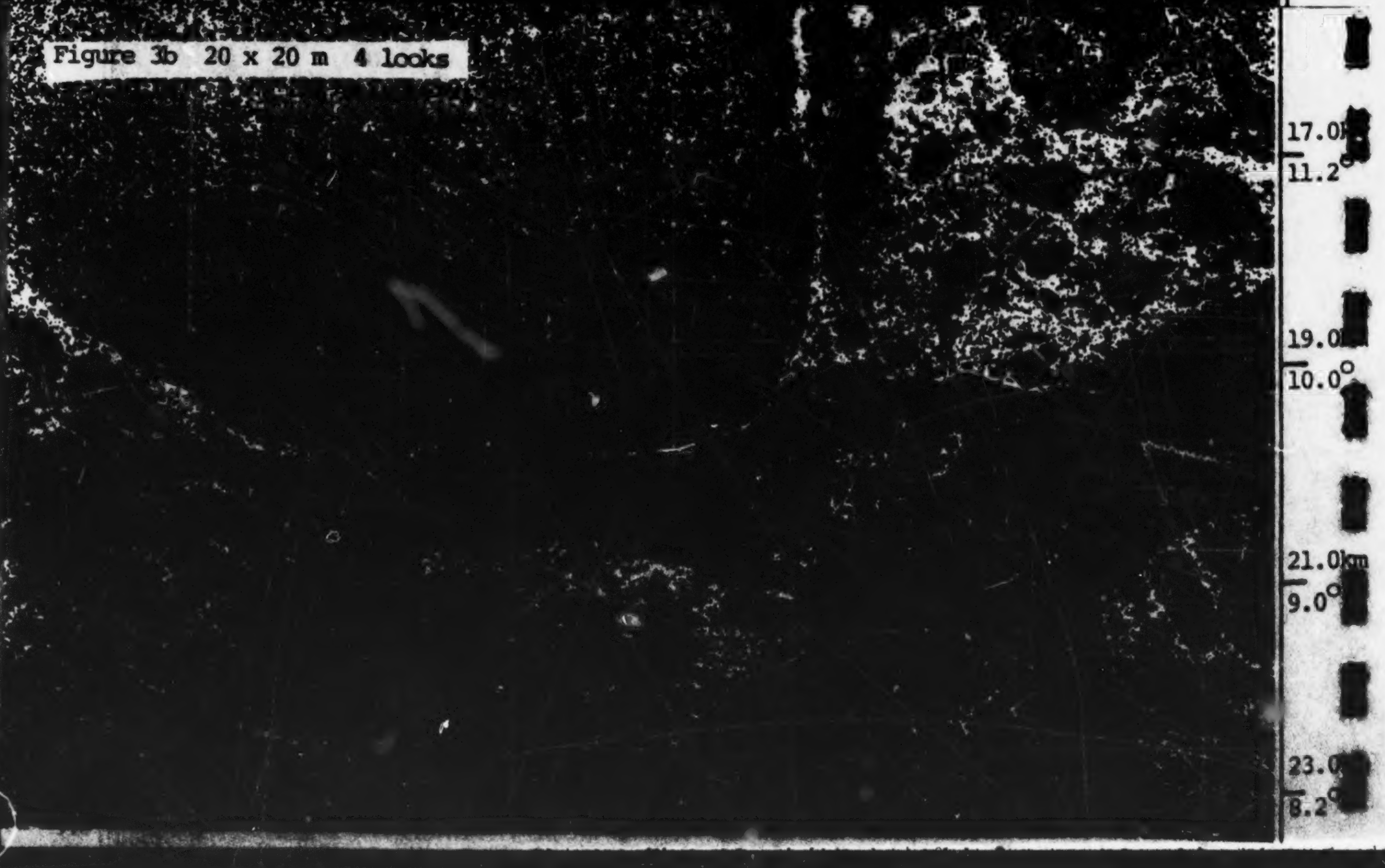
Figure 3b 20 x 20 m 4 looks

17.0km
11.2°
19.0km
10.0°
21.0km
9.0°
23.0
8.2°

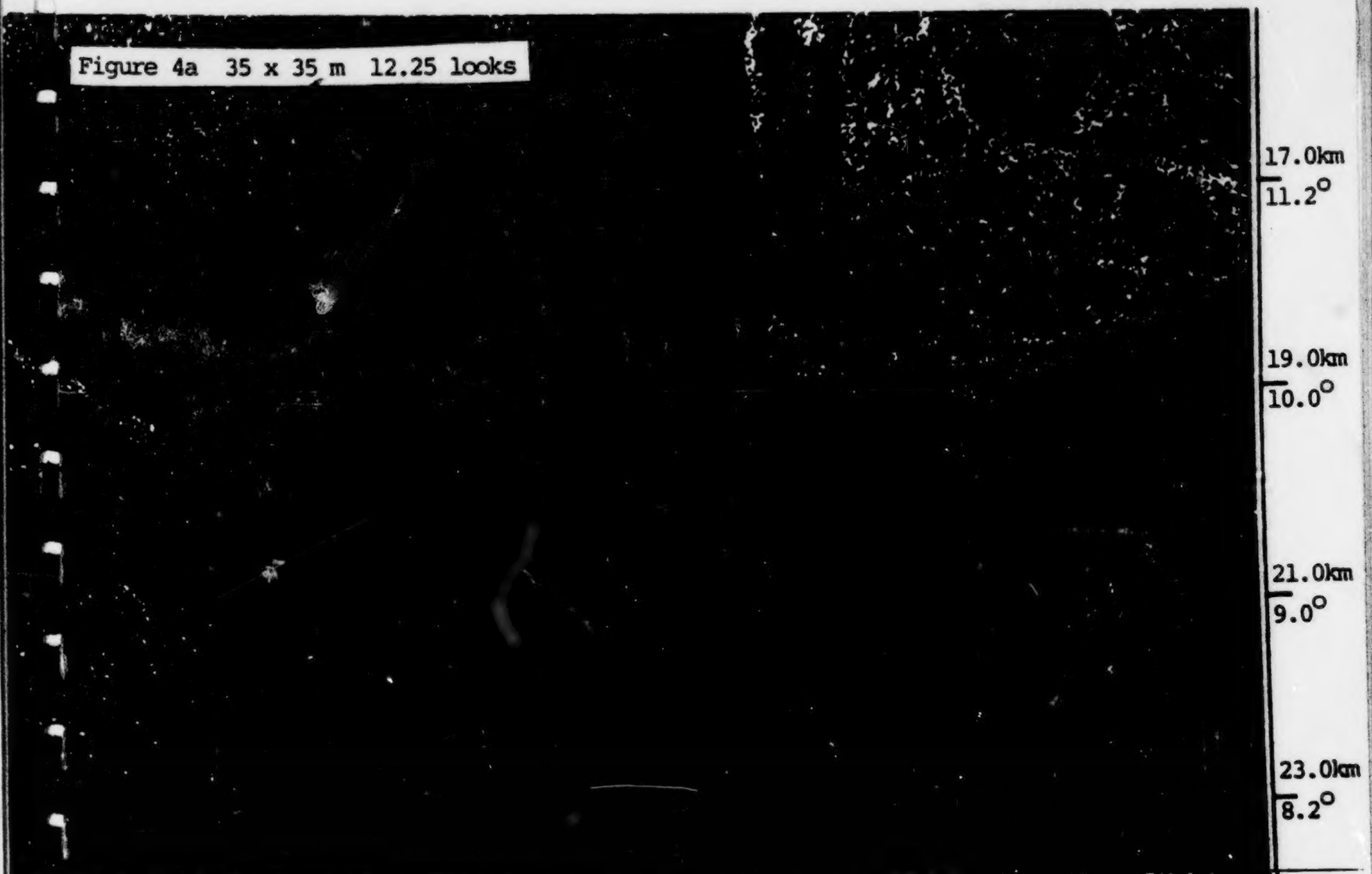
Figure 4a 35 x 35 m 12.25 looks
17.0km
11.2°
19.0km
10.0°
21.0km
9.0°
23.0km
8.2°

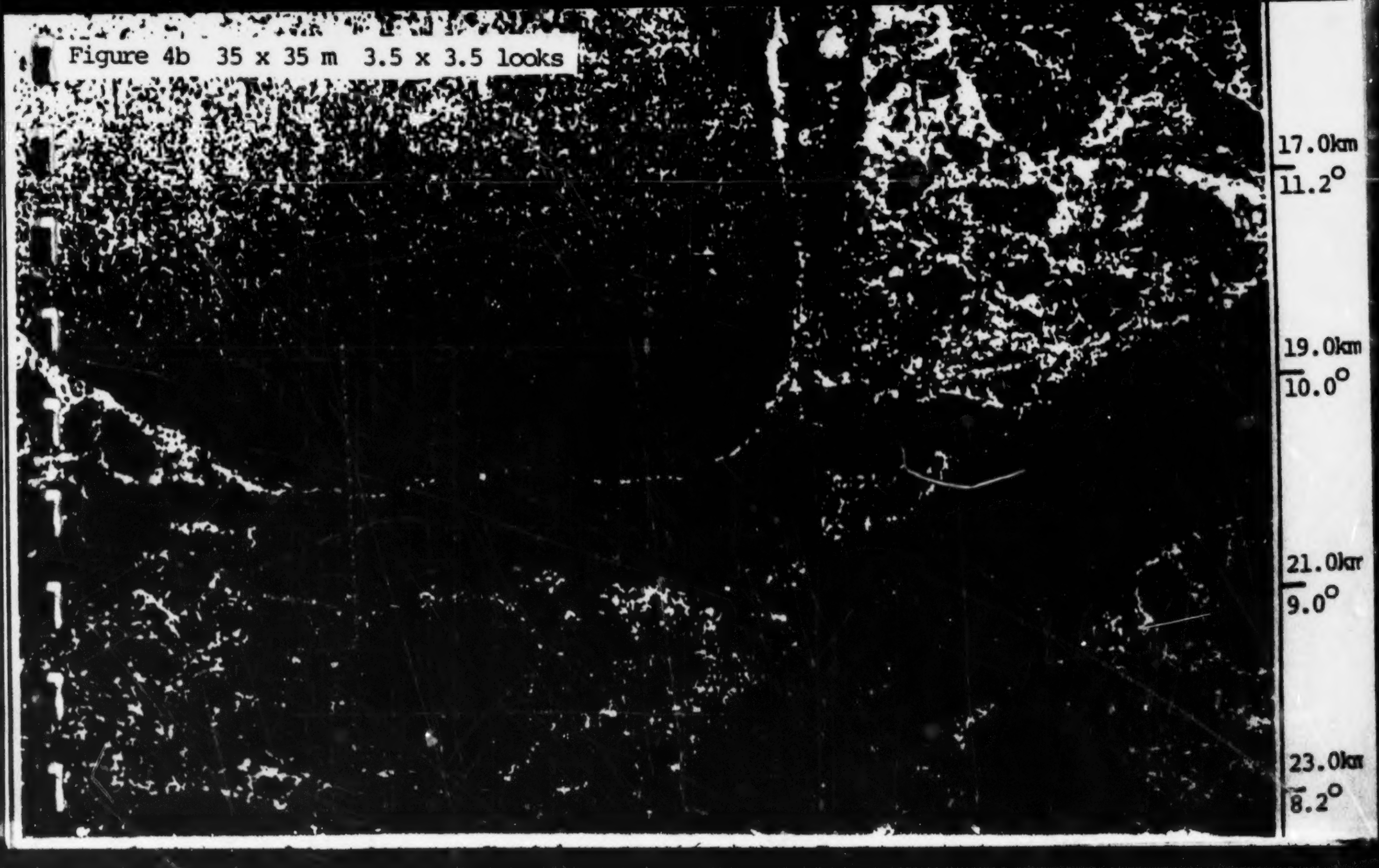
Figure 4b 35 x 35 m 3.5 x 3.5 looks
17.0km
11.2°
19.0km
10.0°
21.0km
9.0°
23.0km
8.2°

SECTION 5.18

EXPERIMENTAL USE OF REAL TIME SAR IMAGERY IN SUPPORT OF OIL EXPLORATION IN THE BEAUFORT SEA

Mercer, J.B., R.T. Lowry and S.K. Leung

EXPERIMENTAL USE OF REAL TIME SAR IMAGERY IN SUPPORT OF OIL EXPLORATION IN THE BEAUFORT SEA

J. B. Mercer, Dome Petroleum Ltd., Calgary, Alberta

- and -

R. T. Lowry and S. K. Leung, Intera Environmental Consultants Ltd., Ottawa, Ontario

ABSTRACT

Synthetic Aperture Radar imagery, generated in real time, has been used for the first time to support an Arctic marine operation. During the latter portion of Dome Petroleum's late season drilling program (November 1979) in the Beaufort Sea, the SAR-580 flew daily missions in order to provide near real time "snap shots" of the ice conditions in the vicinity of the operations. The purpose of the program was to assist both the icebreaker support of the drillship and the subsequent navigation back to harbour.

Near real time imagery was made available to the drillship initially, and later to the icebreaker Kigoriak, by two methods - VHF data link and by "local mail". The former had a time lag of a few minutes; the latter lagged by several hours. The downlink transmission utilized a "slow scan" TV system which transmitted an image of the hard copy output from the SAR real time processor through a VHF voice link to the ship. A reverse process aboard ship produced hard copy prints. The RTP output was generally of superior quality, while the downlink product was degraded both in resolution and grey scale. The undegraded imagery was viewed positively by operations personnel although a number of recommendations were made concerning the ultimate format of the product.

To provide the context for this SAR application, a review of Beaufort Sea ice conditions is presented along with a brief discussion of the problems and techniques for interpretation of the SAR imagery. The SAR, its downlink and operational performance, is described along with an outline of an improved system planned for 1980. The conclusion of marine operations personnel associated with this project was that SAR should form a valuable support tool for future winter arctic operations.

1. INTRODUCTION

Canada currently imports approximately 30% of its oil at world prices. It is therefore imperative to develop domestic sources such as the Beaufort Sea. To discover and extract oil in the presence of continuous ice threat, regular cloud cover, and Arctic nights 3 months long, demands the support of all weather day/night remote sensing systems. Imaging radar holds great promise for this application and in this paper we describe the first use of SAR in the support of non-military operations.

Dome Petroleum's subsidiary, Canmar (Canadian Marine Drilling), has been conducting exploratory drilling operations in the Beaufort Sea since 1976 using ice strengthened drillships and icebreaking support vessels. Restricted normally to the relatively brief open water season during the summer, Canmar was able, as a consequence of the presence of its new icebreaker Kigoriak, to extend operations until the end of November in 1979. During the final week, the operations were supported by daily flights of the SAR-580. This facility, which was brought to the Beaufort by Intera for a joint government-Dome ice modelling experiment, was mobilized earlier, at Dome's request, to support drilling operations.

The ice in the Beaufort exhibits a wide diversity of characteristics. Both the intrinsic properties and surface appearance are seasonally dependent and the notable features, can vary from year to year. We shall describe some of the characteristics. Both the intrinsic properties and surface appearance are seasonally dependent and the notable features, can vary from year to year. We shall describe some of the characteristics, especially as they relate to remote sensing and to drilling operations. A number of more detailed reviews are available (e.g., Kovacs and Mellor 1974; Wadhams 1975).

Typically the southern Beaufort is ice covered for about nine months annually, although about one year in ten the ice cover may remain throughout the year. The ice, during the late winter at least, is characterized by three zones as illustrated in Figure 1.

The landfast zone extends outward from the coast to about the 20 m bathymetric contour. Stabilized against movement by the presence of grounded ridge keels to this depth, the landfast zone grows annually to a thickness of about 2 metres. During the early summer it weakens, fragments and the resulting floes either melt or join the permanent arctic pack ice further offshore.

The permanent pack consists mainly of ice which has survived previous summer melting cycles. The multi-year ice which has thus evolved is characteristically 3 - 5 metres thick in floes which range in size from ten metres to (rarely) tens of km. Normally the multi-year ice appears in a matrix of first year ice, often heavily ridged. The major characteristic of the permanent pack ice found in the Beaufort Gyre is its large scale clockwise motion. (See Figure 1)

The transition zone exists as an interface between the stable landfast ice and the circulating pack ice of the Beaufort Gyre. This zone encompasses areas where most of the hydrocarbon deposits are believed to be situated, and where Canmar's drilling activities are located. It is also the zone of maximum dynamic ice interaction.

The formation of new ice normally commences by mid-October in the southern Beaufort. Freeze-up occurs first in the shallower near-shore regions and its evolution is governed by a number of factors including the local heat budget, the fresh water flow of the Mackenzie River and, the dynamic effects of the winds and currents. This early evolutionary history determines the surface properties of the ice and is fundamental to the appearance of the ice in X-band radar imagery.

As the ice grows to perhaps 30 cm thickness by early November, the dynamic effects produce rafting and subsequently ridging of the ice. Because of the low tensile strength and the susceptibility to fracture a range of thickness and surface conditions are produced, including specular smoothness, microscale roughness (typically 1 - 10 cm) and microscale roughness (typically 10 cm - 10 m) and are distributed on scales of tens of metres to several km. By mid-December the dynamic evolution is restricted to the transition zone although even in the landfast zone the surface characteristics continue to evolve due to brine migration and snow coverage.

The appearance of the ice in the transition zone is characterized therefore by a range of roughness scales and by a range of thicknesses and geometries. Sometimes multi-year ice will intrude upon this scene and be distinguished by its low rolling appearance and smoothed ridges.

Canmar's marine drilling operations are (at present) mainly conducted in open water or loose pack (unconsolidated ice) conditions of the summer season. In 1979 one drillship, aided by the icebreaker Kigoriak and several smaller vessels, was able to continue operations until the end of November in winter ice up to 40 cm thickness. Being statically positioned the drillship capability is limited by the forces exerted upon it by the moving ice (particularly from the side). The function of the icebreakers was to fragment the ice sheet prior to interaction in order to reduce their forces. The purpose of ice reconnaissance and forecast was to enable tactical direction of icebreakers, particularly in the presence of specific ice features such as ridges and rubble fields.

It has been known for many years that radar imagery of sea ice contained a very useful quantity of information on the properties of the ice. This is evidenced by the fact that both Canada and the USSR operationally use imaging radars as a mainstay of their ice condition surveillance systems. Numerous workers have noted however, that relating ice properties to radar return is not a simple task (Gray et al 1977, Dunbar 1975, Lowry et al 1979). Variations occur with radar frequency, polarization, depression angle and resolution as well as ice age, snow cover, and current and past air temperatures. This is an area of active research. See for example, in these proceedings, Hawkins et al (1980), Pearson et al (1980), and Lowry et al (1980).

During this experiment, the SAR-580 was operated in an X-band (9GHZ) H transmit, H receive mode with useful data being collected between 10° and 45° depression angle. The ice in the drilling area, consisted entirely of first year ice. The majority was at least one month old, and had 10 to 20 cm of snow cover. Ice of this type has very low X-band backscatter at aircraft depression angles.

Younger ice which forms in leads, that has yet to have snow fall on it shows a much wider range of backscatter. When first formed, this ice resembles water with no waves and is a total specular reflector (unless deformed), returning no energy to the radar. Normally the air temperature is well below freezing and the ice grows very rapidly. This causes brine to be expelled from the ice, yielding a concentrated brine on the surface where salinities can exceed 100 p.p.t. Very soon after its formation, frost flowers often form on the surface of the leads. These have a size which matches very well the X-band wavelength and as a result are very strong scatterers. Thus new ice can go from being very dark to very bright on X-band imagery, when less than 15 cm thick.

The main visual feature of SAR imagery of ice is the ridging and other deformations that return large amounts of energy. Ridge thickness is typically three to six times the surface soil height (0.5 - 5 m generally) and as such represents an impediment to marine operations, particularly when consolidated. Some work has been done to extract ridge size from radar imagery, with little success, but more work is planned.

2. THE SAR-580 SYSTEM AND THE DOWNLINK

The SAR-580 was operated in the wide swath X-HH mode for this exercise. (Inkster et al 1979). In this mode, 21.5 km of slant range data are collected in uncompressed form on two 70 mm films for post-flight processing on an optical correlator at ERIM. The onboard real time processor (RTP) can produce 2048 pixels for each range scan. The RTP data are processed to 3 m resolution giving a swath width of 6 km. Although these data are limited to 8 bits at the processor output, considerable flexability is provided to position this range of grey scales in the output dynamic range of the radar. In the aircraft the imagery is generated on heat developed dry silver paper exposed by a laser scan system. The line rate output of the RTP is tied to aircraft ground speed. At a maximum ground speed of 180 m/sec (350 knots) the line rate will reach 72 Hz although a more typical value is 60 Hz. (150 m/s). The near edge of the RTP swath was located about 5 km from nadir, corresponding to a 30° depression angle.

Several schemes were considered to transmit RTP radar imagery to the drillship while the aircraft was mapping in the vicinity. A full resolution, wide bandwidth VHF radio link would have given the best fidelity. Unfortunately, because of the longer lead time for its development, it was considered too risky to order one for the November 1979 operations. Instead a Robot slow scan TV system was selected for its simplicity, low cost and off-the-shelf delivery. The system used is described in Figure 2a. A television camera was focused onto the real time processor output and the video was digitized and stored in a 256 x 256 pixel x 6 bit memory. This frozen frame of image was then scanned and transmitted at audio rates through a standard VHF air to ground voice transceiver to the ship. About 30 seconds time was required to "process" each frame. On board the ship the received signal was stored in a similar memory and scanned at television rates to produce a TV image on a video monitor. A hard copy on dry silver paper was obtained using a Tektronix image forming module. The same VHF radios were also used for voice communication between the Convair 580 and the ship. In addition, an audio cassette tape recorder was used on the ship to record the data and voice communication. This served as documentation and as a source for replay into the hard copy machine. The resolution of the hard copy produced is estimated to be in the order of 30 m in range and 40 m in azimuth with about 6 grey shades. This is rather poorer than was expected but, as mentioned, the system was selected to demonstrate feasibility of downlinking imagery to the ships bridge. The resolution was limited by both the 256 x 256 scan memory and the vidicon in the TV camera. The grey scale was limited by (1) the RTP output dry silver paper, (2) the inability of the TV system to resolve grey scales by reflected light off the paper, (3) the frequency response of the Robot unit and (4) hardcopy production on the ships.

During the ship support, flying weather conditions were very favourable so the RTP images collected were flown to the ship by helicopter later the same day. The comparison showed clearly the degradation in going from the RTP output image to the downlink operator. An annotation block was placed on the beginning of the strip and frames were marked off on it. It was then placed on an illuminated stand which was in the field of view of the TV camera. The downlink operator was in voice communications with the ship and with mutually agreed timing, the strip of imagery was transmitted, frame by frame. As one frame was being transmitted, the next frame would be aligned on the light table. It was found to be possible to downlink all the data during a mission with no loitering needed. Although there was a delay of one line in the system, transmission speeds approximated collection speed. The final line was transmitted while the aircraft returned to Inuvik.

The shipboard operation was somewhat different. The audio tape recorder was used to record both the images as they arrived, and the conversation between the operators. Each frame, as it arrived, was placed in a Robot unit 256 x 256 memory. This memory is constantly displayed on a TV screen so the operator could keep watch on interference and other effects and call for retransmission of the scene if needed. Once the scene had been received, a hard copy was made using the Textronics image formation module. If more copies were needed they were made post flight, from the tape recordings.

As the data were received, they were printed and the prints were mosaiced. By this means, before the aircraft had landed in Inuvik, the mosaic was available on board the ship. In spite of the poor quality of these images, some interpretation was possible (see Figure 4). Features such as the track of the drilling operation in the moving ice were clearly visible with other features such as large new leads and large rubble patches also being detected. The mosaics were made available to the ships master to be used in conjunction with the ships radar, weather forecasts, wind speed and, when possible, visual observations to predict ice forces.

As mentioned, during this entire period, the weather conditions remained good so that regular helicopter runs were made from Tuktoyaktuk to the drillship. This allowed daily visual observations by the ships master and the ice observer on board, as well as delivery of the high quality RTP imagery. These factors combined to reduce the value of the downlink data to the ship's master.

As soon as the RTP data arrived, it was mosaiced (see Figure 5) and, when warrented, potentially hazardous ice areas indicated by the imagery were examined visually from the helicopter or directly by one of the icebreakers. The level of interaction with the ship's crew was very encouraging since they already had, in place, a system for handling the hazards posed by the ice. A great deal was learned about the capability of the SAR by the ship's crew, and of the needs of the ship's crew by the SAR operators. The fact that the imagery was collected and available long before the meagre light of mid-day was not lost on the ship's crew.

However, the futility of providing a mere image of the ice that the crew knew was there anyway, was not lost on the remote sensing advocates. As mentioned, this mutual learning was considered to be one of the positive outcomes of this experiment.

The comments of the ship's master have been used as guidelines in designing the equipment to be used in the 1980 trials. Firstly, the swath width of the SAR RTP is to be doubled to enable better mosaics to be constructed. This relates to the master's desire to have the information presented in a more compact way. Further, attempts are to be made to develop video storage and retrieval systems to display on a TV screen, data from several days, at various scales. This allows compact storage and retrieval. It is unlikely that this video system will be available for 1980 drillship support.

3. CONCLUSIONS

The motivation clearly exists to pursue the technological development required if we are to overcome environmental obstacles to extract oil from Canada's Arctic and East Coast frontier regions. In this paper we have described the role of one such technology, SAR, in terms of a specific operation, and in the context of wider use for future Arctic marine operations.

As a result of the operational support described, certain technical deficiencies became apparent. In response to these deficiencies, recommendations for modifications to the SAR-580 RTP, downlink and display were made which are presently underway. This should improve substantially the support planned for Canmar's late season operations in 1980. The intention to proceed with this support reflects the positive opinion of the marine users toward the potential usefulness of SAR in operational roles as described.

4. ACKNOWLEDGEMENTS

This work, funded by Dome Petroleum, was conducted as a pilot project under the SURSAT program (Inkster et al 1980) and the support of the SURSAT Office is gratefully acknowledged. Field operations were greatly aided by both MOT and Dome personnel at Inuvik. The airborne operations were supported by CCRS Air-Ops and the Innotech and Intera crews who operated under difficult conditions. Without the cooperation of the ship's master and crew aboard both the Explorer IV and the Kigoriak, this experiment would not have been possible.

REFERENCES

Dunbar, M., (1975) Interpretation of SLAR Imagery of Sea Ice in Naus Strait and the Arctic Ocean; Journal of Glaciology, v. 15, no. 73, p. 193-213.

Gray, A. L., R. O. Ramseier, W. J. Campbell, (1977): Scatterometer and SLAR Results Obtained Over Arctic Sea-Ice and Their Relevance to the Problems of Arctic Ice Reconnaissance, in Symposium on Remote Sensing, Quebec City, P.Q., p. 424-442.

Hawkins, R. K., C. E. Livingstone, A. L. Gray, T. L. Wilkinson, L. D. Arsenault, D. Pearson, K. Okamoto (1980): Single and Multiple Parameter Microwave Signatures of Sea Ice (In these Proceedings).

Inkster, D. R., R. K. Raney and R. F. Rawson (1979): State of the Art in Airborne Imaging Radar, Proc. 13th International Symposium on Remote Sensing of Environment, Ann Arbor, Michigan, 1979, p. 361-381.

Inkster, D. R., R. T. Lowry, N. A. Prout, R. K. Raney, K. P. B. Thomson (1980): The Airborne SAR Project - Conclusions and Applications, (In these Proceedings).

Kovacs, A. and M. Mellor (1974): Sea Ice Morphology and Ice as a Geologic Agent in the Beaufort Sea, ed. J. C. Reed and J. E. Sater, pp 113-161, Arctic Institute of North America, Arlington, Va.

Lowry, R. T., H. G. Hengeveld, R. A. Shuchman (1980): Optimizing Imaging Radar Parameters for Ice Reconnaissance, (In these Proceedings)

Pearson, D., C. E. Livingston, R. K. Hawkins, K. Okamoto, L. D. Arsenault, T. L. Wilkinson, A. L. Gray (1980): Radar Detection of Sea Ice Ridges and Icebergs in Frozen Oceans at Incidence Angles from 8° to 55°. (In these Proceedings).

Wadhams, P. (1975): Sea Ice Morphology in the Beaufort Sea, Technical Report No. 36, Beaufort Sea Project, Dept. of the Environment, Victoria, B.C.

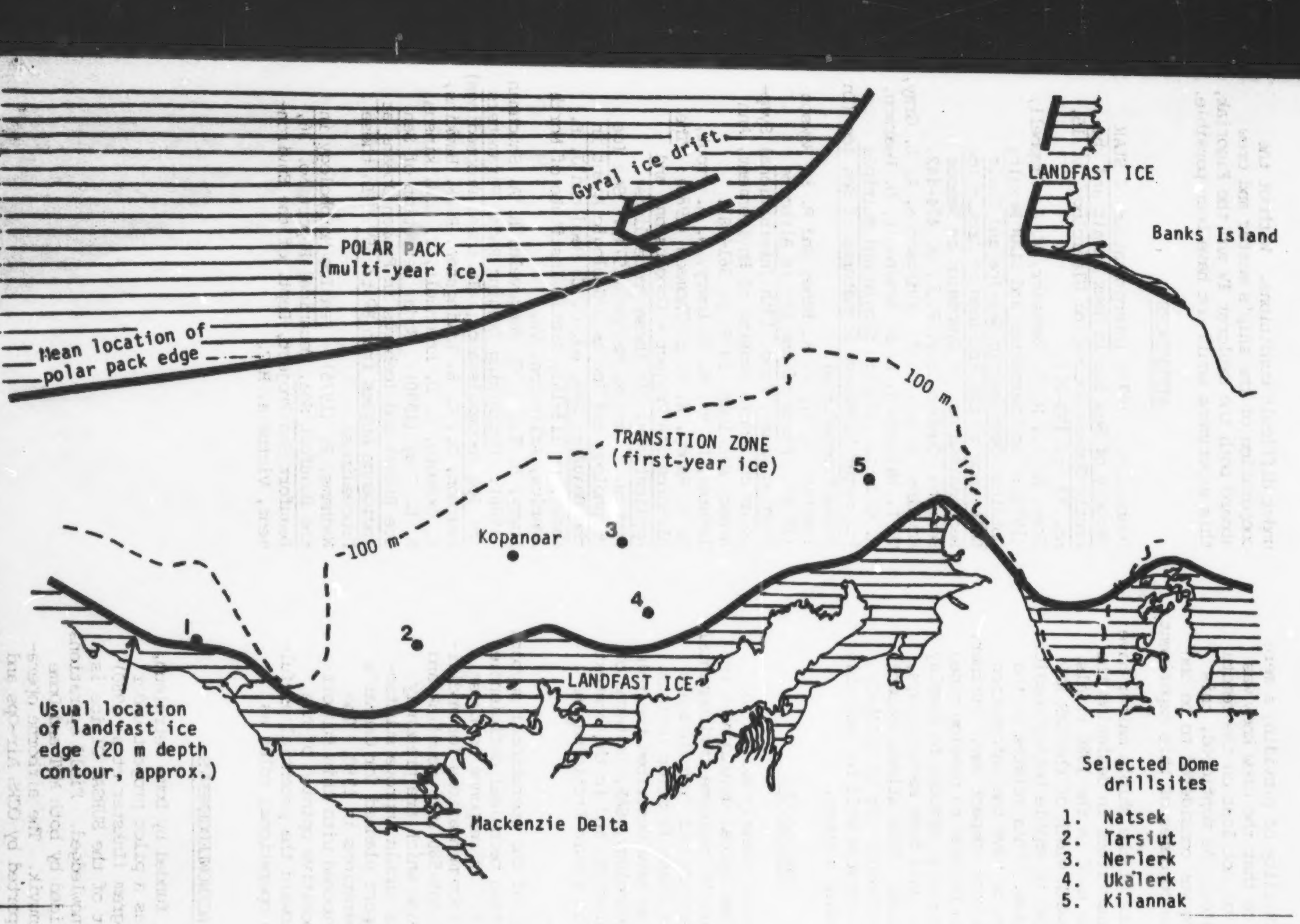
POLAR PACK
(multi-year ice)
Gyral ice drift
Mean location of
polar pack edge
LANDFAST ICE
Banks Island
TRANSITION ZONE
(first-year ice)
100 m
-100 m
Kopanoar
1
2
3
4
5
LANDFAST ICE
Usual location
of landfast ice
edge (20 m depth
contour, approx.)
Mackenzie Delta
Selected Dome
drillsites
1. Natsek
2. Tarsiut
3. Nerlerk
4. Ukalerk
5. Kilannak

Figure 1 Beaufort Sea Winter Ice Regime

During the winter months, the three regions will typically occupy the area shown. Several drill sites, located in between the shore, and the 100 metre water depth line are also indicated.

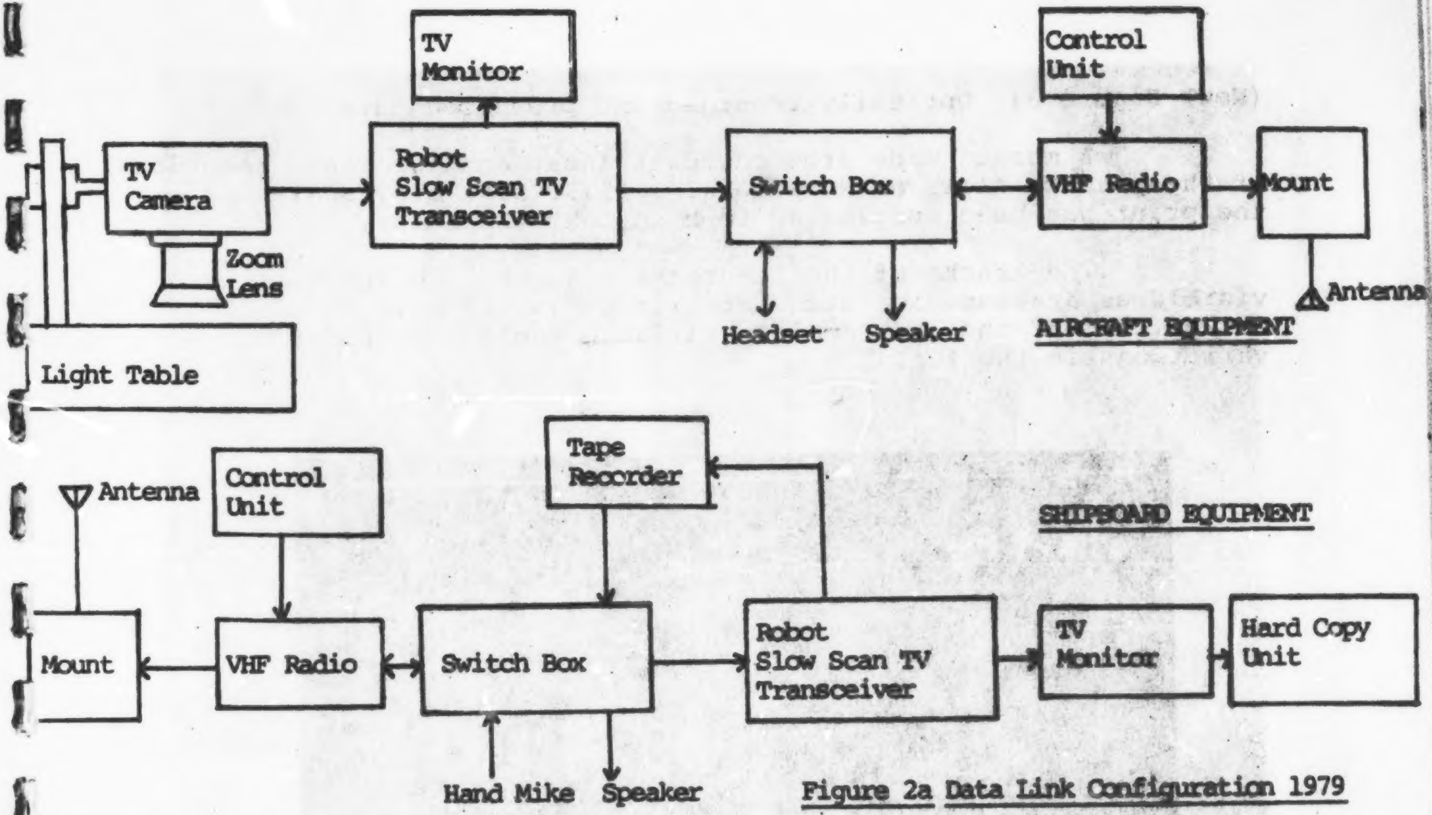
TV Monitor
Control Unit
TV Camera
Robot Slow Scan TV Transceiver
Switch Box
VHF Radio
Mount
Zoom Lens
Antenna
Headset
Speaker
AIRCRAFT EQUIPMENT
Light Table
Tape Recorder
Antenna
Control Unit
SHIPBOARD EQUIPMENT
Mount
VHF Radio
Switch Box
Robot Slow Scan TV Transceiver
TV Monitor
Hard Copy Unit
Hand Mike
Speaker

Figure 2a Data Link Configuration 1979

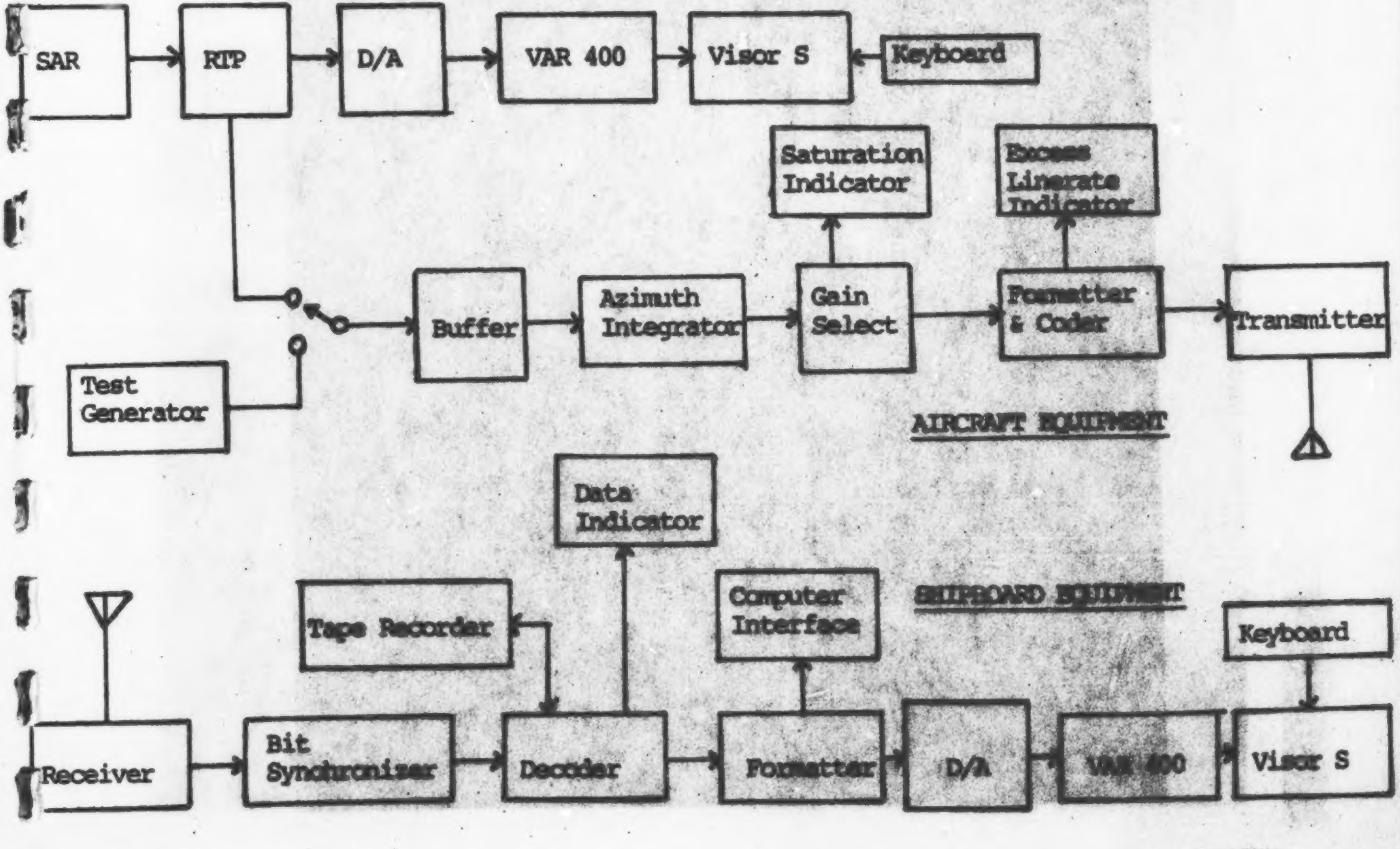
SAR
RTP
D/A
VAR 400
Visor S
Keyboard
Saturation Indicator
Excess Linerate Indicator
Buffer
Azimuth Integrator
Gain Select
Formatter & Coder
Transmitter
Test Generator
AIRCRAFT EQUIPMENT
Data Indicator
Tape Recorder
Computer Interface
SHIPBOARD EQUIPMENT
Keyboard
Receiver
Bit Synchronizer
Decoder
Formatter
D/A
VAR 400
Visor S

Figure 2b Proposed Data Link Configuration 1980

(New) Figure 3: Optically recorded and processed data.

A mosaic made from one pass (near and far range recorders) of the pattern flown on November 27, 1979. The grey scale on the print has been suppressed to highlight the ships.

The tracks of the icebreakers in the ice are still visible as are some ice structures, such as ridges. A 'lower cut' of the grey scales available would show tonal variations in the ice.

FIGURE 3

intera
24 NOVEMBER, 1979
SHIP SUPPORT PHASE
[illegible] LINK IMAGERY

intera
26 NOVEMBER, 1979
SHIP SUPPORT PHASE
REAL TIME IMAGERY

FIGURE 5

SECTION 5.19

AIRBORNE IMPULSE RADAR SOUNDINGS OF SEA ICE

Rossiter, J.R., K.A. Butt, J.B. Gamberg, T.F. Ridings

Sixth Canadian Symposium on Remote Sensing, Halifax, May 21-23, 1980

AIRBORNE IMPULSE RADAR SOUNDING OF SEA ICE

James R. Rossiter, Kenneth A. Butt, J. Brian Gamberg, Terry F. Ridings
Centre for Cold Ocean Resources Engineering
Memorial University of Newfoundland
St. John's, Newfoundland
A1B 3X5

ABSTRACT

Airborne impulse radar, operated from helicopter and Twin-Otter, was used in March-April 1979 to estimate the physical properties of sea ice in the Beaufort Sea and Lake Melville, Labrador. Concurrent measurements included: augered thickness, salinity, temperature, crystal fabric, electrical properties of the ice, simultaneous aerial photography, and synthetic aperture radar imagery.

Impulse radar centre-frequency of 80, 100, and 200 MHz were used. A centre-frequency near 100 MHz appears to give the best trade-off of penetration vs resolution and antenna size. Data collected below 30 m elevation have reduced side-scatter from the ice surface. Speeds below 50 m s^{-1} are required with the current hardware to achieve coherence from scan-to-scan.

Thickness estimates are excellent for fresh and brackish ice, and are good for undeformed first-year sea ice about 1-2 m thick. Areas of fresh water melt pools that have only experienced surface refreezing show thickness profiles that warrant further examination. Bottom returns from multi-year ice are sporadic, although floes up to 14 m have been sounded. Ridges are not usually penetrated, but can be easily detected. Data processing algorithms are under development to characterize the ice further using the strength of the returns. Airborne impulse radar appears useful for routine estimation of the "third-dimension" of ice properties, particularly in conjunction with aerial remote sensing surveys.

INTRODUCTION

As more work is carried out in the Canadian Arctic during winter, there exists a greater need for the ability to make remote estimates of the physical properties of sea ice (Mercer, 1980). The critical properties are the thickness and strength of ice, whether it be for operations on the ice surface, or movement of ice-breaking vessels. Although progress has been made in recent years in the observation and classification of sea ice using remote sensors (Campbell et al., 1975), only limited success has been achieved in remote measurement of ice thickness and strength. This ability is particularly important because of the high variability and dynamic nature of sea ice and the increased industrial activity in Canada's North.

The most successful measurements to date use radar sounders operating in or near the VHF band (Rossiter, 1980), and a number of new instruments are actively being developed which have potential application to the remote determination of sea ice thickness (Rossiter and Bazeley, 1980).

Impulse radar systems, using broadband pulses in the 50 to 500 MHz frequency band, are being used routinely in the Arctic from surface vehicles. Active research work on sea ice is being pursued using these systems both at the Cold Regions Research and Engineering Laboratory in the U.S.A. (e.g. Kovacs and Morey, 1979) and at C-CORE (Rossiter et al., 1977; Butt and Gamberg, 1980).

This paper reports on C-CORE field measurements made in the Beaufort Sea during March 1979 (Rossiter and Butt, 1979) and over Lake Melville, Labrador in April 1979 (Butt et al., 1979). The sites were chosen to coincide in time and place with other investigations, including the SURSAT Project, which involved a number of sea ice studies (including other remote sensing overflights), and a Province of Newfoundland and Labrador study of Lake Melville ice conditions. Results from subsequent analysis of selected sites are presented.

In addition, enhancement of results that can be achieved through data processing are presented. In particular, cross correlation appears promising, and this technique is outlined here.

DATA COLLECTION

Beaufort Sea

The Beaufort Sea field program operated out of the Polar Continental Shelf Project base camp at Tuktoyaktuk, N.W.T. A description of the sites and a summary of the data as collected are presented in a separate report by Rossiter and Butt (1979). The positions of the sites are shown in Figure 1. The local sites, all of which were within a 75 km radius of Tuk, are designated as C-1 through C-6. Besides the radar work, concurrent ice measurements included: augered thickness, salinity, temperature (Snellen and Rossiter, 1980), crystal fabric (Langhorne, 1980; Langhorne et al., 1980), electrical properties of the ice (Davis, 1980), simultaneous aerial photography, and synthetic aperture radar imagery.

An area of multi-year ice, north of the shear zone, approximately 320 km north of Tuk and a few km south of Ice Island T-3, was studied b both C-CORE and SURSAT. Another area of interest was the ice rubble field at Issungnak, located approximately 75 km northwest of Tuk. Since the nature of this ice field restricted most conventional forms of ground truthing, only airborne data were collected.

Lake Melville

The Lake Melville field program operated primarily out of Goose Bay, Labrador. A description of the sites and a summary of the data collected are presented in a separate report by Butt et al. (1979). The positions of the ground truth sites and radar overflights are shown in Figure 2.

Although not shown, SAR overflights were run down the Lake, covering the same area as the impulse radar. Surface truth data, provided by Remotec Applications Inc., consisted of ic thickness and salinity measurements. Remotec also provided a central weather station for temperature and local meteorological data.

RESULTS

Beaufort Sea

The Beaufort Sea field trip included the firs use of impulse radar from a fixed-wing aircra platform, (a de Havilland Twin Otter) (see Figure 3). Although the installation was successful, it must be regarded as experiental. The aircraft was flown at 100 to 140 knots airspeed (50 to 70 m s^{-1}). The scan epetition rate of the impulse radar (51.2 cans/ second) is probably not fast enough for routine fixed-wing use, since only a single scan of data was collected per metre of forard movement. The ice characteristics can change substantially in this distance, giving significant differences in returned signal rom scan to scan, even over relatively uniorm ice.

ata were collected at altitudes from 100 to 00 feet above sea level (30 to 100 m). There were noticeable differences between results from lower and higher level operation, caused rimarily by the larger footprint of the radar at higher altitude. The antenna of the radar is a modified dipole, and the footprint size s the same order of magnitude as the flying eight. It was found reasonably easy operationally to fly for several hours at 30 m eleation.

Measurements were made at a centre frequency f 200 MH.. Analysis of 440 line-km of data imilar to Figure 4 over an area of multi-year ice in the Beaufort Sea indicated that penetration of multi-year ice was not consistent rom floe to floe, or even within the same loe. However, the soundings obtained could be used to calculate a multi-year ice thickess distribution. The thickest floe measured ad a calculated thickness of 13.5 m.

hat study showed the utility of collecting imultaneous imaged data, in this case aerial photography. Photographs were taken both at low level from the aircraft containing the adar, and from 2440 m from a second Otter (Figure 5). Since the radar and photography were taken simultaneously, the flight path of he radar aircraft could be plotted, and the adar record correlated with ice features in the imagery. This allowed significant imrovements to be made in the interpretation f the radar returns.

In particular it was possible to identify ice ypes from the nature of the radar echoes. oughness on the scale of 1 to 10 metres horizontally is usually indicative of multi-year loes, which have a hummocked surface. Firstear ice is either much smoother, or if deformed, much rougher (Figure 4). First-year idges and rubble piles are made up of small ocks of ice which are excellent random scatterers at 100 MHz and give very weak surface echoes.

Lake Melville

The ice in Lake Melville is formed from relatively fresh water, and the salinity is typically less than 2 ppt in the bottom 10 cm of ice layer. There is, however, a horizontal salinity gradient increasing from west to east along the lake. The two most significant runs with the impulse radar were the long runs from North West River to Gull Island at 100 MHz and 200 MHz centre-frequencies. Both of these runs showed the effect of the salinity gradient with reduced penetration at the east end. Overall, the best results were obtained at 100 MHz, where a complete profile of the entire lake thickness was obtained. Ground truthed thickness measurements increased systematically from about 85 cm in the west to about 140 cm in the east. This increase showed up clearly on the radar record. The correct value of the thickness was obtained using the measured travel times and a dielectric constant of 3.2. This value of dielectric constant is consistent with ice of relatively low brine volume.

Important features overflown in this study were so called "ridges" that might better be described as "hummocks". The radar was able to delineate the upper surface relief and width of the features. The surrounding ice showed no appreciable increase in thickness as the radar approached the well-defined edge. It is possible that impulse radar could be used to differentiate these hummocks from true ridges, which would be significantly thicker than surrounding ice and perhaps more difficult to break by ship.

Other features that stood out clearly in both the impulse radar and SAR records were refrozen melt ponds. Although these features were not examined by the surface party, they appeared from the air as circular areas of ice, several tens of metres in diameter, which had melted and later had refrozen to some depth. The impulse radar record showed these features with very pronounced V-shaped "bottom" echoes. Two interpretations are presented by Butt et al. (1979). One is based on the hyperbolic return profiles formed from point targets and a forward antenna velocity. The other relies on the presence of a water layer sandwiched between the refrozen top and original ice surfaces. However, due to slope variations in the hyperbolic tails and the need for a water layer in excess of 1 m thick in some places, neither of the explanations is wholly adequate. These features warrant further field investigation.

4. DATA ENHANCEMENT

As suggested by Rossiter et al. (1977), the radar signal itself may be used to establish crudely the electrical properties of the ice. An attempt has been made to estimate the relative attenuation between the top and bottom ice surface reflections from the return echo strengths (Butt and Gamberg, 1980; Rossiter et al., 1980).

Measurement of the ice attenuation involves computation of the signal losses at each interface of the air-snow-ice layers. For the case of no snow, attenuation can be calculated from:

$$E_b = E_t \times T_{ai} \times R_{iw} \times T_{ia} \times A \times \frac{1}{r^2} \quad (1)$$

where E_b is the received intensity of the bottom echo,

E_t is the intensity of the transmitted signal,

T_{ai} is the transmission coefficient at the air-ice interface,

R_{iw} is the reflection coefficient at the ice-water interface,

T_{ia} is the transmission coefficient at the ice-air interface,

A is the signal attenuation in the ice,

and r is the total signal path.

We usually assume that the geometric spreading losses ($1/r^2$) are compensated for by the time-varying (t^2) gain of the receiver.

Studies indicate that the effective reflection coefficient of a snow layer is significant. If a snow layer is present then the apparent transmission coefficient should be calculated for substitution into (1) (Butt and Gamberg, 1980).

Having calculated the total attenuation and measured the pulse travel time through the medium, an empirical relationship as described by Rossiter et al (1980), can be used to form an estimate of the ice thickness without first having to assume a dielectric constant. The dielectric constant can then, in turn, be calculated. Received signal strength (E_b) is determined from the magnitude of the peak of the cross-correlation between the received signal and an estimate of the transmitted signal (replica pulse). The location of this peak is also used to accurately determine the arrival time of the received pulse.

Figure 6 shows a sample of unprocessed data collected in the Beaufort Sea using the GSSI impulse radar. Figure 7 is the result of the same data set from Figure 6 that has had the cross-correlation technique applied. It clearly demonstrates the feasibility of producing accurate estimates of top and bottom echo arrival times. Due to time-base accurac in the radar system, most thickness results are calculated using a fixed dielectric constant near 4. From our data, this approximation gives thickness estimates accurate to ± 20% or better.

For ice displaying horizontal anisotropy (Kovacs and Morey, 1979; Langhorne, 1980), the orientation of the electric field determines the strength of the return echo. Therefore this factor must be considered in using the strength of the echo to determine ice properties. Initial analytical work (Rossite et al., 1980) indicates that it may be possible to estimate the orientation by using two orthogonal antennas. It would be necessary to measure the return echo from each antenna as well as the cross-completed component. Further work on this approach is underway.

In addition to the approaches presented above, standard signal enhancement techniques can be used on impulse radar data, such as averaging consecutive echoes to reduce random noise and pulse compression to delineate echoes more clearly. Although all the above procedures are still in the developing stages at C-CORE, they appear to offer ways of extracting more information from the return signal. Some techniques will prove too slow or cumbersome to use routinely, but we expect others to become an integral part of future ice sounding equipment and operations.

CONCLUSIONS

It is apparent that under some conditions sea ice can be sounded from airborne platforms. It is also true that not all types of sea ice, in all areas, or at all times, can be sounded by radio techniques. The limitations must be understood by potential users. Airborne use of radar sounders is still in the research stage, but with new types of instrumentation currently being designed, routine operational use is not too far in the future. It is likely that large strides towards an operational system will come not only with new har ware development, but also with greater understanding of the properties of sea ice and wit improvements in interpretation techniques. Al of these steps need to be followed in future research.

ACKNOWLEDGEMENTS

Financial support for this work was received from Department of Supply and Services Contract 1SU78-00347; Canadian Marine Drilling, Ltd.; Esso Resources Canada, Ltd.; and the National Research Council of Canada. Generous logistic support from Polar Continental Shelf Project is gratefully acknowledged. It is a pleasure also to acknowledge the many fruitful discussions on this topic with P. Langhorne, L. Davis, B. Mercer, R. Morey, A. Kovacs, R. Lowry, and our colleagues at C-CORE.

REFERENCES

Butt, K.A., Gamberg, J.B. and Rossiter, J.R. (1979), Remote Estimation of the Properties of Sea Ice, Impulse Radar Study of Lake Melville, Labrador, C-CORE Publication No. 79-7, 248 pp.

Butt, K.A. and Gamberg, J.B. (1980), Technology of an Airborne Impulse Radar, Proc. International Workshop on Remote Estimation of Sea Ice Thickness, St. John's, Sept. 25-26, 1979, In Press.

Campbell, W.J., Ramseier, R.O., Weeks, W.F. and Gloersen, P. (1975), An Integrated Approach to the Remote Sensing of Floating Ice, Proc. Third Canadian Symp. on Remote Sensing, Edmonton, Sept. 22-24, 1975, pp. 39-72.

Davis, J.L. (1980), Electrical Property Measurements of Sea ice In Situ Using a Wideband Borehole Radar and a Time-Domain Reflectometer, Proc. International Workshop on Remote Estimation of Sea Ice Thickness, St. John's, Sept. 25-26, 1979, In Press.

Kovacs, A. and Morey, R.M. (1979), Anisotropic Properties of Sea Ice in the 50- to 150-MHz Range, J. Geophys. Res., vol. 84, pp. 5749-5759.

Langhorne, P.J. (1980), Crystal Anisotropy in Sea Ice, Proc. International Workshop on Remote Estimation of Sea Ice Thickness, St. John's, Sept. 25-26, 1979, In Press.

Langhorne, P.J., Rossiter, J.R. and Keliher, T.E. (1980), Remote Estimation of the Properties of Sea Ice, Ice Core Analysis, Beaufort Sea, March 1979, C-CORE Data Report, in Preparation.

Mercer, J.B. (1980), Remote Sounding of Sea Ice - Past, Present, and Future Applications, Proc. International Workshop on Remote Estimation of Sea Ice Thickness, St. John's, Sept. 25-26, 1979, In Press.

Rossiter, J.R., Langhorne, P., Ridings, T. and Allan, A.J. (1977), Study of Sea Ice Using Impulse Radar, Proc. Fourth Intl. Conf. on Port and Ocean Eng. under Arctic Conditions, St. John's, Sept. 26-30, 1977, pp. 556-567.

Rossiter, J.R. and Butt, K.A. (1979), Remote Estimation of the Properties of Sea Ice, Beaufort Sea Field Trip Report - March 1979, C-CORE Publication No. 79-9, 36 pp.

Rossiter, J.R. (1980), Review of Impulse Radar Sounding of Sea Ice, Proc. International Workshop on Remote Estimation of Sea Ice Thickness, St. John's, Sept. 25-26, 1979, In Press.

Rossiter, J.R., Gamberg, J.B., Gidney, G., Santos, R. and Snellen, J.B. (1980), Remote Estimation of the Properties of Sea Ice, Analytical Techniques for Radar Sounding Data, C-CORE Technical Report, In Preparation.

Rossiter, J.R. and Bazeley, D.P. (1980), ed. Proc. International Workshop on Sea Ice Thickness, St. John's, Sept. 25-26, 1979, C-CORE Publication No. 80-5, In Press.

Snellen, J.B. and Rossiter, J.R. (1980), Remote Estimation of the Properties of Sea Ice, Surface Measurements, Beaufort Sea, March 1979, C-CORE Data Report, In Preparation

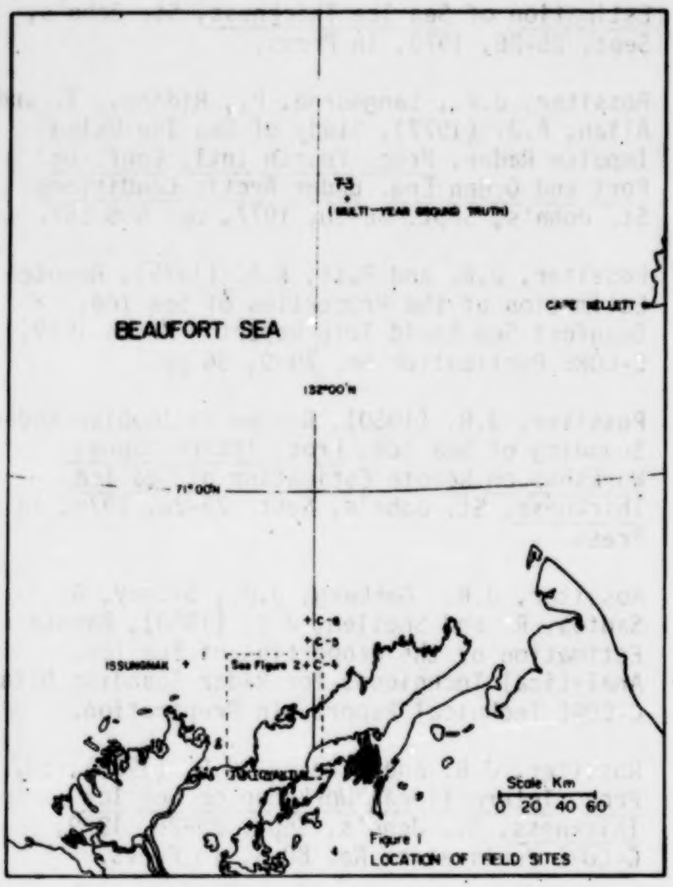
T-3
(MULTI-YEAR GROUND TRUTH)
CAPE KELLETT
BEAUFORT SEA
132°00'W
71°00'N
C-6
C-5
C-4
ISSUNGNAK
See Figure 2
TUKTOYAKTUK
Scale Km
0 20 40 60
Figure 1
LOCATION OF FIELD SITES

Figure 1 Location of field sites for impulse radar experiment, Beaufort Sea, March 1979.

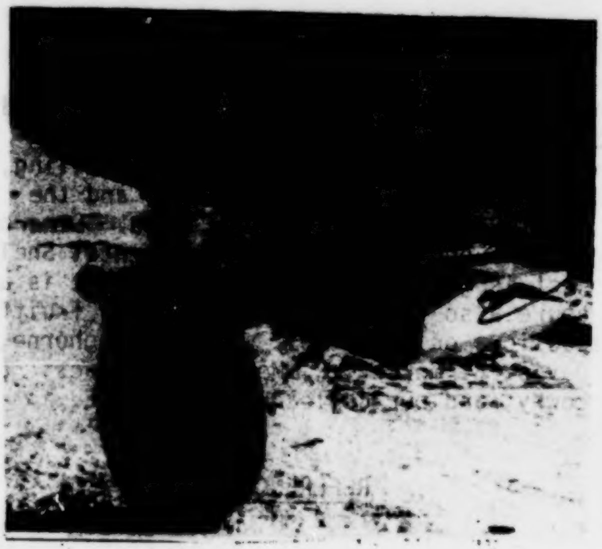

Figure 3 Impulse radar antenna, 200 MHz centre-frequency, mounted under a de Havilland Twin Otter directly aft of the nose wheel. This installation was the first reported use of impulse radar from a fixed-wing aircraft.

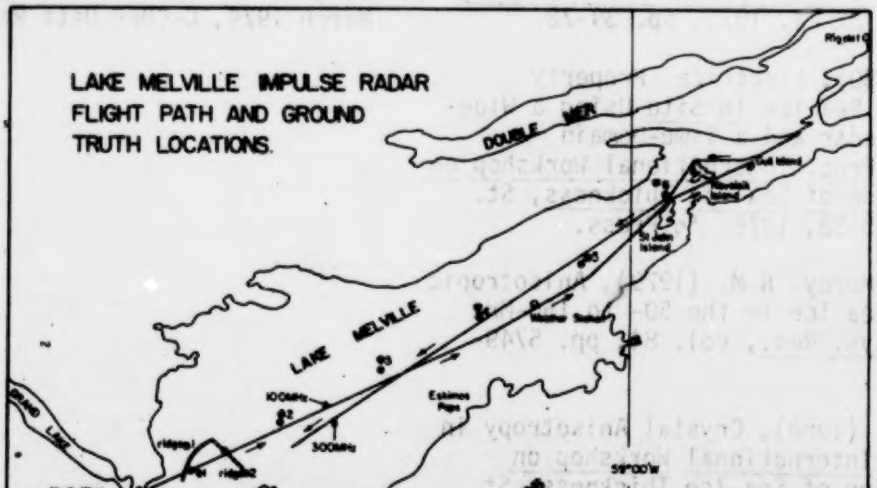
LAKE MELVILLE IMPULSE RADAR FLIGHT PATH AND GROUND TRUTH LOCATIONS.
Rigolet
DOUBLE MER
LAKE MELVILLE
GRAND LAKE
100MHz
300MHz
Eskimo Point
Weather Station
North West River
59°00'W
53°30'N
MEALY MOUNTAINS
GOOSE BAY
Happy Valley
Scale Km
0 10 20
Ground Truth Station
Figure 3(a)

Figure 2 Location of field sites for impulse radar flight paths and ground truth locations, Lake Melville, April 1979.

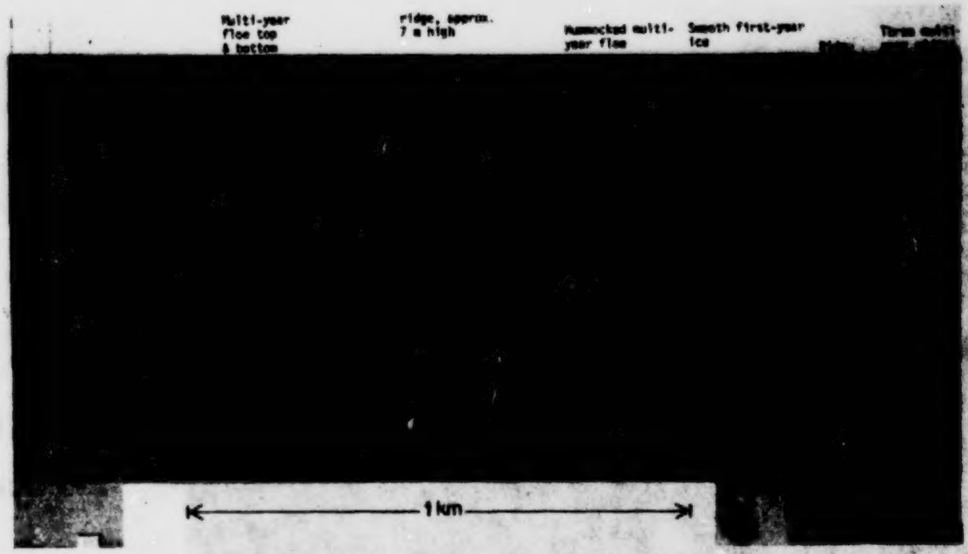

Figure 4 Airborne impulse radar profile taken from a Twin Otter at 30 m elevation and 50 m/s airspeed using a centre frequency of approximately 200 MHz. Multi-year floes typically have moderately rough hummocked upper surface; however, penetration appears to be variable from floe to floe. Reflections from the top of smooth first-year ice are strong; reflections from first-year ridges are very weak due to random scattering. The multi-year floe at the left with a clear bottom echo has an interpreted thickness of 2-3 m, assuming a dielectric constant of 3.5 for the ice. Symbols represent positions on aerial photograph in Figure 5 (Courtesy Canadian Marine Drilling, Ltd.).

Figure 5 Aerial photograph taken simultaneously with the radar record in Figure 4, but at an altitude of 2440 m. Solid line shows the flight path of the radar aircraft, which can be seen circled in the photograph. Various ice features, indicated by the different symbols, can be correlated with the radar record in Figure 4

Figure 6 Airborne impulse radar profile over site C-4, taken from a helicopter flying at approximately 10 m elevation and using a centre frequency of approximately 80 MHz. The horizontal bands marked "A" and "B" are systematic interference from the helicopter. This first-year sea ice had a thickness of approximately 1.15 m. Helicopter altitude increased to the left, beyond 28 sec. travel time. Vertical dashed lines are event markers; hyperbolic echoes are from reflectors placed on the ice surface.

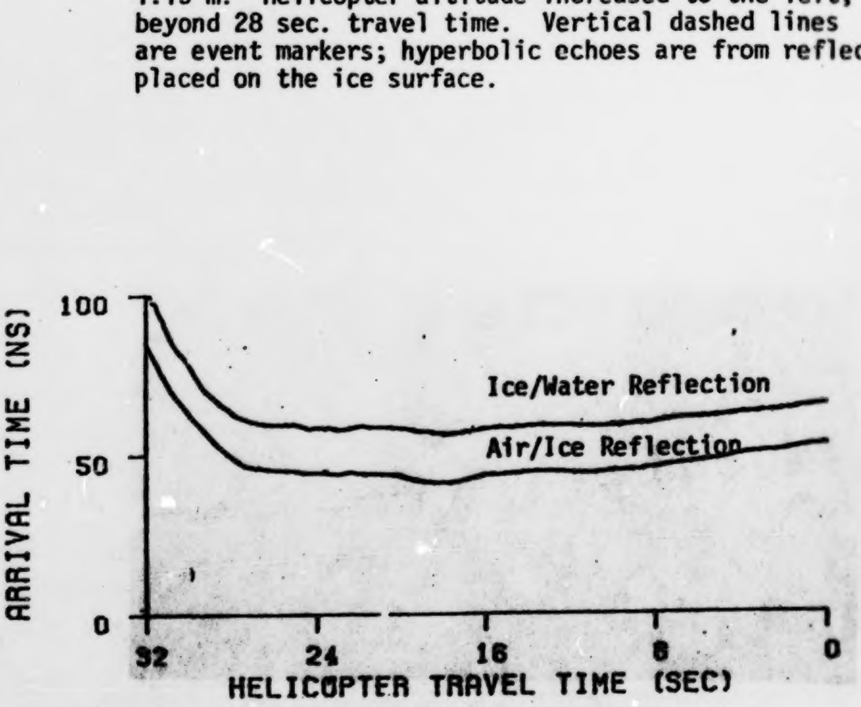

Figure 7 **Pulse arrival times from Figure 6 calculated using cross-correlation technique. Agreement with measured ice thickness was obtained using a dielectric constant of 3.7.**

SECTION 5.20

IMPULSE RADAR PROFILE OVER T-3

Rossiter J.R., K.A. Butt and J.B. Mercer

IMPULSE RADAR PROFILE OVER T-3

James R. Rossiter*, Kenneth A. Butt

C-CORE, Memorial University of Newfoundland
St. John's, Newfoundland, Canada A1B 3X5

and
J. Bryan Mercer

Dome Petroleum Limited
P.O. Box 200
Calgary Alberta
T2P 2H8

On March 17, 1979 an impulse radar profile was run over almost the entire length of Ice Island T-3, which was situated at the time in the Beaufort Sea at approximately 72°37'N, 131°34'W. The most probable flight path is shown in the Plan.

The radar (see Rossiter et al., 1980, for a description) was operated at a centre frequency of approximately 200-300 MHz from a Twin Otter aircraft flying at 30 m (100 feet) elevation and 50 m s^{-1} (100 knots) airspeed. The profile is shown in the figures, from scan 0 on the eastern side of the Island to scan 10,900 at the western edge.

No direct thickness measurements were made to confirm the soundings; however, using a dielectric constant of 3.2, typical for freshwater ice, the ice thickness is between 25 and 30 m along most of the traverse. This thickness compares with measurements made in 1973 by Holdsworth and Traetteberg (1973), giving an average thickness of 30 m and an ablation rate based on 1952 measurements (Crary, 1954) of approximately 1 m per year.

---

*Now with Huntec ('70) Ltd., 25 Howden Road, Scarborough, Ontario, Canada M1R 5A6

Also of interest is the large variation in the strength of the ice bottom echo; for example scans 1400-1500 compared to scans 3100-3200. It is not clear whether this fading is due to geometric effects or due to differing radio wave attenuation for different parts of the Island. There are occasional indications of possible internal reflections from within the ice (e.g. near scan 370), but they are small and relatively weak. At the western end of the Island the top of a large first-year ridge (scan 10,900) shows up quite clearly, followed by top and bottom echoes from first-year sea ice approximately 2 m thick.

These results appear to be the first airborne ice thickness profiling measurements made over an ice island, although Kovacs (1977) reported surface radar soundings. The measurements took only a few minutes of flying time, and therefore the technique has potential for future use in routine operational surveys (e.g. Rossiter and Gustajtis, 1978).

It is expected that further analysis of these records will be carried out for formal publication.

Acknowledgements

We are grateful to Canadian Marine Drilling Ltd., a subsidiary of Dome Petroleum, for the opportunity to make these measurements and permission to publish them. Thanks are also due to Terry Ridings of C-CORE who played an important role in installation and operation of the radar, and to Brian Gamberg of C-CORE who digitized and plotted the data.

C-CORE Publication No. 80-18.

REFERENCES

Crary, A.P., 1954. "Seismic Studies on Fletcher's Ice Island, T-3". Trans A.G.U., vol. 35, pp. 293-300.

Holdsworth, G., and Traetteberg, A., 1973. "The Deformation of an Arctic Ice Island", Proc. 2nd Int'l Conf. Port Ocean Eng. Arctic Conditions, Trondheim, pp. 419-440.

Kovacs, A., 1977. "Iceberg Thickness Profiling", Proc. 4th Int'l Conf. Port Ocean Eng. Arctic Conditions, St. John's pp. 766-774.

Rossiter, James R. and Gustajtis, A.K., 1978. "Iceberg Sounding by Impulse Radar", Nature, vol. 271, pp. 48-50.

Rossiter, James R., Butt, Kenneth A., Gamberg, J. Brian and Ridings, Terry F., 1980. "Airborne Impulse Radar Sounding of Sea Ice", Proc. 6th Con. Symp. Remote Sensing, Halifax, in press (reprinted in this volume).

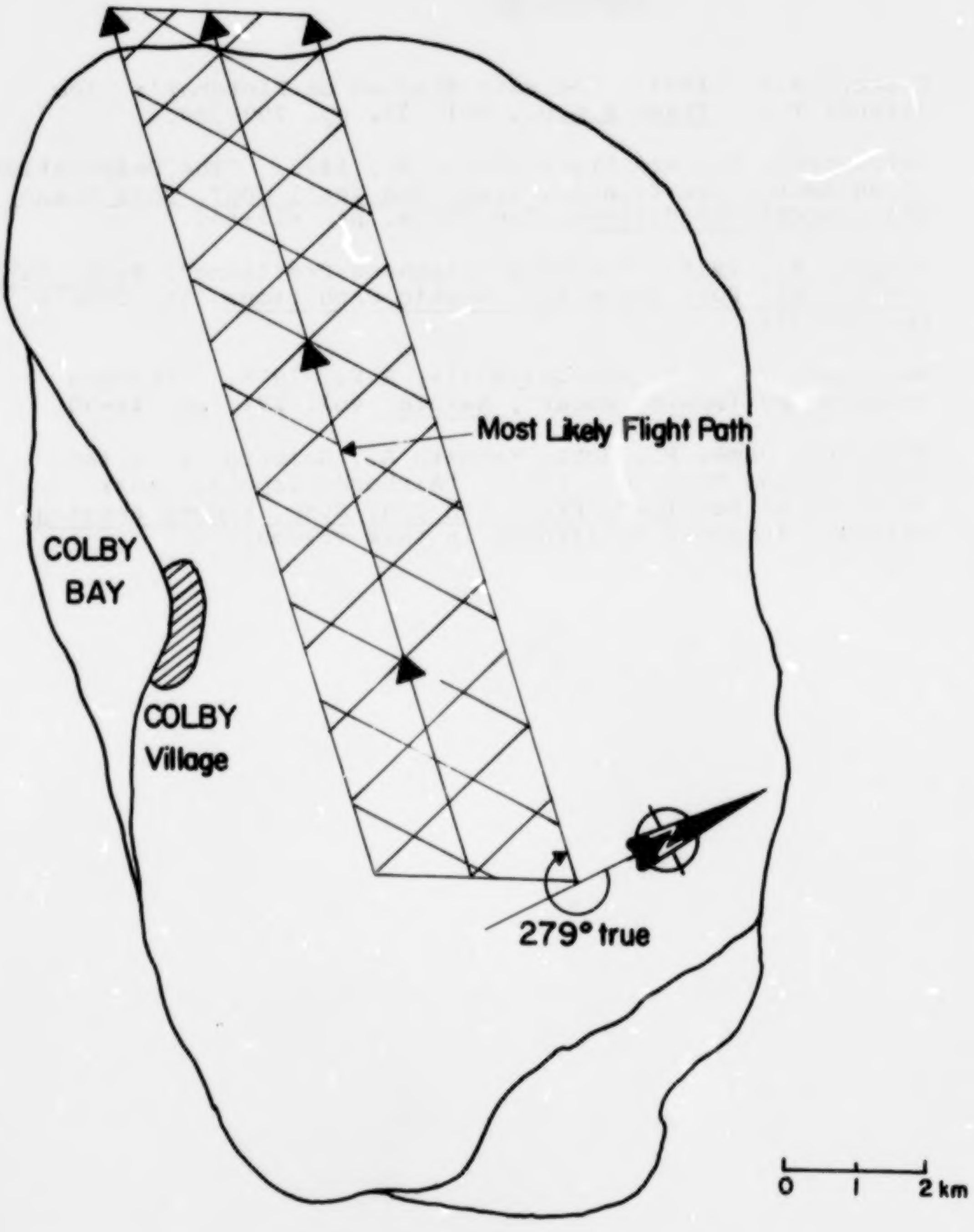
Most Likely Flight Path
COLBY BAY
COLBY Village
279° true
0 1 2 km

Plan view of Ice Island T-3, March 1979, showing boundary (cross-hatched area) of most likely path of Impulse Radar overflight. Arrows indicate direction of flight; centre line shows "true" bearing.

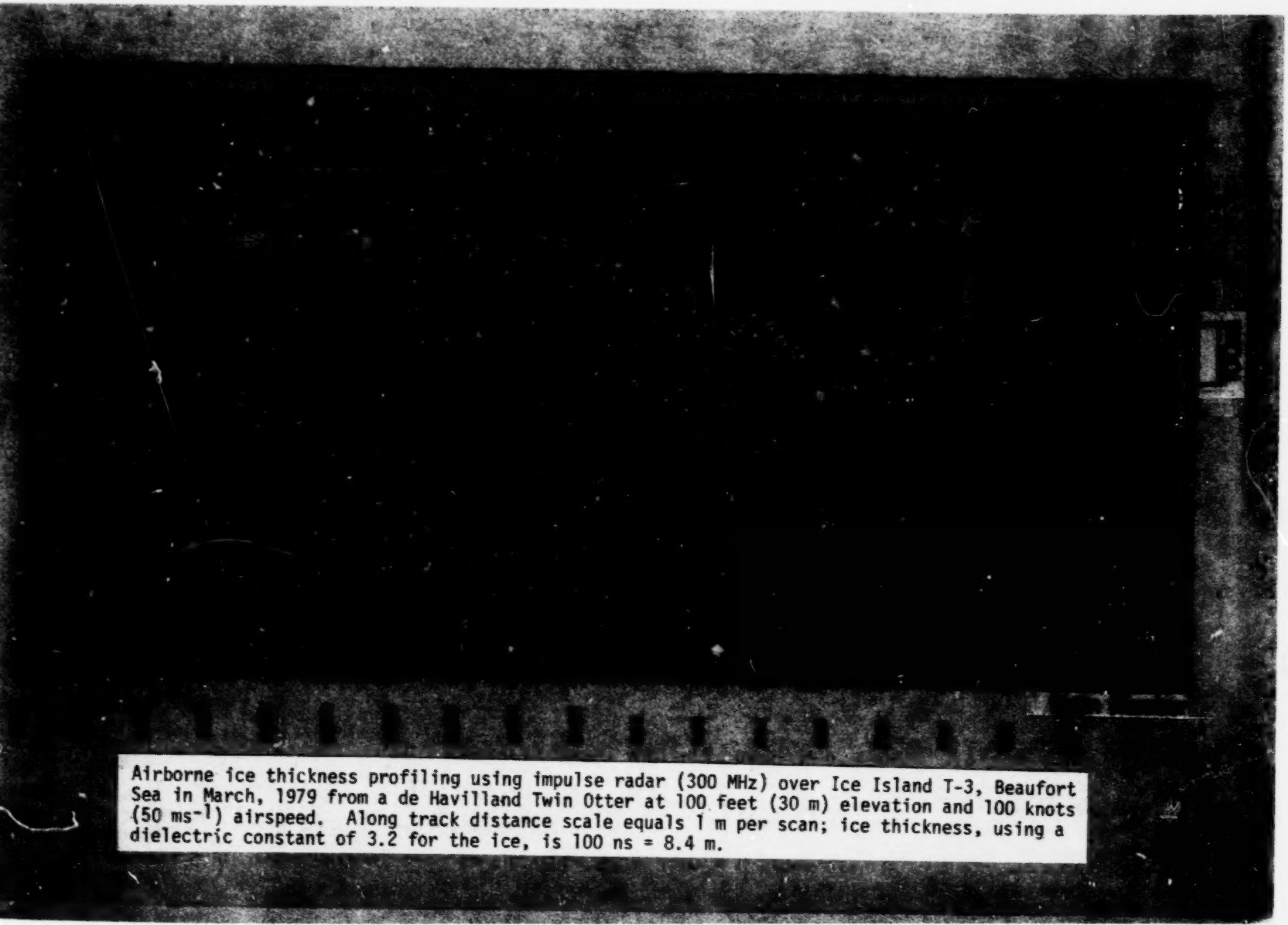

Airborne ice thickness profiling using impulse radar (300 MHz) over Ice Island T-3, Beaufort Sea in March, 1979 from a de Havilland Twin Otter at 100 feet (30 m) elevation and 100 knots (50 ms^{-1}) airspeed. Along track distance scale equals 1 m per scan; ice thickness, using a dielectric constant of 3.2 for the ice, is 100 ns = 8.4 m.

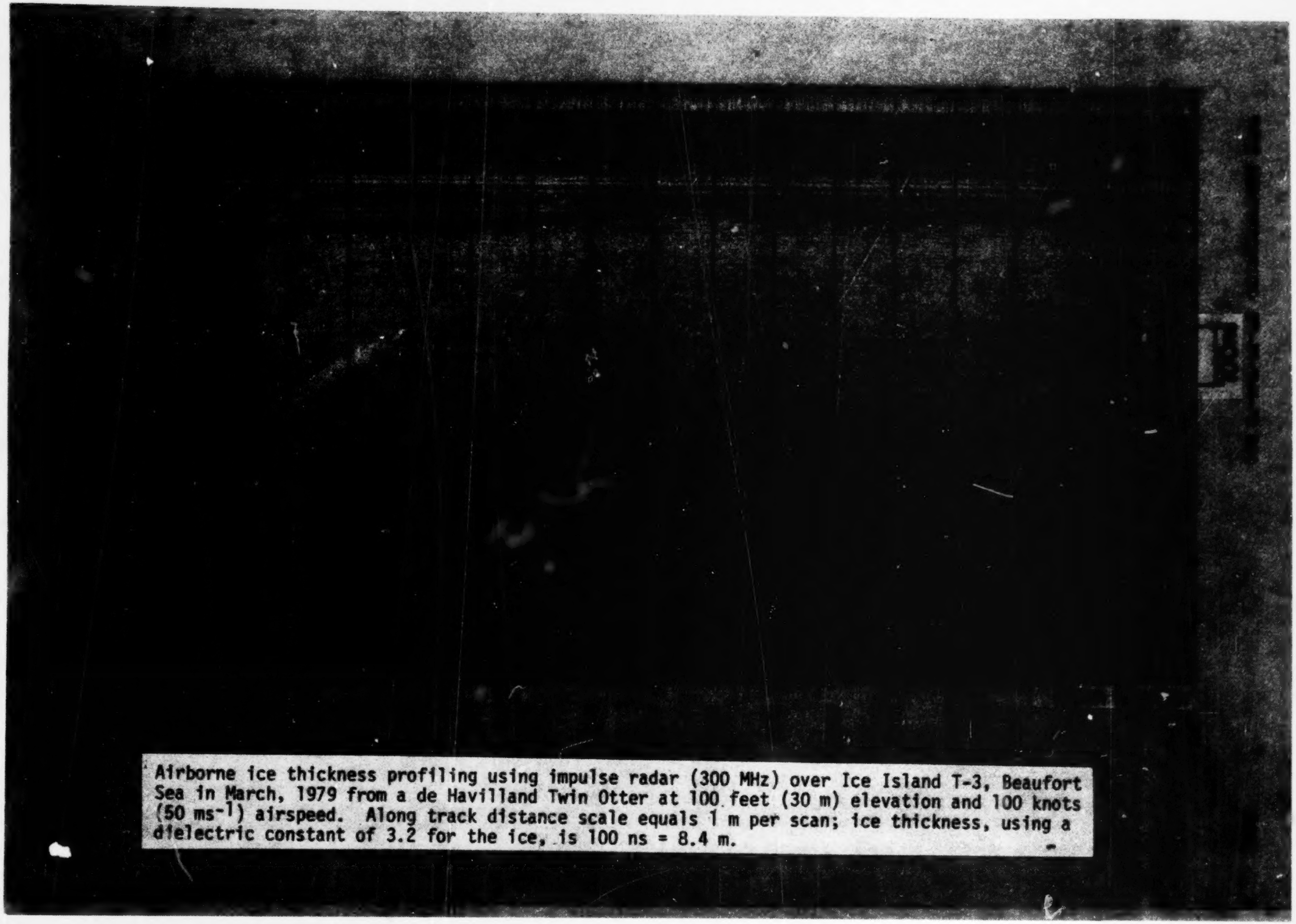

Airborne ice thickness profiling using impulse radar (300 MHz) over Ice Island T-3, Beaufort Sea in March, 1979 from a de Havilland Twin Otter at 100 feet (30 m) elevation and 100 knots (50 ms^{-1}) airspeed. Along track distance scale equals 1 m per scan; ice thickness, using a dielectric constant of 3.2 for the ice, is 100 ns = 8.4 m.

Airborne ice thickness profiling using impulse radar (300 MHz) over Ice Island T-3, Beaufort Sea in March, 1979 from a de Havilland Twin Otter at 100 feet (30 m) elevation and 100 knots (50 ms^{-1}) airspeed. Along track distance scale equals 1 m per scan; ice thickness, using a dielectric constant of 3.2 for the ice, is 100 ns = 8.4 m.

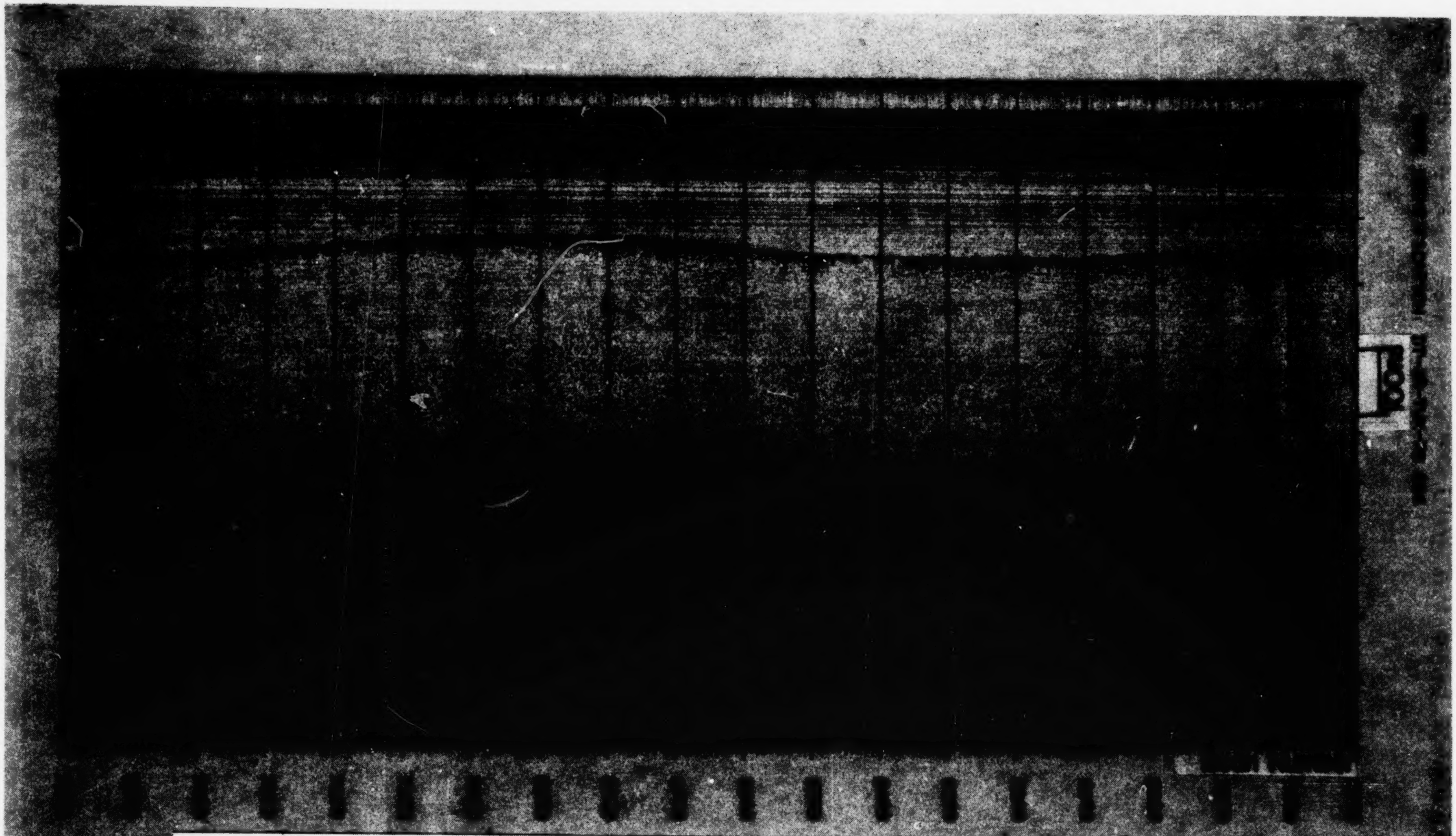

Airborne ice thickness profiling using impulse radar (300 MHz) over Ice Island T-3, Beaufort Sea in March, 1979 from a de Havilland Twin Otter at 100 feet (30 m) elevation and 100 knots (50 ms^{-1}) airspeed. Along track distance scale equals 1 m per scan; ice thickness, using a dielectric constant of 3.2 for the ice, is 100 ns = 8.4 m.

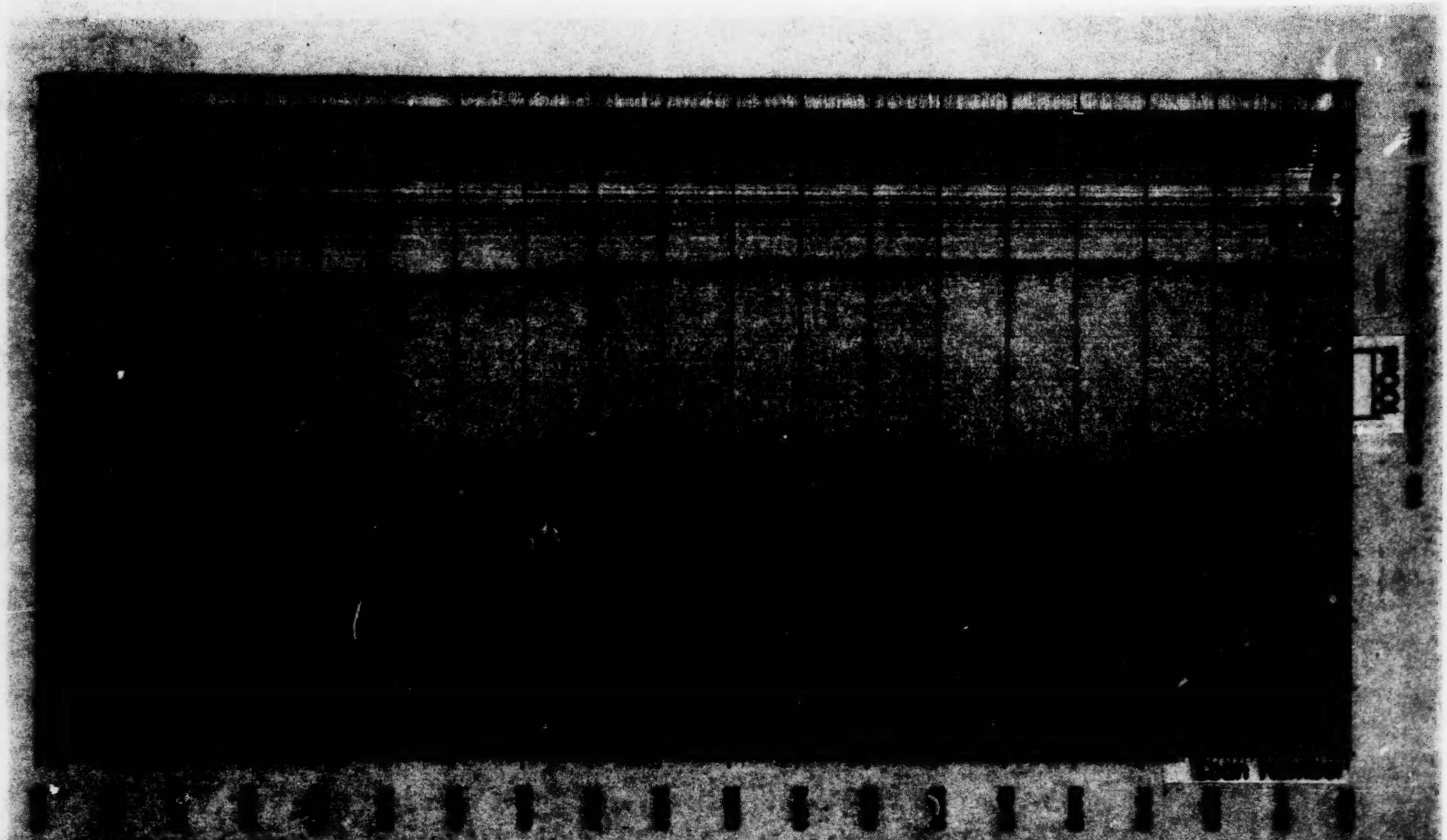

Airborne ice thickness profiling using impulse radar (300 MHz) over Ice Island T-3, Beaufort Sea in March, 1979 from a de Havilland Twin Otter at 100 feet (30 m) elevation and 100 knots (50 ms^{-1}) airspeed. Along track distance scale equals 1 m per scan; ice thickness, using a dielectric constant of 3.2 for the ice, is 100 ns = 8.4 m.

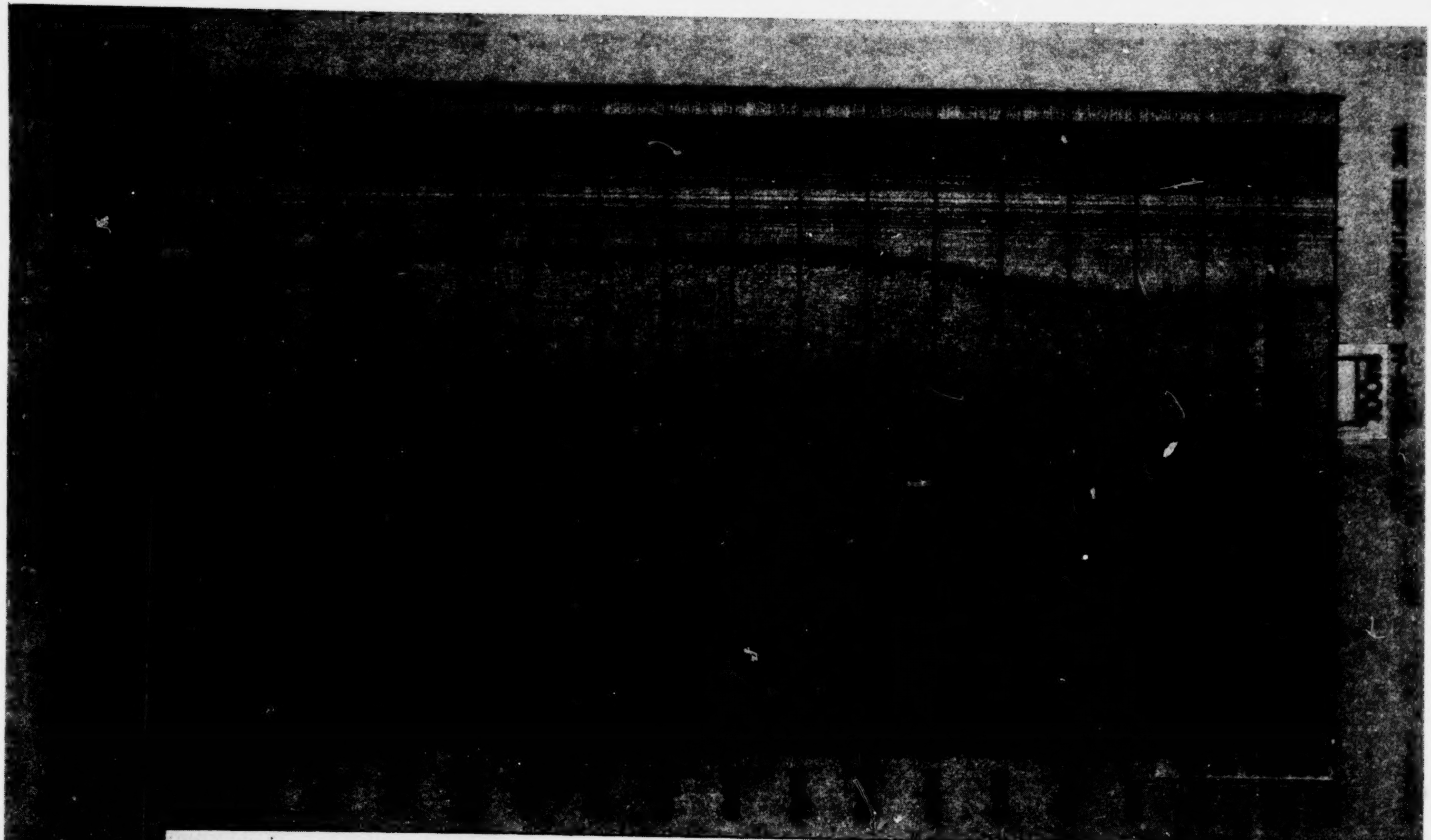

Airborne ice thickness profiling using impulse radar (300 MHz) over Ice Island T-3, Beaufort Sea in March, 1979 from a de Havilland Twin Otter at 100 feet (30 m) elevation and 100 knots (50 ms^{-1}) airspeed. Along track distance scale equals 1 m per scan; ice thickness, using a dielectric constant of 3.2 for the ice, is 100 ns = 8.4 m.

SECTION 5.21

LABRADOR ICE DYNAMICS EXPERIMENT (LIDEX)

Denner, W.W. and T.E. Keliher

LABRADOR ICE DYNAMICS EXPERIMENT (LIDEX)

W.W. Denner
T.E. Keliher

Presented at the SURSAT Workshop on Active and Passive Microwave Measurements of Sea Ice and Icebergs.

23-27 June 1980 Toronto

LABRADOR ICE DYNAMICS EXPERIMENT (LIDEX)

The Labrador Sea and Grand Banks are a very data sparce area, but it is becoming very important to obtain baseline oceanographic, sea ice, and iceberg data for the area. In the last few years the potential for hydrocarbon development has become very attractive, and along with the already existing fishing and shipping to Labrador and the Arctic, indicates an increasing need for information about the area before any more extensive developments take place. One of the most pressing areas has been the lack of current observations especially of the powereful Labrador Current, and sea ice and iceberg drifts rate off Labrador in the winter season. In order to meet this need, the idea of an ice dynamics experiment was brought forth.

The initial concept of this Labrador Ice Dynamics Experiment was to make the measurements very relevant to anticipated economic developments and to encompass as many research interests as possible. A workshop was held in St. John's, Newfoundland on 6-8 March 1980 in order to carry out an assessment of the needs for such an experiment. During the workshop panels were set up on transportation, fisheries, ice conditions, meteorology, oceanography, numerical modelling, remote sensing, and ocean engineering. The conclusion of these panels as well as a summary of the papers presented at the workshop will be contained in the proceedings of the workshop due to be published by the end of the summer.

In order to provide the necessary guidance of such a large experiment both a financial management panel to handle the financing aspects and a scientific panel to handle the technical aspects have been set up. As well it is anticipated to have a LIDEX office set up at Memorial University of Newfoundland to provide a central focus point for the various organizational aspects of the experiment, especially if some cross-pollenization can be carried out with ICEX and MIZEX programs.

A pilot program for LIDEX is planned for March 1981 with the installation of satellite reporting drift buoys, which would be supported by the National Science and Engineering Research Council of Canada. It is also planned to carry out spot current measurements through the ice as well as meteorological measurements when possible. It is also anticipated to have a numerical sea ice model ready for testing at this time.

The main portion of LIDEX is planned for winter 1981/82, however, the difficulty of organizing the large effort may force a delay until winter 1982/83. This main experiment would be more extensive than the pilot experiment with an initial proposal to include bottom mounted, long-term current measurements, integration with remote sensing, and more extensive iceberg monitoring. The program would also concentrate on the study of processes occurring at the ice edge.

SECTION 5.22

THE SPECIAL SENSOR MICROWAVE IMAGER (SSM/I) FOR THE DEFENSE METEOROLOGICAL SATELLITE PROGRAM (DMSP)

Burke, H.K., K.R. Hardy and J.C. Barnes

THE SPECIAL SENSOR MICROWAVE/IMAGER (SSM/I) FOR THE DEFENSE METEOROLOGICAL SATELLITE PROGRAM (DMSP)

by

Hsiao-hua K. Burke,
Kenneth R. Hardy and James C. Barnes
Environmental Research & Technology, Inc.

ABSTRACT

The SSM/I is a seven-channel microwave radiometer system which is to be part of the DMSP. It is planned to be launched during the first quarter of 1983 on the F-8 satellite. The instrument will scan a 1300 kilometer field of view every 1.9 seconds from an altitude of 830 kilometers, sensing radiation energy emitted and reflected from ice, land, ocean, and the atmosphere. The geophysical parameters to be derived from the sensor on an operational basis are rainfall rate, integrated rain and cloud water contents, ocean surface wind speed, sea ice characteristics, and soil moisture. Algorithms to retrieve the geophysical parameters have been developed. The techniques used to develop these algorithms are summarized.

Paper presented at SURSAT Workshop on Active and Passive Microwave Measurements of Sea Ice, AES, Toronto, 23-27 June 1980.

Introduction

Since the early 1970's, microwave radiometers flown on the Nimbus series satellites have been collecting essential sea ice data. The capability of the microwave sensors to observe the Earth's surface during both day and night and in all weather conditions has significantly increased the ice data base. The Special Sensor Microwave/Imager (SSM/I) is a seven-channel passive microwave sensor system designed for future Defense Meteorological Satellite Program (DMSP) missions. The SSM/I could be a vital source of data for ice programs since the system is scheduled to go into operation in early 1983, at a time when it is probable that no other satellite microwave system will be operable.

The baseline design of the SSM/I system was to maximize the overall effectiveness for real-time determination of (1) precipitation over ocean and land with accuracy of ±5 mm/hr, (2) ocean surface wind speed with accuracy of ±2 m/sec, (3) cloud water content with accuracy of $\pm.1\ kg/m^2$, (4) sea ice concentration with accuracy of ±12%, (5) ice edge and age determination and (6) soil moisture content. The characteristics of the sensor are given in Table 1. The highest frequency channels are designed specifically for estimating rain rates over land background to obtain both a better response and spatial resolution than is possible with any previous or current satellite microwave sensors.

The modeling of the microwave signature is done by computing the unit volume properties which govern the propagation of radiation through stratified layers of the atmosphere. In addition, the emissivities are also calculated using appropriate surface models. These properties are then used as input to the radiative transfer calculations which derive the final expected brightness temperatures for the seven channels.

TABLE 1

CHARACTERISTICS OF THE
SPECIAL SENSOR MICROWAVE/IMAGER (SSM/I)

Frequency	Polarization	Approximate Resolution
19.35 GHz	V and H	50 km
22.235 GHz	V	50 km
37 GHz	V and H	25 km
85.5 GHz	V and H	12.5 km

scan: constant look angle with respect to earth surface of 53°
scan swath: approximately 1300 km
scheduled launch: early 1983
satellite: DMSP F-8, altitude 830 km (450 nmi)

Overall Technique for Parameter Retrieval

The SSM/I channel utilization is designed to provide optimum processing time consistent with the accuracies required for the desired geophysical parameters. Over the ocean, data from four channels (19 H, 22 V, 37 V and H) will be utilized; over land six channels will be used (19, 37 and 85 GHz, all dual polarized). The channel utilization is summarized in Table 2. For all parameters other than those of sea ice, a statistical parameter inversion technique will be applied. For sea ice parameters, a deterministic inversion technique will be adopted.

The variability of the climates and seasons in which the parameters must be retrieved has to be taken into consideration for the inversion technique. Clearly, no single set of inversion algorithms could provide reasonable parameter estimates for all regions of the Earth. Because of these difficulties, the globe is divided geographically into three major

TABLE 2

DATA CHANNEL UTILIZATION FOR SSM/I

Parameters/ Frequencies (GHz)	19		22	37		85	
	V	H	V	V	H	V	H
Surface Wind Speed, Ocean		x	x	x	x		
Precipitation Over Ocean		x	x	x	x		
Cloud Water Ocean		x	x	x	x		
Land	x	x		x		x	
Liquid Water Ocean		x	x	x	x		
Land				x	x	x	x
Soil Moisture, Land	x	x					
Precipitation Over Land				x	x	x	x
Sea Ice Conditions							
Concentration		x		x	x		
Age				x			
Edge Location							

regions (tropical, mid-latitude, polar). The regions are, in turn, divided temporarily into seasons. Table 3 demonstrates the 14 different climate zones selected according to latitude and season.

TABLE 3

DEFINITION OF CLIMATE ZONES

	Degrees Latitude	Seasons	Backgrounds
Tropical	0°-20°	Warm (Jun-Nov) Cool (Dec-May)	Land, Ocean
Transition	20°-25°	Averaging Between Tropical and Midlat	
Mid-latitude	25°-55°	Spring/Fall Summer (Jun-Aug) Winter (Nov-Feb)	Land, Ocean*
Transition	55°-60°	Averaging Between Midlat and Polar	
Polar	60°-90°	Cool (May-Oct) Cold (Nov-Apr)	Land, Ocean*

*Including Sea Ice

Adding to the complexity of this scheme is the fact that a sudden transition from one region to the next, tropical to mid-latitude for instance, is undesirable. To smooth the changeover between these regions, a transition region can be defined. Parameters are derived in these regions by means of an averaging process between the parameters as derived for the neighboring regions.

Algorithms for Parameters Other Than Sea Ice

The basic tool used for retrieving the geophysical parameters (other than the ice parameters) from the brightness temperatures is the Statistical Parameter Inversion Method. The method seeks out significant statistical correlations between the simulated brightness temperatures and their associated parameters. To do this, it starts from an ensemble of simulated scenes. These scenes are represented by brightness temperatures associated with the physical parameters. The resulting correlations are contained in a set of matrix elements.

The underlying assumption for this technique is that there exists some linear combination of data elements which will provide a useful estimate of the desired parameters. The format is:

$$P = Co + \sum_{i} Ci * TBi$$

where P is the estimate of the parameter, TBi's are the brightness temperatures, and Ci's are the coefficients.

The matrix elements are computed by first selecting a set of approximately 500 radiosonde records representative of each climate zone. Then based upon the climatology for the climatic zone, a complete set of composite geophysical parameters is generated for each radiosonde record. Using radiative transfer models, brightness temperatures are simulated for each SSM/I channel and each of the 500 cases. From about one-half of the cases, matrix elements are derived by correlating the brightness temperatures with the geophysical parameters. The resulting matrix elements are applied to the brightness temperatures of the remaining 250 cases to compute estimated geophysical parameters. The root mean square error of the difference between these estimated parameters and the geophysical parameters associated with the brightness temperatures can then be computed. It is this rms error which is used to access the accuracy of the algorithm.

The algorithms over land can be summarized as follows. A frozen ground test is carried out first. If the ground is frozen, soil moisture content is set to indeterminate. Otherwise, the HEAVY RAIN test is carried out. If there is heavy rain, soil moisture and cloud water are set to be indeterminate while rain and liquid water are retrieved. A MAYBE RAIN test is finally carried out. If the test fails, rain parameters are set to be zero and soil moisture and cloud water are retrieved. Otherwise, all the parameters are retrieved.

The algorithms over ocean can be summarized as follows. There are tests for NO RAIN, MAYBE RAIN, or HEAVY RAIN. In the NO RAIN case, the rain rate and integrated liquid water are both set to zero and surface wind and cloud water are retrieved. In the MAYBE RAIN case, rain rate, integrated cloud and liquid water, and surface wind are all retrieved. If there is heavy rain, surface wind and integrated cloud water are set to indeterminate, while rain rate and integrated liquid water are retrieved.

Models for Sea Ice Parameters

The up-welling brightness temperature of a scene containing sea water and various amounts of sea ice is a function of the relative fractions of the ice components (e.g., First Year, Multiyear, First Year Thin) and water, their emissivities and thermal temperatures, and the amount of water vapor and liquid water in the atmosphere. Table 4 lists the emissivities of different types of sea ice at 19.35 and 37 GHz. It is shown that the difference between vertical and horizontal emissivities at 37 GHz exhibits significantly less dependence on ice age than the corresponding 19.35 GHz emissivity differences or the vertical and horizontal components of either frequency. This property can be employed to obtain the ice concentration using the deterministic inversion method. In this approach, equations for the microwave brightness temperatures are solved for the fraction of sea ice.

TABLE 4

EMISSIVITIES FOR VARIOUS ICE TYPES AND WATER

Ice Type	MY		FY Ice		FY Thin Ice		Water Calm Sea	
Polarization*	V	H	V	H	V	H	V	H
Frequency, GHz								
19.35	0.86	0.73	0.97	0.84	0.96	0.78	0.60	0.33
37	0.69	0.64	0.97	0.95	0.96	0.87	0.70	0.41
37 (V-H)	0.05		0.02		0.09		0.29	

*V - Vertical; H - Horizontal; 50° Earth Incidence Angle

Gloersen, P.H., J. Zwally, A.T.C. Chang, D.K. Hall, W.J. Campbell and R.O. Ramseier, 1978: Boundary-Layer Meteorology, 13, 339-359.

Ice age determination can be derived from the 37 GHz vertical brightness temperature value and computed value of ice concentration. This is accomplished by computing the effective average ice brightness temperature and comparing that value with the known first year and multiyear brightness temperature values.

The ice edge determination can be carried out using a two-dimensional interpolation technique. If a pixel is ice, the adjacent pixels will be tested. If any of these adjacent pixels is water, the center pixel will be flagged as ice edge.

Status of SSM/I Development

The SSM/I program is a joint effort of the U.S. Air Force and Navy. The prime contractor for the program is Hughes Aircraft Company. Environmental Research & Technology, Inc. (ERT), as a subcontractor, is responsible for algorithm development of parameter extraction, verification, and update components.

The SSM/I, which is scheduled for launch in early 1983 on the DMSP F-8 mission, will be the first microwave sensor system for which the data will be processed in real-time. Although the primary use of the SSM/I will be to provide data to the Air Force Global Weather Central and the Navy Fleet Numerical Weather Center, it is anticipated that the data will also be available to other users, such as the sea ice community.

5.23 - LIST OF WORKSHOP PARTICIPANTS

ATTENDEE	ADDRESS	TELEPHONE NUMBER
Ms. Lyn Arsenault Cold Regions Remote Sensing	Box 526 Stittsville, Ont., KOA 3GO	(613) 836-4003
Mr. J.C. Barnes Environmental Research & Technology, Inc.	696 Virgina Road Concord, Mass. U.S.A., 01742	(617) 369-8910
Mr. Clinton J. Bowly Environmental Research and Technology, Inc.	696 Virginia Road Concord, Mass. U.S.A., 01742	(617) 369-8910
Dr. W. Campbell U.S. Geological Survey	Thompson Science Hall Room 119 Univ. of Puget Sound Tacoma WA, USA, 98416	(206) 593-6517
Dr. Frank Carsey NASA	Goddard Space Flight Centre Greenbelt MD, 20771	(301) 344-8513
Mr. J. Crawford NASA	Langley Research Center Hampton, Virginia U.S.A., 23665	(804) 827-3631
Dr. V. Delnore NASA	Langley Research Center Hampton, Virginia U.S.A., 23665	(804) 827-3631
Dr. W.W.Denner Nfld. Inst. for Cold Ocean Science	Memorial Univ. of Nfld. St. John's Newfoundland, A1B 3X7	(709) 737-8833
Mr. H. Edel Ocean and Aquatic Sciences	Marine Sciences & Information. Directorate 580 Booth Street Ottawa, Ontario, K1A OH3	(613) 995-3966
Dr. T. Grenfell Dept. of Atmospheric Sciences	AK-40, University of Washington Seattle, WA, USA, 98195	(206) 543-9411
Dr. R.K. Hawkins Canada Centre for Remote Sensing	Dept. of Energy, Mines & Resources Limebank Road, Ottawa, Ont.	(613) 998-9060
Mr. H.G. Hengeveld Ice Branch, Atmospheric Environment Service	4905 Dufferin Street Downsview, Ontario M3H 5T4	(416) 667-4724

ATTENDEE	ADDRESS	TELEPHONE NUMBER
Dr. R. Inkster Intera Environmental Consultants Ltd.	Suite 204 2841 Riverside Dr. Ottawa, Ontario, K1V 8N4	(613) 523-5530
Mr. Brian Jonasson Petro-Canada	1350 Guiness House 727 7th Avenue S.W. Calgary, Alberta, T2P 0Z6	(403) 232-8745
Dr. L. Jones NASA	Langley Research Center Mail Stop 490 Hampton, Virginia, U.S.A., 23665	(804) 827-3631
Mr. T. Keliher Nfld. Institute for Cold Ocean Science	Memorial Univ. of Nfld. St. John's Newfoundland, A1B 3X7	(754) 737-8877
Mr. R. Ketchum U.S. Navy	Naval Ocean R&D Activity (NORDA) NSTL Station, Code 332 Mississippi, USA, 39529	(601) 688-4810
Mr. M. Kirby Intera Environmental Consultants Ltd.	2841 Riverside Dr. Suite 204 Ottawa, Ontario, K1V 8N4	(613) 523-5530
Dr. C. Livingstone Canada Centre for Remote Sensing	Dept. of Energy, Mines and Resources 2464 Sheffield Road Ottawa, Ont., K1A 0Y7	(613) 998-9060
Dr. R. Lowry Intera Environmental Consultants Ltd.	2841 Riverside Drive Suite 204 Ottawa, Ontario, K1V 8N4	(613) 523-5530
Mr. C. Luther Office of Naval Research	Code 461 800 N. Quincy Street Arlington, Virginia U.S.A., 22217	(202) 696-4118
Mr. W. Markham Ice Branch, Atmospheric Environment Service	4905 Dufferin Street Downsview, Ontario M3H 5T4	(416) 667-4727
Ms. Lyn McNutt Univ. of Washington	3711 15th Ave. N.E. Seattle, WA, U.S.A.	(206) 543-5276
Dr.B. Mercer Dome Petroleum	P.O. Box 200 Calgary, Alberta, T2P 2H8	(403) 232-6395
Mr. J. Miller Petro-Canada	1350 Guiness House 727 7th Avenue S.W.	(403) 232-8831 (Office) (403) 283-7617 (Home)

ATTENDEE	**ADDRESS**	**TELEPHONE NUMBER**
Dr. R. Moore University of Kansas	Remote Sensing Laboratory University of Kansas 2291 Irving Hill Drive Lawrence, Kansas, USA, 66045	(913) 864-4836
Dr. G. Mourad Battelle Columbus Laboratories	505 King Avenue Columbus, Ohio, USA, 43201	(614) 424-5097
Mr. T. Mullane Ice Forecsting Central Atmospheric Env. Service	Trebla Building 473 Albert Street Ottawa, Ontario, K1A OH3	(613) 996-5236
Dr. V. Neralla Atmospheric Env. Service	4905 Dufferin Street Downsview, Ontario, M3H 5T4	(416) 667-4849
Mr. D. Pearson Intera Environmental Consultants Ltd.	Suite 204 2841 Riverside Dr. Ottawa, Ont., K1V 8N4	(613) 523-5530
Dr. S. Peteherych Atmospheric Environment Service	4905 Dufferin Street Downsview, Ontario M3H 5T4	(416) 667-4815
Dr. R. Ramseier Atmospheric Environment Serv.	c/o Ice Forecasting Central Atmospheric Environment Service Trebla Building 473 Albert Street Ottawa, Ontario, K1A OH3	(613) 996-5630
Dr. J. Rossiter Huntec 70 Limited	25 Howden Road Scarborough, Ontario M1R 5A6	(416) 751-8055
Ms. R. Santos C-CORE	Memorial Univ. of Nfld. St. John's Newfoundland, A1C 5S7	(709) 737-8353
Mr. R. Schertler NASA	Lewis Research Center 2100 Brook Park Road Cleveland, Ohio, U.S.A., 44135	(216) 433-4000 Ex. 754
Mr. D. Schwab Gulf Resources Inc.	Frontier Research Box 130, Calgary, Alberta	(403) 233-3893
Mr. G. Spedding Esso Resources Canada Ltd.	Production Research Division 339-50th Ave. S.W. Calgary, Alberta, T2G 2B3	(403) 259-0335
Dr. Niels Skou Technical Univ. of Denmark	Building 348 DK2800 Lyngby, Denmark	(02) 881444

ATTENDEE	**ADDRESS**	**TELEPHONE NUMBER**
Dr. F. Stone OAO Corporation	50/50 Powder Mill Road Beltsville, Md. U.S.A., 20705	(301) 937-3090
Dr. C. Swift NASA	Langley Research Center Hampton, Virginia, U.S.A., 23665	(804) 827-3631
Dr. G. Tang State University of New York at Buffalo	Dept. of Electrical Engineering 223 Bell Hall Amherst, N.Y., USA, 14260	(716) 636-2424
Mr. M. Warren C-CORE	Memorial Univ. of Nfld. St. John's Newfoundland, A1C 5S7	(709) 726-9209
Mr. E. Wedler Air, Earth and Oceans Ltd.	P.O. Box 54 Oshawa, Ontario, L1H 7K8	(416) 728-4179
Dr. W. Weeks U.S. Army Cold Regions Research and Engineering Laboratory (CRREL)	P.O. Box 282 Hanover, N.H., USA, 03755	(603) 643-3200
Mr. F. Wentz Remote Sensing Systems	Sausalito, California, USA	(415) 332-8911

6. SURSAT ICE EXPERIMENT

6.1 INTRODUCTION

The report on Satellites and Sovereignty published by the Government of Canada (1977) identified marine transportation, resource development and exploitation as major application areas needing ice reports and forecasts.* The need for this information was identified by several departments (Table 6.1).

Table 6.1

List of Departments Requiring Ice Reports and Forecasts

ENERGY, MINES AND RESOURCES	(EM&R)
ENVIRONMENT	(DOE)
FISHERIES AND OCEANS	(DFO)
INDIAN AND NORTHERN AFFAIRS	(DINA)
NATIONAL DEFENCE	(DND)
TRANSPORT	(DOT)

Since the above-mentioned document was published, the Atmospheric Environment Service has created the Canadian Climate Centre. Climate has been identified as an additional application where ice information is required.

In order to plan the ice experiment, the 19 proposals relevant to ice which were received on solicitation by the SURSAT Project Office were combined into 3 experiments. Each experiment covered a particular geographic area representing different ice conditions. These included the Beaufort Sea which has predominantly first-year and multi-year ice; the Baffin-Labrador Seas with predominantly first-year ice, icebergs and a marginal ice zone; and the Gulf of St. Lawrence with predominantly thin first-year ice. Figure 6.1 identifies the different test sites. Unfortunately, the Gulf of St. Lawrence experiment could not be carried out due to technical difficulties (Intera, 1980). All other experiments were carried out to a successful conclusion.

Table 6.2 lists the various agencies which participated in the ice experiment. We were fortunate to have a large international effort as well as an excellent mix between Government, Industry and Academia. The various groups met at several workshops to plan for the experiments. Since the analysis of the vast amount of data which was collected is going to continue, it was felt that certain key activities should be included in the SURSAT final ice report which would permit the design of a straw-man ice information and service system.

---

*Appendix 6.1 Interdepartmental Task Force on Surveillance Satellites - Census of Surveillance Requirements for ice.

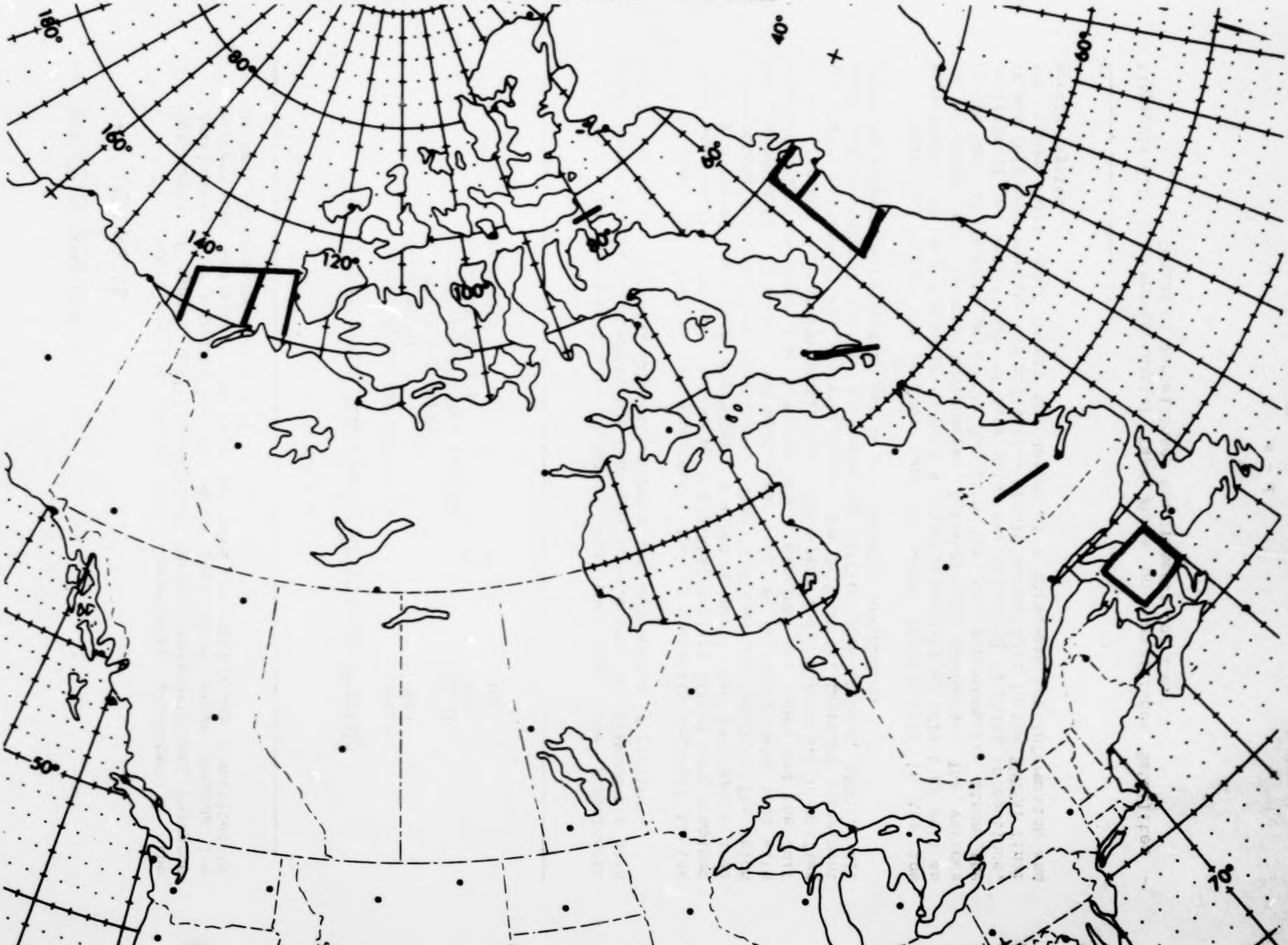
180°
160°
80°
140°
120°
100°
80°
60°
40°
60°
50°
70°

FIGURE 6.1 - LOCATIONS OF SURSAT ICE EXPERIMENT TEST SITES

Table 6.2

Participants in SURSAT Ice Experiment by Agencies Only

GOVERNMENT

Atmospheric Environment Service
Canada Centre for Remote Sensing
Canadian Coast Guard
Communications Research Centre
Defence Research Establishment
Geological Survey of Canada
National Research Council
Ocean & Aquatic Sciences
Polar Continental Shelf Project
NASA Langley
NASA Lewis
NASA Houston
Naval Ocean Research and Development Activity
Office of Naval Research
U.S. Coast Guard
U.S. Geological Survey
Danish Meteorological Institute
Island Command Greenland
Royal Danish Air Force

INDUSTRY

Canadian Marine Drilling
Cold Regions Remote Sensing
Environmental Research Institute of Michigan
Esso Resources Canada
Gulf Canada
Innotech
Intera
Nordco
Petro Canada
Remotech Applications
Steltner Development
Total Eastcan Exploration

UNIVERSITY

C-CORE
Scott Polar Research Institute
Technical University of Denmark
University of Kansas
York University

It should also be pointed out at this time that due to the premature failure of SEASAT-1 no planned ice experiments were carried out, and no airborne and surface information was collected simultaneously with a SEASAT overpass. Planned activities were carried out with NIMBUS-7 using the SMMR 9 (Scanning Multifrequency Microwave Radiometer). Table 6.3 gives the periods at which airborne and surface measurements were carried out with simultaneous NIMBUS-7 SMMR coverage on even Julian days. Most of the analysis using SMMR data will occur well after the publication of this document.

Table 6.3 NIMBUS-7 SMMR COVERAGE

NAME OF EXPERIMENT	DATE	ACTIVITIES	
	1979	Airborne	Surface
SURSAT BEAUFORT	Feb 12	X	
SURSAT BEAUFORT	March	X	X
AES OPERATIONS	All year	X	Some
WIEBS	Dec	X	X
	1980		
AES OPERATIONS	Feb	X	Limited

Table 6.4 gives a listing of the various research projects being carried out as agreed amongst the participants at the workshop held in Toronto on May 30-31, 1979, and partially updated as of December 1, 1980.

Table 6.4

SURSAT ICE PROJECTS

Project No.	Project	Project Team	General Project Area
1+	Statistics of scattering coefficients for varying ice types (scatt, rad, SAR) over specific sites.	*Livingstone, Gray Hawkins, Arsenault, Pearson, Jones	Beaufort and Eastern Arctic
2+	Reconnaissance Ice Parameters (simulate different radar products)	*Lowry, Hengeveld, Klooster	Beaufort
3+	Incidence angle of radar imagery	*Gray, Hengeveld, Schertler, Larson	Beaufort, Baffin Bay
4+	SAR vs SLAR comparison	*Hengeveld, Schertler	Beaufort and Eastern Arctic
5	Digital image processing (SAR) - 4 channel registration and signature	*Lowry, Larson, Kirby	Beaufort and Eastern Arctic
6	Radar return vs ridge parameters	*Mercer, Lowry, Schertler	Beaufort
7+	Surface scattering and airborne TRAMAS	*Onstott	Beaufort
8	Cross correlation of SAR with other data sets, eg. photography (including meltponds)	*Spedding, Mercer, Schwab, Arsenault, Ketchum, Inkster	Beaufort and Eastern Arctic
9+	SEASAT SAR Analysis	*Hengeveld, Peteherych, Spedding Schwab, Kirby	Beaufort
10	NIMBUS-SMMR signatures	*Ramseier, Peteherych, Campbell, Barnes, Neralla, Gloersen	Beaufort and eastern Arctic
11	Digital Landsat vs Radar	*Kirby, Lowry, Larson, Schertler	Beaufort and Eastern Arctic

12	Radar shadows from pressure ridges	*Mercer, Lowry, Gray	Beaufort
13	Ice dynamics from digital SEASAT images	*Ramseier, Campbell, Teleki, Kirby, Neralla, Zwally, Lowry, Lapp	Prince of Wales Strait, Beaufort Sea
14	Iceberg detectability	*Kirby, Gray, Hawkins, Larson	Eastern Arctic
15	Penny Ice Cap	cancelled	
16+	Danish Experiment	*Gray, Gudmandsen, Overgaard, Skou, Sondergaard, Pedersen	Eastern Arctic
17	Swell in ice cover	*Wadhams, Lowry	Eastern Arctic
18	RTP SAR evaluation	*Inkster, Leung	Beaufort and Eastern Arctic
19++	Sea ice thickness by impulse radar techniques	*Rossiter	Beaufort, Lake Melville
30	Iceberg detectability (SLAR)	*Ramseier, Lapp	Eastern Arctic
31	Melt pond dynamics and morphology	*Kirby, Pearson, Ramseier, Lapp	Arctic
32	Dynamics of sea ice with the use of passive microwave data	Neralla, Ramseier, Crawford	Beaufort
33+++	Lake Melville SAR and photoanalysis	*Remotech	Labrador

*Indicates Team Coordinator

+Summary Reports included in the final Sursat documentation

++See Appendix A2 for reports available

+++Part of NORDCO, Lake Melville/Offshore Labrador Experiment

Priority 2 Research Projects

Project No.	Project	Project Team	General Project Area
20	Parameter extraction from SAR imagery'	*Ramseier, Scherter, Inkster, Luther	Beaufort and Eastern Arctic
21	Radar return vs microstructure	*Lowry, *Ramseier, *Gray	Beaufort
22	Radar return vs salinity (scatterometer, SAR)	*Onstott, *Lowry, Luther	Beaufort
23	Freshwater ponds and river channels	*Ramseier, Lowry, Rossiter	Beaufort
24	Ice dynamics from aircraft data (SLAR and SAR)	*Hengeveld, Neralla Mercer	Beaufort
25	MY ice Site 2	Overall effort	
26	FY ice Site 1(A)	Overall effort	
27	MY and FY ice distribution	Overall effort	
28	Snow effect on radar signatures	Overall effort	
29	Study of T-3	*Rossiter, Luther, Hengeveld	Beaufort

6.2 EXPERIMENTAL PROCEDURES

The organization of ice experiments was quite different from the Lands experiments (Intera, 1980). For agriculture, forestry, cartography, geology and similar experiments, individual principal investigators submitted experiment proposals which were evaluated by the Experiment Selection Panel. Usually, the investigator was familiar with the test site and supplied all required ground truthing and analysis facilities in return for the imagery and other data collected by the SAR-580. The ice experiments, however, were organized into several major sorties with the collected data being shared and analyzed by some 40 principal investigators. The main reasons for this approach were the logistical difficulties and expenses involved with both airborne and surface-based measurement operations in the Arctic.

Three ice sorties are described in the Airborne Experiment Plan (Intera, 1978) and in more detail in the SURSAT Ice Experiment Plan (SSPO, 1979). The first experiment, called the Gulf of St. Lawrence Experiment was scheduled for the second and third weeks of February 1979. Unfortunately,

---

*Indicates Team Coordinator

early in February both the SAR-580 and the participating Coast Guard Search and Rescue vessel Alert developed problems, and the sortie was first delayed and then re-scheduled for May 1979. Fortunately, young ice forms, like those typically seen in the Gulf of St. Lawrence, were imaged on the coast of Labrador and along the Greenland coast during Sortie 79-3. Sortie 79-2, the Beaufort Sea ice experiment, was scheduled for March 1979, and operations were successfully completed on schedule. Sortie 79-3, the Eastern Arctic ice experiment, was planned for mid-April and took place on schedule.

Sortie 79-2, the Beaufort Sea ice experiment, was the most ambitious single experiment conducted during the Airborne Sensing Program (ASP). It involved about 100 people including aircrews, six aircraft, two helicopters, and an impressive array of remote sensing and surface truth equipment. The SAR-580, based in Yellowknife, flew three missions over the Southern Beaufort Sea collecting scatterometer data, radiometer data*, photography, and SAR imagery at steep and shallow depression angles and in wide swath mode.

Sortie 79-3 took place in April 1979 along the coast of Labrador to Southern Baffin Island, across Davis Strait to Greenland, north to Thule and finally returning by the north end of Baffin Island. Five remote sensing aircraft from Danish, American and Canadian agencies were involved and the data sets collected generally had coincident coverage by several sensors. Ice and weather conditions were quite different from those experienced in the Beaufort Sea, and this factor has allowed more general conclusions to be drawn regarding the utility of SAR for sea ice reconnaissance.

Since the publication of the Airborne Experiment Plan, additional ice data collections have been planned and conducted. First, during Sortie 78-3, along the east coast of Baffin Island, an opportunity was taken to image grounded icebergs under a variety of sea states. These data have been used to study the detectability of icebergs using SAR. Second, a joint industry-government experiment supported by Petro-Canada was conducted in the Lancaster Sound area in September 1979. The detectability of small icebergs was investigated and the ability of various analysis techniques to re-identify the same berg seen on different days was evaluated. Finally, another joint industry-government project was conducted with CANMAR, the drilling subsidiary of Dome Petroleum. During November and December 1979, the ability of SAR to support drilling and shipping operations in the Beaufort Sea was demonstrated.

6.3 DISCUSSION OF CONTRIBUTIONS TO FINAL SURSAT MEETING.

6.3.1 Summary of the SURSAT active-passive microwave sea ice experiment.

The preliminary results as reported by Hawkins et al (1980) were obtained in March 1979 in the Beaufort Sea and during April 1979 in the eastern Arctic. The objective was to measure the radar backscattering cross section at 13.3 GHz and emissivity at 19.4 GHz at viewing angles appropriate to satellites. Subsequent analysis of the data was an extension of previous work on microwave properties of sea ice. It is the first study correlating both active (scatterometer) and passive (radiometer) microwave data into a sea-ice classification scheme. The detection of ice bergs and ice pressure ridges formed another facet of the study. In each case, the effect of incidence angle and polarization was determined.

---

*19.4 GHz radiometer on loan from NASA Langley.

The extent to which single sensor information can be used to separate ice classes was examined and the advantage of combining data from more than one sensor was assessed. The following classes and subclasses of sea-ice conditions were identified during the experiment using aerial (Dunbar, 1969) photographic methods. The classes are listed generally in order of thickness and age (thicknesses from WMO Sea Ice Nomenclature).

ICE TYPE	THICKNESS
Open sea water	
Frazil	
Grease	
Dark nilas	5 cm
Light nilas	5 cm
Grey	10-15 cm
Grey-white	15-30 cm
Smooth first-year	30 cm-2.0 m
Rough first-year	
Smooth second-year	
Rough second-year	
Smooth multi-year	3 m
Rough multi-year	
Ice island	

Not all classes of ice were studied under the same condition, and/or in the same region but enough overlap in data was obtained to be useful in comparing classes. Included in the list of factors found in the experiment to determine the microwave properties of sea ice are:

1) Surface roughness
2) Temperature history of the ice
3) Temperature, salinity and brine volume fraction controlling the dielectric constant (Vant, 1976)
4) Surface water at ice-snow interface and free water content in snow
5) Internal inhomogeneity and porosity

The Beaufort Sea mission furnished data mainly from older ice forms, classes (i) to (n) above, while the Eastern Arctic mission gave results for ice forms first-year and younger. In addition to this difference, the Beaufort mission results were for surface temperatures colder than -25°C while surface temperatures in the Eastern Arctic were warmer than -5°C under spring break-up conditions. Both effects can easily be seen in the microwave results.

Radiometer measurements were reduced to ice emissivities using the available estimates of the ice surface and sky temperatures. Scatterometer measurements were reduced to backscattering coefficients for the range of incidence angles 0° to 60° for HH and HV polarizations. A statistical data base was established for each ice condition by combining all segments of data for corresponding ice types.

Microwave Emissivity of Sea Ice

In Fig. 2 from Hawkins et al., these proceedings Section 5.1, the results of microwave emissivity measurements are summarized for typical ice thickness estimates for each ice class. The thickness data is inferred based upon microwave signatures and a visual classification of ice types. This diagram shows two contravening tendencies in the emissivity of sea ice with age and thickness. The thinner, younger forms appear to have increasing emissivity with ice thickness while the thicker, older forms show decreasing emissivity with ice thickness. These two trends are indicated by the straight lines running through the data. This characteristic may be a result of a transition from surface emission in the younger, more saline ice to volumetric emission in the older ice classes which allows deeper microwave penetration.

The result of these two trends is to produce inherent ambiguities in the interpretation of microwave radiometric results: confusing younger ice with older, thicker ice types. It is clear that microwave emissivity data alone is insufficient to classify sea-ice data.

Radar Cross Section of Sea Ice

Fig. 3 from Hawkins et al., these proceedings Section 5.1, is a summary of 13.3 GHz backscattering coefficient results from the SURSAT missions. The transmitted radiation was H polarization, and on either axis of the figure the two receive polarizations are plotted for an incidence angle of 45°. At smaller incidence angles, the dB separation of older ice is superior with cross-polarization to like-polarization: otherwise, the group patterns are similar regardless of incidence angle and the dominant effect is an overall displacement to smaller absolute signal for every ice type* when the incidence angle is increased. As can be seen, rough and smooth ice can be separated better with cross-polarization than like-polarization. In this representation the ice island, T3, appears as very old multi-year ice. Young ice shows a higher degree of variability than old ice on this diagram. It should also be noted, that the logarithmic representation of the data distorts the real contrast of the results and that substantially more favourable signal-to-noise conditions exist at low incidence (steep depression) angles. Smaller floe sizes depicted in the wave-broken first-year ice, raise the radar cross section 4-10 dB. It is similar in this respect to the effect of roughness due to pressure ridging. Multi-year ice is weathered sufficiently to make little difference in radar return (approx. 2 dB) for rough and smooth forms. There are inherent ambiguities between grey and grey-white ice, first-year ice and nilas. Groupings with temperature and ice type are evident.

---

*Water is somewhat anomalous in this respect having a much steeper angular dependence than ice and so moves through the cluster diagram and is best separated at higher incidence angles.

Combination of Emissivity and Radar Cross Section Results of Sea Ice

Fig. 6 from Hawkins et al., these proceedings Section 5.1, shows the 19.4 GHz emissivity and 13.3 GHz backscattering coefficient cluster representation of all classes of sea ice for an incidence angle of 45°. In this representation, all classes become separable with the ambiguities among the younger ice forms and old ice now removed. The ice island now is clearly separated from multi-year ice. There is a marginal separation of grey-white and first-year ice forms.

Grey ice appears anomalous in that it does not appear to lie in the aging pattern followed by the younger forms in the progression to first-year. This feature and the large variation of the class perhaps indicates a transition with respect to its microwave response, but more investigation is required to understand this ice class.

The data base consisting of radiometer and scatterometer statistics for the ice classes measured in the Beaufort Sea was used in a simple Euclidean classifier with a high success rate. It now tentatively appears that with surface temperature, emissivity and backscattering coefficient measurements, sea ice may be reliably classified. More sophisticated classification algorithms now being tested have yielded very impressive success rates. More data under differing conditions are required before the utility of this approach can be determined generally.

Iceberg and Pressure Ridging Study

The ice ridge and iceberg study conducted for this project was directed toward the measurement of radar contrast rather than feature detection by absolute cross sections.*

First-year ridges show higher contrast for cross-polarization than like-polarization with contrasts increasing with incidence angle until about 20°. At this point, the radar contrast remains independent of incidence angle over the range of the scatterometer measurements. First-year ridges studied vary in contrast from 0 to 20 dB for HV polarization and 0 to 14 dB for HH polarization.

Ridges in multi-year ice show much lower contrast than first-year ridges ranging from 0 to 8 dB for HV polarization and 0 to 6 dB for HH polarization. This result showed no dependence on incidence angle for the range of angles studied with the scatterometer.

---

*Only a few estimations of emissivity were gathered in the study of icebergs and none for ridges, because these features were normally much smaller than the footprint size of the radiometer.

Radar contrasts for icebergs in smooth first-year ice are of the same order as that seen in the ridging study. They are independent of look angle and range from 0 to 16 dB for HV polarization and 0 to 12 for HH polarization. The contrast depends on iceberg shape, size and weathering.

Recommendations for Future Study:

The work of the SURSAT Active-Passive Sea-Ice Experiment suggests the following recommendations for future study:

A) More attention to be directed toward ground truth information in the overflight region including the following data:

1. Surface temperature
2. Air temperature
3. Ice density
4. Ice thickness
5. Ice salinity
6. Ice brine volume fraction
7. Complex dielectric constant measurements

B) Continued study with particular emphasis on profiling sensor data since this data is most easily quantified and cross compared. In such reconnaissance, the following sensor complement is recommended as a minimum requirement:

1. Wide-angle aerial camera
2. Infra-red profiling thermometer
3. Microwave scatterometer
4. Microwave radiometer
5. Inertial navigation system
6. Radar altimeter

In addition to these primary sensors, valuable complementary data could be obtained by simultaneous measurements with:

1. Impulse radar thickness profilometer
2. Radar surface profilometer
3. SAR imagery
4. SMMR imagery

C) Missions using the sensors described in (B) should gather data for similar ice scenes over the complete seasonal cycle to assess the variation of microwave signatures with seasonal patterns and different geographical areas.

D) Continued analysis is required of current data sets to establish:

1. The effect of snow cover and conditions on sea-ice microwave signatures.
2. The uniqueness of the angular dependence of the backscattering in classifying sea ice.

3. The form and uniqueness of the probability distribution functions for microwave emissivity and backscattering cross section.
4. The cross comparison of profiling sensor and imaging sensor data for (3).
5. The validity of current data for less frequently observed ice forms such as frazil, grease, nilas, grey, grey-white. Much of the optimum data set has now been analyzed but useful data may be retrieved from secondary results still largely untouched.
6. The study of roughness features: ridging, rafting, fractures and edges, to determine their utility in determining floe boundaries and ridge patterns.
7. Theoretical work on the prediction and modelling of microwave scattering coefficient and emissivity by comparing results with empirical data.

6.3.2 Intermediate results of the radar backscatter study of sea ice in the Beaufort Sea.

A team from the University of Kansas (Delker et al, 1980, in these proceedings) conducted a series of backscatter measurements using a surface-based transportable microwave active spectrometer (TRAMAS) system and a helicopter-borne scatterometer (HELOSCAT)* Several ice types were investigated such as lake ice, brackish ice, young sea ice and thick, first-year ice. Effects due to snow cover were also measured. Both like and cross polarized measurements were made at L-band (1.5 GHz) and Ku-X-band (8.5 - 17.5 GHz) frequencies.

The TRAMAS system at L-band was able to distinguish between lake ice and sea ice. Thick first-year and thin sea ice have very similar results at VV polarization. Cross polarization (VH) at incidence angles greater than 40° provided good discrimination of thick FY and thin ice. At frequencies between 8.5 and 17.5 GHz discrimination is possible if one selected the proper incidence angle. The greatest separation occurs at 8.5 GHz with VV polarization. As the frequency increases the difference between returns decreases.

It was also found (Delker, et al, 1980, in these proceedings) that an increase in the salinity caused an increase in the backscatter.

Results on the effect of snow show that an artificially roughened snow surface gave the highest backscatter as compared to the natural snow cover of 4 cm thickness. After removing the snow, the bare-surface lake ice had a dramatically lower backscatter than the snow covered lake. The difference on the average was 8 dB or greater. These results indicate that even cold snow plays an important role on lake ice and has to be accounted for. (Unfortunately, these measurements were not repeated over sea ice. Since the effect is probably due to volume scattering by the snow a similar effect should be expected over sea ice.**)

---

*Bell model 205 helicopter.

**Editor's comments.

The HELOSCAT measurements by Delker et al (1980), were consistent with the one of the TRAMAS system. This is very encouraging since the airborne systems can cover a much greater variety of ice types than the surface-based one.

The frequency response using the TRAMAS system is shown in Figure 5.1 from Delker et al., 1980, these proceedings, Section 5.3. This differs significantly from previous results by Onstott et al. (1979). The slopes for thin and thick FY ice have become negative, as compared to the previous results shown in Figure 6.2. An explanation of this difference has to await the final analysis. The authors have not ruled out calibration errors.

Figure 6.2

SCATTERING COEFFICIENT FREQUENCY RESPONSE OF
THICK FIRST-YEAR AND MULTI-YEAR ICE

IEEE TRANSACTIONS ON GEOSCIENCE ELECTRONICS, VOL. GE-17, NO. 3, JULY 1979

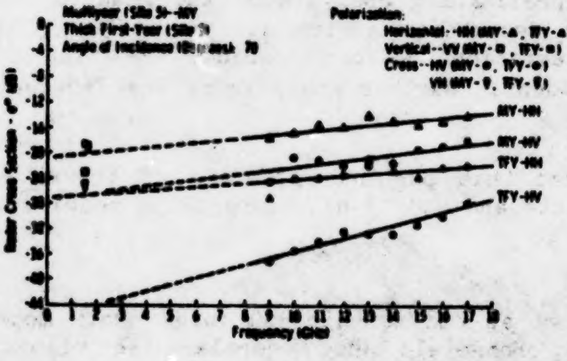

Based on the results of both the surface-based scatterometer and the HELOSCAT, a radar operating at 9 GHz with a large incidence angle would produce the best discrimination.

6.3.3 West Greenland Sea Ice Experiment

Gray et al, 1980 (in these proceedings) had as their objective to study and demonstrate the capabilities of different microwave remote sensors to provide information on the extent, type and thickness of sea ice, particularly to those concerned with shipping. In addition, they also addressed the detection of icebergs. They used both active and passive non-imaging and imaging systems. Besides the instrumentation provided by the Canadian aircraft, the Technical University of Denmark provided their own imaging multifrequency microwave system and a SLAR. The experiment was primarily carried out in the ice marginal zone. Surface ice temperatures were just below the melting point. The ice had undergone significant melting and decay. No significant ground truth was collected due to technical difficulties. Snow surface appeared dry, but the snow-ice interface was not. Snow thickness was about 10 cm and ice thickness 20 cm.

The authors commented on the relative merits of SAR vs SLAR for ice reconnaissance. Generally speaking they feel that a SLAR is satisfactory for estimating ice extent and concentration. In case of very loose pack one could over-estimate the concentration if the average floe size were smaller than the system resolution. SAR permits the identification and also provides an estimation of the presence of different ice types, such as small multi-year ice floes (Ketchum, 1977).

Concerning the detectability of icebergs, the authors make a rather definite observation. They state that "The SLAR results have shown that the detection of icebergs in sea ice should use low depression angles (less than about 8°) to try to increase the iceberg-sea contrast". On 20 February 1980, the Danish experiment which led to the above conclusion was repeated with the SLAR-equipped Electra of AES. A preliminary analysis of the results indicate that icebergs can be detected at depression angles as low as 30-35° (Table 6.4, Project 30). From this observation one can conclude that the iceberg detection is probably system dependent. Further analysis of the February 1980 data set is continuing.

It has also been recognized that our understanding of the effect of snow and wet ice is far from complete and additional research is required.

6.3.4 SAR Versus SLAR Comparison

Based on data sets collected by the Convair-580 (wide swath mode) and NASA's APS-94D on 12 March 1979, Hengeveld and Schertler (see Table 6.4, Project 4) presented following preliminary considerations. At incidence angles of 80-85° the surface topography dominates over the electromagnetic properties of the ice. Comparison of data collected at similar incidence angles, showed significant differences in the detail and definition of topographical features. SAR showed highly detailed spatical definition of small floes less than 33 metres in size and could distinguish between heavily broken-up floes and areas of total rubble. The SLAR spatial characteristics are, of course, dependent on range, but in general showed much poorer spatial definition of surface details. Floes smaller than medium category (100 m) were difficult to resolve and heavily defined floes appeared as rubble areas. However, surface texture appeared very similar on both data sets at all incidence angles, implying that the difference in resolution has little impact on the effect of surface electromagnetic properties which are significant in the classification of ice types.

6.3.5 SEASAT SAR Analysis

As part of project Number 9, Table 6.4, Hengeveld presented the following preliminary conclusions.

FIGURE 6.3 DIGITALLY PROCESSED SEASAT-SAR IMAGE OF CAMBRIDGE BAY, N.W.T.

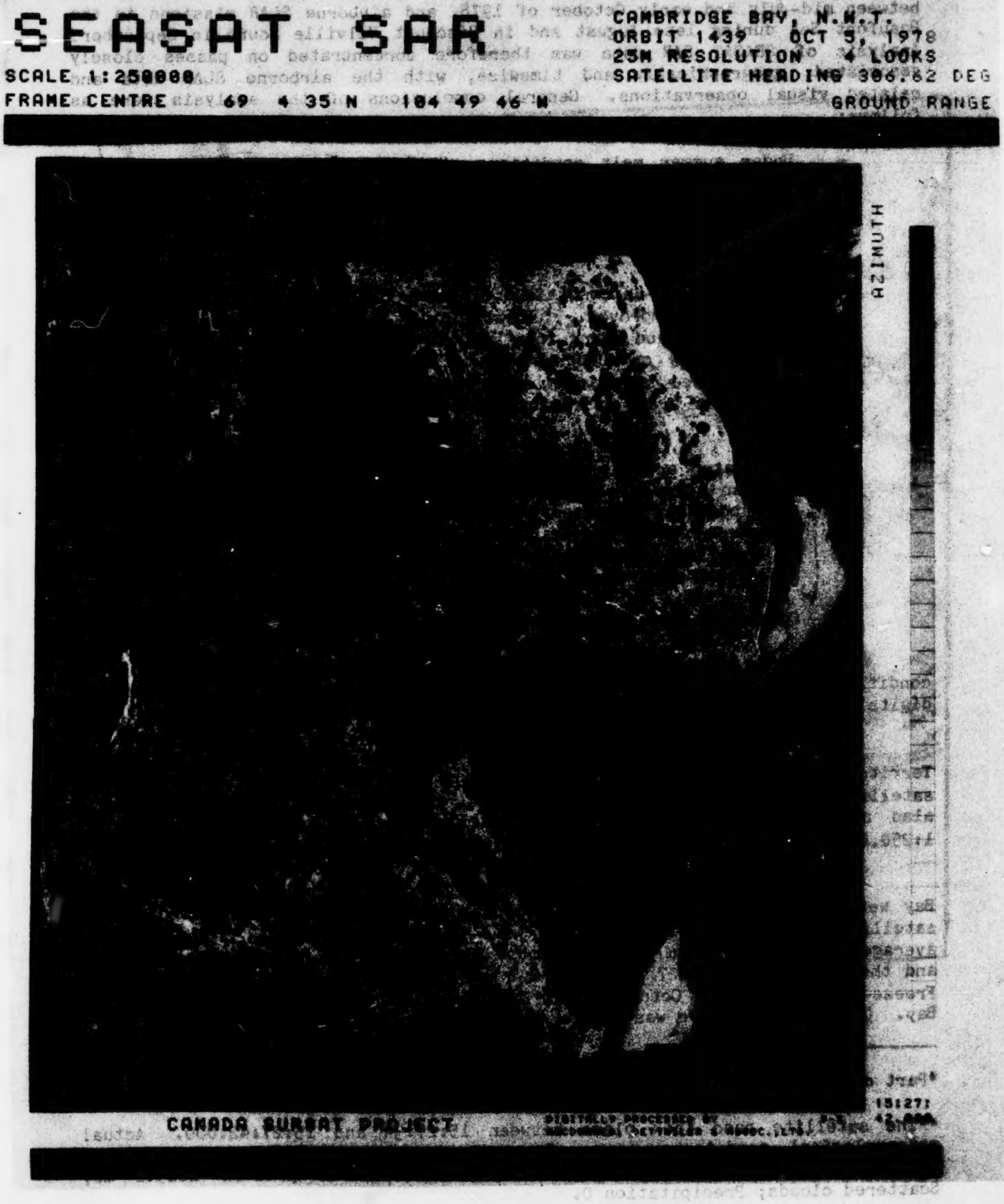
SEASAT SAR
CAMBRIDGE BAY, N.W.T.
ORBIT 1439 OCT 5, 1978
25M RESOLUTION 4 LOOKS
SCALE 1:250000
SATELLITE HEADING 306.62 DEG
FRAME CENTRE 69 4 35 N 104 49 46 W
GROUND RANGE
AZIMUTH
CANADA SURSAT PROJECT
DIGITALLY PROCESSED BY
MACDONALD, DETTWILER & ASSOC. LTD.

Data sets available included 30 SEASAT passes over the western Arctic between mid-July and early October of 1978, and airborne SLAR missions in the Beaufort Sea during late August and in Viscount Melville Sound in September. Analysis of SEASAT SAR data was therefore concentrated on passes closely associated, geographically and timewise, with the airborne SLAR data and related visual observations. General conclusions of the analysis were as follows:

- Under summer melt conditions, SEASAT SAR imagery of sea ice is relatively featureless while airborne SLAR imagery over identical ice fields show topographical features clearly. The effect of the low SAR incidence angle combined with presence of surface melt water is presumed to be responsible for this difference.

- During freeze-up conditions, information available from SEASAT SAR is much improved. Identifiable ice types included old, first-year, and young ice. Smooth floes of second year, often not identifiable on SLAR because of high incidence angles involved, also showed a unique signature. Newly formed ice showed on open-water areas as regions of no sea clutter.

- Open-water areas provided strong sea clutter returns, often more so than adjacent ice surfaces, resulting in a reverse image from that normally observed in SLAR. In the vicinity of ice floes, open water often showed a margin of low sea clutter along one side of the floes. This effect was confirmed in several cases to be associated with wind directions.

- Considerable work remains to be undertaken on the data sets.

To illustrate one of Hengeveld's conclusions during freeze-up conditions, Ramseier and Stasyshyn* presented following analysis of a digitally processed SEASAT-SAR image by MacDonald Dettwiler and Associates.

The image (Fig. 6.3) covers the area around Cambridge Bay, Northwest Territories. It was obtained from orbit 1439, 5 October 1978, with a satellite heading of 306.62 degrees. The corresponding topographic map is also attached Fig. 6.4. Both illustrations are at an original scale of 1:250,000. Cambridge Bay is seen in the radar image as a bright return.

On October 5 the weather conditions in the general area of Cambridge Bay were as follows: The average temperature for the 9 hours preceding the satellite pass** was -14.9°C. The wind was from the NW (320 deg.) at an average speed of 19.8 km/hr, (11 knots) on the average. It was a clear day and the visibility was 27 km or more. Ice formation started on September 24. Freeze-up occurred on October 4 in the inlet at the location of Cambridge Bay. On October 5 there was just a trace of snow on the ice.

---

*Part of SEASAT-1 SAR team validation experiment on ice morphology.

**The satellite pass took place between 15:27:34 and 15:27:42:000. Actual meteorological conditions were: Temperature -15.7 to -14.5°C; Wind speed 10-04 knots; Wind direction 300-320 deg.; Sea level presure 1029.1 mb; Scattered clouds; Precipitation 0.

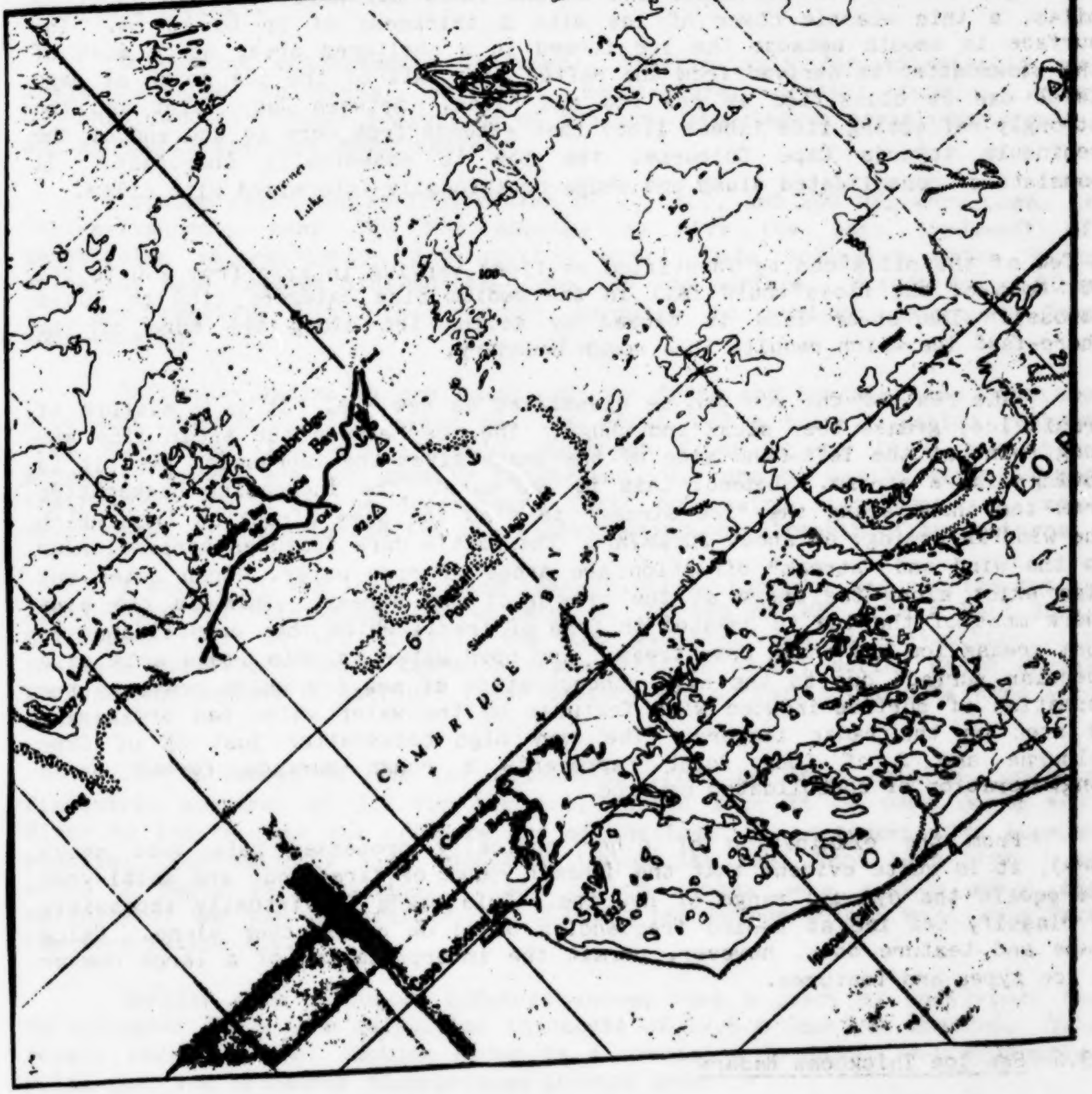
Greiner Lake
Cambridge Bay
Jago Islet
Simpson Rock
CAMBRIDGE BAY
Cape Colquhoun

FIGURE 6.4 - ORIENTATION OF SEASAT SAR IMAGE OF CAMBRIDGE BAY

All water bodies for the large part were ice-covered on October 5, including the lakes covered with fresh-water ice. By closer examination of the lake ice covers some rafting can be observed. Most of the visible rafting is generally parallel to the satellite track, thus performing much as a corner reflector. For example, the line which extends from Jago Islet across the Bay shows variation in intensity. One could speculate that this represents finger rafting. The ice on the lakes and on the inner Bay north of Jago Inlet is nilas, a thin elastic cover of ice with a thickness of up to 10 cm. The surface is smooth because the ice formed in a sheltered area, hence most of the backscatter is derived from the rafted ice. All of the ice south of Jago Islet can be classified as new ice and nilas. Between Jago Islet and the strongly reflecting line (shear line) that extends from here to the end of the peninsula towards Cape Colburne, the ice is essentially shorefast. It consists of consolidated slush and shuga occasionally intermixed with nilas.

A few of the nilas can be identified as floes varying in size from 250 to 750 m. Most of the floes would fall in the medium size category (100 to 500 m across). The shear line is caused by moving ice along the edge of the shore-fast ice which results in a rough boundary.

The rest of the ice can be classified as new ice. It is a mixture of frazil ice, grease ice, slush and shuga. The ice between the shear line and Long Point at the left-hand side of the image gives the impression that it is moving like a stream. Indeed, this is the case. The increasing backscatter from the shore along the "ice stream" is also the same direction from which the wind is coming, at about 20 km/hr. The little dark features perpendicular to the wind and "stream" direction are areas of open water. Open water may also exist along the shore at the origin of the stream. This is the area where most of the ice is created in form of frazil which then consolidates to form grease ice and shuga downstream. Any open water in this image acts as a specular surface due to the high concentration of new ice which prevents the formation of surface-induced wind features on the water which can ordinarily be seen on the radar imagery. The very high backscatter just SE of Cape Colburne and S of Long Point represents a rough surface formed by a conglomeration of consolidated new ice.

From the examination of other optically processed data (not shown here), it is quite evident that the dynamic range of first-year and multi-year ice equals the dynamic range of new ice. This makes it virtually impossible to classify sea ice at L-band frequencies based on backscatter alone. Using shape and texture does, however, permit the interpretation of a large number of ice types and features.

6.3.6 Sea Ice Thickness Radars

During 1979 C-CORE received a contract from the Canadian Government to develop sea ice thickness radar capability in Canada, and in particular to relate airborne impulse radar measurements to actual ice conditions. The field measurements under this program were organized to coincide with the field activities of the SURSAT Project in the Beaufort Sea in March and over Lake Melville in April. By conducting these experiments with those of other investigators it was possible to collect highly complementary data sets over a wide variety of ice types. Moreover, it was possible to pool an extensive set of surface truth measurements.

The program in the Beaufort Sea, run under the auspices of C-CORE, was described by Rossiter and Butt (1979). Particular attention was given to in-situ measurement of the electrical properties of sea ice at HF and VHF frequencies and to understanding the effects on the radar return of the horizontal anisotrophy of first-year sea ice. In addition, the program was the first recorded use of ice sounding radar from a fixed-wing aircraft with real-time readout.

Concurrent measurements included: (particularly for anisotropic sea ice): augered thickness, salinity, temperature, crystal fabric, water currents, and electrical properties of the ice, simultanous aerial photograhy, and synthetic aperture radar imagery.

Impulse radar centre-frequencies of 80, 100, and 200 MHz were used. A centre-frequency near 100 MHz appears to give the best trade-off of penetration vs resolution and antenna size. Data collected below 30 m elevation have reduced side-scatter from the ice surface. Speeds below 50 m s^{-1} are required with the current hardware to achieve coherence from scan-to-scan.

Thickness estimates are excellent for fresh and brackish ice, and are good for underformed first-year sea ice about 1-2 m thick. Bottom returns from multi-year ice are sporadic, although floes up to 14 m have been sounded. Ridges are not usually penetrated, but can be easily detected and their width can often be determined. Data processing algorithms are under development to characterize the ice further using the strength of the returns.

A survey of the ice covering Lake Melville, Labrador was carried out on April 9 and 10, 1979 using impulse radar at 100 and 200 MHz from a Bell 206XL helicopter (Butt et al., 1979). The work was performed in conjunction with the Lake Melville/Offshore Labrador Transportation Study, during which aerial photography, synthetic aperture radar imagery and surface truth data were also gathered.

The thickness of the ice calculated from the radar returns, using a dielectric constant of 3.2 for the ice, varied from 85 cm near North West River to 140 cm near the offshore end of the Lake, in agreement with augered results. The salinity also increased toward the east from less than 1 to about 2 parts per thousand. Clear bottom echoes were weaker where the salinity of the ice was greater. At 200 MHz the bottom echoes were poor from the more saline ice.

Earlier data collected offshore showed that a piece of multi-year ice in Groswater Bay with a calculated thickness of 14.6 m could be sounded. This result indicates that impulse radar is a promising technique for estimating multi-year ice thickness distribution in this area.

Very distinctive signatures were obtained over re-frozen meltponds, and these also show up on the SAR imagery. Unfortunately these were not studied on the surface, and further work will be needed to understand the returns fully.

An International Workshop on the Remote Estimation of Sea Ice Thickness was held in St. John's, Newfoundland, on September 25 and 26, 1979. The sixty participants included both researchers and operational users from North America, Europe, and the Soviet Union. Nineteen invited papers were presented in three sessions: Overview of Problem; Recent Sea Ice Studies; and Ice Sounding Technology. The final session was devoted to a panel discussion, culminating in recommendations for research priorities in this field.

A significant amount of time at the workshop was spent discussing the electrical properties of sea ice, since most of the remote measurement techniques involved radar sounding. Sea ice is a very complex natural material and discussion focused on the high variability of its electrical properties. There is a strong need for standardization of electrical property measurements so that the results from different workers can be compared. The frequency range of interest - approximately 100 MHz - is a very difficulty range in which to work, particularly for making in-situ measurements.

New data on the horizontal electrical anisotropy of sea ice and a new theoretical model were presented. The anisotropy phenomenon appears to be closely related to the structure of the lower part of first-year sea ice. This topic is one of considerable research interest at the moment. In general, it was felt that we have very poor basic understanding of the electrical properties of sea ice, and that the existence of any "quick fix" to remedy this is unlikely.

Discussion concerning the processing of sounding results indicated that significant advances could probably be achieved by appropriate signal processing. This might be pre-processing, post-processing (matched filtering), or use of new "super-resolution" algorithms. Interpretive procedures need to be oriented toward real-time operational output.

There were papers on the use of a laser profilometer and a satellite altimeter to determine statistical ice properties over long tracks. The suggestion was made the inertial systems might be developed to extend these types of measurements for synoptic estimates of ice freeboard and hence thickness.

The majority of sounding results presented were based on a broad-band impulse radar system that has been used for several years. Concern was expressed over the fact that measurements are made in the near field of the antenna without properly allowing for this, and the importance of diffraction effects was noted. Several new systems are under development, including: synthetic pulse radar, a phase measurement system, and a "distributed-source" antenna. In the U.S.S.R. modulated pulse radar and synthetic pulse radar have been used for some years. A new two frequency phase-pulse system is under development in that country. The importance of testing new systems in the real environment was stressed.

Finally the needs of the various users was underlined. It appears that each user has particular needs, and it is possible that these will not all be met by a single instrument. For example, the need of some operators is for good definition of multi-year ice thickness; for others, the design parameters for offshore structures. Some people need operational strategic planning devices; whereas others are more interested in tactical support. The location and time of year of operation are also significant. It seems clear, however, that ice thickness devices should be much more than merely research tools. To this end, the workshop was able to bring together both researchers and those people who will ultimately have to make use of this technology and the data that are collected. The Proceedings, including the written papers and a transcript of the Discussion Session, have been published (C-CORE, 1980).

A number of reports under this program are in the final stages of preparation, as listed in Appendix 6.2. Considerable attention has been devoted in the data analysis to relating airborne data to surface truth measurements and developing analytical algorithms for computer-assisted enhancement and interpretation of ice sounding radar data, including returns from anisotropic sea ice.

More recent work is already in progress at C-CORE: (a) to field evaluate newer ice thickness radars along with the C-CORE airborne impulse radar; (b) to evaluate impulse radar under novel conditions (e.g. from the bow of an ice breaker); and (c) to examine the complementary nature of ice sounding radar profiles and synthetic aperture radar imagery. This latter work is making use of the two simultaneous data sets collected in the Beaufort Sea by SURSAT.

In summary, it appears that it is possible to successfully sound sea ice from helicopters or small fixed-wing aircraft under some conditions. Proper interpretation of the results can give information on the thickness and type of sea ice. Future efforts should be devoted to making operations using ice sounding radars more routine.

6.3.7 Project Ice Map (ASP Final Report)

This joint industry-government research project (Intera, 1980) was organized somewhat differently from the other ASP experiments. Funding for the airborne operations and research was supplied by CANMAR, the drilling subsidiary of Dome Petroleum, and the project was incorporated into the ASP because it was a practical demonstration of the utility of airborne SAR in an operational environment. The project objectives can be stated as follows:

a) to develop a real-time data downlink suitable for transmitting SAR imagery to a drill ship;

b) to demonstrate the potential of this imagery for assisting in drilling and shipping operational decisions;

c) to collect a data set suitable for the development of a site specific ice dynamics model.

The data collection period which lasted from November 25 to December 17, 1979 was successful. The SAR flew missions from a base in Inuvik, N.W.T. to the drilling site, accumulating about 85 hours of air time and mapping about 120,000 km^2 of sea ice during the project.

The downlink developed for the project was a limited resolution slow-scan T.V. system operating over a VHF radio link. Imagery from the real-time processor (RTP) was annotated by an interpreter and transmitted to another interpreter on the bridge of the drill ship. The quality of the transmitted imagery was inferior to the original RTP imagery due to the inherent lower resolution of the system. To compensate for this, the original data were airlifted out to the drilling operation immediately after the SAR-580 landed at Inuvik so the operations people generally had top quality imagery of their site one-to-twc hours after collection.

The SAR imagery was found to be useful for making operational decisions. It was possible to identify heavily ridged areas in the young ice as they approached the drill ship, and the supporting ice breaker and supply vessels could be deployed to break up the thicker ice. When the fleet was returning to harbour at the end of the drilling season, the SAR imagery was used to select a route along existing leads. Because the weather for most of the project was unusually mild and ice conditions rather light, drilling operations could have been conducted safely with support from visual sensors. It is concluded that the SAR will provide extremely valuable tactical support for drilling operations when darkness, cloud or fog preclude other remote sensing techniques.

The modelling data sets consist of nine rectangular mosaics over the drilling operaton, each covering an area of about 10,000 km^2. With separate funding from the Atmospheric Environment Service and the Dept. of Supply and Services, these data are being prepared for input to a site specific ice dynamics model. Data quality appears to be high. The authors are presently developing automated classification procedures to facilitate image interpretation.

6.3.8 Project Berg-Map

Like Project Ice Map (ASP Final Report, 1980) this joint industry-government study was conceived as a pilot project to test the ability of airborne SAR to image icebergs under a variety of conditions. After the encouraging results reported from Sorties 78-3 and 79-2, Petro Canada agreed to supply funding to study tactical ice hazard identification for possible drilling programs in the Lancaster Sound and Davis Strait area. The specific objectives were:

- **a) to evaluate the ability of SAR to detect small icebergs;**
- **b) to study the possibility of re-identifying the same iceberg using imagery collected on consecutive days.**

Data collection for this project took place during September 1979 when a SAR-580 sortie was conducted to Thule, Greenland. Photographic underflights were planned using a Petro Canada Twin Otter for three days. Bad weather prevented the photographic underflights but did not affect SAR-580 operations. Problems with the inertial navigation system seriously restricted the quantity of data collected.

The authors reported that the analysis of these data is in progress, and that the limited data set is adequate for addressing objective a) and considering objective b). Preliminary results indicate that thousands of icebergs, bergy bits and small multi-year floes have been detected, and that features in the order of 10 m in maximum dimension are generally detectable, depending on sea state. In areas where coincident iceberg detection was attempted using an airborne search radar and visual identification, the SAR detected about twice as many bergs as the visual technique.

Based upon their radar appearance, several bergs have been detected on consecutive days. Drift velocities have been calculated for input to an iceberg drift model being developed by Intera for Petro Canada and the results show that iceberg drift patterns in the Bylot Island area are extremely complex. The authors concluded this work with a study of digital pattern recognition techniques applicable to the iceberg identification problem which is presented as a paper in these proceedings by Kirby.

6.4 MARINE (ICE) ENVIRONMENTAL INFORMATION PROGRAM

The Atmospheric Environment Service in partial response to Dome Petroleum's proposal "Description of the Remote Sensing and Modelling Components of the AML-X4 Research Program, Winter 1979-80", Intera's unsolicited proposal to "Develop an Ice Motion Model for Unconsolidated Sea Ice", and the recent advances in technology in support of ice information is in the process of defining a marine ice environmental information service (MIEIS). The responsibilities for providing this service lies partially with the Federal Government and Industry. For example, the Federal Government's responsibility would be to provide global, hemispheric, and regional ice services whereas it would be industry's responsibility to provide site specific ice services for their own operations. In some cases the Federal Government would also provide specific routing of ice services to the Coast Guard and commercial vessels operating in the Gulf of St. Lawrence, for example.

The nature of the ice service would be to provide strategic, tactical and near tactical support under all weather, day and night conditions. In order to provide this service under the above-mentioned circumstances, active and passive microwave sensors will have to be used primarily.

Sea ice research using active and passive microwave sensors started about in the mid sixties, the first published papers dealing with an airborne imaging radar way by Anderson (1966) and using a scatterometer by Rouse (1969). Similarly, the first report on aircraft measurements using a passive microwave imager was by Wilheit et al (1972) and on surface radiometer measurements by Meeks et al (1974). Passive microwave images obtained by the NIMBUS-5 satellite* were first published by Campbell et al. (1974).

---

*Launched 11 December 1972

It is not until late 1986 that the first operational microwave satellite will be available to the civilian community in the form of NOSS (National Oceanographic Satellite System). NOSS will carry a LAMMR (Large Antenna Multifrequency Microwave Radiometer), a scatterometer and two radar altimeters. It is not surprising that it will take 13 years to develop an imaging passive microwave system. For example, it will take 12 years for the scatterometer and altimeter to become operational, having flown for the first time on SKYLAB in 1973. While the capability of these sensors has been clearly demonstrated from SEASAT, operating systems will not exist until NOSS is launched. Consequently, it will probably take about the same amount of time for the imaging radar to become operational. This event could happen sometime in the early 1990's. However, if the new RadarSat program remains on time, it could be as early as 1988 (see Section 7).

In planning a MIEIS the availability of all weather, day and night operating microwave sensors is essential. Current industry projections indicate that year round production of oil in the Beaufort Sea could start as early as 1985 with seasonal production as early as 1983 (Harrison, 1979). Based on this time scale and the previously stated requirements, it is clear that for Canada to have an effective MIEIS it will need an integrated data system which makes use of satellites, airborne platforms and surface-based microwave sensor systems. Figure 6.5 presents a schematic of the data acquisition phase for MIEIS.

Airborne platforms will be required to provide strategic, tactical and near-tactical support. The strategic support would be complimentary to the satellite data. It is envisaged that this would primarily be in a region such as the archipelago where some areas are too small to be viewed by satellites. This could also apply to coastal areas if they are not covered by ground-based systems. However, the main purpose of an aircraft platform would be to provide tactical, and to a lesser degree, near-tactical support. This will require a high-resolution imaging radar, whereas for the tactical support, a low-resolution active and passive imaging system would be required.

From the NOSS program, one could assume that low resolution (about 4.5 by 7 km at 36.5 GHz) data would be available for operational use in 1986. Similarly scatterometer data with a resolution of about 25-50 km would also be available. The passive microwave data would provide ice concentration to about 1% accuracy and the fraction of first-year to multi-year ice to about 10%. A scatterometer would provide some information on ice type, ice concentration, and ice roughness all combined within the backscatter value of σ_0 .A desirable quantity is roughness. Research needs to be carried out to be able to separate out the roughness contribution to σ_0 . It is hoped that by 1986 this problem will have been solved. Combining the multifrequency radiometer measurements with the backscatter value from the scatterometer would provide operational data on ice concentration, fraction of ice type present, and a roughness parameter for a grid size of the order of 40 x 40 km. These data could then be input directly into an operational regional ice model which would provide a forecast on areas which will diverge or converge, on motion vectors, on concentration, on ice type distribution and the location of the ice edge. A significant amount of research is still required in support of the altimeter for applications to sea ice operations. In the past the altimeter has demonstrated that it could locate the ice edge (Brooks et al, 1977).

FIGURE 6.5

MARINE ICE ENVIRONMENT INFORMATION SYSTEM (MIEIS)

DATA ACQUISITION PHASE

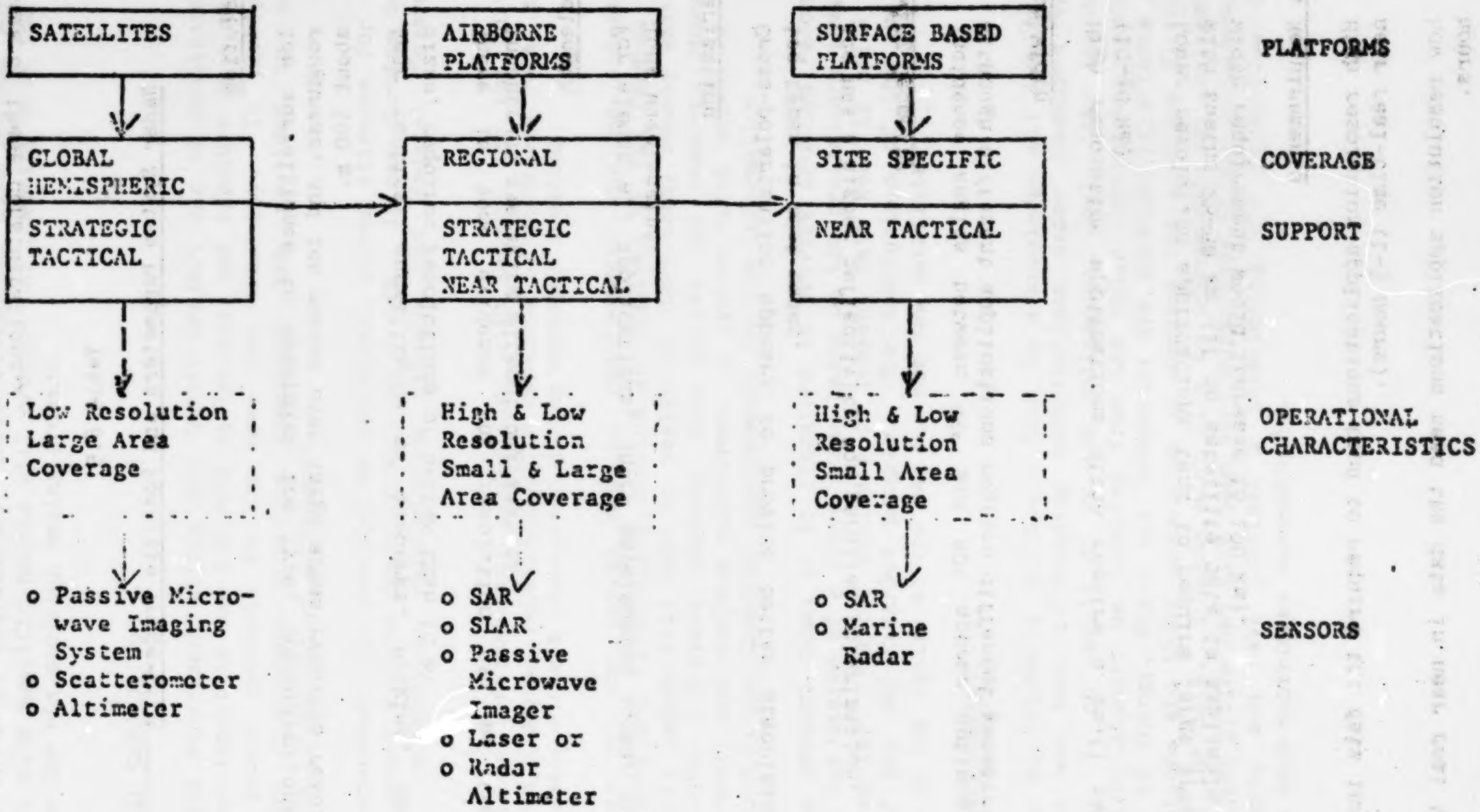
SATELLITES
AIRBORNE PLATFORMS
SURFACE BASED PLATFORMS
PLATFORMS
GLOBAL HEMISPHERIC
REGIONAL
SITE SPECIFIC
COVERAGE
STRATEGIC TACTICAL
STRATEGIC TACTICAL NEAR TACTICAL
NEAR TACTICAL
SUPPORT
Low Resolution Large Area Coverage
High & Low Resolution Small & Large Area Coverage
High & Low Resolution Small Area Coverage
OPERATIONAL CHARACTERISTICS
o Passive Micro-wave Imaging System
o Scatterometer
o Altimeter
o SAR
o SLAR
o Passive Microwave Imager
o Laser or
o Radar Altimeter
o SAR
o Marine Radar
SENSORS

Future operational imaging radars, very likely to be of the SAR type, must consider trade-offs among several system parameters based on the requirements of the users. Table 6.5 (partially modified from INTERA, 1980) presents some of these considerations.

Table 6.5

Radar System Parameters and Possible Trade-Offs

1. Resolution

   a) Ice surveillance to determine ice type, concentrations, surface roughness, and ice motion over large areas requires resolutions of about 100 m.

   b) Near tactical surveillance of icebergs, ridging, small floes sizes, requires resolutions of better than 10 m.

   c) There is some evidence tht resolution can be traded with incoherent averaging without degradation.

2. Wavelength

   a) For almost all applications, short wavelengths appear superior to long wavelengths.

3. Polarization

   a) Cross-polarization appears to provide better discriminations of ice types in most cases.

   b) Ice has a higher reflectivity for parallel polarization.

4. Viewing Geometry

   a) Incidence angles between 45° and 80° appear optimum overall, although different applications require different geometries.

5. Swath Width

   a) High resolution applications often require a small swath width (10-20 km).

   b) Lower resolution applications tend to require large area coverage with swaths 25-50 km (if no satellite data is available the swath width requirement would increase to 100 km).

6. Data Requirements

   a) High resolution applications tend to require the data instantly or near real-time (1-3 hours).

   b) Low resolution applications need the data in near real time (3-6) hours.

The surface-based platforms fall into two categories, the ship or drill rig based marine radars and ground-based shore radars. These are essential. They provide the operator with continuous informtion on ice conditions within a limited radius of operations. These continuous observations supported by operational site specific models will provide the operator with the necessary information for his decision making process.

6.5 GENERAL CONCLUSIONS

The ice experiment within the SURSAT project can be considered to have made a major impact in sea ice data collection, and exposure of a multitude of microwave sensor products to the user ice community. In particular, the Convair 580 instrument platform component has provided an outstanding contribution to the entire experiment.

The experiment has provided an additional strong stimulus for the use of microwave sensor systems operationally in Canada. It has further developed a productive cooperative relationship between the Federal Government and Industry.

The close international cooperation with Denmark and the United States has provided a strong relationship to continue to undertake joint experiments based on research needs identified during workshop sessions.

Because of the varied mission requirements for an operational ice reconnaissance and forecasting service as required by the federal government and industry, Canada will have to design an operational remote sensing system which includes microwave sensors, both active and passive, operating from space, aircraft and surface platforms. A system based solely on satellites will not fulfill the Canadian requirements for ice information.

At the present time, it is premature to provide detailed recommendations concerning the design of a space radar based on the preliminary investigations presented so far. Further analysis of present data sets is still continuing as part of the new RadarSat program. The conclusions of the analysis will contribute to the design of the SAR for the new satellite.

6.6 ACKNOWLEDGEMENTS

It is an extremely difficult task to acknowledge all the agencies and individuals who made outstanding contributions under sometimes very severe conditions. I, on behalf of my ice colleagues, would like to acknowledge: the excellent support we received from the Polar Continental Shelf Project; Department of Energy, Mines and Resources; the outstanding efforts of Intera, CCRS operations and their associates in keeping the airplane flying in order to collect the data. I would also like to acknowledge my colleagues in the SURSAT Project office who have been very supportive to the requirements of the ice community and have provided a stimulating and productive milieu for completing this experiment successfully.

6.7 REFERENCES

Anderson, V.H., 1966. High altitude side-looking radar images of sea ice in the Arctic. Proceedings of the Fourth Symposium on Remote Sensing of Environment, 1966, Ann Arbor, Will Run Laboratories, Institue of Science and Technology, University Michigan, 845-47.

Brooks, R.L., R.O. Ramseier, W.J. Campbell, C.L. Parsons, 1977. Applicability of satellite radar altimetry for monitoring sea ice boundaries and for detecting temporal changes in the thickness of continental ice sheets. American Geophysical Union, Annual Spring Meeting, Washington, D.C. (abstract only).

Butt, Kenneth A., J. Brian Gamberg, James R. Rossiter, 1979. Remote Estimation of the Properties of Sea Ice, Impulse Radar Study of Lake Melville, Labrador. Data Report C-CORE Publication Number 79-7.

Campbell, W.J., P. Gloersen, W. Nordberg and T.T. Wilheit, 1974. Dynamics and morphology of Beaufort sea ice determined from satellites, aircraft, and drifting stations. In Book: Approaches to earth survey problems through use of space technologies. Proceedings of the symposium held in Constance, F.R.G., 23-25 May 1973. Edited by D. Book, with the Assistance of F.W.G. Bakre and S. Ruttenberg. Berlin, Akademie-Verlag, p. 311-27.

C-CORE, 1980. Proceedings of the International Workshop on the remote estimation of sea ice thickness, St. Johns, September 25-26, 1979. Ed. James R. Rossiter and David P. Bazeley, C-CORE Publication Number 80-5, p.505.

Dunbar, M. (1969) A glossary of ice terms (WMO Terminology). Ice Seminar, Special Volume 10, The Canadian Institute of Mining and Metallurgy. pp. 105-110.

Government of Canada, 1977. Satellites and Sovereignty, Report of the Interdepartmental Task Force on Surveillance Satellites, Canada Centre for Remote Sensing, 172 p.

Harrison, G.R., 1979. The need for action-oriented R and D in the Canadian Arctic. Proceedings of Symposium on Marine Transportation and High Arctic Development: Policy Framework and Priorities, held at Montebello, Quebec, 21-23 March 1979, p. 45-58.

Intera, 1980. Airborne SAR Project, Intera Environmental Consultants Ltd., Ottawa, Ontario.

Ketchum, R.D., 1977. An evaluation of side-looking radar imagery of sea ice features and conditions in the Lincoln Sea, Nares Strait and Baffin Bay. NORDA Technical Note 7.

Meeks, D.C., R.O. Ramseier and W.J. Campbell, 1974. A study of microwave emission properties of sea ice - AIDJEX 1972. Proceedings of the Ninth Symposium on Remote Sensing of Environment, 1974, Ann Arbor, Environmental Research Institute of Michigan, p. 307-22.

National Aeronautics and Space Administration, 1979. Ice and Climate experiment, Goddard Space Flight Center, Greenbelt, Maryland.

Onstott, R.G., R.K. Moore and W.F. Weeks, 1979. Surface-based scatterometer results of Arctic Sea ice. IEEE Transactions on Geoscience Electronics, Vol. GE-17, No. 3, p.78-85.

Rossiter, J.R. and K.A. Butt, 1979. Remote Estimation of the Properties of Sea Ice, Beaufort Sea Field Trip Report - March 1979. (C-CORE Data Report, Publication 79--9).

Rouse, J.W. Jr., 1969. Arctic ice type identification by radar. Proceedings of the Institute of Electrical and Electronics Engineers, Vol. 57, No. 4, p. 605-11.

SURSAT Project Office, 1978. SURSAT Ice Experiment, SURSAT Project Office, Ottawa, Ont., p.94.

Vant, M. (1976) A combined empirical and theoretical study of the dielectric properties of sea ice over the frequency range 100 MHz to 40 GHz, Ph.D. Thesis, Carleton University, 462 p.

Wilheit, T.T., W. Nordberg, J.C. Blinn, W.J. Campbell and A.T. Edgerton, 1972. Aircraft measurements of microwave emision from Arctic sea ice. Remote Sensing of Environment, Vol. 2, No. 3, p. 129-39.

Appendix 6.1

Interdepartmental Task Force on Surveillance Satellites

Census of Surveillance Requirements

Application(s): Marine transportation, resource development and exploitation

Department(s): DOT, DOE, DND, DINA, EMR, DFO

Information Required: Ice reports and forecasts

Description of Target(s) or Data Required:

- Extent of ice coverage
- Type, age and thickness of ice
- Distribution and height of ridges
- Snow cover (Eastern seaboard, Gulf of St. Lawrence, Great Lakes and St. Lawrence Seaway only)
- Location, extent and size of leads
- Location and drift of icebergs, bergy bits and growlers
- Location and size of polynias

Characteristics of Target(s):

"Icebergs", "Bergy Bits" and "Growlers" refer to sizes of free-floating masses of ice. Icebergs and bergy bits are large enough to have considerable size above water; growlers are usually awash or nearly so. For navigation purposes, need to distinguish between "first-year" and "multi-year" ice. Knowledge of snow cover, especially wet snow, important for navigation.

Accuracy(ies) Required:

Planning:	10-20 km
Strategic:	500 m
Tactical:	500 m

Area(s) of Interest/Spatial Grid Size(s):

Canadian Arctic; Labrador Sea North of 55°N; Gulf of St. Lawrence and Eastern Seaboard (including Newfoundland waters); Great Lakes and St. Lawrence Seaway; Grand Banks and eastern approaches.

Frequency of Observation Needed:

(see comments)
Planning - twice daily
Planning and strategic - daily
Tactical - continuous surveillance in area within immediate range of ship

Response Time Required:

Strategic: 6 to 24 hours
Tactical: immediate

Data Format(s):

- Photographic imagery or charts for ice coverage
- Telex, imagery, other means for icebergs, bergy bits and growlers.

Special Data Handling/Processing Requirements:

It is frequently desirable to send ice information via pictorial methods directly out to vessels and other users.

Comments:

There are three distinct requirements for ice information:

1) Planning information. This is required for pre-season planning of ship utilization, marine insurance, hull design, regulatory policy design, etc. Data are of a statistical and time series nature, derived from the strategic data base.

2) Strategic. Required for short-term planning for voyages and ice forecasting. Daily coverage is required in all areas. These data are not now available with adequate geographic coverage or frequency.

3) Tactical. This information is in support of a single ship or group of ships travelling together. It is only required within the immediate area of the ship (say 20 km) and is required with minimum delay on a continuous or nearly continuous basis.

Note that wind shifts can cause very rapid movements of ice floes, causing extreme hazard to ships trapped between floes or between ice and shore. Weather forecasts and tactical surveillance are very important in such cases.

Appendix 6.2

Remote Estimation of the Properties of Sea Ice

Publication List - March 1980

The following have already appeared as C-CORE Data Reports.

Rossiter, J.R., and Butt, K.A., "Remote Estimation of the Properties of Sea Ice, Beaufort Sea Field Trip Report - March 1979", 36 pp., C-CORE Publication 79-9.

Butt, K.A., Gamberg, J.B., and Rossiter, J.R., "Remote Estimation of the Properties of Sea Ice, Impulse Radar Study of Lake Melville, Labrador", 248 pp., C-CORE Publication 79-7.

The following will appear in the Proceedings of the International Workshop on the Remote Estimation of Sea Ice Thickness, held in St. John's, September 25-26, 1979. The proceedings were published by C-CORE in May, 1980.

Rossiter, James R., "Review of Impulse Radar Sounding of Sea Ice", C-CORE Publication 79-11.

Butt, K.A., and Gamberg, J.B., "Technology of Airborne Impulse Radar", C-CORE Publication 79-12.

Langhorne, P.J., "Crystal Anistropy in Sea Ice".

Davis, J.L., "Electrical Property Measurements of Sea Ice in situ Using Borehole Radar and TDR Techniques".

The following related reports have been published or were in preparation during spring/summer 1980:

Langhorne, Patricia J., Rossiter, James R., and Keliher, T.E., "Remote Estimation of the Properties of Sea Ice, Ice Crystal Fabrics, Beaufort Sea, March 1979", C-CORE Data Report.

Snellen, Jan and Rossiter, James R., "Remote Estimation of the Properties of Sea Ice, Surface Measurements Beaufort Sea, March 1979, C-CORE Data Report.

Rossiter, James R., and others, "Remote Estimation of the Properties of Sea Ice, Analytical Technique for Radar Sounding Data", C-CORE Technical Report.

The following paper was published for the Sixth Canadian Symposium on Remote Sensing, to be held in Halifax, May 21-23, 1980 and published in these proceedings..

Rossiter, James R., and others, "Airborne Impulse Radar Sounding of Sea Ice".

7. RADAR SATELLITE PROGRAM

At the end of the SURSAT project (31 March 1980) a recommendation in form of a Cabinet Submission was made in support of a Radar Satellite (RadarSat) program. During the next three years, the RadarSat project will carry out research and development in SAR technology, mission requirement studies and aircraft experiments that will define a complete radar satellite spacecraft system, whose primary purpose is sea-ice surveillance. The total funding ($15.6M) for this project is requested in the 1980/81 ICS 5-Year Plan, EMR Project No. 3. Currently $1.7M has been approved by Cabinet committee.

This program is being supplemented by a bilateral SAR satellite mission requirements study between NASA and three agencies of the Canadian goverment:

Department of Energy, Mines and Resources
- Canada Centre for Remote Sensing

Department of the Environment
- Atmospheric Environment Service

Department of Communications
- Communications Research Centre

The primary goal of such a RadarSat program would be to provide timely information on ice and ice covered oceans. Consequently ice, particularly sea ice is becoming the driver for the SAR design and the mission concept. If the program is carried out to its total extent, the RadarSat would provide an operational demonstration for ice information services. The satellite launch is expected to occur in 1988. The full bilateral agreement is then in Appendix 7.1. Appendix 7.2 contains some of the NASA and Canadian background material in support of the bilateral study.

APPENDIX 7.1

Bilateral SAR Satellite Mission Requirements Study

Program Implementation Plan

Approval

NASA:

Anthony J Calio

Anthony J. Calio
Associate Administrator for
Space and Terrestrial Applications

Nov. 26, 1980
Date

DEMR:

John D. Keys
Assistant Deputy Minister
Energy, Mines, and Resources

26 November 1980
Date

BACKGROUND

The discussions among representatives of NASA and the Canadian Department of Energy, Mines and Resources (DEMR)* in Ottawa, July 10, 1980, concluded that NASA and DEMR have a mutual interest in undertaking a bilateral study to define a possible future bilateral NASA/DEMR Synthetic Aperture Radar (SAR) satellite program to satisfy US and Canadian requirements. The goals of such a bilateral SAR satellite program would be to provide timely information on ice and ice covered oceans, to provide research data for analyses of ice and open oceans, and to evaluate the contributions of a SAR satellite system to assessing renewable and non-renewable land resources. As agreed at the July 10 meeting, the designated NASA and DEMR points of contact, Dr. Lawrence R. Greenwood of NASA and Dr. Edryd Shaw of DEMR, have discussed further the objectives and method of implementation for the bilateral study. These discussions have led to the development of the plan proposed herein.

OBJECTIVE

The objective of the bilateral study will be to define the mission requirements that may support a bilateral NASA/DEMR program for the development, launch and exploitation of a SAR satellite system designed to satisfy US and Canadian program goals and objectives.

SCOPE

A study to define the mission requirements will be jointly conducted by NASA and DEMR in accordance with the provisions of the Appendix 1 work statement. The C-band radar described in "A Conceptual Design Study for a SURSAT Remote Sensing Satellite System--Main Report," (Reference 1) will be taken as a baseline SAR system to focus the bilateral study. While not part of the bilateral study activity, it is anticipated that NASA and DEMR will separately conduct studies to define a SAR and a mission concept that is responsive to the mission requirements as jointly defined.

SUPPORTING ACTIVITIES

To support the bilateral study, it is expected that an experimental program including airborne SAR experiments will be conducted. The experiments will be designed to attempt to satisfy both US and Canadian objectives. With regard to experiments involving flights of Canadian aircraft, DEMR will bear the costs of flights over Canada, and NASA will bear the costs of flights over the US.

---

*DEMR is the lead agency acting on behalf of Canadian Federal agencies.

ORGANIZATION

The organizational structure for the bilateral study is shown in Figure 1. The organization involves bilateral bodies at three levels: a Review Board, a Program Board and study teams.

The Review Board (RB) will be composed of NASA and Canadian Government agency officials and will be jointly chaired by NASA and DEMR. It will meet alternately in the US and Canada. The RB will provide general direction for the bilateral study and will review the progress of the bilateral study and plans for the prospective bilateral SAR satellite program periodically, as appropriate. At least two major reviews are anticipated.

The Program Board (PB) will be composed of representatives of NASA and DEMR who will manage the NASA and DEMR study team activities. The PB will be jointly chaired. It will meet in conjunction with mutually agreed critical control milestones to review the progress of the bilateral study, provide direction, address any unresolved problems that arise at the study team level, provide a mechanism for cross fertilization among the study teams and develop a plan for the prospective bilateral SAR satellite program, if practical.

The bilateral study teams will have co-chairmen designated by NASA and DEMR. Study team decisions will be made by consensus. There will be four study teams addressing mission requirements for four discipline areas--ice, oceans, renewable and non-renewable land resources. There will be frequent interaction among the study teams.

INFORMATION EXCHANGE/DELIVERABLES/SCHEDULE

Throughout the study activity, the experimental data, results and recommendations deriving from US and Canadian study and experiment activities will be exchanged without restriction. The final product of the study will consist of a final report and a final Mission Requirements Document. If practical, an overall Implementation Plan, including a recommended division of responsibilities, will also be provided. The proposed schedule for the bilateral study is shown in Figure 2.

RESOURCES

It is understood that NASA and DEMR will bear the costs of their respective activities including the cost of required travel for their personnel (except as stated above regarding the flights of Canadian aircraft over the US). It is further understood that the ability of NASA and DEMR to carry out their responsibilities is subject to the availability of appropriated funds.

CONDITIONS

Following completion of the bilateral study activity, NASA and DEMR will assess and determine their respective interest in proceeding with a bilateral SAR satellite program. It is understood that, while such a program is of potential mutual interest to NASA and DEMR, no commitment on the part of either NASA or DEMR to undertake such a bilateral program is implied by their activities in the bilateral study.

REFERENCE

"A Conceptual Design Study for a SURSAT Remote Sensing Satellite System--Main Report", prepared by Canadian Astronautics Limited for the Canada Centre for Remote Sensing under DSS Contract No. 1 SQ78-00116, March 1980.

FIGURE 1 - STUDY ORGANIZATION

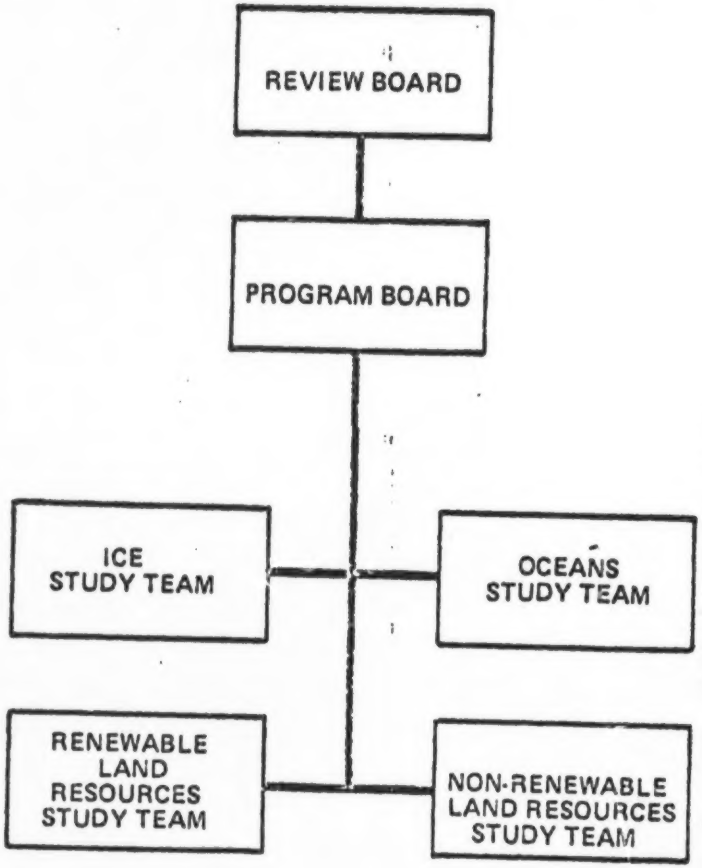
REVIEW BOARD
PROGRAM BOARD
ICE STUDY TEAM
OCEANS STUDY TEAM
RENEWABLE LAND RESOURCES STUDY TEAM
NON-RENEWABLE LAND RESOURCES STUDY TEAM

FIGURE 2 - BILATERAL STUDY SCHEDULE

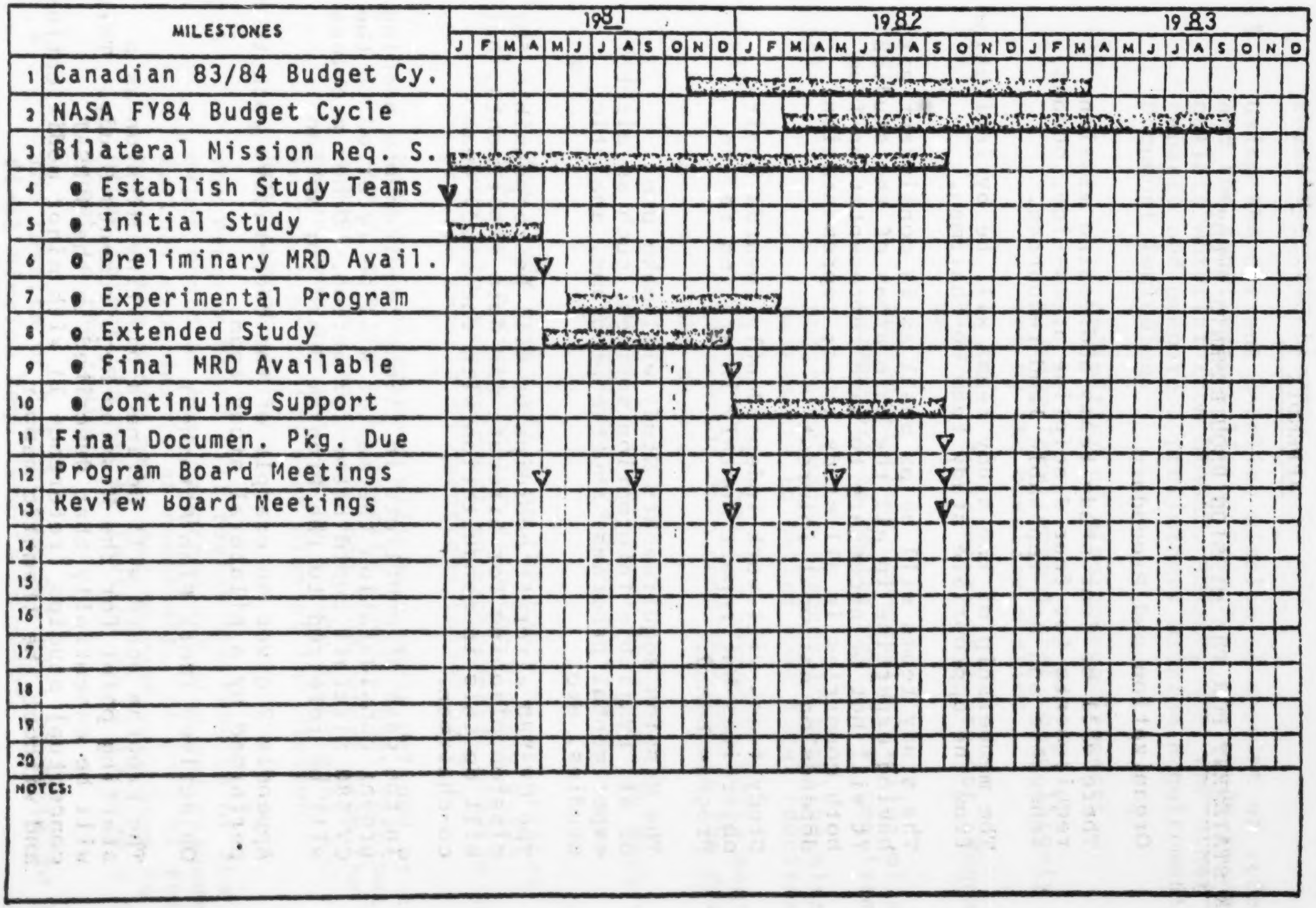

APPENDIX 1

WORK STATEMENT FOR THE MISSION REQUIREMENTS STUDY

1. Organization and Procedure

1.1 There will be four study teams addressing mission requirements for four discipline areas--ice, oceans, renewable and non-renewable land resources.

1.2 The membership of the study teams will be by invitation from the appropriate study team co-chairmen.

1.3 The study teams will be as small as is consistent with having expertise in all the main areas of the studies. It will not be necessary to have representation from both countries in all study areas; representation depends on national interest.

1.4 Study teams will work independently towards their objectives but report monthly in writing to the Program Board.

1.5 The Mission Requirements Study will make use of all available information sources, such as aircraft experimental programs, shuttle programs, analytic studies, etc.

1.6 The CV-580 aircraft coordinator will be responsible for mission planning for aircraft SAR data experiments, but will do this in consultation with the study team co-chairmen.

1.7 In the case of conflicts in flight requirements needing urgent consideration the matter will be referred to the CV-580 aircraft coordinator for action. Other problems will be referred to the Program Board for action.

1.8 Appendix 2 gives an example of the cooperative work to be performed by a bilateral study team.

2. Objectives (Work Plan Attached)

2.1 The Program Board will define a baseline mission as a starting point for the Mission Requirements Study. This will be essentially that described in the SURSAT conceptual studies (reference 1) with minor modifications and without the thematic mapper.

2.2 The study teams will prepare lists of mission requirements with specifications for satellite data and the latitude in these specifications.

2.3 Using the current baseline mission as a point of reference and the requirements listed from 2.2, the study teams will collate material from SEASAT, SURSAT, ASP, and other reports and prepare a preliminary Mission Requirements Document including:

(i) definition of mission requirements

(ii) mission requirements that could largely be met by the baseline mission

(iii) mission requirements that are not adequately met

(iv) suggested minor changes to baseline mission parameters to better meet total requirements

(v) suggested major changes to baseline mission parameters to better meet total requirements

(vi) recommendations for secondary instrumentation to provide data complementary to the prime SAR mission

(vii) areas of uncertainty that require more work on existing data or more data.

2.4 The study teams will, on the basis of priorities decided in consultation with the Program Board formulate and implement an experimental program to provide answers to questions raised by 2.3.

Each such experiment will have goals defined by the study team who will specify exactly what information is sought, the form of the required report from the experiment and the timing of the experiment and report in relation to the work plan of the Mission Requirements Study.

2.5 The Program Board will review the results of the experiments as they progress and plan and conduct further experiments as necessary. As part of this process the study teams may convene workshops to which other scientists may be invited so as to give a broader input to the review.

2.6 The results of 2.3 through 2.5 will be compiled into a final Mission Requirements Document.

2.7 For the remainder of the bilateral study the teams will conclude any outstanding work on the experimental program and associated reports.

WORK PLAN

Month from program start	State of Project
-1	Co-chairmen of the study teams chosen and agreed
-0.5	Study team members chosen and agreed
0	Program start-meeting to review procedures and workplan and to define the baseline mission (Objective 2.1).
1.5	Baseline requirements list completed (Objective 2.2).
4	Preliminary Mission Requirements Document completed (Objective 2.3).
	Experiment plan produced (Objective 2.4). Preparations for implementation started.
*5-14	Data collection for experiments.
8	Interim reports, review, initiation of further experiments if necessary (Objective 2.5).
12	Final Mission Requirements Document completed (Objective 2.6).
16	Data processing completed.
20	Data analysis completed.
21	Experimental reports completed.
	Mission Requirements Definition Study completed (Objective 2.7).

* THE EXPERIMENTS WILL BE STAGGERED THROUGH MONTHS 5 TO 14 BECAUSE OF AIRCRAFT LOGISTICS.

APPENDIX 2

Example of

LEVEL OF CO-OPERATION BETWEEN U.S. & CDN

MISSION REQUIREMENT DEFINITION STUDY - ICE

COORDINATION & COOPERATION IN:

- Identifying research needs
- Planning of experiments and theoretical studies to address these research needs
- Carrying out of these recommended activities
- Joint progress reports on these activities
- Write final documentation on
    - science requirements
    - short and long term applications requirements
    - operational requirements

PREPARE

- Recommendations on the most effective sensor mix (satellite) for our operational demonstration program.

APPENDIX 7.2

Joint NASA/DEMR

SAR Satellite Mission Requirements Study

Program Implementation Plan

Scope/Content

NASA Headquarters

November 26, 1980

Joint SAR Satellite Mission Requirements Study

Objectives

JOINT PROGRAM:

- Provide timely information on ice and ice covered oceans.
- Provide research data for analyses of ice and open oceans.
- Evaluate the contributions of a SAR satellite system to assessing renewable and non-renewable land resources.

JOINT STUDY:

- Define the mission requirements that may support a bilateral NASA/DEMR program for the development, launch, and exploitation of a SAR satellite system designed to satisfy US and Canadian program goals and objectives.

Joint SAR Satellite Mission Requirements Study

Scope

- This plan provides for the definition of mission requirements (research and operational) that may support a future joint SAR satellite program.
- The C-Band SAR described in the SURSAT study will be used as a baseline to focus the joint study.
- The definition of a SAR and a mission concept responsive to the mission requirements as jointly defined is not provided for by this plan.

Joint SAR Satellite Mission Requirements Study

Approach

- Form joint US/Canadian study teams to address in detail the specific research and operational requirements associated with each of the four discipline related areas of interest, i.e., ice, oceans, renewable and non-renewable land resources.

- Establish a Mission Requirements Steering Committee to provide guidance and direction to the study teams and to provide a mechanism for cross fertilization among the study teams.

- Formulate and implement an experimental program utilizing airborne SAR to address questions raised by the study teams.

Joint SAR Satellite Mission Requirements Study

Deliverables

- A Mission Requirements Document including:
    - rank ordering of mission requirements
    - mission requirements that could largely be met by the baseline mission
    - mission requirements that are not adequately met
    - suggested minor changes to baseline mission parameters to better meet total requirements
    - suggested major changes to baseline mission parameters to better meet total requirements
    - recommendations for secondary instrumentation to provide data complementary to the prime SAR mission
    - areas of uncertainty that require more work on existing data or more data.
- A final report covering all aspects of the joint study activity, including the experimental program.

Joint SAR Satellite Mission Requirements Study

Additional Considerations

- The experimental data, results and recommendations deriving from the joint study will be exchanged without restriction .
- NASA and DEMR will bear the costs of their respective activities subject to the availability of appropriated funds.
- At the conclusion of the joint study, NASA and DEMR will address whether or not to proceed with a joint SAR satellite program. No commitment to do so is implied by the joint study.
- The method of implementation for the SAR and mission concept definition studies is TBD.

RADARSAT

CANADIAN OBJECTIVES

- TO PROVIDE RELIABLE TIMELY SOURCE OF ALL-WEATHER SATELLITE DATA TO SUPPORT ARCTIC OPERATIONS.
- TO PROVIDE OCEANS AND LAND RESEARCHERS HIGH QUALITY DIGITAL RADAR DATA FOR DEVELOPMENT OF APPLICATIONS.
- DEVELOP AN INDUSTRIAL TECHNOLOGY BASE TO MEET DOMESTIC NEEDS FOR RADAR SATELLITE SYSTEMS.

CANADIAN ISSUES

- ARCTIC SOVEREIGNTY
  - CANADIAN NEED FOR DATA
  - EXPLOITATION UNDER CANADIAN CONTROL
- INDUSTRIAL DEVELOPMENT
  - REMOTE SENSING SPACE TECHNOLOGY
  - PRIME CONTRACTOR PROGRAM MAINTENANCE
  - GROUND SYSTEMS
  - INFORMATION USE

FRONTIER ENERGY SUPPLIES

ESTIMATED RESERVES*

BEAUFORT SEA/MACKENZIE DELTA

OIL **	32 - 70 Billion Barrels
GAS **	84 - 127 Trillion Cu. Ft.

EAST COAST

OIL	1.9 Billion Barrels
GAS	9.6 Trillion Cu. Ft.

ARCTIC ISLANDS

GAS	14.7 Trillion Cu. Ft.

---

* Dome Petroleum Ltd.

** *DEMR ESTIMATES (ADDED BY EDITORS)*

OIL 6.9- 9.1 BILLION BARRELS

GAS 60 - 76.5 TRILLION Cu. Ft.

TRANSPORTATION SCHEDULE

ICE-BREAKER TANKERS

BEAUFORT OIL -

1985 - 750,000 BBLS/DAY

1990 - 1,500,000 BBLS/DAY

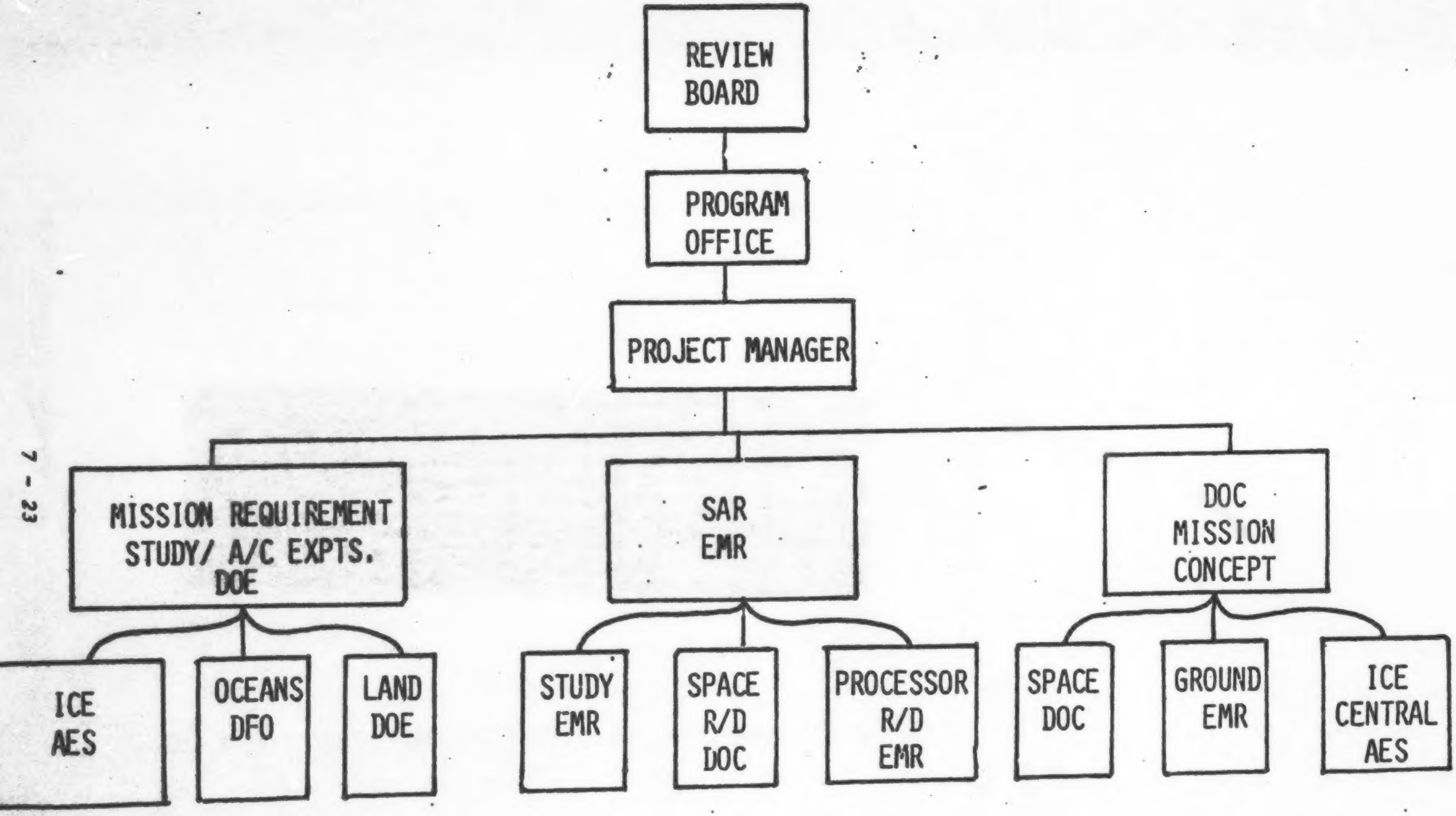
REVIEW BOARD
PROGRAM OFFICE
PROJECT MANAGER
MISSION REQUIREMENT STUDY/ A/C EXPTS. DOE
SAR EMR
DOC MISSION CONCEPT
ICE AES
OCEANS DFO
LAND DOE
STUDY EMR
SPACE R/D DOC
PROCESSOR R/D EMR
SPACE DOC
GROUND EMR
ICE CENTRAL AES

RADARSAT ORGANIZATION (CANADA)

POOR

QUALITY

ORIGINAL